

INFORMATION TO USERS

This manuscript has been reproduced from the microfilm master. UMI films the text directly from the original or copy submitted. Thus, some thesis and dissertation copies are in typewriter face, while others may be from any type of computer printer.

The quality of this reproduction is dependent upon the quality of the copy submitted. Broken or indistinct print, colored or poor quality illustrations and photographs, print bleedthrough, substandard margins, and improper alignment can adversely affect reproduction.

In the unlikely event that the author did not send UMI a complete manuscript and there are missing pages, these will be noted. Also, if unauthorized copyright material had to be removed, a note will indicate the deletion.

Oversize materials (e.g., maps, drawings, charts) are reproduced by sectioning the original, beginning at the upper left-hand corner and continuing from left to right in equal sections with small overlaps. Each original is also photographed in one exposure and is included in reduced form at the back of the book.

Photographs included in the original manuscript have been reproduced xerographically in this copy. Higher quality 6" x 9" black and white photographic prints are available for any photographs or illustrations appearing in this copy for an additional charge. Contact UMI directly to order.

UMI

A Bell & Howell Information Company
300 North Zeeb Road, Ann Arbor MI 48106-1346 USA
313/761-4700 800/521-0600

University of Alberta

**Fe(CO)₄(η^2 -alkyne) Compounds:
An Organometallic Renaissance**

by

Jason Cooke ©

A thesis submitted to the Faculty of Graduate Studies and Research
in partial fulfillment of the requirements for the degree of Doctor of Philosophy

Department of Chemistry

Edmonton, Alberta

Fall, 1998



National Library
of Canada

Acquisitions and
Bibliographic Services

395 Wellington Street
Ottawa ON K1A 0N4
Canada

Bibliothèque nationale
du Canada

Acquisitions et
services bibliographiques

395, rue Wellington
Ottawa ON K1A 0N4
Canada

Your file Votre référence

Our file Notre référence

The author has granted a non-exclusive licence allowing the National Library of Canada to reproduce, loan, distribute or sell copies of this thesis in microform, paper or electronic formats.

The author retains ownership of the copyright in this thesis. Neither the thesis nor substantial extracts from it may be printed or otherwise reproduced without the author's permission.

L'auteur a accordé une licence non exclusive permettant à la Bibliothèque nationale du Canada de reproduire, prêter, distribuer ou vendre des copies de cette thèse sous la forme de microfiche/film, de reproduction sur papier ou sur format électronique.

L'auteur conserve la propriété du droit d'auteur qui protège cette thèse. Ni la thèse ni des extraits substantiels de celle-ci ne doivent être imprimés ou autrement reproduits sans son autorisation.

0-612-34751-6

Canada

University of Alberta

Library Release Form

Name of Author: Jason Cooke

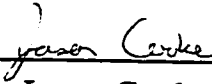
Title of Thesis: Fe(CO)₄(η²-alkyne) Compounds:
An Organometallic Renaissance

Degree: Doctor of Philosophy

Year this Degree Granted: 1998

Permission is hereby granted to the University of Alberta Library to reproduce single copies of this thesis and to lend or sell such copies for private, scholarly, or scientific research purposes only.

The author reserves all other publication and other rights in association with the copyright in the thesis, and except as hereinbefore provided, neither the thesis nor any substantial portion thereof may be printed or otherwise reproduced in any material form whatever without the author's prior written permission.



Jason Cooke

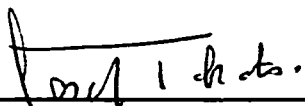
#202, 10810 - 86 Avenue
Edmonton, Alberta
T6E 2N2

Date: July 7, 1998

University of Alberta

Faculty of Graduate Studies and Research

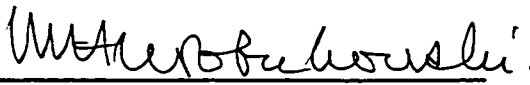
The undersigned certify that they have read, and recommend to the Faculty of Graduate Studies and Research for acceptance, a thesis entitled **Fe(CO)₄(η^2 -alkyne) Compounds: An Organometallic Renaissance** submitted by Jason Cooke in partial fulfillment of the requirements for the degree of Doctor of Philosophy.



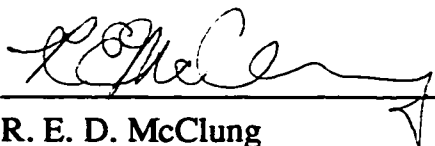
J. Takats (Supervisor)



R. B. Jordan



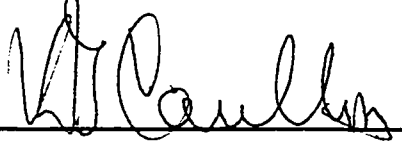
M. Klobukowski



R. E. D. McClung



S. E. Wanke



K. G. Caulton (External Examiner)

Date: June 22, 1998

Abstract

The long elusive $\text{Fe}(\text{CO})_4(\eta^2\text{-C}_2\text{R}_2)$ ($\text{R} = \text{R}' = \text{CF}_3$, **1a**; H , **1c**; Me , **1e**; $\text{R} = \text{H}$, $\text{R}' = \text{CF}_3$, **1b**; $\text{R} = \text{H}$, $\text{R}' = \text{Me}$, **1d**) compounds have been synthesized by carefully controlled low temperature photochemistry. Reaction of isolated **1a-e** with added alkyne demonstrated that the $\text{Fe}(\text{CO})_4(\eta^2\text{-alkyne})$ complexes were intermediates in the coupling of alkynes with carbon monoxide to produce unsaturated cyclic organic molecules, a hitherto unproved postulate first proposed four decades ago. The $\text{Fe}(\text{CO})_4(\eta^2\text{-C}_2\text{R}_2)$ species were also reactive towards carbon monoxide in the absence of added alkyne. The π -acidic alkyne ligands in **1a,b** underwent one migratory insertion of CO to produce $\text{Fe}(\text{CO})_4\{\eta^1, \eta^1\text{-C}(\text{CF}_3)\text{CRC}(\text{O})\}$ ($\text{R} = \text{CF}_3$, **5a**; H , **5b**), and tricarbonylferracyclopenta-3-en-2,5-dione dimers (**6c-e**) were isolated from complexes **1c-e**. The dimeric compounds proved to be quite reactive towards electron rich alkynes and provided a general synthesis of substituted tricarbonyl(*p*-quinone)iron complexes (**4a-h**). Compounds **6d,e** also reacted further with CO to produce tetracarbonylferracyclopenta-3-en-2,5-diones, **7d,e**.

Apart from the ability to undergo facile migratory insertion reactions, the carbonyl ligands in the $\text{Fe}(\text{CO})_4(\eta^2\text{-C}_2\text{R}_2)$ species were also found to be very labile. Phosphine substitution reactions of $\text{Fe}(\text{CO})_4(\eta^2\text{-C}_2(\text{CF}_3)_2)$ (**1a**) were investigated, and a kinetic study revealed a spectacular 3×10^{13} -fold increase in reactivity relative to the parent $\text{Fe}(\text{CO})_5$. Compound **1a** was also more reactive than its Ru and Os counterparts, providing an interesting exception to the usual triad trend for CO substitution in transition metal carbonyl compounds, (1st row) < (2nd row) > (3rd row). The tricyclohexylphosphine ligand provided a felicitous combination of steric and electronic features which allowed the isolation of $\text{Fe}(\text{CO})_2(\text{PCy}_3)(\eta^2\text{-C}_2(\text{CF}_3)_2)$ (**10**), a compound containing a four

electron-donor alkyne which serves as a model for the putative $[\text{Fe}(\text{CO})_3(\eta^2\text{-C}_2(\text{CF}_3)_2)]$ intermediate following CO dissociation from **1a**.

The $\text{Fe}(\text{CO})_4(\eta^2\text{-alkyne})$ species were also found to be useful precursors in the synthesis of a variety of alkyne-bridged heterobimetallic compounds incorporating group nine metals (Co, Rh, Ir). The structural types included dimetallatetrahedranes (**11**), dimetallacyclobutenes (**12**), $\mu\text{-}\eta^1\text{:}\eta^3\text{-dimetalla-cyclopentenones}$ (**13, 16, 17, 24, 27, 31, 32**) and $\mu\text{-}\eta^1\text{:}\eta^1\text{-dimetallacyclo-pentenones}$ (**18, 25, 26**). In the latter two categories, the acyl groups were most frequently bonded to the Fe center, in contrast to the products obtained previously from $\text{Os}(\text{CO})_4(\eta^2\text{-alkyne})$ compounds where the acyl group was bonded to the group nine metal. Low temperature multinuclear NMR experiments revealed that the distinguishing factor between the different metals of the triad was that the $\text{Fe}(\text{CO})_4(\eta^2\text{-alkyne})$ complexes could initiate reactions through facile migratory insertion, while the Os analogs displayed chemistry governed entirely by a carbonyl dissociation pathway. Although all previously mentioned reactions occurred with retention of the coordinated alkyne ligand, the reaction of $\text{Fe}(\text{CO})_4(\eta^2\text{-C}_2\text{Me}_2)$ with $\text{Cp}^*\text{Co}(\text{CO})_2$ produced $\text{Cp}^*\text{CoFe}(\mu\text{-CO})_2(\text{CO})_4$ (**33**), an interesting heterobimetallic compound containing an Fe→Co dative bond supported by a pair of semi-bridging carbonyl ligands.

Acknowledgements

First and foremost, I would like to extend my deepest thanks to Professor Josef Takats for his advice, support, and enthusiasm. Apart from being an excellent mentor, Joe was always willing to lend a helpful, friendly ear to all manner of subjects, personal and professional, and it is this friendship which I consider to be the most important product of my time under his guidance. You would also be hard-pressed to find better hosts for a Christmas party or barbecue than the other members of the Takats family, Mickey, Lisa, and Michael.

I would also like to thank the past and present members of the Takats' research group for making my tenure enjoyable, for their contributions to discussions surrounding the work presented in this Thesis, and for their support and advice when things were not quite working out in the lab. In no particular order, the cast of characters is John Washington, Ken Hoffman, Wenyi Fu, Yimin Sun, Xingwang Zhang, Tianfu Mao, Stefan Haufe, Jean Pearson, Joanne Gainsforth, Quinn Major, Guanyan Lin, and Greg Ferrence. I would also like to thank Andrew McInroy for performing some experiments related to the reaction of $\text{Fe}(\text{CO})_4(\eta^2\text{-C}_2\text{H}_2)$ with alkynes (Chapter 3) and the synthesis of compound **11a*** (Chapter 4) during his short stay with us one summer.

The friendship and camaraderie of many of the other graduate students has been sincerely appreciated over the years. Although the list is too long to divulge in full, particular thanks go to Chris Daley for his hard work at keeping various hockey-related pastimes going for the enjoyment of all, Steve Decker for providing that bone-crushing body check right when it was least expected, and Mike Ferguson for providing a variety of "interesting" subjects for lunch time discussions in the fourth floor lounge. The other regular members of the lunch crowd, Jason Wiles, Chris Lee, and Rob Lam, are thanked for their efforts to keep Mike in check.

A great number of people within the Department of Chemistry assisted with the accumulation of scientific data presented within this Thesis. Specifically, I would like to take this opportunity to extend my gratitude to the staff of the NMR facility, particularly Dr. Tom Nakashima, Gerdy Aarts, Glen Bigam, Tom

Brisbane, and Lai Kong, for their skill, dedication, and patience in collecting numerous NMR spectra. The efforts of Dr. Bob McDonald in determining all of the X-ray crystal structures presented are sincerely appreciated. Additionally, I would like to thank Darlene Mahlow and Andrea Dunn for elemental analysis and the staff of the Mass Spectrometry facility for obtaining mass spectra on compounds that would occasionally hasten the cleaning of their instruments. Finally, I would like to acknowledge the hard work of the staff of the machine, electronic, and glass shops for keeping various pieces of vital scientific equipment functioning, and for granting the occasional rush "ASAP or sooner" work order.

I would also like to thank several of the Professors in the department for their contributions; Bob Jordan for his generous assistance with the analysis of the kinetic experiments carried out in Chapter 4, Marty Cowie for helpful discussions relating to several of the structures presented, and Ted McClung for providing an upgraded and very user-friendly software package for simulating the variable temperature NMR spectra in Chapters 5 and 6.

Finally, I would like to thank my friends and family for their support and encouragement over the duration of my studies at the University of Alberta. My greatest thanks go to my wife, Grace, for her love, understanding, and support, gifts for which I am continually grateful.

Table of Contents

Chapter 1 Introduction

1.1. The Reaction of Alkynes with Binary Carbonyls of the Iron Triad.....	1
1.1.1. Compounds Derived from Iron Carbonyls.....	1
1.1.2. Some Recent Applications to Organic Synthesis.....	8
1.1.3. Reaction of Osmium and Ruthenium Carbonyls with Alkynes....	10
1.2. $M(CO)_4(\eta^2\text{-alkyne})$ Compounds.....	11
1.2.1. Bonding in $M(CO)_4(\eta^2\text{-alkyne})$ Species.....	11
1.2.2. Synthesis of $M(CO)_4(\eta^2\text{-alkyne})$ ($M = Ru, Os$) Compounds.....	16
1.3. Bimetallic Compounds with Alkyne Bridges.....	17
1.3.1. Targeted Synthesis of Alkyne-Bridged Heterobimetallic Compounds.....	17
1.3.2. Reaction of Alkynes on Pre-Formed Bimetallic Frameworks.....	19
1.4. Scope of the Thesis.....	22
1.5. References.....	24

Chapter 2 Low Temperature Photochemical Synthesis of $Fe(CO)_4(\eta^2\text{-RC}\equiv\text{CR}')$ Complexes ($R, R' = CF_3, H, Me; R = H, R' = CF_3, Me$)

2.1. Introduction.....	30
2.2. Synthesis and Characterization of the Title Compounds.....	31
2.2.1. Synthesis of $Fe(CO)_4(\eta^2\text{-alkyne})$ (1).....	31
2.2.2. ^{13}C Exchange and Evidence of Further Reactivity of 1 Towards CO.....	37
2.2.3. Characterization of $Fe(CO)_4(\eta^2\text{-alkyne})$ Compounds (1a-e).....	38
2.3. A Comparison of the Spectroscopic Properties of 1a-e	44
2.3.1. FT-IR Spectra.....	44
2.3.2. ^{13}C NMR Coordination Shifts.....	46
2.3.3. Carbonyl Scrambling in 1a-e	48
2.4. A Triad Comparison of $M(CO)_4(\eta^2\text{-alkyne})$ Compounds.....	49
2.5. Conclusions.....	57

2.6. Experimental Section.....	58
2.6.1. Solvents and General Techniques.....	58
2.6.2. Physical Measurements.....	58
2.6.3. Photochemical Techniques.....	59
2.6.4. Reagents.....	60
2.6.5. Synthetic Procedures.....	61
2.7. References.....	66

Chapter 3 The Intermediacy of Fe(CO)₄(η^2 -alkyne) Complexes and Their Derivatives in the Metal-Mediated Coupling of Alkynes with Carbon Monoxide

3.1. Introduction.....	68
3.2. Reaction of Fe(CO) ₄ (η^2 -alkyne) Compounds (1a-f) with Alkynes.....	69
3.3. Reaction of Fe(CO) ₄ (η^2 -alkyne) Compounds (1a-e) with CO.....	73
3.3.1. Formation of Metallacyclobutenones (5a,b) from 1a,b.....	73
3.3.2. Synthesis of Ferracyclopent-3-en-2,5-diones (6c-e; 7d,e) from 1c-e.....	77
3.4. Proposed Mechanisms for Fe-Mediated Coupling of Alkynes with CO.....	83
3.4.1. Reaction of Fe(CO) ₄ (η^2 -alkyne) Compounds with CO.....	83
3.4.2. Proposed Pathways for Formation of Cyclic Organic Ligands in 2-4.....	85
3.5. Reaction of Compounds 6d,e with Alkynes: A General Synthesis of Substituted Tricarbonyl(<i>p</i> -quinone)iron Complexes.....	90
3.5.1. Synthetic Aspects.....	90
3.5.2. Characterization of the Tricarbonyl(<i>p</i> -quinone)iron Products.....	93
3.6. Conclusions.....	97
3.7. Experimental Section.....	98
3.7.1. Reagents.....	98
3.7.2. Synthetic Procedures.....	98
3.8. References.....	108

**Chapter 4 Reactivity of $\text{Fe}(\text{CO})_4(\eta^2\text{-C}_2(\text{CF}_3)_2)$ Towards Phosphines:
Spectacular Enhancement of Carbonyl Substitutional Lability
by an Alkyne Ligand**

4.1. Introduction	111
4.2. Reaction of $\text{Fe}(\text{CO})_4(\eta^2\text{-HFB})$ (1a) with PR_3 (R = Me, Ph)	112
4.2.1. Synthetic Aspects	112
4.2.2. Characterization of Products	113
4.2.3. Reversible PPh_3 Dissociation from $\text{Fe}(\text{CO})_2(\text{PPh}_3)_2(\eta^2\text{-HFB})$, 9b	116
4.3. Reaction of 1a with Bulky Phosphines (P^tBu_3 and PCy_3)	117
4.3.1. Initial Observations	117
4.3.2. Characterization of Isomeric $\text{Fe}(\text{CO})_3(\text{PCy}_3)(\eta^2\text{-HFB})$, 8c/c'	119
4.3.3. Isolation of Coordinatively Unsaturated $\text{Fe}(\text{CO})_2(\text{PCy}_3)(\eta^2\text{-HFB})$, 10	122
4.3.4. Molecular Structure of $\text{Fe}(\text{CO})_2(\text{PCy}_3)(\eta^2\text{-HFB})$ (10)	125
4.4. Kinetic Studies	128
4.4.1. Determination of the Rate of CO Dissociation from 1a	128
4.4.2. Further Analysis of the Reaction of 1a with PPh_3	135
4.4.3. Further Analysis of the Reaction of 1a with PCy_3	140
4.5. Conclusions	144
4.6. Experimental Section	146
4.6.1. Reagents	146
4.6.2. Synthetic Procedures	146
4.6.3. X-ray Crystal Structure Determination of Compound 10	150
4.6.4. Kinetic Measurements	153
4.7. References	154

Chapter 5 Formation of Heterobimetallic Complexes from the Reaction of $\text{Fe}(\text{CO})_4(\eta^2\text{-C}_2(\text{CF}_3)_2)$ with $\text{Cp}'\text{M}(\text{CO})_2$ ($\text{M} = \text{Co}, \text{Rh}, \text{Ir}$; $\text{Cp}' = \text{Cp}, \text{Cp}^*$)

5.1. Introduction	157
5.2. Reaction of 1a with $\text{Cp}'\text{M}(\text{CO})_2$ ($\text{M} = \text{Co}, \text{Rh}, \text{Ir}$; $\text{Cp}' = \text{Cp}, \text{Cp}^*$)	158
5.2.1. Synthetic Aspects	158
5.2.2. Characterization of Compounds 11a,a*: Dimetallatetrahedranes	159
5.2.3. Initial Characterization of Heterobimetallics 12a-c and 13a-c	161
5.2.4. Molecular Structure of $\text{CpIrFe}(\text{CO})_5(\mu\text{-}\eta^1\text{:}\eta^1\text{-HFB})$ (12c)	165
5.2.5. Molecular Structure of $\text{Cp}^*\text{IrFe}(\text{CO})_4(\mu\text{-}\eta^1\text{:}\eta^3\text{-C}_2(\text{CF}_3)_2\text{C}(\text{O}))$ (13c)	169
5.2.6. Further Spectroscopic Characterization of 12a-c and 13a-c	175
5.3. Variable Temperature ^{13}C NMR Studies on 12b,c and 13a-c	179
5.3.1. Fluxional Behavior of the Heterodimetallacyclobutenes, 12b,c ...	179
5.3.2. Fluxional Behavior of Heterodimetallacyclopentenones 13a-c ...	183
5.4. Low Temperature NMR Studies of the Reaction of 1a with $\text{Cp}'\text{Rh}(\text{CO})_2$	189
5.4.1. Reaction of 1a with $\text{CpRh}(\text{CO})_2$: Detection of an Intermediate Dimetallacyclopentenone in the Formation of a Dimetallacyclobutene	189
5.4.2. Reaction of 1a with $\text{Cp}^*\text{Rh}(\text{CO})_2$	197
5.5. Intermolecular CO Exchange Between 1a and $\text{Os}(\text{CO})_5$	199
5.6. Conclusions	201
5.7. Experimental Section	202
5.7.1. Reagents	202
5.7.2. Synthetic Procedures	202
5.7.3. X-ray Crystal Structure Determination of Compounds 12c and 13c	208
5.7.4. Variable Temperature NMR Studies of Fluxional Processes	213
5.7.5. Variable Temperature NMR Reaction Monitoring	214
5.8. References	215

Chapter 6 Reaction of $\text{Fe}(\text{CO})_4(\eta^2\text{-C}_2\text{H}_2)$ with $\text{Cp}'\text{M}(\text{CO})_2$ ($\text{M} = \text{Co}, \text{Rh}, \text{Ir}$; $\text{Cp}' = \text{Cp}, \text{Cp}^*$): Formation of Dimetallacyclopentenones

6.1. Introduction	219
6.2. Reaction of 1c with $\text{Cp}'\text{M}(\text{CO})_2$ ($\text{M} = \text{Co}, \text{Rh}, \text{Ir}$; $\text{Cp}' = \text{Cp}, \text{Cp}^*$)	220
6.2.1. Synthetic Aspects	220
6.2.2. Spectroscopic Characterization of 16a-c	221
6.2.3. Molecular Structure of 16b	224
6.2.4. Characterization of 17b: Detection of an Isomeric Pair Related by the Orientation of Ligands on the Ancillary Metal Center	228
6.2.5. Initial Characterization of 18c	231
6.2.6. Molecular Structure of 18c	235
6.2.7. Further Spectroscopic Characterization of 18c	239
6.3. Variable Temperature NMR Studies of Molecular Rearrangements	240
6.3.1. Fluxional Turnstile Exchange in 16a-c and 17b,b'	240
6.3.2. Isomerization of 17b,b'	243
6.4. Low Temperature NMR Reaction Monitoring	247
6.4.1. Reaction of 1c with $\text{Cp}^*\text{Rh}(\text{CO})_2$	247
6.4.2. Proposed Mechanisms in the Reaction of 1c with $\text{Cp}^*\text{Rh}(\text{CO})_2$	251
6.4.3. Solvent Dependence of the Reaction of 1c with $\text{Cp}^*\text{Rh}(\text{CO})_2$	256
6.4.4. Reaction of 1c with $\text{Cp}^*\text{Ir}(\text{CO})_2$	257
6.4.5. Conversion of $\mu\text{-}\eta^1\text{:}\eta^1\text{-}$ and $\mu\text{-}\eta^1\text{:}\eta^3\text{-}$ Dimetallacyclopentenones	258
6.5. Conclusions	259
6.6. Experimental Section	261
6.6.1. Reagents	261
6.6.2. Synthetic Procedures	261
6.6.3. X-ray Crystal Structure Determination of Compounds 16b and 18c	265
6.6.4. Variable Temperature NMR Studies of Fluxional Processes	270
6.6.5. Variable Temperature NMR Reaction Monitoring	270
6.7. References	273

**Chapter 7 Heterobimetallic Compounds Derived from $\text{Fe}(\text{CO})_4(\eta^2\text{-RCCR}')$
($\text{R} = \text{H}$, $\text{R}' = \text{CF}_3, \text{Me}$; $\text{R}, \text{R}' = \text{Me}$)**

7.1. Introduction	276
7.2. Reaction of $\text{Fe}(\text{CO})_4(\eta^2\text{-TFP})$ (1b) with $\text{Cp}'\text{M}(\text{CO})_2$ ($\text{M} = \text{Co}, \text{Rh}, \text{Ir}$; $\text{Cp}' = \text{Cp}, \text{Cp}^*$): Competing Formation of Dimetallacyclopentenones	277
7.2.1. Initial Observations	277
7.2.2. Reaction of $\text{Fe}(\text{CO})_4(\eta^2\text{-TFP})$ (1b) with $\text{Cp}^*\text{Rh}(\text{CO})_2$	277
7.2.3. Molecular Structure of 24b	278
7.2.4. Reaction of 1b with $\text{Cp}'\text{M}(\text{CO})_2$ ($\text{Cp}'\text{M} = \text{Cp}^*\text{Co}, \text{CpRh}, \text{Cp}^*\text{Ir}$)	281
7.2.5. Mechanistic Implications of the Product Distributions	286
7.2.6. Identification of the Thermodynamic Products from 25c and 26c	291
7.3. Reaction of $\text{Fe}(\text{CO})_4(\eta^2\text{-RCCMe})$ ($\text{R} = \text{H}$, 1d; Me, 1e) with $\text{Cp}'\text{M}(\text{CO})_2$	292
7.3.1. Initial Observations	292
7.3.2. Characterization of the Products from the Reaction of 1d with $\text{Cp}'\text{Rh}(\text{CO})_2$ ($\text{Cp}' = \text{Cp}, \text{Cp}^*$)	293
7.3.3. Unexpected Formation of $\text{Cp}^*\text{CoFe}(\mu\text{-CO})_2(\text{CO})_4$, 33, via Alkyne Loss	293
7.3.4. Molecular Structure of $\text{Cp}^*\text{CoFe}(\mu\text{-CO})_2(\text{CO})_4$, 33	295
7.4. Conclusions	301
7.5. Experimental Section	303
7.5.1. Reagents	303
7.5.2. Synthetic Procedures	303
7.5.3. X-ray Crystal Structure Determination of Compounds 24b and 33c	311
7.6. References	316
 Chapter 8 Conclusions	 318
8.1. References	324

List of Tables

Table 2-1	Reaction Conditions and Product Yields in the Synthesis of 1a-e	33
Table 2-2	FT-IR Spectra (pentane, cm^{-1}) of 1a-e	40
Table 2-3	^1H and ^{19}F NMR Spectra (CD_2Cl_2) of 1a-e	41
Table 2-4	$^{13}\text{C}\{^1\text{H}\}$ NMR Spectra (CD_2Cl_2 , ppm) of 1a-e	42
Table 2-5	FT-IR Alkyne Coordination Shifts ($\Delta(\nu_{\text{C-C}})$, cm^{-1}) in 1a-d	45
Table 2-6	^{13}C NMR Alkyne Coordination Shifts ($\Delta(\delta_{\text{C}_{\text{alk}}})$, ppm) in 1a-e	47
Table 2-7	FT-IR in the Carbonyl Region of $\text{M}(\text{CO})_4(\eta^2\text{-RC}\equiv\text{CR}')$ Species...	51
Table 2-8	Comparison of Activation Energies (ΔG^\ddagger , kJ/mol) for Carbonyl Scrambling in $\text{M}(\text{CO})_4(\eta^2\text{-C}_2\text{H}_x)$ ($x = 2,4$).....	52
Table 2-9	Spectroscopic Features of $\text{M}(\text{CO})_4(\eta^2\text{-RC}\equiv\text{CR}')$ Species.....	54
Table 2-10	Spectroscopic Features of $\text{M}(\text{CO})_4(\eta^2\text{-C}_2(\text{SiMe}_3)_2)$ Species.....	55
Table 3-1	$^{13}\text{C}\{^1\text{H}\}$ NMR Spectra (δ , ppm) of $\text{Fe}(\text{CO})_4\{\eta^1, \eta^1\text{-}(\text{O})\text{CCRCR}'\text{C}(\text{O})\}$ Species.....	79
Table 3-2	$^{13}\text{C}\{^1\text{H}\}$ NMR Spectra (CD_2Cl_2 , 400.1 MHz) of ^{13}CO Enriched 6c-e	81
Table 3-3	FT-IR Spectra (ν , cm^{-1}) of 4a-h	94
Table 3-4	^1H NMR Chemical Shifts in 4a-h (CD_2Cl_2 , 400.1 MHz).....	95
Table 3-5	^{13}C NMR Chemical Shifts in 4a-h (CD_2Cl_2 , 100.6 MHz).....	96
Table 4-1	FT-IR Spectra (ν , cm^{-1}) of $\text{Fe}(\text{CO})_{4-x}(\text{PR}_3)_x(\eta^2\text{-HFB})$ ($x = 1, 2$)....	114
Table 4-2	Selected Interatomic Distances (\AA) and Angles (deg.), Compound 10	126
Table 4-3	Kinetic Results for Reactions of PR_3 with 1a in CD_2Cl_2	130
Table 4-4	Comparison of the Reactivity of $\text{M}(\text{CO})_4\text{L}$ Systems with PPh_3	132
Table 4-5	Kinetic Results from Analysis of the Formation of 8b and 9b from 1a and PPh_3 in CD_2Cl_2	139
Table 4-6	Crystallographic Experimental Details for Compound 10	151

Table 4-7	Atomic Coordinates and Equivalent Isotropic Displacement Parameters for Compound 10	152
Table 5-1	^{19}F NMR Data (δ, ppm) for $\text{Cp}'\text{MM}'(\text{CO})_5(\text{HFB})$	162
Table 5-2	FT-IR Spectra (pentane, cm^{-1}) of 12a-c	162
Table 5-3	FT-IR Spectra (pentane, cm^{-1}) of 13a-c	163
Table 5-4	Limiting ^{13}C NMR for 12a-c and 13a-c (CD_2Cl_2)	164
Table 5-5	Selected Interatomic Distances (\AA) in Compound 12c	166
Table 5-6	Selected Interatomic Angles (deg.) in Compound 12c	167
Table 5-7	Selected Interatomic Distances (\AA) in Compound 13c	170
Table 5-8	Selected Interatomic Angles (deg.) in Compound 13c	171
Table 5-9	Activation Parameters for Carbonyl Scrambling in 12b,c	182
Table 5-10	Activation Parameters for Pair-wise Carbonyl Scrambling in Alkyne-Bridged Heterobimetallic Compounds	183
Table 5-11	Activation Parameters for Carbonyl Scrambling in 13a-c	187
Table 5-12	Crystallographic Experimental Details for Compound 12c	209
Table 5-13	Atomic Coordinates and Equivalent Isotropic Displacement Parameters for Compound 12c	210
Table 5-14	Crystallographic Experimental Details for Compound 13c	211
Table 5-15	Atomic Coordinates and Equivalent Isotropic Displacement Parameters for Compound 13c	212
Table 5-16	Summary of the Rate Constants for Pair-wise (k_1) and Turnstile (k_2) Carbonyl Scrambling in 12b,c and 13a-c	213
Table 6-1	^1H and $^{13}\text{C}\{^1\text{H}\}$ NMR Spectra of the C_2H_2 Moiety in 16a-c and Representative $\text{MM}'\text{L}_n(\mu\text{-}\eta^1\text{:}\eta^3\text{-C}_2\text{H}_2\text{C}(\text{O}))$ Species	222
Table 6-2	Limiting $^{13}\text{C}\{^1\text{H}\}$ NMR Spectra of 16a-c in the Carbonyl Region	223
Table 6-3	FT-IR Spectra (CH_2Cl_2, cm^{-1}) of 16a-c	224
Table 6-4	Selected Interatomic Distances (\AA) in Compound 16b	225
Table 6-5	Selected Interatomic Angles (deg.) in Compound 16b	226

Table 6-6	Comparison of Metrical Parameters in MM'L _n (μ-η ¹ :η ³ -C ₂ R ₂ C(O)) Compounds.....	227
Table 6-7	Selected ¹ H and ¹³ C{ ¹ H} NMR Data for 17b/b' and 16b	229
Table 6-8	¹ H and ¹³ C{ ¹ H} NMR Data for MM'L _n (μ-η ¹ :η ¹ -C ₂ H ₂ C(O))	232
Table 6-9	Selected Interatomic Distances (Å) in Compound 18c	236
Table 6-10	Selected Interatomic Angles (deg.) in Compound 18c	237
Table 6-11	Comparison of Metrical Parameters in MM'L _n (μ-η ¹ :η ¹ -C ₂ H ₂ C(O)) Compounds.....	238
Table 6-12	Activation Parameters for Turnstile Exchange in 16a-c and 17b/b'	241
Table 6-13	Crystallographic Experimental Details for Compound 16b	266
Table 6-14	Atomic Coordinates and Equivalent Isotropic Displacement Parameters for Compound 16b	267
Table 6-15	Crystallographic Experimental Details for Compound 18c	268
Table 6-16	Atomic Coordinates and Equivalent Isotropic Displacement Parameters for Compound 18c	269
Table 6-17	Summary of the Rate Constants Determined by Spectral Simulation for Turnstile Carbonyl Scrambling in 16a-c and 17b,b'	270
Table 7-1	Selected Interatomic Distances (Å) in Compound 24b	279
Table 7-2	Selected Interatomic Angles (deg.) in Compound 24b	280
Table 7-3	Selected NMR Data for MM'L _n (μ-η ¹ :η ³ -CH _β CRC(O)) Species..	284
Table 7-4	Selected NMR Data for MM'L _n (μ-η ¹ :η ¹ -C(O)CH _α CR) Species..	285
Table 7-5	Selected Interatomic Distances (Å) in Compound 33	296
Table 7-6	Selected Interatomic Angles (deg.) in Compound 33	297
Table 7-7	Crystallographic Experimental Details for Compound 24b	312
Table 7-8	Atomic Coordinates and Equivalent Isotropic Displacement Parameters for Compound 24b	313
Table 7-9	Crystallographic Experimental Details for Compound 33	314
Table 7-10	Atomic Coordinates and Equivalent Isotropic Displacement Parameters for Compound 33	315

List of Figures

Figure 1-1	Reaction of $\text{Fe}_3(\text{CO})_{12}$ with $\text{PhC}\equiv\text{CPh}$	3
Figure 1-2	Molecular Structure of $\text{Fe}_2(\text{CO})_8(\text{Ph}_2\text{PC}\equiv\text{C}^t\text{Bu})$	7
Figure 2-1	FT-IR Monitoring of the Photolysis of $\text{Fe}(\text{CO})_5$ and TFP in Pentane.....	34
Figure 2-2	Comparison of the Photolyses of $\text{Fe}(\text{CO})_5$ with (a) HFB and (b) TFP.....	35
Figure 2-3	Representative FT-IR Spectra (pentane) for 1a,c,e	39
Figure 2-4	$^{13}\text{C}\{^1\text{H}\}$, APT and ^{13}C NMR Spectra of 1d at -80°C	43
Figure 2-5	Immersion Well Photochemical Reactor.....	60
Figure 3-1	Examples of $\mu\text{-}\eta^2\text{:}\eta^2\text{-Metallacyclobutenones}$	76
Figure 3-2	Variable Temperature ^{13}C NMR (CD_2Cl_2 , 100.6 MHz) of Compound 6e in the Carbonyl Region.....	80
Figure 3-3	Proposed Dimeric Structure for 6c-e	82
Figure 3-4	^{13}C NMR (100.6 MHz, CD_2Cl_2) of the CR Resonances in 6c-e	84
Figure 3-5	Solution IR Spectra Before and after Addition of C_2Et_2 to 1c	88
Figure 4-1	^{19}F NMR Monitored Reaction of 1a with PMe_3 in CD_2Cl_2	113
Figure 4-2	Molecular Structure of Compound 9c	119
Figure 4-3	^{13}C NMR of 8c/c' Formed by Reaction of ^{13}CO Enriched 1a with Excess PCy_3 After 4 h at -40°C	120
Figure 4-4	Molecular Structure of Compound 10	126
Figure 4-5	Integrated Intensity vs. Time Plot for Disappearance of 1a	129
Figure 4-6	Integrated Intensity vs. Time Plot for the Reaction of PPh_3 (0.20 M) with 1a (0.025 M) at -36.7°C in CD_2Cl_2	138
Figure 4-7	Integrated Intensity vs. Time Plot for the Reaction of PCy_3 (0.30 M) with 1a (0.025 M) at -33.5°C in CD_2Cl_2 Modelled to Scheme 4-3.....	142

Figure 4-8	Integrated Intensity vs. Time Plot for the Reaction of PCy ₃ (0.30 M) with 1a (0.025 M) at -33.5°C in CD ₂ Cl ₂ Modelled to Scheme 4-4.....	142
Figure 4-9	Integrated Intensity vs. Time Plot for the Early Stages of the Reaction of PCy ₃ (0.30 M) with 1a (0.025 M) at -38.5°C in CD ₂ Cl ₂	143
Figure 5-1	Proposed Dimetallatetrahedrane Structures for 11a,a*	160
Figure 5-2	Proposed Dimetallacyclobutene Structures for 12a-c	163
Figure 5-3	Molecular Structure of Compound 12c	166
Figure 5-4	Molecular Structure of Compound 13c	170
Figure 5-5	Variable Temperature ¹³ C NMR (toluene- <i>d</i> ₈) of 12b	180
Figure 5-6	Variable Temperature ¹³ C NMR (toluene- <i>d</i> ₈) of 13b	184
Figure 5-7	¹³ C NMR Monitored Reaction of 1a with CpRh(CO) ₂ in CD ₂ Cl ₂	190
Figure 5-8	¹⁹ F NMR Monitored Reaction of 1a with CpRh(CO) ₂ in CD ₂ Cl ₂	191
Figure 5-9	¹³ C NMR Monitored Reaction of 1a with Os(CO) ₅ in CD ₂ Cl ₂	200
Figure 6-1	Molecular Structure of Compound 16b	225
Figure 6-2	Isomeric Forms of CpRhFe(CO) ₄ (μ-η ¹ :η ³ -C ₂ H ₂ C(O)) (17b/b')...	229
Figure 6-3	¹³ C{ ¹ H} NMR of 16b in the Carbonyl Region at -80°C.....	230
Figure 6-4	Molecular Structure of Compound 18c	236
Figure 6-5	Variable Temperature ¹³ C NMR of 17b/b' in the Carbonyl Region.....	242
Figure 6-6	Variable Temperature ¹ H NMR of 17b/b' (toluene- <i>d</i> ₈).....	244
Figure 6-7	High Temperature ¹³ C NMR Spectra of 17b/b' (toluene- <i>d</i> ₈).....	245
Figure 6-8	¹ H NMR Monitored Reaction of 1c with Cp [*] Rh(CO) ₂ in CD ₂ Cl ₂	248

Figure 6-9	^{13}C NMR Monitored Reaction of 1c with $\text{Cp}^*\text{Rh}(\text{CO})_2$ in CD_2Cl_2	253
Figure 6-10	Plausible Structure for Compound 23	258
Figure 7-1	Molecular Structure of Compound 24b	279
Figure 7-2	Proposed Structures for 24a , 26a,c , 27b , and 28b	283
Figure 7-3	Proposed Structure for 25c	286
Figure 7-4	Possible Structures for Compound 33	295
Figure 7-5	Molecular Structure of Compound 33	296
Figure 7-6	Bonding Description of Compound 33	299
Figure 7-7	Molecular Structure of $\text{Cp}^*\text{FeCo}(\mu\text{-CO})_2(\text{CO})_4$	300
Figure 7-8	Bonding Model for $\text{Cp}^*\text{FeCo}(\mu\text{-CO})_2(\text{CO})_4$	300

List of Schemes

Scheme 1-1	Reaction of $\text{Fe}_2(\text{CO})_6(\mu\text{-}\eta^2\text{:}\eta^2\text{-C}_2\text{Ph}_2)$ with C_2Ph_2	5
Scheme 1-2	In-Plane Metal-Alkyne Bonding Components.....	12
Scheme 1-3	Valence Bond Representations of Metal-Alkyne Bonding Extremes.....	12
Scheme 1-4	Metal-Alkyne Interactions Perpendicular to the $\pi_{\parallel}/\pi_{\parallel}^*$ Plane.....	13
Scheme 1-5	Interaction Diagram for an $\text{M}(\text{CO})_4(\eta^2\text{-alkyne})$ Complex.....	14
Scheme 1-6	Reaction of $\text{Os}(\text{CO})_4(\eta^2\text{-RC}_2\text{R}')$ with ML_n Reagents.....	18
Scheme 1-7	Reaction of $\text{Os}(\text{CO})_4(\eta^2\text{-C}_2\text{H}_2)$ with $\text{Ru}(\text{CO})_4(\eta^1\text{-dppm})$	19
Scheme 1-8	Reaction of $\text{Fe}_2(\text{CO})_7(\mu\text{-dppm})$ with C_2H_2	21
Scheme 2-1	Valence Bond Description of the Rehybridization of Triply- Bonded Carbons in Two- and Four-Electron Donor Alkynes.....	46
Scheme 3-1	Reaction of 1a,c,e,f with C_2R_2	70
Scheme 3-2	Possible Mechanisms for the Reaction of 1a with HFB.....	86
Scheme 3-3	Proposed Mechanism for Alkyne Exchange in 1	88
Scheme 3-4	Proposed Mechanism for Formation of 4a	89
Scheme 4-1	Dissociative Mechanism for Initial Reaction of 1a with PR_3	130
Scheme 4-2	Dissociative Mechanism for Subsequent Reaction of 8b with PR_3	136
Scheme 4-3	Proposed Mechanism for Initial Formation of 8c Followed by Isomerization to 8c' in the Reaction of 1a with PCy_3	140
Scheme 4-4	Proposed Mechanism for Competing Axial and Equatorial CO Dissociation from 1a in the Reaction with PCy_3	141
Scheme 5-1	Reaction of $\text{Ru}(\text{CO})_4(\eta^2\text{-HFB})$ with $\text{Cp}'\text{M}(\text{CO})_2$	157
Scheme 5-2	Reaction of 1a with $\text{Cp}'\text{M}(\text{CO})_2$	158
Scheme 5-3	Resonance Structures Describing the Bonding of the $\mu\text{-}\eta^1\text{:}\eta^3\text{-Dimetallacyclopentenone}$ Ring System in 13c	174

Scheme 5-4	Sequence of Appearance of Products in the Reaction of 1a with $\text{CpRh}(\text{CO})_2$ at Low Temperature in CD_2Cl_2	192
Scheme 5-5	Proposed Mechanism for Intermolecular Carbonyl Exchange Between 1a and $\text{CpRh}(\text{CO})_2$	193
Scheme 5-6	Proposed Mechanism for Formation of 12c and 14 from M	194
Scheme 5-7	Proposed Mechanism for Formation of 14 from a Ferracyclobuteneone Intermediate.....	195
Scheme 6-1	Reaction of $\text{Os}(\text{CO})_4(\eta^2\text{-C}_2\text{H}_2)$ with Organometallic Reagents..	219
Scheme 6-2	Reaction of $\text{Fe}(\text{CO})_4(\eta^2\text{-C}_2\text{H}_2)$ (1c) with $\text{Cp}'\text{M}(\text{CO})_2$	220
Scheme 6-3	Two Resonance Structures Describing the Bonding of the $\mu\text{-}\eta^1\text{:}\eta^3$ -Dimetallacyclopentenone Ring Systems in 16a-c	222
Scheme 6-4	Resonance Structures Describing the Bonding of the Unsaturated Organic Fragment in a $\mu\text{-}\eta^1\text{:}\eta^1$ -Dimetallacyclopentenone.....	231
Scheme 6-5	Low Temperature Reaction of 1a with $\text{Cp}^*\text{Rh}(\text{CO})_2$ in CD_2Cl_2	249
Scheme 6-6	Proposed Mechanism of Formation for 18b and 19b	254
Scheme 7-1	Proposed Reaction Sequence for Formation of 26a,c and 28b	287
Scheme 7-2	Proposed Reaction Sequence for Formation of 24a,b and 27b	289
Scheme 7-3	Proposed Reaction Sequence for Formation of 25c	289
Scheme 7-4	Further Reaction of the Mixture of 25c and 26c	291

List of Abbreviations and Symbols

Å	Angström(s)	esd	estimated standard deviation
ac	acyl	Et	ethyl, CH ₃ CH ₂ -
alk	alkyne	<i>et al.</i>	<i>et alii</i> (and others)
Anal.	analysis	eV	electron volts
APT	attached proton test	FAB	fast atom bombardment
atm	atmosphere(s)	FT	Fourier transform
av	average	F.W.	formula weight
ax	axial	Fig.	Figure
BPR	Berry pseudo-rotation	GWV	Glasswerk Wertheim
br	broad	h	hour(s)
<i>ca.</i>	<i>circa</i> (approximately)	HFB	hexafluorobut-2-yne, C ₂ (CF ₃) ₂
Calc.	calculated	hν	radiation
<i>cf.</i>	<i>confer</i> (compare)	Hz	Hertz
Cp	cyclopentadienyl, η ⁵ -C ₅ H ₅	<i>i.e.</i>	<i>id est</i> (that is)
Cp*	pentamethylcyclopentadienyl, η ⁵ -C ₅ (CH ₃) ₅	ⁱ Pr	isopropyl, (CH ₃) ₂ CH-
Cy	cyclohexyl, C ₆ H ₁₁ -	IR	infrared
δ	chemical shift (ppm)	<i>J</i>	coupling constant
Δ	coordination shift	K	Kelvin
d	doublet	λ	wavelength
dmpm	bis(dimethylphosphino)-methane, Me ₂ PCH ₂ PMe ₂	μL	microliters
dppm	bis(diphenylphosphino)-methane, Ph ₂ PCH ₂ PPh ₂	m	multiplet (NMR spectra)
ε	molar extinction coefficient	m	medium (IR spectra)
e ⁻	electron	M	molecular ion (mass spectra)
<i>e.g.</i>	<i>exempli gratia</i> (for example)	Me	methyl, CH ₃ -
E.I.	electron impact	mg	milligrams
eq	equatorial	MHz	megahertz
Eq.	Equation	mL	milliliters
		mM	millimolar (concentration)
		mmol	millimoles

MO	molecular orbital
MS	mass spectrometry
min	minute(s)
nm	nanometers
NMR	nuclear magnetic resonance
ν	frequency
Ph	phenyl, C ₆ H ₅ -
ⁿ Pr	propyl, CH ₃ CH ₂ CH ₂ -
ppm	parts per million
q	quartet
qq	quartet of quartets
r.t.	room temperature
Ref.	Reference
s	second(s)
s	singlet (NMR spectra)
s	strong (IR spectra)
SST	Spin Saturation Transfer
sept	septet
sh	shoulder
t	triplet
T	temperature
^t Bu	tertiary-butyl, (CH ₃) ₃ C-
TFP	trifluoropropyne, HC≡CCF ₃
UV	ultra-violet
v	very
vs.	versus
w	weak
W	watts
[X]	concentration of species "X"

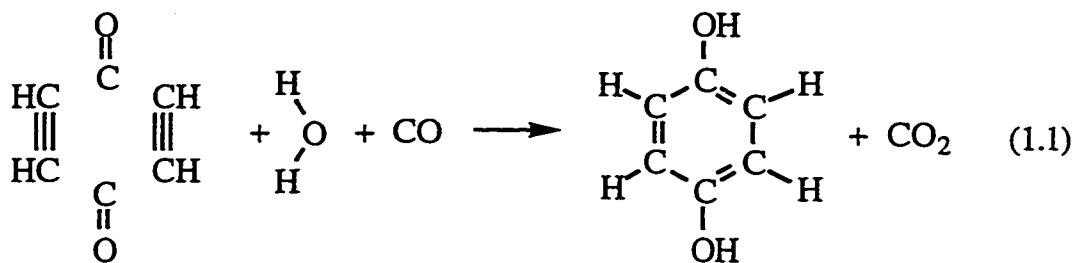
Chapter 1

Introduction

1.1. The Reaction of Alkynes with Binary Carbonyls of the Iron Triad

1.1.1. Compounds Derived from Iron Carbonyls

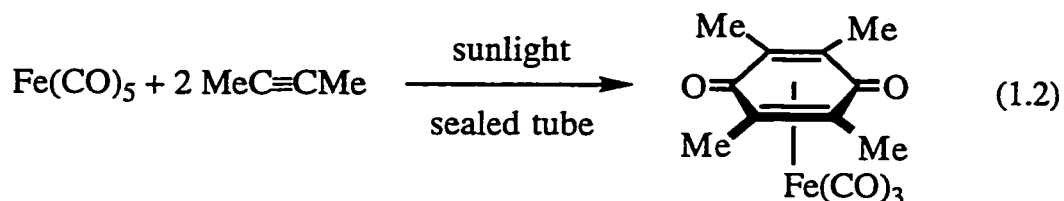
Walter Reppe, regarded as one of the "fathers" of modern organometallic chemistry, conducted some of the first reactions between transition metal carbonyl compounds and unsaturated organic substrates in the 1940s. One study involved the reaction between alkaline solutions of $\text{H}_2\text{Fe}(\text{CO})_4$ and acetylene, producing hydroquinone and various organometallic compounds. The organic product was clearly built up from the linking of molecules of acetylene and carbon monoxide, envisioned by Reppe as Eq. 1.1.¹



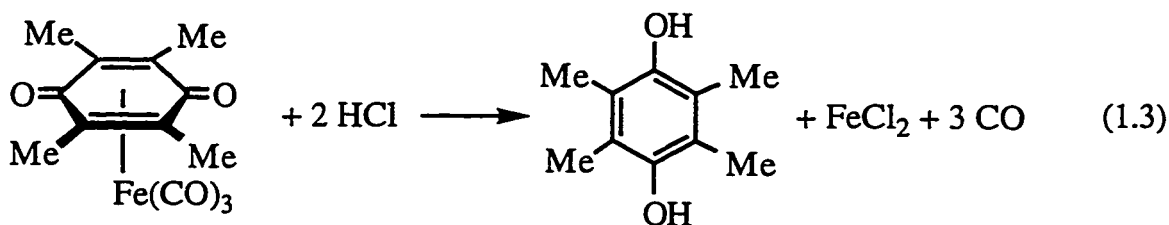
The yield of hydroquinone was relatively poor, and the mechanism of the reaction was unclear, but it seemed likely that the role of the iron carbonyl complex was more significant than simply acting as a source of carbon monoxide.² Nonetheless, Reppe's discovery stimulated many other researchers to continue work in this field, and subsequent publications began to shed light on the structures of the organometallic compounds which were potentially involved in the transformation described in Eq. 1.1.³⁻⁵ It was also found that the reaction could be made partially catalytic in the presence of complex salts, with the primary advantage being the low cost of $\text{Fe}(\text{CO})_5$ over other processes involving Rh or Ru compounds.⁶

It became clear that the alkaline conditions of Reppe's synthesis were important in the reduction of the organic moiety, a complication avoided by

performing the reactions in aprotic solvents. One of the earliest such examples was quite elegant in its simplicity. Dissolution of $\text{Fe}(\text{CO})_5$ in neat but-2-yne in a glass tube followed by exposure to sunlight produced an unstable, easily oxidized, organoiron complex.⁷ Following oxidation of the iron center, the recovery of tetramethyl-1,4-benzoquinone clearly demonstrated that the cyclic organic ligand was built up on the iron center by coupling two equivalents each of alkyne and CO ligands (Eq. 1.2).



Interestingly, treatment of the organometallic compound with HCl resulted in the isolation of tetramethylhydroquinone (Eq. 1.3).



The hydroquinone could also be directly recovered, without detection of an intermediate iron carbonyl complex, by introducing methanolic HCl into the $\text{Fe}(\text{CO})_5/\text{C}_2\text{Me}_2$ reaction medium. This observation prompted the suggestion that tricarbonyl(*p*-quinone)iron species were conceivably potential intermediates in Reppe's synthesis of hydroquinones,⁷ although the latter occurred under alkaline, rather than acidic, conditions and likely involved $\text{H}_2\text{Fe}(\text{CO})_4$ in the reduction of the quinone ligand.⁶ Unfortunately, the methodology of Eq. 1.2 was not universal in its application and only alkyl substituted alkynes such as pent-2-yne and hex-3-yne were found to react similarly with $\text{Fe}(\text{CO})_5$ under mild conditions.^{7,8}

Thermal activation of iron carbonyls was another means of inducing the linking of coordinated carbon monoxide with alkynes. Hübel has reviewed this subject in detail, noting that $\text{Fe}_2(\text{CO})_9$ was reactive at room temperature while $\text{Fe}_3(\text{CO})_{12}$ and $\text{Fe}(\text{CO})_5$ required heating to temperatures of 60 - 100°C and 150°C, respectively, to produce alkyne-containing products.^{9,10} Not surprisingly, the harsh conditions in the latter case resulted in significantly different compounds than the unstable *p*-quinone complexes of Eq. 1.2. The reactions were frequently quite complicated and produced mixtures of compounds which could only be isolated, often in low yield, following painstaking chromatographic separation. Figure 1-1 provides an example of such a system, and demonstrates the structural diversity and types commonly encountered.¹⁰

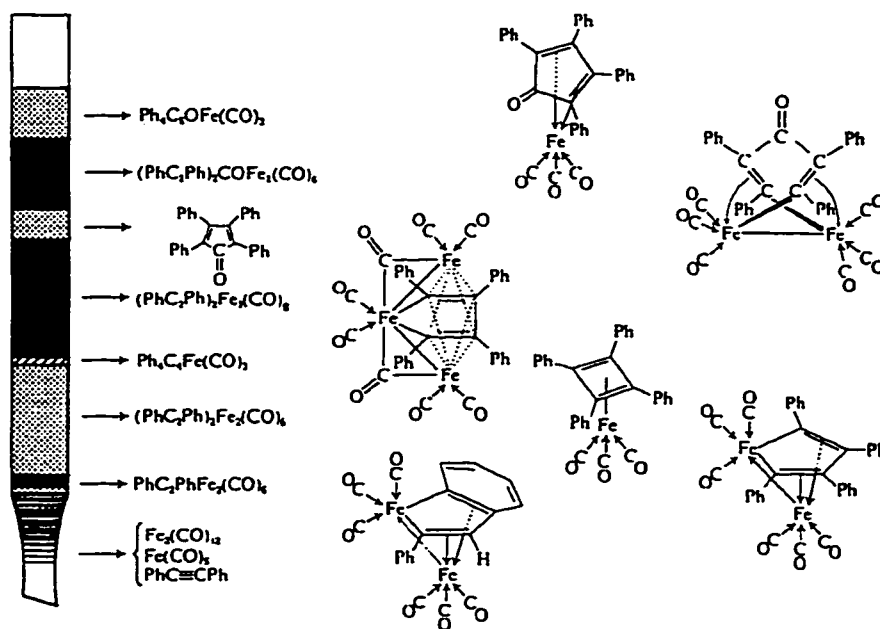
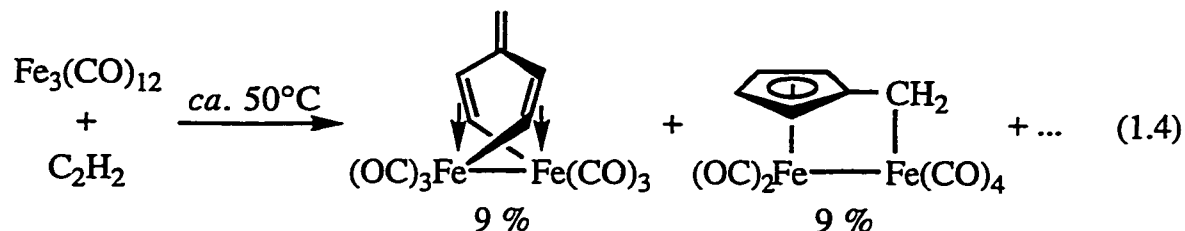


Figure 1-1. Reaction of $\text{Fe}_3(\text{CO})_{12}$ with $\text{PhC}\equiv\text{CPh}$ (Fig. 1 from Ref. 10).

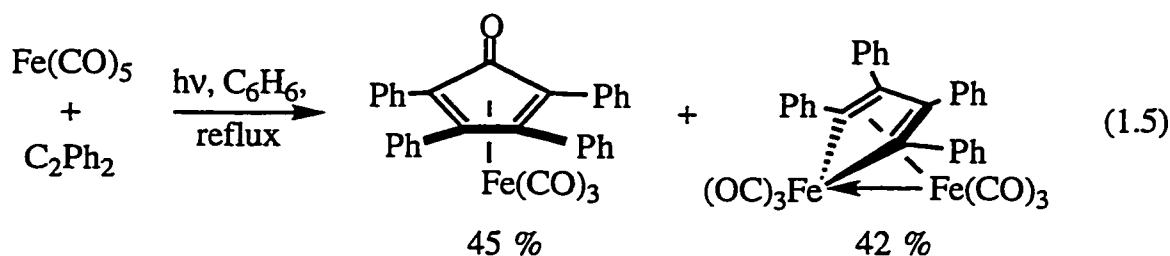
In addition to a variety of organometallic products, cyclic organic compounds such as substituted benzenes, cyclopentadienones, quinones, and hydroquinones were often isolated. Further, it was noted that disubstituted alkynes tended to give higher yields than terminal alkynes, and the latter produced a variety of positional isomers, indicating that the alkynes were frequently not incorporated in a regiospecific manner.¹⁰ The reaction of terminal alkynes was also found to

produce products resulting from hydrogen migrations. Indeed, acetylene reacted with $\text{Fe}_3(\text{CO})_{12}$ to produce at least 11 compounds which included the novel heterocycles shown in Eq. 1.4.¹¹



In contrast, $\text{Fe}_2(\text{CO})_9$ gave primarily $\text{Fe}(\text{CO})_3\{\eta^4\text{-C}_6\text{H}_6\text{C}(\text{O})\}$ ($\text{C}_6\text{H}_6\text{C}(\text{O}) =$ tropone) along with unidentified polymeric materials.¹¹

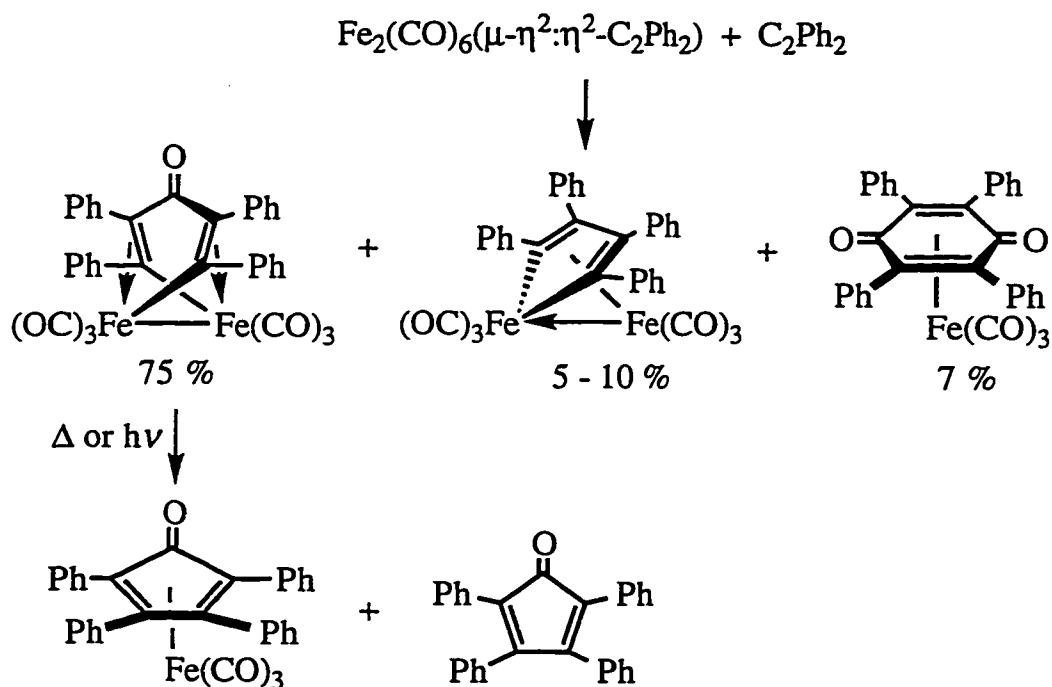
The most commonly observed products from the thermal reactions were dinuclear ferroles, $\text{Fe}_2(\text{CO})_6(\mu\text{-}\eta^1, \eta^1\text{:}\eta^4\text{-C}_4\text{R}_4)$, and mononuclear cyclopentadienone complexes, $\text{Fe}(\text{CO})_3\{\eta^4\text{-C}_4\text{R}_4(\text{O})\}$; the latter, acetylene based product was formed in low yield when C_2H_2 was reacted with $\text{Fe}(\text{CO})_5$ in a sealed pressure-vessel at 70 - 120°C.¹¹ Photolysis of $\text{Fe}(\text{CO})_5$ with C_2Ph_2 in refluxing benzene also produced these structural types, Eq. 1.5, prompting Schrauzer to suggest that a reactive $[\text{Fe}(\text{CO})_4]$ intermediate was produced by all three binary iron carbonyls.¹²



The above compounds were also formed by treatment of $\text{Fe}(\text{CO})_5$ and C_2Ph_2 at 140 - 160°C in an autoclave.⁸

Although the harsher reaction conditions necessary for thermal activation of $\text{Fe}(\text{CO})_5$ and $\text{Fe}_3(\text{CO})_{12}$ resulted in relatively poor product control, greater selectivity was attained with $\text{Fe}_2(\text{CO})_9$ which underwent a relatively clean

reaction with bulky alkynes at ambient temperature. Bis(trimethylsilyl)acetylene produced $\text{Fe}(\text{CO})_4(\eta^2\text{-C}_2(\text{SiMe}_3)_2)^{10,13}$ and bis(*tert*-butyl)acetylene afforded primarily $\text{Fe}_2(\text{CO})_6(\mu\text{-}\eta^2\text{:}\eta^2\text{-C}_2^t\text{Bu}_2)$, along with minor amounts of the mononuclear η^2 -alkyne complex.¹⁴ The dinuclear compound is interesting because it contains an Fe–Fe double bond, as does the previously isolated $\text{Fe}_2(\text{CO})_4(\mu\text{-}\eta^2\text{:}\eta^2\text{-C}_2^t\text{Bu}_2)_2$.¹⁵ The latter compound, synthesized from $\text{Fe}_3(\text{CO})_{12}$ and C_2^tBu_2 in refluxing methylcyclohexane, was surprisingly stable and could be sublimed at 175°C in air without decomposition. In contrast, Hübel found that $\text{Fe}_2(\text{CO})_6(\mu\text{-}\eta^2\text{:}\eta^2\text{-C}_2^t\text{Bu}_2)$ and its diphenylacetylene analog were reactive towards alkynes at ambient temperature, producing several of the compound types presented in Figure 1-1.¹⁶ In particular, $\text{Fe}_2(\text{CO})_6(\mu\text{-}\eta^2\text{:}\eta^2\text{-C}_2\text{Ph}_2)$ gave both high product yield and modest selectivity (Scheme 1-1).^{10,16}

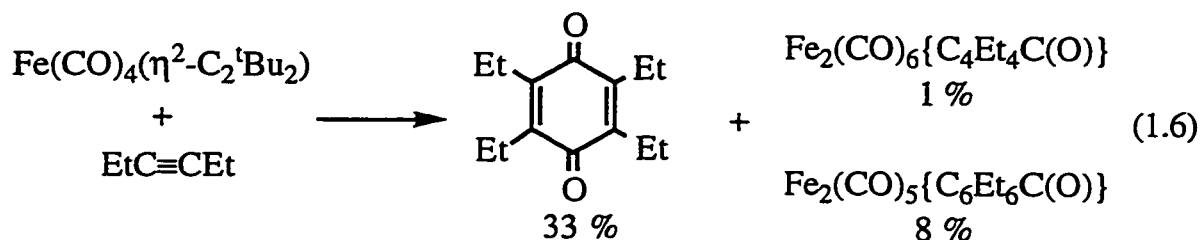


Scheme 1-1. Reaction of $\text{Fe}_2(\text{CO})_6(\mu\text{-}\eta^2\text{:}\eta^2\text{-C}_2\text{Ph}_2)$ with C_2Ph_2 .^{10,16}

Although the major "fly-over-bridged" dinuclear species formally requires only the insertion of a second mole of CO to form a *p*-quinone product, it was found that heating and irradiation led to cyclopentadienone compounds, even when the

reaction was carried out under CO, demonstrating that the dinuclear compound was not an intermediate in the formation of $\text{Fe}(\text{CO})_3\{\eta^4\text{-(O)CC}_4\text{Ph}_4\text{C(O)}\}$. However, treatment under reducing or alkaline conditions did produce both the free quinone and hydroquinone, indicating that the dinuclear compounds could be used as stoichiometric precursors in such transformations.¹⁰ The interesting fly-over-bridged bimetallic compound was also formed in moderate yield directly from $\text{Fe}_2(\text{CO})_9$ and C_2Ph_2 after 24 h at ambient temperature¹⁷ and was the subject of intense structural,¹⁸ ^{13}C NMR,¹⁷⁻¹⁹ photochemical,²⁰ and theoretical^{21,22} scrutiny several years following its initial isolation.¹²

Both mononuclear compounds, $\text{Fe}(\text{CO})_4(\eta^2\text{-C}_2\text{R}_2)$ ($\text{R} = \text{SiMe}_3, \text{tBu}$), could also be formed by irradiation of $\text{Fe}(\text{CO})_5$ in hexanes at ambient temperature, but were found to be thermally unstable.^{10,13} The alkyne ligands were quite labile, and were easily substituted by PPh_3 ^{10,13} and other alkynes.¹⁰ In the latter case, the initial products were presumed to be the corresponding $\text{Fe}(\text{CO})_4(\eta^2\text{-C}_2\text{R}'_2)$ complexes, but these compounds escaped detection and immediately formed coupling products (Eq. 1.6).¹⁰



As the above reaction produced tetraethyl-1,4-benzoquinone as the major product, it appeared likely that the putative $\text{Fe}(\text{CO})_4(\eta^2\text{-C}_2\text{R}'_2)$ ($\text{R}' = \text{Me}, \text{Et}$) species were initial intermediates in the production of $\text{Fe}(\text{CO})_3\{\eta^4\text{-(O)CC}_4\text{R}'_4\text{C(O)}\}$ by Eq. 1.2.²³ However, the proposed intermediates were never observed, and, as $\text{Fe}(\text{CO})_4(\eta^2\text{-C}_2\text{R}_2)$ ($\text{R} = \text{SiMe}_3, \text{tBu}$) did not undergo coupling reactions which retained the bulky alkynes, the involvement of $\text{Fe}(\text{CO})_4(\eta^2\text{-alkyne})$ complexes in processes leading to compounds such as $\text{Fe}(\text{CO})_3\{\eta^4\text{-(O)CC}_4\text{R}'_4\text{C(O)}\}$ remained unproven.^{2,24}

The lack of structurally characterized examples of $\text{Fe}(\text{CO})_4(\eta^2\text{-alkyne})$ complexes prompted Carty to prepare a novel compound, $\text{Fe}_2(\text{CO})_8(\text{Ph}_2\text{PC}\equiv\text{C}^t\text{Bu})$, which included both $\text{Fe}(\text{CO})_4(\text{phosphine})$ and $\text{Fe}(\text{CO})_4(\eta^2\text{-alkyne})$ moieties.²⁵

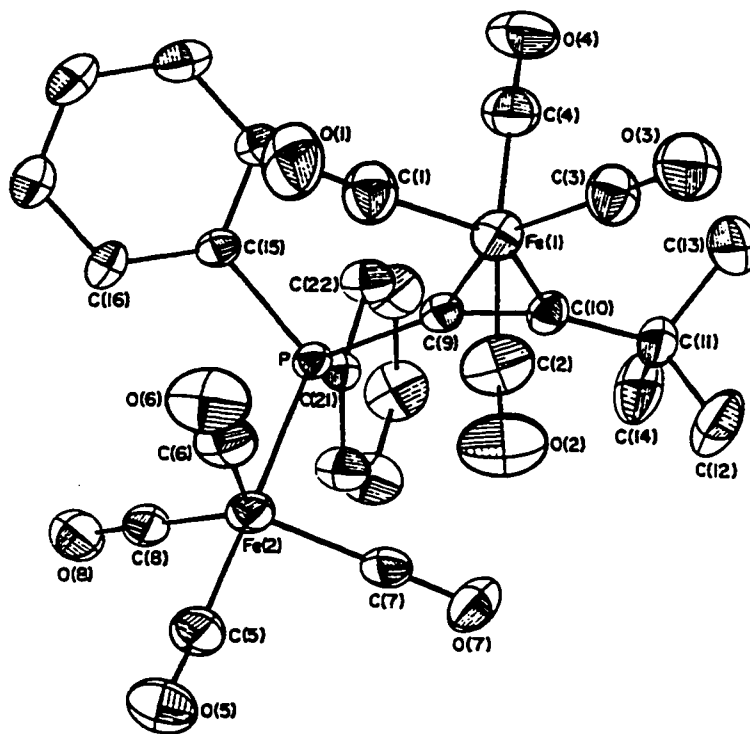


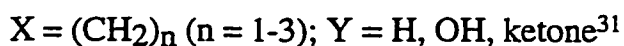
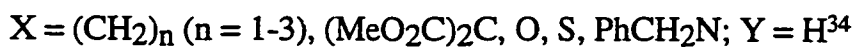
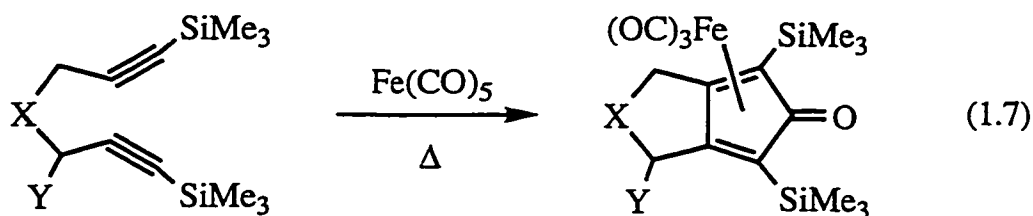
Figure 1-2. Molecular Structure of $\text{Fe}_2(\text{CO})_8(\text{Ph}_2\text{PC}\equiv\text{C}^t\text{Bu})$ (Fig. 1 from Ref. 25).

The analysis of the structure led Carty to conclude that the bonding characteristics of the alkyne were not significantly different than those of an olefin, and that the apparent instability of $\text{Fe}(\text{CO})_4(\eta^2\text{-alkyne})$ complexes was thus due to a "hyper-reactivity of these species towards further acetylene addition rather than the instability of the iron(0)-acetylene bond".²⁵ Berke and co-workers subsequently validated this proposal by preparing a variety of $\text{Fe}(\text{CO})_2\text{L}_2(\eta^2\text{-alkyne})$ (L = phosphine, phosphite) compounds by displacement of dinitrogen from $(\mu\text{-N}_2)(\text{Fe}(\text{CO})_2\text{L}_2)_2$.²⁶⁻²⁹ Although terminal alkynes frequently underwent subsequent rearrangements to acetylide-hydride or vinylidene compounds, nevertheless it was clear that the replacement of carbonyls by ligands which do not undergo migratory insertions is an important

contributor to the increased stability of the $\text{Fe}(\text{CO})_2\text{L}_2(\eta^2\text{-alkyne})$ complexes. However, at the start of this research, examples of the simple ternary $\text{Fe}(\text{CO})_4(\eta^2\text{-alkyne})$ compounds were still limited to the previously mentioned examples involving bulky $\text{C}_2(\text{SiMe}_3)_2$, C_2^tBu_2 , and novel $\{(\text{OC})_4\text{FePPh}_2\}-\text{C}\equiv\text{C}^t\text{Bu}$ ligands.

1.1.2. Some Recent Applications to Organic Synthesis

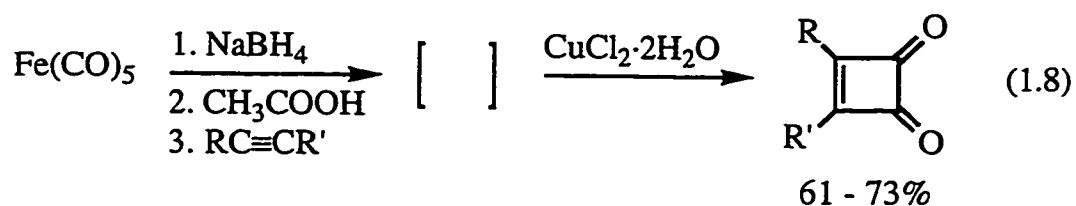
Although the thermal chemistry of iron carbonyls with alkynes tended to be complicated and usually provided mixtures of products, it has proven possible to make use of the ability of the low valent Fe template to link alkynes with carbon monoxide by engineering systems which distinctly favor one product. Pearson and Knölker have carried out independent studies on the thermal reaction of functionalized diynes with $\text{Fe}(\text{CO})_5$ with practical application to organic synthesis, namely [2+2+1] intramolecular coupling to produce bicyclic compounds containing cyclopentadienone moieties (Eq. 1.7).³⁰⁻³⁵



The resulting 3,4-annulated 2,5-disilylcyclopentadienones could often be cleaved from the metal by oxidation with trimethylamine-*N*-oxide to produce useful substrates for natural products synthesis.³¹⁻³⁵ The trimethylsilyl groups were easily functionalized with various electrophiles and the free organic compounds could undergo Diels-Alder cycloadditions to produce more complex polycyclic systems.³⁵ In fact, one of the primary advantages of the coordinated $\text{Fe}(\text{CO})_3$ group is that the reactive cyclopentadienone moiety is stabilized and can be modified without the concern of a competing dimerization.³⁰

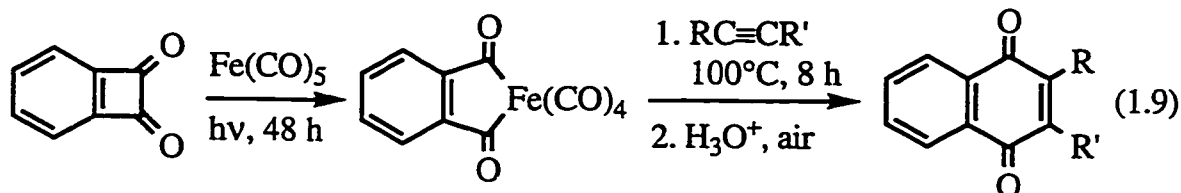
It was also established that the substituents need not be limited to silyl groups, and a recent study has extended the synthesis to terminal diynes and those capped by phenyl and $-(\text{CH}_2)_3\text{CH}=\text{CH}_2$ groups.³² Furthermore, the stereochemical directing power of the $\text{Fe}(\text{CO})_3$ moiety has proven to be useful in cases involving modification of the "Y" substituent prior to decomplexation.³¹ The success of the iron-mediated cyclizations was no doubt due to the design of the substrate, as the ligand's orientation facilitated the intramolecular coordination of the second alkyne moiety preceding cyclization.³³ Pearson has noted that analogous reactions of mono-alkynes are often inefficient,³⁰ but other workers have found that the reactions proceeded in reasonable yield when the alkyne was activated by electron withdrawing groups such as ^tBuO ,³⁶ Cl ,³⁷ or CF_3 .³⁸

Periasamy has recently reported the interesting synthesis of cyclobutenediones *via* iron carbonyl species (Eq. 1.8).



The system was quite tolerant towards the nature of the alkyne substituents, as both unmasked hydroxyl groups and alkene double bonds emerged unaltered from the reaction vessel. The main organometallic compound in solution was identified by UV spectroscopy as $[\text{HFe}_3(\text{CO})_{11}]^-$, and it was speculated that dinuclear ferracycles could be potential intermediates.³⁹ However, the iron carbonyl compounds which formed were not isolated, but rather were decomposed *in situ* with $\text{CuCl}_2 \cdot 2\text{H}_2\text{O}$ to isolate the free organic product. The reaction was also found to proceed if $\text{NaHFe}(\text{CO})_4$ was treated with MeI in THF, heated with the alkyne, and then oxidized with $\text{CuCl}_2 \cdot 2\text{H}_2\text{O}$.⁴⁰ Although similar treatment of $[\text{R}_4\text{N}]\text{HFe}(\text{CO})_4$ with MeI in acetonitrile produced $\text{Fe}(\text{CO})_4(\text{NCMe})$,⁴¹ it was not clear that " $\text{Fe}(\text{CO})_4$ " or the THF solvate was the reactive species in Periasamy's reaction media.⁴⁰

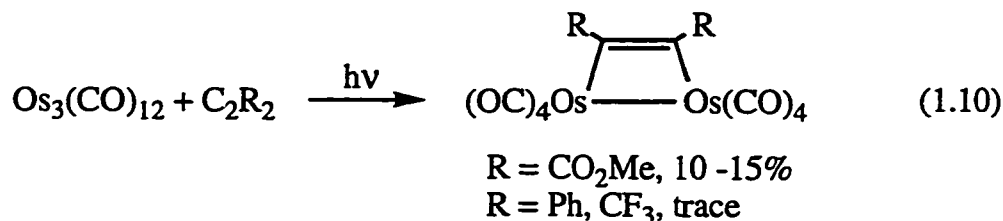
Liebeskind has reported the use of cyclobutenediones as precursors in the synthesis of naphtho- and benzoquinones.⁴² For example, prolonged photolysis of benzocyclobutenedione and $\text{Fe}(\text{CO})_5$ produced a stable phthaloyliron compound which reacted with a variety of alkynes at 100°C to produce a black precipitate, which in turn yielded naphthoquinones in good yield following acidic work-up in air (Eq. 1.9).



Unfortunately, the phthaloyliron precursors were more difficult to synthesize than their $\text{Co}(\text{Cl})(\text{PPh}_3)_2$ analogs, the latter of which formed under milder conditions and could be activated with AgBF_4 to undergo the corresponding conversions to naphthoquinones. The Co-mediated reaction was also applied to the synthesis of substituted 1,4-benzoquinones.⁴²

1.1.3. Reaction of Osmium and Ruthenium Carbonyls with Alkynes

Ruthenium and osmium carbonyls also react with alkynes to produce a variety of compounds, many of which are similar to their iron analogs. However, unlike Fe, the penta- and nonacarbonyls of the heavier group 8 metals are unstable under ambient conditions, and thus the majority of compounds resulted from the reaction of $\text{M}_3(\text{CO})_{12}$ ($\text{M} = \text{Ru}, \text{Os}$) with alkynes. As with the iron carbonyls, bimetallic $\text{M}_2(\text{CO})_6(\mu\text{-}\eta^1, \eta^1\text{:}\eta^4\text{-C}_4\text{R}_4)$ compounds and mononuclear cyclopentadienone complexes, $\text{M}(\text{CO})_3\{\eta^4\text{-C}_4\text{R}_2(\text{O})\}$, were isolated,⁴³⁻⁵¹ but a larger number of cluster compounds were observed^{48,49,52-56} than with $\text{Fe}_3(\text{CO})_{12}$, which more readily fragmented into mono- and dinuclear compounds. Photochemical reactions have been studied more recently,⁵⁷ and introduced some interesting structural types which were absent in the iron chemistry, the most significant of which were the octacarbonyldiosmacyclobutenes (Eq. 1.10).^{57,58}

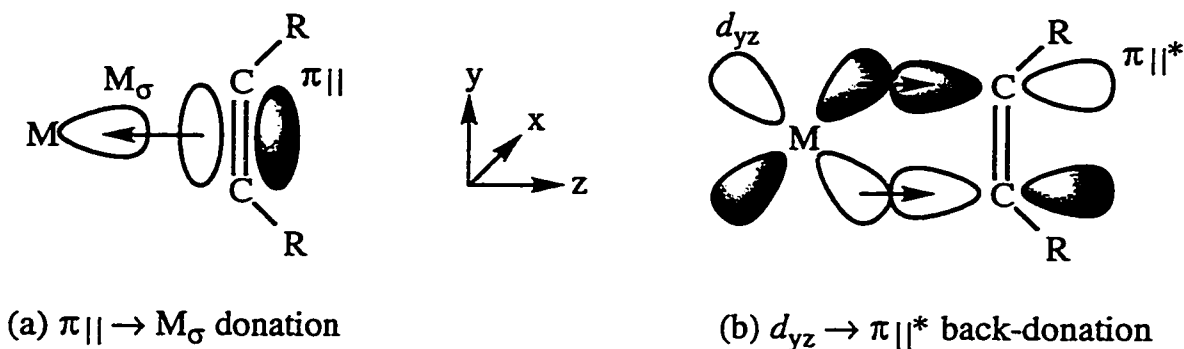


Unfortunately, the interesting alkyne-bridged bimetallics were isolated in very low yields. The photochemistry of $\text{Os}_3(\text{CO})_{12}$ was quite complex and very dependent on the alkyne, with acetylene in particular providing a myriad of products.⁵⁸ An interesting contrast was provided by C_2Ph_2 and $\text{C}_2(\text{SiMe}_3)_2$ which produced $\text{Os}(\text{CO})_3\{\eta^4\text{-C}_4\text{Ph}_4\text{C}(\text{O})\}$ ⁵⁰ and $\text{Os}(\text{CO})_4(\eta^2\text{-C}_2(\text{SiMe}_3)_2)$, respectively.⁵⁹ The latter compound and its Ru analog, prepared by low temperature photolysis of $\text{Ru}(\text{CO})_5$,⁵⁹ provided the first examples of $\text{M}(\text{CO})_4(\eta^2\text{-alkyne})$ ($\text{M} = \text{Ru}, \text{Os}$) species and added to the small collection of examples already available for Fe (*vide supra*).

1.2. $\text{M}(\text{CO})_4(\eta^2\text{-alkyne})$ Compounds

1.2.1. Bonding in $\text{M}(\text{CO})_4(\eta^2\text{-alkyne})$ Species

A cursory analysis of the formulation " $\text{M}(\text{CO})_4(\eta^2\text{-alkyne})$ ", where M is a group 8 transition metal, suggests that the alkyne should formally donate two electrons to the metal center so that the complex may obey the 18-electron rule. As such, the situation is initially analogous to metal-olefin bonding and thus is readily described by the familiar Dewar-Chatt-Duncanson model.^{60,61} The interaction is composed of two distinct components, donation and back-donation, which reinforce one another in a synergic fashion. The donation of electron density from the alkyne is accomplished by overlap of the in-plane, or parallel, π orbital with an empty metal valence orbital of σ symmetry (Scheme 1-2a). At the same time, metal electron density is transferred back onto the alkyne *via* overlap of a metal d_π orbital (d_{yz}) with the in-plane π^* orbital of the alkyne (Scheme 1-2b). The donation component (a) has overall σ symmetry while the back-donation interaction (b) has π symmetry.



Scheme 1-2. In-Plane Metal-Alkyne Bonding Components

An additional feature of note is that the back-donation component (b) populates an anti-bonding orbital and consequently decreases the level of carbon-carbon multiple bonding present in the alkyne. As the $\pi_{||}^*$ orbital becomes increasingly populated, the alkyne carbons rehybridize from sp towards sp^2 . Accordingly, the substituents bend back away from linearity. This feature is well recognized in the solid-state structures of the related $M(\text{CO})_4(\eta^2\text{-olefin})$ compounds.⁶²

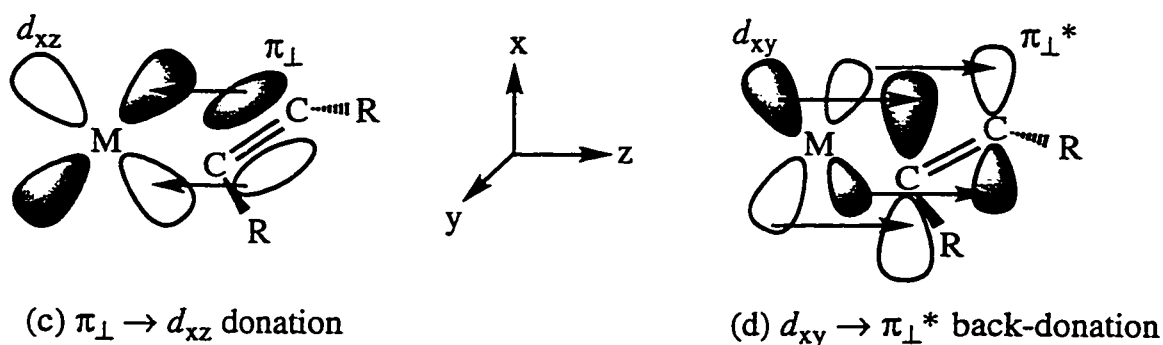
Clearly, the relative contribution of the two bonding components will greatly affect the strength and character of the metal-alkyne interaction. For example, an electron rich alkyne (*eg.* C_2Me_2) functioning as a two electron donor will serve as a good σ -donor to the metal center, and will thus emphasize interaction (a). The weak π -acidity of this type of alkyne will render the back-bonding component (b) less important. On the other hand, an alkyne bearing electron withdrawing substituents (*eg.* $\text{C}_2(\text{CF}_3)_2$) will be a weaker electron donor but a strong π -acceptor, and interaction (b) will be of greatest importance. The two possible extremes can be represented in valence-bonding terms by structures **A** and **B** in Scheme 1-3 below.



Scheme 1-3. Valence Bond Representations of Metal-Alkyne Bonding Extremes

Structure **A** represents donation of alkyne electron density to the metal with little or no π back-donation while **B** represents the extreme of strong π back-donation from the metal to an electron accepting alkyne. Indeed, as the $\pi_{||}^*$ orbital becomes more highly populated with increasing levels of back-donation from the metal, the alkyne carbon-carbon triple bond is reduced to a double bond and formal metal-carbon single bonds are formed. In this regard, strongly π -acidic alkynes coordinated to transition metals are often considered as metallacyclopropene structures much in the same way that π -acidic olefins are represented as metallacyclopropanes.⁶³

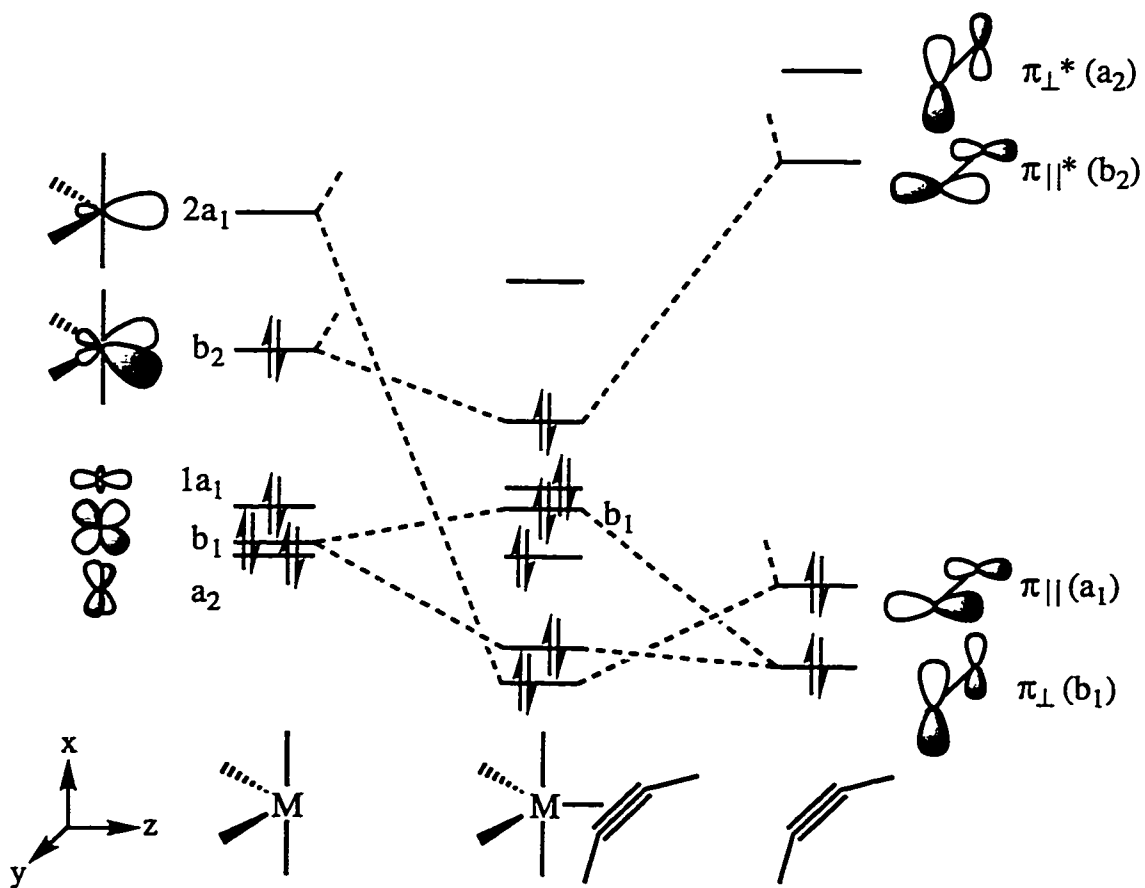
However, unlike an olefin, an alkyne possesses a second π/π^* set which is perpendicular to the plane containing $\pi_{||}$ and $\pi_{||}^*$. We must thus go beyond the basic Dewar-Chatt-Duncanson model to fully appreciate the additional orbital interactions that may arise. In particular, the filled π_{\perp} orbital is arranged so that it may interact strongly with a metal d_{xz} orbital (d_{xz} in Scheme 1-4c).



Scheme 1-4. Metal-Alkyne Interactions Perpendicular to the $\pi_{||}/\pi_{||}^*$ Plane

If the d_{xz} orbital is empty, as is the case for an early transition metal, the second alkyne electron pair is donated and the alkyne functions as a net four electron donor.⁶⁴ However, if the metal d_{xz} orbital is also filled, as in late transition metal compounds for instance, interaction (c) is destabilizing because the d_{xz} and π_{\perp} electron pairs repel one another. This situation has been referred to as four electron destabilization.^{65,66} The final component (d) is a δ interaction which can largely be neglected due to the poor overlap of the π_{\perp}^* and d_{xy} orbitals.⁶²

With a basic understanding of the general bonding properties present in metal-alkyne compounds, we can now consider the bonding of an alkyne to an $M(\text{CO})_4$ moiety. It is most convenient to use the fragment approach advocated by Hoffman in his analysis of the bonding of organometallic compounds.⁶⁷ In his development of the isolobal analogy, Hoffman compiled a library describing the frontier orbitals of a variety of ML_n fragments.⁶⁸ Thus, we can easily take the molecular orbital (MO) diagram provided for a C_{2v} - $M(\text{CO})_4$ fragment⁶⁹ and consider its interaction with the frontier orbitals of an alkyne perturbed to C_{2v} geometry.⁶⁵ The result is the derivation of the important MOs in an $M(\text{CO})_4(\eta^2\text{-alkyne})$ complex (Scheme 1-5), remembering that bonding interactions occur between overlapping orbitals of similar symmetry and energy in the two fragments.



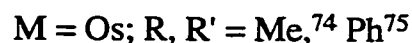
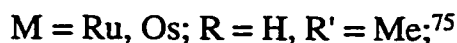
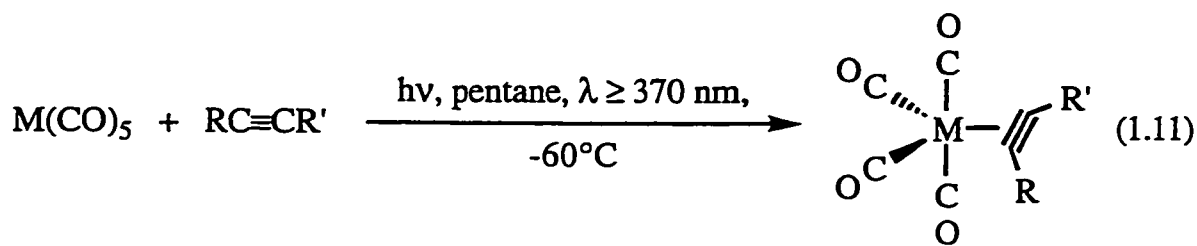
Scheme 1-5. Interaction Diagram for an $M(\text{CO})_4(\eta^2\text{-alkyne})$ Complex

Two significant bonding interactions occur. The empty, high-lying $2a_1$ orbital of the $M(CO)_4$ fragment interacts strongly with the filled $\pi_{||}$ orbital of the alkyne in the same manner described above for the donation component in Scheme 1-2a. Similarly, the filled metal-based orbital of b_2 symmetry overlaps with the $\pi_{||}^*$ orbital of the alkyne in a back-bonding interaction analogous to that in Scheme 1-2b. Although qualitative, the above treatment provides justification for the parallel orientation of the alkyne with respect to the equatorial plane in the trigonal bipyramidal structure.⁷⁰ If the alkyne were to be rotated by 90° to form a plane with the axial carbonyls, the $\pi_{||}^*$ orbital would interact with the metal b_1 orbital which is already heavily involved in back-bonding with the axial carbonyls. The resulting competition would reduce the level of π back bonding to the alkyne and weaken the overall bonding to the metal. Note also that there are no available empty orbitals in the metal fragment which can overlap with the π_{\perp} orbital, and thus the alkyne remains a net two electron donor. If the electrons in the π_{\perp} orbital were included in the electron count, the complex would have 20 valence electrons.

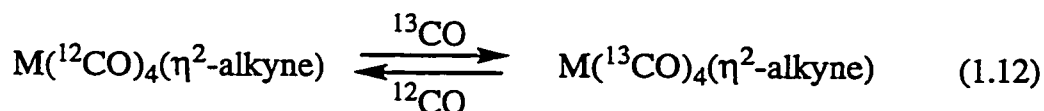
In the first approximation, the filled $1a_1$, b_1 , and a_2 set of orbitals are unperturbed by the bonding of the alkyne to the $M(CO)_4$ fragment. However, upon close inspection, it is clear that the filled π_{\perp} set will interact with the filled b_1 (" d_{xz} ") orbital in a repulsive manner, raising the energy of the b_1 orbital in the complex. The $1a_1$ orbital also experiences a repulsive interaction with filled $\pi_{||}$ orbital, but this repulsion is off-set by the strong bonding interaction between $2a_1$ and $\pi_{||}$. Furthermore, the repulsion experienced by $1a_1$ is also present in $M(CO)_4(\eta^2\text{-olefin})$ compounds.⁶⁹ Accordingly, when compared with their olefin analogs, the only difference in the MO diagrams is that the olefin compounds do not have $\pi_{\perp}/\pi_{\perp}^*$ orbitals, and thus display no destabilizing interactions that are not off-set by strong bonding overlaps. The potential effect of the "four electron destabilization" on the spectroscopic characteristics and reactivity of the compounds is discussed further in Sections 2.3 and Sections 3.4 and 4.4, respectively.

1.2.2. Synthesis of $M(\text{CO})_4(\eta^2\text{-alkyne})$ ($M = \text{Ru, Os}$) Compounds

Further work in our laboratories has extended the photochemical synthesis of $M(\text{CO})_4(\eta^2\text{-alkyne})$ ($M = \text{Ru, Os}$) compounds (Eq. 1.11).⁷¹⁻⁷⁵



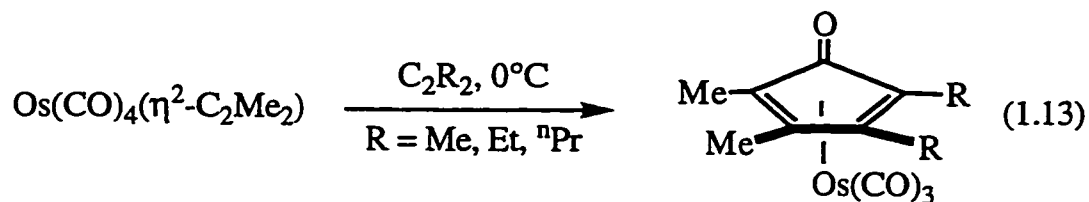
However, unlike $\text{Fe}(\text{CO})_4(\eta^2\text{-C}_2(\text{SiMe}_3)_2)$, which could be prepared by UV irradiation at room temperature,¹³ the photolyses would only afford the thermally unstable $M(\text{CO})_4(\eta^2\text{-alkyne})$ ($M = \text{Ru, Os}$) compounds if the reaction and work-up were conducted at low temperature. A variety of alkyne coupling products or unidentified compounds from thermal decomposition predominated under different conditions.⁷⁴⁻⁷⁷ One of the most interesting features of the compounds is that they were observed to readily exchange their carbonyl ligands with ^{13}CO (Eq. 1.12).



Additionally, the apparent "stability" of many of the species was improved under a CO atmosphere, suggesting that the lability of the carbonyl ligands was the source of the thermal decomposition of the compounds.⁷²

Interestingly, isolated $\text{Os}(\text{CO})_4(\eta^2\text{-C}_2\text{Me}_2)$ reacted with electron rich alkynes C_2R_2 ($R = \text{Me, Et, } n\text{Pr}$) to form the cyclopentadienone complexes $\text{Os}(\text{CO})_3\{\eta^4\text{-C}_4\text{Me}_2\text{R}_2\text{C}(\text{O})\}$, finally providing a clear demonstration of the

intermediacy of an $M(\text{CO})_4(\eta^2\text{-alkyne})$ compound in an alkyne-CO coupling reaction (Eq. 1.13).⁷⁴

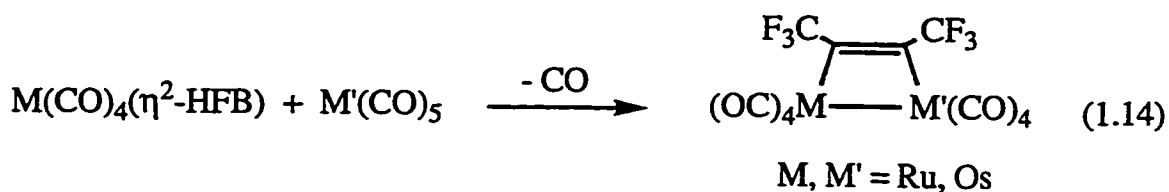


The method was also extended to the general synthesis of $M(\text{CO})_3\{\eta^4\text{-C}_4\text{R}_4\text{C}(\text{O})\}$ compounds using *in situ* photochemical generation of $M(\text{CO})_4(\eta^2\text{-C}_2\text{R}_2)$ in the presence of excess alkyne.⁷⁴ However, the procedure proved to be limited to cases where the alkyne was electron rich and bore aliphatic substituents. For example, even though $\text{Os}(\text{CO})_3\{\eta^4\text{-C}_4\text{Ph}_4\text{C}(\text{O})\}$ has been successfully synthesized by photolysis of $\text{Os}_3(\text{CO})_{12}$ in the presence of excess C_2Ph_2 ,⁵⁰ $\text{Os}(\text{CO})_4(\eta^2\text{-C}_2\text{Ph}_2)$ does not afford the expected alkyne coupling product upon thermal reaction with C_2Ph_2 .⁷⁴ $\text{Os}(\text{CO})_4(\eta^2\text{-C}_2\text{H}_2)$ is similarly unreactive towards added alkynes,⁷⁷ and the Ru analog decomposes above -30°C .⁷² Although the thermal decomposition routes of the alkyne compounds are generally complicated, $\text{Ru}(\text{CO})_4(\eta^2\text{-HFB})$ (HFB = $\text{C}_2(\text{CF}_3)_2$) undergoes a clean conversion to $\text{Ru}_2(\text{CO})_6(\mu\text{-}\eta^1, \eta^1:\eta^4\text{-C}_4(\text{CF}_3)_4)$ upon refluxing in toluene.⁷⁸

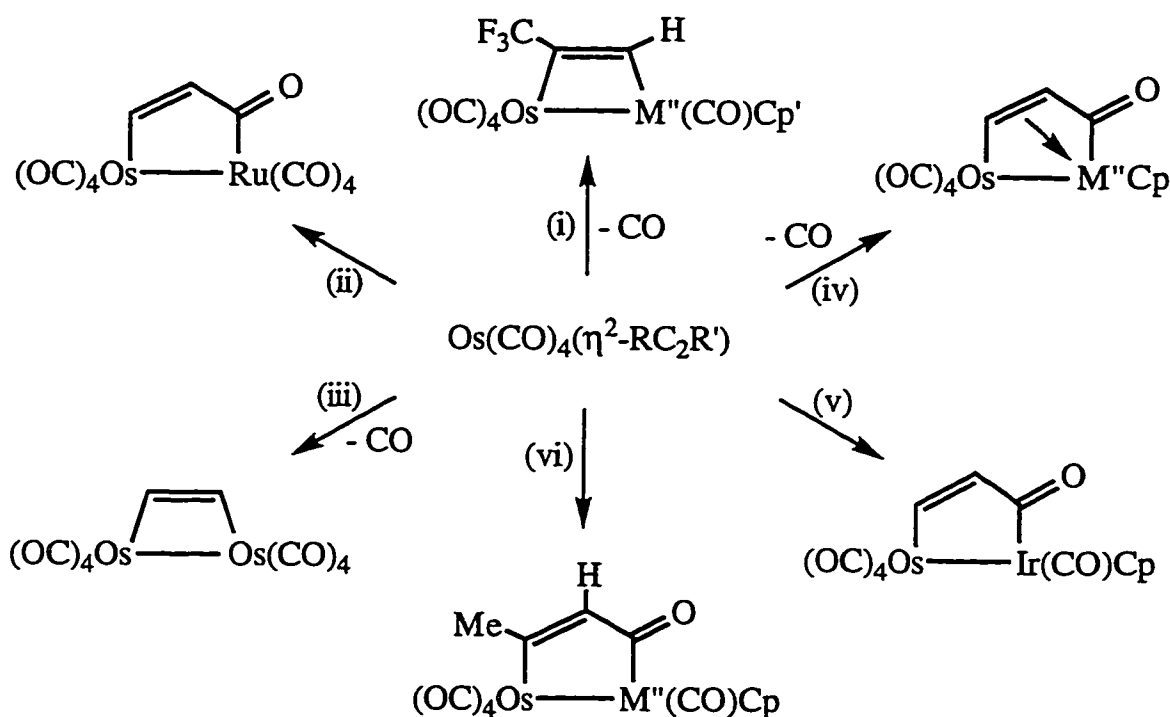
1.3. Bimetallic Compounds with Alkyne Bridges

1.3.1. Targeted Synthesis of Alkyne-Bridged Heterobimetallic Compounds

Even more interesting than the reaction of $\text{Os}(\text{CO})_4(\eta^2\text{-C}_2\text{Me}_2)$ with C_2R_2 (Eq. 1.12) was the observation that the $M(\text{CO})_4(\eta^2\text{-alkyne})$ species were reactive towards other electronically saturated late transition metal compounds. This serendipitous discovery came during the photochemical preparation of $\text{Ru}(\text{CO})_4(\eta^2\text{-HFB})$, where it was observed that the ruthenium-alkyne product would combine with unreacted $\text{Ru}(\text{CO})_5$ or deliberately added $\text{Os}(\text{CO})_5$ to produce the dimetallacyclobutenes $\text{MRu}(\text{CO})_8(\mu\text{-}\eta^1:\eta^1\text{-HFB})$ (Eq. 1.14).⁷¹



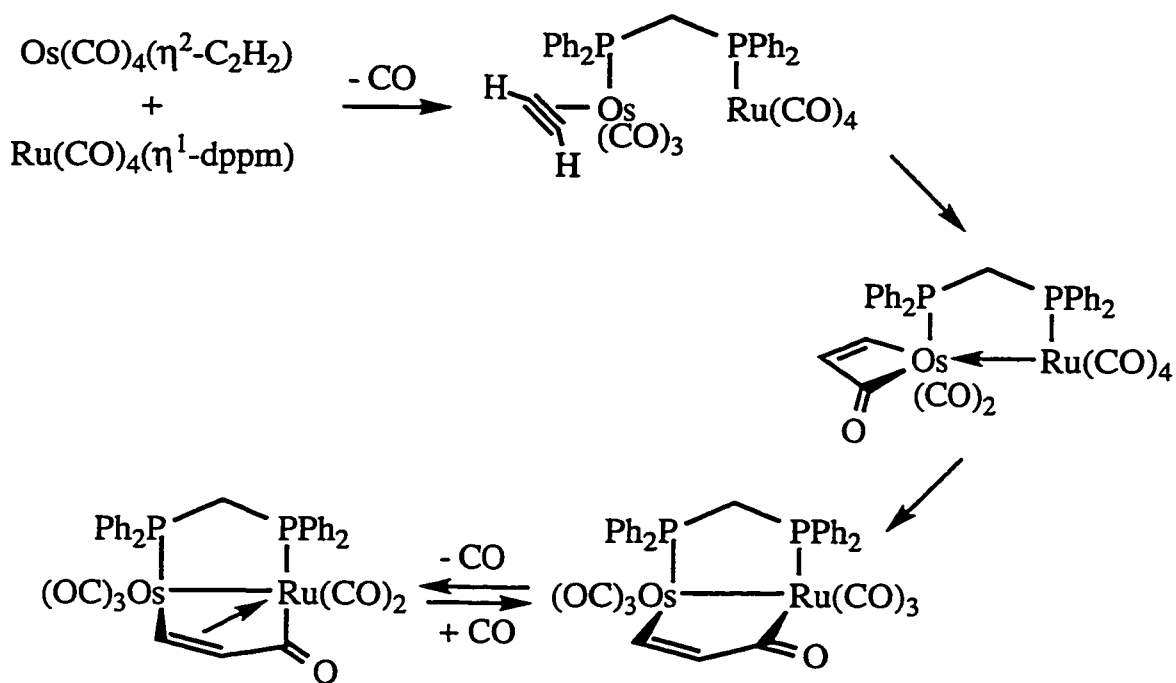
It was also found that $\text{Os}(\text{CO})_4(\eta^2\text{-HFB})$ would react with $\text{Os}(\text{CO})_5$ at 60°C to produce the diosmacyclobutene analog in far better yield than was possible from the photolysis of $\text{Os}_3(\text{CO})_{12}$ in the presence of HFB (Eq. 1.10). Subsequent development of this chemistry with the other available $M(\text{CO})_4(\eta^2\text{-alkyne})$ compounds and $\text{Cp}'\text{M}''(\text{CO})_2$ ($\text{Cp}' = \text{Cp, Cp}^*$; $\text{M}'' = \text{Co, Rh, Ir}$) led to a diverse range of products which commonly included dimetallacyclopentenone structures resulting from migratory CO insertion (Scheme 1-6).^{72,77,79}



Scheme 1-6. Reaction of $\text{Os}(\text{CO})_4(\eta^2\text{-RC}_2\text{R}')$ with ML_n Reagents.^{72,77}

(i) $\text{Cp}'\text{M}''(\text{CO})_2$, $\text{Cp}'\text{M}'' = \text{CpRh, Cp}^*\text{Rh, Cp}^*\text{Ir}$. (ii) $\text{Ru}(\text{CO})_5$. (iii) $\text{Os}(\text{CO})_5$.
 (iv) $\text{CpM}''(\text{CO})_2$, $\text{M}'' = \text{Co, Rh}$. (v) $\text{CpIr}(\text{CO})_2$. (vi) $\text{CpM}''(\text{CO})_2$, $\text{M}'' = \text{Co, Rh, Ir}$.

Low temperature reaction monitoring by multinuclear NMR provided evidence that the reactions were initiated by CO dissociation from the $M(\text{CO})_4(\eta^2\text{-alkyne})$ species, which is fascinating when it is noted that the $\mu\text{-}\eta^1\text{:}\eta^1$ -dimetallacyclopentenones such as $\text{OsRu}(\text{CO})_8(\mu\text{-}\eta^1\text{:}\eta^1\text{-C}_2\text{H}_2\text{C}(\text{O}))$ are formed without net CO loss. Further work revealed that the reaction of $\text{Os}(\text{CO})_4(\eta^2\text{-C}_2\text{H}_2)$ with $M(\text{CO})_4(\eta^1\text{-dppm})$ ($M = \text{Fe}, \text{Ru}$) also proceeded *via* initial CO loss from the osmium-alkyne compound, and careful monitoring of the reaction resulted in the detection of a variety of intermediates along the reaction pathway (Scheme 1-7).⁸⁰ All compounds indicated were detected by multinuclear NMR spectroscopy.



Scheme 1-7. Reaction of $\text{Os}(\text{CO})_4(\eta^2\text{-C}_2\text{H}_2)$ with $\text{Ru}(\text{CO})_4(\eta^1\text{-dppm})$.

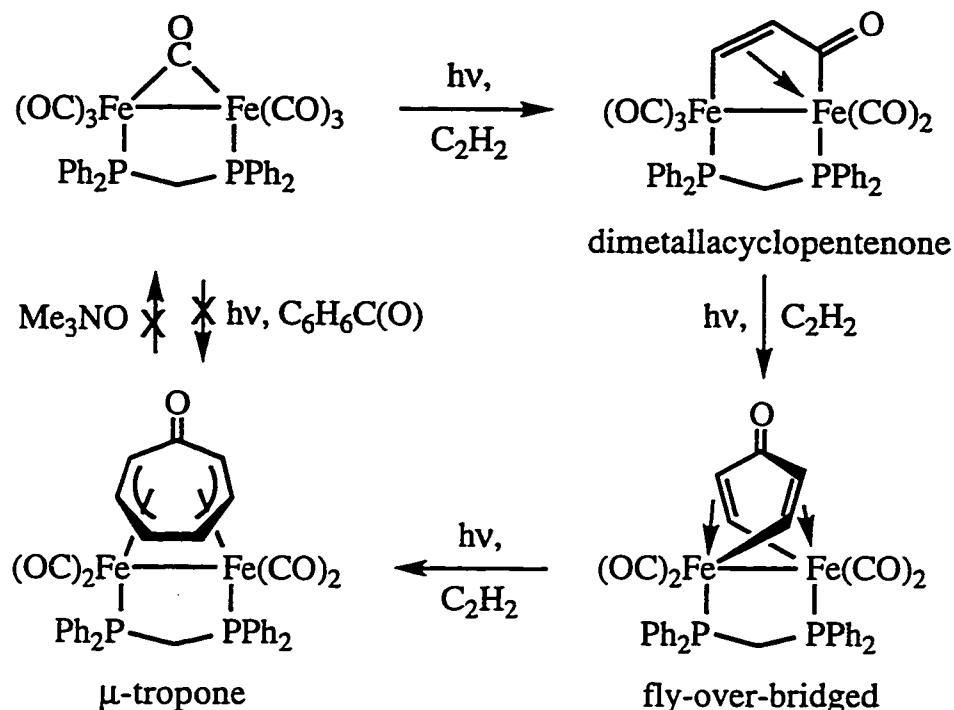
1.3.2. Reaction of Alkynes on Pre-Formed Bimetallic Frameworks

Bimetallic compounds are commonly thought of as a bridge between mononuclear and cluster compounds, and provide one of the simplest models for the adsorption and transformation of surface-bound molecules.⁸¹⁻⁸³ Working catalysts can involve either homo- or heterogeneous mixtures of more than one

metal species, and studying simpler models can be an efficient way of gaining insight into the transformations observed in the more complex systems.⁸⁴ The synthesis of heterobimetallic compounds is thus an important method of investigating the different types of transformations which are possible at each metal center, and is also important in determining if the different metals can act in a cooperative manner to transform substrates. Dimetallacyclobutenes are commonly proposed as the initial products of alkyne adsorption on a surface,⁸⁵ and compounds such as those in Eq. 1.14 can provide an initial model of such behavior.⁷¹

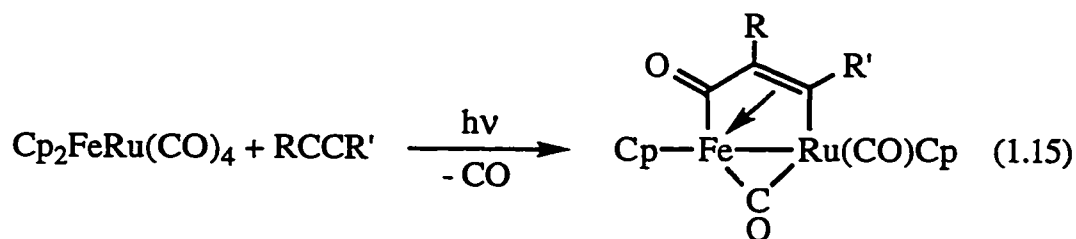
Although a large amount of research has been performed on the coordination and modification of alkynes on dinuclear frameworks, much of the work has been conducted on homobimetallic compounds.⁸⁵⁻⁹⁵ One of the more versatile systems was formed by photolysis of $\text{Cp}_2\text{Ru}_2(\text{CO})_4$ in the presence of diphenylacetylene; the resulting $\text{Cp}_2\text{Ru}_2(\text{CO})(\mu\text{-CO})(\mu\text{-}\eta^1\text{:}\eta^3\text{-C}_2\text{Ph}_2\text{C(O)})$ complex underwent a variety of chemical reactions as a result of the lability of C_2Ph_2 .^{84,88,96} The diphosphine-bridged $\text{Fe}_2(\text{CO})_7(\mu\text{-dppm})$ also made for an interesting study as it reacted sequentially with acetylene to build up a seven-membered tropone ring, which surprisingly could not be liberated from the dinuclear framework (Scheme 1-8).^{89,93} The corresponding reaction with diphenylacetylene proceeded *via* a dimetallacyclopentenone, but afforded the ferrole compound $\text{Fe}_2(\text{CO})_4(\mu\text{-dppm})(\mu\text{-}\eta^1, \eta^1\text{:}\eta^4\text{-C}_4\text{Ph}_4)$ rather than a fly-over bridge or tropone species, a result attributed to steric factors.⁹³ $\text{Ru}_2(\text{CO})_7(\mu\text{-dppm})$ reacts with alkynes in a much more facile manner than its di-iron analog, requiring only mild thermal activation rather than UV irradiation, to produce a dimetallacyclopentenone with acetylene⁹⁰ and a dimetallacyclobutene with $\text{C}_2(\text{CO}_2\text{Me})_2$.⁹⁷ The diruthenacyclopentenone underwent further reaction with acetylene upon irradiation, producing a mixture of a fly-over bridge species $\text{Ru}_2(\text{CO})_4(\mu\text{-dppm})(\mu\text{-}\sigma, \sigma'\text{:}\eta^2, \eta^{2'}\text{-C}_4\text{H}_4\text{C(O)})$ and the ruthenole $\text{Ru}_2(\text{CO})_4(\mu\text{-dppm})(\mu\text{-}\eta^1, \eta^1\text{:}\eta^4\text{-C}_4\text{H}_4)$.⁹⁷ A range of compounds have also been prepared from "A-frame" $\text{M}_2(\mu\text{-dppm})_2$ frameworks,⁹⁸ but these compounds generally do not promote coupling of alkynes with carbon monoxide ligands,

$\text{Ru}_2(\text{dppm})_2(\text{CO})_5$ and $\text{Ru}_2(\text{dmpm})_2(\text{CO})_5$ providing noteworthy exceptions.^{85,91,92}



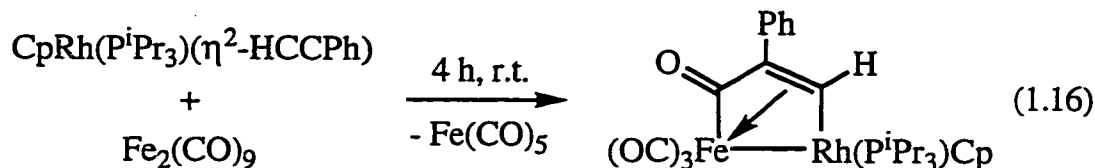
Scheme 1-8. Reaction of $\text{Fe}_2(\text{CO})_7(\mu\text{-dppm})$ with C_2H_2 .^{89,93}

Despite the wealth of chemistry described between alkynes and pre-formed dinuclear centers, one limitation in the methodology is that suitable heterobimetallic starting materials⁹⁹⁻¹⁰² are less commonly available outside the realm of "A-frame" chemistry.¹⁰³⁻¹⁰⁷ Knox and co-workers found that $\text{Cp}_2\text{FeRu}(\text{CO})_4$ was much more reactive towards alkynes than the Fe_2 or Ru_2 analogs, and discovered that the dimetallacyclopentenone products were formed regioselectively with the acyl group bonded to Fe (Eq. 1.15).^{99,100}



Furthermore, many of the transformations of the heterodimetallacyclopentenones imitated their homobimetallic analogs, prompting Knox to comment that the heteronuclear system imposed no significant restraints on the chemistry while providing the advantage of enhanced reactivity.⁹⁹ Shaw also observed that $\text{Fe}(\text{CO})_3(\mu\text{-dppm})(\mu\text{-CO})\text{Pt}(\text{PPh}_3)$ reacted with alkynes under mild conditions, again to provide dimetallacyclopentenones in which the acyl group was bonded to the iron center.^{101,102}

Finally, although mononuclear compounds occasionally react with alkynes to afford alkyne-bridged homodinuclear products,¹⁰⁸⁻¹¹⁰ there are relatively few examples of reactions analogous to Eq. 1.14 and Schemes 1-6 and 1-7. One example was reported by Werner, and involved the reaction of electronically saturated $\text{CpRh}(\text{P}^i\text{Pr}_3)(\eta^2\text{-HC}_2\text{Ph})$ with $\text{Fe}_2(\text{CO})_9$ to produce $\text{CpRh}(\text{P}^i\text{Pr}_3)\text{Fe}(\text{CO})_3(\mu\text{-}\eta^1\text{:}\eta^3\text{-CHCPhC(O)})$ and $\text{Fe}(\text{CO})_5$ (Eq. 1.16).¹¹¹



Beck reported the synthesis of alkyne-bridged heterobimetallic compounds by reaction of anionic organometallic nucleophiles such as $[\text{Re}(\text{CO})_5]^-$ with cationic Mo and W electrophiles containing a coordinated alkyne.^{112,113} Stone successfully synthesized $\text{Pt}_2(\text{COD})_2(\mu\text{-}\eta^1\text{:}\eta^1\text{-HFB})$ by combining $\text{Pt}(\eta^4\text{-C}_8\text{H}_{12})(\eta^2\text{-HFB})$ and $\text{Pt}(\eta^4\text{-C}_8\text{H}_{12})_2$,¹¹⁴ but the method was not reported to generate compounds with two different metal centers.¹¹⁴ Thus, $\text{M}(\text{CO})_4(\eta^2\text{-alkyne})$ compounds provide one of the most versatile methods of incorporating two different late transition metal centers into a heterobimetallic system.

1.4. Scope of the Thesis

The chemistry of alkynes and the carbonyls of the group eight transition metals has been exhaustively studied, and the advent of a convenient synthesis of $\text{M}(\text{CO})_4(\eta^2\text{-alkyne})$ ($\text{M} = \text{Ru}, \text{Os}$) compounds has allowed for a delineation of the importance of these compounds in alkyne-coupling reactions for the heavier

metals of the triad.⁷⁴ Furthermore, a comprehensive study of the properties of the $M(\text{CO})_4(\eta^2\text{-alkyne})$ complexes has revealed that their enhanced reactivity is due to facile carbonyl dissociation, a characteristic that has been exploited in the synthesis of alkyne-bridged heterobimetallic compounds.^{71-73,75,77,79,80} However, despite the wealth of information and isolated compounds from the reaction of binary iron carbonyls with alkynes, only a few examples of the corresponding $\text{Fe}(\text{CO})_4(\eta^2\text{-alkyne})$ archetype exist,^{10,13,14,25} and the steric bulk of the coordinated alkyne largely negates any reactivity leading to modification of the organic substrate in these cases.

The success of the preparation of $M(\text{CO})_4(\eta^2\text{-alkyne})$ ($M = \text{Ru}, \text{Os}$) compounds can be traced to the low temperature at which the photochemistry was conducted. This procedure even allowed isolation of the reactive $\text{Os}(\text{CO})_4(\eta^2\text{-C}_2\text{Me}_2)$, which converted to the more stable $\text{Os}(\text{CO})_3\{\eta^4\text{-C}_4\text{Me}_4\text{C}(\text{O})\}$ on warming.⁷⁴ However, early work on extending the low temperature photochemistry to the lightest member of the triad, $\text{Fe}(\text{CO})_5$, resulted in slow reaction times and copious production of intractable byproducts.⁷⁵ Nonetheless, the isolation of stable $\text{Fe}(\text{CO})_4(\eta^2\text{-alkyne})$ complexes with bulky alkynes suggests that the paucity of such compounds in the literature is not necessarily due to the thermodynamic instability of the Fe-alkyne bond, but rather may reflect a "hyper-reactivity" of these compounds with free alkynes.²⁵ As such, there is no reason, *a priori*, why $\text{Fe}(\text{CO})_4(\eta^2\text{-alkyne})$ compounds cannot be synthesized, providing that suitable preparative conditions can be found. Thus, it is the objective of this thesis to re-examine the low temperature photochemistry of $\text{Fe}(\text{CO})_5$ in the presence of alkynes and, if successful, to survey the reactivity of the long elusive $\text{Fe}(\text{CO})_4(\eta^2\text{-alkyne})$ compounds to hopefully provide answers to some old problems and to develop new chemistry in an age-old field.

1.5. References

1. Reppe, W.; Vetter, H. *Ann. Chem.* **1953**, 582, 133.
2. Pino, P.; Braca, G. In *Organic Synthesis via Metal Carbonyls*; I. Wender and P. Pino, Eds.; Wiley-Interscience: New York, 1977; Vol. 2; pp 419 and references therein.
3. Sternberg, H. W.; Friedel, R. A.; Markby, R.; Wender, I. *J. Am. Chem. Soc.* **1956**, 78, 3621.
4. Clarkson, R.; Jones, E. R. H.; Wailes, P. C.; Whiting, M. C. *J. Am. Chem. Soc.* **1956**, 78, 6206.
5. Case, J. R.; Clarkson, R.; Jones, E. R. H.; Whiting, M. C. *Proc. Chem. Soc.* **1959**, 150.
6. Reppe, W.; Kutepow, N. v.; Magin, A. *Angew. Chem. Int. Ed. Engl.* **1969**, 8, 727.
7. Sternberg, H. W.; Markby, R.; Wender, I. *J. Am. Chem. Soc.* **1958**, 80, 1009.
8. Hübel, W.; Braye, H.; Clauss, A.; Weiss, E.; Krüerke, U.; Brown, D. A.; King, G. S. D.; Hoogzand, C. *J. Inorg. Nucl. Chem.* **1959**, 9, 204.
9. Hübel, W.; Braye, H. *J. Inorg. Nucl. Chem.* **1959**, 10, 250.
10. Hübel, W. In *Organic Synthesis via Metal Carbonyls*; I. Wender and P. Pino, Eds.; Wiley-Interscience: New York, 1968; Vol. 1; pp 273 and references therein.
11. Weiss, E.; Hübel, W.; Merényi, R. *Chem. Ber.* **1962**, 95, 1155.
12. Schrauzer, G. N. *J. Am. Chem. Soc.* **1959**, 81, 5307.
13. Pannell, K. H.; Crawford, G. M. *J. Coord. Chem.* **1973**, 2, 251.
14. Cotton, F. A.; Jamerson, J. D.; Stults, B. R. *J. Am. Chem. Soc.* **1976**, 98, 1774.
15. Nicholas, K.; Bray, L. S.; Davis, R. E.; Pettit, R. *J. Chem. Soc., Chem. Commun.* **1971**, 608.
16. Subsequent to Hübel's initial and exhaustive research, Cotton re-investigated the reaction of $C_2^tBu_2$ with $Fe_2(CO)_9$ and found that the compound initially proposed by Hübel to be $Fe_2(CO)_7(C_2^tBu_2)$ was, in fact, $Fe_2(CO)_6(\mu-\eta^2-\eta^2-C_2^tBu_2)$.¹⁴ The reactive diphenylacetylene analog

referred to as $\text{Fe}_2(\text{CO})_7(\text{C}_2\text{Ph}_2)$ in Ref. 10 is thus presumably $\text{Fe}_2(\text{CO})_6(\mu\text{-}\eta^2\text{:}\eta^2\text{-C}_2\text{Ph}_2)$. Interestingly, the latter formulation appears in one of Hübel's early articles (Fig. 4 in Ref. 9), but it is unclear why the " $\text{Fe}_2(\text{CO})_7(\text{C}_2\text{R}_2)$ " formulation was favored in later reports.

17. Hickey, J. P.; Wilkinson, J. R.; Todd, L. J. *J. Organomet. Chem.* **1975**, *99*, 281.
18. Cotton, F. A.; Hunter, D. L.; Troup, J. M. *Inorg. Chem.* **1976**, *15*, 63.
19. Aime, S.; Milone, L.; Sappa, E. *J. Chem. Soc., Dalton Trans.* **1976**, 838.
20. Osella, D.; Botta, M.; Gobetto, R.; Amadelli, R.; Carassiti, V. *J. Chem. Soc., Dalton Trans.* **1988**, 2519.
21. Thorn, D. L.; Hoffmann, R. *Inorg. Chem.* **1978**, *17*, 126.
22. Casarin, M.; Ajò, D.; Vittadini, A.; G., G.; Bertocello, R.; Osella, D. *Inorg. Chem.* **1986**, *25*, 511.
23. Orgel, L. E. In *International Conference on Co-ordination Chemistry*; Spec. Publ. No. 13, The Chemical Society: London, 1959; pp 93.
24. Parshall, W.; Ittel, S. D. *Homogeneous Catalysis*; Wiley-Interscience: New York, 1992; Vol. 2, pp 205-207.
25. Carty, A. J.; Smith, W. F.; Taylor, N. J. *J. Organomet. Chem.* **1978**, *146*, C1.
26. Birk, R.; Berke, H.; Huttner, G.; Zsolnai, L. *Chem. Ber.* **1988**, *121*, 471.
27. Birk, R.; Grössmann, U.; Hund, H.-U.; Berke, H. *J. Organomet. Chem.* **1988**, *345*, 321.
28. Grössmann, U.; Hund, H.-U.; Bosch, H. W.; Schmalte, H.; Berke, H. *J. Organomet. Chem.* **1991**, *408*, 203.
29. Gauss, C.; Veghini, D.; Berke, H. *Chem. Ber.* **1997**, *130*, 183.
30. Pearson, A. J.; Shively, R. J., Jr.; Dubbert, R. A. *Organometallics* **1992**, *11*, 4096.
31. Pearson, A. J.; Shively, R. J., Jr. *Organometallics* **1994**, *13*, 578.
32. Pearson, A. J.; Perosa, A. *Organometallics* **1995**, *14*, 5178.
33. Knölker, H.-J.; Heber, J.; Mahler, C. H. *Synlett* **1992**, 1002.
34. Knölker, H.-J.; Heber, J. *Synlett* **1993**, 924.
35. Knölker, H.-J.; Baum, E.; Heber, J. *Tetrahedron Lett.* **1995**, *36*, 7647.

36. Fornals, D.; Pericàs, M. A.; Serratosa, F.; Font-Altaba, M.; Solans, X. *J. Chem. Soc. Perkin Trans. I* **1987**, 2749.
37. Krespan, C. G. *J. Org. Chem.* **1975**, *40*, 261.
38. Boston, J. L.; Sharp, D. W. A.; Wilkinson, G. *J. Chem. Soc.* **1962**, 3488.
39. Periasamy, M.; Rameshkumar, C.; Radhakrishnan, U. *Tetrahedron. Lett.* **1997**, *38*, 7229.
40. Periasamy, M.; Radhakrishnan, U.; Brunet, J.-J.; Chauvin, R.; El-Zaizi, A. W. *J. Chem. Soc., Chem. Commun* **1996**, 1499.
41. Whitmire, K. H.; Lee, T. R.; Lewis, E. S. *Organometallics* **1986**, *5*, 987.
42. Liebeskind, L. S.; Baysdon, S. L.; South, M. S.; Iyer, S.; Leeds, J. P. *Tetrahedron* **1985**, *41*, 5839.
43. Dodge, R. P.; Mills, O. S.; Schomaker, V. *Proc. Chem. Soc.* **1963**, 380.
44. Bruce, M. I.; Knight, J. R. *J. Organomet. Chem.* **1968**, *12*, 411.
45. Sears, C. T.; Stone, F. G. A. *J. Organomet. Chem.* **1968**, *11*, 644.
46. Bruce, M. I.; Cooke, M.; Westlake, D. J. *J. Chem. Soc. (A)* **1969**, 987.
47. Gambino, O.; Vaglio, G. A.; Ferrari, R. P.; Getini, G. *J. Organomet. Chem.* **1971**, *30*, 381.
48. Ferrari, R. P.; Vaglio, G. A. *Gazz. Chim. Ital.* **1975**, *105*, 939.
49. Adams, R. D.; Selegue, J. P. In *Comprehensive Organometallic Chemistry*; G. Wilkinson, F. G. A. Stone and E. W. Abel, Eds.; Pergamon Press: Oxford, 1983; Vol. 4; pp 1033-1039.
50. Burke, M. R.; Funk, T.; Takats, J. *Organometallics* **1994**, *13*, 2109.
51. Haines, R. J. In *Comprehensive Organometallic Chemistry II*; G. Wilkinson, F. G. A. Stone and E. W. Abel, Eds.; Pergamon: Oxford, 1995; Vol. 7; pp 654-655.
52. Cetini, G.; Gambino, O.; Sappa, E.; Valle, M. *J. Organomet. Chem.* **1969**, *17*, 437.
53. Bruce, M. I. In *Comprehensive Organometallic Chemistry*; G. Wilkinson, F. G. A. Stone and E. W. Abel, Eds.; Pergamon Press: Oxford, 1983; Vol. 4; pp 858-863.
54. Raithby, P. R.; Rosales, M. J. *Adv. Inorg. Chem. Radiochem.* **1985**, *29*, 169.
55. Deeming, A. J. *Adv. Organomet. Chem.* **1986**, *26*, 1.

56. Poë, A. J.; Sampson, C. N.; Smith, R. T. *J. Am. Chem. Soc.* **1986**, *108*, 5459.
57. Burke, M. R.; Takats, J. *J. Organomet. Chem.* **1986**, *302*, C25.
58. Burke, M. R. PhD Thesis, University of Alberta, 1987.
59. Ball, R. G.; Burke, M. R.; Takats, J. *Organometallics* **1987**, *6*, 1918.
60. Chatt, J.; Duncanson, L. A. *J. Chem. Soc.* **1953**, 2939.
61. Dewar, M. J. S. *J. Am. Chem. Soc.* **1979**, *101*, 783 and references therein.
62. Mingos, D. M. P. In *Comprehensive Organometallic Chemistry*; G. Wilkinson, F. G. A. Stone and E. W. Abel, Eds.; Pergamon Press: Oxford, 1983; Vol. 3; pp 1.
63. Bender, B. R.; Norton, J. R.; Miller, M. M.; Anderson, O. P.; Rappé, A. K. *Organometallics* **1992**, *11*, 3427 and references therein.
64. Templeton, J. L. *Adv. Organomet. Chem.* **1989**, *29*, 1.
65. Marinelli, G.; Streib, W.; Huffman, J. C.; Caulton, K. G.; Gagné, M. R.; Takats, J.; Dartiguenave, M. *Polyhedron* **1990**, *9*, 1867.
66. Caulton, K. G. *New. J. Chem.* **1994**, *18*, 25.
67. Hoffmann, R. *Science* **1981**, *211*, 995.
68. Hoffmann, R. *Angew. Chem. Int. Ed. Engl.* **1982**, *21*, 711.
69. Albright, T. A.; Hoffmann, R.; Thibeault, J. C.; Thorn, D. C. *J. Am. Chem. Soc.* **1979**, *101*, 3801.
70. Rossi, A. R.; Hoffmann, R. *Inorg. Chem.* **1975**, *14*, 365.
71. Gagné, M. R.; Takats, J. *Organometallics* **1988**, *7*, 561.
72. Burn, M. J.; Kiel, G.-Y.; Seils, F.; Takats, J.; Washington, J. *J. Am. Chem. Soc.* **1989**, *111*, 6850.
73. Hoffman, K. MSc. Thesis, University of Alberta, 1994.
74. Washington, J.; McDonald, R.; Takats, J.; Menashe, N.; Reshef, D.; Shvo, Y. *Organometallics* **1995**, *14*, 3996.
75. Kiel, G.-Y. unpublished results.
76. Gagné, M.; Takats, J. unpublished work.
77. Washington, J. PhD Thesis, University of Alberta, 1994.
78. Senzaki, Y.; McCormick, F. B.; Gladfelter, W. L. *Materials* **1992**, *4*, 748.
79. Takats, J. *J. Cluster Science* **1992**, *3*, 479.
80. Mao, T. PhD Thesis, University of Alberta, 1996.

81. Muetterties, E. L.; Rhodin, T. N.; Band, E.; Brucker, C. F.; Pretzer, W. R. *Chem. Rev.* **1979**, *79*, 91.
82. *The Chemistry of Heteronuclear Clusters and Multimetallic Catalysts*; Proceedings of the Seminar Held at Albertus Magnus College, Königstein, FRG, Sept 7-11, 1987; Adams, R.D., Herrmann, W.A., Eds. *Polyhedron*, **1988**, *7*, 2251-2462.
83. Maitlis, P. M.; Long, H. C.; Quyoun, R.; Turner, M. L.; Wang, Z.-Q. *J. Chem. Soc. Chem. Comm.* **1996**, 1.
84. Knox, S. A. R. *Pure Appl. Chem.* **1984**, *56*, 89.
85. Mirza, H. A.; Vittal, J. J.; Puddephatt, R. J. *Organometallics* **1994**, *13*, 3063 and references therein.
86. Dyke, A. F.; Knox, S. A. R.; Naish, P. J.; Taylor, G. E. *J. Chem. Soc., Chem. Commun.* **1980**, 409.
87. Dickson, R. S.; Gatehouse, B. M.; Nesbit, M. C.; Pain, G. N. *J. Organomet. Chem.* **1981**, *215*, 97.
88. Dyke, A. F.; Knox, S. A. R.; Naish, P.; Taylor, G. E. *J. Chem. Soc., Dalton Trans.* **1982**, 1297.
89. Hogarth, G.; Knox, S. A. R.; Lloyd, B. R.; Macpherson, K. A.; Morton, D. A. V.; Orpen, A. G. *J. Chem. Soc., Chem. Commun.* **1988**, 360.
90. Kiel, G.-Y.; Takats, J. *Organometallics* **1989**, *8*, 839.
91. Johnson, K. A.; Gladfelter, W. L. *J. Am. Chem. Soc.* **1991**, *113*, 5097.
92. Johnson, K. A.; Gladfelter, W. L. *Organometallics* **1992**, *11*, 2534.
93. Knox, S. A. R.; Lloyd, B. R.; Morton, D. A. V.; Orpen, A. G.; Turner, M. L.; Hogarth, G. *Polyhedron* **1995**, *14*, 2723.
94. Casey, C. P.; Cariño, R. S.; Sakaba, H.; Hayashi, R. K. *Organometallics* **1996**, *15*, 2640.
95. Casey, C. P.; Cariño, R. S.; Sakaba, H. *Organometallics* **1997**, *16*, 419.
96. Knox, S. A. R. *J. Organomet. Chem.* **1990**, *400*, 255.
97. Sandercock, P. M. L. MSc. Thesis, University of Alberta, 1990.
98. George, D. S. A.; McDonald, R.; Cowie, M. *Can. J. Chem.* **1996**, *74*, 2289 and references therein.

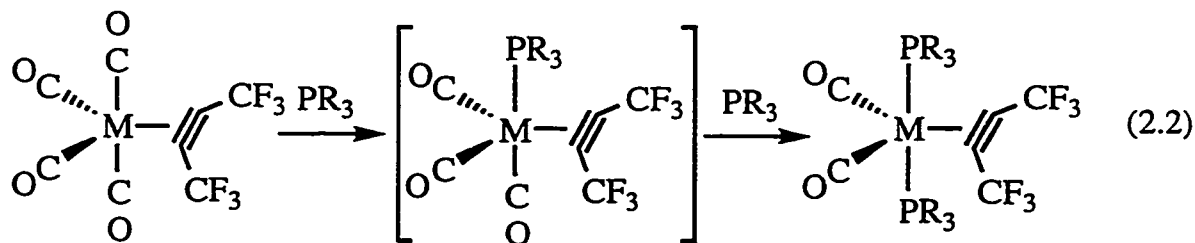
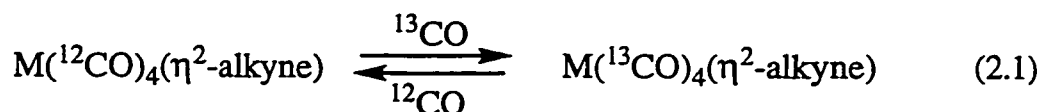
99. Gracey, B. P.; Knox, S. A. R.; Macpherson, K. A.; Orpen, A. G. *J. Organomet. Chem.* **1984**, *272*, C45.
100. Gracey, B. P.; Knox, S. A. R.; Macpherson, K. A.; Orpen, A. G.; Stobart, S. *R. J. Chem. Soc., Dalton Trans.* **1985**, 1935.
101. Fontaine, X. L. R.; Jacobson, G. B.; Shaw, B. L.; Thornton-Pett, M. *J. Chem. Soc., Chem. Commun.* **1987**, 662.
102. Fontaine, X. L. R.; Jacobsen, G. B.; Shaw, B. L.; Thornton-Pett, M. *J. Chem. Soc., Dalton Trans.* **1988**, 741.
103. Antonelli, D. M.; Cowie, M. *Inorg. Chem.* **1990**, *29*, 4039.
104. Hilts, R. W.; Franchuk, R. A.; Cowie, M. *Organometallics* **1991**, *10*, 304.
105. Wang, L.-S.; Cowie, M. *Can. J. Chem.* **1995**, *73*, 1058.
106. Wang, L.-S.; Cowie, M. *Organometallics* **1995**, *14*, 2374.
107. Antwi-Nsiah, F. H.; Oke, O.; Cowie, M. *Organometallics* **1996**, *15*, 506.
108. Rausch, M. D.; Galinger, R. G.; Gardner, S. A.; Brown, R. K.; Wood, J. S. *J. Am. Chem. Soc.* **1977**, *99*, 7870.
109. Dickson, R. S.; Mok, C.; Pain, G. *J. Organomet. Chem.* **1979**, *166*, 385.
110. Koie, Y.; Shinoda, S.; Saito, Y.; Fitzgerald, B. J.; Pierpont, C. G. *Inorg. Chem.* **1980**, *19*, 770.
111. Otto, H.; Garcia Alonso, F. G.; Werner, H. *J. Organomet. Chem.* **1986**, *306*, C13.
112. Beck, W.; Müller, H.-J.; Nagel, U. *Angew. Chem. Int. Ed. Engl.* **1986**, *25*, 734.
113. Müller, H.-J.; Polborn, K.; Steimann, M.; Beck, W. *Chem. Ber.* **1989**, *122*, 1901.
114. Boag, N. M.; Green, M.; Stone, F. G. A. *J. Chem. Soc. Chem. Commun.* **1980**, 1281.

Chapter 2

Low Temperature Photochemical Synthesis of $\text{Fe}(\text{CO})_4(\eta^2\text{-RC}\equiv\text{CR}')$ ($\text{R}, \text{R}' = \text{CF}_3, \text{H}, \text{Me}; \text{R} = \text{H}, \text{R}' = \text{CF}_3, \text{Me}$) Complexes

2.1. Introduction

The first ternary ruthenium and osmium tetracarbonyl-alkyne compounds were prepared in our laboratories in the late 1980s.¹⁻³ Low temperature photolysis of $\text{M}(\text{CO})_5$ ($\text{M} = \text{Ru}, \text{Os}$) in the presence of excess alkyne proved to be the synthetic method of choice in preparing a modest range of $\text{M}(\text{CO})_4(\eta^2\text{-RC}\equiv\text{CR}')$ ($\text{M} = \text{Ru}, \text{Os}; \text{R} = \text{R}' = \text{CF}_3, \text{H}; \text{R} = \text{CF}_3, \text{R}' = \text{H}. \text{M} = \text{Os}, \text{R} = \text{Me}, \text{R}' = \text{H}, \text{Me}$) species.²⁻⁶ The initial focus of subsequent studies was to explore the physical properties and synthetic applications of this new class of compounds. In general, the reactivity patterns were consistent with facile CO loss from the $\text{M}(\text{CO})_4(\eta^2\text{-alkyne})$ complexes. For example, the compounds readily exchanged with ^{13}CO in solution (Eq. 2.1)^{2,3} and underwent carbonyl substitution reactions with phosphines (Eq. 2.2).⁷



$\text{M} = \text{Ru}, \text{Os}; \text{R} = \text{Me}, \text{Ph}.$

In the case of osmium in particular, the facility of CO dissociation at relatively low temperatures (*ca.* 0°C) contrasts with $\text{Os}(\text{CO})_5$ and related $\text{Os}(\text{CO})_4(\eta^2\text{-alkene})$ compounds which generally require more robust thermal activation to accomplish the same result. Iron pentacarbonyl and tetracarbonyliron(olefin) species are also relatively unreactive towards thermal carbonyl substitution, and it was thus

clearly of interest to complete the triad of $M(\text{CO})_4(\eta^2\text{-alkyne})$ compounds to discover if the incorporation of an alkyne would have a similar labilizing effect on iron carbonyl bonds.

The only obstacle remaining was that preliminary work carried out almost a decade ago⁸ on synthesizing the iron member of the $M(\text{CO})_4(\eta^2\text{-HFB})$ (HFB = $\text{C}_2(\text{CF}_3)_2$) series of compounds suggested that a conventional synthesis *via* low temperature photolysis of $\text{Fe}(\text{CO})_5$ was fraught with difficulties. Under similar conditions employed in the preparation of the Ru and Os congeners, only a small amount of $\text{Fe}(\text{CO})_4(\eta^2\text{-HFB})$ was isolated from a large quantity of intractable byproduct after 0.75g $\text{Fe}(\text{CO})_5$ was irradiated in the presence of excess HFB for several days. Thus, it was our aim to revisit the low temperature photochemistry of $\text{Fe}(\text{CO})_5$ with alkynes to hopefully complete the triad of $M(\text{CO})_4(\eta^2\text{-alkyne})$ species. A preliminary account of this investigation has been published.⁹

2.2. Synthesis and Characterization of the Title Compounds

2.2.1. Synthesis of $\text{Fe}(\text{CO})_4(\eta^2\text{-alkyne})$ (1)

Low temperature photochemistry has emerged as an excellent technique for the preparation of $M(\text{CO})_4(\eta^2\text{-alkyne})$ compounds from photo-labile $M(\text{CO})_5$ ($M = \text{Ru}, \text{Os}$).^{2,3,6} The use of a green-glass filter ($\lambda \geq 370 \text{ nm}$) resulted in the activation of the metal pentacarbonyl starting material towards replacement of a single carbonyl by an alkyne without inducing additional CO loss in the desired $M(\text{CO})_4(\eta^2\text{-RC}\equiv\text{CR}')$ product. The reactions were conveniently conducted in pentane, which enabled solvent removal by bulb-to-bulb distillation at -78°C and the isolation of the volatile, thermally sensitive $M(\text{CO})_4(\eta^2\text{-alkyne})$ materials by sublimation onto a cold finger maintained at dry-ice temperature. As mentioned in the Introduction, an early attempt at producing $\text{Fe}(\text{CO})_4(\eta^2\text{-HFB})$ by this method resulted in isolation of a negligible quantity of the desired material from 0.75 g $\text{Fe}(\text{CO})_5$. However, as photochemical activation of iron pentacarbonyl was successful in the past,¹⁰ it seemed reasonable that it should be possible to prepare $\text{Fe}(\text{CO})_4(\eta^2\text{-alkyne})$ species in an analogous manner to the Ru and Os congeners.

Photochemistry is often quite sensitive to the concentration of reagents in solution, and consequently the first modification that was made was to reduce the scale of the reaction so that the concentration of $\text{Fe}(\text{CO})_5$ would be more comparable to that in the successful syntheses employing $\text{M}(\text{CO})_5$ ($\text{M} = \text{Ru}, \text{Os}$). HFB was chosen as the initial alkyne reactant as the corresponding Ru and Os complexes were the most thermally stable of the $\text{M}(\text{CO})_4(\eta^2\text{-RC}\equiv\text{CR}')$ series.³ Under these conditions, formation of the desired product was observed, but the reaction was still quite slow and required at least six hours of photolysis at -50°C to achieve *ca.* 50% conversion. Although encouraging, the synthesis was still not acceptable at this stage as it proved impractical to reduce the concentration $\text{Fe}(\text{CO})_5$ to sufficiently low levels to enable isolation of pure product. Even with prolonged reaction times, a mixture of $\text{Fe}(\text{CO})_5$ and $\text{Fe}(\text{CO})_4(\eta^2\text{-HFB})$ was obtained following sublimation. Thus, the primary hurdle at this stage was to discover a means of promoting greater photochemical efficiency.

Accordingly, the second modification was to make use of a uranium glass filter ($\lambda \geq 330 \text{ nm}$) which would allow irradiation with higher energy photons than the green-glass filter, while hopefully alleviating problems of secondary photoreaction which might be encountered with a harsher filter such as pyrex ($\lambda \geq 280 \text{ nm}$). Gratifyingly, the use of the uranium glass filter produced a significant improvement in the rate of photolysis of $\text{Fe}(\text{CO})_5$ without adversely influencing the stability of the desired product. Further fine-tuning of the quantity of $\text{Fe}(\text{CO})_5$ ultimately allowed for the production of $\text{Fe}(\text{CO})_4(\eta^2\text{-HFB})$ (**1a**) on a 0.25g scale in 84% yield.

The revised synthetic method was subsequently applied to a modest range of alkynes and resulted in the successful synthesis of $\text{Fe}(\text{CO})_4(\eta^2\text{-RC}\equiv\text{CR}')$ (**1a-e**) (Eq. 2.3) in moderate to good yields (Table 2-1). The quantity of $\text{Fe}(\text{CO})_5$ ranged from 120 to 225 mg in 115 mL of pentane, so that the concentration of $\text{Fe}(\text{CO})_5$ varied between 5 and 10 mM (Table 2-1). The thermal conditions of the photolysis were quite critical, especially in the synthesis of **1c**. Photolysis at -70°C gave isolated yields greater than 70%, whereas a rise of only 10°C dropped the yield to below 30% due to a competing thermal reaction of **1c** with excess acetylene (see Chapter 3).

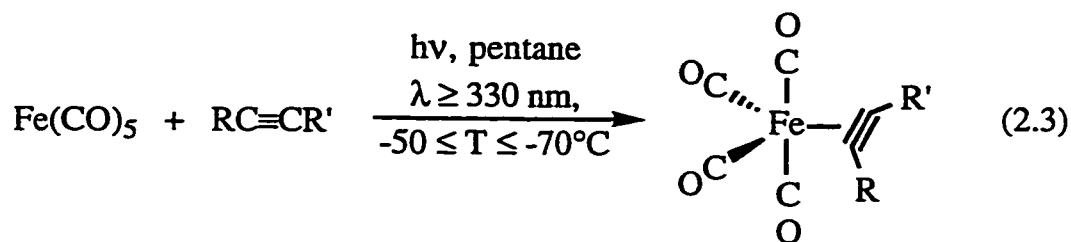


Table 2-1. Reaction Conditions and Product Yields in the Synthesis of **1a-e**.

Compound	R	R'	T (°C)	mass of Fe(CO) ₅ (mg)	[Fe(CO) ₅] (mM)	Yield (%)
1a	CF ₃	CF ₃	-50	119 ^a	5.3	84
1b	H	CF ₃	-70	119	5.3	65
1c	H	H	-70	179	7.9	75
1d	H	Me	-70	119 ^a	5.3	81
1e	Me	Me	-70	224	9.9	57

^adenotes the initial concentration (see Section 2.6.5).

Generally, the alkyne was present in excess to ensure as complete a reaction as possible. However, in the case of **1d**, it was found that if propyne was present in too large a concentration, the reaction was plagued by formation of a large quantity of black, tar-like residue which interfered with the sublimation of the organometallic product. In this instance, the gaseous alkyne was admitted in short bursts while the reaction was monitored carefully by IR spectroscopy to track the level of conversion of Fe(CO)₅ to **1d**. Regrettably, the "trial and error" nature of this procedure occasionally resulted in low product yield if too much propyne was added, but more often than not the synthesis was successful. In reactions employing hexafluorobut-2-yne, trifluoropropyne, acetylene, and but-2-yne, the reactions proceed smoothly provided the alkyne was present in excess; the exact quantity did not appear to be significant. An intractable brown/black residue remained following all reactions, the composition of which was not investigated further. Nonetheless, the residue must have been the product of secondary reaction between the organometallic product and alkyne since irradiation of pentane solutions of propyne or acetylene in the absence of

$\text{Fe}(\text{CO})_5$ did not produce any observable changes. Furthermore, the large quantity of the intractable residue relative to the quantity of $\text{Fe}(\text{CO})_5$ employed suggests that this process may be catalytic in nature; this is not particularly unexpected given the propensity of transition metal catalyzed polymerization and cyclization of alkynes.¹¹

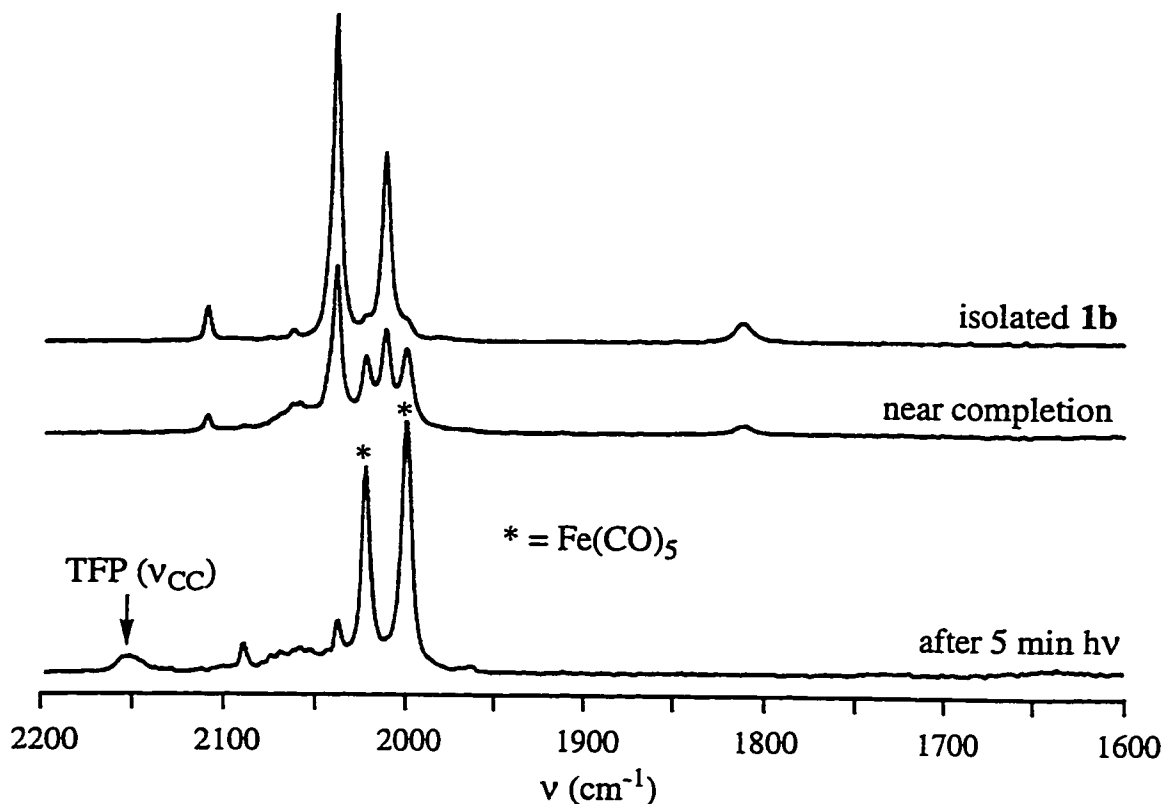


Figure 2-1. FT-IR Monitoring of the Photolysis of $\text{Fe}(\text{CO})_5$ and TFP in Pentane.

As in the syntheses of the $\text{Os}(\text{CO})_4(\eta^2\text{-alkyne})$ compounds, it was found that only the use of low boiling alkynes¹² would result in successful isolation of an $\text{Fe}(\text{CO})_4(\eta^2\text{-alkyne})$ product. For example, $\text{Fe}(\text{CO})_4(\eta^2\text{-C}_2\text{Et}_2)$ (**1f**) can be generated *in situ*, but cannot be isolated because of the high boiling point of hex-3-yne (81 - 82°C). Attempts at isolating **1f** ultimately met with failure as a viscous black oil was obtained following removal of the pentane solvent; in the final sublimation step, the oil refluxed off the cold finger of the sublimation probe without any separation of organometallic product from the excess alkyne. Thus,

synthetic applications of **1f** are limited to reactions that can occur in the presence of excess hex-3-yne (see Chapter 3 for an example).

The reactions were conveniently monitored by FT-IR spectroscopy in the carbonyl region (2200 - 1600 cm^{-1}) by the consumption of $\text{Fe}(\text{CO})_5$ at 2022 and 2000 cm^{-1} (Figure 2-1). The growth of the product was also monitored, but in the syntheses of **1b,c,e**, the spectrum was frequently complicated by the presence of other bands and lower intensity of the bands due to the product than anticipated. Figure 2-2 provides a comparison between the photolyses of $\text{Fe}(\text{CO})_5$ with HFB and TFP near the completion of a reaction employing identical initial amounts of $\text{Fe}(\text{CO})_5$. Note the apparently lower concentration of **1b** compared to **1a**. Although initially ominous, the reaction mixtures faithfully afforded good yields of the desired $\text{Fe}(\text{CO})_4(\eta^2\text{-alkyne})$ products following work-up, which suggested that a reaction was occurring between the excess alkyne and **1b,c,e** in the warm IR cell. This phenomenon has been observed before in the preparation of $\text{Os}(\text{CO})_4(\eta^2\text{-C}_2\text{Me}_2)$,⁶ and the consequence of this type of behavior for compounds **1** will be discussed in greater detail in Chapter 3.

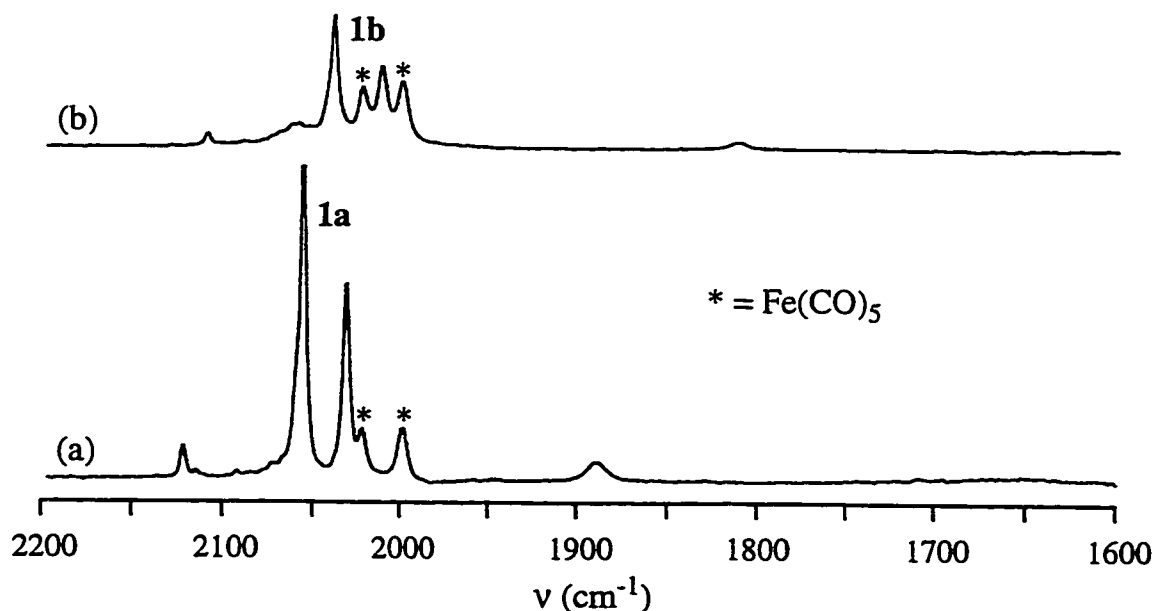


Figure 2-2. Comparison of the Photolyses of $\text{Fe}(\text{CO})_5$ with (a) HFB and (b) TFP.

The isolated materials are all volatile, off-white to pale yellow substances which are thermally sensitive to varying degrees. Although they form solid films at -78°C , upon warming they liquefy with decomposition. The stability order is **1a** (r.t.) > **1b** \approx **1c** (ca. 0°C) > **1d** \approx **1e** (ca. -20°C), with the indicated temperatures marking the point at which decomposition is observed in pentane solution. Clearly, the π -acidity of the alkyne has an important influence on the thermal stability of the complex; this contrast is most marked for **1a** and **1e** where the former bears electron withdrawing substituents and the latter contains an electron donating alkyne. Although no effort has been made to more accurately gauge the decomposition temperatures or melting points, from a synthetic standpoint **1a-e** are best handled as pentane solutions at -78°C . The most stable member of the series, **1a**, can be stored for months as such while **1b,c** will survive for a week at -78°C before being noticeably degraded. On the contrary, **1d,e** are not amenable to storage and are best used within several hours following isolation; even overnight storage in a -80°C freezer results in noticeable decomposition by morning. Furthermore, FT-IR spectra of **1d,e** must be recorded in a cell that has been pre-cooled with pentane at -78°C in order to avoid significant decomposition. An added difficulty is that the yield of product is not readily determined as weighing is essentially impossible; **1a** can be quickly weighed as an oil under an inert atmosphere but some decomposition is inevitable. Thus, the concentration of **1a-e** in pentane solution was determined by titration with $\text{Cp}^*\text{Rh}(\text{CO})_2$ (see Chapters 5, 6, and 7).

In qualitative terms, the thermal stabilities of **1a-e** are more comparable with the heavier Os congeners than with the second row Ru analogs. The latter compounds are very unstable and successful isolation of $\text{Ru}(\text{CO})_4(\eta^2\text{-RC}\equiv\text{CR}')$ is generally only possible when R or R' is an electron withdrawing CF_3 group;^{3,4} $\text{Ru}(\text{CO})_4(\eta^2\text{-C}_2\text{H}_2)$ can be prepared, but decomposes spontaneously above -30°C .² By comparison, $\text{Os}(\text{CO})_4(\eta^2\text{-C}_2\text{H}_2)$ and **1c** degrade only near 0°C . Further comparisons within the triad of available $\text{M}(\text{CO})_4(\eta^2\text{-alkyne})$ compounds will be discussed in Section 2.4.

2.2.2. ^{13}CO Exchange and Evidence of Further Reactivity of **1** Towards CO

Following the successful synthesis of the $\text{Fe}(\text{CO})_4(\eta^2\text{-alkyne})$ complexes, it was immediately of interest to investigate whether or not the carbonyl ligands were labile as in the Ru and Os analogs. The most thermally stable members of the Fe series, **1a-c**, rapidly incorporate the isotopic label when placed under an atmosphere of ^{13}CO (Eq. 2.1). Interestingly, the exchange reactions occur at significantly lower temperatures than were observed for the heavier members of the triad. For example, $^{12}/^{13}\text{CO}$ exchange is complete in **1a,c** after several hours at *ca.* -20°C while the corresponding reaction takes place at 0°C in the Os analogs. In fact, ^{13}CO incorporation was even observed in samples which were exposed to a ^{13}CO atmosphere then stored overnight at -80°C ! Qualitatively, these results imply that the carbonyl ligands in **1** are even more labile than their Ru and Os counterparts, which is fascinating when one considers that the CO ligands in $\text{Fe}(\text{CO})_5$ are less labile than in $\text{Os}(\text{CO})_5$.¹³ A full discussion of the implications of this result and quantification of the rates of carbonyl loss is presented in Chapter 4.

However, an important difference between **1** and $\text{Os}(\text{CO})_4(\eta^2\text{-alkyne})$ compounds quickly emerged. While a CO atmosphere was found to stabilize the osmium compounds, preventing decomposition *via* CO loss,² the Fe complexes underwent competing reactions with carbon monoxide to form yellow products with greatly different physical and spectroscopic properties from those of **1**. In the case of **1a**, this process was relatively slow and only became apparent at ambient temperature, but for **1b-e**, these reactions occurred at much lower temperatures. By exercising care, ^{13}CO enriched **1b,c** could be prepared, providing the reaction temperatures did not exceed -10 and -20°C , respectively. However, $^{12}/^{13}\text{CO}$ exchange in the more thermally unstable **1d,e** was more difficult to achieve as the formation of the yellow byproducts dominated these reactions. Ultimately, ^{13}CO enriched **1d** could be prepared in low yield, but **1e** could only be enriched with relatively low levels of ^{13}CO . The nature of the products of the unexpected, but ultimately very interesting, reaction of **1a-e** with CO will be discussed in detail in the following Chapter.

2.2.3. Characterization of $\text{Fe}(\text{CO})_4(\eta^2\text{-alkyne})$ Compounds (1a-e)

Unfortunately, the low thermal stabilities and melting points of the compounds made elemental analysis and mass spectrometry all but useless in confirming the molecular compositions of 1a-e. The reason for the former is obvious given that the compounds all decompose upon warming to ambient temperature, but the difficulty in obtaining satisfactory mass spectra only serves to underline the challenge of working with thermally sensitive species. Attempts were made to obtain electron impact mass spectra by cooling a Schlenk tube containing either 1a or 1c to liquid nitrogen temperature and connecting the tube directly to the inlet of the mass spectrometer. The ionization voltage was 70 eV and scans were made continuously after the cold bath was removed. In the case of the more stable 1a, the parent molecular ion was not detected and the highest m/z fragment corresponded to $\text{Fe}(\text{CO})_2(\text{HFB})^+$. Series of ions were detected for $\text{M}^+ - n \text{CO} - m \text{F}$ ($n = 2 - 4$, $m = 0, 1$) and $\text{M}^+ - \text{HFB} - n \text{CO}$; ($n = 0 - 3$). The free HFB ligand was also detected and the base peak corresponded to $\text{HFB}^+ - 2 \text{F}$. The solid Ru and Os analogs displayed similar series of ligand loss, but the molecular ion was detected in both cases.³ The current lack of a low energy ionization source in the MS laboratories may have contributed to the absence of a detectable molecular ion peak in 1a.

For the less stable but more volatile 1c, a very weak molecular ion was detected with an intensity 2.4% of the base peak ($\text{Fe}(\text{CO})^+$) along with the series $\text{M}^+ - n \text{CO}$ ($n = 1 - 4$) for the subsequent loss of four carbonyl ligands. Peaks were also detected for $\text{M}^+ - \text{C}_2\text{H}_2 - n \text{CO}$ ($n = 0 - 4$) from initial loss of the acetylene ligand, but more troubling was the presence of a clear peak at $m/z = 196$ for $\text{Fe}(\text{CO})_5^+$ at 25.6% relative abundance. One possible explanation is that once the acetylene ligand is lost from the iron center, any carbon monoxide present in the mass spectrometer stream was readily scavenged, leading to $\text{Fe}(\text{CO})_5^+$. However, as peaks corresponding to much greater m/z values than the parent ion were also detected in appreciable quantities, it seems reasonable to suggest that thermal decomposition was also occurring in the inlet stream, possibly leading directly to the production of $\text{Fe}(\text{CO})_5^+$ from the unidentified products of thermal decomposition. The level of thermal decomposition was

reinforced by the observation of a dark brown film in the inlet tubing and at the probe tip following the run. Apart from the above difficulties in dealing with the volatile, thermally sensitive $\text{Fe}(\text{CO})_4(\eta^2\text{-alkyne})$ compounds in pure form, the remainder of the spectroscopic characterization of the complexes proved relatively straightforward providing that care was exercised in preparing the relevant samples at low temperature.

The IR spectra (Figure 2-3, Table 2-2) showed three terminal carbonyl stretches in a weak/strong/medium intensity pattern for each compound.

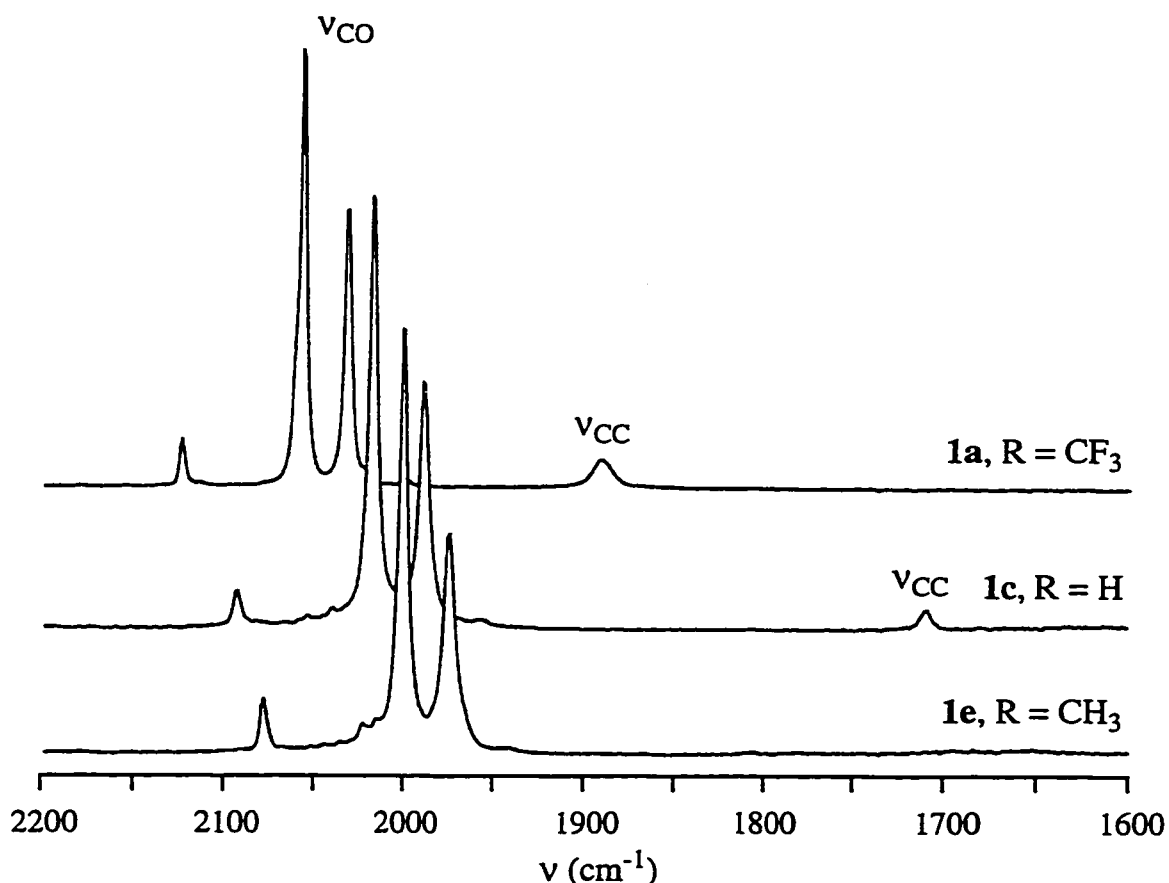


Figure 2-3. Representative FT-IR Spectra (pentane) for **1a,c,e**.

Since four carbonyl stretches are expected, two are overlapping, most likely at the most intense absorption. Similar observations have been made for certain $\text{M}(\text{CO})_4(\eta^2\text{-alkyne})$ species ($\text{M} = \text{Ru}, \text{Os}$).^{4,6} Most telling is the observation of a weak band at high frequency corresponding to the symmetrical stretch of the

mutually *trans* axial carbonyls. Indeed, it is this feature which confirms the proposed trigonal-bipyramidal structure in which the alkyne occupies an in-plane equatorial position, as has been observed in the solid-state structures of $\text{Os}(\text{CO})_4(\eta^2\text{-C}_2(\text{SiMe}_3)_2)^1$ and $\text{M}(\text{CO})_4(\eta^2\text{-HFB})$ ($\text{M} = \text{Ru}, \text{Os}$).¹⁴ In addition to the carbonyl stretches, a weak band was observed to lower frequency in **1a-d**; this band did not shift upon ^{13}C O enrichment and thus is attributed to the alkyne carbon-carbon stretch. The ν_{CC} stretch was not observed **1e** and was also absent in the IR spectrum of $\text{Os}(\text{CO})_4(\eta^2\text{-C}_2\text{Me}_2)$.⁶

Table 2-2. FT-IR Spectra (pentane, cm^{-1}) of **1a-e**.

Compound	R	R'	ν_{CO}	ν_{CC}
1a	CF ₃	CF ₃	2125(w), 2058(s), 2033(m)	1890 (w)
1b	H	CF ₃	2111(w), 2040(s), 2013(m)	1812(vw)
1c	H	H	2094(w), 2018(s), 1989(m)	1709(vw)
1d	H	Me	2086(w), 2009(s), 1981(m)	1873(vw)
1e	Me	Me	2079(w), 2001(s), 1975(m)	–

The ^1H and ^{19}F NMR spectra (Table 2-3) displayed the anticipated pattern of signals for the alkyne substituents. Singlets were observed for **1a,c,e** in accord with the C_{2v} geometry of the compound, while the unsymmetrical $\text{HC}\equiv\text{CR}$ ($\text{R} = \text{CF}_3, \text{Me}$) in **1b,d** afforded a more complicated signal pattern. A doublet was observed for the downfield (δ 6.46) *CH* proton in **1b** with a corresponding quartet in the ^{19}F NMR for the CF_3 group; both shared a common $^4J_{\text{HF}}$ coupling constant of 2.7 Hz which compares with the values observed in $\text{M}(\text{CO})_4(\eta^2\text{-TFP})$ ($\text{M} = \text{Ru}, 2.9 \text{ Hz}^4; \text{Os}, 1.8 \text{ Hz}^8; \text{TFP} = \text{trifluoropropyne}$). The ^1H NMR of **1d** consisted of a doublet (δ 4.21) and quartet (δ 2.47) in a 1:3 ratio, and the $^4J_{\text{HH}}$ coupling constant of 2.6 Hz is similar to the 2 Hz value in $\text{Os}(\text{CO})_4(\eta^2\text{-HC}\equiv\text{CMe})$.⁸ The downfield shift of the *CH* protons relative to the free alkyne in the ^1H NMR of **1c,d** is in accord with rehybridization of the alkyne carbon from sp to sp^2 upon coordination to the metal.

Table 2-3. ^1H and ^{19}F NMR Spectra (CD_2Cl_2) of **1a-e**.

Compound	R	R'	δ (^1H) (ppm) ^a	$^4J_{\text{HX}}$ (Hz)	δ (^{19}F) (ppm) ^a
1a^b	CF ₃	CF ₃	–	–	-56.10 (s)
1b^c	H	CF ₃	6.46 (d)	2.7	-54.06 (d)
1c^d	H	H	5.19 (s)	–	–
1d^d	H	CH ₃	4.21 (q), 2.47 (d)	2.6	–
1e^d	CH ₃	CH ₃	2.26 (s)	–	–

^aletter in parenthesis denotes multiplicity. ^bat -40°C. ^cat -60°C. ^dat -80°C.

The ^{13}C NMR spectra (Table 2-4) further corroborate the structural assignments. Four resonances were observed in the ^{13}C NMR of **1a**, with a pair of resonances for the alkyne carbons appearing in the upfield portion of the spectrum. The quartet at δ 121.35 ($^1J_{\text{CF}} = 267$ Hz) is characteristic of the CF₃ group while the AA'X₃X_{3'} pattern at δ 88.51 (qq, $^2J_{\text{CF}} = 50$ Hz, $^3J_{\text{CF}} = 6$ Hz) corresponds to the quaternary carbons; both appeared as singlets in the ^{19}F -decoupled spectrum. The magnitude of the carbon-fluorine coupling constants is identical to that in the previously characterized $\text{M}(\text{CO})_4(\eta^2\text{-HFB})$ ($\text{M} = \text{Ru}, \text{Os}$) complexes.³ The downfield pair of equal intensity singlets (δ 205.77, 199.20) correspond to the carbonyl ligands (*c.f.* δ 210 ppm in $\text{Fe}(\text{CO})_5$).¹⁵ In the ^{13}CO enriched material, both were pseudo-triplets ($^2J_{\text{CC}} = 10$ Hz) due to coupling to an equivalent pair of neighboring nuclei, thus confirming the presence of four terminal carbonyl ligands in axial and equatorial pairs.

Although further assignment is somewhat ambiguous in the current case, the carbonyl resonance to lowest field in $\text{M}(\text{CO})_4(\eta^2\text{-HFB})$ ($\text{M} = \text{Ru}, \text{Os}$) was broadened by unresolved coupling to fluorine in the CF₃ groups and was thus assigned to the equatorial carbonyls.³ In line with these expectations, the C_s symmetric **1b** displayed a 1:1:2 pattern for two inequivalent equatorial and a pair of equivalent axial carbonyls. As with **1a**, all signals were pseudo triplets ($^2J_{\text{CeqCax}} = 10$ Hz) in the ^{13}CO enriched material, suggesting that the $^2J_{\text{CeqCeq}}$ coupling constant was too small to be detected. After extended acquisition, resonances for the CH and CCF₃ carbons were detected at δ 82.65 (q, $^3J_{\text{CF}} = 7$

Hz) and 74.96 (q, $^2J_{CF} = 49$ Hz) ppm; the magnitude of $^{2,3}J_{CF}$ is essentially identical to that in the Ru⁴ and Os⁸ analogs. In the $^{13}\text{C}\{^{19}\text{F}\}$ spectrum, both resonances appeared as doublets as a result of coupling to the CH proton. The downfield CH signal had a large $^1J_{CH}$ coupling constant of 237 Hz while the upfield CCF₃ signal showed smaller $^2J_{CH}$ coupling of 22 Hz.

Table 2-4. $^{13}\text{C}\{^1\text{H}\}$ NMR Spectra (CD₂Cl₂, ppm) of **1a-e**.

	R	R'	$\delta \text{CO}_{\text{eq}}$	$\delta \text{CO}_{\text{ax}}$	δCR	$\delta \text{CR}'$	δCX_3
1a^a	CF ₃	CF ₃	205.77	199.20	88.51 ^b		121.35 ^c
1b^d	H	CF ₃	209.78 ^e , 208.62 ^e	203.02 ^f	82.65 ^g	74.96 ^h	122.00 ⁱ
1c^j	H	H	213.3 ^k	208.1 ^k	62.81		–
1d^l	H	CH ₃	212.06		48.75	71.86	14.09
1e^l	CH ₃	CH ₃	213.21		57.96		13.46

^arecorded at -40°C. ^bquartet of quartets, $^2J_{CF} = 50$ Hz, $^3J_{CF} = 6$ Hz. ^cquartet, $^1J_{CF} = 267$ Hz. ^dat -60°C. ^eintensity one. ^fintensity two. ^gquartet, $^3J_{CF} = 7$ Hz. ^hquartet, $^2J_{CF} = 49$ Hz. ⁱquartet, $^1J_{CF} = 264$ Hz. ^jat -115°C. ^kbroad. ^lat -80°C.

At -115°C, Fe(CO)₄(η^2 -C₂H₂) (**1c**) displayed a single resonance for the equivalent CH carbons at δ 62.81, while the carbonyl ligands appeared as a pair broadened singlets at δ 213.3 and 208.1; at -40°C, the carbonyl ligands presented one sharp coalesced singlet at δ 210.97 in accord with rapid intramolecular carbonyl exchange (*vide infra*). Similarly, the averaged CO resonance was detected at δ 213.21 in **1e** while CMe signal was found upfield at δ 57.96 ppm. The characterization of the propyne complex **1d**, as with **1b** discussed above, is more complex due to the asymmetry of the alkyne. Four singlets were observed in the $^{13}\text{C}\{^1\text{H}\}$ NMR spectrum at δ 212.06, 71.86, 48.75, and 14.09 ppm, the furthest downfield of which is due to the averaged carbonyl ligands. The furthest upfield signal can be confidently assigned to the carbon of the methyl group on the basis of chemical shift. In order to assign the remaining two resonances, an APT{¹H} ^{13}C NMR spectrum was obtained (Figure 2-4).

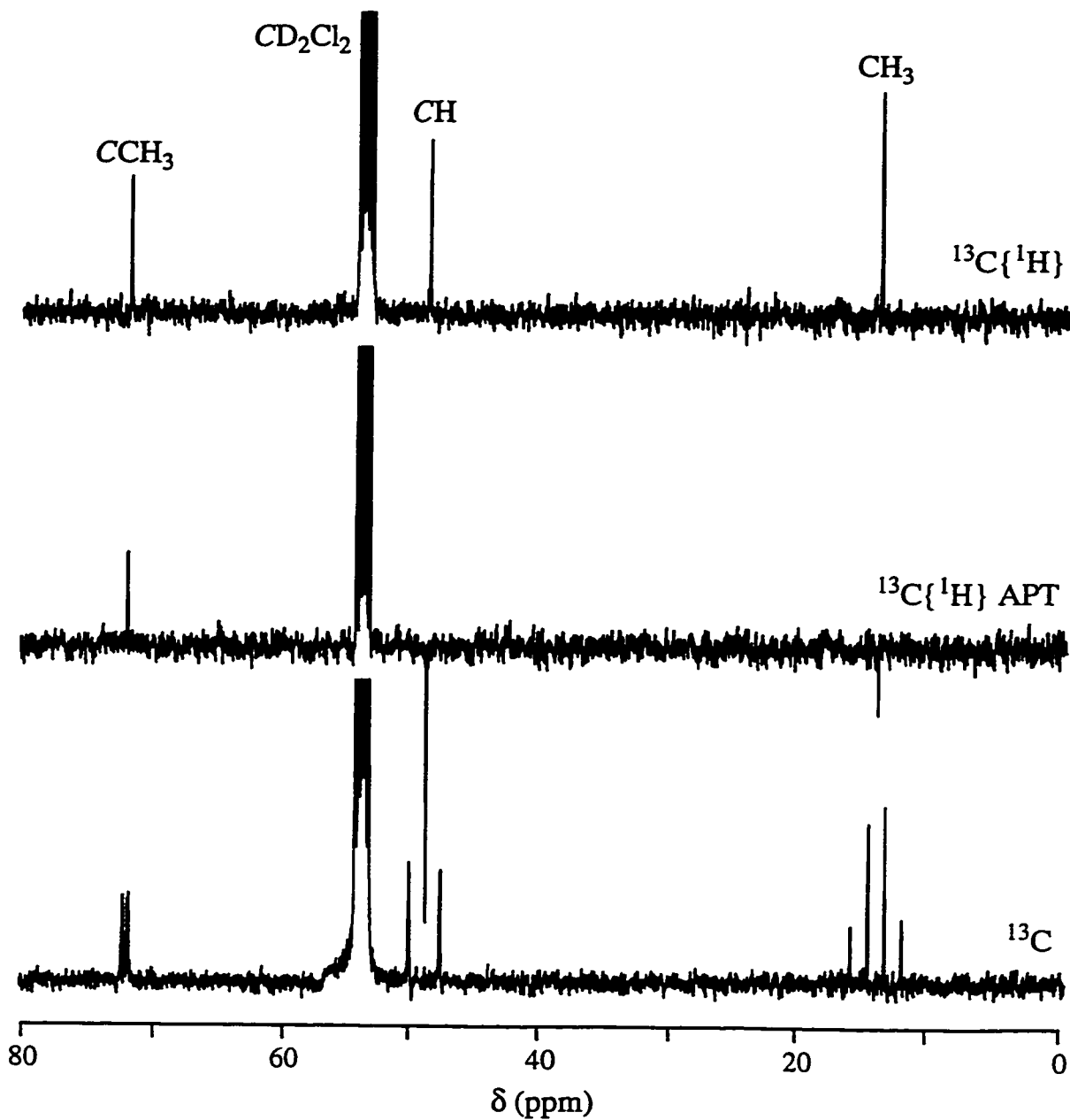


Figure 2-4. 100.6 MHz $^{13}\text{C}\{^1\text{H}\}$, APT and ^{13}C NMR Spectra of **1d** at -80°C .

The APT spectrum clearly demonstrated that the resonance at δ 71.86 had the same phase as the solvent (CD_2Cl_2) peak, and was thus due to the quaternary carbon, while the signal at δ 48.75 had the opposite phase and consequently was the CH resonance; the signal at δ 14.09 for the methyl group also had a phase opposite to CD_2Cl_2 as expected. Confirmation of the APT experiment was

obtained *via* the proton-coupled ^{13}C NMR spectrum in which both signals appeared as doublets of quartets. The downfield CMe resonance had coupling constants of $^2J_{\text{C}(\text{CH})} = 34$ Hz and $^2J_{\text{C}(\text{CH}_3)} = 9$ Hz, respectively, while the upfield CH signal had values of $^1J_{\text{CH}} = 242$ Hz and $^3J_{\text{C}(\text{CH}_3)} = 4$ Hz. The distinguishing feature between the two resonances is the much larger magnitude of the $^1J_{\text{CH}}$ coupling constant at the CH signal, which further confirms the assignment of the δ 48.75 resonance as belonging to the CH carbon.

2.3. A Comparison of the Spectroscopic Properties of 1a-e

2.3.1. FT-IR Spectra

In comparing the physical characteristics of the $\text{Fe}(\text{CO})_4(\eta^2\text{-alkyne})$ compounds, a correlation was noted between the π -acidity of the alkyne ligand and the thermal stability of the complex. Predictably, correlations have also been observed between various spectroscopic characteristics and the π -acidity of the coordinated alkyne. For instance, referring to Figure 2-3 and Table 2-2, it is clear that as the substituents of the alkyne progress from electron withdrawing (CF_3) to electron donating (Me), the carbonyl stretches shift to lower frequency by *ca.* 50 cm^{-1} when comparing the extremes of **1a** and **1e**. This observation is in accord with the well-known synergic model for bonding of carbonyl ligands;¹⁶ that is, the more π -acidic the alkyne, the greater is the competition for metal electron density, and thus the higher is the ν_{CO} stretching frequency. Interestingly, comparable $\text{Fe}(\text{CO})_4(\eta^2\text{-olefin})$ compounds display similar IR frequencies to **1a-e**; for example, the IR bands of a series of fluoro-olefin complexes are within 10 cm^{-1} of those of **1a**,¹⁷ and $\text{Fe}(\text{CO})_4(\eta^2\text{-C}_2\text{H}_4)$ (2088, 2013, 2007, 1986 cm^{-1} in heptane)¹⁸ shows an even closer correlation to the band positions of the acetylene complex **1c**. The closeness of the carbonyl stretching frequencies suggests that similarly substituted olefins and alkynes have comparable π -acidities when coordinated to an $\text{Fe}(\text{CO})_4$ fragment, which renders the CO lability in **1a-e** even more remarkable.

At a cursory glance, there does not appear to be a readily definable trend between either the ν_{CC} (Table 2-2) or δ CR (Table 2-4) parameters. However, it is well established¹ that a proper comparison may only be drawn after considering

the coordination shift (Δ) which compares the pertinent frequency or chemical shift of the free alkyne to that of the coordinated ligand in the complex (Tables 2-5 and 2-6).

Table 2-5. FT-IR Alkyne Coordination Shifts ($\Delta(\nu_{\text{C-C}})$, cm^{-1}) in **1a-d**.

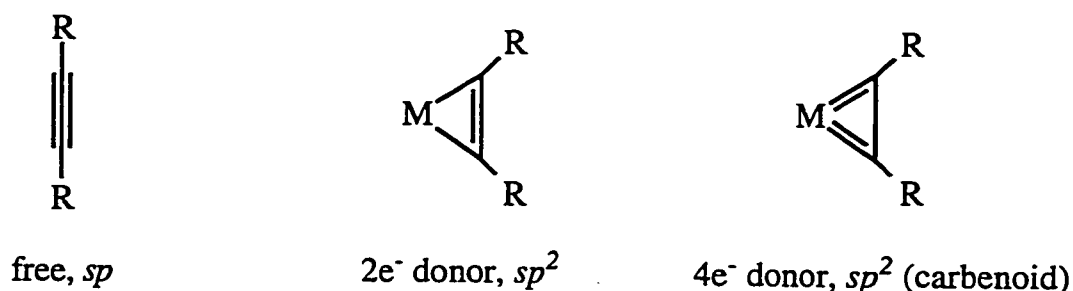
Compound	R	R'	$\nu_{\text{C-C}}(\text{free})$	$\nu_{\text{C-C}}(\text{complex})$	$\Delta(\nu_{\text{C-C}})^{\text{a}}$
1a	CF ₃	CF ₃	2300 ¹⁹	1890	410
1b	H	CF ₃	2165 ¹⁹	1812	353
1c	H	H	1974 ²⁰	1709	265
1d	H	Me	2142 ²¹	1873	269

$$^{\text{a}}\Delta(\nu_{\text{C-C}}) = \nu_{\text{C-C}}(\text{free}) - \nu_{\text{C-C}}(\text{complex})$$

Not surprisingly, the carbon-carbon stretching frequency decreases upon coordination to the metal center as a result of the reduction in the carbon-carbon bond order as per the Dewar-Duncanson-Chatt model for metal-alkyne bonding (Scheme 1-2). The perfluorinated hexafluorobut-2-yne ligand in **1a** shows the greatest coordination shift as a consequence of greater π -back donation from the metal, and thus may be considered to achieve the metallacyclopropene extreme of M-alkyne bonding (Scheme 1-3). The value of $\Delta(\nu_{\text{C-C}})$ decreases steadily as the electron-withdrawing CF₃ groups are replaced by one and two protons in **1b** and **1c**, respectively, as the alkyne becomes more electron rich and the complex drifts away from a metallacyclopropene bonding description. However, a slight reversal in the trend occurs at the propyne complex; the substitution of a methyl group for a proton in **1c** would be expected to further reduce the π -acidity of the alkyne, yet **1d** shows a slightly larger coordination shift than **1c**. This reinforces the synergic nature of the metal-alkyne bonding interaction and suggests that the reduction in π -acidity is off-set by an increase in the forward donation of electron density from propyne to Fe ($\pi_{\parallel} \rightarrow M_{\sigma}$ in Scheme 1-2a). A similar reversal in $\Delta(\nu_{\text{C-C}})$ is observed between Os(CO)₄(η^2 -C₂H₂) and Os(CO)₄(η^2 -HC≡CMe) (*vide infra*).

2.3.2. ^{13}C NMR Coordination Shifts

Templeton has described an analogous correlation to $\Delta(\nu_{\text{C-C}})$ that relates the ^{13}C NMR chemical shift of the alkyne carbons (C_{alk}) to the number of electrons formally donated.²² Mo and W compounds were studied with a variety of alkynes including HFB, acetylene, propyne and but-2-yne. The triply-bonded carbons in free alkynes tend to resonate upfield of alkenes owing to anisotropic effects;²³ thus, a downfield shift is commonly observed as the carbons rehybridize upon coordination to the metal center.²⁴



Scheme 2-1. Valence Bond Description of the Rehybridization of Triply-Bonded Carbons in Two- and Four-Electron Donor Alkynes.

Two electron donor alkyne carbons were typically found in the region between δ 98 and 126 ppm while four electron donation resulted in a dramatic downfield shift.²⁵ For example, the CH carbons resonate at δ 106 and 98 ppm in $\text{CpW}(\text{CO})(\text{NO})(\eta^2\text{-C}_2\text{H}_2)$, corresponding to coordination shifts of -34 and -26 ppm, respectively, for the two-electron alkyne ligand. On the other hand, the four electron alkyne in $\text{CpW}(\text{CO})(\text{Me})(\eta^2\text{-C}_2\text{H}_2)$ takes on metal-carbon double bond (carbenoid) character and the CH carbons are found far downfield at δ 192 and 187, $\Delta(\delta_{C_{\text{alk}}}) = -120, -115$ ppm. The coordination shifts in compounds **1a-e** are listed in Table 2-6.

The fluorinated alkynes in **1a,b** largely conform to Templeton's predictions. Coordination of the alkyne causes a downfield shift, and the larger shift for the HFB ligand reflects its greater π -acidity compared with TFP. However, it should be noted that the alkyne carbons in each fall outside the range mentioned above for the Mo and W species and are shifted towards the upfield end of the

spectrum. Furthermore, the more electron rich alkynes (C_2H_2 , $HCCMe$, and C_2Me_2) display a *positive* coordination shift; that is, the alkyne carbons are found further upfield in **1c-e** than in the free ligand. A similar observation was made for $Os(CO)_4(\eta^2-C_2Me_2)$, and it was suggested that this could be a reflection of the $4e^-$ destabilization between the metal-based d -orbitals and the π -set on the alkyne oriented perpendicular to the plane of coordination (π_{\perp} in Scheme 1-5).⁶ This suggestion makes intuitive sense if one considers that the " $4e^-$ destabilization", *i.e.* the projection of metal-based d electrons into the region of space occupied by the alkyne ligand, would manifest itself in shielding effects in the ^{13}C NMR which could outweigh expected rehybridization effects. Thus, in the absence of $4e^-$ destabilization, a more negative $\Delta(\delta_{C_{alk}})$ value would be expected for **1a,b**.

Table 2-6. ^{13}C NMR Alkyne Coordination Shifts ($\Delta(\delta_{C_{alk}})$, ppm) in **1a-e**.

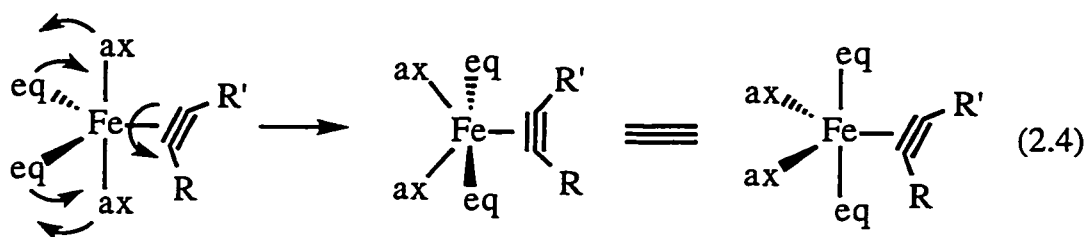
Compound	R	R'	$\delta_{C_{alk}(free)}$	$\delta_{C_{alk}(complex)}$	$\Delta(\delta_{C_{alk}})^a$
1a	CF ₃	CF ₃	71.4 ²⁶	88.5	-17.1
1b	H	CF ₃	75.9, 69.2 ⁸	82.7, 75.0	-6.8, -5.8
1c	H	H	71.9 ⁸	62.8	+9.1
1d	H	Me	67.2, 80.2 ⁸	48.8, 71.9	+18.4, +8.3
1e	Me	Me	74.6 ⁶	58.0	+16.6

$$^a\Delta(\delta_{C_{alk}}) = \delta_{C_{alk}(free)} - \delta_{C_{alk}(complex)}$$

Another observation of note is that the value of the $^1J_{CH}$ coupling constant in **1d** (242 Hz) is only 6 Hz smaller than that in free propyne (248 Hz), but 22 Hz greater than that found in cyclopropene (220 Hz).²⁷ This suggests that the compounds containing electron rich alkynes should not be described as true metallacyclopropenes, but still indicates some rehybridization of the alkyne carbon from sp towards sp^2 upon coordination to the $Fe(CO)_4$ fragment because $^1J_{CH}$ is directly related to the proportion of s -character in the C–H bond.²⁵

2.3.3. Carbonyl Scrambling in 1a-e

Transition metal species with trigonal bipyramidal structures, such as $\text{Fe}(\text{CO})_5$ and its derivatives, often display remarkably facile carbonyl scrambling in solution. Indeed, $\text{Fe}(\text{CO})_5$ displays a sharp singlet in its ^{13}C NMR spectrum down to -170°C .²⁸ Thus, it is not surprising that **1a-e** all display carbonyl fluxionality to differing extents; the dynamic behaviour manifests itself in the ^{13}C NMR spectrum by the averaging of the distinct carbonyl ligands either observed (**1a-c**) or anticipated (**1d,e**) in the ground state structure. Following from detailed investigations conducted on a series of $\text{Fe}(\text{CO})_4(\eta^2\text{-olefin})$ complexes^{29,30} and a corresponding investigation of the triad of $\text{M}(\text{CO})_4(\eta^2\text{-C}_2(\text{SiMe}_3)_2)$ ($\text{M} = \text{Fe}, \text{Ru}, \text{Os}$) compounds,¹ the most likely mechanism is a coupled alkyne-Berry pseudo-rotation (BPR) (Eq. 2.4).



The key feature of the above mechanism is that the exchange of axial and equatorial carbonyl ligands is accompanied by a rotation of the alkyne ligand. Rapid rotation of the alkyne in the absence of the BPR would result in a 1:1 pattern of resonances in **1c-e** rather than the single resonance observed at the fast exchange limit.

As with the physical and spectroscopic features of **1a-e** discussed above, the fluxional behavior of the compounds is dependent upon the π -acidity of the alkyne ligand. For instance, while **1a** is rigid on the NMR time scale below 0°C , at ambient temperature the carbonyl resonances are noticeably broader, and their pseudo-triplet splitting pattern is no longer resolved. Unfortunately, the moderate thermal instability of **1a** at ambient temperature precluded a determination of activation parameters, but qualitatively it is apparent that the carbonyl ligands are just entering into measurable exchange at ambient temperature. Conversely, the

signals for **1b** begin to broaden above -40°C but thermal decomposition above *ca.* 0°C prevents achieving coalescence. In stark contrast to the fluorinated alkyne complexes, **1c** displayed two broad resonances of equal intensity only when cooled to just above the freezing point (-115°C) of its solution in CD_2Cl_2 . The two signals coalesced at -100°C , which corresponds to $\Delta G^{\ddagger}_{173} = 32 \pm 2$ kJ/mol from the two site exchange approximation.³¹ Compounds **1d,e** displayed sharp singlets at -80°C , corresponding to the fast exchange limit for carbonyl fluxionality; limiting spectra could not be achieved down to -110°C due to the facility of the axial/equatorial carbonyl exchange in these electron rich alkyne complexes.

Thus, a clear qualitative trend has emerged - the more π -acidic the alkyne, the higher is the energy barrier to intramolecular carbonyl exchange. The trend may be rationalized by considering that the exchange mechanism presented in Eq. 2.4 is accompanied by a 90° rotation of the alkyne as the carbonyl ligands shift positions. The rotation of the alkyne in this manner requires that the $d\pi/\pi_{||}^*$ overlap (Scheme 1-2b) be broken, and clearly the stronger the back-bonding component, the less readily the rotation can be achieved. Thus, as the π -accepting characteristics of the alkyne decrease from HFB through to but-2-yne, the alkyne will rotate more freely and the carbonyl ligands will exchange more readily. It should be noted that the $\pi_{||} \rightarrow M\sigma$ donation component is not affected by rotation of the alkyne as the orbitals involved have cylindrical symmetry.²⁹ The trend is also in full agreement with observations reported for a wide range of $\text{Fe}(\text{CO})_4(\eta^2\text{-olefin})$ complexes wherein the activation barrier to carbonyl exchange was found to increase with increasing π -acceptor ability of the olefin ligand.^{29,30}

2.4. A Triad Comparison of $\text{M}(\text{CO})_4(\eta^2\text{-alkyne})$ Compounds

Transition-metal complexes have perhaps the most diverse bonding and reactivity patterns of any group in the periodic table, and a necessary consequence of this myriad of traits is that their properties are often influenced by a series of subtle and competing factors. It has long been recognized that comparisons of the metal-dependent properties of a triad of homologous

compounds serve as one of the best methods of interpreting the hierarchy of factors which determine the structures and reactivities of the complexes. While a previous publication¹ established a framework for the elucidation of the important properties which influence metal-alkyne bonding in $M(\text{CO})_4(\eta^2\text{-C}_2(\text{SiMe}_3)_2)$ ($M = \text{Fe, Ru, Os}$), the synthesis of **1a-e** has completed a triad of compounds which also differ in the electronic characteristics of the coordinated alkyne. A brief discussion of the influence that the different metals of the group 8 triad have on the physical and spectroscopic features of this new series of $M(\text{CO})_4(\eta^2\text{-alkyne})$ complexes is thus warranted.

For any of the alkynes studied here, the thermal stabilities of the compounds qualitatively follow the general trend $\text{Os} > \text{Fe} \gg \text{Ru}$ with the exception of the strongly π -acidic HFB ligand where the order is $\text{Os} > \text{Ru} > \text{Fe}$. The implication, nonetheless, is that **1a-e** are generally similar to their third row congeners while the 2nd row Ru species are far less robust. However, the thermal decomposition of the compounds tends to follow complicated routes, and a clear rationale for the above trend is not immediately obvious. Yet, it should be noted that a similar trend exists for the triad of $M(\text{CO})_4(\eta^2\text{-olefin})$ compounds where, in particular, the Os derivatives are stable at ambient temperature while the Ru congeners can be employed as $\text{Ru}(\text{CO})_4$ transfer reagents owing to the facility of alkene dissociation.³² Furthermore, $\text{Fe}(\text{CO})_5$ is the least reactive of the metal pentacarbonyls followed by $\text{Os}(\text{CO})_5$, while $\text{Ru}(\text{CO})_5$ can only exist in the presence of a protective CO atmosphere. In this sense, the similar thermal stabilities of **1a-e** with respect to their Os congeners is perhaps not unexpected.

A comparison of the frequencies of the terminal carbonyl bands in the FT-IR produces a curious result (Table 2-7). In general, the bands lie to lower frequency for the Fe complexes than either the Os or Ru compounds; this is particularly evident in the high frequency band attributed to the symmetrical stretching of the axial carbonyls. In a qualitative sense, this suggests that Fe has slightly greater back-bonding interactions with its attendant carbonyl ligands than do its Ru or Os counterparts. There are two possible ways the alkyne ligand could contribute to this outcome. One possibility is that the alkyne donates proportionally greater electron density to the Fe center, thus emphasizing

interaction (a) in Scheme 1-2, and produces an excess of electron density at the metal center which is relieved by enhanced back-bonding to the carbonyl ligands. On the other hand, it is equally possible that the alkynes rely more heavily on back-bonding with the Ru and Os centers, and thus compete with the carbonyl ligands for the available metal electron density.

Table 2-7. FT-IR in the Carbonyl Region of $M(\text{CO})_4(\eta^2\text{-RC}\equiv\text{CR}')$ Species.

M	R	R'	ν_{CO} (cm^{-1})
Fe	CF ₃	CF ₃	2125(w), 2058(s), 2033(m)
Ru ³	CF ₃	CF ₃	2143(w), 2073(vs), 2042(s)
Os ³	CF ₃	CF ₃	2149(w), 2069(vs), 2061(s), 2029(s)
Fe	H	CF ₃	2111(w), 2040(s), 2013(m)
Ru ⁴	H	CF ₃	2131(vw), 2056(s), 2025(m)
Os ⁸	H	CF ₃	2136(w), 2054(s), 2047(m), 2013(s)
Fe	H	H	2094(w), 2018(s), 1989(m)
Ru ²	H	H	2115(w), 2036(s), 2028(m), 2002(s)
Os ²	H	H	2122(w), 2036(s), 2027(m), 1994(s)
Fe	H	Me	2086(w), 2009(s), 1981(m)
Os ⁸	H	Me	2113(w), 2028(s), 2021(m), 1990(s)
Fe	Me	Me	2079(w), 2001(s), 1975(m)
Os ⁶	Me	Me	2106(w), 2020(vs), 1988(m)

In the triad comparison of $M(\text{CO})_4(\eta^2\text{-C}_2(\text{SiMe}_3)_2)$ ($M = \text{Fe}, \text{Ru}, \text{Os}$),¹ a similar dilemma was noted. However, it was possible to distinguish between the two possibilities by focussing on a property that depends heavily on the back-donation component of the bonding interaction, the activation free energy for coupled alkyne rotation-carbonyl scrambling *via* BPR (Eq. 2.4). Although not rigorously examined for all cases, the activation free energy for the complete triad of $M(\text{CO})_4(\eta^2\text{-C}_2\text{H}_2)$ species is available (Table 2-8); the reported values for the ethylene analogs are provided for comparison.

Table 2-8. Comparison of Activation Free Energies (ΔG^\ddagger , kJ/mol) for Carbonyl Scrambling in $M(\text{CO})_4(\eta^2\text{-C}_2\text{H}_x)$ ($x = 2,4$).

M	$M(\text{CO})_4(\eta^2\text{-C}_2\text{H}_2)^a$	Δ^b	$M(\text{CO})_4(\eta^2\text{-C}_2\text{H}_4)^a$	Δ^b
Fe	32 (173)	8	29 (144) ³³	4
Ru	40 (240) ⁸		33 (178) ⁸	8
Os	52 (280) ⁸	12	41 (218) ⁸	

^anumber in brackets denotes the temperature (K) at which ΔG^\ddagger was determined; the estimated error in the activation energies is ± 2 kJ/mol.³¹

^b Δ = difference in ΔG^\ddagger between species of different rows.

The alkyne species generally mirror the trend seen for the ethylene complexes, with the barrier increasing according to Fe < Ru < Os in each, reflecting increasingly greater levels of π -back donation to the alkyne as the triad is descended. It is noteworthy that ΔG^\ddagger is greater for the acetylene complexes than ethylene compounds, and that the relative magnitudes of the differences, Δ , appear to be subtly different, with a 4 kJ/mol difference between the Fe and Ru ethylene species, but an 8 kJ/mol difference for the acetylene compounds. A corresponding difference between the Ru and Os species exists. This likely reflects the greater π -acidity of acetylene¹⁶ relative to ethylene as stronger back-bonding would be expected to increase the barrier to rotation. A limited qualitative comparison is also available for the HFB complexes. The carbonyl resonances in **1a** begin to broaden at ambient temperature while those in $M(\text{CO})_4(\eta^2\text{-HFB})$ are static, even upon warming.³ Again, this result suggests that the back-bonding trend is Fe < Ru, Os in the HFB compounds.

In the triad comparison of $M(\text{CO})_4(\eta^2\text{-C}_2(\text{SiMe}_3)_2)$, the weakness of the Ru-alkyne interaction was related to the σ component of the metal-alkyne interaction, bearing in mind the back-bonding trend.¹ From this, it can be inferred that, in the present case, the σ interaction likely follows Ru \ll Fe, Os, as the Ru complexes are generally less thermally stable than their Fe congeners, despite the fact that they exhibit demonstrably greater back-bonding interactions with the

alkyne. Indeed, it is plausible that the σ component in the Fe complexes is more important than in the third row Os compounds, given that the latter back-bond more readily to the coordinated alkyne yet share comparable thermal stabilities with their Fe analogs. Furthermore, it has been noted that the discontinuity at the second row metal in terms of thermal stability is not restricted to the group eight metals.¹ However, care should be taken in extending this argument too far, for while it is true that $\text{Ru}(\text{CO})_4(\eta^2\text{-HC}\equiv\text{CR})$ ($\text{R} = \text{H}, \text{CF}_3$) appear to decompose largely *via* alkyne dissociation, the Fe and Os compounds follow more complicated routes involving initial CO loss. Additionally, decomposition of $\text{Ru}(\text{CO})_4(\eta^2\text{-HFB})$ occurs *via* dissociation of a carbonyl ligand and formation of a fly-over bridged bimetallic species.³⁴

The triad comparison can be extended to the spectroscopic properties $\Delta(\nu_{\text{C-C}})$ and $\Delta(\delta_{\text{C}_{\text{alk}}})$ which map the nature of the metal-alkyne interaction in a more quantitative fashion (Table 2-9). Given a particular metal, the trends in spectroscopic properties generally mirror those discussed in Section 2.3. That is, $\Delta(\nu_{\text{C-C}})$ decreases in the order $\text{HFB} > \text{TFP} > \text{C}_2\text{H}_2 \approx \text{MeCCH}$ as the alkyne becomes less π -acidic, and the $\Delta(\delta_{\text{C}_{\text{alk}}})$ criterion generally shows a negative to positive shift following the sequence $\text{HFB} < \text{TFP} < \text{C}_2\text{H}_2 < \text{MeCCH} < \text{C}_2\text{Me}_2$.

A more interesting comparison can be drawn between the metal-dependent properties within the triad of a particular $\text{M}(\text{CO})_4(\eta^2\text{-alkyne})$ compound. In general, the following conclusions can be drawn about the metal-dependency of the spectroscopic markers. $\Delta(\nu_{\text{C-C}})$ decreases in the order $\text{Os} > \text{Ru} > \text{Fe}$ for all species studied, clearly suggesting that the Os and Ru species are capable of better back-bonding interactions with the alkyne than is Fe. As mentioned above, this trend is mirrored in ΔG^\ddagger for coupled alkyne rotation-carbonyl exchange which more readily measures back-bonding in the absence of σ -bonding effects. In this regard, it is clear that π back-bonding alone is not the determining factor for thermal stability as $\Delta(\nu_{\text{C-C}})_{\text{Ru}} > \Delta(\nu_{\text{C-C}})_{\text{Fe}}$ in both the TFP and acetylene cases, yet $\text{Ru}(\text{CO})_4(\eta^2\text{-TFP})$ rapidly decomposes above -20°C ⁴ while the Fe compound is stable to at least 0°C . Additionally, $\text{Ru}(\text{CO})_4(\eta^2\text{-C}_2\text{H}_2)$ is only stable to -30°C while $\text{Fe}(\text{CO})_4(\eta^2\text{-C}_2\text{H}_2)$ more closely resembles $\text{Os}(\text{CO})_4(\eta^2\text{-C}_2\text{H}_2)$, decomposing near 0°C .²

Table 2-9. Spectroscopic Features of $M(\text{CO})_4(\eta^2\text{-RC}\equiv\text{CR}')$ Species.

M	R	R'	$\nu_{\text{C-C}}$ (cm^{-1})	$\Delta(\nu_{\text{C-C}})^{\text{a}}$ (cm^{-1})	$\delta_{\text{C}_{\text{alk}}}$ (ppm)	$\Delta(\delta_{\text{C}_{\text{alk}}})^{\text{b}}$ (ppm)
Fe	CF ₃	CF ₃	1890	410	88.5	-17.1
Ru ³	CF ₃	CF ₃	1856, 1818	444, 482	94.1	-22.7
Os ³	CF ₃	CF ₃	1810, 1802	490, 498	92.5	-21.1
Fe	H	CF ₃	1812	353	82.7, 75.0	-6.8, -5.8
Ru ⁴	H	CF ₃	1771	394	89.5, 81.5	-13.6, -12.3
Os ⁸	H	CF ₃	1735	430	89.4, 81.8	-13.5, -12.6
Fe	H	H	1709	265	62.8	+9.1
Ru ²	H	H	1670	304	70.1	+1.8
Os ²	H	H	1642	332	73.5	-1.6
Fe	H	Me	1873	269	48.8, 71.9	+18.4, +8.3
Os ⁸	H	Me	1766	376	58.0, 84.5	+9.2, -4.3
Fe	Me	Me	-	-	58.0	+16.6
Os ⁶	Me	Me	-	-	69.7	+5.9

$$^{\text{a}}\Delta(\nu_{\text{C-C}}) = \nu_{\text{C-C}}(\text{free}) - \nu_{\text{C-C}}(\text{complex}). \quad ^{\text{b}}\Delta(\delta_{\text{C}_{\text{alk}}}) = \delta_{\text{C}_{\text{alk}}}(\text{free}) - \delta_{\text{C}_{\text{alk}}}(\text{complex}).$$

The $\Delta(\delta_{\text{C}_{\text{alk}}})$ parameter is generally similar for the Ru and Os compounds while the Fe complexes generally display more disparate values as the alkyne becomes less π -acidic. For example, when comparing the Fe and Os species, $\Delta(\delta_{\text{C}_{\text{alk}}})$ differs by +4.0 and +6.8 ppm for the HFB and TFP substituted species, respectively, and reaches an average value of +10.7 ppm for the acetylene, propyne, and but-2-yne complexes. It is interesting to note that the triad trend for $\delta_{\text{C}_{\text{alk}}}$ (Fe < Ru < Os) is completely opposite to that commonly observed for carbon atoms bonded to group eight metals; generally, an upfield shift is observed as the triad is descended. This is a well recognized feature for carbonyl ligands¹⁵ and also exists for the $M(\text{CO})_4(\eta^2\text{-C}_2\text{H}_4)$ triad (*i.e.* $\delta_{\text{C}_{\text{olefin}}} = 88.1, \text{Fe}^{33}; 26.3, \text{Ru}^8; 10.9, \text{Os}^8$). The reversal of the regular triad trend for $\delta_{\text{C}_{\text{alk}}}$ therefore argues for the added influence of $4e^-$ interaction in the $M(\text{CO})_4(\eta^2\text{-alkyne})$ complexes. This correlation suggests greater shielding of the alkyne carbons in the Fe case by the

more compact $3d$ orbitals (specifically the b_1 orbital in Scheme 1-5) and potentially a greater destabilizing interaction with the filled π_{\perp} orbital. Bearing in mind the discontinuity at the second row in the thermal stabilities of the $M(\text{CO})_4(\eta^2\text{-alkyne})$ compounds, it is clear that $\Delta(\delta_{\text{C}_{\text{alk}}})$ does not measure the complete metal-alkyne bonding interaction, but serves as a potential indicator of the level of repulsive d_{π}/π_{\perp} interaction.

One final topic deserving discussion is how the series of $M(\text{CO})_4(\eta^2\text{-RC}\equiv\text{CR}')$ ($R, R' = \text{CF}_3, \text{H}, \text{Me}$) compounds relates to the previously analyzed triad of $M(\text{CO})_4(\eta^2\text{-C}_2(\text{SiMe}_3)_2)$ complexes. A summary of the relevant spectroscopic features for the latter is presented in Table 2-10 for comparison.

Table 2-10. Spectroscopic Features of $M(\text{CO})_4(\eta^2\text{-C}_2(\text{SiMe}_3)_2)$ Species.¹

M	$\Delta G^{\ddagger a}$ (kJ/mol)	$\nu_{\text{C-C}}$ (cm^{-1})	$\Delta(\nu_{\text{C-C}})^b$ (cm^{-1})	$\delta_{\text{C}_{\text{alk}}}$ (ppm)	$\Delta(\delta_{\text{C}_{\text{alk}}})^c$ (ppm)
Fe	38	1875	233	87.8	+25.2
Ru	38	1860	248	89.5	+23.5
Os	46	1809	299	92.7	+20.3

^afor alkyne coupled-BPR. ^b $\Delta(\nu_{\text{C-C}}) = 2108 - \nu_{\text{C-C}}(\text{complex})$. ^c $\Delta(\delta_{\text{C}_{\text{alk}}}) = 113.0 - \delta_{\text{C}_{\text{alk}}(\text{complex})}$.

The activation free energy for coupled alkyne rotation-carbonyl exchange established the back-bonding trend as $\text{Fe} \approx \text{Ru} < \text{Os}$ in these compounds,¹ which differs only slightly from the $\text{Fe} < \text{Ru} < \text{Os}$ sequence for the $M(\text{CO})_4(\eta^2\text{-C}_2\text{H}_2)$ complexes (Table 2-8). Additionally, the barrier to carbonyl exchange is slightly lower (with the exception of $M = \text{Fe}$) than for the acetylene species, suggesting a somewhat diminished emphasis on back-donation in the $\text{C}_2(\text{SiMe}_3)_2$ complexes. This contention is borne out by the $\Delta(\nu_{\text{C-C}})$ criterion as the $\text{C}_2(\text{SiMe}_3)_2$ compounds display smaller coordination shifts by some $30 - 50 \text{ cm}^{-1}$. The *ca.* 6 kJ/mol increase for carbonyl exchange in $\text{Fe}(\text{CO})_4(\eta^2\text{-C}_2(\text{SiMe}_3)_2)$ compared to **1c** may be a consequence of increased steric hindrance of the accompanying alkyne rotation in the former compound. The $\Delta(\delta_{\text{C}_{\text{alk}}})$ parameter is some 16 - 22

ppm more positive for $M(\text{CO})_4(\eta^2\text{-C}_2(\text{SiMe}_3)_2)$ than $M(\text{CO})_4(\eta^2\text{-C}_2\text{H}_2)$. This has been rationalized by considering that the quaternary carbons in the free alkyne are found some 35 ppm to lower field than carbon substituted alkynes due to a $p\pi\text{-d}\pi$ conjugative interaction between the carbon-carbon triple bond and the SiMe_3 moiety which serves to reduce the overall π -bond order in the free alkyne.¹

In terms of physical characteristics, the thermal stability of $\text{Ru}(\text{CO})_4(\eta^2\text{-C}_2(\text{SiMe}_3)_2)$ ($< -20^\circ\text{C}$)¹ is quite similar to the TFP and acetylene compounds which decompose above -20°C ⁴ and -30°C ² respectively. However, some differences exist for the first and third row complexes of the bulky bis-trimethylsilylacetylene ligand. While the corresponding acetylene and TFP compounds rapidly decompose at ambient temperature, $\text{Os}(\text{CO})_4(\eta^2\text{-C}_2(\text{SiMe}_3)_2)$ is quite stable and the Fe congener only decomposes slowly under these conditions.³⁵ Furthermore, the carbonyl ligands in $\text{Os}(\text{CO})_4(\eta^2\text{-C}_2(\text{SiMe}_3)_2)$ exchange with ^{13}CO only after the complex is warmed to $+35^\circ\text{C}$ in marked contrast to $\text{Os}(\text{CO})_4(\eta^2\text{-HC}\equiv\text{CR})$ ($\text{R} = \text{H}, \text{CF}_3$) where exchange is complete after *ca.* 2 h at 0°C .²⁶ Additionally, although Pannell and Crawford noted that $\text{Fe}(\text{CO})_4(\eta^2\text{-C}_2(\text{SiMe}_3)_2)$ loses CO more readily than the coordinated alkyne under mass spectrometric conditions, they were unable to illustrate this phenomenon chemically as reaction with PPh_3 produced $\text{Fe}(\text{CO})_3(\text{PPh}_3)_2$ exclusively.³⁵

Thus, although the series of $M(\text{CO})_4(\eta^2\text{-RC}\equiv\text{CR}')$ ($\text{R}, \text{R}' = \text{CF}_3, \text{H}, \text{Me}$) compounds appear to have properties dominated by electronic characteristics, substituent bulk should not be discounted as an additional stabilizing influence. In this regard, it hardly seems coincidental that the only $\text{Fe}(\text{CO})_4(\eta^2\text{-alkyne})$ compounds detected prior to this work included bulky SiMe_3 ³⁵ or tBu ^{36,37} substituents. Furthermore, it is interesting to note that the hex-3-yne complex **1f** survives for a longer period of time at ambient temperature than its but-2-yne congener **1e**, suggesting that the larger ethyl groups in the former provide some additional thermal stability.

2.5. Conclusions

It has been demonstrated that the long elusive $\text{Fe}(\text{CO})_4(\eta^2\text{-alkyne})$ compounds can be readily synthesized in good yield under the appropriate photochemical and thermal conditions. In common with their Ru and Os analogs, the attendant carbonyl ligands are labile, and exchange at much lower temperatures than were observed for the heavier members of the triad. The modest range of alkynes which can be incorporated differ markedly in their electronic characteristics, and a comparison of the influence of the alkyne substituents on the physical and chemical characteristics of the $\text{Fe}(\text{CO})_4(\eta^2\text{-alkyne})$ complexes has been presented. The availability of the new series of iron-alkyne complexes has completed a triad of homologous compounds and has allowed for a study of the metal-dependent characteristics of the important spectroscopic markers and bonding interactions in $\text{M}(\text{CO})_4(\eta^2\text{-alkyne})$ species.

2.6. Experimental Section

2.6.1. Solvents and General Techniques

All solvents were dried and distilled under nitrogen from an appropriate drying agent prior to use. Pentane was stirred over concentrated sulphuric acid for several cycles, trace acid was neutralized with aqueous sodium bicarbonate, then washed with distilled water and finally dried over sodium sulphate before being distilled from calcium hydride. Dichloromethane (CH_2Cl_2) was also distilled from calcium hydride. CD_2Cl_2 was dried with P_2O_5 and vacuum distilled before being stored over molecular sieves under nitrogen. Toluene-d₈ was dried over molecular sieves and degassed by three freeze-pump-thaw cycles prior to use.

All glassware was pretreated by soaking in a KOH/alcohol (either EtOH or *i*PrOH) solution followed by a dilute HCl solution; the glassware was then rinsed three times with distilled water and dried overnight at 175°C before use. Any intractable material in reaction vessels (especially photochemical reactors) which was not soluble in organic solvents was conveniently removed by washing with a *ca.* 5% solution of hydrogen peroxide in concentrated sulphuric acid before receiving the above treatment.

All reactions were carried out under argon or nitrogen atmosphere using standard Schlenk techniques. The argon or nitrogen gas was purified by passage through a heated (100°C) column of BASF Cu catalyst (R3 - 11) and a column of Mallinkrodt Aquasorb (P_2O_5 on an inert support) to remove trace oxygen and moisture respectively before being admitted to the Schlenk line.

2.6.2. Physical Measurements

Fourier transformed infrared (FT-IR) spectra were recorded either on a Bomem MB-100 or Nicolet MX-1 spectrometer over the range 2200 - 1600 cm^{-1} . Solution samples and background solvent were held between KBr plates with a path length of 0.1 mm. NMR spectra were obtained on a Bruker WH-200, AM-300, AM-400 or Varian UNITY-500 spectrometer. ^1H and ^{13}C NMR chemical shifts (δ) were internally referenced to solvent and are reported in ppm relative to tetramethylsilane (TMS). ^{19}F NMR chemical shifts were referred externally to

CFCl_3 and ^{31}P NMR chemical shifts were externally referenced to 85% H_3PO_4 . The NMR sample tubes were either sealed with a serum stopper or flame-sealed under vacuum. Electron impact mass spectra were recorded on an AEI-MS50 spectrometer operating at 70 eV. For highly volatile samples, the probe was cooled to liquid nitrogen temperature before evacuating the antechamber of the mass spectrometer; this was conveniently achieved by attaching a sealed Schlenk tube containing a small amount of sample directly to the probe inlet. Fast atom bombardment mass spectra (FAB-MS) were recorded on a modified AEI-MS9 mass spectrometer with positive xenon ionization (+FAB). Elemental analyses were performed by the Microanalytical Laboratory of the Department of Chemistry.

2.6.3. Photochemical Techniques

Low temperature photochemistry was conducted using the immersion well photolysis reactor shown in Figure 2.5. The reactor consisted of an outside cooling jacket and a cooled cut-off filter insert connected to either an MGM Lauda Klein-Kryomat or Julabo F83-MW refrigerated circulating bath with methanol or ethanol, respectively, functioning as the circulating/cooling solution. The system was cooled and maintained at a constant temperature (between -50°C and -70°C) while the solution inside the reactor chamber was stirred vigorously with a magnetic stir-bar. Pentane (115 mL), $\text{Fe}(\text{CO})_5$ (80 - 150 μL), and excess alkyne were added to the cooled reactor. A slow stream of nitrogen gas (*ca.* 1 bubble/s) was passed through the solution to remove CO liberated during the photolysis. A Phillips HPK 125 W mercury vapor lamp was employed as the irradiation source, and the wavelength of the incident radiation was controlled by the composition of the cut-off filter, with uranium glass ($\lambda \geq 330 \text{ nm}$) being the material of choice. Irradiation was continued until IR spectroscopy indicated that the reaction was complete; the work-up procedure varied slightly for each compound and shall be described separately in section 2.6.5.

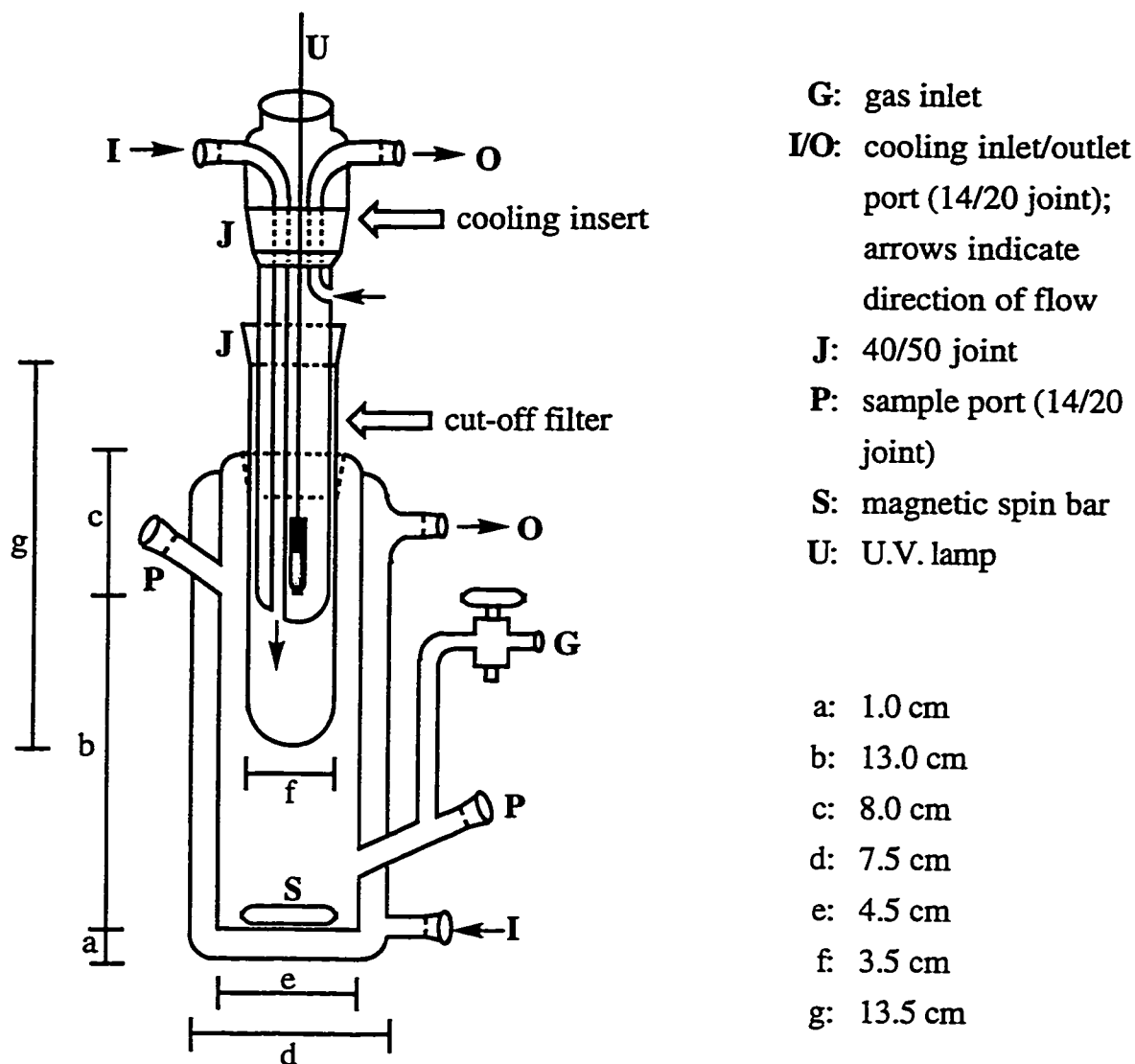


Figure 2-5. Immersion Well Photochemical Reactor.

2.6.4. Reagents

The gaseous alkynes $C_2(CF_3)_2$ (HFB) and $HC\equiv CCF_3$ (TFP) were purchased from Farchan Chemical Co. while propyne (99%) was purchased from Wiley Organics; all were used without subsequent purification. In the case of propyne, it was found that very poor results were obtained if the gas was shipped stabilized with an inert volatile hydrocarbon such as propane. Acetylene was purchased from Linde Gas Products and was passed through a dry ice/acetone trap to remove the acetone stabilizer before being admitted to the photochemical

reactor. But-2-yne and hex-3-yne were purchased from Aldrich Chemical Co. and used without further purification. $\text{Fe}(\text{CO})_5$ was purchased from Johnson-Matthey, Inc. and was filtered prior to use. ^{13}CO (99.5 %) was purchased from Isotec, Inc.

2.6.5. Synthetic Procedures

Synthesis of $\text{Fe}(\text{CO})_4(\eta^2\text{-HFB})$ (1a). $\text{Fe}(\text{CO})_5$ (80 μL , 119 mg, 0.607 mmol) was dissolved in 115 mL pentane at -50°C in an immersion well photochemical reactor equipped with a uranium glass cut-off filter. Hexafluorobut-2-yne (HFB) was bubbled through the solution for five minutes and a slow (*ca.* 1 bubble/2 s) N_2 flow was maintained for the duration of the photolysis. The solution was irradiated for 1 h, at which point IR spectroscopy indicated near consumption of $\text{Fe}(\text{CO})_5$. A 40 μL (60 mg, 0.304 mmol) portion of $\text{Fe}(\text{CO})_5$ was added and irradiation was continued until IR spectroscopy indicated that the reaction was complete (*ca.* 1 h). The solution was transferred cold into a 200 mL round-bottom flask and freeze-thaw degassed once. Pentane and excess HFB were removed by bulb-to-bulb distillation to leave a greenish-brown residue; the distilling flask was maintained at a temperature of -78°C while the distillate was collected in a liquid nitrogen trap. The product was purified by sublimation onto a dry-ice cooled cold-finger at 10^{-3} torr by allowing the dry-ice/acetone bath surrounding the flask to slowly warm from -78°C to -10°C . The pale yellow sublimate was washed from the probe with 50 mL pentane, and removal of the pentane *in vacuo* at -78°C provided $\text{Fe}(\text{CO})_4(\eta^2\text{-HFB})$ (1a) (252 mg, 0.764 mmol, 84 %) as a thermally sensitive yellow oil that could be quickly weighed at room temperature; however, titration of the product with $\text{Cp}^*\text{Rh}(\text{CO})_2$ is the desired means of determining the yield (see Chapter 5). $\text{Fe}(^{13}\text{CO})_4(\eta^2\text{-HFB})$ was prepared by submitting a pentane solution of 1a to three freeze-thaw degassing cycles and stirring the solution in the dark for 3 hours at $-10^\circ\text{C} \leq T \leq -20^\circ\text{C}$ under 1 atm of ^{13}CO .

F.W. 329.9

IR (pentane) ν_{CO} 2125(w), 2058(s), 2033(m); ν_{CC} 1890(w).

$$\epsilon_{2058} = 8.8 \times 10^3 \text{ M}^{-1} \text{ cm}^{-1}; \epsilon_{2032} = 6.1 \times 10^3 \text{ M}^{-1} \text{ cm}^{-1}$$

$^{13}\text{C}\{^1\text{H}\}$ NMR (CD_2Cl_2 , 100.6 MHz, -40°C) δ 205.77 (s, 2CO_{eq}), 199.20 (s, 2CO_{ax}), 121.35 (q, $^1J_{\text{CF}} = 267$ Hz, CF_3), 88.51 (qq, $^2J_{\text{CF}} = 50$ Hz, $^3J_{\text{CF}} = 6$ Hz, $\equiv\text{CCF}_3$).

$^{13}\text{C}\{^1\text{H}\}$ NMR (CD_2Cl_2 , 100.6 MHz, -40°C , ^{13}CO enriched) δ 205.75 (t, $^2J_{\text{CC}} = 10$ Hz, 2CO_{eq}), 199.17 (t, $^2J_{\text{CC}} = 10$ Hz, 2CO_{ax}).

$^{13}\text{C}\{^{19}\text{F}\}$ NMR (CD_2Cl_2 , 100.6 MHz, -40°C) δ 205.76 (s, 2CO_{eq}), 199.19 (s, 2CO_{ax}), 121.35 (s, CF_3), 88.51 (s, $\equiv\text{CCF}_3$).

^{19}F NMR (CD_2Cl_2 , 376.5 MHz, -40°C) δ -56.10 (s).

EI-MS: $\text{M}^+ - n\text{CO} - m\text{F}$ ($n = 2 - 4$, $m = 0, 1$); $\text{M}^+ - \text{HFB} - n\text{CO}$; ($n = 0 - 3$); HFB^+ ; $\text{HFB}^+ - 2\text{F}$ (base peak).

Synthesis of $\text{Fe}(\text{CO})_4(\eta^2\text{-HC}\equiv\text{CCF}_3)$ (1b**).** Under similar conditions as for the preparation of **1a**, 120 μL (179 mg, 0.913 mmol) $\text{Fe}(\text{CO})_5$ was converted into **1b** (156 mg, 0.596 mmol, 65 %) in the presence of excess trifluoropropyne following a total of 1 h 30 min of irradiation at -70°C . As with **1a**, it is best to begin the photolysis with 80 μL $\text{Fe}(\text{CO})_5$ and add a second portion (40 μL) when IR spectroscopy indicates consumption of the original amount. ^{13}CO enriched material was prepared by submitting a pentane solution of **1b** to three freeze-thaw degassing cycles and placing under 1 atm of ^{13}CO for 4 h at $-45^\circ\text{C} < T < -35^\circ\text{C}$. It is important to repurify the product by sublimation as described above to remove byproducts which may form during $^{12}/^{13}\text{CO}$ exchange (see Chapter 3).

F.W. 261.9

IR (pentane) ν_{CO} 2111(w), 2040(s), 2013(m); ν_{CC} 1812(vw).

$$\epsilon_{2040} = 9.8 \times 10^3 \text{ M}^{-1} \text{ cm}^{-1}; \epsilon_{2023} = 5.6 \times 10^3 \text{ M}^{-1} \text{ cm}^{-1}$$

^1H NMR (CD_2Cl_2 , 400.1 MHz, -60°C) δ 6.46 (d, $^4J_{\text{HF}} = 2.7$ Hz, CH).

$^{13}\text{C}\{^1\text{H}\}$ NMR (CD_2Cl_2 , 100.6 MHz, -60°C) δ 209.78 (s, CO_{eq}), 208.62 (s, CO_{eq}), 203.02 (s, 2CO_{ax}), 122.00 (q, $^1J_{\text{CF}} = 264$ Hz, CF_3), 82.65 (q, $^3J_{\text{CF}} = 7$ Hz, $\equiv\text{CH}$), 74.96 (q, $^2J_{\text{CF}} = 49$ Hz, $\equiv\text{CCF}_3$).

$^{13}\text{C}\{^1\text{H}\}$ NMR (CD_2Cl_2 , 100.6 MHz, -80°C , ^{13}CO enriched) δ 210.38 (t, $^2J_{\text{C}_{\text{eq}}\text{C}_{\text{ax}}} = 10$ Hz, CO_{eq}), 209.23 (t, $^2J_{\text{C}_{\text{eq}}\text{C}_{\text{ax}}} = 10$ Hz, CO_{eq}), 203.53 (t, $^2J_{\text{C}_{\text{ax}}\text{C}_{\text{eq}}} = 10$ Hz, 2CO_{ax}).

$^{13}\text{C}\{^{19}\text{F}\}$ NMR (CD_2Cl_2 , 100.6 MHz, -60°C) δ 209.80 (s, CO_{eq}), 208.63 (s, CO_{eq}), 203.04 (s, 2CO_{ax}), 122.02 (s, CF_3), 82.67 (d, $^1J_{\text{CH}} = 237$ Hz, $\equiv\text{CH}$), 74.99 (d, $^2J_{\text{CH}} = 22$ Hz, $\equiv\text{CCF}_3$).

^{19}F NMR (CD_2Cl_2 , 376.5 MHz, -60°C) δ -54.06 (d, $^4J_{\text{HF}} = 2.7$ Hz, CF_3).

Synthesis of $\text{Fe}(\text{CO})_4(\eta^2\text{-C}_2\text{H}_2)$ (1c). Under similar conditions to that for the preparation of 1a, 120 μL (179 mg, 0.913 mmol) $\text{Fe}(\text{CO})_5$ was converted to 1c (133 mg, 0.686 mmol, 75 %) following 50 min irradiation. Acetylene was purged through the solution for 10 min and a slow (*ca.* 1 bubble/2 s) flow was maintained. It is essential that the bath not warm above -65°C during the course of the reaction; the indicated quantity of $\text{Fe}(\text{CO})_5$ is considered optimum. $\text{Fe}(^{13}\text{CO})_4(\eta^2\text{-C}_2\text{H}_2)$ was prepared by submitting a pentane solution of 1c to three freeze-thaw degassing cycles and stirring under 1 atm of ^{13}CO for 3 hours at $-25 < T < -15^\circ\text{C}$. The solution may yellow during this treatment (see Chapter 3), but this material is insoluble in pentane and precipitates to the bottom of the flask. Providing care is taken in extracting the solution by syringe, no further purification is required.

F.W. 193.9

IR (pentane) ν_{CO} 2094(w), 2018(s), 1989(m); ν_{CC} 1709(vw).

$$\epsilon_{2018} = 8.4 \times 10^3 \text{ M}^{-1} \text{ cm}^{-1}; \epsilon_{1989} = 4.6 \times 10^3 \text{ M}^{-1} \text{ cm}^{-1}$$

^1H NMR (CD_2Cl_2 , 400.1 MHz, -80°C) δ 5.19 (s).

$^{13}\text{C}\{^1\text{H}\}$ NMR (CD_2Cl_2 , 100.6 MHz, -115°C , ^{13}CO enriched) δ 213.3 (br s, CO_{eq}), 208.1 (br s, CO_{ax}), 62.81 (s, $\equiv\text{CH}$); (-40°C) δ 210.97 (s, CO_{av}), 63.09 (s, $\equiv\text{CH}$).

EI-MS: M^+ (2.4% of base); $\text{M}^+ - n\text{CO}$ ($n = 1 - 4$); $\text{M}^+ - 2\text{H}$; $\text{M}^+ - 2\text{H} - \text{CO}$; $\text{Fe}(\text{CO})_5^+ - m\text{CO}$ ($m = 0 - 5$; $m = 4$, base peak). Peaks at higher molecular weights were also detected, suggesting decomposition in the inlet stream.

Synthesis of $\text{Fe}(\text{CO})_4(\eta^2\text{-HC}\equiv\text{CMe})$ (1d). Under the same conditions as for the preparation of **1c**, 80 μL (119 mg, 0.607 mmol) $\text{Fe}(\text{CO})_5$ was converted into **1d** (102 mg, 0.491 mmol, 81 %) following 45 min of irradiation. The best results are obtained under relatively low concentrations of propyne as large quantities of photochemical byproducts plague isolation if a large excess of propyne is present initially; it is essential, however, to maintain a sufficient quantity of propyne to enable successful preparation of the desired compound. As it is difficult to precisely gauge the quantity of propyne that is admitted to the reaction vessel in the above manner, the product yield can vary between 40 and 80%. Extreme care must be exercised in handling this thermally sensitive compound as decomposition rapidly ensues above *ca.* -20°C . ^{13}C -enriched **1d** was prepared in low yield by submitting a pentane solution to three freeze-thaw degassing cycles, placing under 1 atm of ^{13}C O for 1 h at -10°C , and resubliming the product as described above to remove byproducts which form during $^{12}/^{13}\text{C}$ O exchange (see Chapter 3).

F.W. 207.9

IR (pentane) ν_{CO} 2086(w), 2009(s), 1981(m); ν_{CC} 1873(vw).

$$\epsilon_{2009} = 8.2 \times 10^3 \text{ M}^{-1} \text{ cm}^{-1}; \epsilon_{1981} = 4.3 \times 10^3 \text{ M}^{-1} \text{ cm}^{-1}$$

^1H NMR (CD_2Cl_2 , 400.1 MHz, -80°C) δ 4.21 (q, $^4J_{\text{HH}} = 2.6$ Hz, CH), 2.47 (d, $^4J_{\text{HH}} = 2.6$ Hz, CH_3).

$^{13}\text{C}\{^1\text{H}\}$ NMR (CD_2Cl_2 , 100.6 MHz, -80°C) δ 212.06 (s, CO_{av}), 71.86 (s, $\equiv\text{CCH}_3$), 48.75 (s, $\equiv\text{CH}$), 14.09 (s, CH_3).

^{13}C NMR (CD_2Cl_2 , 100.6 MHz, -80°C) δ 212.09 (s, CO_{av}), 71.94 (dq, $^2J_{\text{C}(\text{CH})} = 34$ Hz, $^2J_{\text{C}(\text{CH}_3)} = 9$ Hz, $\equiv\text{CCH}_3$), 48.81 (dq, $^1J_{\text{CH}} = 242$ Hz, $^3J_{\text{C}(\text{CH}_3)} = 4$ Hz, $\equiv\text{CH}$), 14.11 (q, $^1J_{\text{CH}} = 132$ Hz, CH_3).

Synthesis of $\text{Fe}(\text{CO})_4(\eta^2\text{-C}_2\text{Me}_2)$ (1e). Under the same conditions as for the preparation of **1c**, 150 μL (224 mg, 1.14 mmol) $\text{Fe}(\text{CO})_5$ was converted into **1e** (144 mg, 0.649 mmol, 57 %) in the presence of excess but-2-yne (0.5 mL, 6.4 mmol) following 35 minutes of irradiation. Extreme care must be exercised in handling this thermally sensitive compound as decomposition rapidly ensues above *ca.* -20°C .

F.W. 221.9

IR (pentane) ν_{CO} 2079(w), 2001(s), 1975(m).

$$\epsilon_{2002} = 7.9 \times 10^3 \text{ M}^{-1} \text{ cm}^{-1}; \epsilon_{1976} = 4.2 \times 10^3 \text{ M}^{-1} \text{ cm}^{-1}$$

^1H NMR (CD_2Cl_2 , 400.1 MHz, -80°C) δ 2.26 (s).

$^{13}\text{C}\{^1\text{H}\}$ NMR (CD_2Cl_2 , 100.6 MHz, -80°C) δ 213.21 (s, CO_{av}), 57.96 (s, $\equiv\text{CCH}_3$), 13.46 (s, CH_3).

Synthesis of $\text{Fe}(\text{CO})_4(\eta^2\text{-C}_2\text{Et}_2)$ (1f**).** Under the same conditions as for the preparation of **1c**, 100 μL (149 mg, 0.766 mmol) $\text{Fe}(\text{CO})_5$ was converted into **1f** in the presence of excess hex-3-yne (0.5 mL, 4.4 mmol) following 30 min of irradiation. Compound **1f** cannot be isolated as a pure material as the high boiling point of hex-3-yne ($81 - 82^\circ\text{C}$) prevents its removal under vacuum at low temperature.

F.W. 249.9

IR (pentane) ν_{CO} 2080(w), 2002(s), 1975(m).

2.7. References

1. Ball, R. G.; Burke, M. R.; Takats, J. *Organometallics* **1987**, *6*, 1918.
2. Burn, M. J.; Kiel, G.-Y.; Seils, F.; Takats, J.; Washington, J. *J. Am. Chem. Soc.* **1989**, *111*, 6850.
3. Gagné, M. R.; Takats, J. *Organometallics* **1988**, *7*, 561.
4. Hoffman, K. MSc. Thesis, University of Alberta, 1994.
5. Takats, J. *J. Cluster Science* **1992**, *3*, 479.
6. Washington, J.; McDonald, R.; Takats, J.; Menashe, N.; Reshef, D.; Shvo, Y. *Organometallics* **1995**, *14*, 3996.
7. Mao, T. PhD Thesis, University of Alberta, 1996.
8. Kiel, G.-Y. unpublished results.
9. Cooke, J.; Takats, J. *J. Am. Chem. Soc.* **1997**, *119*, 11088.
10. King, R. B. In *The Organic Chemistry of Iron*; E. A. Koerner Von Gustorf, F.-W. Grevels and I. Fischler, Eds.; Academic Press: New York, 1978; Vol. 1; pp 397.
11. Heck, R. F. *Organotransition Metal Chemistry: A Mechanistic Approach*; Academic Press: New York, 1974, pp 174.
12. Washington, J. PhD Thesis, University of Alberta, 1994.
13. Shen, J. K.; Gao, Y. C.; Shi, Q. Z.; Basolo, F. *Inorg. Chem.* **1989**, *28*, 4304.
14. Marinelli, G.; Streib, W.; Huffman, J. C.; Caulton, K. G.; Gagné, M. R.; Takats, J.; Dartiguenave, M. *Polyhedron* **1990**, *9*, 1867.
15. Mann, B. E.; Taylor, B. F. *¹³C NMR Data for Organometallic Compounds*; Academic: New York, 1981, pp 14, 15, 166.
16. Mingos, D. M. P. In *Comprehensive Organometallic Chemistry*; G. Wilkinson, F. G. A. Stone and E. W. Abel, Eds.; Pergamon Press: Oxford, 1983; Vol. 3; pp 1.
17. Fields, R.; Germain, M. M.; Haszeldine, R. N.; Wiggans, P. W. *J. Chem. Soc. (A)* **1970**, 1969.
18. Murdoch, H. D.; Weiss, E. *Helv. Chim. Acta* **1963**, *46*, 1588.
19. Berney, C. V.; Cousins, L. R.; Miller, F. A. *Spectrochim. Acta* **1963**, *19*, 2019.

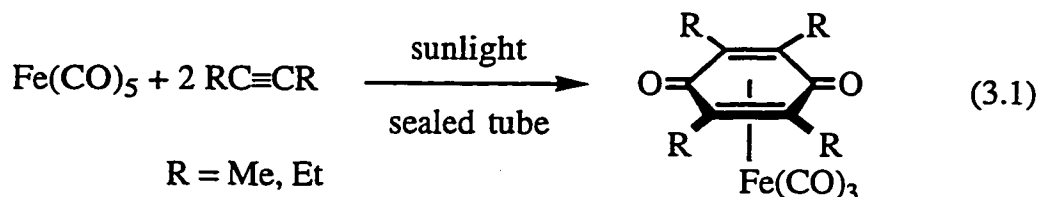
20. Brodersen, S. In *Topics in Current Physics*; A. Weber, Ed.; Springer-Verlag: New York, 1979; Vol. 11; pp 44.
21. Meyer, A.; Bigorgne, M. *Organometallics* **1984**, *3*, 1112.
22. Templeton, J. L.; Ward, B. C. *J. Am. Chem. Soc.* **1980**, *102*, 3288.
23. Silverstein, R. M.; Bassler, G. C.; Morrill, T. C. *Spectrometric Identification of Organic Compounds*; 5th ed.; Wiley: New York, 1991, pp 174, 239.
24. Chisholm, M. H.; Clark, H. C.; Manzer, L. E.; Stothers, J. B. *J. Am. Chem. Soc.* **1972**, *94*, 5087.
25. Templeton, J. L. *Adv. Organomet. Chem.* **1989**, *29*, 1.
26. Washington, J. unpublished results.
27. Breitmaier, E.; Voelter, W. *Carbon-13 NMR Spectroscopy*; VCH: Weinheim, 1987, pp 133-155.
28. Jesson, J. P. *J. Am. Chem. Soc.* **1973**, *95*, 1344.
29. Kruczynski, L.; LiShingMan, L. K. K.; Takats, J. *J. Am. Chem. Soc.* **1974**, *96*, 4006.
30. Wilson, S. T.; Coville, N. J.; Shapely, J. R.; Osborn, J. A. *J. Am. Chem. Soc.* **1974**, *96*, 4038.
31. Sandström, J. *Dynamic NMR Spectroscopy*; Academic Press: London, 1982, Chp 7.
32. Grevels, F.-W.; Reuvers, J. G. A.; Takats, J. *J. Am. Chem. Soc.* **1981**, *103*, 4069.
33. von Büren, M.; Cosandey, M.; Hansen, H.-J. *Helv. Chim. Acta* **1980**, *63*, 738.
34. Senzaki, Y.; McCormick, F. B.; Gladfelter, W. L. *Materials* **1992**, *4*, 748.
35. Pannell, K. H.; Crawford, G. M. *J. Coord. Chem.* **1973**, *2*, 251.
36. Cotton, F. A.; Jamerson, J. D.; Stults, B. R. *J. Am. Chem. Soc.* **1976**, *98*, 1774.
37. Hübel, W. In *Organic Synthesis via Metal Carbonyls*; I. Wender and P. Pino, Eds.; Wiley-Interscience: New York, 1968; Vol. 1; pp 273 and references therein.

Chapter 3

**The Intermediacy of $\text{Fe}(\text{CO})_4(\eta^2\text{-alkyne})$ Complexes and Their Derivatives
in the Metal-Mediated Coupling of Alkynes with Carbon Monoxide**

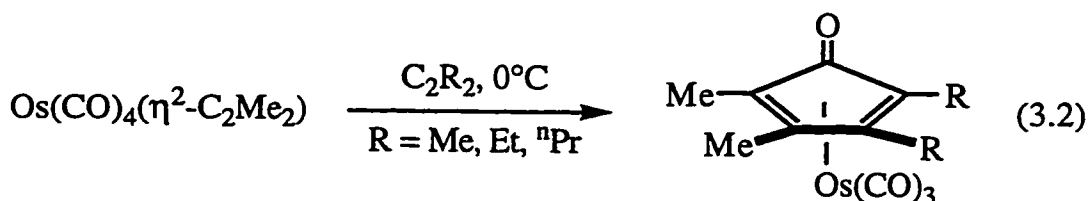
3.1. Introduction

One of the earliest examples of a reaction between an iron carbonyl and an alkyne serves as an elegant reminder of the occasional simplicity of organometallic reactions; simply sealing $\text{Fe}(\text{CO})_5$ and neat C_2R_2 ($\text{R} = \text{Me}, \text{Et}$) in a glass tube and exposing to sunlight produced an organoiron complex containing a *p*-quinone ligand derived from the coupling of two equivalents each of alkyne and CO ligands (Eq. 3.1).¹



While $\text{Fe}(\text{CO})_4(\eta^2\text{-alkyne})$ species have been postulated as intermediates in such reactions,^{2,3} there were only two well documented examples of this type of complex prior to this work. Both incorporated bulky substituents (SiMe_3 ,⁴ tBu ^{3,5}) and neither were reported to produce coupling products with CO, a likely consequence of their steric bulk.

Despite the wealth of available examples of group 8 metal carbonyl-mediated cyclization reactions (Chapter 1), it was only recently that an $\text{M}(\text{CO})_4(\eta^2\text{-alkyne})$ species was demonstrated to be an immediate precursor in such a reaction. Isolated $\text{Os}(\text{CO})_4(\eta^2\text{-C}_2\text{Me}_2)$ was observed to react with electron rich alkynes C_2R_2 ($\text{R} = \text{Me}, \text{Et}, \text{}^n\text{Pr}$) to form the cyclopentadienone complexes $\text{Os}(\text{CO})_3\{\eta^4\text{-C}_4\text{Me}_2\text{R}_2(\text{O})\}$ (Eq. 3.2).⁶



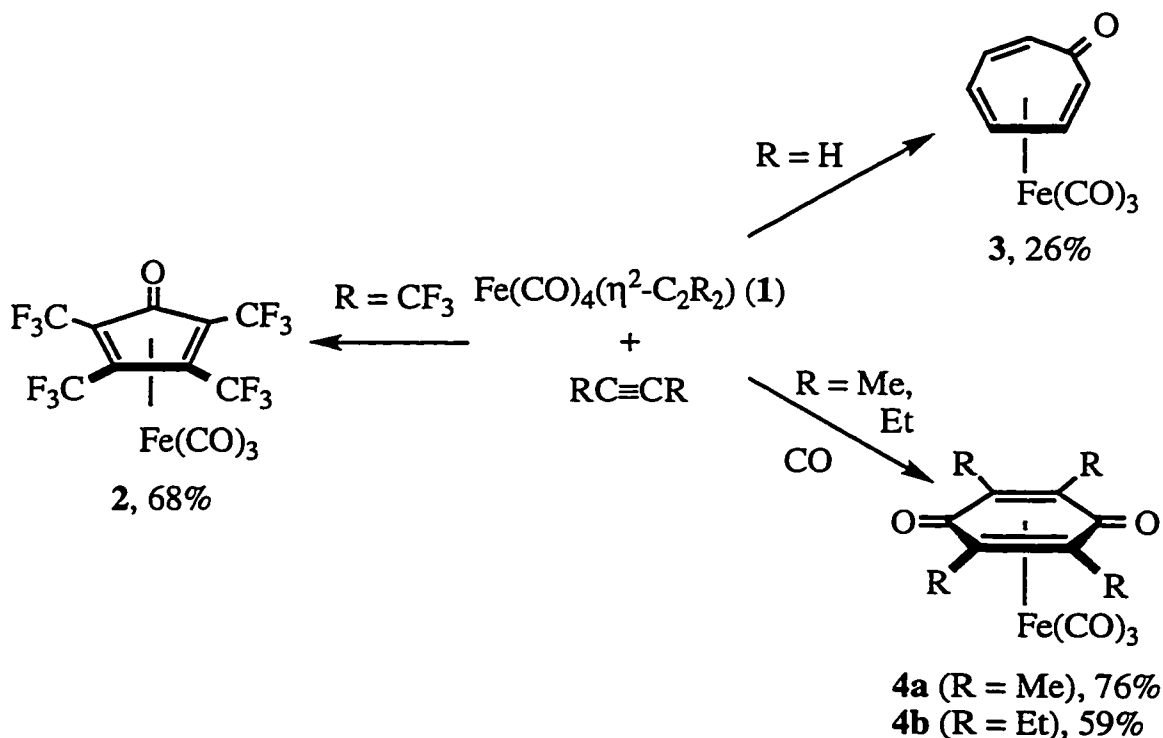
Thus, it was clearly of interest to investigate the reactivity of the newly available $\text{Fe}(\text{CO})_4(\eta^2\text{-alkyne})$ complexes (**1a-f**) with alkynes, for it has yet to be demonstrated that such compounds are the actual intermediates in iron-mediated alkyne coupling reactions. Furthermore, the reactivity of **1a-e** towards added CO (see Section 2.2.2) has been investigated given its potential importance in understanding how coordinated alkynes are linked with carbon monoxide and whether such species are potential precursors for further coupling reactions. A preliminary account of this investigation has been published.⁷

3.2. Reaction of $\text{Fe}(\text{CO})_4(\eta^2\text{-alkyne})$ Compounds (**1a-f**) with Alkynes

The first indication that $\text{Fe}(\text{CO})_4(\eta^2\text{-alkyne})$ compounds are indeed reactive towards alkynes came during the low temperature photochemical preparation of **1b,c,e**. As described in Section 2.2.1, when FT-IR spectra were recorded as the reactions proceeded, the bands due to **1b,c,e** appeared at lower intensity than was anticipated and the spectra were complicated by the presence of other bands (Figure 2-2). However, following work-up the reaction mixtures provided good yields of the desired $\text{Fe}(\text{CO})_4(\eta^2\text{-alkyne})$ products, suggesting that a reaction was occurring between the excess alkyne and **1b,c,e** in the warm IR cell. The strongly π -acidic HFB complex **1a** did not display this behavior, and the FT-IR spectra of reaction mixtures containing the propyne compound **1d** only displayed the above complications if a large excess of propyne was present. In order to more fully understand the above observations, and to hopefully demonstrate that $\text{Fe}(\text{CO})_4(\eta^2\text{-alkyne})$ compounds were indeed intermediates in reactions such as Eq. 3.1, the reaction of isolated **1a-e** with added alkyne was investigated.

Compound **1a** undergoes a slow reaction with HFB at ambient temperature, producing the cyclopentadienone complex **2** after stirring overnight in a sealed tube (Scheme 3-1). Tricarbonyl(cyclopentadienone)iron complexes are among the most prevalent products of reaction of alkynes with iron carbonyls, and a large number of examples have been compiled.^{3,8-15} Compound **2** was first isolated in 60% yield from the high temperature bomb reaction of neat $\text{Fe}(\text{CO})_5$ with excess HFB¹⁶ and its solid-state structure has been determined.¹⁷ Its IR and

^{19}F NMR spectra agree with those reported in the literature,¹⁶ and additional confirmation of the structure was obtained *via* ^{13}C NMR spectroscopy. Fluorine decoupling was employed to aid in the observation of the carbon atoms of the cyclopentadienone backbone. Singlet resonances were observed at δ 163.86 ($\text{C}=\text{O}$), 90.14 (C_{inner}) and 66.40 (C_{outer}); the "inner" and "outer" labels refer to the diene portion of the molecule, the "outer" carbons being attached to the ketone carbonyl.^{6,18,19} The above data bears comparison to the $\text{M}(\text{CO})_3\{\eta^4\text{-C}_4\text{Ph}_4\text{C}(\text{O})\}$ ($\text{M} = \text{Fe}, \text{Ru}, \text{Os}$) family of compounds whose ^{13}C NMR data have been reported.¹⁸ In particular, the pertinent resonances for $\text{Fe}(\text{CO})_3\{\eta^4\text{-C}_4\text{Ph}_4\text{C}(\text{O})\}$ are δ 170.6, 104.7 and 83.0 ppm. The fact that the resonances in **2** are further upfield than those in the phenyl-substituted analog can be attributed to the stronger π -acidity of the ring system in **2**, which imparts more sp^3 character to the diene carbons as more metal electron density is back-donated to the ring.



Scheme 3-1. Reaction of **1a,c,e,f** with C_2R_2 .

Treatment of **1b** with excess trifluoropropyne led to the formation of an intractable brown powder on warming from -78°C to room temperature, without detection of a complex analogous to **2**. Similarly, when a pentane solution of isolated **1c** was saturated with acetylene and allowed to slowly warm from -78°C , the colorless solution began to turn yellowish orange at -60°C with rapid formation of a brownish black precipitate by -40°C . In this case, though, extraction of the residue gave an air-stable orange material in 26% yield which was subsequently identified as $\text{Fe}(\text{CO})_3\{\eta^4\text{-C}_6\text{H}_6\text{C}(\text{O})\}$ (**3**) ($\text{C}_6\text{H}_6\text{C}(\text{O}) =$ tropone) by comparison of its characteristic IR,²⁰ ^1H NMR²¹ and ^{13}C NMR²² spectra reported previously in the literature. The intractable black precipitate has so far defied characterization, but most probably contains some polymeric material.²³ The facile reaction of **1c** with C_2H_2 is in notable contrast to $\text{Os}(\text{CO})_4(\eta^2\text{-C}_2\text{H}_2)$ which does not react with excess acetylene.⁶ Furthermore, it explains why the photochemical reactor must be kept at temperatures below -65°C in the synthesis of **1c** (Section 2.2.1).

It is most interesting that the reaction of **1c** with C_2H_2 yields **3** as the exclusive organometallic product, since $\text{Fe}(\text{CO})_5$ produces primarily the cyclopentadienone species $\text{Fe}(\text{CO})_3\{\eta^4\text{-C}_4\text{H}_4\text{C}(\text{O})\}$ along with trace amounts of $\text{Fe}_2(\text{CO})_6(\mu\text{-}\eta^1, \eta^1:\eta^4\text{-C}_4\text{H}_4)$ and **3** when heated under acetylene pressure.²³ The cycloheptatrienone complex **3** was obtained, as the only tractable product, by treating $\text{Fe}_2(\text{CO})_9$ with C_2H_2 (22 atm) at ambient temperature.²⁰ Thus, the thermal conditions of the reaction are important factors in determining the eventual products, with **3** being favored from intermediate **1c** under mild conditions. The cyclopentadienone complex dominates under harsher conditions and, as such, is likely formed from a different intermediate than **1c**.

Knox *et. al* have implicated a di-iron complex in the formation of tropone from $\text{Fe}_2(\text{CO})_9$ following the completion of a study illustrating the step-wise build-up of the cycloheptatrienone on $\text{Fe}_2(\text{CO})_7(\mu\text{-dppm})$.²⁴ However, the ready formation of **3** from **1c** suggests that the tropone ring is more likely to form at a mononuclear iron center. In the case of the thermal reaction of acetylene with diironnonacarbonyl, tropone formation presumably occurs *via* formation of short-lived intermediate **1c** following the fragmentation of $\text{Fe}_2(\text{CO})_9$ into $[\text{Fe}(\text{CO})_4]$ and

$\text{Fe}(\text{CO})_5$. In this regard, it seems more than a coincidence that the isolated yields of **3** (ca. 25%) from the reaction of **1c** with C_2H_2 mirrors that reported for the preparation from $\text{Fe}_2(\text{CO})_9$ (28%).²⁰ Additionally, Birk and co-workers have recently reported the formation of $\text{Fe}(\text{CO})_2(\text{PEt}_3)\{\eta^4\text{-C}_6\text{H}_6\text{C}(\text{O})\}$ in 7% yield by reaction of $\{\text{Fe}(\text{CO})_2(\text{PEt}_3)_2\}_2(\mu\text{-N}_2)$ under prolonged acetylene purge at room temperature.²⁵ Although $\text{Fe}(\text{CO})_2(\text{PEt}_3)_2(\eta^2\text{-C}_2\text{H}_2)$ is accessible on warming $\{\text{Fe}(\text{CO})_2(\text{PEt}_3)_2\}_2(\mu\text{-N}_2)$ from -20°C under 1 atm C_2H_2 , the authors did not seem to implicate the η^2 -acetylene species in the formation of the troponone complex.

$\text{Fe}(\text{CO})_4(\eta^2\text{-C}_2\text{R}_2)$ (R = Me, Et) species have also been proposed as intermediates in the formation of 1,4-benzoquinones *via* unstable $\text{Fe}(\text{CO})_3\{\eta^4\text{-(O)CC}_4\text{R}_4\text{C}(\text{O})\}$ (R = Me (**4a**); Et (**4b**)) complexes.^{2,3} Furthermore, as $\text{Os}(\text{CO})_4(\eta^2\text{-C}_2\text{Me}_2)$ reacts with electron rich alkynes to generate the cyclopentadienone species $\text{Os}(\text{CO})_3\{\eta^4\text{-C}_4\text{Me}_2\text{R}_2\text{C}(\text{O})\}$ (Eq. 3.2),⁶ it was obviously of interest to determine whether **1e** would react further with added alkyne and, if so, which ligand type would be favored - cyclopentadienone, quinone or perhaps even cycloheptatrienone as per compound **3** discussed above. Attempts at reacting isolated **1e** with an added excess of C_2Me_2 resulted predominantly in intractable material, with no evidence for a cyclopentadienone or *p*-quinone species. However, **1e** reacts cleanly with but-2-yne at low temperature under a CO atmosphere to produce the *p*-quinone complex **4a** in 76% isolated yield (Scheme 3-1), thus clearly demonstrating the intermediacy of **1e** in the synthesis of **4a** from $\text{Fe}(\text{CO})_5$ and C_2Me_2 (Eq. 3.1).¹ The lack of tractable product in the reaction carried out under N_2 atmosphere can be attributed to the necessity of an additional mole of CO in forming **4a**; presumably, in its absence, the required CO is scavenged from unreacted **1e** leading largely to decomposition.

Compound **1d** similarly formed an intractable brown solid when exposed to excess propyne under nitrogen atmosphere, but in this case carrying out the reaction under CO did not lead to an isolable organometallic product. However, the *p*-quinone complex $\text{Fe}(\text{CO})_3\{\eta^4\text{-(O)CC}_4\text{Et}_4\text{C}(\text{O})\}$ (**4b**) could be isolated following the *in situ* generation of $\text{Fe}(\text{CO})_4(\eta^2\text{-C}_2\text{Et}_2)$ at low temperature in the presence of excess hex-3-yne and subsequent warming of the solution to room

temperature under an atmosphere of CO. The lack of formation of a quinone complex from **1c** suggests that electron rich substituents may be important in producing these somewhat unstable species. Although first reported nearly four decades ago,¹ compounds **4a,b** have yet to be characterized by modern spectroscopic methods and a brief discussion of their IR and NMR spectra is included in Section 3.5.2.

3.3. Reaction of $\text{Fe}(\text{CO})_4(\eta^2\text{-alkyne})$ Compounds (**1a-e**) with CO

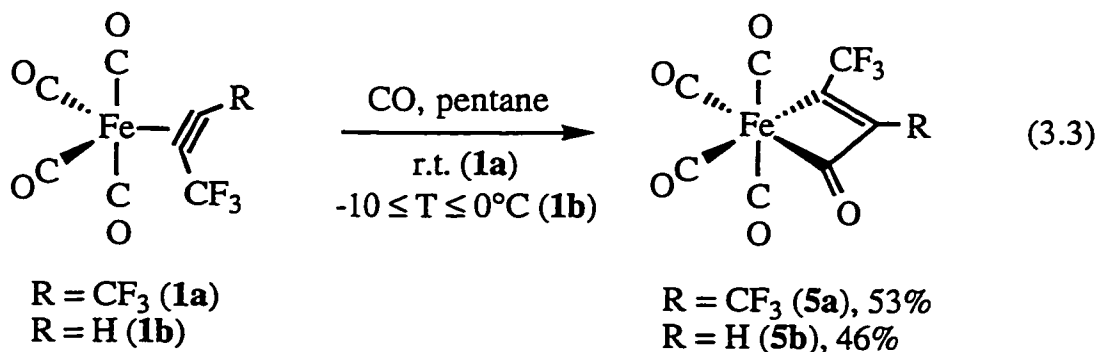
The formation of *p*-quinone species from **1e,f** seems to imply that CO insertion precedes alkyne incorporation in these reactions. It was thus important to corroborate that CO would react with $\text{Fe}(\text{CO})_4(\eta^2\text{-alkyne})$ complexes in the absence of excess alkyne. Indeed, during the ^{13}C O exchange reactions of **1a-e** discussed in Section 2.2.2, new compounds were observed to form if the temperature exceeded certain rigid limits. In the case of the electron rich **1e**, only very low levels of ^{13}C O could be incorporated because copious amounts of yellow precipitate formed on warming **1e** above -30°C under a ^{13}C O atmosphere. This behavior is in stark contrast to the $\text{Os}(\text{CO})_4(\eta^2\text{-alkyne})$ congeners which are actually stabilized under a CO atmosphere.²⁶ Thus, **1a-e** were reacted with carbon monoxide so as to discover the nature of these unanticipated products.

3.3.1. Formation of Metallacyclobutenones (**5a,b**) from **1a,b**

The most thermally stable member of the series, **1a**, undergoes a slow reaction with CO, eventually resulting in a mixture of a new product **5a** and unreacted **1a** after several days at ambient temperature. Prolonged stirring does not lead to further conversion, and heating the solution leads only to deposition of intractable brown material without evidence for increased formation of product. Fortunately, **5a** is less volatile than **1a** and its isolation is possible by removing the excess reactant by sublimation at -20°C . The trifluoropropyne complex **1b** is much more reactive towards CO, being consumed after 3.5 h at $-10 \leq T \leq 0^\circ\text{C}$. The pentane-soluble product (**5b**) is readily separated from an intractable yellow precipitate which forms during the course of the reaction. Compound **5a** is stable in air for short periods at ambient temperature; both elemental analysis and mass spectrometry suggest the composition

$\text{Fe}(\text{CO})_5(\text{HFB})$. In contrast, **5b** is thermally unstable, even under an inert atmosphere. Consequently, a satisfactory elemental analysis could not be obtained, but an adequate mass spectrum, consistent with an $\text{Fe}(\text{CO})_5(\text{TFP})$ formulation, was obtained using the method outlined in Section 2.2.3.

The IR spectra of each compound are similar and display three terminal CO stretching bands in a medium/medium-strong/very strong intensity pattern. In accord with the weaker electron-accepting ability of TFP compared with HFB, the bands in **5b** (2118, 2062, 2046 cm^{-1}) lie to slightly lower wavenumber than those in **5a** (2126, 2074, 2057 cm^{-1}). Additionally, a signal of medium intensity was detected in the acyl region of the spectrum (1762 cm^{-1} , **5a**; 1760 cm^{-1} , **5b**) and was confirmed to belong to a carbonyl group as the correct isotopic shift was observed upon ^{13}C O enrichment. The HFB complex **5a** displayed an additional, very weak, band at 1629 cm^{-1} which did not shift under the same treatment, suggesting a carbon-carbon stretch and consequently the presence of an olefinic moiety in the compound. Thus, the IR characteristics of **5a,b** suggest that they are ferracyclobut-3-en-2-one complexes formed by the migratory insertion of carbon monoxide into the Fe-alkyne bond (Eq. 3.3).



The ruthenium analog of **5a** is known, as is a structurally characterized PMe_3 -substituted variant.²⁷ The former has an IR spectrum similar to that of **5a** with one exception - four terminal CO bands are observed in accord with the proposed C_s symmetry of the compound. It is thus likely that two bands are accidentally overlapping at the most intense absorptions in **5a,b**. Indeed, in the comparable perfluorinated ferracyclopentan-2-one complex $\text{Fe}(\text{CO})_4\{\eta^1, \eta^1-(\text{CF}_2)_3\text{C}(\text{O})\}$,

only three terminal CO bands are observed in the IR spectrum; furthermore, the acyl stretch was reported at 1734 cm^{-1} (Nujol mull) in general agreement with the pentane solution values for **5a,b**.²⁸

In accord with the ferracyclobutenone formulation, the ^{19}F NMR spectrum of **5a** consists of two equally intense quartets due to the inequivalency of the trifluoromethyl groups. The ^{19}F NMR spectrum of **5b** is a doublet ($^4J_{\text{HF}} = 2.0$ Hz) and the CH proton in the ^1H NMR resonates as a quartet at δ 7.16 ppm, the downfield shift in accord with the CH group being sp^2 hybridized and adjacent to an electron withdrawing group.

While the ^{13}C NMR spectrum of a ^{13}CO enriched sample proved instrumental in confirming the structure of the Ru analog, primarily due to the observation of large $^2J_{\text{CC}(\text{trans})}$ coupling between the resonance of the acyl group and the carbonyl *trans* to it,²⁷ the corresponding spectrum for **5a** is quite complex as a result of observable coupling between mutually *cis* carbonyls. All signals appeared as poorly resolved multiplets as a result, but the anticipated 2:1:1:1 intensity pattern was observed. Unfortunately, unlike the Ru analog, there was no large $^2J_{\text{CC}}$ coupling which would readily identify the equatorial carbonyl *trans* to the acyl group; the magnitudes of the *trans* and *cis* $^2J_{\text{CC}}$ coupling constants are apparently similar in the case of Fe.²⁹ However, in both the Fe and Ru complexes, one signal (δ 196.2 in **5a**) had a relative integration of approximately 0.8 unless a 10 s delay was introduced between pulses. This signal was one of the doublets observed in the Ru compound and was assigned to the acyl group in that complex; a similar assignment is corroborated in the current case. The TFP compound **5b** displayed a similar relaxation-delay dependent integration of one signal at δ 198.58.

Although difficulty was encountered in detecting the carbon resonances of the HFB moiety in **5a**, it was relatively easy to detect the CH signal in **5b** due to the intensity enhancement effect of NOE.³⁰ The chemical shift of the CH carbon (δ 158.64) is some 15 ppm downfield of the range anticipated for sp^2 carbon atoms adjacent to an acyl group in organic compounds,³⁰ while the quartet appearance and $^3J_{\text{CF}}$ coupling constant of 8 Hz are similar to that for the CH group in the parent **1b**. Upon ^{19}F decoupling, the CCF_3 resonance was

detected at δ 156.11. An initial hint that the CH group was adjacent to the acyl moiety was the lack of J_{CH} coupling to the acyl carbonyl in this proton-coupled spectrum. If the CH group were bonded to the metal, large $^3J_{CH}$ coupling approaching 15 Hz would be anticipated due to the *trans* orientation of the proton and acyl carbon on the olefinic moiety; on the other hand, a geminal arrangement would result in much smaller coupling of 0 - 2 Hz.³¹

Further confirmation of the proposed substitution pattern was achieved by collecting an extended $^{13}C\{^1H\}$ NMR spectrum on ^{13}CO enriched **5b**. In accord with the connectivity of the acyl and CH carbons, the CH resonance appeared as a complex multiplet due to $^1J_{CC}$ coupling of *ca.* 35 - 40 Hz magnitude. The complexity of the signal pattern reflects the fact that the ^{13}CO incorporation level was less than 100%, in theory leading to a doublet of quartets pattern overlapping on the original quartet ($^3J_{CF} = 8$ Hz). Nonetheless, the magnitude of the additional coupling ($^1J_{CC} \approx 35 - 40$ Hz) is in full agreement with the range of $^1J_{CC}$ (42 - 51 Hz) found for the C_{ac} -CH bond in $CpMOs(CO)_5\{\mu-\eta^1:\eta^1-(O)CCHCMe\}$ ($M = Co, Rh, Ir$)³² and thus clearly confirms that the CH carbon is bonded to the acyl carbon.

Metallacyclobutenones are relatively rare in the literature. Bimetallic examples with a $\mu-\eta^2:\eta^2$ -metallacyclobutenone ring, where the olefinic double bond is π -bonded to a second metal, have been reported (Figure 3-1),³³⁻³⁶ and Chetcuti has noted that it is interesting that the bulk of these complexes are derived from electron-withdrawing alkynes.³⁷

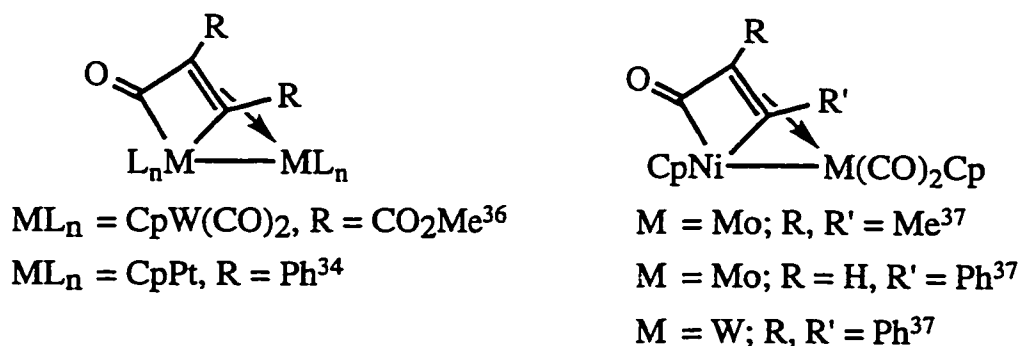
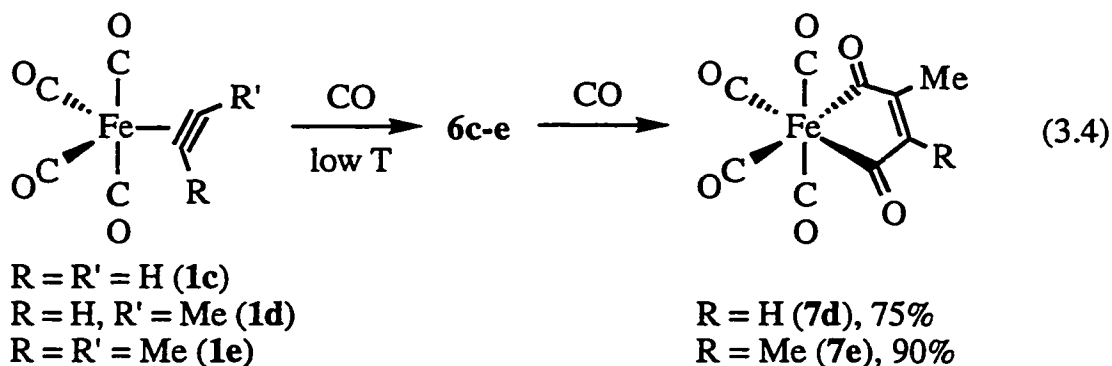


Figure 3-1. Examples of $\mu-\eta^2:\eta^2$ -Metallacyclobutenones.

A few examples of mononuclear metallacyclobutenones incorporating electron deficient alkynes are also known.^{27,38-43} However, to the best of our knowledge, **5a,b** and $\text{Ru}(\text{CO})_3\text{L}\{\eta^1:\eta^1\text{-C}_2(\text{CF}_3)_2\text{C}(\text{O})\}$ ($\text{L} = \text{CO}, \text{PMe}_3$)²⁷ are the first such species to be demonstrably formed *via* migratory CO insertion into a pre-existing metal-alkyne bond at a mononuclear center, a concept proposed by Bird three decades ago,⁴⁴ and one often implicated in mechanisms involving the coupling of alkynes with carbon monoxide leading to cyclic organic products.^{6,45,46}

3.3.2. Synthesis of Ferracyclopent-3-en-2,5-diones (**6c-e**; **7d,e**) from **1c-e**

The more electron rich iron-alkyne compounds are also reactive towards carbon monoxide to differing extents. The most spectacular example is the but-2-yne complex **1e**, which rapidly deposits a bright yellow precipitate (**6e**) when a CO-saturated pentane solution is warmed to -30°C . The propyne analog **1d** is slightly less reactive, producing a pentane-soluble beige compound (**6d**) when warmed to -10°C , and the acetylene complex **1c** is even less reactive, depositing a beige precipitate (**6c**) slowly when warmed to 0°C . Products **6c-e** can be isolated in good yield provided that fairly strict thermal limits are not exceeded. However, above -20°C , **6e** undergoes further reaction with CO to produce the previously known tetracarbonyl-3,4-dimethylferracyclopenta-3-en-2,5-dione **7e**, also available in 11% yield by extended photolysis of $\text{Fe}(\text{CO})_5$ in acetone in the presence of *cis*-3-dibromobut-2-ene.⁴⁷ The corresponding reaction of CO with **6d** occurs at *ca.* 0°C , producing tetracarbonyl-3-methylferracyclopenta-3-en-2,5-dione (**7d**) (Eq. 3.4).



Compound **6c** is more resistant to further reaction with CO, and tends to decompose if warmed to ambient temperature, even under a CO atmosphere. No evidence was found for formation of the acetylene analog of **7d,e**. Compounds **6d,e** are also thermally unstable; stirring each in CH₂Cl₂ at ambient temperature produces **7d,e** in addition to an intractable brown-black solid. The characterization of **6c-e** is deferred until after a brief discussion of the spectroscopic characteristics of the thermodynamic products **7d,e**.

As mentioned above, the stable end-product (**7e**) from the reaction of **6e** with CO has been isolated previously in low yield by a quite different synthetic route.⁴⁷ In fact, substituted tetracarbonylferracyclopenta-3-en-2,5-dione complexes are fairly well known in the literature, having been isolated either as very minor products of thermal reaction of iron carbonyls with alkynes,³ by oxidation of {R₂(OH)₂C₄}Fe₂(CO)₆ in acidic media,⁴⁸ or as one of up to ten products from the reaction of Fe(CO)₅ with alkynes and solid NaOH in refluxing methanol.⁴⁹ The crystal structures of Fe(CO)₄{η¹,η¹-(O)CCHCHC(O)}⁵⁰ and its diethyl-substituted variant⁴⁹ have been published. The unsymmetrical analog **7d** has also been mentioned briefly in an early communication,⁴⁸ but no spectroscopic or analytical data were published. Accordingly, full characterization of **7d** was carried out, and the previously unreported ¹³C NMR spectrum of **7e** was also collected for comparison.

Both compounds displayed four terminal CO stretching bands in the IR spectrum, in addition to a single (**7e**) or a pair of acyl bands (**7d**). The ¹H NMR spectrum of **7d** consisted of a low field singlet of intensity one at δ 7.20 for the CH proton and a high field singlet at δ 2.03 for the methyl group; the former is quite similar to the δ 7.54 value reported for Fe(CO)₄{η¹,η¹-(O)CCHCHC(O)}⁵⁰ while the latter agrees with the δ 1.95 value in **7e**. The ¹³C NMR data (Table 3-1) are fully consistent with the proposed structure. The most notable feature is that the acyl carbonyls resonate in the far downfield region of the spectrum, suggesting carbenoid character due to partial Fe-C_{ac} double bonding. A similar conclusion was reached in the crystallographic study of Fe(CO)₄{η¹,η¹-(O)CCHCHC(O)}.⁵⁰ The terminal carbonyl groups are found at virtually the same chemical shift in all three compounds, and the asymmetry of **7d** allows for the

distinction between axial and equatorial groups which was previously not possible in the C_{2v} symmetrical $\text{Fe}(\text{CO})_4\{\eta^1, \eta^1\text{-(O)CCHCHC(O)}\}$. Additionally, there is a close correlation between the chemical shifts of the olefinic carbons in **7d** and the symmetrical compounds, with the *CH* resonances being found upfield of the *CMe* signals.

Table 3-1. $^{13}\text{C}\{^1\text{H}\}$ NMR Spectra (δ , ppm) of $\text{Fe}(\text{CO})_4\{\eta^1, \eta^1\text{-(O)CCRCR}'\text{C(O)}\}$.

	R	R'	CO_{ac}	CO_{ax}	CO_{eq}	<i>CMe</i>	<i>CH</i>
a	H	H	245.1	201.5	199.4	–	162.3
7d^b	H	Me	243.82, 242.50	202.57	200.38, 200.16	175.57	159.19 ^c
7e^b	Me	Me	242.07	202.91	200.40	169.58	–

^ain CDCl_3 , data from Ref. 50. ^bin CD_2Cl_2 . ^copposite phase in the APT spectrum.

The intermediate compounds, **6c-e**, were slightly more challenging to characterize. The elemental compositions and electron impact (EI) mass spectra were consistent with a species of basic formula " $\text{Fe}(\text{CO})_5(\text{alkyne})$ ", suggesting a metallacyclobutenone structure. However, the IR spectra were substantially different than those of **5a,b**. The highest frequency CO bands in **6c-e** were well below 2100 cm^{-1} , in contrast to the high frequency stretches at *ca.* 2120 cm^{-1} in **5a,b**. The intensity patterns in **6c-e** resembled those of **4a,b**, suggesting the presence of an $\text{Fe}(\text{CO})_3$ group. Furthermore, two or three bands were observed between *ca.* $1850 - 1760\text{ cm}^{-1}$. These lie to higher energy than the acyl bands in the metallacyclobutenones, but to lower frequency than anticipated for terminal carbonyls. The ^1H NMR spectra also did not fit a metallacyclobutenone formulation, as the *CH* proton in **6d** resonated much further upfield (δ 4.39) than in **5b** (δ 7.16). Furthermore, only one singlet resonance was observed for **6c** at δ 4.39, rather than the two doublets expected for a ferracyclobutenone. A single resonance was also observed for the two methyl groups in **6e**, suggesting that the alkyne moiety in this compound was also symmetrical.

The ^{13}C NMR spectra (Table 3-2), obtained with ^{13}CO enriched material, provided the clinching spectroscopic proof. At -40°C , compounds **6c,e** displayed

2:3 patterns in the carbonyl region, with the signals of intensity two appearing at *ca.* δ 229 ppm relative to the singlet of intensity three at approximately δ 206 ppm. The latter is typical of an $\text{Fe}(\text{CO})_3$ moiety undergoing rapid scrambling of the carbonyl ligands,¹⁹ and, consistent with this proposal, cooling the samples to -110 and -100°C respectively resulted in decoalescence and the appearance of a 1:2 pattern; no change was observed in the downfield singlet of intensity two apart from a slight temperature dependence of the chemical shift (Figure 3-2).

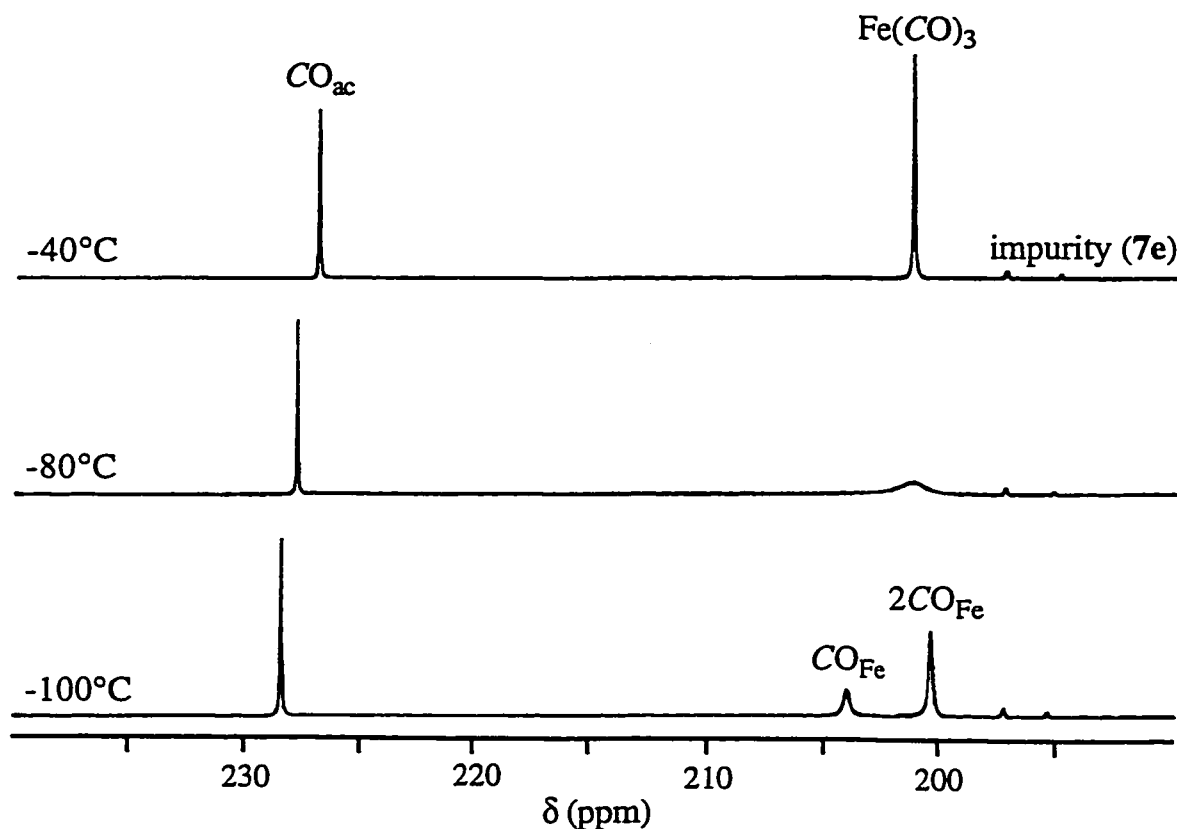


Figure 3-2. Variable Temperature ^{13}C NMR (CD_2Cl_2 , 100.6 MHz) of Compound **6e** in the Carbonyl Region.

The quaternary carbons derived from the symmetrical alkyne moieties were detected as singlets at δ 39.22 (**6c**) and 67.10 (**6e**). In accord with the pattern suggested by the IR spectra, the downfield signals are thus assigned to a pair of equivalent acyl carbonyls. In agreement with this proposal, the CH and CMe signals displayed characteristic $^1J_{\text{CC}}$ coupling constants of 39 and 38 Hz

magnitude respectively. The ^{13}C NMR spectrum of **6d** has features similar to those of **6c,e**. The low temperature limiting spectrum gave a 1:1:1 pattern for the terminal carbonyls, due to the asymmetry of the propyne moiety, and both CR groups were coupled to acyl carbonyls. Thus, compounds **6c-e** contain a ferracyclopenta-3-en-2,5-dione ring.

Table 3-2. $^{13}\text{C}\{^1\text{H}\}$ NMR Spectra (CD_2Cl_2 , 400.1 MHz) of ^{13}C O Enriched **6c-e**.

Compound	$\delta \text{CO}_{\text{ac}}$	$\delta \text{CO}_{\text{ax}}$	$\delta \text{CO}_{\text{eq}}$	δCMe	δCH
6c	228.81	206.8 ^a	204.7 ^a	–	39.22 ^{b,c}
6d	230.55, 227.41	207.14 ^d	204.92, 204.06 ^d	62.44 ^e	47.69 ^{c,f}
6e	229.51	207.57 ^c	204.24 ^c	67.10 ^g	–

^aat -110°C . ^bappeared as a pseudo doublet, $^1J_{\text{CC}} = 39$ Hz. ^copposite phase in the corresponding APT spectrum. ^dat -100°C . ^epseudo doublet, $^1J_{\text{CC}} = 34$ Hz. ^fpseudo doublet, $^1J_{\text{CC}} = 38$ Hz. ^gwith ^{13}C satellites, $^1J_{\text{CC}} = 38$ Hz.

However, unlike compounds **7** discussed above, the current species are distinguished by the presence of only three terminal carbonyl ligands. At first glance, this would render the Fe center unsaturated with a 16 electron count, but the position of the CR resonances, 100 - 120 ppm further upfield in **6c-e** than in their tetracarbonyl analogs (Table 3-1), clearly implies that there is a significant change in the nature of the olefinic moiety. In fact, upfield shift of olefinic carbon resonances is a well-recognized spectroscopic marker for coordination to a transition metal.⁵¹ On this basis, a dimeric structure is proposed for **6c-e**, Figure 3-3, in which the electron deficiency at one iron is removed by coordination of the olefinic function of the other. Apart from the clear ^{13}C NMR evidence, it has proven difficult to confirm the dimeric nature of **6c-e** by other methods. For example, the electron impact (EI) mass spectra of **6c-e** display peaks due only to " $\text{Fe}(\text{CO})_3\{\eta^1, \eta^1\text{-}(\text{O})\text{CCR}'\text{C}(\text{O})\}$ ", while fast atom bombardment (FAB) reveals peaks up to 1.5 times the predicted molecular mass. The former observation clearly suggests that the dimer is readily cleaved into its monomeric constituents while the latter is likely a result of the thermal instability of the compounds as they must be introduced into an inert matrix prior to obtaining the FAB spectrum

at ambient temperature. Finally, attempts to obtain crystals suitable for X-ray crystallography have thus far met with failure, again largely due to the slow thermal decomposition of the dimers to the thermodynamically stable **7** under crystal growth conditions.

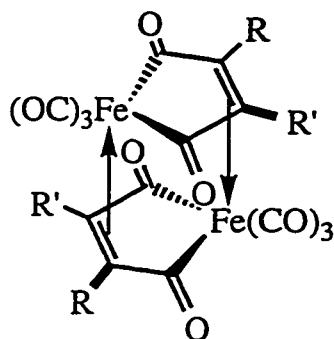


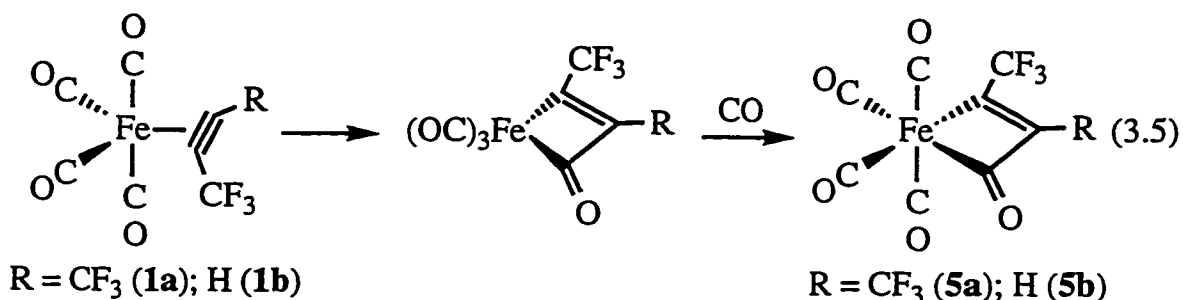
Figure 3-3. Proposed Dimeric Structure for **6c-e**.

It is interesting to note that only one of the two possible isomers are observed for the unsymmetrical compound **6d**, and it is suggested that this is the C_i isomer, as depicted in Figure 3-3. Although its C_2 counter-part would have an identical ^{13}C NMR pattern, it seems likely that steric effects would be present if the methyl substituents were both present on the same side of the structure. This perhaps explains why **6e** converts readily to **7e** on warming above -20°C in the presence of CO while **6c** does not form the corresponding tetracarbonylferracyclopenta-3-en-2,5-dione under the same conditions; the methyl substituents in **6e** may sterically restrict the degree of iron-olefin bonding that can be achieved, ultimately enhancing separation of the dimer into its monomeric components which readily react with an additional ligand. In this sense, it is interesting to note that the coordination shift (relative to compounds **7**) in **6c** is $+123.1$ ppm compared with $+102.5$ ppm in **6e**; the larger magnitude in the case of **6c** suggests greater rehybridization of the CH carbons from sp^2 towards sp^3 and thus stronger Fe-CH bonding than the Fe-CMe bonding present in **6e**.

3.4. Proposed Mechanisms for Fe-Mediated Coupling of Alkynes with CO

3.4.1. Reaction of $\text{Fe}(\text{CO})_4(\eta^2\text{-alkyne})$ Compounds with CO

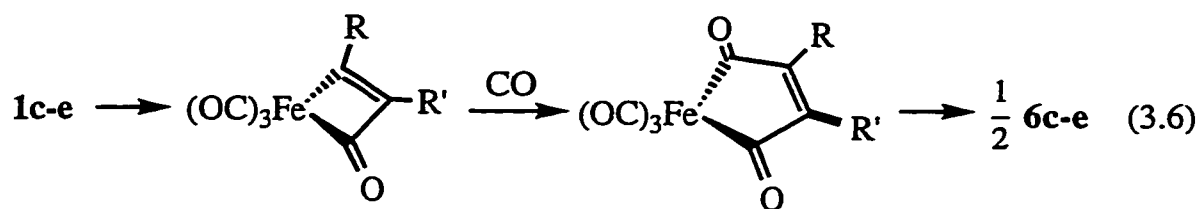
The first question to be addressed is why it is the more electron rich alkynes in complexes **1c-e** that undergo two sequential migratory CO insertions to produce **6c-e** while the more π -acidic alkynes in **1a,b** produce the metallacyclobutenones **5a,b**. In this context, it is important to remember that the key element which is likely to influence the initial reactivity of the iron-alkyne compounds is the so-called "four electron destabilization" present between the filled π_{\perp} orbital of the alkyne and the corresponding filled d -orbital on the metal center (see Section 1.2.1). The filled/filled repulsion in the iron complexes is apparently sufficient to weaken the Fe–C_{alkyne} bond and render it nucleophilic to facilitate migratory insertion of a carbonyl and to produce the metallacyclobutene, which has no residual repulsive interactions between filled orbitals on the metal and ligand. In the case of the π -acidic alkynes in **5a,b**, the creation of a strong Fe–C(CF₃) σ -bond appears to be sufficient to stabilize the inherently strained four-membered metallacycle (Eq. 3.5).



In the case of the unsymmetrical TFP ligand, the regioselective migration of the CH carbon is consistent with the normal substituent dependence for alkyl group migration.⁵²

Apparently, with less electron-withdrawing or electron-donating substituents, the bond strain present in the four-membered ring is sufficient to overcome the weaker Fe–CH or Fe–CMe bonds, promoting a second migration and formation of a ferracyclopenta-3-en-2,5-dione ring. The uptake of an

additional mole of CO at this stage still leaves the active species unsaturated, a situation rectified by dimerization to form **6c-e** (Eq. 3.6).



When the reaction was carried out under a ^{13}CO atmosphere, it was possible to qualitatively gauge the relative rate of CO exchange (Section 2.2.2) compared to CO insertion. The CH signal of **6c** appeared as a pseudo doublet in the ^{13}C NMR spectrum due to the high level of ^{13}CO incorporation into the metallacycle. In contrast, the CMe carbons of **6e** exhibited a singlet with weak ^{13}C satellites (Figure 3-4).

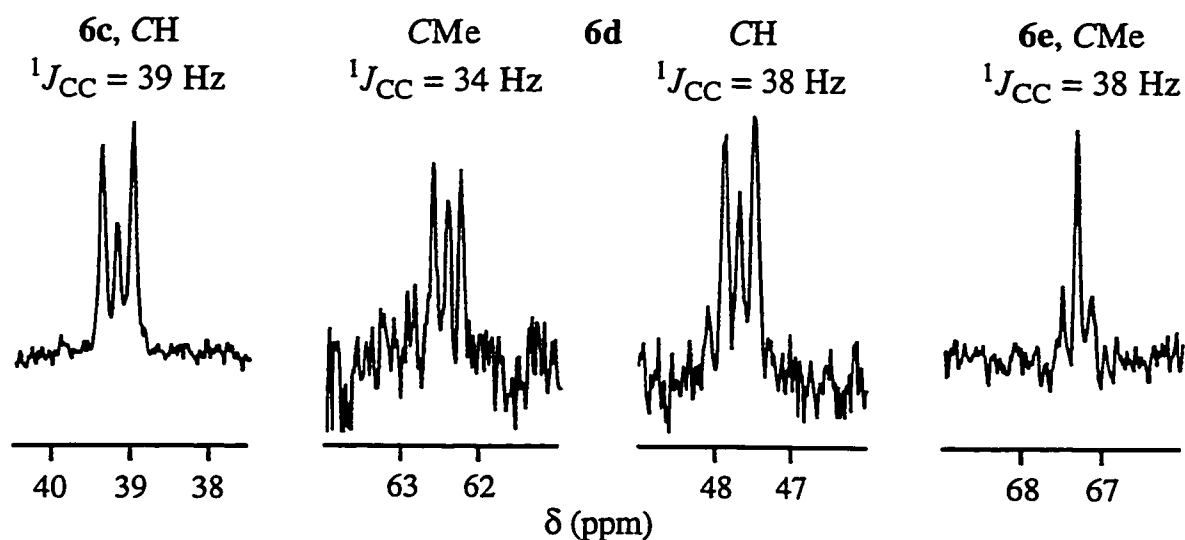


Figure 3-4. ^{13}C NMR (100.6 MHz, CD_2Cl_2) of the CR Resonances in **6c-e**.

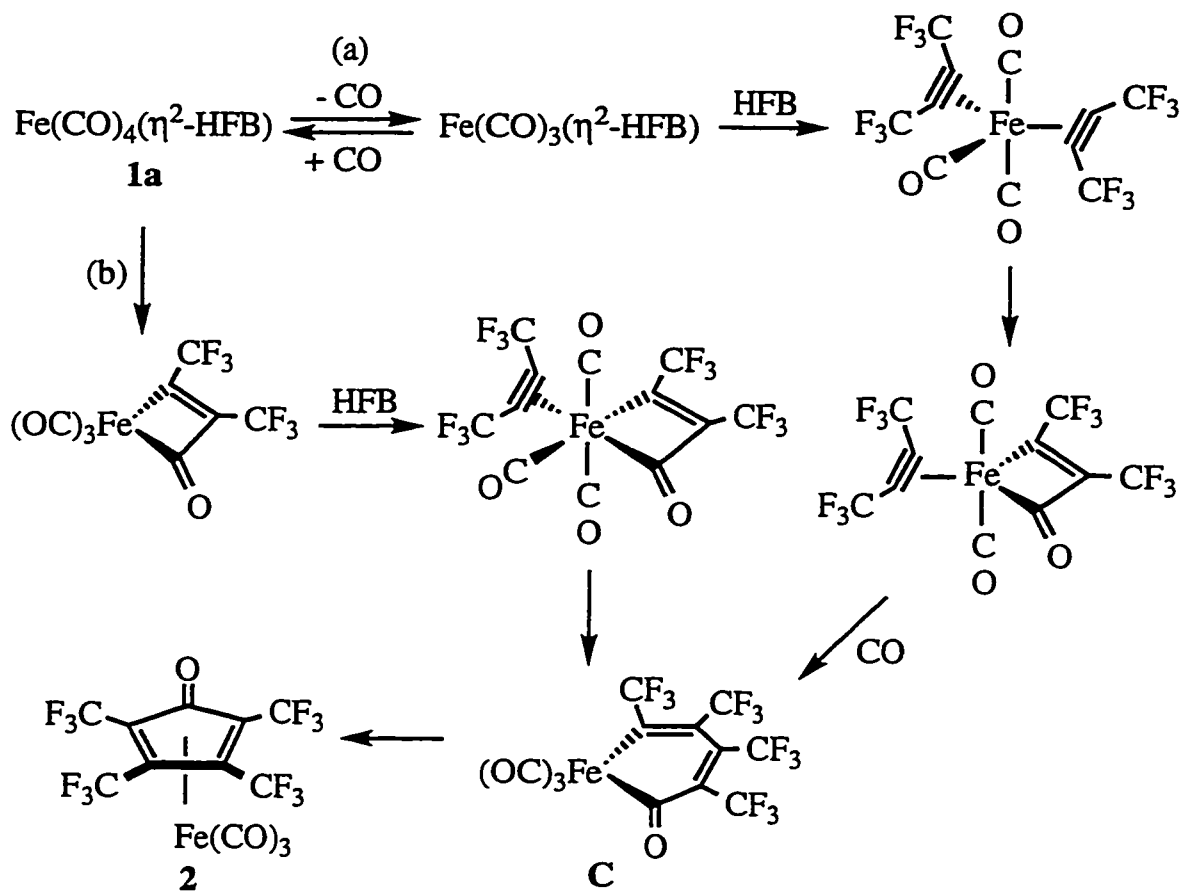
The latter observation reinforces the rapidity of the reaction of $Fe(CO)_4(\eta^2-C_2Me_2)$ with CO; very little ^{13}CO exchange occurs (*ca.* 20% based on the relative intensity of the satellites) as "CO insertion" is more facile. Complex **6d** displays a pattern similar to that of **6c**, consistent with a high level of ^{13}CO

incorporation into the acyl groups. Bearing in mind the more rapid formation of **6d** compared with **6c**, the order of reactivity towards CO is $1e \gg 1d > 1c$ which suggests that the greater the initial $4e^-$ destabilization in the $\text{Fe}(\text{CO})_4(\eta^2\text{-alkyne})$ complex, the greater is the rate of migratory CO insertion to remove the destabilizing filled/filled interaction. It is also clear that the iron-alkyne bonds are more labile towards migratory CO insertion than their third row congeners as no reaction is observed when $\text{Os}(\text{CO})_4(\eta^2\text{-alkyne})$ species are exposed to CO.

3.4.2. Proposed Pathways for Formation of Cyclic Organic Ligands in 2-4.

With an appreciation for the types of cyclic products available from the reaction of compounds **1** with alkynes and their independent reactivity towards carbon monoxide, it is possible to propose the mechanisms by which such transformations probably occur. Beginning with compound **2**, derived from the π -acidic hexafluorobut-2-yne complex **1a**, two probable routes can be envisioned. Washington *et al.* proposed initial CO dissociation followed by alkyne coordination and coupling to rationalize the formation of the $\text{Os}(\text{CO})_3\{\eta^4\text{-C}_4\text{Me}_2\text{R}_2(\text{O})\}$ complexes described in Eq. 3.2, and it seems reasonable that such a mechanism could apply to **1a** given the even greater lability of its attendant carbonyl ligands (Scheme 3-2a). On the other hand, the fact that **1a** reacts with CO to form **5a** suggests that the coordination of the second alkyne may occur following initial migratory CO insertion (Scheme 3-2b) into the Fe-alkyne bond; both mechanisms proceed through a common intermediate labelled **C**, and it is only the mode of initiation that differs. Washington and co-workers reasoned that, following initial CO loss and uptake of additional alkyne, the "CO insertion" step in route (a) was brought about by stronger four-electron destabilization as a result of having two alkynes within the coordination sphere of a d^8 metal. As suggested in section 3.4.1, it is possible that **1a** is sufficiently destabilized with only one alkyne coordinated to facilitate initial alkyne migration onto a terminal CO (route (b)) which frees a coordination site, removing the offending source of the destabilizing interaction in doing so. The vacant site is then occupied by a second alkyne which readily couples with the existing organic fragment; of paramount importance in the formation of the

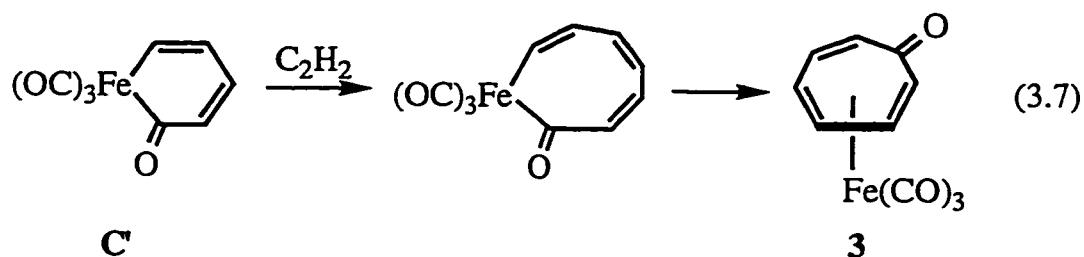
cyclopentadienone ring is the stability of the initial tricarbonylferracyclobuteneone species towards further "CO insertion". Path (b) has the additional advantage of not requiring scavenging of previously dissociated CO to complete the cycle. However, given the much greater rate of $^{12}/^{13}\text{C}$ exchange in **1a** compared with CO insertion to form **5a**, route (a) should not be entirely discounted.



Scheme 3-2. Possible Mechanisms for the Reaction of **1a** with HFB.

The build-up of the tropone ring system in **3** likely follows a route analogous to (b) in Scheme 3-2, with the exception that a further mole of acetylene is taken into the vacant coordination site and inserted into the Fe–CH bond of **C'** prior to cyclization (Eq. 3.7). Presumably, as with the formation of **2** discussed above, the initial ferracyclobutenone ring system must be relatively

stable towards further "CO insertion". Although it is true that only the tricarbonylferracyclopenta-3-en-2,5-dione dimer is produced from reaction of **1c** with CO, the relative slowness of this reaction compared to **1d,e** under the same conditions suggests a reluctance to undergo the second migratory insertion. However, the relatively low yield of **3** (*ca.* 25%) and abundance of black, intractable, and presumably²³ polymeric material, suggests that another pathway is also available from **1c**, but it is unclear how this process is initiated or perpetuated.



At this juncture it is notable that none of **1a-e** react cleanly with a different added alkyne, even in the presence of CO, and products resulting from alkyne exchange predominate in certain cases. Thus, combining either **1c** or **1e** with C_2Et_2 , with or without added CO, afforded the tetraethyl-*p*-quinone complex **4b** as the major species in solution. In fact, upon adding C_2Et_2 to a solution of $\text{Fe(CO)}_4(\eta^2\text{-C}_2\text{H}_2)$ (**1c**), the intensity of the IR bands due to the acetylene complex decreased, and those due to $\text{Fe(CO)}_4(\eta^2\text{-C}_2\text{Et}_2)$ (**1f**) predominated (Figure 3-5). This observation is analogous to that reported by Hübel for the reaction of C_2Et_2 with $\text{Fe(CO)}_4(\eta^2\text{-C}_2^t\text{Bu}_2)$ (Chapter 1, Eq. 1.6).³ The likely mechanism for this mode of reactivity is given in Scheme 3-3. In line with the facile CO lability in compounds **1**, it is proposed that CO dissociation initiates the reaction and that the incoming alkyne $\text{C}_2\text{R}'_2$ occupies the vacant coordination site. The resulting increase in $4e^-$ destabilization is not relieved by a coupling reaction with CO at this stage, but rather leads to dissociation of the original alkyne, $\text{C}_2\text{R}'_2$. The newly formed $[\text{Fe(CO)}_3(\eta^2\text{-C}_2\text{R}'_2)]$ is then free to react with additional $\text{C}_2\text{R}'_2$, and CO liberated in the first step, to form products such as **4b** ($\text{R}' = \text{Et}$). It is unlikely that migratory CO insertion initiates alkyne exchange as

the resulting unsaturated ferracyclobutenone would be expected to couple with the entering alkyne. This type of reactivity is in notable contrast to that of $\text{Os}(\text{CO})_4(\eta^2\text{-C}_2\text{Me}_2)$ which reacts with C_2R_2 to form the cyclopentadienone complexes $\text{Os}(\text{CO})_3\{\eta^4\text{-C}_4\text{Me}_2\text{R}_2(\text{O})\}$ (Eq. 3.2),⁶ and further suggests that the Fe-alkyne bonds in **1** are more labile than those in the third row Os counterparts.

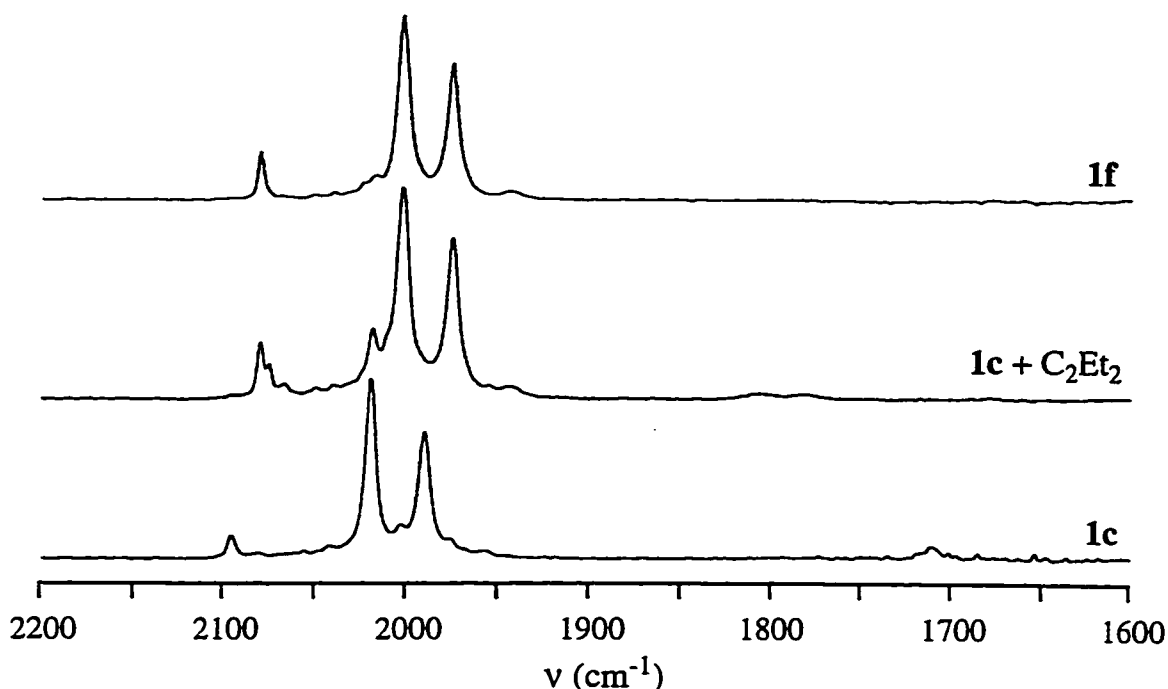
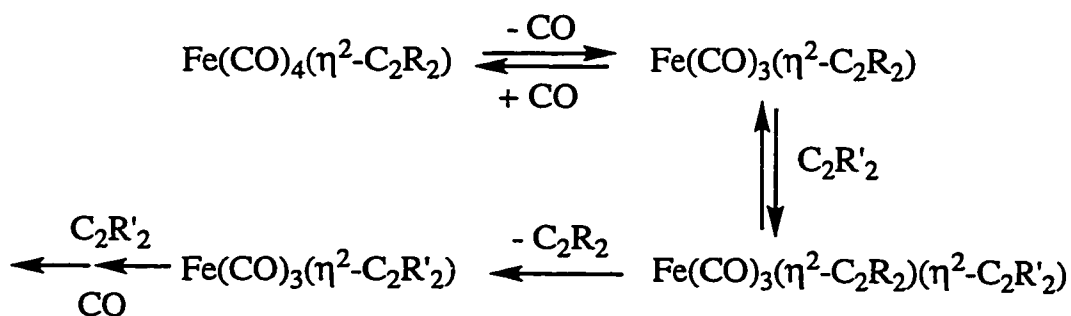
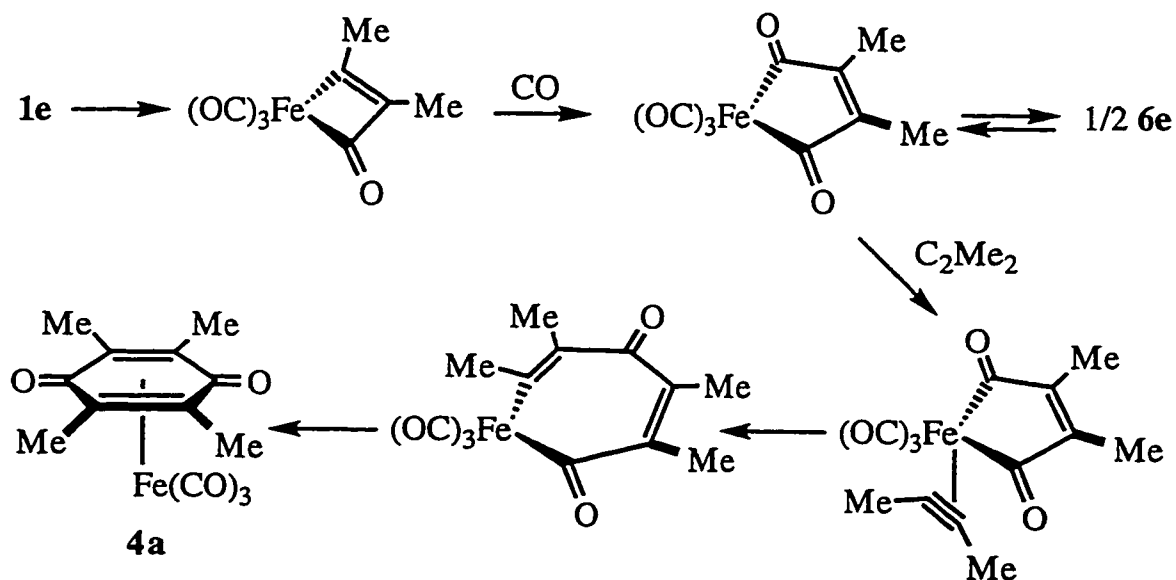


Figure 3-5. Solution IR Spectra Before and after Addition of C_2Et_2 (0.1 M) to **1c** (0.01 M) in Pentane.



Scheme 3-3. Proposed Mechanism for Alkyne Exchange in **1**.

Although compounds **2** and **3** appear to follow similar reaction pathways, most likely involving initial migratory CO-insertion into the Fe-alkyne bond, the formation of the *p*-quinone complexes **4a,b** probably follows a different route. Given that the synthesis of **4a** from **1e** requires an additional mole of CO and that reaction of **1e** with CO is very facile, it seems probable that the ferracyclopenta-3-en-2,5-dione product **6e** is an intermediate on the reaction pathway. This proposal is readily verified. Addition of C₂Me₂ to a CH₂Cl₂ solution of **6e** at -30°C results in rapid darkening of the color of solution from yellow to orange and the resulting IR spectrum is identical to that of isolated **4a**. Thus, the *p*-quinone ring system is built up first by sequential migration of each end of the alkyne onto a terminal carbonyl ligand to form a ferracyclopenta-3-en-2,5-dione ring as in Eq. 3.6 (*vide supra*). The incoming alkyne coordinates at the open site on the monomer, and then couples with an acyl group to form an unstable ferracyclohepta-3,6-dien-2,5-dione ring, closure of which results in the final *p*-quinone complex **4a** (Scheme 3-4).



Scheme 3-4. Proposed Mechanism for Formation of **4a**.

Unsaturated ferracyclopenta-3-en-2,5-dione species have been previously suggested in the formation of *p*-quinones at an Fe center. Soon after the

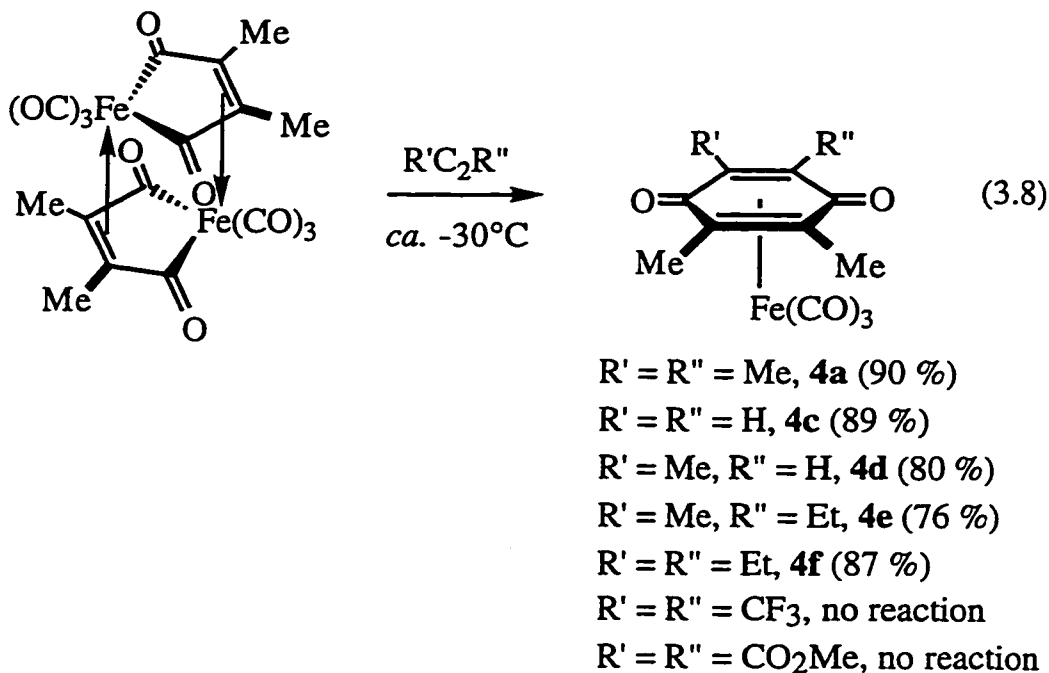
publication of the reaction in Eq. 3.1, Orgel proposed $\text{Fe}(\text{CO})_4(\eta^2\text{-C}_2\text{Me}_2)$ and " $\text{Fe}(\text{CO})_2\{\eta^1, \eta^1\text{-(O)CCMeCMeC(O)}\}$ " as potential intermediates.² Heck has also commented on the potential intermediacy of this type of "maleoyliron" compound, noting that since isolated species such as **7** do not react further with alkynes, the actual intermediate is likely a CO-dissociated form.⁵³ Other reviewers have noted that, despite much speculation, the path by which *p*-quinones and the related hydroquinones form in syntheses from metal carbonyls is not clear.^{45,54} Thus, the isolation of **1e** and **6e** finally identify the actual reaction pathway for formation of the *p*-quinone complex **4a**, nearly four decades after its initial isolation.

3.5. Reaction of Compounds **6d,e** with Alkynes: A General Synthesis of Substituted Tricarbonyl(*p*-quinone)iron Complexes

3.5.1. Synthetic Aspects

Although the ready reaction of the isolated dimeric species **6e** with but-2-yne provided confirmatory proof of the mode of formation of **4a**, it also immediately suggested a general synthetic route to unsymmetrically substituted tricarbonyliron(*p*-quinone) complexes. Namely, if C_2Me_2 reacted readily with the intermediate dimeric species, then it logically followed that other alkynes should do so. Accordingly, **6e** was reacted with a variety of alkynes; the results are summarized in Equation 3.8. The successful reactions all took place at approximately -30°C and clearly demonstrated the high reactivity of the stabilized $[\text{Fe}(\text{CO})_3\{\eta^1, \eta^1\text{-(O)CCMeCMeC(O)}\}]$ intermediate. The synthesis appears to be limited to relatively electron rich alkynes, as attempts to react **6e** with either $\text{C}_2(\text{CF}_3)_2$ or $\text{C}_2(\text{CO}_2\text{Me})_2$ resulted only in decomposition of the dimer. Nonetheless, the above method is an excellent means of targeting *p*-quinone complexes with a 2,3-Me-5-R'-6-R" substitution pattern, especially given the lack of success in doing so by reacting **1e** with $\text{C}_2\text{R}'_2$ under a CO atmosphere (*vide supra*). Liebeskind has recently shown that related substituted phthaloyliron compounds can couple with alkynes to produce substituted naphthoquinones, but the reactions required temperatures of 100°C to initiate the reaction (Chapter 1, Eq. 1.9).⁵⁵ Maitlis has also reported the synthesis of an

inseparable mixture of 2,3-diethyl-5,6-dimethyl-1,4-benzoquinone and tetramethyl-1,4-benzoquinone from an amorphous solid believed to contain a 3,4-dimethylrhodacyclopenta-3-en-2,5-dione species.⁵⁶

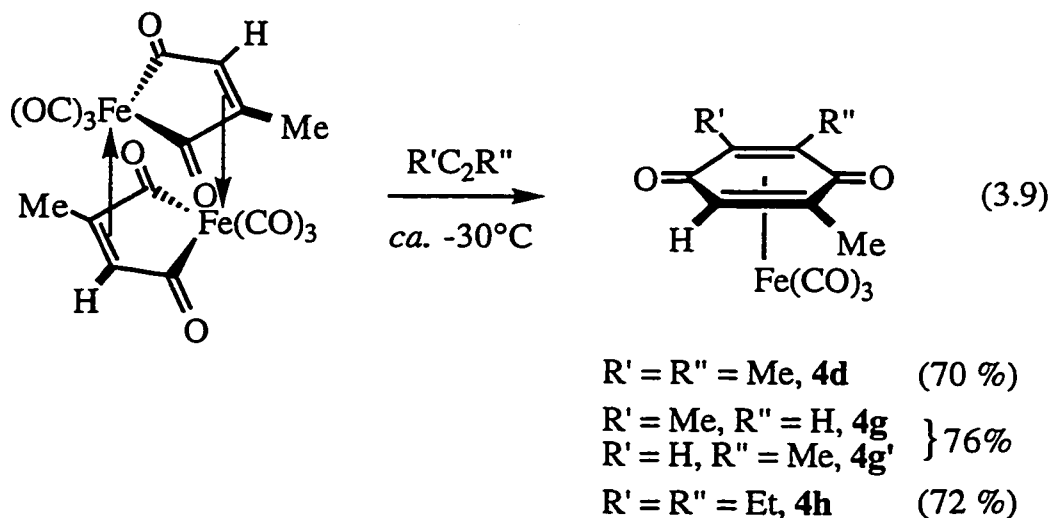


The isolated compounds **4c-f** are all air and thermally sensitive to varying degrees, with greater levels of alkyl substitution affording enhanced stability. Complex **4c** is the least stable member of the series, decomposing in an inert atmosphere within minutes at ambient temperature or pyrophorically if exposed to air. On the other hand, complexes **4e,f** are stable at room temperature under a nitrogen atmosphere and can be handled quickly in air, with prolonged exposure causing decomposition to a black solid. The relatively low stability of compounds **4** can be traced to the lack of conjugation of the two carbon-carbon double bonds in the ring system; in contrast, $\text{Fe}(\text{CO})_3$ fragments are known to form particularly strong bonding interactions with *cis*-conjugated dienes as is the case in complexes **2** and **3**.⁵⁷

The successful incorporation of unsymmetrically substituted alkynes into the *p*-quinone framework raised the question as to whether the dimers derived from acetylene (**6c**) and propyne (**6d**) would also react with alkynes to allow

greater flexibility in the substitution patterns available. Unfortunately, **6c** proved unreactive towards all alkynes save but-2-yne which afforded the unstable complex **4c**, a compound more readily synthesized from **6e**. This result reinforces the conclusion derived from the observation that **6c** is also unreactive towards CO; that is, the olefinic moiety in **6c** is more strongly coordinated than in the dimethyl-substituted **6e**. The fact that **6c** reacts with but-2-yne but not the ethyl-substituted pent-2-yne and hex-3-yne suggests that the approach of the alkyne may be sterically hindered in some manner, while the lack of reactivity of acetylene and propyne likely reflects the need for at least two stabilizing alkyl substituents in the final *p*-quinone product.

Despite the general lack of success at producing *p*-quinone products from **6c**, the propyne-derived analog **6d** proved reactive towards the same range of alkynes as **6e** with the exception of acetylene (Eq. 3.9).



The lack of reaction of acetylene with **6d** reinforces the contention that at least two alkyl substituents are required to stabilize coordination of the *p*-quinone ring to the $\text{Fe}(\text{CO})_3$ fragment in this type of complex. As will be shown in section 3.5.2, complex **4g** was obtained as a mixture of two isomers, demonstrating a lack of regioselectivity in cases where neither of the original alkynes employed is symmetrical. Furthermore, the formation of this complex contrasts with the reaction of **1d** with propyne which leads predominantly to intractable materials,

even in the presence of added CO. As discussed above for the reaction of **1c** with acetylene, this may reflect the possibility that **1d** can react with propyne prior to reacting with CO, ultimately in a manner which does not lead to isolable organometallic products. Finally, in line with the general trends established for the stabilities of **4c-f**, compound **4g** decomposes rapidly at ambient temperature, even under an inert atmosphere, while the 2,3-diethyl-5-methyl-1,4-benzoquinone complex **4h** can be handled in air for short periods without noticeable degradation.

3.5.2. Characterization of the Tricarbonyl(*p*-quinone)iron Products

The molecular formulation of compounds **4e,f,h** was readily confirmed by both mass spectrometry and elemental analysis, although some care was needed owing to their slight thermal instability and air sensitivity. The relative ease of cleavage of the *p*-quinone ring from the Fe center was evident in the mass spectra which detected intense signals derived from the free *p*-quinone ligand in addition to peaks attributable to the organometallic species and those resulting from loss of terminal carbonyls. However, the extreme thermal instability of compounds **4c,d,g** prevented characterization by these methods.

The IR spectra of **4a-h** confirm a tricarbonyl formulation at the Fe center. Also, two bands were generally observed in the 1650 - 1610 cm⁻¹ region for the symmetric and asymmetric stretching of the ketone groups. In the case of **4b**, coordination of the *p*-quinone to the metal center renders the previously IR inactive symmetrical stretching mode observable because a change in dipole moment is achieved; this agrees with what is observed in free 2,6-disubstituted-1,4-benzoquinones⁵⁸ where the same criterion applies. The average frequencies of the ketone stretches generally decrease with increasing levels of alkyl substitution, a pattern also reported for the free 1,4-benzoquinone ligands.⁵⁹ Furthermore, a corresponding trend emerges for the band positions due to the Fe(CO)₃ moiety; again, increasing levels of alkyl substitution result in a decrease in the terminal CO stretching frequencies. The observed trend is in line with expectations of the metal-ligand bonding interaction depending heavily on σ -donation. Hence, the more donating the *p*-quinone ligand is to the strongly

accepting Fe(CO)₃ moiety, the lower are the terminal CO stretching frequencies. Table 3-3 illustrates this trend; the compounds have been ordered according to increasing levels of alkyl substitution and thus decreasing ν_{CO} .

Table 3-3. FT-IR Spectra (ν , cm⁻¹) of **4a-h**.

	R	R'	R''	ν_{CO}	$\nu(\text{C}=\text{O})$	
4c^a	Me	Me	H	H	2082(vs), 2027(s)	1648(sh), 1630(m)
4g^a	Me	H	Me	H	2082(vs), 2028(s), 2006(s)	1630 (m, br)
4d^a	Me	Me	Me	H	2077(vs), 2023(s)	1635(m), 1615(m)
4h^a	Me	H	Et	Et	2076(vs), 2022(s)	1635(m), 1611(m)
4a^b	Me	Me	Me	Me	2067(vs), 2014(s), 2010(sh)	1638(w, br)
4e^a	Me	Me	Me	Et	2072(vs), 2017(s)	1630(w), 1609(w)
4f^a	Me	Me	Et	Et	2072 (vs), 2020 (s)	1632(w), 1608(w)
4b^b	Et	Et	Et	Et	2067(vs), 2014(s), 2008(s)	1645(w), 1620(w)

^aCH₂Cl₂. ^bpentane.

The sequence of thermal stabilities nicely mirrors the above trend, where the least stable species **4c,g** have the highest ν_{CO} values while the more stable tetraalkyl complexes **4a,b,e,f** have lower CO stretching frequencies. This may also explain why electron poor alkynes are unreactive towards **6c-e**, as electron withdrawing substituents might render the *p*-quinone ring too electron poor to stabilize the Fe(CO)₃ fragment. Qualitatively, though, there is a difference in stability between the derivatives containing methyl and ethyl substituents, suggesting that substituent bulk may also play a role.

The ¹H NMR data of **4a-h** (Table 3-4) agree with the proposed formulations. The CH resonances in **4c,d,g,h** are all further upfield by some 1.5 ppm compared with the δ 6.8 to 6.5 range found in substituted free 1,4-benzoquinones,⁵⁸ the upfield shift being characteristic of the bonding of an olefinic moiety to a metal center. The downfield shift of the methyl groups bonded to quaternary carbons in the *p*-quinone ring relative to those within ethyl groups is also common.³⁰ More importantly, the ethyl substituted complexes reveal a pair of doublets of quartets ($^2J_{\text{HH}} = 12.5$ Hz, $^3J_{\text{HH}} = 7.5$ Hz) for each

methylene group. Coordination to the metal center removes the mirror plane defined by the ring carbons, and consequently renders the CH₂ protons diastereotopic. The two-bond H-H coupling constant of 12.5 Hz between the adjacent methylene protons agrees with that commonly observed in aliphatic organic compounds, as does the ³J_{HH} coupling constant of 7.5 Hz to the protons of the neighboring methyl group.³⁰

Table 3-4. ¹H NMR Chemical Shifts (δ, ppm) in 4a-h (CD₂Cl₂, 400.1 MHz).

	R	R'	R''	H	CH ₂ Me ^a	Me	CH ₂ Me ^b	
4a	Me	Me	Me	Me	—	—	1.98	—
4b	Et	Et	Et	Et	—	2.90 2.10	—	1.26
4c	Me	Me	H	H	4.93	—	2.01	—
4d	Me	Me	Me	H	4.96	—	2.03 1.95 1.95	—
4e	Me	Me	Me	Et	—	2.84 1.92	2.04 2.01 2.00	1.15
4f	Me	Me	Et	Et	—	2.60 2.16	2.01	1.24
4g	Me	H	Me	H	4.96	—	1.97	—
4g'	Me	H	H	Me	5.21	—	1.89	—
4h	Me	H	Et	Et	5.06	2.71 2.55 2.11 2.09	1.98	1.24 1.19

^adoublet of quartets, ²J_{HH} = 12.5 Hz, ³J_{HH} = 7.5 Hz. ^btriplet, ³J_{HH} = 7.5 Hz.

The ¹³C NMR data (Table 3-5) also agree with the proposed structures. In compounds 4c,d,g,h, the CH carbons are readily identified as they are found in the opposite phase in the corresponding APT spectra. In accord with the ¹³C NMR spectra of free *p*-quinones, the alkyl-substituted quaternary carbons resonate further downfield than unsubstituted ring carbons.⁶⁰ Assignment of the quaternary carbon resonances bearing ethyl and methyl groups, such as 4e,h, is based on the observation that δ C_{Et} in 4b is further downfield than δ C_{Me} in 4a.

While this criterion can also be applied to **4f**, the assignment is somewhat ambiguous as the chemical shifts of the quaternary carbons differ by a mere 0.4 ppm. As in the free ligands, the different substitution patterns have a significant influence on the chemical shifts of the olefinic carbons while the ketone carbons remain largely unperturbed.

Table 3-5. ^{13}C NMR Chemical Shifts (δ , ppm) in **4a-h** (CD_2Cl_2 , 100.6 MHz).

	R	R'	R''	COFe	C=O	CEt	CMe	CH^a	
4a	Me	Me	Me	Me	207.12	163.12	–	99.01	–
4b	Et	Et	Et	Et	207.32	162.44	104.78	–	–
4c	Me	Me	H	H	206.00	163.63	–	109.08	75.88
4d	Me	Me	Me	H	206.42	163.01 162.89	–	105.56 103.56 96.96	76.64
4e	Me	Me	Me	Et	207.42	163.71 163.06	103.12	100.61 100.01 98.58	–
4f	Me	Me	Et	Et	207.07	162.60	101.84	101.42	–
4g	Me	H	Me	H	205.74	162.78	–	102.10	85.19
4g'	Me	H	H	Me	205.74	163.30 162.24	–	104.77	82.79
4h	Me	H	Et	Et	206.45	162.75 162.19	107.98 105.92	100.84	82.08

^aassignment confirmed by APT.

The olefinic carbons within the *p*-quinone ring display the anticipated upfield shift upon coordination to the metal center. However, the coordination shifts are not as substantial as those of the coordinated olefin moieties in **6c-e** compared to the free ring carbons in **7** ($\Delta \approx +100 - 120$ ppm) (*vide supra*). For example, the CMe carbons in free duroquinone resonate at δ 140.4 ppm⁶⁰ compared with δ 99.0 in **4a** ($\Delta = +41.4$ ppm); similarly, the CMe and CH carbons resonate at δ 145.8 and 133.8 respectively in 2,6-dimethyl-1,4-benzoquinone⁶⁰ compared to δ 104.8 and 82.8 in **4g'** ($\Delta = +41.0, 51.0$ ppm). The ketone carbons also show a significant upfield shift of some 25 ppm when compared with alkyl-

substituted 1,4-benzoquinones where the ketone carbonyls typically resonate in a very narrow window between δ 186 and 189 ppm.⁶⁰

3.6. Conclusions

The available synthesis of the $\text{Fe}(\text{CO})_4(\eta^2\text{-alkyne})$ compounds **1a-e** has finally enabled confirmation of early proposals^{2,3} that such compounds are intermediates in iron-mediated coupling reactions of alkynes and carbon monoxide, ultimately leading to the production of cyclic organic ligands. In the case of **1c** and **1e**, the remarkably low temperatures at which the reactions occur clearly demonstrate why such species remained undetected in early thermal reactions of alkynes with iron carbonyls. Moreover, the diversity of the products, ranging from cyclopentadienone (**2**) to tropone (**3**) to *p*-quinone (**4a,b**) complexes, provides a reminder of the remarkable range of transformations that are possible. The observation that **1a-e** are also quite reactive towards carbon monoxide, in the absence of added alkyne, provided initial clues as to the mechanisms by which compounds **2-4** formed. More importantly, perhaps, the identity of a second previously unknown and unproven intermediate was detected in the elegantly simple synthesis of tricarbonyl(tetramethyl-1,4-benzoquinone)iron from $\text{Fe}(\text{CO})_5$ and but-2-yne under gentle sunlight irradiation, a reaction that was first discovered at the dawn of modern organometallic chemistry. The intermediate tricarbonyl-3,4-dimethylferracyclopenta-3-en-2,5-dione dimer proved to be reactive towards alkynes other than but-2-yne, and provided a general synthesis of a modest range of substituted tricarbonyl(*p*-quinone)iron complexes (**4c-h**).

3.7. Experimental Section

Unless otherwise noted, the general synthetic techniques and physical measurements employed were as described in Sections 2.6.1 and 2.6.2. Although compounds **2**,¹⁶ **4a,b**,¹ and **7e**⁴⁷ have been synthesized previously by other methods, their spectroscopic data have not been reported and are thus provided here. Assignments specified in ¹³C{¹H} NMR for C/CH₂ vs. CH/CH₃ were confirmed by obtaining an APT spectrum.

3.7.1. Reagents

Compounds **1a-f** were prepared according to the procedures described in Chapter 2. Pent-2-yne was purchased from Aldrich Chemical Co. and used without further purification. Carbon monoxide gas (Matheson) was H.P. grade and used without further purification.

3.7.2. Synthetic Procedures

Synthesis of Fe(CO)₃{η⁴-C₄(CF₃)₄C(O)} (**2**) from **1a**. HFB was bubbled for 1 min through a solution of **1a** (32 mg, 0.097 mmol) dissolved in 20 mL pentane in a sealed Carius tube. The initially colorless solution was allowed to stir at room temperature overnight. The pentane was removed and the orange residue was sublimed at 75°C *in vacuo* before being washed from the water-cooled probe with pentane. Concentration of the solution and crystallization at -80°C yielded 32.6 mg (0.066 mmol, 68 %) of a bright yellow powder which contained predominantly **2** along with a minor byproduct. The byproduct has similar volatility and solubility properties and is thus not readily separated. Attempts to purify the mixture by chromatography met with failure. Compound **2** was first isolated in 60% yield from the high temperature bomb reaction of neat Fe(CO)₅ with excess HFB¹⁶ and its solid-state structure has been determined.¹⁷

F.W. 491.9

IR (pentane) ν_{CO} 2118(s), 2076(s), 2066(m); ν_{C=O/CC} 1740(w), 1725(w).¹⁶

¹⁹F NMR (188.3 MHz, CD₂Cl₂) δ -53.0 (m), -56.7 (m).

¹³C{¹⁹F} NMR (100.6 MHz, CD₂Cl₂) δ 200.45 (s, CO_{Fe}), 163.86 (s, C=O), 121.88 (s, CF₃), 121.51 (s, CF₃), 90.14 (s, C_{inner}), 66.40 (s, C_{outer}).

Reaction of C₂H₂ with 1c. Acetylene was bubbled for 10 min through a solution of **1c** (27 mg, 0.139 mmol) dissolved in 15 mL pentane at -78°C, and a slow (*ca.* 1 bubble/s) flow was maintained. The initially colorless solution was allowed to slowly warm; by -60°C the solution became a deep yellowish orange color and by -40°C a copious amount of brownish black precipitate had formed. After warming to 0°C, the intractable black precipitate was extracted exhaustively with pentane to yield 9.0 mg (0.037 mmol, 26 %) of an orange powder of Fe(CO)₃{η⁴-C₆H₆C(O)} (**3**) which was first prepared from Fe₂(CO)₉ under 22 atm C₂H₂ at ambient temperature.²⁰ The identity of the product was confirmed by comparison of the characteristic IR,²⁰ ¹H NMR²¹ and ¹³C NMR²² spectra reported previously in the literature. The intractable black precipitate has so far defied characterization, but is believed to contain polymeric materials.²³

Synthesis of Fe(CO)₃{η⁴-(O)CC₄Me₄C(O)} (**4a**) from **1e**. Excess but-2-yne was added to **1e** (18 mg, 0.081 mmol) dissolved in 20 mL pentane at -78°C. The solution was freeze-thaw degassed three times and placed under 1 atm CO. Storage at -80°C overnight afforded a bright yellow precipitate; to ensure complete reaction, the solution was allowed to warm with stirring to -15°C before being returned to -80°C for crystallization. Fe(CO)₃{η⁴-(O)CC₄Me₄C(O)} (**4a**) was isolated as a bright yellow powder by inverse filtration (18.7 mg, 0.061 mmol, 76 %). Compound **4a** was first prepared by exposing a mixture of Fe(CO)₅ and but-2-yne to sunlight in a sealed tube.¹ The material is somewhat thermally unstable and degrades rapidly in air.

F.W. 304.1

IR (pentane) ν_{CO} 2067(vs), 2014(s), 2010(sh); ν(C=O) 1638(w, br).

¹H NMR (400.1 MHz, CD₂Cl₂, -60°C) δ 1.98 (s).

¹³C{¹H} NMR (100.6 MHz, CD₂Cl₂, -60°C) δ 207.12 (s, CO_{Fe}), 163.12 (s, C=O), 99.01 (s, CMe), 13.27 (s, Me).

Synthesis of Fe(CO)₃{η⁴-(O)CC₄Et₄C(O)} (**4b**) from **1f**. A 115 mL solution of **1f** (formed *in situ* from Fe(CO)₅ (149 mg, 0.766 mmol) and an excess of hex-3-yne (500 μL, 4.4 mmol)) was freeze-thaw degassed and placed under 1

atm CO. The solution was stirred at room temperature for 4 h before being filtered through a cotton pad to remove fine intractable particles. Crystallization at -80°C afforded a golden brown powder of $\text{Fe}(\text{CO})_3\{\eta^4\text{-(O)CC}_4\text{Et}_4\text{C(O)}\}$ (**4b**) (123.8 mg). Concentration of the mother liquor and recrystallization at -80°C afforded another 51.3 mg (total yield = 175.1 mg, 0.451 mmol, 59 % from $\text{Fe}(\text{CO})_5$). Compound **4b** was first prepared by exposing a mixture of $\text{Fe}(\text{CO})_5$ and hex-3-yne to sunlight in a sealed tube.¹ The material degrades slowly upon standing in air.

F.W. 359.9

IR (pentane) ν_{CO} 2067(vs), 2014(s), 2008(s); $\nu_{\text{(C=O)}}$ 1645(w), 1620(w).

^1H NMR (400.1 MHz, CD_2Cl_2 , -60°C) δ 2.90 (dq, $^2J_{\text{HH}} = 12.5$ Hz, $^3J_{\text{HH}} = 7.5$ Hz, 4H, CHH), 2.10 (dq, $^2J_{\text{HH}} = 12.5$ Hz, $^3J_{\text{HH}} = 7.5$ Hz, 4H, CHH), 1.26 (t, $^3J_{\text{HH}} = 7.5$ Hz, 12H, CH_3).

$^{13}\text{C}\{^1\text{H}\}$ NMR (100.6 MHz, CD_2Cl_2 , -60°C) δ 207.32 (s, CO_{Fe}), 162.44 (s, C=O), 104.78 (s, CEt), 21.92 (s, CH_2), 14.24 (s, CH_3).

Reaction of 1a with CO. A 15 mL pentane solution of **1a** (30 mg, 0.091 mmol) was sealed inside a small Carius tube equipped with a stir bar. The solution was freeze-thaw degassed three times and *ca.* 1.5 atm CO was added. The initially colorless solution was stirred for four days at room temperature until the IR spectrum indicated no further change; heating the solution caused decomposition without producing more product. The pentane and excess **1a** were removed *in vacuo* at $T \leq -20^{\circ}\text{C}$ and the beige product was purified by sublimation onto a dry-ice cooled cold-finger at ambient temperature. The product was washed from the probe with 20 mL pentane, the solution was concentrated and recrystallization at -80°C afforded 17.1 mg of a beige powder of $\text{Fe}(\text{CO})_4\{\eta^1, \eta^1\text{-C}_2(\text{CF}_3)_2\text{C(O)}\}$ (**5a**) (0.048 mmol, 53 %). ^{13}CO enriched material was prepared as above.

F.W. 357.9

Anal. Calcd for $\text{C}_9\text{F}_6\text{FeO}_5$: C, 30.20. Found: C, 30.21.

IR (pentane) ν_{CO} 2126(m), 2074(ms), 2057(vs); ν_{acyl} 1762(m); ν_{CC} 1629(vw).

$^{13}\text{C}\{^1\text{H}\}$ NMR (CD_2Cl_2 , 100.6 MHz, ^{13}CO enriched) δ 202.9 (m, 2CO, CO_{ax}), 200.6 (m, CO_{eq}), 196.8 (m, CO_{eq}), 196.2 (m, CO_{ac}). The δ 196.2 resonance had an integration of 0.8 unless a 10 s delay was introduced between pulses.

^{19}F NMR (CD_2Cl_2 , 376.5 MHz) δ -60.01 (q, $^5J_{\text{FF}} = 8.1$ Hz), -63.38 (q, $^5J_{\text{FF}} = 8.1$ Hz).

EI-MS: M^+ ; $\text{M}^+ - n \text{CO}$ ($n = 1 - 5$); $\text{M}^+ - \text{F} - m \text{CO}$ ($m = 2 - 5$); $\text{M}^+ - \text{CO} - \text{HFB}$.

Reaction of 1b with CO. A 10 mL pentane solution of **1b** (26 mg, 0.099 mmol) was purged with CO at -30°C and allowed to warm slowly. The initially colorless solution began to turn yellow at -10°C and was maintained at $-10 \leq T \leq 0^\circ\text{C}$ for 3.5 hours until IR spectroscopy indicated consumption of **1b**. The yellow supernatant was filtered from an intractable yellow precipitate (11.6 mg), and recrystallization at -80°C afforded 13.3 mg of a beige powder of $\text{Fe}(\text{CO})_4\{\eta^1, \eta^1\text{-C}(\text{CF}_3)\text{CHC}(\text{O})\}$ (**5b**) (0.046 mmol, 46 %). The product is volatile and can be purified by sublimation if required. The beige solid is thermally sensitive and decomposes as a solid upon standing at ambient temperature; consequently a satisfactory elemental analysis could not be obtained. ^{13}CO enriched material was prepared as above.

F.W. 289.9

IR (pentane) ν_{CO} 2118 (m), 2062 (ms), 2046 (vs); ν_{acyl} 1760 (m).

^1H NMR (CD_2Cl_2 , 200.1 MHz) δ 7.16 (q, $^4J_{\text{HF}} = 2.0$ Hz, CH).

$^{13}\text{C}\{^1\text{H}\}$ NMR (CD_2Cl_2 , 100.6 MHz, -60°C) δ 204.60 (s, 2 CO_{ax}), 202.00 (s, CO_{eq}), 198.78 (s, CO_{ac}), 198.56 (s, CO_{eq}), 158.64 (q, $^3J_{\text{CF}} = 8$ Hz, CH). The CCF_3 and CF_3 resonances were not detected.

$^{13}\text{C}\{^{19}\text{F}\}$ NMR (CD_2Cl_2 , 100.6 MHz, -60°C) δ 204.62 (s, 2 CO_{ax}), 202.01 (s, CO_{eq}), 198.77 (s, CO_{eq}), 198.58 (s, CO_{ac}), 158.64 (d, $^1J_{\text{CH}} = 169$ Hz, CH), 156.11 (br, CCF_3). The CF_3 resonance was not detected.

$^{13}\text{C}\{^1\text{H}, ^{19}\text{F}\}$ NMR (CD_2Cl_2 , 100.6 MHz, -60°C) δ 204.66 (s, 2 CO_{ax}), 202.04 (s, CO_{eq}), 198.72 (s, CO_{ac}), 198.60 (s, CO_{eq}), 158.65 (s, CH), 156.16 (s, CCF_3).

$^{13}\text{C}\{^1\text{H}\}$ NMR (CD_2Cl_2 , 100.6 MHz, ^{13}CO enriched, -60°C) δ 204.59 (s, 2 CO_{ax}), 201.99 (s, CO_{eq}), 198.74 (s, CO_{ac}), 198.56 (s, CO_{eq}), 158.64 (m, $^1J_{\text{CC}} \approx 35 - 40$

Hz, CH). The δ 198.74 signal had an integration of *ca.* 0.75 unless a 10 s delay was introduced between pulses.

^{19}F NMR (CD_2Cl_2 , 188.3 MHz) δ -67.12 (d, $^4J_{\text{HF}} = 2.0$ Hz, CF_3).

EI-MS: M^+ ; $\text{M}^+ - n \text{CO}$ ($n = 1 - 4$); $\text{M}^+ - \text{TFP} - m \text{CO}$ ($m = 1 - 4$); $\text{C}_5\text{HF}_3\text{O}_2^+$ (base peak).

Reaction of 1c with CO. A 50 mL pentane solution of 1c (155 mg, 0.799 mmol) was purged with CO for 30 minutes at -78°C . The initially colorless solution was stored at *ca.* -35°C for two days, at which point a copious amount of beige precipitate has deposited and the IR spectrum indicated very little starting material remaining. The solution was stored overnight at -80°C , and the beige product (6c) (126.9 mg, 0.286 mmol, 71%) was collected by inverse filtration. The solid is air sensitive and somewhat thermally unstable, decomposing slowly to unknown products at room temperature even under inert atmosphere; an analytically pure sample was not obtained despite many attempts. The solid is not amenable to characterization by either EI or FAB MS; when EI was used, only peaks attributable to half of the dimer were observed, and when FAB was attempted, peaks up to triple the monomer FW were detected, suggesting decomposition in the matrix. ^{13}C enriched material was prepared as above.

F.W. 443.8

Anal. Calcd for $\text{C}_{14}\text{H}_4\text{Fe}_2\text{O}_{10}$: C, 37.88; H 0.91. Found: C, 36.73; H 0.75.

IR (CH_2Cl_2) ν_{CO} 2085(m), 2025(s); ν_{acyl} 1837(w), 1817(w), 1760(vw).

^1H NMR (CD_2Cl_2 , 400.1 MHz, -60°C) δ 4.39 (s).

$^{13}\text{C}\{^1\text{H}\}$ NMR (CD_2Cl_2 , 100.6 MHz, ^{13}C enriched): (-110°C) δ 228.81 (s, 2CO_{ac}), 206.8 (br, CO_{Fe}), 204.7 (br, 2CO_{Fe}). (-80°C) δ 228.52 (s, 2CO_{ac}), 205.6 (br, $3\text{CO}_{\text{Fe(av)}}$). (-40°C) δ 228.14 (s, 2CO_{ac}), 205.84 (s, $3\text{CO}_{\text{Fe(av)}}$), 39.22 ("d", $^1J_{\text{CC}} = 39$ Hz, CH).

Reaction of 1d,e with CO. A 50 mL pentane solution of 1d (63 mg, 0.303 mmol) was purged with CO for 30 minutes at -78°C . The initially colorless solution was warmed to -10°C and stirred at this temperature for 1.5 h until IR

spectroscopy indicated that formation of $\text{Fe}(\text{CO})_4\{\eta^1, \eta^1\text{-(O)CCMeCHC(O)}\}$ (**7d**) had begun. The solution was stored at -80°C overnight, and the beige product (**6d**) (44.0 mg, 0.093 mmol, 61%) was collected by inverse filtration. In a similar fashion, **1e** (108 mg, 0.487 mmol) was converted to bright yellow **6e** (93.7 mg, 0.187 mmol, 77%) which began to precipitate from solution as the temperature exceeded -30°C . The reaction was complete after 5 hours at $-30 \leq T \leq -20^\circ\text{C}$; warming the vessel above this temperature results in competing production of **7e**. Both materials are thermally sensitive and decompose at room temperature even under inert atmosphere; the decomposition is more rapid if exposed to air. As with **6c** described above, neither compound was amenable to EI- or FAB-MS. Compounds **7d,e**, respectively, are the primary products of thermal decomposition in solution. ^{13}C O enriched material was prepared as above.

$[\text{Fe}(\text{CO})_3\{\eta^1, \eta^1\text{-(O)CCMeCHC(O)}\}]_2$ (**6d**):

F.W. 471.9

Anal. Calcd for $\text{C}_{16}\text{H}_8\text{Fe}_2\text{O}_{10}$: C, 40.72; H 1.71. Found: C, 40.94; H 1.33.

IR (CH_2Cl_2) ν_{CO} 2081(s), 2020(vs); ν_{acyl} 1850(vw), 1796(m), 1767(m).

^1H NMR (CD_2Cl_2 , 400.1 MHz, -60°C) δ 4.39 (s, CH), 2.03 (s, Me).

$^{13}\text{C}\{^1\text{H}\}$ NMR (CD_2Cl_2 , 100.6 MHz, -60°C): δ 230.16 (s, CO_{ac}), 227.00 (s, CO_{ac}), 205.6 (br, $\text{CO}_{\text{Fe(av)}}$), 62.29 (s, CMe), 47.69 (s, CH), 12.17 (s, Me).

$^{13}\text{C}\{^1\text{H}\}$ NMR (CD_2Cl_2 , 100.6 MHz, ^{13}C O enriched): (-100°C) δ 230.55 (s, CO_{ac}), 227.41 (s, CO_{ac}), 207.14 (brs, CO_{Fe}), 204.92 (brs, CO_{Fe}), 204.06 (brs, CO_{Fe}), 62.44 ("d", $^1J_{\text{CC}} = 34$ Hz, CMe), 47.69 ("d", $^1J_{\text{CC}} = 38$ Hz, CH), 11.87 (s, Me).

$[\text{Fe}(\text{CO})_3\{\eta^1, \eta^1\text{-(O)CCMeCMeC(O)}\}]_2$ (**6e**):

F.W. 499.9

Anal. Calcd for $\text{C}_{18}\text{H}_{12}\text{Fe}_2\text{O}_{10}$: C, 43.24; H 2.42. Found: C, 42.96; H 1.98.

IR (CH_2Cl_2) ν_{CO} 2078(m), 2017(s); ν_{acyl} 1795(mw), 1758(sh).

^1H NMR (CD_2Cl_2 , 400.1 MHz, -100°C) δ 1.98 (s).

$^{13}\text{C}\{^1\text{H}\}$ NMR (CD_2Cl_2 , 100.6 MHz, ^{13}C O enriched) -100°C : δ 229.51 (s, 2CO_{ac}), 207.57 (s, CO_{Fe}), 204.24 (s, 2CO_{Fe}). -40°C : δ 228.93 (s, 2CO_{ac}),

205.79 (s, 3CO_{Fe}), 67.37 (s, with ¹³C satellites, ¹J_{CC} = 38 Hz, CMe), 10.48 (s, Me).

Synthesis of Fe(CO)₄{η¹,η¹-(O)CCRCMeC(O)} (R = H, 7d; Me, 7e) from 1d,e. Freshly sublimed 1d (48 mg, 0.231 mmol) in 40 mL pentane was purged with CO for 30 minutes at -78°C. Upon warming to 0°C and storing overnight at *ca.* 5°C, IR spectroscopy indicated that the reaction was complete. The solution was concentrated to *ca.* 20 mL before being recrystallized at -80°C to afford a beige powder of Fe(CO)₄{η¹,η¹-(O)CCHCMeC(O)} (7d) (45.9 mg, 0.174 mmol, 75%). In a similar fashion, 1e (144 mg, 0.649 mmol) was converted to beige flakes of Fe(CO)₄{η¹,η¹-(O)CCMeCMeC(O)} (7e) (162.1 mg, 0.583 mmol, 90%) after warming the initial yellow slurry of 6e to +10°C for 6 h under CO. Compound 7e can also be synthesized in 11% yield by extended photolysis of Fe(CO)₅ in acetone in the presence of *cis*-,3-dibromobut-2-ene.⁴⁷

Fe(CO)₄{η¹,η¹-(O)CCHCMeC(O)} (7d):

F.W. 264.0

Anal. Calcd for C₉H₄FeO₆: C, 40.95; H, 1.53. Found: C, 40.89; H, 1.52.

IR (pentane) ν_{CO} 2113(m), 2057(sh), 2053(s), 2029(vs); ν_{acyl} 1685(sh), 1667(m).

¹H NMR (CD₂Cl₂, 200.1 MHz) δ 7.20 (s, CH), 2.03 (s, Me).

¹³C{¹H} NMR (CD₂Cl₂, 75.5 MHz) δ 243.82 (s, CO_{ac}), 242.50 (s, CO_{ac}), 202.57 (s, 2CO_{ax}), 200.38 (s, CO_{eq}), 200.16 (s, CO_{eq}), 175.57 (s, CMe), 159.19 (s, CH), 13.60 (s, Me).

EI-MS: M⁺ (9.0% of base); M⁺ - n CO (n = 1 - 6) (n = 1, base peak).

Fe(CO)₄{η¹,η¹-(O)CCMeCMeC(O)} (7e):

F.W. 278.0

IR (pentane) ν_{CO} 2112(m), 2053(m), 2050(s), 2027(vs); ν_{acyl} 1663(w).

¹H NMR (CD₂Cl₂, 200.1 MHz) δ 1.95 (s).

¹³C{¹H} NMR (CD₂Cl₂, 75.5 MHz) δ 242.07 (s, 2CO_{ac}), 202.91 (s, 2CO_{ax}), 200.40 (s, 2CO_{eq}) 169.58 (s, CMe), 12.35 (s, Me).

General Synthesis of $\text{Fe}(\text{CO})_3\{\eta^4\text{-(O)CC}_4\text{MeRR'R''C(O)}\}$ (4a,c-h) from 6d,e. An excess of $\text{R}'\text{C}\equiv\text{CR}''$ was added to a CH_2Cl_2 solution of 50 - 100 mg of 1d,e at -30°C . The solution quickly changed color from yellow to orange and IR spectroscopy indicated consumption of the starting material. The solution was concentrated to *ca.* 1 mL at $T \leq -20^\circ\text{C}$ and pentane (*ca.* 5 mL) was added. The results ranged from immediate precipitation (4c) to microcrystal formation following overnight storage at -80°C (4f). All $\text{Fe}(\text{CO})_3\{\eta^4\text{-(O)CC}_4\text{MeRR'R''C(O)}\}$ products are air sensitive to various degrees, decomposing pyrophorically in the case of 4c. Additionally, all are somewhat thermally unstable in the order $4\text{c} \approx 4\text{g/g}' < 4\text{d} < 4\text{a} \approx 4\text{h} < 4\text{e} \approx 4\text{f}$; the earlier members of the series decompose in an inert atmosphere within minutes at ambient temperature while the latter can be handled quickly in air. As a result, neither 4c, 4d nor 4g/g' could be characterized by elemental analysis or mass spectrometry.

4c: R = Me, R' = R'' = H; thermally sensitive yellow powder, 89 %.

F.W. 276.0

IR (CH_2Cl_2) ν_{CO} 2082(vs), 2027(s); $\nu_{\text{(C=O)}}$ 1648(sh), 1630(m).

^1H NMR (CD_2Cl_2 , 400.1 MHz, -60°C) δ 4.93 (s, CH), 2.01 (s, Me).

$^{13}\text{C}\{^1\text{H}\}$ NMR (CD_2Cl_2 , 100.6 MHz, -60°C) δ 206.00 (s, $\text{CO}_{\text{Fe(av)}}$), 163.63 (s, C=O), 109.08 (s, CMe), 75.88 (s, CH), 13.45 (s, Me).

4d: R = R' = Me, R'' = H; thermally sensitive yellow-brown oil, 80 %.

F.W. 290.0

IR (CH_2Cl_2) ν_{CO} 2077(vs), 2023(s); $\nu_{\text{(C=O)}}$ 1635(m), 1615(m).

^1H NMR (CD_2Cl_2 , 400.1 MHz, -60°C) δ 4.96 (s, CH), 2.03 (s, Me), 1.95 (s, 6H, 2Me).

$^{13}\text{C}\{^1\text{H}\}$ NMR (CD_2Cl_2 , 100.6 MHz, -60°C) δ 206.42 (s, $\text{CO}_{\text{Fe(av)}}$), 163.01 (s, C=O), 162.89 (s, C=O), 105.56 (s, CMe), 103.56 (s, CMe), 96.96 (s, CMe), 76.64 (s, CH), 16.45 (s, Me), 13.45 (s, Me), 13.10 (s, Me).

4e: R = R' = Me, R'' = Et; beige powder, 76%.

F.W. 318.1

Anal. Calcd for $C_{14}H_{14}FeO_5$: C, 52.86; H 4.44. Found: C, 52.50; H 4.13.

IR (CH_2Cl_2) ν_{CO} 2072(vs), 2017(s); $\nu_{(C=O)}$ 1630(w), 1609(w).

1H NMR (CD_2Cl_2 , 400.1 MHz, $-60^\circ C$) δ 2.84 (dq, $^2J_{HH} = 12.5$ Hz, $^3J_{HH} = 7.5$ Hz, 2H, CHH), 2.04 (s, Me-C), 2.01 (s, Me-C), 2.00 (s, Me-C), 1.92 (m, CHH), 1.15 (t, $^3J_{HH} = 7.5$ Hz, 3H, CH_3-CH_2).

$^{13}C\{^1H\}$ NMR (CD_2Cl_2 , 100.6 MHz, $-20^\circ C$) δ 207.42 (s, $COFe(av)$), 163.71 (s, C=O), 163.06 (s, C=O), 103.12 (s, CR), 100.61 (s, CR), 100.01 (s, CR), 98.58 (s, CR), 22.06 (s, CH_2), 13.50 (s, Me), 13.35 (s, Me), 12.99 (s, Me), 12.64 (s, Me).

EI-MS: M^+ (0.7%), $M^+ - n CO - m H$ ($n = 1-3$, $m = 0, 2$), $C_6O_2Me_3Et^+$, $C_5OMe_3Et^+$, $C_4OMe_2Et^+$, CO^+ (base peak).

4f: R = Me, R' = R'' = Et; yellow-orange micro-crystals, 87 %.

F.W. 332.2

Anal. Calcd for $C_{15}H_{16}FeO_5$: C, 54.24; H 4.86. Found: C, 54.12; H 4.58.

IR (pentane) ν_{CO} 2065(vs), 2013(s), 2006(s); $\nu_{(C=O)}$ 1647(w), 1627(w).

(CH_2Cl_2) ν_{CO} 2072(vs), 2020(s); $\nu_{(C=O)}$ 1632(w), 1608(w).

1H NMR (CD_2Cl_2 , 400.1 MHz, $-60^\circ C$) δ 2.60 (dq, $^2J_{HH} = 12.5$ Hz, $^3J_{HH} = 7.5$ Hz, CHH), 2.16 (dq, $^2J_{HH} = 12.5$ Hz, $^3J_{HH} = 7.5$ Hz, CHH), 2.01 (s, 6H, Me-C), 1.24 (t, $^3J_{HH} = 7.5$ Hz, CH_3-CH_2).

$^{13}C\{^1H\}$ NMR (CD_2Cl_2 , 100.6 MHz, $-20^\circ C$) δ 207.07 (s, $COFe(av)$), 162.60 (s, C=O), 101.84 (s, CR), 101.42 (s, CR), 21.22 (s, CH_2), 14.01 (s, Me), 13.14 (s, Me).

EI-MS: M^+ (8.2%), $M^+ - n CO - m H$ ($n = 1 - 3$, $m = 0, 2$) ($n = 3$, $m = 2$; base peak), $C_6O_2Me_2Et_2^+$, $C_4OMeEt_2^+$.

4g/g': thermally sensitive beige powder, 76 %.

F.W. 276.0

IR (CH_2Cl_2) ν_{CO} 2082(vs), 2028(s), 2006(s); $\nu_{(C=O)}$ 1630(m,br).

R = H, R' = Me, R'' = H; C_2 isomer (4g) (major, ca. 60 %):

1H NMR (CD_2Cl_2 , 400.1 MHz, $-60^\circ C$) δ 5.21 (s, CH), 1.89 (s, Me).

$^{13}C\{^1H\}$ NMR (CD_2Cl_2 , 100.6 MHz, $-60^\circ C$) δ 205.74 (s, $COFe(av)$), 162.78 (s, C=O), 102.10 (s, CMe), 85.19 (s, CH), 16.15 (s, Me).

R = R' = H, R'' = Me; C_s isomer (**4g'**) (minor, ca. 40 %):

¹H NMR (CD₂Cl₂, 400.1 MHz, -60°C) δ 4.96 (s, CH), 1.97 (s, Me).

¹³C{¹H} NMR (CD₂Cl₂, 100.6 MHz, -60°C) δ 205.74 (s, COFe(av)), 163.30 (s, C=O), 162.24 (s, C=O), 104.77 (s, CMe), 82.79 (s, CH), 16.63 (s, Me).

4h: R = H, R' = R'' = Et; beige powder, 72 %.

F.W. 318.1

Anal. Calcd for C₁₄H₁₄FeO₅: C, 52.86; H 4.44. Found: C, 52.75; H 4.45.

IR (CH₂Cl₂) ν_{CO} 2076(vs), 2022(s); ν_(C=O) 1635(m), 1611(m).

¹H NMR (CD₂Cl₂, 400.1 MHz, -60°C) δ 5.06 (s, CH), 2.71 (dq, ²J_{HH} = 12.5 Hz, ³J_{HH} = 7.5 Hz, CHH), 2.55 (dq, ²J_{HH} = 12.5 Hz, ³J_{HH} = 7.5 Hz, CHH), 2.11 (dq, ²J_{HH} = 12.5 Hz, ³J_{HH} = 7.5 Hz, CHH), 2.09 (dq, ²J_{HH} = 12.5 Hz, ³J_{HH} = 7.5 Hz, CHH), 1.98 (s, 3H, Me-C), 1.24 (t, ³J_{HH} = 7.5 Hz, CH₃-CH₂), 1.19 (t, ³J_{HH} = 7.5 Hz, CH₃-CH₂).

¹³C{¹H} NMR (CD₂Cl₂, 100.6 MHz, -60°C) δ 206.45 (s, COFe(av)), 162.75 (s, C=O), 162.19 (s, C=O), 107.98 (s, CR), 105.92 (s, CR), 100.84 (s, CR), 82.08 (s, CH), 21.83 (s, CH₂), 21.43 (s, CH₂), 16.35 (s, Me), 14.29 (s, Me), 13.89 (s, Me).

EI-MS: M⁺ (9.5%), M⁺ - n CO (n = 1 - 3) (n = 3, base peak), C₆O₂HMeEt₂⁺, C₅OHMeEt₂⁺, C₄OHEt₂⁺.

3.8. References

1. Sternberg, H. W.; Markby, R.; Wender, I. *J. Am. Chem. Soc.* **1958**, *80*, 1009.
2. Orgel, L. E. In *International Conference on Co-ordination Chemistry*; Spec. Publ. No. 13, The Chemical Society: London, 1959; pp 93.
3. Hübel, W. In *Organic Synthesis via Metal Carbonyls*; I. Wender and P. Pino, Eds.; Wiley-Interscience: New York, 1968; Vol. 1; pp 273 and references therein.
4. Pannell, K. H.; Crawford, G. M. *J. Coord. Chem.* **1973**, *2*, 251.
5. Cotton, F. A.; Jamerson, J. D.; Stults, B. R. *J. Am. Chem. Soc.* **1976**, *98*, 1774.
6. Washington, J.; McDonald, R.; Takats, J.; Menashe, N.; Reshef, D.; Shvo, Y. *Organometallics* **1995**, *14*, 3996.
7. Cooke, J.; Takats, J. *J. Am. Chem. Soc.* **1997**, *119*, 11088.
8. Fornals, D.; Pericàs, M. A.; Serratos, F.; Font-Altava, M.; Solans, X. *J. Chem. Soc. Perkin Trans. I* **1987**, 2749.
9. Krespan, C. G. *J. Org. Chem.* **1975**, *40*, 261.
10. Pearson, A. J.; Shively, R. J., Jr.; Dubbert, R. A. *Organometallics* **1992**, *11*, 4096.
11. Pearson, A. J.; Shively, R. J., Jr. *Organometallics* **1994**, *13*, 578.
12. Pearson, A. J.; Perosa, A. *Organometallics* **1995**, *14*, 5178.
13. Knölker, H.-J.; Heber, J.; Mahler, C. H. *Synlett* **1992**, 1002.
14. Knölker, H.-J.; Heber, J. *Synlett* **1993**, 924.
15. Knölker, H.-J.; Baum, E.; Heber, J. *Tetrahedron Lett.* **1995**, *36*, 7647.
16. Boston, J. L.; Sharp, D. W. A.; Wilkinson, G. *J. Chem. Soc.* **1962**, 3488.
17. Bailey, N. A.; Mason, R. *Acta Cryst.* **1966**, *21*, 652.
18. Burke, M.; Funk, T.; Takats, J. *Organometallics* **1994**, *13*, 2109.
19. Kruczynski, L.; Takats, J. *Inorg. Chem.* **1976**, *15*, 3140.
20. Weiss, E.; Hübel, W. *Chem. Ber.* **1962**, *95*, 1179.
21. Hunt, D. F.; Farrant, G. C.; Rodeheaver, G. T. *J. Organomet. Chem.* **1972**, *38*, 349.
22. Johnson, B. F. G.; Lewis, J.; McArdle, P.; Norton, J. R. *J. Chem. Soc., Dalton Trans.* **1974**, 1253.

23. Weiss, E.; Hübel, W.; Merényi, R. *Chem. Ber.* **1962**, *95*, 1155.
24. Knox, S. A. R.; Lloyd, B. R.; Morton, D. A. V.; Orpen, A. G.; Turner, M. L.; Hogarth, G. *Polyhedron* **1995**, *14*, 2723.
25. Birk, R.; Berke, H.; Huttner, G.; Zsolnai, L. *Chem. Ber.* **1988**, *121*, 471.
26. Burn, M. J.; Kiel, G.-Y.; Seils, F.; Takats, J.; Washington, J. *J. Am. Chem. Soc.* **1989**, *111*, 6850.
27. Cooke, J.; Gagné, M. R.; Mao, T.; Takats, J.; Bond, A. H.; Rogers, R. D. manuscript in preparation.
28. Karel, K.; Tulip, T. H.; Ittel, S. D. *Organometallics* **1990**, *9*, 1276.
29. Mann, B. E.; Taylor, B. F. *¹³C NMR Data for Organometallic Compounds*; Academic: New York, 1981, pp 23.
30. Silverstein, R. M.; Bassler, G. C.; Morrill, T. C. *Spectrometric Identification of Organic Compounds*; 5th ed.; Wiley, Chp. 4 and 5: New York, 1991.
31. Breitmaier, E.; Voelter, W. *Carbon-13 NMR Spectroscopy*; VCH: Weinheim, 1987, pp 133-155.
32. Washington, J. PhD Thesis, University of Alberta, 1994.
33. Azar, M. C.; Chetcuti, M. J.; Eigenbrot, C.; Green, K. A. *J. Am. Chem. Soc.* **1985**, *107*, 7209.
34. Boag, N. M.; Goodfellow, R. J.; Green, M.; Hessner, B.; Howard, J. A. K.; Stone, F. G. A. *J. Chem. Soc., Dalton Trans.* **1983**, 2585.
35. Dickson, R. S.; Evans, G. S.; Fallon, G. D. *Aust. J. Chem.* **1985**, *38*, 273.
36. Finnimore, S. R.; Knox, S. A. R.; Taylor, G. E. *J. Chem. Soc., Chem. Commun.* **1980**, 411.
37. Chetcuti, M. J.; Eigenbrot, C.; Green, K. A. *Organometallics* **1987**, *6*, 2298.
38. Burt, R.; Cooke, M.; Green, M. *J. Chem. Soc. (A)* **1970**, 2981.
39. Padolik, L. L.; Gallucci, J.; Wojcicki, A. *J. Organomet. Chem.* **1990**, *383*, C1.
40. Padolik, L. L.; Gallucci, J.; Wojcicki, A. *J. Am. Chem. Soc.* **1993**, *115*, 9986.
41. Corrigan, P. A.; Dickson, R. S.; Fallon, G. D.; Michel, L. J.; Mok, C. *Aust. J. Chem.* **1978**, *31*, 1937.
42. Corrigan, P. A.; Dickson, R. S. *Aust. J. Chem.* **1979**, *32*, 2147.
43. Wong, W.; Singer, S. J.; Pitts, W. D.; Watkins, S. F.; Baddley, W. H. *J. Chem. Soc., Chem. Commun.* **1972**, 672.

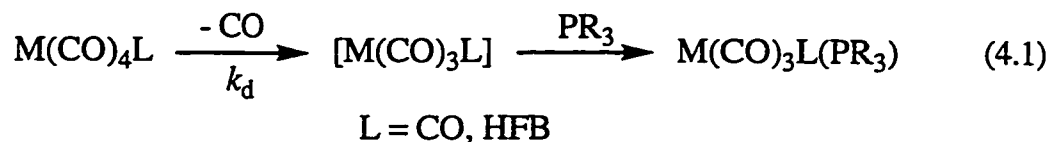
44. Bird, C. W.; Briggs, E. M.; Hudec, J. J. *J. Chem. Soc.(C)* **1967**, 1862.
45. Pino, P.; Braca, G. In *Organic Synthesis via Metal Carbonyls*; I. Wender and P. Pino, Eds.; Wiley-Interscience: New York, 1977; Vol. 2; pp 419.
46. Otsuka, S.; Nakamura, A. *Adv. Organomet. Chem.* **1975**, *14*, 245.
47. Grevels, F.-W.; Buchkremer; Koerner von Gustorf, E. A. *J. Organomet. Chem.* **1976**, *111*, 235.
48. Case, J. R.; Clarkson, R.; Jones, E. R. H.; Whiting, M. C. *Proc. Chem. Soc.* **1959**, 150.
49. Aime, S.; Milone, L.; Sappa, E. *J. Chem. Soc. Dalton Trans.* **1979**, 1664.
50. Hoffman, K.; Weiss, E. *J. Organomet. Chem.* **1977**, *128*, 399.
51. Grevels, F.-W.; Reuvers, J. G. A.; Takats, J. *J. Am. Chem. Soc.* **1981**, *103*, 4069 and references therein.
52. Axe, F. U.; Marynick, D. S. *J. Am. Chem. Soc.* **1988**, *110*, 3728, and references therein.
53. Heck, R. F. *Organotransition Metal Chemistry: A Mechanistic Approach*; Academic Press: New York, 1974, pp 239-240.
54. Parshall, W.; Ittel, S. D. *Homogeneous Catalysis*; Wiley-Interscience: New York, 1992; Vol. 2, pp 205-207.
55. Liebeskind, L. S.; Baysdon, S. L.; South, M. S.; Iyer, S.; Leeds, J. P. *Tetrahedron* **1985**, *41*, 5839.
56. Kang, J. W.; McVey, S.; Maitlis, P. M. *Can. J. Chem.* **1968**, *46*, 3189.
57. Mingos, D. M. P. In *Comprehensive Organometallic Chemistry*; G. Wilkinson, F. G. A. Stone and E. W. Abel, Eds.; Pergamon Press: Oxford, 1983; Vol. 3; pp 62.
58. Rieker, A.; Rundel, W.; Kessler, H. *Z. Naturforsch., B.* **1969**, *24*, 547.
59. Bruce, J. M. In *Rodd's Chemistry of Carbon Compounds*; S. Coffey, Ed.; Elsevier: New York, 1974; Vol. III, Part B, Chp. 8; pp 33.
60. Berger, S.; Rieker, A. *Tetrahedron* **1972**, *28*, 3123.

Chapter 4

Reactivity of $\text{Fe}(\text{CO})_4(\eta^2\text{-C}_2(\text{CF}_3)_2)$ Towards Phosphines: Spectacular Enhancement of Carbonyl Substitutional Lability by an Alkyne Ligand

4.1. Introduction

The reactivity patterns of $\text{M}(\text{CO})_4(\eta^2\text{-alkyne})$ ($\text{M} = \text{Ru}, \text{Os}$) complexes suggest that the reactions are initiated by facile CO dissociation. For example, the compounds readily exchange with ^{13}CO in solution^{1,2} and undergo carbonyl substitution reactions with phosphines.³ Furthermore, a detailed kinetic study of the carbonyl substitution chemistry of $\text{M}(\text{CO})_4(\eta^2\text{-HFB})$ ($\text{M} = \text{Ru}, \text{Os}$) has recently been conducted, and the dissociative mechanism was confirmed.⁴ Interestingly, a profound metal dependence of the rate of CO loss was discovered. When compared with $\text{M}(\text{CO})_5$, the rate of CO dissociation in $\text{M}(\text{CO})_4(\eta^2\text{-HFB})$ was accelerated by factors of 2×10^2 for ruthenium and, more significantly, by 1×10^7 for Os (Eq. 4.1).

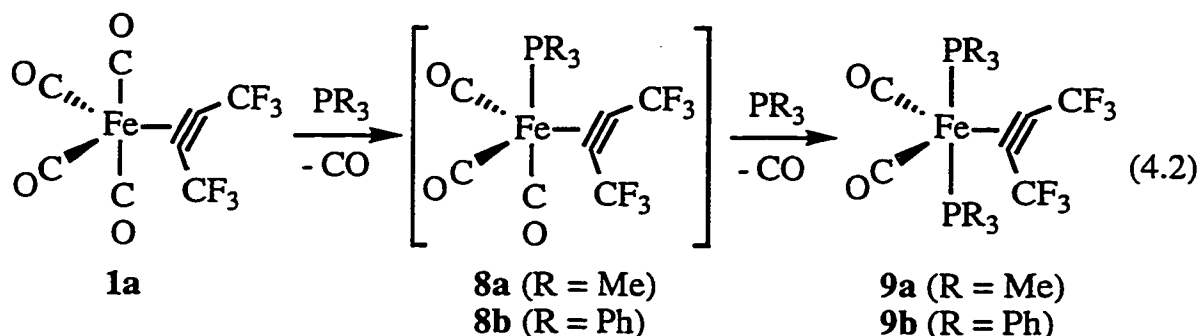


As discussed in Chapter 2, $\text{Fe}(\text{CO})_4(\eta^2\text{-HFB})$ (**1a**) also exchanges with ^{13}CO , but the exchange is much faster than in its second and third row congeners. This qualitatively implies that the iron complex is undergoing even more facile CO dissociation, which is fascinating when one considers that the carbonyl ligands in $\text{Fe}(\text{CO})_5$ are less labile than those in $\text{Os}(\text{CO})_5$.⁵ Given this intriguing metal dependence, it was naturally of interest to complete the kinetic study by investigating the reactivity of **1a** towards phosphines. A study incorporating results presented in this chapter has been published.⁴

4.2. Reaction of $\text{Fe}(\text{CO})_4(\eta^2\text{-HFB})$ (**1a**) with PR_3 ($\text{R} = \text{Me}, \text{Ph}$)

4.2.1. Synthetic Aspects

In agreement with the greater facility of ^{13}C O exchange in $\text{Fe}(\text{CO})_4(\eta^2\text{-alkyne})$ complexes, **1a** is much more reactive towards phosphines than its second and third row congeners. On warming reaction mixtures of **1a** and PR_3 from -78°C , the initially colorless solutions gave way to a bright yellow ($\text{R} = \text{Me}$) or bright orange ($\text{R} = \text{Ph}$) color beginning at a remarkably low temperature of *ca.* -35°C . In contrast, the reactions of $\text{M}(\text{CO})_4(\eta^2\text{-HFB})$ ($\text{M} = \text{Ru}, \text{Os}$) with trimethyl- and triphenylphosphine occurred between 0 and $+10^\circ\text{C}$.³ As with the ruthenium and osmium compounds, the reaction did not stop with substitution of one CO ligand, but continued to afford $\text{Fe}(\text{CO})_2(\text{PR}_3)_2(\eta^2\text{-HFB})$ (**9a**, $\text{R} = \text{Me}$; **9b**, $\text{R} = \text{Ph}$) as yellow (**9a**) or orange (**9b**) powders, respectively (Eq. 4.2).



Addition of one equivalent of phosphine generated a mixture of unreacted **1a**, a small amount of the monosubstituted **8** and large quantities of disubstituted **9**. When the reaction of **1a** with excess PMe_3 was followed by ^{19}F NMR spectroscopy, the monosubstituted **8a** could be readily identified (*vide infra*) by its characteristic doublet resonance at $\delta -54.49$ ppm ($^4J_{\text{PF}} = 0.7$ Hz) (Figure 4-1). The reaction was complete within 90 min at -35°C , and the final *bis*-phosphine complex **9a** was present in greater concentration than **8a** in all recorded spectra. This generally agrees with the behavior of the ruthenium and osmium counterparts and qualitatively suggests that the second substitution step with **1a** is as rapid or more rapid than the first. Finally, it should be noted that the

retention of the HFB ligand in **8,9** contrasts with $\text{Fe}(\text{CO})_4(\eta^2\text{-C}_2(\text{SiMe}_3)_2)$ which afforded $\text{Fe}(\text{CO})_3(\text{PPh}_3)_2$ when reacted with PPh_3 .⁶

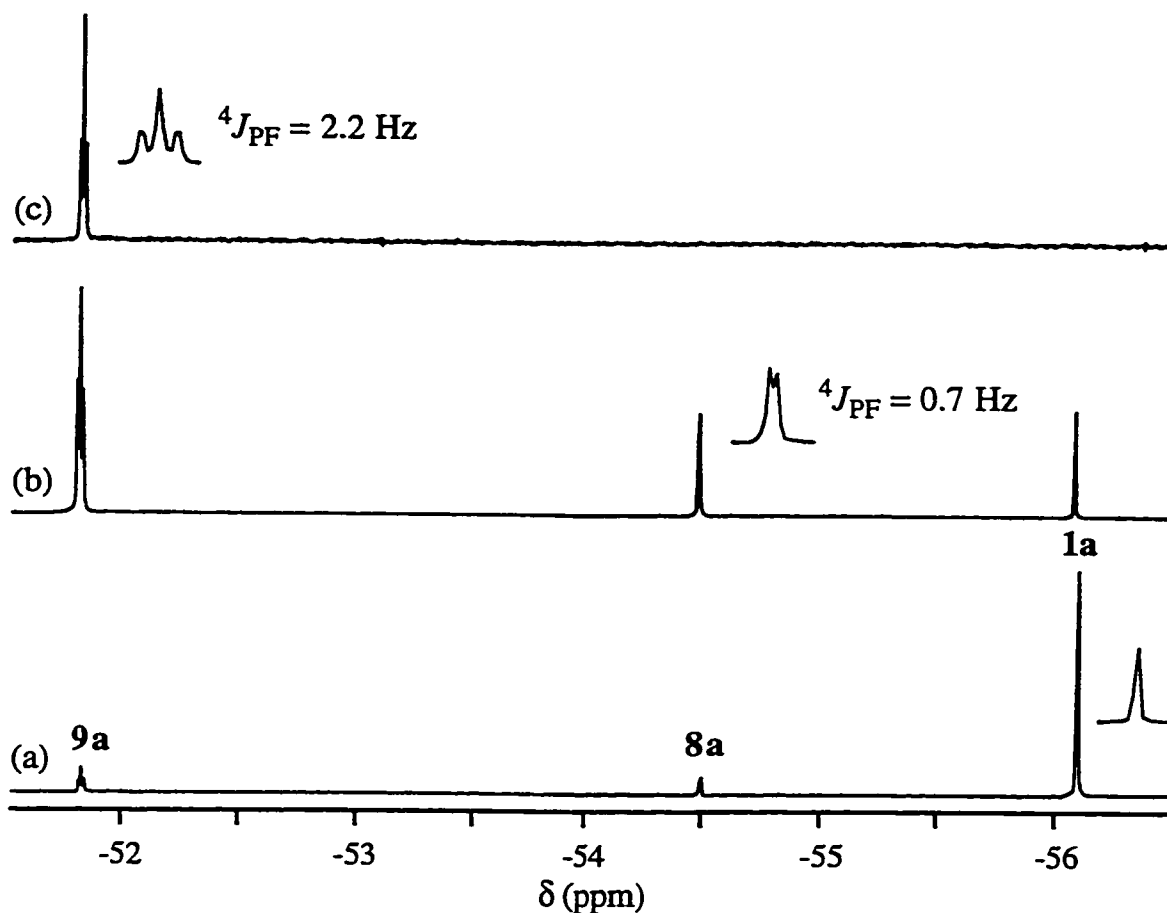


Figure 4-1. ^{19}F NMR Monitored Reaction of **1a** with PMe_3 in CD_2Cl_2 .
 (a) Initial, -60°C . (b) After 30 min at -35°C . (c) After 90 min at -35°C .

4.2.2. Characterization of Products

The IR spectra of the $\text{Fe}(\text{CO})_3(\text{PR}_3)(\eta^2\text{-HFB})$ (**8a**, $\text{R} = \text{Me}$; **8b**, $\text{R} = \text{Ph}$) species show the expected tricarbonyl band pattern for the proposed C_s structure. In accord with the substitution of a carbonyl by an electron-donating phosphine ligand, the average CO stretching frequencies have shifted to lower energy by *ca.* 50 cm^{-1} when compared to **1a** (Table 4-1).

Table 4-1. FT-IR Spectra (ν , cm^{-1}) of $\text{Fe}(\text{CO})_{4-x}(\text{PR}_3)_x(\eta^2\text{-HFB})$ ($x = 1, 2$).

Compound	x	R	ν_{CO}	$\nu_{\text{C-C}}$	$\Delta(\nu_{\text{C-C}})^a$
1a^b	0	–	2125(w), 2058(s), 2033(m)	1890(w)	410
8a^b	1	Me	2069(s), 2010(s), 1979(vs)	1858(w)	442
8b^b	1	Ph	2068(vs), 2012(s), 1982(s)	1848(w)	452
9a^b	2	Me	1989(m), 1924(s)	1823(w) 1780(vw)	477 520
9b^c	2	Ph	1989(m), 1922(s)	1809(w, br) 1775(w)	491 525

^a $\Delta(\nu_{\text{C-C}}) = \nu_{\text{C-C}}(\text{free}) (2300 \text{ cm}^{-1})^7 - \nu_{\text{C-C}}(\text{complex})$. ^bpentane. ^c CH_2Cl_2 .

In the disubstituted complexes **9a,b**, the IR spectra display the expected two band carbonyl pattern, again to lower frequency than that for the monosubstituted complexes. The band pattern is similar to that of $\text{Fe}(\text{CO})_2(\text{PPh}_3)_2(\eta^2\text{-C}_2\text{Ph}_2)$ which was isolated from the reduction of $\text{Fe}(\text{CO})_2(\text{PPh}_3)_2\text{Br}_2$ in the presence of diphenylacetylene.⁸ As the coordination shift criterion $\Delta(\nu_{\text{C-C}})$ (see Section 2.3) demonstrates, the alkyne carbon-carbon stretching frequencies have also shifted to lower energy, indicating that the increased electron density on the metal is also transmitted to the alkyne through enhanced back-bonding. Unexpectedly, there is little difference between the ν_{CO} and $\nu_{\text{C-C}}$ stretching frequencies in the PMe_3 - and PPh_3 -substituted complexes. The disubstituted complexes display two $\nu_{\text{C-C}}$ bands, a result attributed to Fermi resonance coupling with another IR active vibration of the same symmetry. This phenomenon has been seen previously in a variety of η^2 -alkyne complexes, including $\text{M}(\text{CO})_4(\eta^2\text{-HFB})$ ($\text{M} = \text{Ru}, \text{Os}$)² and $\text{M}'\text{Cl}(\text{PPh}_3)_2(\eta^2\text{-C}_2\text{R}_2)$ ($\text{M}' = \text{Rh}, \text{Ir}$; $\text{R} = \text{CF}_3, \text{Ph}, \text{Et}$).⁹ The Ru and Os analogs display similar spectroscopic characteristics and coordination shifts relative to their $\text{M}(\text{CO})_4(\eta^2\text{-HFB})$ ($\text{M} = \text{Ru}, \text{Os}$) parents.³ In keeping with the triad comparison presented in Chapter 2, the heavier congeners show larger coordination shifts than the Fe compounds.

The NMR features of the phosphine-substituted complexes are as expected. The ^{19}F NMR spectra of **8a,b** appear as a doublets due to coupling to

the single phosphorus nucleus ($^4J_{PF} = 0.7$ Hz, **8a**; 1.8 Hz, **8b**). The single resonance in the ^{19}F NMR confirms that the phosphine is located in the axial position, as expected on the basis of both steric and electronic arguments.¹⁰ The corresponding signal in the ^{31}P NMR spectra appears as a broadened singlet; the anticipated septet is not resolved. The ^{13}C NMR spectrum recorded on a ^{13}CO enriched sample of **8a** provides further confirmation of the molecular geometry. Two resonances are observed at δ 211.68 and 202.90 in a 2:1 ratio. The signal of unit intensity is a doublet with a large carbon-phosphorus coupling constant ($^2J_{PC} = 73$ Hz), confirming that the axial carbonyl lies *trans* to the phosphine.¹¹ The signal of intensity two displays a smaller *cis* coupling of $^2J_{PC} = 33$ Hz. Additional coupling ($^2J_{CC} = 8$ Hz) was observed between the axial and equatorial carbonyls with the correct splitting pattern.

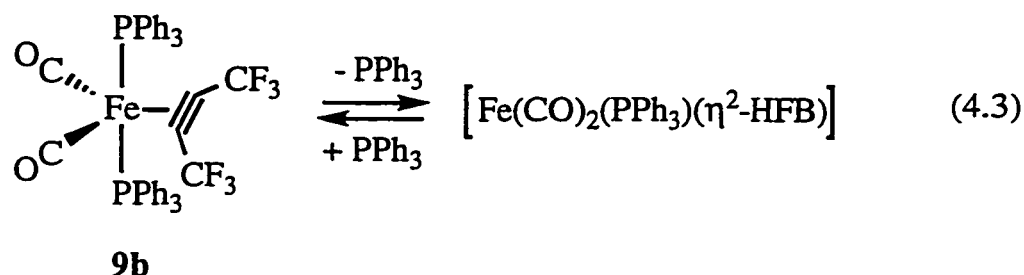
Both $\text{Fe}(\text{CO})_2(\text{PR}_3)_2(\eta^2\text{-HFB})$ complexes have similar NMR features in accord with a structure of C_{2v} symmetry. The ^{19}F NMR spectra display a single triplet resonance, and the ^{31}P NMR spectra consist of a single septet for **9a** and a broad, unresolved singlet for **9b** in accord with equivalent CF_3 and PR_3 groups, respectively. Furthermore, the ^{13}C NMR spectra consist of a single triplet resonance in the CO region (δ 218.00, **9a**; 218.54, **9b**) with a coupling constant ($^2J_{PC} = 28$ Hz) that is consistent with a mutually *cis* arrangement of carbonyl and phosphine ligand. Complexes **1a**, **8** and **9** also demonstrate the well known trend for δ_{CO} , $\text{Fe} > \text{Ru} > \text{Os}$,¹¹ and δ_{CO} also generally shifts further downfield with increasing levels of phosphine substitution.¹² Thus, the CO resonances in **8a** are some 5 ppm downfield of those in **1a**, and the lone triplet in **9a** is 6 ppm downfield of the equatorial CO signal of **8a**. Finally, the fact that $\delta_{\text{CO(ax)}} < \delta_{\text{CO(eq)}}$ in **8a** supports the assignment of the upfield CO resonance in **1a** to the axial carbonyls (Section 2.2.3).

The observation of a pseudotriplet due to virtual coupling^{13,14} for the methyl protons in **9a** confirms the *trans* relationship of the phosphines in the disubstituted compounds. A similar observation was made in the characterization of $\text{Os}(\text{CO})_2\{\text{P}(\text{OMe})_3\}_2(\eta^2\text{-HFB})$, prepared by prolonged UV photolysis of *trans*- $\text{Os}(\text{CO})_3\{\text{P}(\text{OMe})_3\}_2$ in neat hexafluorobut-2-yne.¹⁵ Berke and co-workers have successfully prepared $\text{Fe}(\text{CO})_2(\text{PR}'_3)_2(\eta^2\text{-alkyne})$ ($\text{R}' = \text{Et}, \text{OMe}$; alkyne = C_2Ph_2 ,

PhCCH, C₂H₂) complexes from {Fe(CO)₂(PR'₃)₂}₂(μ-N₂),^{16,17} and the structurally characterized examples display the mutually *trans* diaxial arrangement of phosphines predicted for **9a,b**.^{16,18}

4.2.3. Reversible PPh₃ Dissociation from Fe(CO)₂(PPh₃)₂(η²-HFB), **9b**

Both disubstituted complexes are stable as solids at room temperature, but **9b** shows evidence for reversible phosphine dissociation in solution. Namely, when the IR spectrum of the compound was obtained as a KBr pellet, two terminal CO bands were observed at 1987 and 1919 cm⁻¹. However, when orange **9b** was dissolved in CH₂Cl₂, the bands at 1989 and 1922 cm⁻¹ were accompanied by two weak terminal CO bands at 2016 and 1954 cm⁻¹. As these new bands are at higher frequency than the original bands of **9b**, it seems reasonable to suggest that phosphine dissociation has occurred to generate a small equilibrium amount of Fe(CO)₂(PPh₃)(η²-HFB) (Eq. 4.3).



In accord with this suggestion, the ³¹P NMR spectrum of **9b** was broad at room temperature, but sharpened to a narrow singlet at -60°C, suggesting rapid exchange with a second species at higher temperature. When excess PPh₃ was added to the NMR tube, the ³¹P NMR resonance due to free PPh₃ was broad at room temperature but sharp at -60°C, indicating that the exchange behavior involves free PPh₃. Phosphine dissociation has also been reported recently by Caulton and co-workers for Ru(CO)₂(P^tBu₂Me)₂(η²-C₂Ph₂) and was attributed to steric repulsion between the bulky phosphines and coordinated diphenylacetylene.¹⁹ Support for steric arguments in this case and for **9b** comes from the observation that both Ru(CO)₂(PEt₃)₂(η²-C₂Ph₂) and Fe(CO)₂(PMe₃)₂(η²-HFB) (**9a**) are stable toward phosphine dissociation.

Although attempts to isolate the phosphine-dissociated product were unsuccessful, the reversible nature of the second substitution step allowed for the formulation of a synthetic strategy for the *in situ* formation of **8b**. We reasoned that, in the presence of CO, any **9b** formed during the initial stages of the reaction would convert back to **8b**, presumably *via* the " $\text{Fe}(\text{CO})_2(\text{PPh}_3)(\eta^2\text{-HFB})$ " intermediate, thereby liberating PPh_3 . Thus, as long as the stoichiometry between **1a** and PPh_3 was 1:1, the presence of a CO atmosphere would ensure formation of **8b** only, and this was indeed the case. It was found that **8b** itself was quite unstable in the absence of a CO atmosphere and could not be isolated pure. Unfortunately, loss of CO to form " $\text{Fe}(\text{CO})_2(\text{PPh}_3)(\eta^2\text{-HFB})$ " was not clean, and **8b** decomposed upon warming.

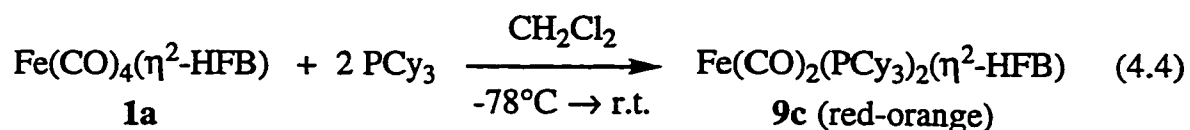
4.3. Reaction of **1a** with Bulky Phosphines (P^tBu_3 and PCy_3)

4.3.1. Initial Observations

The interesting observation that compound **9b** reversibly loses PPh_3 in solution was tempered by the fact that the dissociated product could not be isolated or characterized. Since it was argued that steric factors were controlling this behavior, **1a** was reacted with the much more sterically demanding P^tBu_3 in the hopes of stabilizing the putative " $\text{Fe}(\text{CO})_2(\text{PR}_3)(\eta^2\text{-HFB})$ " compound. Unfortunately, and in complete contrast to the reaction with the smaller triphenylphosphine ligand, slow warming of a solution of **1a** in the presence of one or two equivalents of P^tBu_3 from -30°C to room temperature induced complete decomposition of the iron-alkyne compound.

However, **1a** did react with PCy_3 in CH_2Cl_2 under the same low temperature conditions noted for PMe_3 and PPh_3 . As in the previous cases, addition of two equivalents of PCy_3 was required to consume all of **1a**. Initially, a pale yellow solution formed which, upon warming to room temperature, progressively darkened to a deep purple color. Even more intriguing was the fact that, when the solvent was stripped, the purple solution deposited a reddish orange solid which promptly turned purple upon redissolution in CH_2Cl_2 . Cooling the solution to -78°C returned the orange color and addition of pentane

precipitated a reddish-orange solid which had a molecular composition consistent with $\text{Fe}(\text{CO})_2(\text{PCy}_3)_2(\eta^2\text{-HFB})$ (**9c**) (Eq. 4.4).²⁰



An IR spectrum of the orange-red solid (KBr pellet) showed two terminal CO bands at 1973 and 1899 cm^{-1} ,²⁰ while the purple CH_2Cl_2 solution revealed a distinct shift to higher frequency by some 30 - 40 cm^{-1} . As discussed previously for **9b**, these observations clearly suggest that the orange and purple species are related by reversible phosphine dissociation but that the equilibrium strongly favors " $\text{Fe}(\text{CO})_2(\text{PCy}_3)_2(\eta^2\text{-HFB})$ " for the bulkier tricyclohexylphosphine ligand. Also, the ^{31}P NMR spectrum of **9c** was temperature dependent, displaying a sharp singlet at δ 55.51 ppm at -80°C and a very broad signal at δ 61 ppm at ambient temperature.²⁰

An X-ray crystallography study of the orange compound has confirmed the anticipated *trans*- $\text{Fe}(\text{CO})_2(\text{PCy}_3)_2(\eta^2\text{-HFB})$ structure for **9c** (Figure 4-2).²¹ The phosphine ligands are noticeably bent back away from the HFB ligand, a feature reflected in the P(1)-Fe-P(2) angle of $168.20(5)^\circ$.²¹ This contrasts with the essentially linear P-Fe-P angles in $\text{Fe}(\text{CO})_2(\text{PEt}_3)_2(\eta^2\text{-PhCCH})$ ($177.1(1)^\circ$)¹⁶ and $\text{Fe}(\text{CO})_2\{\text{P}(\text{OMe})_3\}_2(\eta^2\text{-C}_2\text{Ph}_2)$ ($177.4(1)^\circ$).¹⁸ The phosphine ligands are also tilted significantly towards C(2)O(2); the P(1)-Fe-C(1) and P(2)-Fe-C(1) angles are essentially right at $90.89(13)$ and $89.14(13)^\circ$ while the P(1)-Fe-C(2) and P(2)-Fe-C(2) angles are compressed to $83.74(13)$ and $84.89(13)^\circ$. The corresponding angles in $\text{Fe}(\text{CO})_2(\text{PEt}_3)_2(\eta^2\text{-PhCCH})$ and $\text{Fe}(\text{CO})_2\{\text{P}(\text{OMe})_3\}_2(\eta^2\text{-C}_2\text{Ph}_2)$ range between $89.5(1)$ and $92.0(1)^\circ$.^{16,18} Although not shown in Figure 4-2, the hydrogen atoms on the cyclohexyl ring carbons adjacent to a CF_3 group approach to within ≈ 2.4 Å of the fluorine atoms. For example, the axial hydrogen on C(26) has close contacts of 2.50 and 2.65 Å with F(1) and F(3), respectively, as does the axial hydrogen of C(46) with F(4) and F(6) at 2.65 Å each.

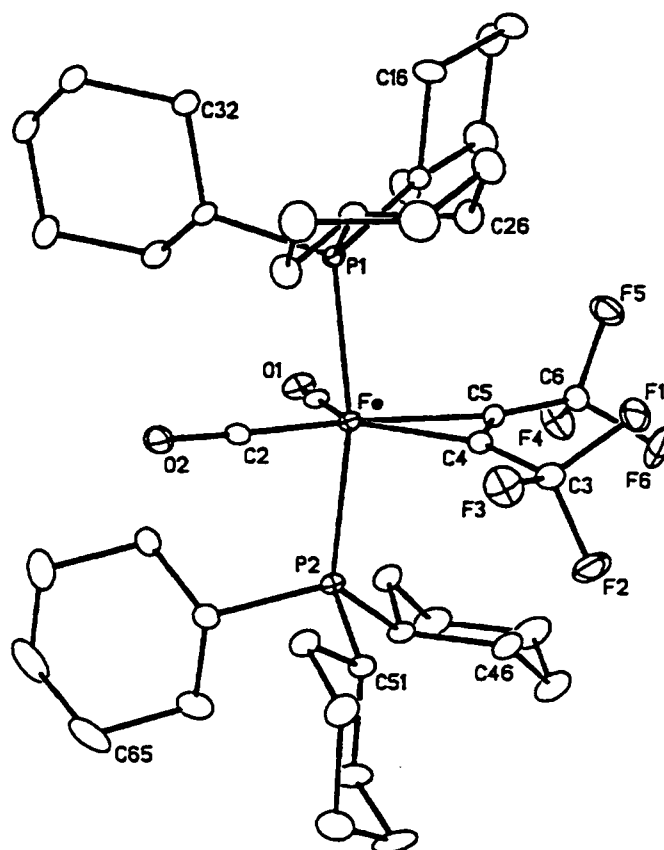


Figure 4-2. Molecular Structure of Compound **9c**.²¹

One of the closest approaches is made by the hydrogen on the *ipso* carbon C(51) to F(2) at 2.44 Å. All of the noted contacts are significantly less than the sum of the van der Waals radii of hydrogen (1.20 - 1.45 Å) and fluorine (1.50 - 1.60 Å).²² Overall, it is clear that the inclusion of the two bulky PCy₃ groups in **9c** results in a significant amount of steric strain in the molecule.

4.3.2. Characterization of Isomeric Fe(CO)₃(PCy₃)(η²-HFB), **8c/c'**

Given the apparent tendency of **9c** to exist in its dissociated form, it seemed reasonable that it should be possible to isolate and characterize the purple compound providing that the second equivalent of PCy₃ could be eliminated. However, initial efforts met with failure. Thus, simple reaction of **1a** with one equivalent of PCy₃ led to the recovery of **9c** along with unreacted **1a**.²⁰ In the hopes of discovering more about the course of the reaction so as to develop a

strategy to isolate the intriguing purple compound, the reaction of **1a** with excess PCy₃ was monitored by multinuclear NMR spectroscopy.

As in the benchtop experiments, following consumption of **1a** after *ca.* 1 h at -30°C, the solution was yellow and two products were detected by ¹⁹F NMR spectroscopy in a *ca.* 25:75 % ratio. A doublet was observed for the minor species, a result consistent with the anticipated axially substituted Fe(CO)₃(PCy₃)(η²-HFB) (**8c**). However, rather than observing a broadened singlet for the anticipated *trans*-Fe(CO)₂(PCy₃)₂(η²-HFB) (**9c**), the major product gave rise to a pair of multiplets of equal intensity. The downfield signal was a quartet (⁵J_{FF} = 5.1 Hz) and the upfield signal appeared as a quartet of doublets (⁵J_{FF} = 5.1 Hz, ⁴J_{PF} = 3.3 Hz), clearly suggesting that the new species contained an unsymmetrical HFB ligand. The fact that the upfield signal was split into a doublet by phosphorus coupling implied that the major species contained one PCy₃ ligand as well.

In order to obtain further structural information, ¹³CO enriched **1a** was reacted under the same conditions and gave surprising results (Figure 4-3).

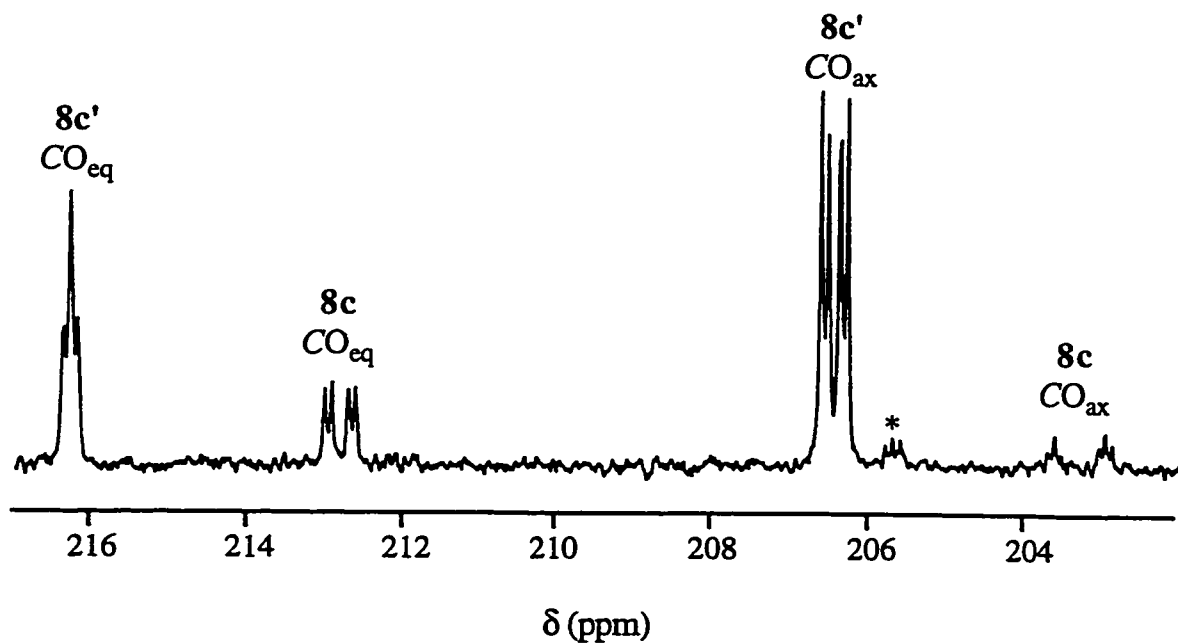
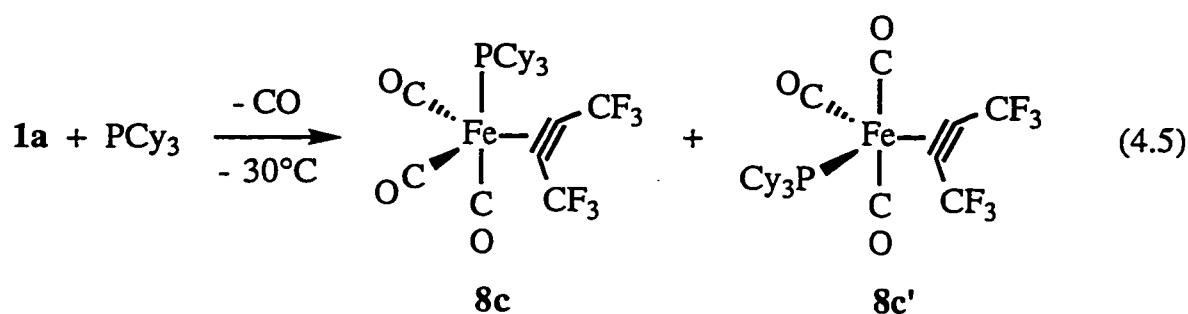


Figure 4-3. ¹³C NMR of **8c/c'** Formed by Reaction of ¹³CO Enriched **1a** with Excess PCy₃ After 4 h at -40°C (* = CO_{eq}, Unreacted **1a**).

Both species were found to contain three carbonyl ligands, two of which were equivalent in each. The ^{13}C NMR spectrum of the minor species **8c** was similar to that of the PMe_3 complex **8a**. Signals were observed in a 2:1 ratio at δ 212.82 (dd, $^2J_{\text{PC}} = 31$ Hz, $^2J_{\text{CC}} = 9$ Hz) and 203.35 (dt, $^2J_{\text{PC}} = 68$ Hz, $^2J_{\text{CC}} = 9$ Hz); the large phosphorus-carbon coupling of the latter signal confirms the structural assignment as the axially-substituted product. In contrast, the major species **8c'** displayed resonances at δ 216.26 and 206.52 in a 1:2 ratio. Based on the criterion established by **8a**, $\delta \text{CO}_{\text{eq}} > \delta \text{CO}_{\text{ax}}$, the chemical shifts suggest a single equatorial and a pair of equivalent axial carbonyls consistent with equatorial PCy_3 substitution (Eq. 4.5).



The downfield resonance was a triplet ($^2J_{\text{CC}} = 9$ Hz) while the upfield signal appeared as a doublet of doublets ($^2J_{\text{PC}} = 24$ Hz and $^2J_{\text{CC}} = 9$ Hz); the small phosphorus-carbon coupling reinforces the conclusion that both carbonyls are *cis* with respect to the equatorial phosphine. A selective ^{13}C - ^{13}C decoupling experiment was also performed to support the assignment of the carbonyls. Irradiation of the signal at δ 216.3 caused the signal at δ 206.5 to collapse to a doublet. Furthermore, the ^{31}P NMR spectrum showed a single resonance at δ 65.04 which was split into a triplet ($^2J_{\text{PC}(\textit{cis})} = 24$ Hz), confirming that the phosphine was coupled to equivalent axial carbonyls.

It is most interesting that the reaction strongly favors **8c'** since, with PMe_3 and PPh_3 , only axial-substituted compounds were observed. Given the similar basicity of PCy_3 and PMe_3 , this likely reflects a steric preference, and suggests that the equatorial position is more favored in this regard. Although this contrasts with common expectations for trigonal bipyramidal compounds,¹⁰ it appears

reasonable for **8c'** when one considers that the CF₃ groups of the HFB ligand are bent back, away from the equatorial site, as is observed in the sterically encumbered **9c** (Figure 4-2). In fact, the "pocket" of space open in the equatorial site would be quite large (*i.e.* C(2)–Fe–C(4) = 117.4(2)°)²¹ compared to the 90° angle between axial and equatorial sites in an ideal trigonal bipyramid. Thus, the placement of a smaller CO ligand in the axial site and the bulky PCy₃ in the equatorial site might reduce steric interactions with the HFB ligand.

Upon warming the sample to 0°C, the signals in the ¹³C NMR all broadened, suggesting that chemical exchange was occurring between the two isomers. Furthermore, the signal due to free ¹³CO in solution also broadened, indicating that the carbonyls in Fe(CO)₃(PCy₃)(η²-HFB) were labile as expected. Contrary to the formation of **9c**, further reaction under the conditions of the sealed NMR tube was not possible as the ¹³CO present in solution apparently inhibited further substitution.

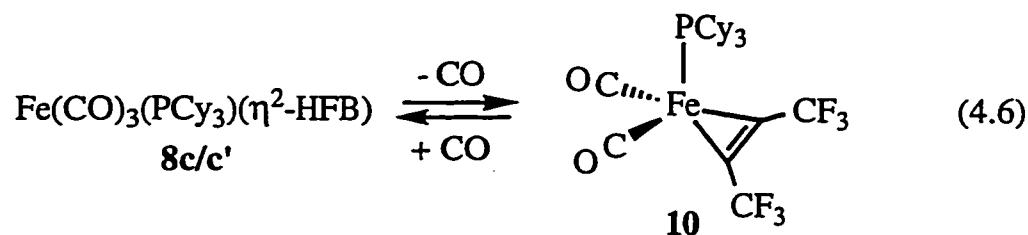
4.3.3. Isolation of Coordinatively Unsaturated Fe(CO)₂(PCy₃)(η²-HFB), **10**

The suppression of further substitution by CO in the formation of **8c/c'** hinted that it might be possible to eliminate formation of the red-orange **9c** if **1a** was reacted with one equivalent of PCy₃ under a CO atmosphere. As with the triphenylphosphine system, allowing the reaction to equilibrate under CO on the benchtop successfully produced **8c/c'** *in situ* and in a similar ratio to that detected in the sealed NMR tube reaction. The yellow compound could be recovered from pentane at -78°C, but warming the solid above *ca.* 0°C resulted in rapid formation of a purple/brown powder. Similarly, warming a pentane solution of **8c/c'** to ambient temperature resulted in a rapid color change to deep purple, and removal of the solvent *in vacuo* left an oily purple residue. Unlike previous attempts, there was no trace of orange-red solid, and the new compound, **10**, was isolated analytically pure.

The air-stable purple compound was quite soluble in pentane, but could be crystallized from a concentrated solution at -80°C. The resulting deep purple crystalline solid was opaque and almost black in color. Addition of one equivalent of PCy₃ in CH₂Cl₂ to a pentane solution of **10** followed by cooling to

-78°C resulted in a color change to orange, and recrystallization at the same temperature afforded **9c** in good yield. Similarly, exposing a pentane solution of the purple compound to a stream of CO resulted in the rapid reformation of **8c/c'**. Thus, the new purple compound is clearly the sought after $\text{Fe}(\text{CO})_2(\text{PCy}_3)(\eta^2\text{-HFB})$ (**10**), a formulation supported by elemental analysis.

As mentioned previously, the IR spectrum of the purple compound revealed two terminal CO bands to higher frequency than solid **9c** in accord with **10** being related to **9c** by phosphine loss. The ^{19}F NMR and ^{31}P NMR spectra at + 20°C consisted of singlets at δ -57.03 and 49.93 ppm, respectively, suggesting a C_s structure (Eq. 4.6).



Importantly, the latter signal was sharp with a half-height width of 7 Hz, in distinct contrast to the ^{31}P NMR spectrum of **9c** which displayed a very broad signal at δ 61 ppm at ambient temperature ($\Delta\nu_{1/2} \approx 1 \times 10^4$ Hz).²⁰ Thus, compound **10** retains its phosphine ligand in solution.

A clear issue to be resolved is whether the HFB ligand in **10** functions as a two electron donor, keeping the iron center both coordinatively and electronically unsaturated, or whether the alkyne π_{\perp} MO also becomes involved in bonding to provide an electron-precise compound containing a four-electron donor alkyne.²³ A comparison of the carbon-carbon stretching frequency provides an initial clue, for the band in **10** (1734 cm^{-1}) is found to lower wavenumber than the ν_{CC} stretch in **8c/c'** (1840 cm^{-1}) by 106 cm^{-1} , thus suggesting additional metal-alkyne bonding in **10**.

Another criterion, introduced by Templeton, is the relationship between the ^{13}C NMR chemical shift of the alkyne carbons and the number of electrons formally donated.²⁴ Two electron donor alkyne carbons are typically found in

the region between δ 98 and 126 ppm while four electron donation results in a dramatic downfield shift between δ 175 and 226 ppm as the carbon atoms become carbenoid in character (Scheme 2-1). In order to establish a benchmark for a two-electron alkyne in the current system, a $^{13}\text{C}\{^{19}\text{F}\}$ spectrum was collected on a concentrated sample of $\text{Fe}(\text{CO})_3(\text{PCy}_3)(\eta^2\text{-HFB})$. The alkyne carbons of **8c'** were detected as doublets at δ 104.23 and 91.85 ($^2J_{\text{PC}} = 6, 9$ Hz respectively) in accord with Templeton's criteria. The fact that the resonances are further downfield than those in **1a** agrees with greater π back-donation to the alkyne due to the presence of electron donor PCy_3 , as discussed for the $\Delta(\nu_{\text{C-C}})$ trends in **8a,b** (Section 4.2.2).

The ^{13}C NMR spectrum of compound **10** showed three resonances at δ 216.73 (d, $^2J_{\text{PC}} = 28$ Hz), 171.1 (m), and 123.84 (q, $^1J_{\text{CF}} = 270$ Hz) in addition to upfield resonances for the carbons in the phosphine ligand. The downfield doublet is due to a pair of equivalent carbonyl ligands, and the observed coupling to phosphorus agrees with a *cis* arrangement between the phosphine and carbonyls; the signal intensity also increased dramatically when a spectrum was recorded on ^{13}CO enriched material. The quartet at δ 123.84 ppm is assigned to the carbon of the trifluoromethyl group on the basis of the characteristic $^1J_{\text{CF}}$ coupling constant, which leaves the multiplet at δ 171.1 as belonging to the internal alkyne carbons. To further confirm the assignments, ^{19}F decoupling was employed; the multiplet at δ 171.1 resolved into a doublet ($^2J_{\text{PC}} = 7$ Hz) and the quartet for the CF_3 group expectedly became a singlet. Thus, the ^{13}C NMR characteristics of the HFB ligand in compound **10** conforms to that predicted for a four-electron donor alkyne. Similar low field resonances were detected at *ca.* δ 187 in $\text{Fe}(\eta^2\text{-C}_2\text{R}_2)\{(\text{PMe}_2\text{CH}_2)_3\text{SiMe}\}$ ($\text{R} = \text{Et}, \text{Ph}$) where the alkynes also act as four electron donors.²⁵

The C_s structure proposed in Eq. 4.6 is consistent with other examples of $d^8\text{-ML}_3(\eta^2\text{-alkyne})$ complexes of group 9 metals²⁶ and, more importantly, with the group 8 examples $\text{M}(\text{CO})(\text{P}^i\text{Pr}_3)_2(\eta^2\text{-C}_2\text{Ph}_2)$ ($\text{M} = \text{Ru}, \text{Os}$),²⁷ and $\text{Fe}\{\text{P}(\text{OMe})_3\}_3(\eta^2\text{-C}_2\text{R}_2)$ ($\text{R} = \text{Me}, \text{Et}, \text{Ph}$).²⁸ The ruthenium and osmium compounds were formed by reaction of $\text{RuH}(\eta^2\text{-H}_2\text{BH}_2)(\text{CO})(\text{P}^i\text{Pr}_3)_2$ and $\text{OsH}_4(\text{CO})(\text{P}^i\text{Pr}_3)_2$, respectively, with excess diphenylacetylene while the purple

iron complexes were produced in low (< 4 %) yield by the reduction of $\text{FeCl}_2\{\text{P}(\text{OMe})_3\}_3$ in the presence of alkynes. The most notable difference between the aforementioned compounds and **10** is that the former all react *irreversibly* with CO to produce *trans*- $\text{M}(\text{CO})_2(\text{PR}_3)_2(\eta^2\text{-C}_2\text{R}_2)$ compounds analogous to **9a-c**. In the case of compound **10**, it would appear that, due to the felicitous stereo-electronic properties of the PCy₃ ligand, the CO-dissociated form is the thermodynamic product.

4.3.4. Molecular Structure of $\text{Fe}(\text{CO})_2(\text{PCy}_3)(\eta^2\text{-HFB})$ (**10**)

Although the spectroscopic and analytical data are in agreement with the proposed structure for compound **10**, it was clearly of interest to seek further corroboration by X-ray diffraction techniques. A single crystal was grown from a concentrated pentane solution at -35°C , and the resulting molecular structure is presented in Figure 4-4. Selected interatomic distances and angles are provided in Table 4-2. The geometry can be described as square-pyramidal, where C(1), C(2), C(3), and C(4) form the base and P is the apex. However, contrary to typical square-pyramidal coordination where the apical ligand is perpendicular to the base,¹⁰ the angles in the present complex show severe but interesting deviations. Thus, while the angles between the carbonyls and phosphine are near 90° ($\text{P-Fe-C}(1) = 90.17(12)^\circ$ and $\text{P-Fe-C}(2) = 91.61(12)^\circ$), the angles between the phosphine and the alkyne ligand open up considerably ($\text{P-Fe-C}(4) = 116.62(11)^\circ$ and $\text{P-Fe-C}(5) = 120.48(12)^\circ$), with the result that the Fe-P vector bends significantly towards the carbonyl ligands.

The structure is closely related to the two known group eight examples, $\text{Os}(\text{CO})(\text{P}^i\text{Pr}_3)_2(\eta^2\text{-C}_2\text{Ph}_2)$ ²⁷ and $\text{Fe}\{\text{P}(\text{OMe})_3\}_3(\eta^2\text{-C}_2\text{Ph}_2)$.²⁸ The former compound has essentially the same geometry as **10** with the exception that one of the basal carbonyls is replaced by a phosphine. In common with **10**, the angle between the apical phosphorus and carbonyl is $88.2(1)^\circ$ and the alkyne is bent away from the apical position with $\text{P-Os-C}_{\text{alk}}$ angles of $101.3(1)$ and $128.9(1)^\circ$. The presence of the bulky alkyne in a basal position causes the alkyne to twist so that the larger of the aforementioned angles belongs to the carbon adjacent to the phosphine; the twisting is thus likely the result of a steric interaction between the

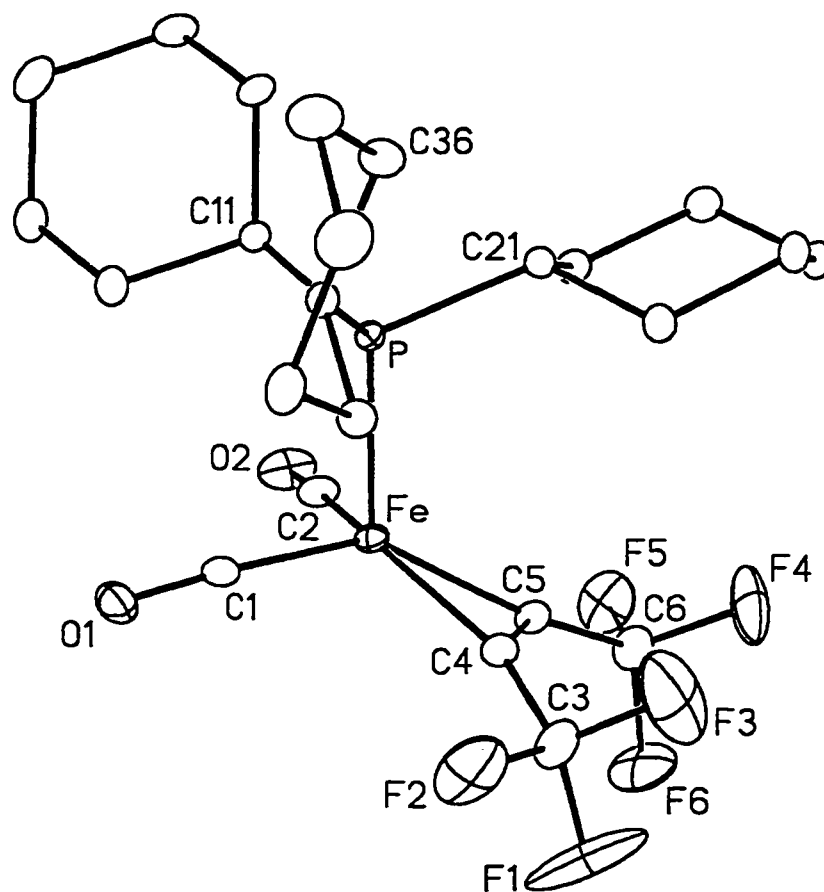


Figure 4-4. Molecular Structure of Compound 10.

Table 4-2. Selected Interatomic Distances (Å) and Angles (deg.), Compound 10.

Fe–P	2.2101(10)	P–Fe–C(5)	120.48(12)
Fe–C(1)	1.759(4)	C(1)–Fe–C(2)	103.3(2)
Fe–C(2)	1.778(4)	C(1)–Fe–C(4)	104.5(2)
Fe–C(4)	1.864(4)	C(2)–Fe–C(5)	101.3(2)
Fe–C(5)	1.871(4)	C(4)–Fe–C(5)	40.5(2)
C(4)–C(5)	1.294(5)	Fe–C(1)–O(1)	175.9(3)
C(1)–O(1)	1.154(5)	Fe–C(2)–O(2)	176.8(3)
C(2)–O(2)	1.144(5)	Fe–C(4)–C(5)	70.0(2)
P–Fe–C(1)	90.17(12)	Fe–C(5)–C(4)	69.5(2)
P–Fe–C(2)	91.61(12)	C(3)–C(4)–C(5)	136.2(4)
P–Fe–C(4)	116.62(11)	C(4)–C(5)–C(6)	138.0(4)

phosphine and the phenyl substituent of the alkyne. Unfortunately, only a preliminary X-ray study was completed on $\text{Fe}\{\text{P}(\text{OMe})_3\}_3(\eta^2\text{-C}_2\text{Ph}_2)$,²⁸ with the lone datum reported being the alkynic carbon-carbon distance of 1.332(10) Å. The carbon-carbon separation is similar to that in Os compound (1.318(5) Å) and slightly longer than is found in **10** (1.294(5) Å).

In accord with the IR and ¹³C NMR spectroscopic characteristics, the HFB ligand in compound **10** shows the expected features of a four electron alkyne. Namely, the C(4)–C(5) separation is lengthened by some 0.03 Å when compared with that in **9c** (1.267(5) Å²¹) and is also longer than the C–C distance in $\text{M}(\text{CO})_4(\eta^2\text{-HFB})$ (M = Ru, Os) (1.276(6) Å, Ru; 1.276(19) Å, Os).²⁶ More importantly, the Fe–C(4) and Fe–C(5) distances (1.864(4), 1.871(4) Å) are much shorter than in the disubstituted complex **9c** (1.991(4), 2.030(4) Å)²¹ and other examples of two-electron alkyne ligands bonded to iron, namely 2.046(8), 2.014(8) Å in $\text{Fe}(\text{CO})_2(\text{PEt}_3)_2(\eta^2\text{-PhCCH})$ ¹⁶ and 2.048(2) Å $\text{Fe}(\text{CO})_2\{\text{P}(\text{OMe})_3\}_2(\eta^2\text{-C}_2\text{Ph}_2)$.¹⁸ The iron-carbon distances are also much shorter than in $\text{Fe}(\text{NO})_2(\text{PPh}_3)(\eta^2\text{-C}_2(\text{CN})_4)$ (2.029(7) and 2.101(6) Å), an olefin compound which adopts a similar geometry to **10**.²⁹ Shortened Os–C_{alk} bond lengths were noted also by Oro in his discussion of the $\text{Os}(\text{CO})(\text{P}^i\text{Pr}_3)_2(\eta^2\text{-C}_2\text{Ph}_2)$ structure.²⁷

This feature agrees with alkyne carbons in **10** taking on a measure of iron-carbon double bond character (Scheme 2-1) through interaction of the π_{\perp} MO with the iron center. Despite the increase in the iron-alkyne bonding character in **10**, the bend-back angles to the CF₃ groups are not greatly affected, as they measure 136.2(4) and 138.0(4)° compared with 133.7(4) and 137.8(4)° in **9c**.²¹ Similar features were noted in a comparison of two- and four-electron HFB ligands in Mo and W compounds. The C–C bond length was found to increase slightly from the 1.28 Å benchmark for a two-electron compound to between 1.30 and 1.34 Å in four-electron HFB complexes with little change in the bend-back angle for the CF₃ groups (137 - 140°). The most important structural feature was the contraction of the M–C_{alk} bond length by approximately 0.10 Å in compounds containing four-electron donor HFB ligands.²³

An additional feature of note is that the Fe–P bond length (2.2101(10) Å) is considerably shorter, by *ca.* 0.15 Å, than those in **9c** (2.3629(11) and 2.3503(12) Å).²¹ This could be the result of reduced steric strain between the cyclohexyl and trifluoromethyl groups compared with the disubstituted complex. The closest approach of a hydrogen in the PCy₃ ligand to the fluorine atoms of HFB in **10** is 2.88 Å. This value is at the cusp of the sum of the van der Waals radii of hydrogen (1.20 - 1.45 Å) and fluorine (1.50 - 1.60 Å),²² thus suggesting minimal steric strain, whereas in **9c** the closest approach was \approx 2.4 Å. On the other hand, the short Fe–P separation might reflect better bonding interactions with the apical phosphine ligand in **10**. Indeed, a common feature of group 9 ML₃(η^2 -alkyne) species is an especially short metal-apical ligand bond length.²⁶ Also distinctive is the near right-angle between the apical ligand and the non-alkyne basal ligands, compared with the more open angle to the alkyne carbons which ranges between 110 and 120° in most of the complexes.^{26,30,31} Thus, compound **10** resembles the known structures of *d*⁸-ML₃(η^2 -alkyne) compounds of group 8 and 9 metals but not the square-planar configurations of *d*⁸ platinum complexes. A detailed analysis of the relationship between distorted square pyramidal and square planar geometries of ML₃(η^2 -alkyne) complexes has been conducted in a previous study.²⁶

4.4. Kinetic Studies

4.4.1. Determination of the Rate of CO Dissociation from **1a**

The fact that **1a** reacts smoothly with PR₃ (R = Me, Ph) at *ca.* -35°C reflects a phenomenal increase in the substitutional lability of the iron-carbonyl bonds in Fe(CO)₄(η^2 -HFB) compared with Fe(CO)₅, which undergoes slow thermal substitution by phosphines only at temperatures near 100°C where the reaction is complicated by decomposition of the metal pentacarbonyl.³² Qualitatively, the result also suggests that **1a** is more reactive than its second and third row congeners which undergo reaction between 0 and 10°C, and it was therefore crucial to quantify the effect by carrying out a kinetic study to compliment the work completed earlier by Pearson and Jordan on the M(CO)₄(η^2 -HFB) (M = Ru, Os) compounds.⁴

Attempts were made to study the reaction by low temperature IR spectroscopy, but it was found that the reaction was simply too fast for IR monitoring, even at the low temperature limit of our system, *ca.* -20°C . Fortunately, the presence of trifluoromethyl groups in **1a** rendered the system easy to monitor by ^{19}F NMR, a qualitative example of which has already been provided in Figure 4-1. The reaction was followed between -30 and -40°C for a range of phosphines (PPh_3 , PCy_3 , P(OPh)_3) which were chosen to provide a modest range of steric and electronic characteristics and to match those used for the kinetic study on the ruthenium analog.⁴ When the disappearance of reactant **1a** was plotted against the time of the reaction (Figure 4-5), it was found that the observed rate was independent of both the nature and concentration of the entering group (Table 4-3), thus initially satisfying the conditions for a dissociative mechanism in which the rate determining step is loss of CO from **1a**.³³

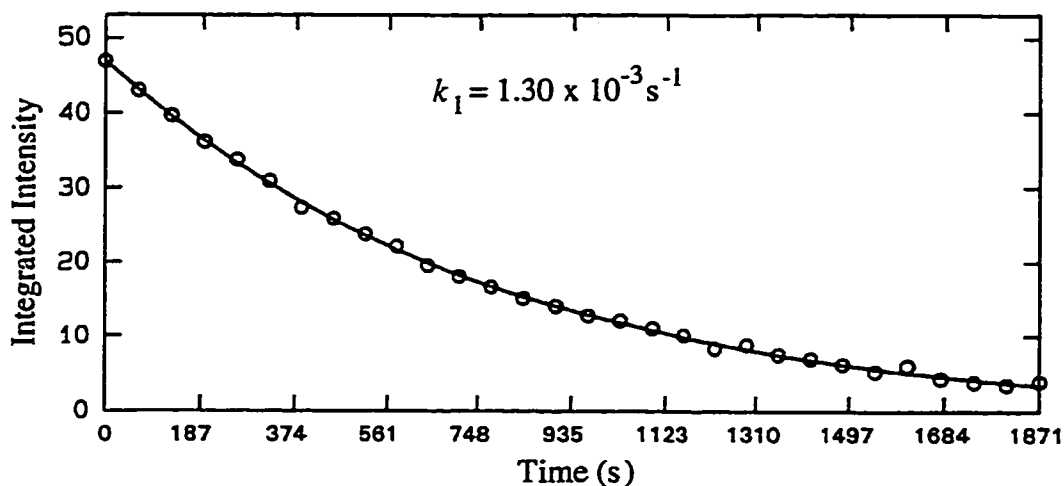


Figure 4-5. Integrated Intensity vs. Time Plot for Disappearance of **1a**. Kinetic Run Conditions were 0.30 M PPh_3 :0.025 M **1a** at -33.5°C in CD_2Cl_2 .

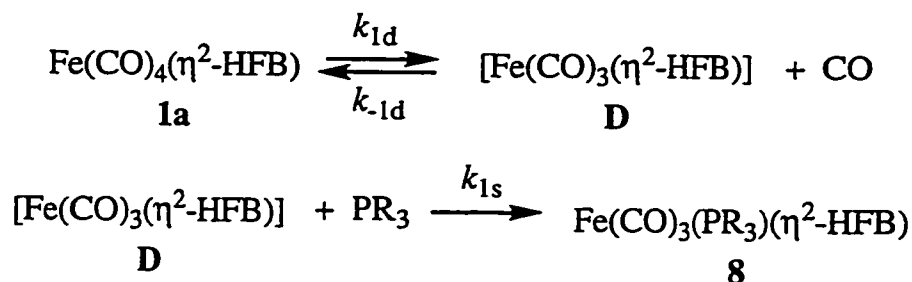
Scheme 4-1 details the proposed mechanism which is initiated by CO loss from **1a** followed by rapid reaction of the putative $[\text{Fe}(\text{CO})_3(\eta^2\text{-HFB})]$ intermediate (**D**) with phosphine.

Table 4-3. Kinetic Results for Reactions of PR₃ with **1a** in CD₂Cl₂.^a

PR ₃	T (°C)	[PR ₃] (M)	10 ³ x k ₁ (s ⁻¹) ^b
PCy ₃	-33.5	0.30	1.34 ± 0.05
P(OPh) ₃	-33.5	0.30	1.22 ± 0.05
PPh ₃	-33.5	0.30	1.30 ± 0.03
PPh ₃	-33.7	0.20	1.28 ± 0.05
PPh ₃	-33.7	0.10	1.30 ± 0.05
PPh ₃	-30.7	0.20	2.16 ± 0.06
PPh ₃	-36.7	0.20	0.69 ± 0.03
PPh ₃	-39.9	0.20	0.38 ± 0.07

^aThe solution initially contained 2.5 x 10⁻² M **1a** and the indicated [PR₃].

^bErrors are one standard deviation determined from least-squares fits of the integrated intensity for 30 points covering ≈ 90% reaction (eg. Figure 4-5).

**Scheme 4-1.** Dissociative Mechanism for Initial Reaction of **1a** with PR₃.

The rate of disappearance of **1a** is given by

$$-d[\mathbf{1a}]/dt = k_{1d}[\mathbf{1a}] - k_{-1d}[\mathbf{D}][\text{CO}] \quad (4.7)$$

and the rate laws governing intermediate **D** are

$$d[\mathbf{D}]/dt = k_{1d}[\mathbf{1a}] \quad (4.8)$$

$$-d[\mathbf{D}]/dt = k_{-1d}[\mathbf{D}][\text{CO}] + k_{1s}[\mathbf{D}][\text{PR}_3] \quad (4.9)$$

The application of the steady state assumption³³ to the concentration of the dissociative intermediate **D** gives

$$[\mathbf{D}] = \frac{k_{1d}[\mathbf{1a}]}{k_{-1d}[\text{CO}] + k_{1s}[\text{PR}_3]} \quad (4.10)$$

which substituted back into Eq. 4.7 provides

$$\begin{aligned} -d[\mathbf{1a}]/dt &= k_{1d} \left(1 - \frac{k_{-1d}[\text{CO}]}{k_{-1d}[\text{CO}] + k_{1s}[\text{PR}_3]} \right) [\mathbf{1a}] \\ &= \frac{k_{1d}k_{1s}[\text{PR}_3]}{k_{-1d}[\text{CO}] + k_{1s}[\text{PR}_3]} [\mathbf{1a}] \end{aligned} \quad (4.11)$$

and thus the result

$$-d[\mathbf{1a}]/dt = k_1[\mathbf{1a}] \quad (4.12)$$

where

$$k_1 = \frac{k_{1d}k_{1s}[\text{PR}_3]}{k_{-1d}[\text{CO}] + k_{1s}[\text{PR}_3]} \quad (4.13)$$

Furthermore, under the experimental conditions of $[\text{PR}_3] \gg [\text{CO}]$ and $k_{1s} > k_{-1d}$, the observations indicate that $k_{1s}[\text{PR}_3] \gg k_{-1d}[\text{CO}]$ so that Eq. 4.13 reduces to

$$k_1 = k_{1d} \quad (4.14)$$

and the observed rate constant k_1 provides the rate of CO dissociation from **1a**.

A least-squares regression analysis of the temperature dependence³³ of k_1 (Eq. 4.15) provides activation parameters of $\Delta H^\ddagger = 88 \pm 2 \text{ kJ}\cdot\text{mol}^{-1}$ and $\Delta S^\ddagger = 70 \pm 10 \text{ J}\cdot\text{mol}^{-1}\cdot\text{K}^{-1}$ for this process.

$$\ln \left(\frac{k_1}{T} \right) = \ln \left(\frac{k_b}{h} \right) - \left(\frac{\Delta H^\ddagger}{RT} \right) + \left(\frac{\Delta S^\ddagger}{R} \right) \quad (4.15)$$

Notably, ΔS^\ddagger is large and positive as expected for a dissociative mechanism.³³ A comparison of the values determined for a series of $\text{M}(\text{CO})_4\text{L}$ ($\text{M} = \text{Fe}, \text{Ru}, \text{Os}$; $\text{L} = \text{CO}, \text{HFB}, \text{PPh}_3$) compounds⁴ is presented in Table 4-4. The results are quite spectacular; the inclusion of the HFB ligand in the $\text{Fe}(\text{CO})_4\text{L}$ framework renders **1a** approximately *30 trillion times* more reactive than the parent pentacarbonyl towards CO substitution and reduces the activation enthalpy by nearly 80

$\text{kJ}\cdot\text{mol}^{-1}$. When taken in the context of the triad as a whole, it becomes clear that the alkyne has a profound influence on the reactivity sequence, reversing the $\text{Fe} < \text{Os} \ll \text{Ru}$ trend for the metal pentacarbonyls to $\text{Fe} \gg \text{Ru} > \text{Os}$ in the $\text{M}(\text{CO})_4(\eta^2\text{-HFB})$ complexes. This is not the case with classical, two-electron donor ligands such as PPh_3 where the trend remains $\text{Fe} < \text{Os} \ll \text{Ru}$ and the rates of CO dissociation actually decrease by one or two orders of magnitude.

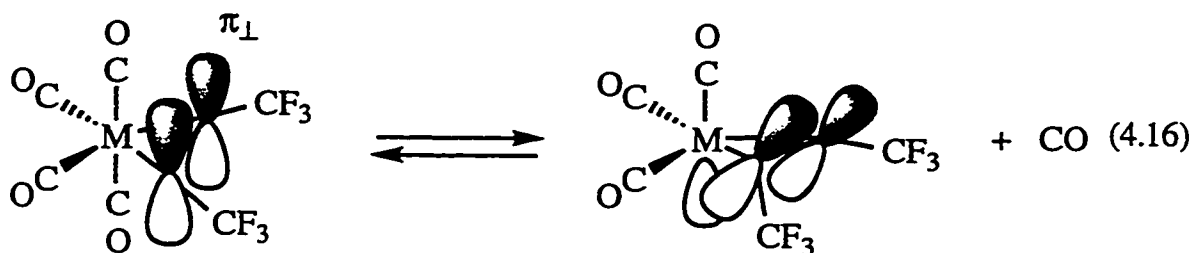
Table 4-4. Comparison of the Reactivity of $\text{M}(\text{CO})_4\text{L}$ Systems with PPh_3 .^a

M	L	k_1 (s^{-1}) (25°C)	$k_{\text{HFB}}/k_{\text{L}}$	ΔH^\ddagger ($\text{kJ}\cdot\text{mol}^{-1}$)	ΔS^\ddagger ($\text{J mol}^{-1}\cdot\text{K}^{-1}$)
Fe	HFB	9.5	–	88 ± 2	70 ± 10
Fe	CO	$\approx 3 \times 10^{-13}$	$\approx 3 \times 10^{13}$	≈ 167	≈ 75
Fe	PPh_3	5.4×10^{-15}	1.8×10^{15}	176 ± 5	73 ± 11
Ru	HFB	1.25×10^{-2}	–	104 ± 2	66 ± 9
Ru	CO	7.0×10^{-5}	1.8×10^2	114.5 ± 3.9	60 ± 12
Ru	PPh_3	3.2×10^{-6}	3.9×10^3	126 ± 1	72 ± 4
Os	HFB	3.5×10^{-3}	–	99.5 ± 0.8	42 ± 3
Os	CO	3.3×10^{-10}	1.1×10^7	133 ± 3	21 ± 7
Os	PPh_3	1.3×10^{-12}	2.6×10^9	168 ± 3	92 ± 8

^aValues for the $\text{M}(\text{CO})_4\text{L}$ systems other than **1a** were taken from Ref. 4.

Despite the remarkable metal dependence of carbonyl lability of the $\text{M}(\text{CO})_4(\eta^2\text{-HFB})$ compounds, their spectroscopic characteristics reveal no significant differences that could account for the profound differences in reactivity. For example, the ν_{CO} stretches in the IR spectra are quite similar (Table 2-7). Furthermore, although a solid state structure is not available for **1a**, the X-ray crystal structures of Ru and Os($\text{CO})_4(\eta^2\text{-HFB})$ ²⁶ showed no significant differences in metrical parameters and the M–CO distances are the same, to within 0.01 Å, of those in the parent $\text{M}(\text{CO})_5$ compounds.^{34,35} Thus, there are no apparent ground state characteristics that account for the metal-dependent trend in carbonyl lability.

A more viable explanation emerges when one considers the nature of the proposed intermediates following CO dissociation from $M(CO)_4(\eta^2\text{-HFB})$ and $M(CO)_5$. Namely, the alkyne ligand has the potential to stabilize the putative $[M(CO)_3(\eta^2\text{-HFB})]$ intermediate through involvement of the filled π_{\perp} orbital on the alkyne (Eq. 4.16).



Indeed, Mingos has noted that "the additional π -donor interaction available to acetylene confers upon it unusual properties since it can function simultaneously as a π -acceptor and π -donor ligand."³⁶ Because no such interaction is possible in $[M(CO)_4]$, the transition state in the alkyne compounds is stabilized and the activation enthalpy is lower when compared with the metal pentacarbonyls. A recent computational study on model $M(CO)_4(\eta^2\text{-C}_2\text{H}_2)$ compounds reproduced the experimental metal-dependent trend and confirmed that the energy of the $[M(CO)_3(\eta^2\text{-C}_2\text{H}_2)]$ intermediates is lower than that of $[M(CO)_4]$.³⁷ Furthermore, dissociation of an axial CO was found to be more favorable than an equatorial one by *ca.* 40 - 80 $\text{kJ}\cdot\text{mol}^{-1}$, a direct consequence of the filled π_{\perp} orbital's ability to stabilize the resulting intermediate from loss of an axial ligand.

Compound **10** provides a clear model for the intermediate proposed in Eq. 4.16. Fortuitously, the PCy_3 ligand provides the correct combination of electronic and steric properties to allow the isolation of this reactive species. In the context of Eq. 4.16, a better description of the structure of **10** might be to consider the phosphine and carbonyls as occupying axial and equatorial sites, respectively, in a trigonal bipyramid. The mid-point of the C(4)–C(5) vector occupies the third equatorial site and the entire alkyne moiety is bent down towards the remaining vacant axial site. In other words, the main structural

change relative to tricarbonyl **8c** is a bending down of the alkyne to interact with the vacant metal orbital following dissociation of the axial carbonyl.

It is also gratifying to note that the calculated geometry of the CO-dissociated $[\text{Fe}(\text{CO})_3(\eta^2\text{-C}_2\text{H}_2)]$ intermediate bears many similarities to the X-ray crystal structure of **10**. Namely, the calculated structure adopts a C_s geometry resembling a distorted square-based pyramid. The angle between the apical and basal CO ligands is 93.3° while the acetylene ligand is bent away from the apical carbonyl by an angle of 117.6° . Furthermore, the C–C bond length is lengthened by 0.05 \AA compared to the $\text{Fe}(\text{CO})_4(\eta^2\text{-C}_2\text{H}_2)$ species, and the Fe–C_{acetylene} bond length contracts to 1.904 \AA from 2.140 \AA upon CO dissociation.³⁷

Although the above rationalizes the greater carbonyl lability in the $\text{M}(\text{CO})_4(\eta^2\text{-HFB})$ compounds relative to $\text{M}(\text{CO})_5$, the origin of the metal dependence in the carbonyl substitution reactions is less straightforward. One reason for this is that while the Ru and Os systems are all diamagnetic, the lowest energy form of $[\text{Fe}(\text{CO})_4]$ is a triplet³⁸⁻⁴⁰ in contrast to $[\text{Fe}(\text{CO})_3(\eta^2\text{-C}_2\text{H}_2)]$ (and thus presumably **D**) which has been calculated to have a singlet ground state.³⁷ Although Decker and Klobukowski have cautioned that the difference in ground state electronic structure of the $[\text{M}(\text{CO})_4]$ intermediates renders rationalization of CO dissociation trends a complex affair,³⁷ it is generally assumed that CO dissociation from $\text{Fe}(\text{CO})_5$ proceeds *via* the spin-allowed path to the singlet.^{4,41} It is thus unlikely that the large activation enthalpy for CO substitution in $\text{Fe}(\text{CO})_5$ is due to formation of triplet $[\text{Fe}(\text{CO})_4]$ by a spin-forbidden process.

Despite the above ambiguity, the tremendous acceleration of CO dissociation in $\text{Fe}(\text{CO})_4(\eta^2\text{-HFB})$ relative to its Os analog can be traced to the lower energy of the empty $3d$ orbital which interacts with the filled alkyne π_{\perp} orbital in the dissociative intermediate. The smaller size and lower energy of the $3d$ LUMO in the Fe species compared to the $5d$ orbital in the Os congener results in a better energy match and orbital overlap with π_{\perp} , and consequently a stronger interaction, which reduces the energy of $[\text{Fe}(\text{CO})_3(\eta^2\text{-HFB})]$ more than $[\text{Os}(\text{CO})_3(\eta^2\text{-HFB})]$. As a result, the activation enthalpy in the Fe complex is reduced relative to that of its osmium counterpart. However, it is unclear why $\text{Ru}(\text{CO})_4(\eta^2\text{-HFB})$ undergoes significantly less acceleration compared to

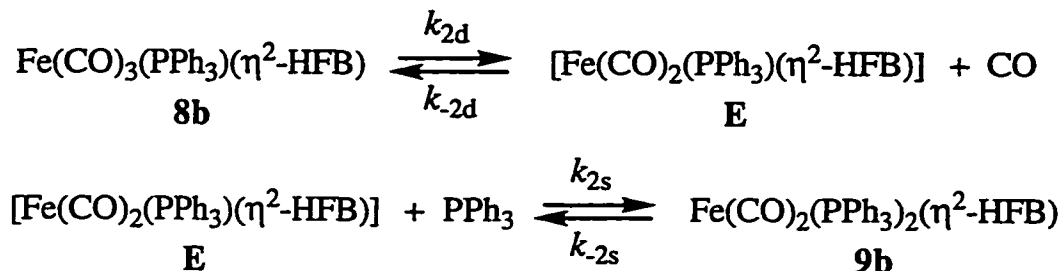
$\text{Ru}(\text{CO})_5$ as the energy of the $4d$ orbitals are expected to be similar in energy to those of the $5d$ orbitals in the Os compound. Although the qualitative predictions were quantified in the computational study, the MO energy gaps were found to be disconcertingly basis set dependent, and consequently it has been suggested that extreme caution should be exercised in relating the calculated MO gaps to chemical phenomena.³⁷

Interestingly, Basolo has noted that the rate of CO substitution generally follows the trend (1st row) < (2nd row) > (3rd row), regardless of mechanism and the metal triad to which it is applied.⁴² However, the exact source of the trend has been the subject of some debate. Recent theoretical results have revealed that relativistic effects are important for the increased M–CO bond strengths of the third row metals, for in the absence of these contributions the M–CO bond strengths decrease monotonically as one descends a triad.^{43,44} Accordingly, it is both experimentally observed and theoretically predicted that 2nd row metal complexes are generally the most substitutionally labile of any triad. The reactivity of the $\text{M}(\text{CO})_4(\eta^2\text{-HFB})$ species thus provides a noteworthy exception to this trend as it is the 1st row complex **1a** which is much more reactive than its 2nd and 3rd row congeners.

4.4.2. Further Analysis of the Reaction of **1a** with PPh_3

As mentioned in Section 4.2.1, the reaction of **1a** with PPh_3 ultimately affords the disubstituted complex **9b** (Eq. 4.2). Thus, the rate of formation of **8b** can be expected to be complicated by the competing rate of a second phosphine substitution to give **9b**. Indeed, as the kinetic reactions were followed by ^{19}F NMR, the monosubstituted compound **8b** was generally present in lower concentration than **9b**. Although the reactant **1a** was entirely consumed over the course of the reaction, an equilibrium was established between **8b** and **9b**. This behavior differs markedly from the Ru and Os chemistry where the reactions proceed to completion.⁴ However, the current results are understandable when it is recalled that the second phosphine ligand in **9b** is labile (Eq. 4.3), and that **8b** can be isolated *in situ* from a 1:1 mixture of **1a** and PPh_3 if the reaction is conducted under CO. In the present case, the fact that the kinetic reactions were

carried out in vacuum-sealed NMR tubes allowed for a build up of a low-pressure CO atmosphere (*ca.* 0.4 atm, *vide infra*) which is sufficient to inhibit complete formation of **9b**. The proposed reaction sequence is summarized in Scheme 4-2.



Scheme 4-2. Dissociative Mechanism for Subsequent Reaction of **8b** with PR₃.

The same general analysis presented in Eqs. 4.7-4.13 applies to the present case with suitable modifications. Bearing in mind that **8b** will initially form at the same rate as **1a** is consumed, the rate law governing the production of **8b** is

$$d[\mathbf{8b}]/dt = k_1[\mathbf{1a}] - k_{2d}[\mathbf{8b}] + k_{-2d}[\mathbf{E}][\text{CO}] \quad (4.17)$$

To evaluate $[\mathbf{E}]$, a steady-state approximation may be applied to the total rate of change of $[\mathbf{E}]$

$$d[\mathbf{E}]/dt = k_{2d}[\mathbf{8b}] + k_{-2s}[\mathbf{9b}] - (k_{-2d}[\text{CO}][\mathbf{E}] + k_{2s}[\text{PPh}_3][\mathbf{E}]) = 0 \quad (4.18)$$

Solving for $[\mathbf{E}]$ and substituting into Eq. 4.17 gives

$$d[\mathbf{8b}]/dt = k_1[\mathbf{1a}] + \left(\frac{k_{-2d}k_{-2s}[\text{CO}][\mathbf{9b}] - k_{2d}k_{2s}[\text{PPh}_3][\mathbf{8b}]}{k_{-2d}[\text{CO}] + k_{2s}[\text{PPh}_3]} \right) \quad (4.19)$$

which reduces to

$$d[\mathbf{8b}]/dt = k_1[\mathbf{1a}] + \left(\frac{\frac{k_{-2d}k_{-2s}[\text{CO}]}{k_{2s}[\text{PPh}_3]}[\mathbf{9b}] - k_{2d}[\mathbf{8b}]}{\frac{k_{-2d}[\text{CO}]}{k_{2s}[\text{PPh}_3]} + 1}} \right) \quad (4.20)$$

Application of the criterion $k_{-2d}[\text{CO}] \ll k_{2s}[\text{PPh}_3]$ has the result that the denominator approaches unity so that

$$d[\mathbf{8b}]/dt = k_1[\mathbf{1a}] + k_{-2} \frac{[\text{CO}]}{[\text{PPh}_3]}[\mathbf{9b}] - k_2[\mathbf{8b}] \quad (4.21)$$

where

$$k_2 = k_{2d} \text{ and } k_{-2} = \frac{k_{-2s}k_{-2d}}{k_{2s}}$$

Similarly, the rate law governing the production of $\mathbf{9b}$ is

$$d[\mathbf{9b}]/dt = k_{2s}[\mathbf{E}][\text{PPh}_3] - k_{-2s}[\mathbf{9b}] \quad (4.22)$$

which gives

$$d[\mathbf{9b}]/dt = k_2[\mathbf{8b}] - k_{-2} \frac{[\text{CO}]}{[\text{PPh}_3]}[\mathbf{9b}] \quad (4.23)$$

Due to the complexity of equations 4.21 and 4.23, numerical integration methods proved convenient in the analysis of the evolution of $\mathbf{8b}$ and $\mathbf{9b}$ during the course of the reaction. One difficulty encountered was that both equations have a dependence on $[\text{CO}]$. Given that the solubility of CO in a variety of non-aqueous solvents is *ca.* 7 mM under 1 atm CO,^{45,46} application of Henry's law provides

$$\begin{aligned} [\text{CO}] &= P_{\text{CO}} K_{\text{H}}(\text{CO}) \\ &= P_{\text{CO}} (7 \times 10^{-3} \text{ M}\cdot\text{atm}^{-1}) \end{aligned} \quad (4.24)$$

so that the number of moles of CO in solution (n_l) is

$$n_l = V_l P_{\text{CO}} (7 \times 10^{-3} \text{ M}\cdot\text{atm}^{-1}) \quad (4.25)$$

for a solution volume V_l . The derivation of the pressure of CO above the solution (P_{CO}) is more complicated. The total number of moles of CO (n_{tot}) available at any one point is given by

$$n_{\text{tot}} = n_l + n_g \quad (4.26)$$

where n_g is the number of moles of CO in the gas phase. Application of Eq. 4.26 and the ideal gas law gives

$$n_{\text{tot}} = \left(V_l (7 \times 10^{-3} \text{ M}\cdot\text{atm}^{-1}) + \frac{V_g}{RT} \right) P_{\text{CO}} \quad (4.27)$$

for a head-space volume V_g . From the reaction stoichiometry, it follows that

$$n_{tot} = V_l ([8b] + 2[9b]) \quad (4.28)$$

Combining Eqs. 4.27 and 4.28 thus provides

$$P_{CO} = ([8b] + 2[9b]) \left(7 \times 10^{-3} \text{ M}\cdot\text{atm}^{-1} + \frac{V_g}{V_l RT} \right)^{-1} \quad (4.29)$$

Thus, Eqs. 4.12, 4.21, 4.23, 4.24, and 4.29 were used to model Scheme 4-2, using $V_l = 0.45 \text{ mL}$ and $V_g = 1.0 \text{ mL}$ for the sealed NMR tubes used in the reactions. An additional complication was that the T_1 of reactant **1a** was found to be longer than that of **9b**, leading to slightly lower integration of the former due to incomplete relaxation. Thus, the data for **1a** was fit using a scaling factor with the value of k_1 constrained to be identical to that presented in Table 4-3. The preliminary results are presented in Table 4-5, and an example of a fit of the model to the experimental data is presented in Figure 4-6.

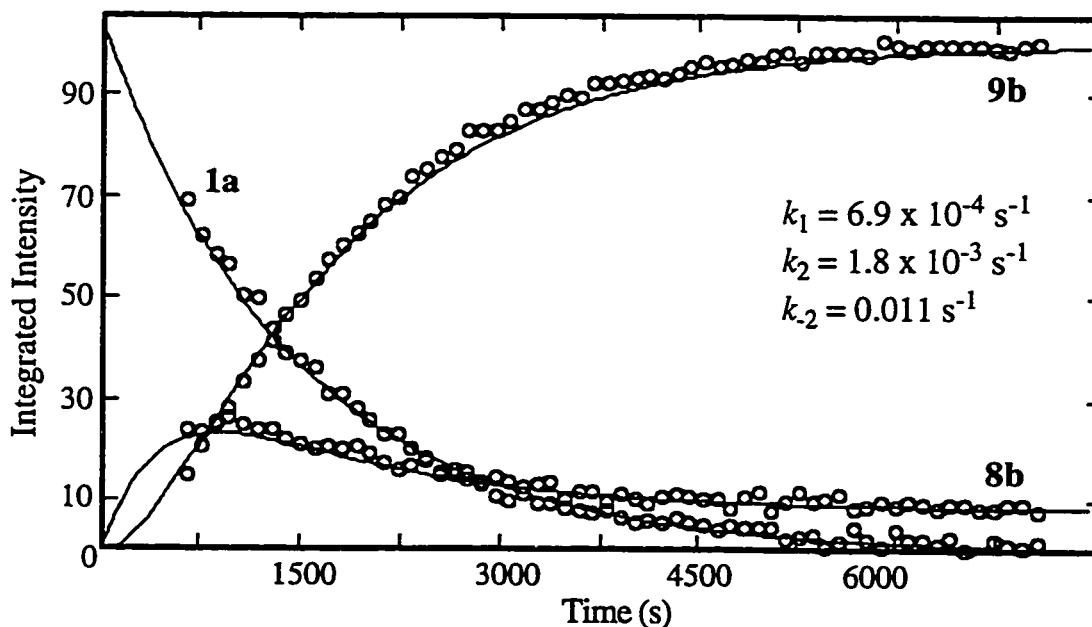


Figure 4-6. Integrated Intensity vs. Time Plot for the Reaction of PPh_3 (0.20 M) with **1a** (0.025 M) at -36.7°C in CD_2Cl_2 .

Table 4-5. Kinetic Results from Analysis of the Formation of **8b** and **9b** from **1a** and PPh₃ in CD₂Cl₂.^a

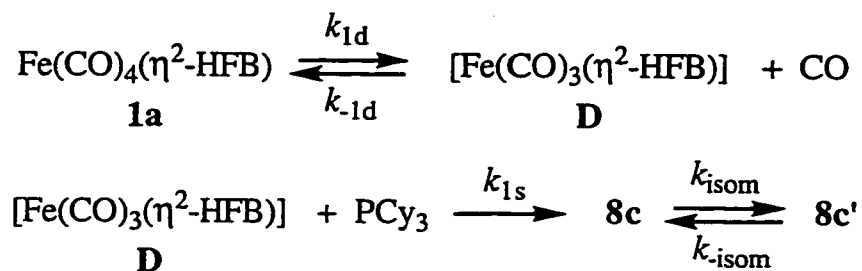
T (°C)	[PPh ₃] (M)	10 ³ x k ₂ (s ⁻¹) ^b	10 ³ x k ₋₂ (s ⁻¹) ^b	[CO] _{final} (mM)	P _{CO} (final) (atm)
-30.7	0.20	4.2	32	2.7	0.39
-33.5	0.30	3.1	21	2.8	0.40
-33.7	0.20	3.2	22	2.8	0.40
-33.7	0.10	2.9	14	2.7	0.39
-36.7	0.20	1.8	11	2.7	0.39
-39.9	0.20	1.0	5.0	2.8	0.40

^aThe solution initially contained 2.5×10^{-2} M **1a** and the indicated [PPh₃]. ^bThe rate constants were determined by visual comparison of calculated and experimental curves (eg. Figure 4-6).

The final calculated [CO] in solution was small (ca. 3 mM for P_{CO} ≈ 0.4 atm from Eq. 4.29), justifying the assumption made in Eq. 4.21. The most important result is that k_2 is approximately two to three times larger than k_1 (Table 4-3), confirming the results suggested qualitatively in the synthetic study. Additionally, the lack of dependence of k_2 on the concentration of PPh₃ implies a dissociative mechanism as expected. An analysis of the temperature dependence of k_2 (Eq. 4.15) provided activation parameters of $\Delta H^\ddagger = 64 \pm 9$ kJ·mol⁻¹ and $\Delta S^\ddagger = -24 \pm 59$ J·mol⁻¹·K⁻¹. The lower magnitude of ΔH^\ddagger is also in accord with the greater facility of the second phosphine substitution. Although a negative ΔS^\ddagger is commonly a marker for an associative mechanism, very little can be deduced in the present case owing to the large accompanying error. Nonetheless, the data collected in the kinetic runs support the mechanism proposed in Scheme 4-2. More reliable quantitative results would require a systematic variation of the concentration of the iron complexes in order to overcome the complications resulting from the reversibility of the second phosphine substitution.

4.4.3. Further Analysis of the Reaction of 1a with PCy₃

The reaction of **1a** with PCy₃ also formed an equilibrium mixture of two products, but, as described in Section 4.3.1, both products (**8c/c'**) were the result of substitution of one carbonyl by PCy₃ in axial and equatorial sites, respectively. Given that the disappearance of **1a** in reaction with PCy₃ follows Eq. 4.12 and it has been hypothesized that only dissociation of an axial carbonyl (Eq. 4-16) should result in acceleration of the rate of carbonyl substitution, it was clearly of interest to discover whether it was possible to rule out equatorial CO dissociation from **1a** as leading to the formation of **8c'**. Thus, two models were considered. The first (Scheme 4-3) suggests initial formation of the axial isomer **8c** followed by a more rapid isomerization step to the equatorial **8c'**, a proposal supported by the fact that **8c** and **8c'** are known to undergo exchange on the NMR time scale at *ca.* 0°C (*vide supra*).



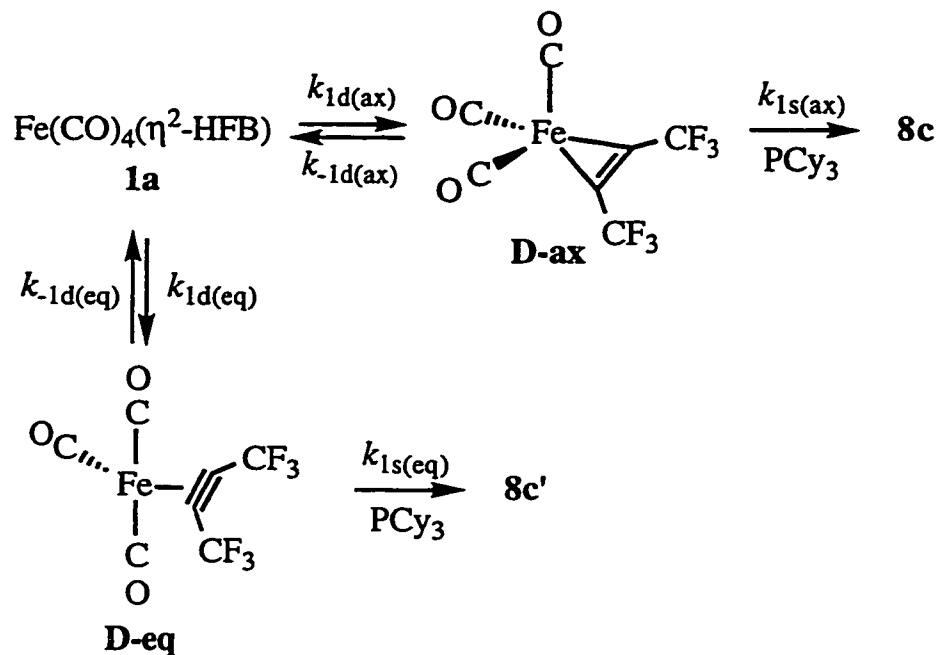
Scheme 4-3. Proposed Mechanism for Initial Formation of **8c** Followed by Isomerization to **8c'** in the Reaction of **1a** with PCy₃.

Following the same assumptions in the derivation of Eqs. 4.7-13, the rate laws governing the formation of **8c** and **8c'** are

$$d[\mathbf{8c}]/dt = k_1[\mathbf{1a}] - k_{isom}[\mathbf{8c}] \quad (4.30)$$

$$d[\mathbf{8c}']/dt = k_{isom}[\mathbf{8c}] - k_{-isom}[\mathbf{8c}'] \quad (4.31)$$

The second possibility is that **8c** and **8c'** form from different CO-dissociated intermediates; in other words, there are competing rates of axial and equatorial CO dissociation from **1a**. This mechanism is summarized in Scheme 4-4.



Scheme 4-4. Proposed Mechanism for Competing Axial and Equatorial CO Dissociation from **1a** in the Reaction with PCy_3 .

In this case, assuming steady-state behaviour for intermediates **D-ax** and **D-eq**, the rate laws governing the formation of **8c** and **8c'** are

$$d[\mathbf{8c}]/dt = k_{1d(ax)}[\mathbf{1a}] \quad (4.32)$$

$$d[\mathbf{8c}']/dt = k_{1d(eq)}[\mathbf{1a}] \quad (4.33)$$

where

$$k_{1d(ax)} + k_{1d(eq)} = k_{1d} = k_1 \quad (4.34)$$

since

$$-d[\mathbf{1a}]/dt = (k_{1d(ax)} + k_{1d(eq)})[\mathbf{1a}] \quad (4.35)$$

Additionally, the final ratio of the products follows

$$\frac{[\mathbf{8c}']}{[\mathbf{8c}]} = \frac{k_{1d(eq)}}{k_{1d(ax)}} \quad (4.35)$$

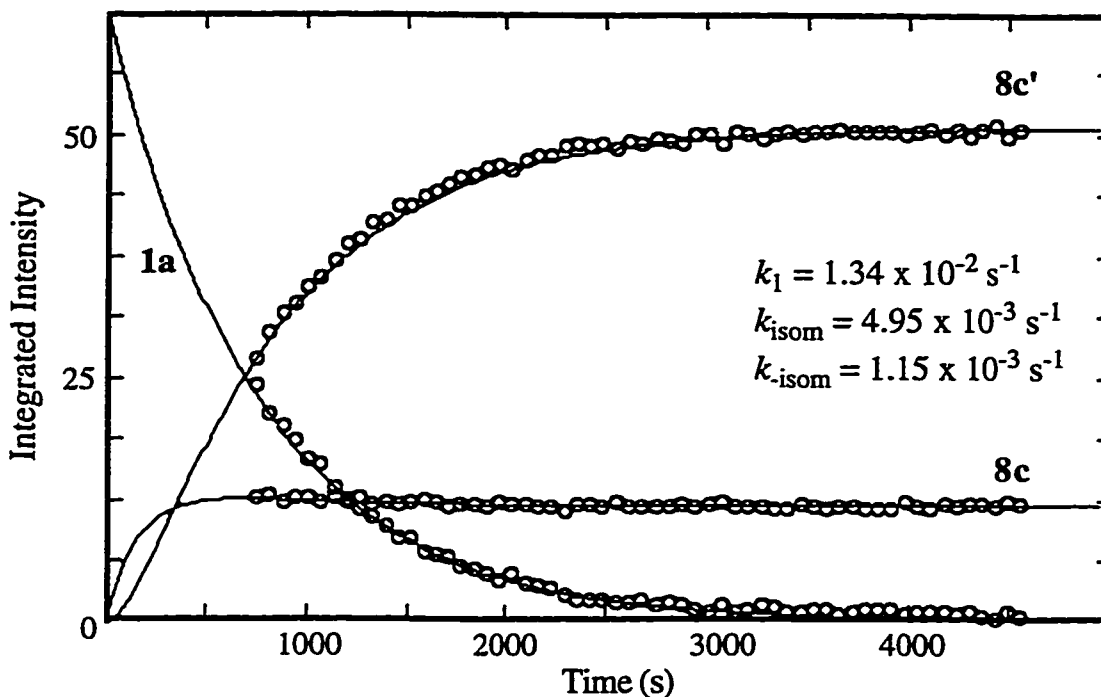


Figure 4-7. Integrated Intensity vs. Time Plot for the Reaction of PCy₃ (0.30 M) with 1a (0.025 M) at -33.5°C in CD₂Cl₂ Modelled to Scheme 4-3.

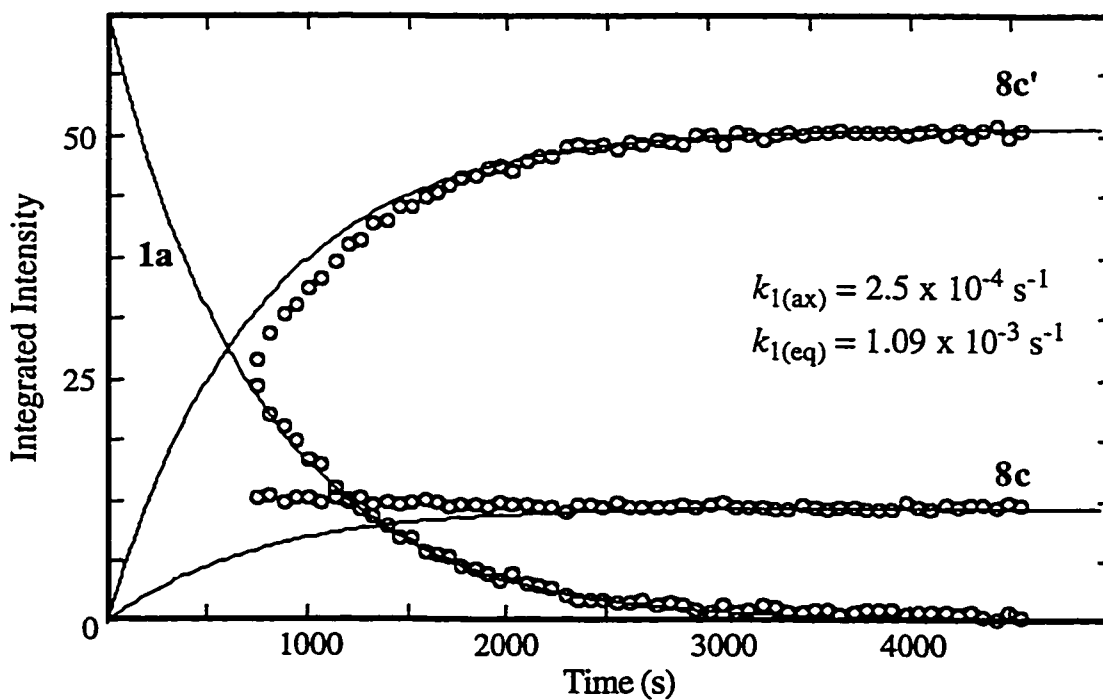


Figure 4-8. Integrated Intensity vs. Time Plot for the Reaction of PCy₃ (0.30 M) with 1a (0.025 M) at -33.5°C in CD₂Cl₂ Modelled to Scheme 4-4.

Both models were then applied to the experimental data from the run at -33.5°C ; the results are shown in Figures 4-7 and 4-8. Clearly, the experimental data are best fit by the model in Scheme 4-3, especially in terms of the evolution of the axial isomer **8c**. One feature distinguishing the time evolution of **8c** and **8c'** in the two schemes is that the mechanism of Scheme 4-3 implies that in the initial stages of the reaction, $[\mathbf{8c}]$ should be greater than $[\mathbf{8c}']$ for a short period. The same is not true of the mechanism from Scheme 4-4, where $[\mathbf{8c}]$ is less than $[\mathbf{8c}']$ throughout. Thus, it should be possible to more readily discriminate between the two mechanisms based on the evolution of the products in the early stages of the reaction.

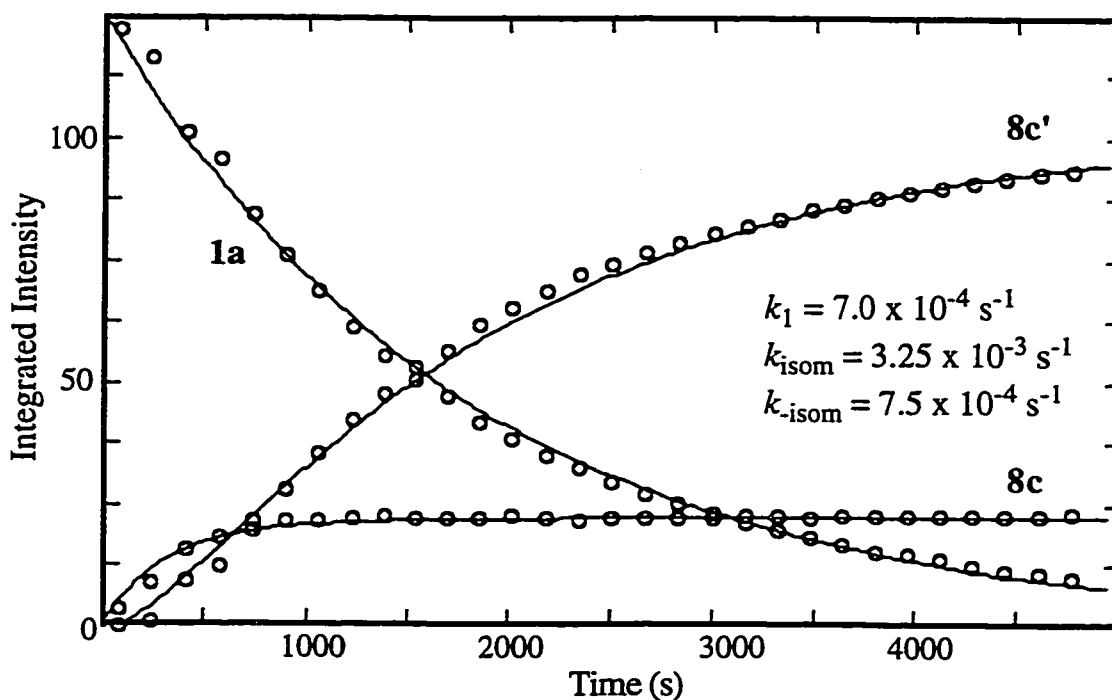


Figure 4-9. Integrated Intensity vs. Time Plot for the Early Stages of the Reaction of PCy_3 (0.30 M) with **1a** (0.025 M) at -38.5°C in CD_2Cl_2 .

In order to achieve this experimentally, the NMR probe was allowed to equilibrate at a temperature of $-39.5 \pm 0.2^{\circ}\text{C}$ and then cooled to -80°C prior to sample introduction; it proved impossible to monitor the early stages of the reaction if the sample was introduced at the desired temperature as the reaction

had already passed the desired point by the time that monitoring could commence. The temperature was then increased slowly to the calibrated temperature while spectra were collected. A second calibration following the run gave a probe temperature of $-37.5 \pm 0.2^\circ\text{C}$, resulting in a mean temperature of $-38.5 \pm 1.4^\circ\text{C}$. Despite the large magnitude of the thermal drift, the experiment was successful in monitoring the early stage of the reaction where $[\mathbf{8c}] > [\mathbf{8c}']$ (Figure 4-9), confirming that the mechanism of Scheme 4-3 is the most likely. This result lends further credence to the theory presented in Section 4.4.1; that is, only dissociation of an axial carbonyl in $\mathbf{1a}$ can be stabilized by interaction with the filled π_{\perp} orbital of HFB (Eq. 4.16), and thus the equatorially-substituted isomer $\mathbf{8c}'$ must form subsequently from $\mathbf{8c}$. This also agrees with the observation that the axial sites undergo preferential ^{13}CO enrichment over the equatorial sites in $\text{Ru}(\text{CO})_4(\eta^2\text{-HFB})$.⁴⁷ The $\mathbf{8c}/\mathbf{8c}'$ isomerization could occur by an intramolecular rearrangement such as a Berry pseudo-rotation (BPR) (Eq. 2.4), or possibly by a CO dissociation/association process *via* compound $\mathbf{10}$.

Finally, the formation of products in the reaction of $\mathbf{1a}$ with $\text{P}(\text{OPh})_3$ was also complicated by formation of an equatorial isomer analogous to $\mathbf{8c}'$. However, the reaction did not cease with incorporation of one phosphite and proceeded to give exclusively *trans*- $\text{Fe}(\text{CO})_2\{\text{P}(\text{OPh})_3\}_2(\eta^2\text{-HFB})$. In this case, the concentration of the equatorial isomer was also greater than the axial in the initial $\text{Fe}(\text{CO})_3\{\text{P}(\text{OPh})_3\}(\eta^2\text{-HFB})$ products, but the overall concentration of the monosubstituted species was small relative to that of the major disubstituted product at all points during the reaction. In this sense, the reaction of $\mathbf{1a}$ with $\text{P}(\text{OPh})_3$ shares characteristics of both previously studied systems with the exception that the second substitution step appears to be irreversible, or at least much less so than was observed with PPh_3 . This may be due to the fact that $\text{P}(\text{OPh})_3$ is less sterically hindered than PPh_3 .⁴⁸

4.5. Conclusions

$\text{Fe}(\text{CO})_4(\eta^2\text{-HFB})$ ($\mathbf{1a}$) undergoes carbonyl substitution reactions with phosphines at much lower temperatures than its Ru and Os congeners. A kinetic study confirmed a dissociative mechanism and quantified the increase in carbonyl

lability with the result that compound **1a** is over 30 trillion times more reactive towards carbonyl substitution than $\text{Fe}(\text{CO})_5$. The phenomenal acceleration of the rate of CO dissociation has been rationalized by stabilization of the $[\text{Fe}(\text{CO})_3(\eta^2\text{-HFB})]$ intermediate by interaction of the second π set of the alkyne with the vacated metal orbital. Interesting differences also emerged in the behavior of the phosphine substituted products, especially when tricyclohexylphosphine was employed. While PPh_3 and PMe_3 occupied axial positions exclusively, the greater steric demands of PCy_3 resulted in the equatorial isomer of $\text{Fe}(\text{CO})_3(\text{PCy}_3)(\eta^2\text{-HFB})$ (**8c'**) being more favored than the axial isomer. Additionally, the bulky phosphine enabled the isolation of the CO-dissociated compound $\text{Fe}(\text{CO})_2(\text{PCy}_3)(\eta^2\text{-HFB})$ (**10**) in which the alkyne functions as a four-electron donor to the Fe center. Accordingly, compound **10** provides an empirical model for the proposed $[\text{Fe}(\text{CO})_3(\eta^2\text{-HFB})]$ intermediate resulting from CO dissociation from **1a**.

4.6. Experimental Section

Unless otherwise noted, the general synthetic techniques and physical measurements employed are as described in Sections 2.6.1 and 2.6.2.

4.6.1. Reagents

Compound **1a** was prepared according to the procedure described in Chapter 2. The ligands PMe_3 , PPh_3 , PCy_3 , and P(OPh)_3 were purchased from Aldrich Chemical Co. and used without further purification. The trialkylphosphines were stored and handled under an inert atmosphere.

4.6.2. Synthetic Procedures

Reaction of $\text{Fe}(\text{CO})_4(\eta^2\text{-HFB})$ (1a**) with PMe_3 .** Trimethylphosphine (18 μL , 0.17 mmol) was added *via* micro-syringe into a flask containing **1a** (28 mg, 0.084 mmol) dissolved in 10 mL pentane at -78°C . The colorless solution was allowed to warm slowly, and gradually became bright yellow at *ca.* -35°C . After slowly warming to room temperature, the flask was cooled to -30°C and the solvent was removed *in vacuo*. The yellow product was dried *in vacuo* for 2 h at this temperature, and crystallization from pentane at -80°C afforded $\text{Fe}(\text{CO})_2(\text{PMe}_3)_2(\eta^2\text{-HFB})$ (**9a**) (28.0 mg, 0.0657 mmol, 78%) as moderately air-stable yellow crystals. If less than two equivalents of PMe_3 were employed, $\text{Fe}(\text{CO})_3(\text{PMe}_3)(\eta^2\text{-HFB})$ (**8a**) could be detected both by IR and NMR spectroscopy. However, the major product was **9a** along with unreacted **1a**.

$\text{Fe}(\text{CO})_3(\text{PMe}_3)(\eta^2\text{-HFB})$ (**8a**) (*in situ*):

F.W. 378.0

IR (pentane) 2069(s), 2010(s), 1979(vs); $\nu_{\text{C-C}}$ 1858(w).

^{13}C NMR (CD_2Cl_2 , 100.6 MHz, ^{13}C enriched, -60°C) δ 211.68 (dd, $^2J_{\text{PC}} = 28$ Hz, $^2J_{\text{CC}} = 8$ Hz, 2CO_{eq}), 202.90 (dt, $^2J_{\text{PC}} = 73$ Hz, $^2J_{\text{CC}} = 8$ Hz, CO_{ax}).

^{19}F NMR (CD_2Cl_2 , 188.3 MHz, -60°C) δ -54.49 (d, $^4J_{\text{PF}} = 0.7$ Hz).

^{31}P NMR (CD_2Cl_2 , 81.0 MHz) δ 22.48 (br s).

$\text{Fe}(\text{CO})_2(\text{PMe}_3)_2(\eta^2\text{-HFB})$ (**9a**):

F.W. 426.1

Anal. Calcd. for $C_{12}H_{18}F_6FeO_2P_2$: C, 33.83; H, 4.27. Found: C, 33.81; H, 4.13.

IR (pentane) ν_{CO} 1989(m), 1924(s); ν_{CC} 1823(w), 1780(vw).

1H NMR (CD_2Cl_2 , 200 MHz) δ 1.17 (t, $J_{PH} = 3.9$ Hz).

^{13}C NMR (CD_2Cl_2 , 75.5 MHz) δ 218.00 (t, $^2J_{PC} = 28$ Hz, $2CO_{eq}$), 17.49 (d, $^1J_{PC} = 14$ Hz, $P(CH_3)_3$). The HFB carbons were not observed.

^{19}F NMR (CD_2Cl_2 , 188.3 MHz) δ -52.16 (t, $^4J_{PF} = 2.2$ Hz).

^{31}P NMR (CD_2Cl_2 , 81.0 MHz) δ 21.36 (sept, $^4J_{PF} = 2.2$ Hz).

EI-MS: M^+ (28.1% of base); $M^+ - 2 CO$; $M^+ - 2CO - HFB$ (base peak).

Reaction of $Fe(CO)_4(\eta^2\text{-HFB})$ (1a) with PPh_3 . Two equivalents of triphenylphosphine (31.0 mg, 0.118 mmol) were dissolved in a small amount of cold CH_2Cl_2 and transferred into a stirred solution of 1a (20 mg, 0.061 mmol) in 10 mL CH_2Cl_2 at $-78^\circ C$. The colorless solution was allowed to warm slowly to room temperature and became deep orange in color at approximately $-35^\circ C$. The CH_2Cl_2 was removed *in vacuo* and the orange residue was recrystallized from CH_2Cl_2 /pentane to afford an orange powder of $Fe(CO)_2(PPh_3)_2(\eta^2\text{-HFB})$ (9b) (42.1 mg, 0.0527 mmol, 89 %).

F.W. 798.5

Anal. Calcd. for $C_{42}H_{30}F_6FeO_2P_2$: C, 63.18; H, 3.79. Found: C, 63.26; H, 3.69.

IR (CH_2Cl_2) ν_{CO} 1989(m), 1922(s); ν_{CC} 1809(w, br), 1775(w).

(KBr) 1987(m), 1919(s), 1808(w, br), 1773(w), 1435(w), 1226(s), 1107(m), 1085(mw), 741(w), 694(m).

^{13}C NMR (CD_2Cl_2 , 100.6 MHz, ^{13}CO enriched, $-60^\circ C$) δ 218.54 (t, $^2J_{PC} = 28$ Hz, $2CO_{eq}$).

^{19}F NMR (CD_2Cl_2 , 188.3 MHz, $-60^\circ C$) δ -50.50 (t, $^4J_{PF} = 1.8$ Hz).

^{31}P NMR (CD_2Cl_2 , 81.0 MHz, $-60^\circ C$) δ 61.88 (br s).

$Fe(CO)_3(PPh_3)(\eta^2\text{-HFB})$ (8b) was formed *in situ* by slowly warming a CH_2Cl_2 solution containing one equivalent of PPh_3 and 1a under a CO atmosphere from $-78^\circ C$ to $-10^\circ C$. The resulting yellow compound was pentane soluble, but degraded rapidly in the absence of a CO atmosphere and could not be isolated as a solid.

F.W. 564.2

IR (pentane) ν_{CO} 2068(vs), 2012(s), 1982(s); ν_{CC} 1848(w).

(CH_2Cl_2) ν_{CO} 2067(vs), 2009(ms), 1980(s); ν_{CC} 1842(w).

^{19}F NMR (CD_2Cl_2 , 188.3 MHz, -60°C) δ -53.81 (d, $^4J_{\text{PF}} = 1.1$ Hz).

^{31}P NMR (CD_2Cl_2 , 81.0 MHz, -60°C) δ 57.64 (sept, $^4J_{\text{PF}} = 1.1$ Hz).

Synthesis of $\text{Fe}(\text{CO})_3(\text{PCy}_3)(\eta^2\text{-HFB})$ (8c/c'**).** One equivalent of tricyclohexylphosphine (93.6 mg, 0.338 mmol) was dissolved in 5 mL CH_2Cl_2 and transferred into a stirred solution of **1a** (112 mg, 0.339 mmol) in 20 mL CH_2Cl_2 at -78°C . The solution was allowed to warm, becoming yellow near -35°C and then brown by -10°C . A stream of CO was admitted at this temperature, resulting in a rapid return of the bright yellow color. The CH_2Cl_2 was removed *in vacuo* at -78°C and the yellow residue was warmed under vacuum to *ca.* -10°C to removed excess **1a**. The yellow film was extracted into pentane at -10°C , resulting in a brown colored solution. The solvent was concentrated to *ca.* 1 mL under a rapid stream of CO, returning the yellow color, and recrystallization at -78°C afforded a thermally sensitive yellow powder of $\text{Fe}(\text{CO})_3(\text{PCy}_3)(\eta^2\text{-HFB})$ as a mixture of axial (**8c**) and equatorial (**8c'**) isomers in a *ca.* 25:75% ratio. The compound was stable in solution under a CO atmosphere, but converted rapidly to **10** upon warming under N_2 ; solid $\text{Fe}(\text{CO})_3(\text{PCy}_3)(\eta^2\text{-HFB})$ also converted to **10** above *ca.* 0°C and could not be isolated at ambient temperature.

F.W. 579.2

IR (pentane) ν_{CO} 2063(m), 1995(vs), 1987(m) 1973 (m); ν_{CC} 1840(vw).

(CH_2Cl_2) ν_{CO} 2063(w), 1997(s), 1978(sh); ν_{CC} 1837(w).

ax- $\text{Fe}(\text{CO})_3(\text{PCy}_3)(\eta^2\text{-HFB})$ (**8c**):

^{13}C NMR (CD_2Cl_2 , 100.6 MHz, ^{13}CO enriched, -40°C) δ 212.82 (dd, $^2J_{\text{PC}} = 31$ Hz, $^2J_{\text{CC}} = 9$ Hz, 2CO_{eq}), 203.35 (dt, $^2J_{\text{PC}} = 68$ Hz, $^2J_{\text{CC}} = 9$ Hz, CO_{ax}).

^{13}C NMR (CD_2Cl_2 , 100.6 MHz, -60°C) δ 212.63 (d, $^2J_{\text{PC}} = 31$ Hz, 2CO_{eq}), 203.21 (d, $^2J_{\text{PC}} = 68$ Hz, CO_{ax}). The CF_3 and CCF_3 resonances were not observed.

$^{13}\text{C}\{^{19}\text{F}\}$ NMR (CD_2Cl_2 , 100.6 MHz, -60°C) δ 212.62 (d, $^2J_{\text{PC}} = 31$ Hz, 2CO_{eq}), 203.20 (d, $^2J_{\text{PC}} = 68$ Hz, CO_{ax}). The CF_3 and CCF_3 resonances were not observed.

^{19}F NMR (CD_2Cl_2 , 188.3 MHz, -40°C) δ -53.35 (d, $^4J_{\text{PF}} = 1.6$ Hz).

^{31}P NMR (CD_2Cl_2 , 81.0 MHz, -40°C , ^{13}C enriched) δ 56.76 (dt, $^2J_{\text{PC}(\text{trans})} = 68$ Hz, $^2J_{\text{PC}(\text{cis})} = 31$ Hz).

eq- $\text{Fe}(\text{CO})_3(\text{PCy}_3)(\eta^2\text{-HFB})$ (**8c'**):

^{13}C NMR (CD_2Cl_2 , 100.6 MHz, ^{13}C enriched, -40°C) δ 216.26 (t, $^2J_{\text{CC}} = 9$ Hz, CO_{eq}), 206.52 (dd, $^2J_{\text{PC}} = 24$ Hz, $^2J_{\text{CC}} = 9$ Hz, 2CO_{ax}).

^{13}C NMR (CD_2Cl_2 , 100.6 MHz, -60°C) δ 216.19 (s, CO_{eq}), 206.29 (d, $^2J_{\text{PC}} = 25$ Hz, 2CO_{ax}), 123.26 (q, $^1J_{\text{CF}} = 269$ Hz, CF_3), 104.23 (m, CCF_3), 91.84 (m, CCF_3).

$^{13}\text{C}\{^{19}\text{F}\}$ NMR (CD_2Cl_2 , 100.6 MHz, -60°C) δ 216.18 (s, CO_{eq}), 206.29 (d, $^2J_{\text{PC}} = 25$ Hz, 2CO_{ax}), 123.25 (s, CF_3), 104.23 (d, $^2J_{\text{PC}} = 6$ Hz, CCF_3), 91.85 (d, $^2J_{\text{PC}} = 9$ Hz, CCF_3).

^{19}F NMR (CD_2Cl_2 , 188.3 MHz, -40°C) δ -52.35 (q, $^5J_{\text{FF}} = 5.1$ Hz, CF_3), -52.35 (qd, $^5J_{\text{FF}} = 5.1$ Hz, $^4J_{\text{PF}} = 3.3$ Hz, CF_3).

^{31}P NMR (CD_2Cl_2 , 81.0 MHz, -40°C , ^{13}C enriched) δ 65.04 (t, $^2J_{\text{PC}(\text{cis})} = 24$ Hz).

Synthesis of $\text{Fe}(\text{CO})_2(\text{PCy}_3)(\eta^2\text{-HFB})$ (10**).** A 10 mL pentane solution of **8c** was prepared from PCy_3 (92.7 mg, 0.334 mmol) and **1a** (112 mg, 0.339 mmol). The solvent was removed *in vacuo* at ambient temperature, producing a deep purple oily film. The residue was redissolved in pentane and the procedure was repeated. Recrystallization from *ca.* 1 mL pentane at -80°C produced air stable, dark purple $\text{Fe}(\text{CO})_2(\text{PCy}_3)(\eta^2\text{-HFB})$ (**10**) (151.8 mg, 0.274 mmol, 82 %).

F.W. 551.2

Anal. Calcd. for $\text{C}_{24}\text{H}_{33}\text{F}_6\text{FeO}_2\text{P}$: C, 52.00; H, 6.00. Found: C, 52.28; H, 6.27.

IR (pentane) ν_{CO} 2009(m), 1948(s); ν_{CC} 1734(w).

(CH_2Cl_2) ν_{CO} 2005(m), 1939(s); ν_{CC} 1732(w).

(KBr disk) ν_{CO} 2011(s), 1955(s); ν_{CC} 1724(m).

$^{13}\text{C}\{^1\text{H}\}$ NMR (CD_2Cl_2 , 100.6 MHz, ^{13}C enriched) δ 216.70 (d, $^2J_{\text{PC}} = 28$ Hz, CO).

^{13}C NMR (CD_2Cl_2 , 100.6 MHz, -60°C) δ 216.73 (d, $^2J_{\text{PC}} = 28$ Hz, CO), 171.1 (m, CCF_3), 123.84 (q, $^1J_{\text{CF}} = 270$ Hz, CCF_3).

$^{13}\text{C}\{^{19}\text{F}\}$ NMR (CD_2Cl_2 , 100.6 MHz, -60°C) δ 216.73 (d, $^2J_{\text{PC}} = 28$ Hz, CO), 171.12 (d, $^2J_{\text{PC}} = 7$ Hz, CCF_3), 123.84 (s, CCF_3).

^{19}F NMR (CD_2Cl_2 , 188.3 MHz) δ -57.03 (s).

^{31}P NMR (CD_2Cl_2 , 81.0 MHz) δ 49.93 (brs).

Synthesis of $\text{Fe}(\text{CO})_2(\text{PCy}_3)_2(\eta^2\text{-HFB})$ (9c**).** A 0.5 mL solution of tricyclohexylphosphine (10.9 mg, 0.0389 mmol) in CH_2Cl_2 was added to a stirred solution of **10** (20.2 mg, 0.0364 mmol) dissolved in 5 mL pentane at ambient temperature. Reddish orange micro-crystals of $\text{Fe}(\text{CO})_2(\text{PCy}_3)_2(\eta^2\text{-HFB})^{20}$ (**9c**) (26.8 mg, 0.0321 mmol, 86 %) were recovered following recrystallization from CH_2Cl_2 /pentane at -78°C .

4.6.3. X-ray Crystal Structure Determination of Compound **10**

Dark purple single crystals were grown by cooling a concentrated pentane solution of **10** at -35°C . The X-ray data collection and structure refinement were carried out by Dr. Bob McDonald at the Structure Determination Laboratory, Department of Chemistry, University of Alberta. The crystal was mounted on a thin glass fibre and transferred to the goniometer of a Siemens P4/RA diffractometer⁴⁹ where it was kept under a stream of cooled nitrogen gas. The structure was solved using direct methods techniques (*SHELXS-86*⁵⁰) and refined by full-matrix least-squares on F^2 (*SHELXL-93*⁵¹). All non-hydrogen atoms were located. The geometrically constrained hydrogen atoms were placed in calculated positions appropriate for sp^3 carbons. A summary of data collection parameters is given in Table 4-6. The final atomic coordinates and equivalent isotropic displacement parameters are given in Table 4-7. Selected interatomic distances and angles are provided in Table 4-2.

Table 4-6. Crystallographic Experimental Details for Compound 10

Formula	C ₂₄ H ₃₃ F ₆ FeO ₂ P
Formula weight.	554.32
Crystal dimensions (mm)	0.36 x 0.30 x 0.16
Crystal system	triclinic
Space group	<i>P</i> $\bar{1}$ (No. 2)
Unit cell parameters ^a	
<i>a</i> , Å	9.7035 (4)
<i>b</i> , Å	11.1394 (5)
<i>c</i> , Å	13.3961 (5)
α , deg	74.027 (4)
β , deg	86.904 (4)
γ , deg	66.043 (4)
<i>V</i> , Å ³	1269.42 (9)
<i>Z</i>	2
ρ_{calc} , g cm ⁻³	1.450
μ , mm ⁻¹	5.933
Radiation, λ (Å)	graphite-monochromated CuK α (1.54178)
Temperature, °C	-60
Scan type	$\theta - 2\theta$
Data collection 2θ limit, deg	115.0
Total data collected	3641 ($0 \leq h \leq 10$, $-10 \leq k \leq 11$, $-14 \leq l \leq 14$)
Independent reflections	3400
Number of observations (<i>NO</i>)	3056 [$F_o^2 \geq 2\sigma(F_o^2)$]
Absorption correction method	Gaussian integration (face-indexed)
Range of transmission factors	0.4412 - 0.2063
data/restraints/parameters	3399 [$F_o^2 \geq -3\sigma(F_o^2)$]/0/307
Goodness-of-fit (<i>S</i>) ^b	1.024 [$F_o^2 \geq -3\sigma(F_o^2)$]
Final <i>R</i> indices ^c	
$F_o^2 \geq 2\sigma(F_o^2)$	$R_1 = 0.0443$, $wR_2 = 0.1087$
all data	$R_1 = 0.0505$, $wR_2 = 0.1140$
Largest difference peak and hole	0.716 and -0.484 e Å ⁻³

^aObtained from least-squares refinement of 34 reflections with $54.3^\circ < 2\theta < 57.9^\circ$.

^b $S = [\sum w(F_o^2 - F_c^2)^2 / (n - p)]^{1/2}$ (*n* = number of data; *p* = number of parameters varied; $w = [\sigma^2(F_o^2) + (0.0600P)^2 + 1.9765P]^{-1}$ where $P = [\text{Max}(F_o^2, 0) + 2F_c^2] / 3$).

^c $R_1 = \sum ||F_o| - |F_c|| / \sum |F_o|$; $wR_2 = [\sum w(F_o^2 - F_c^2)^2 / \sum w(F_o^4)]^{1/2}$.

Table 4-7. Atomic Coordinates and Equivalent Isotropic Displacement Parameters for Compound 10

Atom	x	y	z	$U_{eq}, \text{\AA}^2$
Fe	0.09666(6)	0.50133(5)	-0.14822(4)	0.0245(2)*
P	0.29413(9)	0.38224(8)	-0.22271(6)	0.0211(2)*
F1	-0.3459(4)	0.6953(5)	-0.2534(5)	0.162(3)*
F2	-0.2449(4)	0.4934(3)	-0.2523(3)	0.0966(12)*
F3	-0.2246(6)	0.6355(7)	-0.3758(3)	0.167(3)*
F4	-0.0770(5)	0.8813(3)	-0.3481(2)	0.1074(14)*
F5	0.0128(4)	0.8669(3)	-0.2036(3)	0.0840(10)*
F6	-0.2121(4)	0.8953(3)	-0.2166(3)	0.0900(11)*
O1	0.0704(3)	0.2540(3)	-0.0221(2)	0.0485(8)*
O2	0.2832(4)	0.5514(4)	-0.0143(3)	0.0609(9)*
C1	0.0860(4)	0.3491(4)	-0.0730(3)	0.0310(9)*
C2	0.2138(4)	0.5296(4)	-0.0678(3)	0.0353(9)*
C3	-0.2249(5)	0.6067(4)	-0.2757(4)	0.0463(11)*
C4	-0.0856(4)	0.5962(4)	-0.2291(3)	0.0300(9)*
C5	-0.0311(4)	0.6809(4)	-0.2187(3)	0.0300(9)*
C6	-0.0772(5)	0.8306(4)	-0.2468(4)	0.0479(11)*
C11	0.4732(4)	0.3044(3)	-0.1397(3)	0.0240(8)*
C12	0.6191(4)	0.2324(4)	-0.1887(3)	0.0322(9)*
C13	0.7567(4)	0.1907(5)	-0.1159(3)	0.0432(10)*
C14	0.7484(5)	0.0982(5)	-0.0110(3)	0.0500(11)*
C15	0.6022(5)	0.1654(4)	0.0378(3)	0.0445(11)*
C16	0.4645(4)	0.2085(4)	-0.0350(3)	0.0365(9)*
C21	0.3260(4)	0.4973(3)	-0.3414(3)	0.0251(8)*
C22	0.3625(4)	0.6095(4)	-0.3186(3)	0.0305(8)*
C23	0.3952(4)	0.6982(4)	-0.4172(3)	0.0353(9)*
C24	0.2666(4)	0.7586(4)	-0.5011(3)	0.0385(10)*
C25	0.2338(5)	0.6460(4)	-0.5237(3)	0.0348(9)*
C26	0.1964(4)	0.5608(4)	-0.4254(3)	0.0298(8)*
C31	0.2826(4)	0.2388(3)	-0.2619(3)	0.0255(8)*
C32	0.1213(4)	0.2553(4)	-0.2867(3)	0.0294(8)*
C33	0.1253(5)	0.1217(4)	-0.2999(3)	0.0370(9)*
C34	0.2245(5)	0.0798(5)	-0.3862(4)	0.0501(12)*
C35	0.3832(5)	0.0665(4)	-0.3662(3)	0.0473(11)*
C36	0.3819(5)	0.1983(4)	-0.3511(3)	0.0352(9)*

^aAnisotropically-refined atoms are marked with an asterisk (*). The form of the anisotropic displacement parameter is: $\exp[-2\pi^2(h^2a^*{}^2U_{11} + k^2b^*{}^2U_{22} + l^2c^*{}^2U_{33} + 2klb^*c^*U_{23} + 2hla^*c^*U_{13} + 2hka^*b^*U_{12})]$.

4.6.4. Kinetic Measurements

Samples were prepared by adding 225 μL of a cold (-78°C) stock solution of **1a** (0.050M in CD_2Cl_2) and 225 μL of a cold (-78°C) stock solution of the appropriate phosphine (also in CD_2Cl_2) to an pre-cooled thick-walled NMR tube ($\approx 3\text{mm}$ I.D., 5mm O.D.). The contents of the NMR tube were then subjected to three freeze-thaw degassing cycles and the tube was flame sealed under vacuum following the final thaw cycle. The ^{19}F NMR spectra were obtained at standardized time intervals on a Bruker WH-200 spectrometer. Temperatures were monitored by the use of an external Sensotek BAT-10 copper thermocouple inserted into a toluene solution in a 5 mm O.D. NMR tube. The temperature at the probe was allowed to equilibrate for 10 minutes and was monitored until a steady reading was obtained over a ten minute interval. The temperature was re-measured following the completion of the experiments in order to ascertain any thermal drift ($\leq 0.2^\circ\text{C}$ in general) and the mean temperature was then used for subsequent calculations. The integrated peak intensities were determined using a common set of spectral processing parameters for each series of experiments. The data was analyzed on an IBM-486 type computer using locally-developed software written in BASIC (Prof. R.B. Jordan) by least-squares methods based on the Marquardt algorithm.⁴ Reaction profile modelling was accomplished using the fourth order Runge-Kutta method for numeric integration on an Apple Macintosh PowerPC computer with the generous assistance of Prof. R.B. Jordan. The kinetic results are summarized in Tables 4-3 and 4-5 and examples of common reaction profiles are provided in Figures 4-5 to 4-9.

4.7. References

1. Burn, M. J.; Kiel, G.-Y.; Seils, F.; Takats, J.; Washington, J. *J. Am. Chem. Soc.* **1989**, *111*, 6850.
2. Gagné, M. R.; Takats, J. *Organometallics* **1988**, *7*, 561.
3. Mao, T. PhD Thesis, University of Alberta, 1996.
4. Pearson, J.; Cooke, J.; Takats, J.; Jordan, R. B. *J. Am. Chem. Soc.* **1998**, *120*, 1434.
5. Shen, J. K.; Gao, Y. C.; Shi, Q. Z.; Basolo, F. *Inorg. Chem.* **1989**, *28*, 4304.
6. Pannell, K. H.; Crawford, G. M. *J. Coord. Chem.* **1973**, *2*, 251.
7. Berney, C. V.; Cousins, L. R.; Miller, F. A. *Spectrochim. Acta* **1963**, *19*, 2019.
8. Vancheesan, S. *Indian J. Chem.* **1983**, *22A*, 54.
9. van Gaal, H. L. M.; Graef, M. W. M.; van der Ent, A. *J. Organomet. Chem.* **1977**, *131*, 453.
10. Rossi, A. R.; Hoffmann, R. *Inorg. Chem.* **1975**, *14*, 365 and references therein.
11. Mann, B. E.; Taylor, B. F. *¹³C NMR Data for Organometallic Compounds*; Academic: New York, 1981, pp 23.
12. Alex, R. F.; Pomeroy, R. K. *Organometallics* **1987**, *6*, 2437.
13. Anderson, R. A.; Jones, R. A.; Wilkinson, G. *J. Chem. Soc., Dalton Trans.* **1977**, 446.
14. Harris, R. K. *Can. J. Chem.* **1964**, *42*, 2275.
15. Burt, R.; Cooke, M.; Green, M. *J. Chem. Soc. (A)* **1970**, 2981.
16. Birk, R.; Berke, H.; Huttner, G.; Zsolnai, L. *Chem. Ber.* **1988**, *121*, 471.
17. Birk, R.; Grössmann, U.; Hund, H.-U.; Berke, H. *J. Organomet. Chem.* **1988**, *345*, 321.
18. Meier-Brooks, F.; Albrecht, R.; Weiss, E. *J. Organomet. Chem.* **1992**, *439*, 65.
19. Ogasawara, M.; Macgregor, S. A.; Streib, W. E.; Folting, K.; Eisenstein, O.; Caulton, K. G. *J. Am. Chem. Soc.* **1996**, *118*, 10189.
20. Washington, J. unpublished results.
21. McDonald, B.; Takats, J.; Washington, J. unpublished results.

22. Huheey, J. E.; Keiter, E. A.; Keiter, R. L. *Inorganic Chemistry: Principles of Structure and Reactivity*; 4th ed.; HarperCollins: New York, 1993, pp 292.
23. Templeton, J. L. *Adv. Organomet. Chem.* **1989**, *29*, 1.
24. Templeton, J. L.; Ward, B. C. *J. Am. Chem. Soc.* **1980**, *102*, 3288.
25. Boncella, J. M.; Green, M. L. H. *J. Organomet. Chem.* **1987**, *325*, 217.
26. Marinelli, G.; Streib, W.; Huffman, J. C.; Caulton, K. G.; Gagné, M. R.; Takats, J.; Dartiguenave, M. *Polyhedron* **1990**, *9*, 1867.
27. Espuelas, J.; Esteruelas, M. A.; Lahoz, F. J.; López, A. M.; Oro, L. A.; Valero, C. *J. Organomet. Chem.* **1994**, *468*, 223.
28. Harris, T. V.; Rathke, J. W.; Muetterties, E. L. *J. Am. Chem. Soc.* **1978**, *100*, 6966.
29. Li, L.; Enright, G. D.; Preston, K. F. *Organometallics* **1994**, *13*, 4686.
30. Capelle, B.; Dartiguenave, M.; Dartiguenave, Y.; Beauchamp, A. L. *J. Am. Chem. Soc.* **1983**, *105*, 4662.
31. Rappoli, B. J.; Churchill, M. R.; Janik, T. S.; Rees, W. M.; Atwood, J. D. *J. Am. Chem. Soc.* **1987**, *109*, 5145.
32. Siefert, E. E.; Angelici, R. J. *J. Organomet. Chem.* **1967**, *8*, 374.
33. Jordan, R. B. *Reaction Mechanisms of Inorganic and Organometallic Systems*; Oxford University Press: New York, 1991, Chp 1-3.
34. Huang, J.; Hedberg, K.; Pomeroy, R. K. *Organometallics* **1988**, *7*, 2049.
35. Huang, J.; Hedberg, K.; Pomeroy, R. K. *Inorg. Chem.* **1990**, *29*, 3923.
36. Mingos, D. M. P. In *Comprehensive Organometallic Chemistry*; G. Wilkinson, F. G. A. Stone and E. W. Abel, Eds.; Pergamon Press: Oxford, 1983; Vol. 3; pp 59.
37. Decker, S.; Klobukowski, M., submitted for publication.
38. Barton, T. J.; Grinter, R.; Thomson, A. J.; Davies, B.; Poliakoff, M. *J. Chem. Soc., Chem. Commun.* **1977**, 841.
39. Poliakoff, M.; Turner, J. J. *J. Chem. Soc., Dalton Trans.* **1974**, 2276.
40. Poliakoff, M.; Weitz, E. *Acc. Chem. Res.* **1987**, *20*, 408.
41. Lewis, K. E.; Golden, D. M.; Smith, G. P. *J. Am. Chem. Soc.* **1984**, *106*, 3905.
42. Basolo, F. *Polyhedron* **1990**, *9*, 1503.
43. Ziegler, T.; Tschinke, V.; Ursenbach *J. Am. Chem. Soc.* **1987**, *109*, 4825.

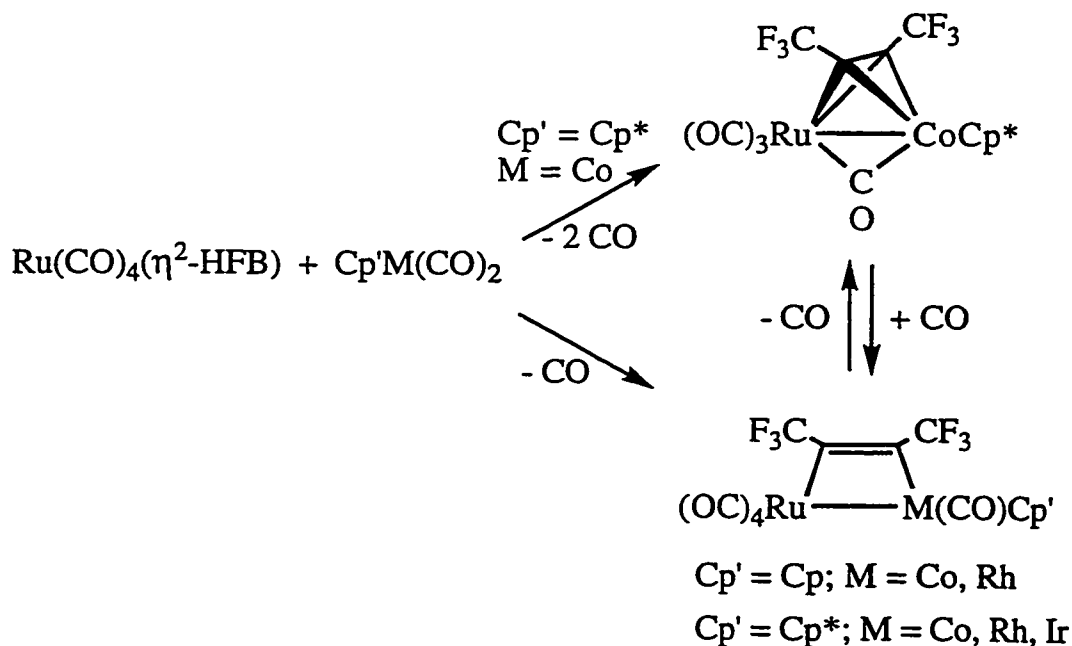
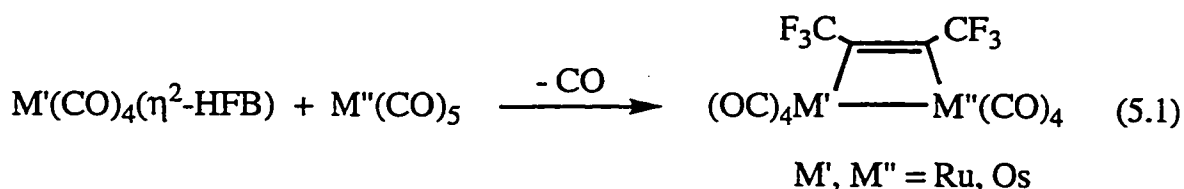
44. Li, J.; Schreckenbach, G.; Ziegler, T. *J. Am. Chem. Soc.* **1995**, *117*, 486.
45. Poë, A. J.; Sampson, C. N.; Smith, R. T.; Zheng, Y. *J. Am. Chem. Soc.* **1993**, *115*, 3174 and references therein.
46. Nudelman, N. S.; Doctorovich, F. *J. Chem. Soc. Perkin Trans. 2* **1994**, 1233 and references therein.
47. Jacke, J.; Takats, J. unpublished results.
48. Tolman, C. A. *Chem. Rev.* **1977**, *77*, 313.
49. Programs for diffractometer operation, data collection, data reduction, and absorption correction were those supplied by Siemens.
50. Sheldrick, G. M. *Acta Crystallogr.* **1990**, *A46*, 467.
51. Sheldrick, G.M. *SHELXL-93*. Program for crystal structure determination. University of Göttingen, Germany, 1993.

Chapter 5

**Formation of Heterobimetallic Complexes from the Reaction of
 $\text{Fe}(\text{CO})_4(\eta^2\text{-C}_2(\text{CF}_3)_2)$ with $\text{Cp}'\text{M}(\text{CO})_2$ ($\text{M} = \text{Co}, \text{Rh}, \text{Ir}$; $\text{Cp}' = \text{Cp}, \text{Cp}^*$)**

5.1. Introduction

The preceding chapter established the remarkable lability of the carbonyl ligands in $\text{Fe}(\text{CO})_4(\eta^2\text{-HFB})$ (**1a**) in substitution reactions with phosphines. The analogous ruthenium and osmium compounds also undergo CO dissociation under relatively mild thermal conditions, and a fascinating consequence of this behavior is that the metal-alkyne compounds readily react with other 18-electron transition metal species to afford a variety of alkyne-bridged homo- and heterobimetallic complexes (Eq. 5.1 and Scheme 5-1).^{1,2}



Scheme 5-1. Reaction of $\text{Ru}(\text{CO})_4(\eta^2\text{-HFB})$ with $\text{Cp}'\text{M}(\text{CO})_2$.

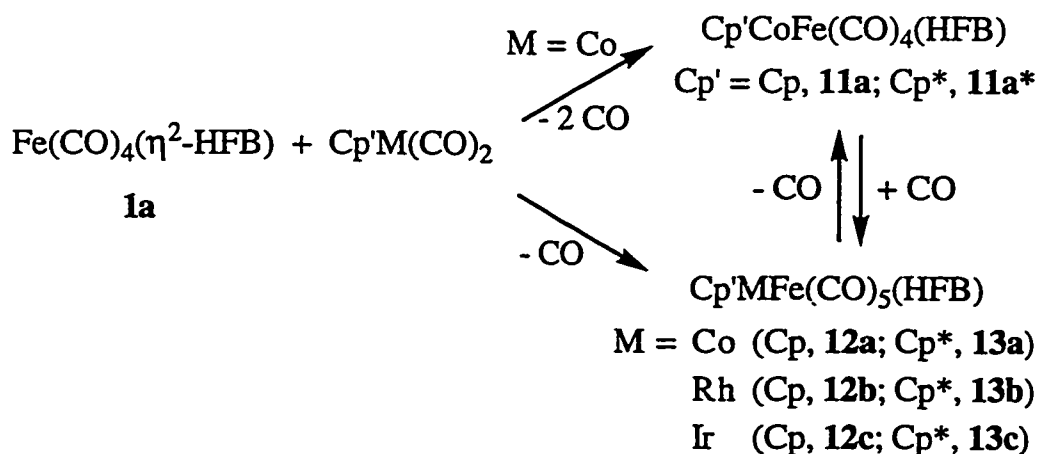
It was thus naturally of interest to investigate whether **1a** would react similarly and provide access to a new series of iron-containing heterobimetallic compounds. A preliminary account of this investigation has been published.³

5.2. Reaction of **1a** with $\text{Cp}'\text{M}(\text{CO})_2$ ($\text{M} = \text{Co, Rh, Ir}$; $\text{Cp}' = \text{Cp, Cp}^*$)

5.2.1. Synthetic Aspects

The initial discovery that $\text{M}(\text{CO})_4(\eta^2\text{-alkyne})$ compounds are reactive towards other 18 electron organometallic complexes came during the photochemical preparation of $\text{Ru}(\text{CO})_4(\eta^2\text{-HFB})$, when it was observed that the ruthenium-alkyne product would combine with unreacted $\text{Ru}(\text{CO})_5$ or deliberately added $\text{Os}(\text{CO})_5$ to produce the dimetallacyclobutenes $\text{M}'\text{Ru}(\text{CO})_8(\mu\text{-}\eta^1\text{:}\eta^1\text{-HFB})$ (Eq. 5.1).¹ In contrast, compound **1a** is unreactive towards the entire triad of group eight metal pentacarbonyls. In some ways, this resembles the behavior of $\text{Os}(\text{CO})_4(\eta^2\text{-HFB})$ which is unreactive towards $\text{Ru}(\text{CO})_5$ and reacts with $\text{Os}(\text{CO})_5$ only above $+60^\circ\text{C}$. The modest thermal instability of **1a** precludes similar high temperature treatment.

However, **1a** does react cleanly with all six variants of $\text{Cp}'\text{M}(\text{CO})_2$ ($\text{M} = \text{Co, Rh, Ir}$; $\text{Cp}' = \text{Cp, Cp}^*$) to form brightly colored products (Scheme 5-2) in high yield (72 - 96 %).



Scheme 5-2. Reaction of **1a** with $\text{Cp}'\text{M}(\text{CO})_2$.

Elemental analysis and mass spectrometry confirmed that the products were bimetallic compounds with the indicated molecular compositions. As shown in the Scheme, reaction of **1a** with $\text{Cp}'\text{Co}(\text{CO})_2$ initially afforded **11a** ($\text{Cp}' = \text{Cp}$) and **11a*** ($\text{Cp}' = \text{Cp}^*$) which converted to **12a** and **13a** upon treatment with CO, and reverted to **11a,a*** when stirred in solution under static vacuum. In the case of **11a**, it was not possible to entirely shift the equilibrium towards **12a** under 1 atm. CO, and a *ca.* 1:2 mixture of **11a**:**12a** resulted. In contrast, the Rh- and Ir-derived complexes **12b,c** and **13b,c** are stable towards CO loss at ambient temperature, even upon prolonged stirring under static vacuum.

Interestingly, and contrary to expectation, there was a marked dependence of the reaction completion time on the nature of $\text{Cp}'\text{M}(\text{CO})_2$. Firstly, the electron rich $\text{Cp}^*\text{M}(\text{CO})_2$ compounds all reacted more quickly than their Cp analogs, suggesting a dependence of the reaction on the nucleophilicity of the entering metal species. For instance, the reaction of **1a** and $\text{Cp}^*\text{Rh}(\text{CO})_2$ commenced at *ca.* -40°C while that with $\text{CpRh}(\text{CO})_2$ began above -20°C . More interestingly, the reactions also showed a metal dependence, being quickest for the Rh compounds and slowest for Ir within each Cp/Cp* series. For example, the order of reactivity with $\text{CpM}(\text{CO})_2$ was clearly established, by the completion times of the analogous reactions at room temperature, to be Rh (*ca.* 1h) > Co (*ca.* 4 h) >> Ir (*ca.* 3 days). A similar metal-dependent trend was found for the Cp* series, suggesting that the reactions were not necessarily occurring under conditions of rate-limiting CO loss from compound **1a**.

5.2.2. Characterization of Compounds **11a,a***: Dimetallatetrahedranes

Both $\text{Cp}'\text{CoFe}(\text{CO})_4(\text{HFB})$ ($\text{Cp}' = \text{Cp}$, **11a**; Cp^* , **11a***) compounds displayed one singlet in their ^{19}F NMR spectra, clearly suggesting that the HFB ligand lies perpendicular to a mirror plane in the complex. The IR spectra consisted of three high frequency bands (2071 , 2029 , and 2015 cm^{-1} , **11a**; 2071 , 2022 , and 2003 cm^{-1} , **11a***) as would be expected for three terminal CO ligands on the Fe center. A weaker band was found to lower frequency at 1914 and 1887 cm^{-1} , respectively, suggesting the presence of a bridging CO ligand. In keeping with the greater electron releasing nature of the Cp* ligand relative to

Cp, the μ -CO band in **11a*** was shifted to lower frequency than in **11a**. Transmission of this electronic effect to the Fe center was evident as two Fe–CO stretches were shifted to lower wavenumber in **11a***. All of the above features agree with the spectroscopic characteristics of the previously characterized $\text{Cp}^*\text{CoRu}(\text{CO})_3(\mu\text{-CO})(\mu\text{-}\eta^2\text{:}\eta^2\text{-HFB})$ (Scheme 5-1), and consequently a similar structure is proposed for **11a,a*** (Figure 5-1).

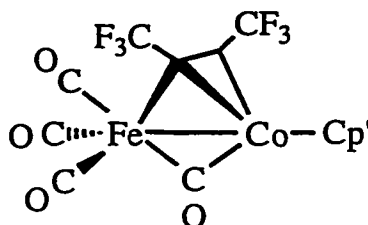


Figure 5-1. Proposed Dimetallatetrahedrane Structures for **11a,a***.

The alkyne shares each of its two available π sets with the two different metal centers, contributing two electrons to each, and thus functions as a net four-electron donor to the bimetallic complex. The preference of the alkyne to orient itself perpendicular to the metal-metal bond rather than the parallel fashion favored for 2nd and 3rd row metals (Eq. 5.1, Scheme 5-1) may be because the shorter metal-metal bond anticipated between two first row metals does not readily support a $\mu\text{-}\eta^1\text{:}\eta^1\text{-alkyne}$ bridge. Indeed, a wide range of dicobaltatetrahedranes have been isolated incorporating the $\text{Co}_2(\text{CO})_6$ fragment, but $\text{Co}_2(\text{CO})_7(\mu\text{-}\eta^1\text{:}\eta^1\text{-RCCR})$ structures are unknown.⁴ In contrast, dimetallacyclobutenes abound for rhodium and iridium bimetallics.^{5,6}

The ^{13}C NMR spectra in the carbonyl region agree with the proposed structure, as three resonances were observed in a 1:1:2 ratio at the low temperature limit (-100°C). The furthest downfield signal (δ 220.37, **11a**; 228.17, **11a***) is assigned to the bridging CO ligand while the remaining 1:2 pattern is due to an $\text{Fe}(\text{CO})_3$ group with C_s symmetry. In accord with these assignments, the two upfield resonances collapsed and coalesced to an average resonance (δ 204.52, **11a**; 205.70, **11a***) upon warming as the $\text{Fe}(\text{CO})_3$ moiety expectedly⁷ underwent fluxional exchange; the downfield resonance for the bridging

carbonyl remained sharp throughout this process. The bridging alkyne carbons were detected at δ 73.53 (**11a**) and 70.36 (**11a***) in a $^{13}\text{C}\{^{19}\text{F}\}$ NMR experiment. The chemical shifts are some 15 ppm downfield of those in the structurally characterized $\text{Cp}^*\text{RhRu}(\text{CO})_3(\mu\text{-CO})(\mu\text{-}\eta^2\text{:}\eta^2\text{-HFB})$ analog (δ 56.96, d, $^1J_{\text{RhC}} = 22 \text{ Hz}$)² and quite similar to that in free HFB (δ 71.4).⁸ An upfield shift is predicted as the alkyne carbons would be expected to take on sp^3 character upon coordination of the HFB moiety in a $\mu\text{-}\eta^2\text{:}\eta^2$ fashion, and thus the similarity of the chemical shifts in **11a,a*** to free HFB likely reflects a balance between rehybridization effects and the removal of diamagnetic anisotropy which causes an upfield shift in the free alkyne.⁹

5.2.3. Initial Characterization of Heterobimetallics **12a-c** and **13a-c**

Compounds **12a-c** and **13a-c** have identical molecular compositions, $\text{Cp}'\text{MFe}(\text{CO})_5(\text{HFB})$, determined by elemental analysis and mass spectrometry. The ^1H NMR spectra were largely unremarkable as they consisted of a single resonance for the protons of the Cp (**12a-c**) or Cp* (**13a-c**) ligands. However, the ^{19}F NMR spectra provided useful structural information. Two resonances were observed in accord with the presence of an unsymmetrical HFB ligand. A comparison of chemical shift parameters with the known $\text{Cp}'\text{MRu}(\text{CO})_5(\mu\text{-}\eta^1\text{:}\eta^1\text{-HFB})$ (Cp' = Cp, Cp*; M = Co, Rh, Ir) species^{1,2} is presented below (Table 5-1). The resonances can be assigned rigorously for the cases where M = Rh as distinctive $^3J_{\text{RhF}}$ coupling was observed to the CF_3 group attached to the Rh-bonded alkyne carbon. For the Co- and Ir-containing bimetallics, the assignments are based on the observation that the chemical shift of the trifluoromethyl group proximal to the group 8 metal (M') remained roughly constant at δ -58 ppm. The remaining downfield resonances are then assigned to the CF_3 groups adjacent to the group nine metal, resulting in the general trend $\text{Co} > \text{Rh} > \text{Ir}$ for $\delta(\text{CF}_3)_\text{M}$. Furthermore, the chemical shifts of the CF_3 groups are very similar to those of the previously characterized ruthenium dimetallacyclobutenes,^{1,2} and thus initially suggest similar structures for **12a-c** and **13a-c**.

The IR spectra (Table 5-2) of **12a-c** each show five terminal carbonyl stretches and one much weaker band to lower frequency which did not shift

upon ^{13}C O enrichment. The latter is thus a νCC band and is distinctive of hexafluoro-but-2-yne when bridging either group 8 or group 9 metals.^{1,10}

Table 5-1. ^{19}F NMR Data (δ , ppm) for $\text{Cp}^*\text{MM}'(\text{CO})_5(\text{HFB})$.^a

	Cp'	M	M'	M-C-CF ₃	M'-C-CF ₃	$^5J_{\text{FF}}$ (Hz)
12a	Cp	Co	Fe ^b	-52.7	-57.0	10.9
13a	Cp*	Co	Fe ^b	-51.5	-58.7	11.5
	Cp	Co	Ru	-55.5	-57.8	12.0
	Cp*	Co	Ru ^b	-52.5	-58.3	12.4
12b	Cp	Rh	Fe	-55.0 ^c	-57.8	11.7
13b	Cp*	Rh	Fe	-53.7 ^d	-58.7	12.1
	Cp*	Rh	Ru	-53.6 ^d	-57.5	13.0
12c	Cp	Ir	Fe	-56.8	-57.5	12.4
13c	Cp*	Ir	Fe	-55.5	-57.7	12.5
	Cp*	Ir	Ru	-55.5	-57.1	13.0

^a CD_2Cl_2 , at ambient temperature unless otherwise noted. ^b-60°C.

^cAdditional doublet coupling of $^3J_{\text{RhF}} = 3.0$ Hz. ^d $^3J_{\text{RhF}} = 3.4$ Hz.

Table 5-2. FT-IR Spectra (pentane, cm^{-1}) of **12a-c**.

Compound	νCO	νCC
12a	2093(s), 2042(s), 2031(vs), 2024(vs), 2008(m) ^a	1635(vw)
12b	2093(s), 2043(vs), 2028(vs), 2019(m), 2012(m)	1635(vw)
12c	2094(s), 2043(s), 2023(vs), 2015(s), 2004(m)	1626 (w)

^aassignment uncertain; see Section 5.7.2.

The νCC stretches are some 13 - 14 cm^{-1} to higher frequency than were observed for the analogous $\text{Cp}^*\text{MRu}(\text{CO})_5(\mu\text{-}\eta^1\text{-}\eta^1\text{-HFB})$ species, reflecting a dependence of the alkyne bonding on the heterodinuclear framework. The presence of five terminal νCO and one olefinic νCC stretch in the IR spectra thus confirm that compounds **12a-c** are indeed the anticipated heterodimetallacyclobutenes (Figure 5-2).

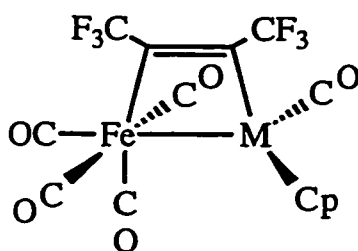


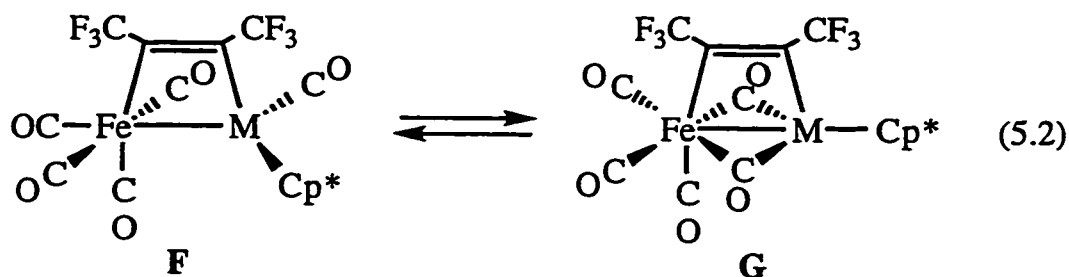
Figure 5-2. Proposed Dimetallacyclobutene Structures for **12a-c**.

However, the IR spectra of compounds **13a-c** are markedly different from their Cp congeners (Table 5-3). The FeCo species **13a** displays a total of six bands, three of which are found in the bridging CO stretching region, while the heavier compounds **13b,c** show no fewer than nine carbonyl stretching bands in addition to a very weak, low frequency band attributed to the ν_{CC} stretch of the coordinated alkyne. As with **12a-c**, this low frequency band did not shift upon ^{13}C O enrichment.

Table 5-3. FT-IR Spectra (pentane, cm^{-1}) of **13a-c**.

	ν_{CO}	ν_{CC}
13a	2064(s), 2019(s), 1972(m), 1790(w), 1762(w), 1754(sh)	–
13b	2082(m), 2063(vs), 2031(m), 2024(vs), 2012(m), 1996(w), 1957(m), 1790(w), 1761(w), 1753(sh)	1625(vw)
13c	2084(m), 2062(vs), 2032(m), 2016(vs), 2002(m), 1988(w), 1971(m), 1793(w), 1761(m)	1617(vw)

The presence of a distinct ν_{CC} band in **13b,c** suggests an alkyne-bridged structure analogous to that of **12a-c**, while the large number of CO stretching bands is rationalized by the presence of isomers in solution. In particular, the presence of bands in the bridging carbonyl region of the spectrum suggested an equilibrium mixture of isomeric all-terminal (**F**) and doubly-CO bridged (**G**) dimetallacyclobutenes (Eq. 5.2). For example, the $\mu\text{-CO}$ bands in **13c** compare well with the 1787 cm^{-1} value in $\text{Cp}^*\text{Ir}(\mu\text{-CO})_2\text{Fe}_2(\text{CO})_7$, a structure containing similar ligands in which an Fe–Ir bond is supported by a pair of bridging COs.¹¹



The pattern of **13a** can also be rationalized by Eq. 5.2 providing it is assumed that the ν_{CC} stretch was too weak to be observed and the equilibrium heavily favors the bridged isomer **G**, as would be expected for a bimetallic compound containing two first row metals.¹²⁻¹⁴ However, the presence of a low frequency shoulder in the IR spectra of both **13a** and **13b** remains unexplained, as this provides one more carbonyl stretch in the bridging region than can be explained by Eq. 5.2. Furthermore, the simplicity of both the ^1H and ^{19}F NMR spectra from ambient temperature to -80°C requires that the equilibrium be fast on the NMR time scale.

In the hopes of obtaining further structural information, ^{13}C NMR spectra were collected on ^{13}CO enriched samples of **12a-c** and **13a-c**. The bimetallic complexes were anticipated^{1,2} to exhibit carbonyl fluxionality and the spectra were indeed temperature dependent. Discussion of the fluxional behavior is deferred to Section 5.3; for the moment, attention is focussed on the low temperature limiting spectra which could be achieved in all cases. The relevant data are collected in Table 5-4.

Table 5-4. Limiting ^{13}C NMR for **12a-c** and **13a-c** (CD_2Cl_2 , 100.6 MHz).

	Cp'	M	$\delta(\text{CO}_{\text{Fe}})$	$\delta(\text{CO}_{\text{M}})$	T (K)
12a	Cp	Co	214.55, 212.02, 206.11, 202.36	196.58	213
13a	Cp*	Co	217.30, 214.61, 208.42, 203.39	198.88	213
12b	Cp	Rh	208.72, 207.05, 206.64, 203.67	189.19 ^a	173
13b	Cp*	Rh	216.62, 212.81, 209.89, 204.09	186.41 ^b	213
12c	Cp	Ir	210.35, 207.54 (2CO), 201.87	169.37	173
13c	Cp*	Ir	218.91, 211.10, 210.70, 204.15	165.66	203

^adoublet, $^1J_{\text{RhC}} = 80$ Hz. ^bdoublet, $^1J_{\text{RhC}} = 81$ Hz.

As expected, the dimetallacyclobutenes **12a-c**, having no symmetry, show a five signal pattern for each of the distinct carbonyls shown in Figure 5-2. Surprisingly, compounds **13a-c** have an identical pattern. The terminal carbonyls bonded to the group 9 metal are readily identified on the basis of chemical shift. Also, compounds **12b** and **13b** displayed large $^1J_{\text{RhC}}$ coupling of approximately 80 Hz, and the Co-carbonyl resonances of **12a** and **13a** showed a temperature dependence, unrelated to the fluxional processes (*vide infra*), due to interaction with the ^{59}Co quadrupole.¹⁵ The presence of a terminal M–CO resonance in **13a-c** implies that if the equilibrium proposed in Eq. 5.2 is occurring, the product distribution must shift entirely towards **F** at low temperature. In the case of **13a**, this is particularly strange as there was no evidence for the all-terminal isomer in the solution FT-IR spectrum at ambient temperature. Although isomer distributions can be solvent dependent, the appearance of the solution IR spectra of **13a-c** were not affected by a change from pentane to CH_2Cl_2 . Thus, while limiting ^{13}C NMR spectra in the carbonyl region further confirm the nature of **12a-c**, few additional clues are provided as to the structures of **13a-c**.

Accordingly, determination of the molecular geometry of **13a-c** by X-ray crystallography was desirable and suitable crystals were obtained for **13c**. Although compounds **12a-c** are well defined by their spectroscopic characteristics, the molecular structure of **12c** was determined for comparison with its Cp^* congener and shall be discussed first.

5.2.4. Molecular Structure of $\text{CpIrFe}(\text{CO})_5(\mu\text{-}\eta^1\text{:}\eta^1\text{-HFB})$ (**12c**)

The molecular structure of **12c** is presented in Figure 5-3, and selected interatomic distances and angles are provided in Tables 5-5 and 5-6. The structure was well-defined with respect to the ligands surrounding the two metal centers, but a rotational disorder was detected in the CF_3 groups. The latter may be due to the desire of the bulky trifluoromethyl groups to minimize non-bonded contacts between fluorines. In both models, the CF_3 groups interlock in a "cog-wheel" fashion.

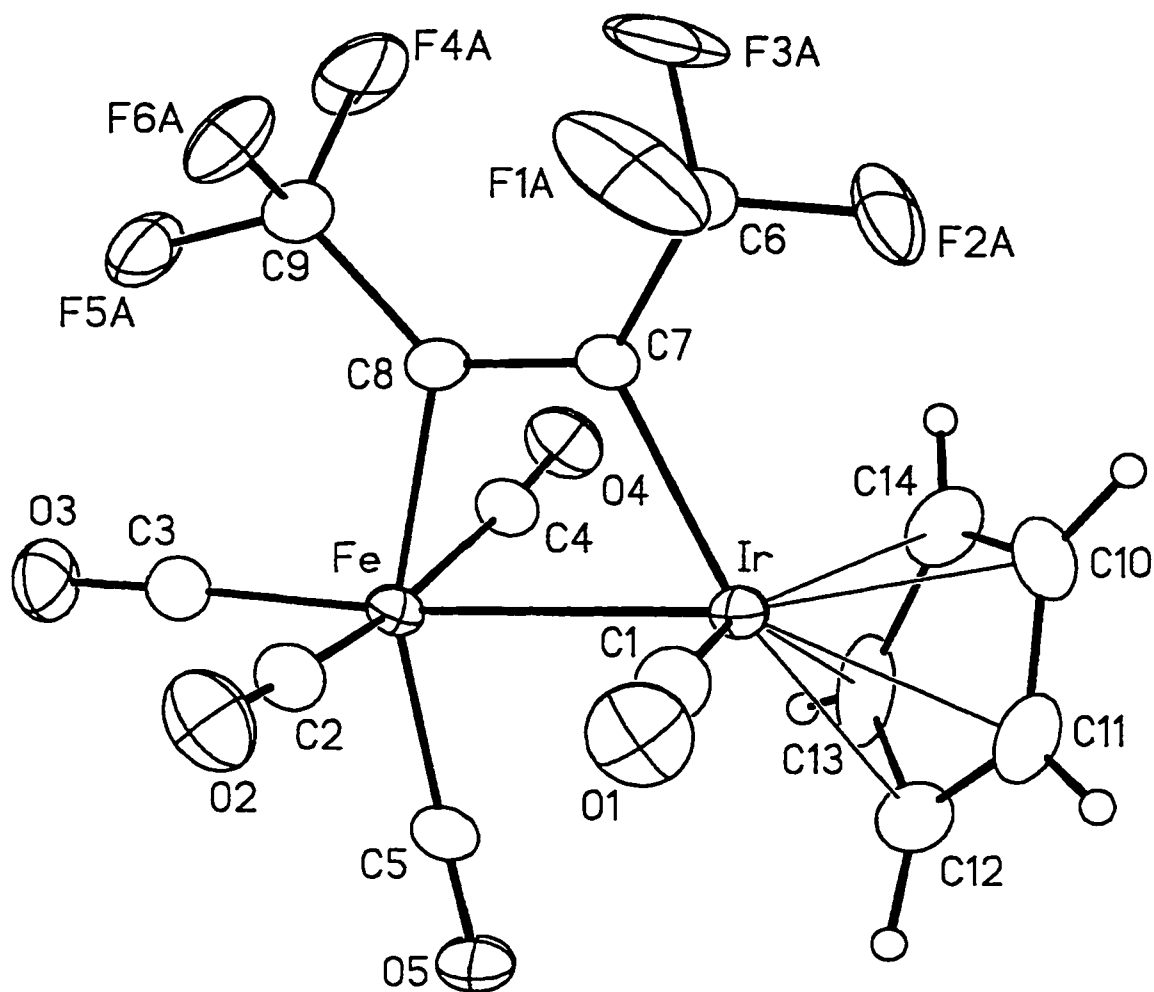


Figure 5-3. Molecular Structure of Compound 12c.

Table 5-5. Selected Interatomic Distances (Å) in Compound 12c.

Fe–Ir	2.7049(10)	Fe–C(8)	2.022(7)
Ir–C(1)	1.823(9)	C(1)–O(1)	1.154(12)
Ir–C(7)	2.058(7)	C(2)–O(2)	1.120(11)
Fe–C(2)	1.816(9)	C(3)–O(3)	1.137(11)
Fe–C(3)	1.805(9)	C(4)–O(4)	1.125(11)
Fe–C(4)	1.815(8)	C(5)–O(5)	1.116(9)
Fe–C(5)	1.833(7)	C(7)–C(8)	1.317(10)

Table 5-6. Selected Interatomic Angles (deg.) in Compound **12c**.

Fe–Ir–C(1)	95.5(3)	C(3)–Fe–C(8)	103.0(3)
Fe–Ir–C(7)	68.4(2)	C(4)–Fe–C(5)	96.7(3)
Ir–Fe–C(2)	88.8(3)	C(4)–Fe–C(8)	80.6(3)
Ir–Fe–C(3)	174.8(3)	C(5)–Fe–C(8)	158.5(3)
Ir–Fe–C(4)	84.7(3)	Ir–C(1)–O(1)	175.2(9)
Ir–Fe–C(5)	86.6(3)	Fe–C(2)–O(2)	176.5(9)
Ir–Fe–C(8)	71.9(2)	Fe–C(3)–O(3)	177.6(8)
C(1)–Ir–C(7)	88.6(4)	Fe–C(4)–O(4)	176.4(8)
C(2)–Fe–C(3)	91.9(4)	Fe–C(5)–O(5)	178.9(8)
C(2)–Fe–C(4)	166.6(3)	Ir–C(7)–C(8)	112.0(5)
C(2)–Fe–C(5)	94.6(4)	Fe–C(8)–C(7)	107.7(5)
C(2)–Fe–C(8)	86.2(3)	C(6)–C(7)–C(8)	126.8(7)
C(3)–Fe–C(4)	93.5(4)	C(7)–C(8)–C(9)	128.1(7)
C(3)–Fe–C(5)	98.5(4)		

The alkyne bridges the two metal centers in an $\eta^1:\eta^1$ fashion, as predicted. The C(7)–C(8) vector lies in the same plane as the Ir–Fe vector; the C(7)–Ir–Fe–C(8) and Fe–Ir–C(7)–C(8) torsion angles are $-0.6(3)^\circ$ and $1.0(5)^\circ$, respectively. This is typical of bimetallic complexes containing a $\mu\text{-}\eta^1:\eta^1\text{-C}_2(\text{CF}_3)_2$ ligand.¹⁶⁻¹⁸ Furthermore, the Ir–Fe–C(8) and Fe–C(8)–C(7) angles sum to 179.6° , and the Fe–Ir–C(7) and Ir–C(7)–C(8) angles sum to 180.4° , demonstrating that the C(7)–C(8) vector is also parallel to the metal-metal bond. This result is interesting given that the alkyne is skewed towards the Fe center because the Fe–C(8) bond (2.022(7) Å) is shorter than the Ir–C(7) bond (2.058(7) Å) by 0.03 Å. In other heterobimetallic compounds containing a $\mu\text{-}\eta^1:\eta^1$ -alkyne ligand, it is common for the alkyne to "tilt" slightly towards one of the disparate metal centers. For instance, in $\text{Cp}^*\text{RhRu}(\text{CO})_4\text{L}(\mu\text{-HFB})$ (L = CO,¹⁷ PMe₃¹⁹), the alkyne "tilts" slightly towards the group nine metal as the sum of the Rh–Ru–C(alk) and Ru–C(alk)–Calk' angles is roughly 176° while the Ru–Rh–C(alk)' and Rh–C(alk)'–

C(alk) angles sum to 184° . A similar situation results in $\text{Cp}^*\text{IrOs}(\text{CO})_5(\mu\text{-}\eta^1\text{:}\eta^1\text{-CHC}(\text{CF}_3))$, with corresponding angle sums of 177° and 183° .⁸

The Fe–Ir bond distance of $2.7049(10)$ Å suggests an Fe–Ir single bond and compares favorably with the $2.7178(9)$ Å separation reported in $\text{CpFe}(\text{CO})(\mu\text{-CO})(\mu\text{-CF}_2)\text{Ir}(\text{CO})(\text{Cl})(\text{PMe}_2\text{Ph})_2$.²⁰ The distance is also similar to that found in $\text{Cp}^*\text{Ir}(\mu\text{-CO})_2\text{Fe}_2(\text{CO})_7$ for the unsupported Fe–Ir bond ($2.698(7)$ Å); the CO-bridged intermetallic separation is significantly shorter at $2.616(7)$ Å in this complex.¹¹ The Ir–C(7) bond length, $2.058(7)$ Å, is quite similar to that found for the Ir–C(sp^2) single bonds in $\text{Cp}^*\text{IrOs}(\text{CO})_5(\mu\text{-}\eta^1\text{:}\eta^1\text{-CHC}(\text{CF}_3))$ ($2.055(8)$ Å)⁸ and $\text{Ir}_2\text{Cp}_2(\text{CO})_2(\mu\text{-C}_6\text{F}_4)$ ($2.045(3)$ and $2.024(2)$ Å).²¹ The Fe–C(8) bond length of $2.022(7)$ Å is within the range of Fe–C(sp^2) bond lengths²² and compares well with the corresponding separations of $2.021(3)$ and $2.022(3)$ Å in $\text{Fe}_2(\text{CO})_8(\mu\text{-}\eta^1\text{:}\eta^1\text{-C}_6\text{F}_4)$.²³ The C(7)–C(8) interatomic distance of $1.317(10)$ Å is significantly longer than the 1.276 Å found in structurally characterized examples of $\text{M}(\text{CO})_4(\eta^2\text{-HFB})$ ($\text{M} = \text{Ru}, \text{Os}$),²⁴ but very similar to other localized C–C double bonds derived from the HFB ligand, which generally range from 1.32 – 1.36 Å.^{16-19,25}

The trifluoromethyl substituents are bent back to similar degrees, although the C(6)–C(7)–C(8) and C(7)–C(8)–C(9) angles are larger than the 120° anticipated for idealized sp^2 hybridization of the C(7) and C(8) atoms. It has been suggested that this general feature of $\mu\text{-}\eta^1\text{:}\eta^1\text{-C}_2(\text{CF}_3)_2$ ligands is likely a combination of steric and electronic effects.¹⁸ The steric component results from the desire of the bulky trifluoromethyl groups to attain the maximum possible separation while the electronic component may be a compensation for the compressed M–C(alk)–C(alk) angles ($107.7(5)$ and $112.0(5)^\circ$ presently) which result from the alkyne bridging the metal centers.

The geometry of the Ir center resembles that of a three-legged piano stool, and the Fe center is pseudo-octahedral, the greatest deviation being the Ir–Fe–C(8) angle of $71.9(2)^\circ$. More interesting is the clear upward bend of carbonyls C(2)O(2) and C(4)O(4). This is typical of heterodinuclear $\text{Cp}'\text{MM}'(\text{CO})_5$ frameworks containing a $\mu\text{-}\eta^1\text{:}\eta^1$ -bridge (bridge = C_2R_2 or $\text{C}_2\text{R}_2\text{C}(\text{O})$) and Washington has recently drawn an analogy between such complexes and

pseudo-octahedral $M(\text{CO})_4\text{L}$ ($\text{L} = \text{olefin, alkyne}$) systems which display a similar deflection of their axial ligands in the direction of the equatorial metallacyclic ring system.⁸ In the present case, $\text{C}(2)\text{O}(2)$ and $\text{C}(4)\text{O}(4)$ are the axial substituents bending towards the equatorial Ir and $\text{C}(8)$ substituents on the Fe center which are part of a dimetallacyclobutene ring. At $166.6(3)^\circ$, the $\text{C}(2)\text{-Fe-C}(4)$ angle defines a rather large deflection from linearity and is similar to the $166.8(4)^\circ$ angle found in $\text{CpRhOs}(\text{CO})_5(\mu\text{-}\eta^1\text{:}\eta^1\text{-}(\text{O})\text{CCHCMe})$.⁸ The homobimetallic $\text{Fe}_2(\text{CO})_8(\mu\text{-}\eta^1\text{:}\eta^1\text{-C}_6\text{F}_4)$ also exhibits this structural feature with corresponding $(\text{O})\text{C}\text{-Fe-C}(\text{O})$ angles of $170.8(2)$ and $172.9(2)^\circ$.²³

It is also interesting to note that the $\text{C}(2)\text{-Fe-C}(8)$ and $\text{C}(4)\text{-Fe-C}(8)$ angles, $86.2(3)^\circ$ and $80.6(3)^\circ$, are not equivalent, with the result that $\text{C}(4)\text{O}(4)$ is bent further towards the bridging HFB ligand than is $\text{C}(2)\text{O}(2)$. However, the $\text{C}(2)\text{-Fe-C}(5)$ and $\text{C}(4)\text{-Fe-C}(5)$ angles, $94.6(4)^\circ$ and $96.7(3)^\circ$, are more or less equivalent, implying that the entire $\text{Fe}(\text{CO})_4$ moiety is slightly canted relative to the plane defined by Ir, Fe, $\text{C}(7)$, and $\text{C}(8)$. Despite the distortions around the Fe center, the $\text{Fe-C}(\text{O})$ separations are similar and compare with those in $\text{Fe}_2(\text{CO})_8(\mu\text{-}\eta^1\text{:}\eta^1\text{-C}_6\text{F}_4)$ which ranged between $1.806(4)$ and $1.829(4)$ Å.²³

5.2.5. Molecular Structure of $\text{Cp}^*\text{IrFe}(\text{CO})_4(\mu\text{-}\eta^1\text{:}\eta^3\text{-C}_2(\text{CF}_3)_2\text{C}(\text{O}))$ (**13c**)

The molecular structure of compound **13c** is shown in Figure 5-4 and a selection of interatomic distances and angles is provided in Tables 5-7 and 5-8. It is evident that the structure is markedly different from that of **12c**, discussed in the previous section, and is not the doubly-CO bridged isomeric structure **G** (Eq. 5.2) proposed on the basis of IR spectroscopy. The distinguishing feature is the "insertion" of a CO ligand at the Fe center to generate a dimetallacyclopentenone. The resulting $\text{C}_2(\text{CF}_3)_2\text{C}(\text{O})$ moiety is bonded to iron in an η^3 fashion, and $\text{C}(7)$ bridges the two metal centers. In retrospect, although the previous bimetallic compounds derived from $\text{Ru}(\text{CO})_4(\eta^2\text{-HFB})$ all contain bridging alkyne ligands, the formation of a CO-inserted isomer presently is not entirely surprising given the facility of migratory CO insertion in compounds **1a-e** (Chapter 3). Furthermore, the vast majority of bimetallic carbonyl compounds containing iron and an alkyne adopt $\mu\text{-}\eta^1\text{:}\eta^3$ -dimetallacyclopentenone structures.²⁶⁻³³

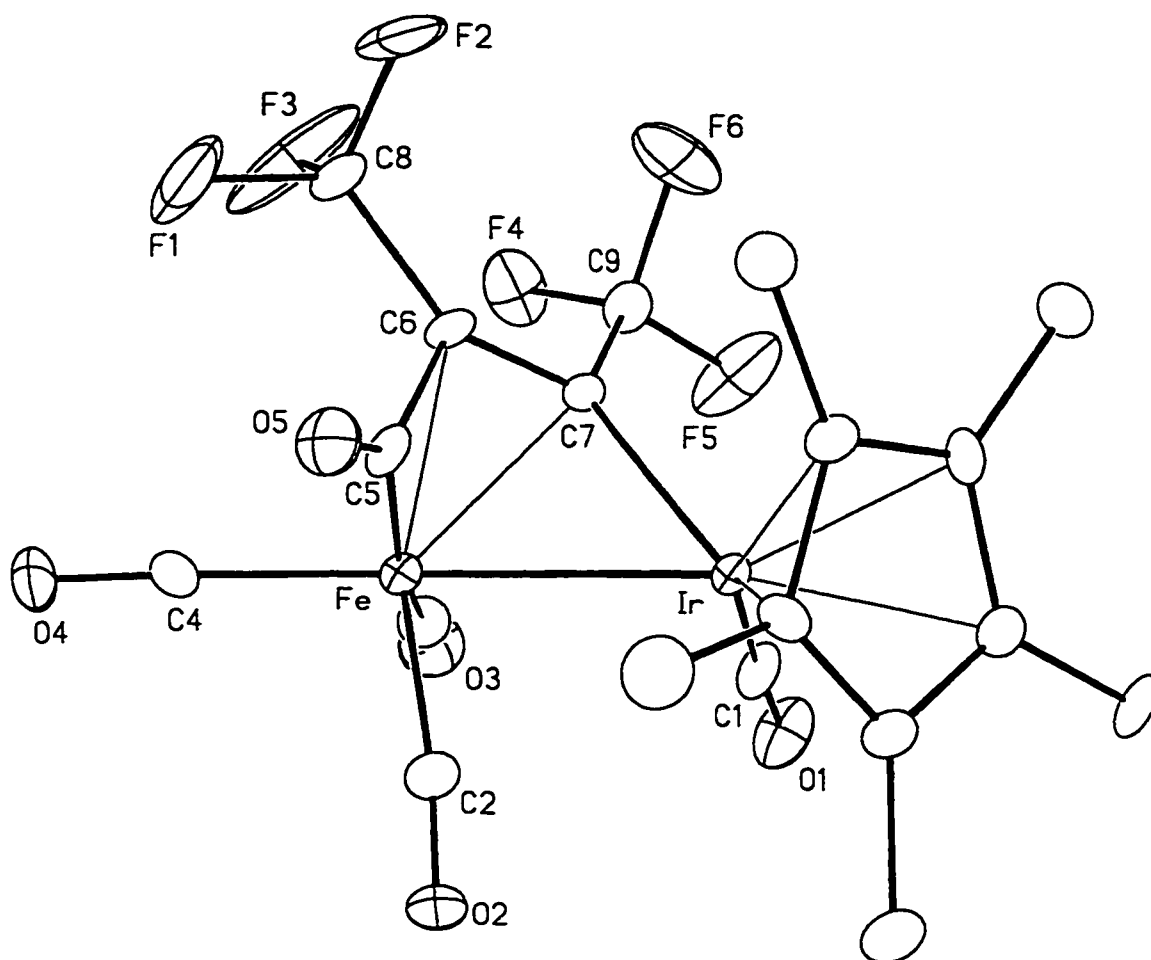


Figure 5-4. Molecular Structure of Compound 13c.

The hydrogen atoms on the methyl groups have been omitted for clarity.

Table 5-7. Selected Interatomic Distances (Å) in Compound 13c.

Fe–Ir	2.6995(15)	Fe–C(7)	2.096(9)
Ir–C(1)	1.826(12)	C(1)–O(1)	1.163(12)
Ir–C(7)	2.037(9)	C(2)–O(2)	1.143(12)
Fe–C(2)	1.788(11)	C(3)–O(3)	1.129(14)
Fe–C(3)	1.857(13)	C(4)–O(4)	1.132(13)
Fe–C(4)	1.781(12)	C(5)–O(5)	1.181(12)
Fe–C(5)	1.913(11)	C(5)–C(6)	1.493(13)
Fe–C(6)	2.094(10)	C(6)–C(7)	1.396(13)

Table 5-8. Selected Interatomic Angles (deg.) in Compound 13c.

Fe–Ir–C(1)	87.9(3)	C(4)–Fe–C(5)	89.2(5)
Fe–Ir–C(7)	50.2(3)	C(4)–Fe–C(6)	101.1(5)
Ir–Fe–C(2)	76.4(7)	C(4)–Fe–C(7)	134.0(4)
Ir–Fe–C(3)	99.2(4)	C(5)–Fe–C(6)	43.5(4)
Ir–Fe–C(4)	167.1(4)	C(5)–Fe–C(7)	73.7(4)
Ir–Fe–C(5)	79.4(3)	C(6)–Fe–C(7)	38.9(4)
Ir–Fe–C(6)	74.9(3)	Ir–C(1)–O(1)	175.1(9)
Ir–Fe–C(7)	48.3(2)	Ir–C(7)–C(6)	117.4(7)
C(2)–Fe–C(3)	100.6(5)	Fe–C(2)–O(2)	171.6(11)
C(2)–Fe–C(4)	98.5(5)	Fe–C(3)–O(3)	177.6(11)
C(2)–Fe–C(5)	95.5(5)	Fe–C(4)–O(4)	177.7(11)
C(2)–Fe–C(6)	113.4(5)	Fe–C(5)–O(5)	147.0(9)
C(2)–Fe–C(7)	124.8(4)	Fe–C(5)–C(6)	74.7(6)
C(3)–Fe–C(4)	93.5(6)	C(5)–C(6)–C(7)	112.8(8)
C(3)–Fe–C(5)	163.1(5)	C(6)–C(5)–O(5)	136.5(10)
C(3)–Fe–C(6)	119.7(5)	C(6)–C(7)–C(9)	119.4(8)
C(3)–Fe–C(7)	92.7(5)	C(7)–C(6)–C(8)	129.6(9)

The geometry surrounding Ir is similar to that in **12c**, whereas that around Fe is more complicated but may still be described as a distorted octahedron if one takes the coordinated olefin moiety, C(6)–C(7), as a single coordination site. The Cp* ring is oriented such that it is on the same side of the complex as the acyl group, presumably to minimize steric interaction with the bulky trifluoromethyl group on the bridging C(7) carbon. The three carbonyl groups on Fe form a facial arrangement, and the distortion of the octahedron can be readily seen by the C(2)–Fe–C(3) and C(2)–Fe–C(4) angles which open to 100.6(5)° and 98.5(5)° respectively. The Ir–Fe–C(2) angle is compressed to 76.4(7)° but C(2)O(2) does not appear to be semi-bridging. The olefinic portion of the bridging group is twisted with respect to the metal-metal bond, as seen by the Ir–Fe–C(6)–C(7) torsion angle of -40.4(5)°.

The Fe–Ir bond distance of 2.6995(15) Å compares favorably with the 2.7049(10) Å separation in **12c**. The Fe–C(2) and Fe–C(4) bond lengths are equal at 1.788(11) and 1.781(12) Å, respectively, while the Fe–C(3) bond distance is significantly longer at 1.857(13) Å. Interestingly, although the Cp* ligand is electron releasing relative to Cp because of its electron donating methyl substituents, the Ir–C(1) bond length in the present complex (1.826(12) Å) is identical to that in **12c** (1.823(9) Å). Indeed, the Ir center is similar in both complexes as each supports a terminal carbonyl ligand, a metal-metal bond and a σ -bonded carbon in addition to the Cp or Cp* ligand. The fact that no difference in Ir–C(1) distance is detected between the Cp and Cp* substituted centers suggests that the Ir centers are electronically similar in both species.

The Fe–C(5) distance, 1.913(11) Å, is similar to that found in systems with a $(\mu\text{-}\eta^1\text{:}\eta^3\text{-C}_2\text{R}_2\text{C(O)})$ ring system, namely 1.928(3) and 1.922(3) Å in the two crystallographically distinct forms of $\text{Fe}_2(\text{CO})_5(\mu\text{-dppm})(\mu\text{-}\eta^1\text{:}\eta^3\text{-C}_2\text{H}_2\text{C(O)})$ ^{32,33} and 1.913(9) Å in $(\text{Ph}_3\text{P})\text{PtFe}(\text{CO})_2(\mu\text{-dppm})(\mu\text{-}\eta^1\text{:}\eta^3\text{-C}_2\text{H}_2\text{C(O)})$,^{30,31} but is shorter than the 1.957(7) Å value in $\text{CpRh}(\text{P}^i\text{Pr}_3)\text{Fe}(\text{CO})_3(\mu\text{-}\eta^1\text{:}\eta^3\text{-CHCPhC(O)})$.²⁹ The Fe–C(5) bond length is also some 0.08 - 0.09 Å shorter than the Fe–C(O) bond lengths in a series of perfluorinated mono- and di-acyl ferracycles, $\text{Fe}(\text{CO})_4(\eta^1, \eta^1\text{-}(\text{O})\text{C}(\text{CF}_2)_x\{\text{C}(\text{O})\}_y)$ ($x = 2, y = 1; x = 3, y = 0, 1$)³⁴ and 0.10 Å shorter than reported partial Fe–C_{acyl} double bonds in $\text{Fe}(\text{CO})_4\{\eta^1, \eta^1\text{-}(\text{O})\text{CCHCHC}(\text{O})\}$ (2.016(3) Å).³⁵ Sappa *et al.*³⁶ subsequently reported the structure of the diethyl analog and concluded that the Fe–C_{acyl} bond lengths of 2.003(5) and 2.014(5) Å were within the range of values found for Fe–C(*sp*²) bonds, which are still 0.09 Å longer than the Fe–C(5) bond length in **13c**.

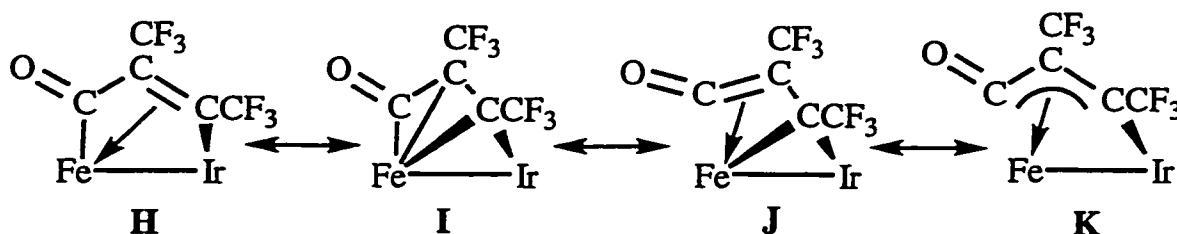
The Ir–C(7) bond length, 2.037(9) Å, is slightly shorter than in **12c**, 2.058(7) Å. The bridging moiety is defined by C(5)–C(6) and C(6)–C(7) interatomic distances of 1.493(13) and 1.396(13) Å, respectively. The latter is significantly longer than the 1.317(10) Å found in **12c**, demonstrating that the carbon-carbon bond order decreases upon coordination to the iron center. The C(5)–C(6) bond is longer than that found in α, β -unsaturated ketones (1.465(18) Å)³⁷ and in other structurally characterized examples of $(\mu\text{-}\eta^1\text{:}\eta^3\text{-}$

$C_2R_2C(O)$) ring systems bearing electron withdrawing groups, namely $Cp_2Ru_2(CO)_2(\mu-\eta^1:\eta^3-C_2Ph_2C(O))$ (1.461(5) Å)^{26,27} and $CpRh(P^iPr_3)Fe(CO)_3(\mu-\eta^1:\eta^3-CHCPhC(O))$ (1.469(8) Å).²⁹ However, the C(5)–C(6) interatomic distance is identical, within error, to that found in $Cp_2Rh_2(CO)_2(\mu-\eta^1:\eta^1-C_2(CF_3)_2C(O))$ (1.499(8) Å)²⁵ and thus suggests a carbon-carbon single bond. Indeed, the separation is similar to the median value reported for (O)C–C(sp^3) bonds in cyclopentanones (1.514(16) Å³⁷) but somewhat shorter than the (O)C–CF₂ distances (1.549(2) - 1.561(3) Å) in $Fe(CO)_4(\eta^1,\eta^1-(O)C(CF_2)_x\{C(O)\}_y)$ (x = 2, y = 1; x = 3, y = 0, 1).³⁴ As the latter distances are some 0.03 - 0.05 Å longer than typical for the organic model, the fact that the C(5)–C(6) bond is some 0.03 Å longer than in the mentioned ($\mu-\eta^1:\eta^3-C_2R_2C(O)$) ring systems may simply reflect the strong electron withdrawing characteristics of the CF₃ substituent on C(6).

The Fe–C(6) and Fe–C(7) distances are equal, within error, at 2.094(10) and 2.096(9) Å, respectively, and are 0.07 Å longer than the Fe–C single bond distance of 2.022(7) Å in **12c**. In $CpRh(P^iPr_3)Fe(CO)_3(\mu-\eta^1:\eta^3-CHCPhC(O))$, the corresponding Fe–C distances are 2.124(5) and 2.063(6) Å, with the carbon bearing the electron withdrawing phenyl ring resting at greater distance from the iron center.²⁹ In $Fe_2(CO)_5(\mu-dppm)(\mu-\eta^1:\eta^3-C_2H_2C(O))$ ^{32,33} and $(Ph_3P)PtFe(CO)_2(\mu-dppm)(\mu-\eta^1:\eta^3-C_2H_2C(O))$,^{30,31} the Fe–CH distances range between 2.084(3) and 2.114(9) Å, agreeing with the values reported presently. One final interesting feature is that the C(8)–C(6)–C(7)–C(9) torsion angle is essentially zero (0.1(18)°), clearly demonstrating that the alkyne ligand distorts in a fashion that keeps the substituents co-planar with the carbon-carbon bond.

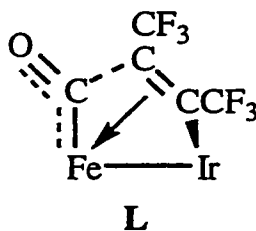
The bonding of $\mu-\eta^1:\eta^3$ -dimetalla-cyclopentenones has been described by Knox²⁶ as consisting of resonance structures **H** - **K** (Scheme 5-3). Namely, the decrease in the C(6)–C(7) bond order with longer than usual Fe–C single bonding distances supports the presence of resonance structure **H** rather than **I**, but the expansion of the C(6)–C(5)–O(5) angle (136.5(10)°) by some 16° relative to ideal sp^2 hybridization suggests that the ketene structure **J** is also a significant contributor. It has generally been accepted that canonical form **K** is the best

overall description of the structure,²⁶ but this leaves one feature, the short Fe–C(5) distance, unexplained.



Scheme 5-3. Resonance Structures Describing the Bonding of the $\mu\text{-}\eta^1\text{:}\eta^3$ -Dimetallacyclopentenone Ring System in **13c**.

Perhaps the most relevant comparison is that the Fe–C(5) bond is some 0.14 Å shorter than the 2.057(7) Å value for the Fe–C_{acyl} bond length in Cp*IrFe(CO)₅($\mu\text{-}\eta^1\text{:}\eta^1\text{-C}_2\text{H}_2\text{C(O)}$) (**18c**, Chapter 6). Thus, the implication is that some measure of iron-carbon multiple bonding is present, and suggests another representation of the structure (**L**).

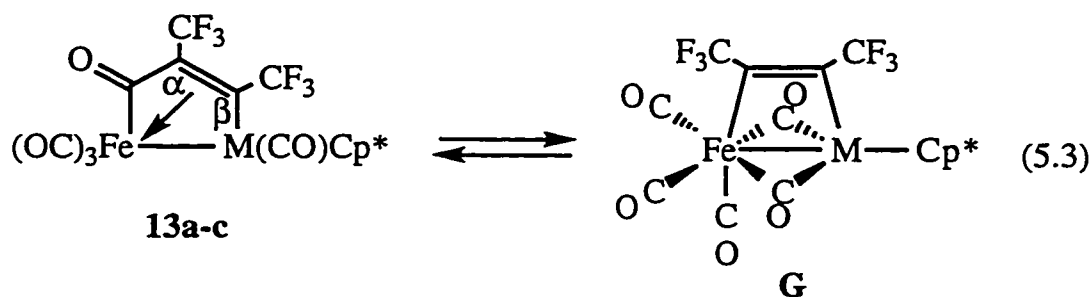


Structure **L** reflects π -back donation from the Fe center into the π^* orbital of the acyl carbonyl, indicating that the acyl group retains some of its terminal carbonyl character after being coupled to the alkyne. This contention is supported by the fact that the Fe–C(5) bond is lengthened by only 0.056 Å when compared with terminal carbonyl Fe–C(3), and the C(5)–O(5) bond is also shorter than the acyl C–O bond lengths in $\mu\text{-}\eta^1\text{:}\eta^1$ -dimetallacyclopentenones (Table 6-11, Section 6.2.6). Furthermore, the Fe–C(5)–O(5) angle is 147.0(9)°, indicating significant *sp* hybridization and reinforcing terminal carbonyl character. The Fe–C(3) bond distance is also longer than the other terminal carbonyls on the Fe center,

reflecting the well-known *trans*-influence³⁸ as C(3)O(3) and C(5)O(5) compete for electron density *via* π -back donation. Finally, **L** provides a rationalization for the lengthened C(5)–C(6) separation.

5.2.6. Further Spectroscopic Characterization of 12a-c and 13a-c

The X-ray diffraction study of compound **13c** clearly established a dimetallacyclopentenone structure in the solid state, and the spectroscopic data presented earlier can also be adapted to this formulation in solution. For instance, ¹⁹F NMR spectrum indicates a pair of inequivalent CF₃ groups and the low temperature limiting ¹³C NMR spectrum in the carbonyl region is consistent with a compound bearing a terminal iridium carbonyl and three terminal iron carbonyls. The acyl group in iron-containing μ - η^1 : η^3 -dimetallacyclopentenones is typically found between δ 210 and 235 ppm^{27,28,33} and thus the furthest downfield carbonyl signal in **13c** (δ 218.91) could be assigned to the acyl moiety. The solution IR spectra, however, still suggest an equilibrium involving a dimetallacyclobutene isomer, primarily because of the observation of the ν_{CC} stretch at 1617 cm⁻¹ (Table 5-3). Thus, incorporating the solid state structure of **13c**, Eq. 5.2 can be revised to



The IR predictions based on these two isomeric forms are as follows; compound **13c** is expected to give rise to four terminal CO stretches while the CO-bridged isomer **G** is predicted to provide three terminal CO stretches and two lower frequency bands for the bridging carbonyls. The resulting total of seven terminal CO bands and two bridging CO bands is exactly what is observed (Table 5-3). Furthermore, since the acyl band in μ - η^1 : η^3 -dimetallacyclopentenones is commonly found higher than 1700 cm⁻¹,^{27,28,33} it is possible to explain the

appearance of three low frequency CO bands in the solution IR spectrum of compound **13b**. The IR of the Co analog also contains an additional low energy stretch attributed to the acyl group of a dimetallacyclopentenone, but contains far fewer terminal stretching bands, suggesting a large amount of coincidental overlap of terminal CO stretching bands in the IR spectrum.

In the hopes of obtaining a clean IR spectrum of the dimetallacyclopentenone isomers, spectra were obtained on the stable **13b,c** in the solid state. Unexpectedly, the bridging CO bands remained in KBr pellet IR spectra, which bear a superficial resemblance to the CH₂Cl₂ solution spectra. While these results seem anomalous in the light of the crystal structure determination on **13c**, Dickson *et al.* observed a similar phenomenon in the characterization of Cp₂Rh₂(CO)₂(μ-η¹:η¹-C₂(CF₃)₂C(O)).²⁵ In this case also, the solid state X-ray structure exhibited terminal carbonyls only, while the IR data suggested significant concentrations of a doubly CO-bridged isomer, both in solution and in the solid state. It was suggested that simple grinding of the solid in the preparation of the IR sample was sufficient to overcome the apparently very low barrier to interconversion between the two isomers.²⁵

Thus, we have the interesting situation that while the equilibrium proposed in Eq. 5.3 appears to predominate at ambient temperature, the ¹³C NMR spectra of ¹³CO enriched **13a-c** clearly suggest that only the dimetallacyclopentenone structure is present at low temperature. To further define the spectroscopic features of the dimetallacyclopentenone structure, the ¹³C{¹⁹F} NMR spectra were collected at low temperature, the rationale being that the olefinic carbons in μ-η¹:η³-dimetallacyclopentenones generally display two widely separated resonances in the ¹³C NMR spectrum.^{27,28,33} The carbon adjacent to the acyl group (C_α) is generally found upfield as it resembles a coordinated olefin, while the other (C_β) tends to resonate downfield owing to its similarity to a bridging alkylidene (resonance structure I, Scheme 5-3). Thus, ¹³C{¹⁹F} NMR spectra were collected at low temperature to better determine if the solid state structure was retained in solution.

In addition to the carbonyl resonances, compound **13b** displayed a singlet at δ 56.47 and a doublet at δ 153.60. The ¹J_{RhC} coupling constant of 38 Hz in

the latter is typical of carbons bridging dinuclear centers containing rhodium, *cf.* $\text{Cp}_2\text{Rh}_2(\text{CO})_2(\mu\text{-CH}_2)$ where $^1J_{\text{RhC}} = 29$ Hz.³⁹ Similar spectroscopic characteristics were found for the bridging moiety in $\text{CpRh}(\text{P}^i\text{Pr}_3)\text{Fe}(\text{CO})_3(\mu\text{-}\eta^1:\eta^3\text{-CHCPhC(O)})$,²⁹ ($\delta(\text{C}_\beta) = 156.33$, $^1J_{\text{RhC}} = 34$ Hz), and in $\text{CpRh}(\text{PR}_3)\text{Os}(\text{CO})_3(\mu\text{-}\eta^1:\eta^3\text{-C}_2\text{H}_2\text{C(O)})$ ($\text{R}_3 = \text{Me}_2\text{Ph}$, MePh_2) where $\delta(\text{C}_\beta) = 156.0$ ($^1J_{\text{RhC}} = 35$ Hz) in both complexes.⁴⁰ Compound **13a** displayed singlets at δ 57.90 and 155.92 as did **13c** at δ 59.09 and 130.53. As expected, the chemical shift of the bridging carbon (C_β) depends on the metal to which it is attached, and follows the usual trend $\text{Co} > \text{Rh} > \text{Ir}$.¹⁵ Finally, the carbons of the HFB moiety were not detected at ambient temperature, implying that the dimetallacyclopentenone ring undergoes significant rearrangement upon warming as suggested in Eq. 5.3.

The carbons of the CF_3 groups were also detected as singlets in the $^{13}\text{C}\{^{19}\text{F}\}$ NMR spectra, and selective ^{19}F decoupling in **13b** provided assignment of the individual trifluoromethyl resonances. Irradiation of the signal in the ^{19}F NMR spectrum belonging to the CF_3 group on the bridging carbon (Table 5-1) caused the δ 126.75 signal to sharpen to a singlet while the δ 121.58 signal became a quartet ($^1J_{\text{CF}} = 273$ Hz). Similarly, decoupling the upfield quartet in the ^{19}F NMR resulted in the δ 121.58 signal appearing as a singlet while that at δ 126.75 became a quartet ($^1J_{\text{CF}} = 273$ Hz). Accordingly, the δ 126.75 signal is assigned to the trifluoromethyl group on the bridging carbon (C_β) and the signal at δ 121.58 is due to the CF_3 moiety adjacent to the acyl group. The CF_3 signals in **13a** and **13c** were assigned by comparison to those in **13b**.

$^{13}\text{C}\{^{19}\text{F}\}$ NMR spectra were also recorded on the dimetallacyclobutenes **12b,c** at ambient temperature. The CF_3 resonances in each were readily observed, but the olefinic CCF_3 signals could not be detected. Consequently, the spectra were collected on the more sensitive 500 MHz spectrometer. After overnight acquisition, **12c** displayed sharp, intense signals for the trifluoromethyl carbons at δ 125.04 and 120.80 while the internal alkyne carbons appeared as a sharp singlet at δ 105.21 and a broad resonance at δ 129.7 ppm. The similarity in chemical shift of the alkyne carbons is in agreement with a dimetallacyclobutene

formulation.^{8,41} For **12b**, the two CF₃ groups appeared as singlets at δ 122.59 and 120.86, and the Rh-bonded CCF₃ carbon was observed as a broadened doublet at δ 122.18 ($^1J_{\text{RhC}} = 26$ Hz). The remaining CCF₃ signal was not detected. Thus, the spectrum was collected at lower temperature.

Cooling **12b** to -20°C resulted in the acquisition of an adequate spectrum within a few hours. Two sharp doublets had emerged from the baseline at δ 126.59 ($^2J_{\text{RhC}} = 10$ Hz) and 121.76 ($^1J_{\text{RhC}} = 28$ Hz) for the olefinic carbons. The downfield CCF₃ signal is thus due to the Fe-bonded carbon, although coupling to rhodium was still observed through the carbon-carbon double bond. In Cp*RhOs(CO)₅(μ - η^1 : η^1 -CHCCF₃), a similar pattern was displayed where $^1J_{\text{RhC}} = 25$ Hz and $^2J_{\text{RhC}} = 6$ Hz at the CH and CCF₃ carbons respectively,⁸ and in the more closely related Cp*RhRu(CO)₅(μ - η^1 : η^1 -HFB), resonances were found at δ 129.03 ($^1J_{\text{RhC}} = 29$ Hz) and 123.03 ($^2J_{\text{RhC}} = 6$ Hz) for the Rh-bonded and Ru-bonded alkyne carbons respectively.² The similarity of the chemical shift of the downfield resonance in **12c** (δ 129.7) to the Fe-bonded carbon in **12b** (δ 126.59) suggests an analogous assignment, leaving the upfield singlet, δ 105.21, as belonging to the Ir-bonded carbon. Furthermore, the fact that the iridium-bonded carbon is shifted some 16.5 ppm further upfield than the Rh-bonded carbon agrees with the comparable situation in Cp*IrOs(CO)₅(μ - η^1 : η^1 -CHC(CF₃)) wherein the CH carbon resonated at δ 110.9, some 19.9 ppm upfield of its Rh analog.⁸

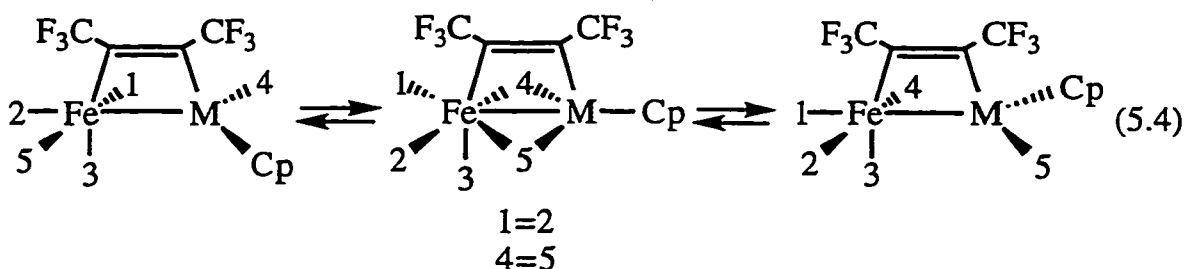
Thus, it would appear that **12b,c** retain their dimetallacyclobutene structure in solution. However, the temperature dependence of the ¹³C NMR spectra of **12b** and the broadness of the downfield CCF₃ resonance in **12c** suggests that some form of fluxionality involving the alkyne moiety may also be occurring at ambient temperature. Isomerization, such as in Eq. 5.3, appears unlikely as the IR spectra contained bands consistent only with the metallacyclobutene formulation of the complex. As it is likely that any fluxional process would involve movement of the carbonyl ligands in any structural change, a complete study of the variable temperature ¹³C NMR behavior of the carbonyl ligands was undertaken. Corresponding experiments were performed on the dimetallacyclo-

pentenones **13a-c** to shed light on the nature of the isomerization process detected by IR spectroscopy.

5.3. Variable Temperature ^{13}C NMR Studies on **12b,c** and **13a-c**

5.3.1. Fluxional Behavior of the Heterodimetallacyclobutenes, **12b,c**

The ^{13}C NMR spectra of **12b,c** vary reversibly with temperature in agreement with intramolecular carbonyl exchange (Figure 5-5). As the samples were progressively warmed from their limiting spectra (Table 5-4), three CO_{Fe} signals and the CO_{M} resonance broadened and coalesced in pairs indicating that pair-wise exchange^{42,43} was occurring in a truncated merry-go-round fashion (Eq. 5.4).^{44,45} It is important to note that these changes occurred at temperatures below those at which the alkyne carbon signals of **12b** and **12c** broadened. Accordingly, this fluxional process does not involve the alkyne ligand.



Thus, CO 4 exchanges with CO 5 and 1 exchanges with 2, but no exchange occurs between these pairs. The carbonyl resonance to lowest field, which initially remains distinct, is assigned to the invariant CO(3). The similarity of the chemical shifts of the two mutually *trans* carbonyls on the iron center (1 and 5) in both complexes prevent individual assignments. However, spectral simulation (*vide infra*) confirms that 2 is the furthest upfield iron carbonyl (δ 204.49). As expected, the 1/2 signals reemerge at the average of their static positions, δ 205.9 ppm at 0°C in **12b** and δ 205.5 ppm at +10°C in **12c**. For the more disparate 4/5 signals, the averaged resonance is found at δ 198 ppm at 0°C in **12b** and δ 188 ppm at +80°C in **12c**. The observed chemical shifts agree with the averages calculated from the resonances in the limiting spectra.

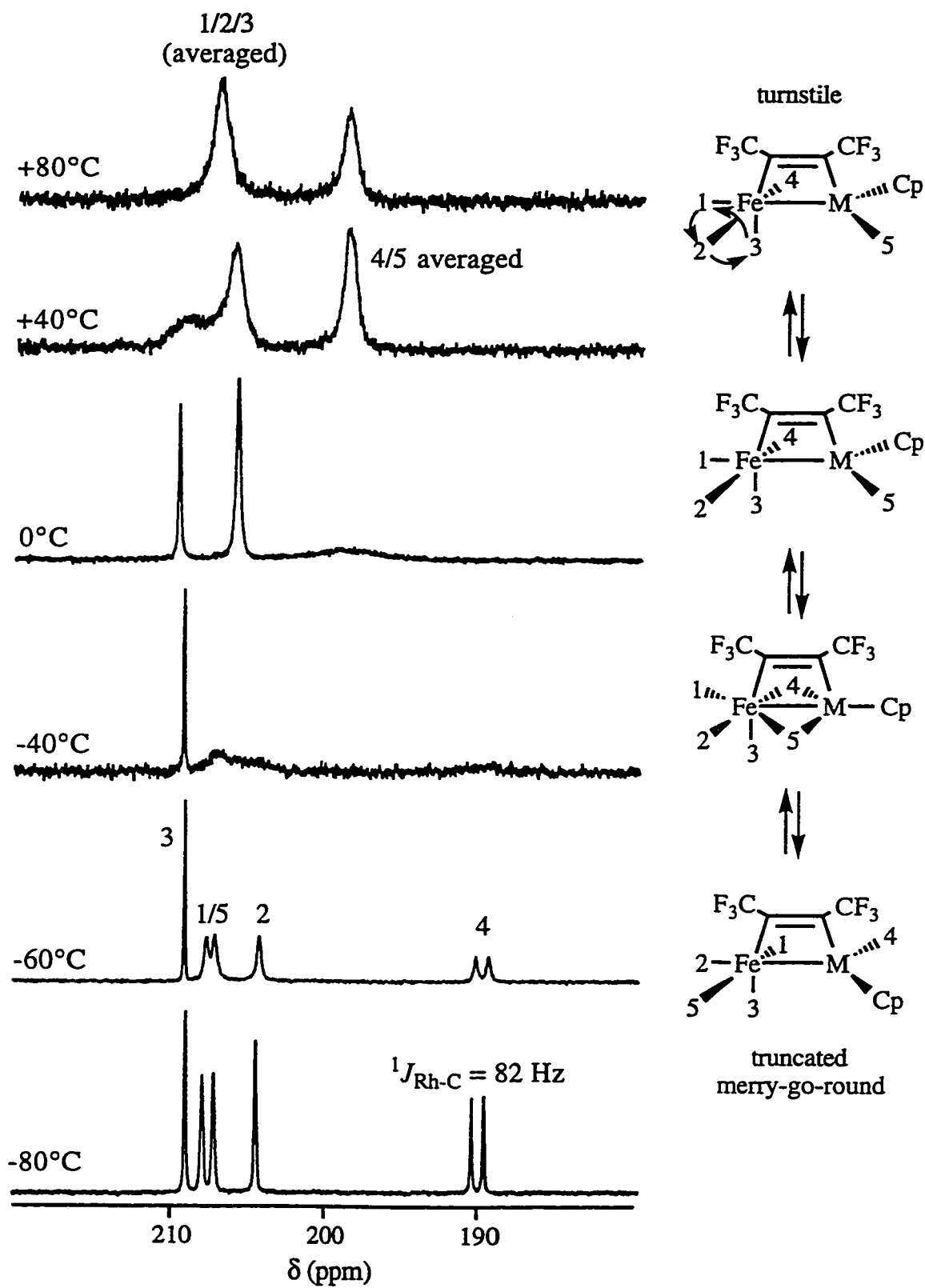
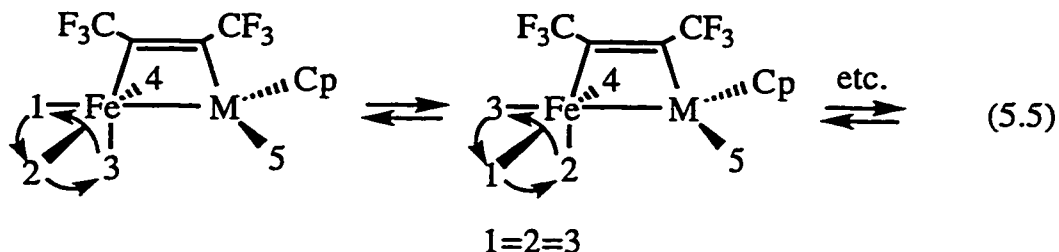


Figure 5-5. Variable Temperature ^{13}C NMR (toluene- d_8 , 100.6 MHz) of **12b**.

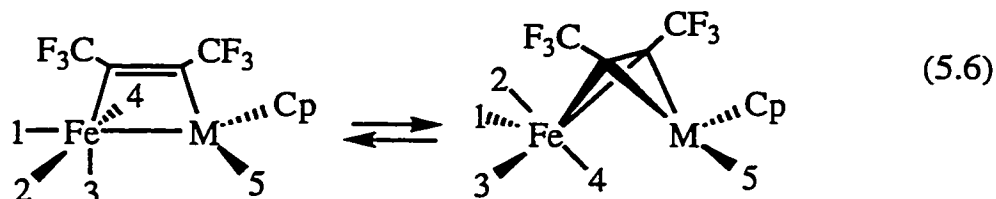
Above 0°C, the previously invariant resonance 3 begins to broaden in tandem with the averaged 1/2 signal, marking the onset of the familiar turnstile, or trigonal twist, mechanism within an Fe(CO)₃ group (Eq. 5.5).⁷



In both compounds, a fascinating result is that the turnstile exchange serves only to exchange the carbonyls labelled 1-3 and does not involve COs 4 or 5 at temperatures up to +80°C. At this temperature, two broadened resonances were observed at δ 207.2 and 198.8, corresponding to the averaged 1-3 and 4/5 resonances respectively. Again, the calculated average chemical shifts from the limiting spectra agree well with the observed positions. Thus, the action of the turnstile does not bring about global CO exchange, which suggests that it acts selectively on one specific face of the distorted Fe octahedron. Although quite common for iron carbonyls, the corresponding turnstile rotation was not observed in Cp*MRu(CO)₅(μ - η^1 : η^1 -HFB)^{1,2} or Cp*MOs(CO)₅(μ - η^1 : η^1 -TFP)⁸ which incorporate the heavier metals of the group 8 triad.

Above +80°C, the averaged resonances in both samples, rather than continuing to sharpen as would be expected, were seen to broaden again. This suggests that a turnstile may begin to operate on the other face of the Fe center as this would bring CO 4 (and by extension 5) into exchange with 1-3, thus causing global CO migration. Another possible explanation of the global carbonyl exchange is rotation of the coordinated alkyne accompanied by cleavage of the Fe-M bond (Eq. 5-6). The iron moiety in the resulting 2,4-dimetallabicyclo[1.1.0]butane resembles an Fe(CO)₄(η^2 -olefin) compound, and would thus be expected to undergo rapid carbonyl exchange by olefin-coupled Berry pseudo-rotation,^{46,47} leading to the averaging of carbonyls 1 - 4. The conversion of the dimetallacyclobutene to the bicyclic isomer would also account

for the fact that the alkyne carbons are broad at ambient temperature (*vide supra*). Casey has observed a similar transformation of $\text{Cp}^*_2\text{Re}_2(\text{CO})_4(\mu\text{-}\eta^1\text{:}\eta^1\text{-C}_2(\text{CO}_2\text{Me})_2)$ to $\text{Cp}^*_2\text{Re}_2(\text{CO})_4(\mu\text{-}\eta^2\text{:}\eta^2\text{-C}_2(\text{CO}_2\text{Me})_2)$ and has determined the solid-state structure of the latter compound.^{48,49} Compound **12c** was stable at elevated temperatures as a spectrum collected following cooling of the sample was identical to that obtained initially. However, after treatment at $+100^\circ\text{C}$, **12b** had darkened in color and new signals were observed upon cooling to -80°C , indicating that some thermal decomposition had occurred also.



The experimental spectra were successfully simulated using the model in Eqs. 5.4 and 5.5, and a summary of the activation parameters determined from a non-linear least-squares fit of the exchange rates to the exponential form of the Eyring equation is presented in Table 5-9. The turnstile exchange processes in **12b** and **12c** have similar activation enthalpies and entropies, which is not surprising as they occur at structurally similar Fe centers.

Table 5-9. Activation Parameters for Carbonyl Scrambling in **12b,c**.^{a,b}

	Pair-wise Exchange		Turnstile Exchange	
	ΔH^\ddagger (kJ·mol ⁻¹)	ΔS^\ddagger (J·mol ⁻¹ ·K ⁻¹)	ΔH^\ddagger (kJ·mol ⁻¹)	ΔS^\ddagger (J·mol ⁻¹ ·K ⁻¹)
12b	37 ± 2	-31 ± 6	51 ± 4	-35 ± 12
12c	41 ± 4	-36 ± 17	48 ± 6	-38 ± 22

^aA summary of the rate constants determined from spectral simulation at given temperatures is provided in Table 5-16. ^bErrors are non-linear errors (*ca.* 3-4 standard deviations) determined from non-linear least-squares analysis.

Pair-wise exchange is slightly more facile in **12b** than in **12c**, demonstrating the generally accepted trend for cluster compounds whereby it becomes

increasingly difficult to bridge metals with carbonyls as one descends the triad.¹²⁻¹⁴ Table 5-10 provides a comparison of activation parameters determined for pair-wise carbonyl exchange in **12b,c** and related compounds.

Table 5-10. Activation Parameters for Pair-wise Carbonyl Scrambling in Alkyne-Bridged Heterobimetallic Compounds.

Compound	ΔH^\ddagger (kJ·mol ⁻¹)	ΔS^\ddagger (J·mol ⁻¹ ·K ⁻¹)	ΔG^\ddagger (kJ·mol ⁻¹) ^a
12b	37	-31	44 (205) ^b
12c	41	-36	49 (205) ^b
Cp*RhRu(CO) ₅ (μ-η ¹ :η ¹ -HFB) ²	–	–	34 (193) ^c
Cp*IrRu(CO) ₅ (μ-η ¹ :η ¹ -HFB) ²	–	–	38 (218) ^c
Cp*RhOs(CO) ₅ (μ-η ¹ :η ¹ -TFP) ⁸	23	-41	32 (205) ^b
Cp*IrOs(CO) ₅ (μ-η ¹ :η ¹ -TFP) ⁸	39	-32	45 (205) ^b
CpRhOs(CO) ₅ (μ-η ¹ :η ¹ -TFP) ⁸	45	-33	51 (205) ^b

^aThe number in brackets indicates the temperature. ^bCalculated from $\Delta G^\ddagger = \Delta H^\ddagger - T\Delta S^\ddagger$; T = 205 K was chosen for comparison with the Cp*MRu(CO)₅(μ-η¹:η¹-HFB) compounds. ^cCalculated from the two-site approximation.⁵⁰

The ΔG^\ddagger values are larger in **12b,c** than their Cp*MRu(CO)₅(μ-η¹:η¹-HFB) analogs, but this likely reflects activation of pair-wise exchange in the latter by the electron-releasing Cp* ligand.^{44,51} In this regard, it is noteworthy that pair-wise exchange is much more facile in Cp*RhOs(CO)₅(μ-η¹:η¹-TFP) than in CpRhOs(CO)₅(μ-η¹:η¹-TFP).

5.3.2. Fluxional Behavior of the Heterodimetallacyclopentenones, **13a-c**

As with **12b,c**, the ¹³C NMR spectra of **13b,c** vary reversibly with temperature, suggesting intramolecular carbonyl scrambling. However, the spectra of **13a** are more complicated as warming leads to facile CO loss and formation of **11a***. The general behavior of the dimetallacyclopentenones (Figure 5-6) is similar to the isomeric dimetallacyclobutenes, with the main exception that turnstile exchange involving the Fe(CO)₃ group occurs at much lower

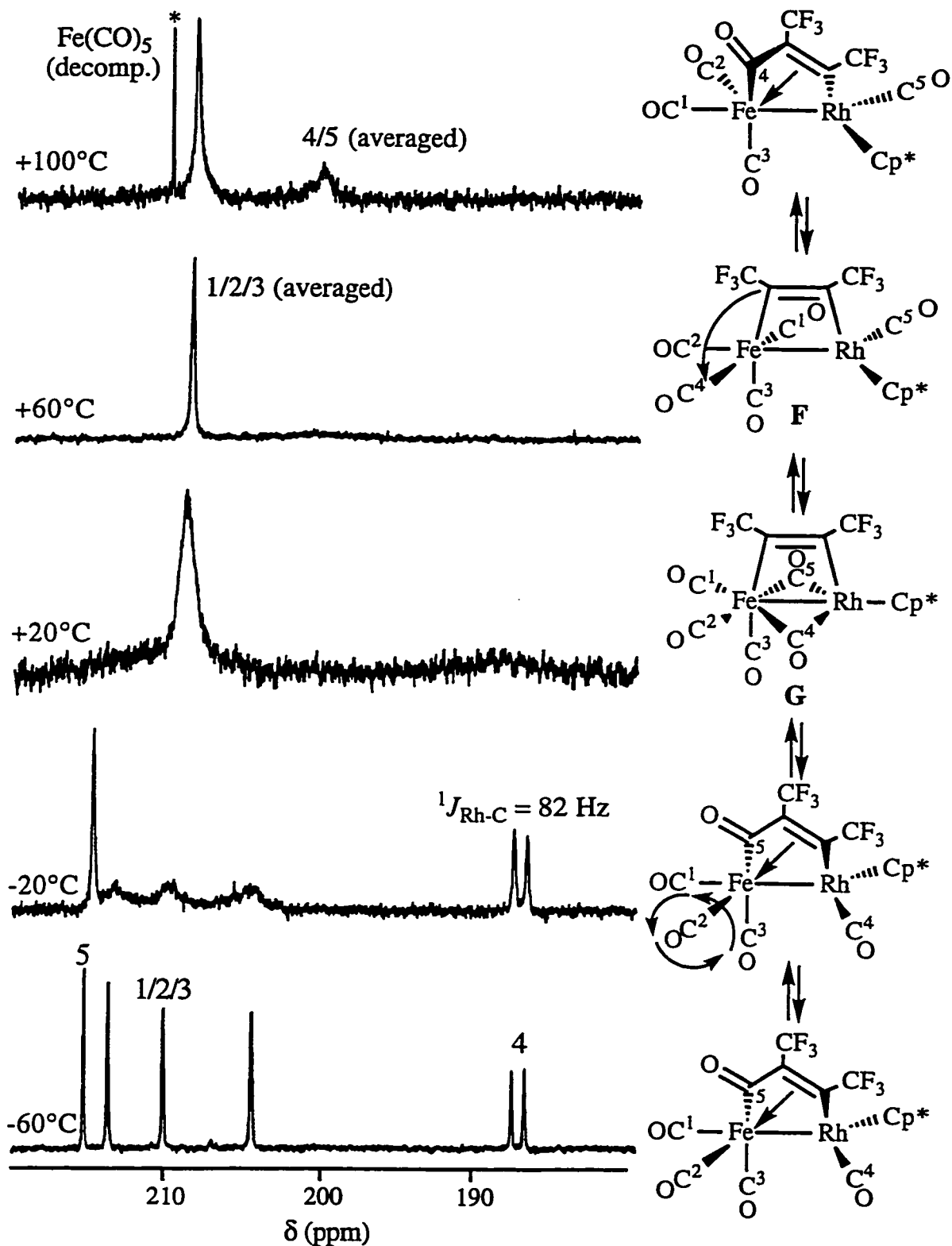


Figure 5-6. Variable Temperature ^{13}C NMR (toluene- d_8 , 100.6 MHz) of 13b.

temperature in **13a-c**. As the samples were progressively warmed, the carbonyls of the $\text{Fe}(\text{CO})_3$ group coalesced, and the $\text{M}-\text{CO}$ (**4**) and acyl (**5**) signals began to broaden. At higher temperatures ($+80^\circ\text{C}$, **13b**; $+100^\circ\text{C}$, **13c**) a broad resonance was detected at the calculated average position (δ 201, **13b**; δ 191, **13c**) suggesting that, as with **12b,c**, the acyl and $\text{M}-\text{CO}$ carbonyls exchange without involving the remaining three carbonyls on the Fe center.

This behavior is consistent with the coupled turnstile/truncated merry-go-round mechanism proposed for **12b,c** with two caveats. The first is that turnstile exchange commenced *prior* to pair-wise exchange in **13a-c**. However, this is not surprising as a facial arrangement of carbonyl ligands exists in an unencumbered region of space in the dimetallacyclopentenone structure (Figure 5-4). More importantly, pair-wise exchange in **13a-c** is initiated by the ejection of the acyl carbonyl from the bridging moiety to form an alkyne-bridged bimetallic **F** which is analogous to **12b,c**. Indeed, what is more surprising is the facility of the process, although the ease of $\text{C}_{\text{acyl}}-\text{C}_{\text{alk}}$ bond cleavage can be rationalized by considering the long $\text{C}(5)-\text{C}(6)$ bond distance in the molecular structure of **13c** (Section 5.2.5). Once formed, the dimetallacyclobutene is free to undergo truncated merry-go-round exchange *via* intermediate **G**. The mechanism of Figure 5-6 can thus be viewed as building upon that in Figure 5-5 with the extra step of reversible migratory CO insertion to form the dimetallacyclopentenones **13a-c** from dimetallacyclobutenes **F**.

As was the case with **12b,c**, carbonyls **1-3** do not enter into exchange with **4** or **5**, allowing for the separate exchange behaviour observed in the ^{13}C NMR spectra. The reason for this is that if the μ -HFB ligand in **F** was to migrate onto CO **2**, this would place a bulky CF_3 group in the proximity of the Cp^* ring, leading to a sterically unfavorable interaction. Thus, pair-wise intermetallic CO exchange is observed which moves the Cp^* ring to the opposite side of the molecule and allows migratory insertion onto the formerly $\text{Rh}-\text{CO}$ (**5**) in **F'**.

Furthermore, it appears that **G** is not simply a fleeting intermediate in this fluxional process, but rather forms in sufficient concentration to be observed in equilibrium with **13a-c** in the FT-IR spectra (*vide supra*). A similar phenomenon was encountered in the characterization of $(\mu\text{-C}_7\text{H}_7)\text{FeM}(\text{CO})_4(\text{PPh}_3)$ ($\text{M} = \text{Rh}$,

Ir) compounds where the IR spectra suggested the presence of all-terminal and CO-bridged isomers, but the low temperature limiting ^{13}C NMR spectra displayed a pattern which showed a single resonance of intensity three for the $\text{Fe}(\text{CO})_3$ group and a separate signal for the terminal M-CO.^{52,53} The authors concluded that the isomer exchange must have been very rapid, even at the low temperature limit, as a resonance for the bridging carbonyl was not observed. A feature supporting this contention was that the averaged $\text{Fe}(\text{CO})_3$ group appeared as a doublet ($J_{\text{RhC}} = 7.1$ Hz) in the low temperature limiting spectrum of the FeRh compound.⁵² The lack of Rh coupling at the iron carbonyls in **13b**, in conjunction with the appearance of distinct CCF_3 resonances, consistent only with a dimetallacyclopentenone formulation at low temperature, indicates that the isomerization occurs only at higher temperatures in **13a-c**.

In the case of **13b**, a further increase in temperature results in broadening of the averaged signal for the $\text{Fe}(\text{CO})_3$ group. When spectra were recorded at 50.3 MHz, a globally averaged resonance was detected at $+110^\circ\text{C}$ as a 14 Hz doublet in rough agreement with expectations based on the low temperature limiting spectrum. However, thermal decomposition was also rampant at this high temperature. Global averaging can be accounted for by considering a trigonal twist on the Fe face adjacent to the Cp^* ligand, *i.e.* the 1, 3, 5 face in **F** in Figure 5-6, or a process similar to that described in Eq. 5.6. The broadening of the $\text{Fe}(\text{CO})_3$ resonance at high temperature in **13c** can be explained similarly, but with the limitation that the rate of exchange is insufficient to result in a fully averaged spectrum.

The fluxional processes were simulated and lineshape analysis provided activation parameters (Table 5-11). The turnstile exchange processes again have similar activation parameters for the three different heteronuclear frameworks. Interestingly, ΔH^\ddagger for pair-wise CO exchange is found to follow the *opposite* trend to **12b,c**, namely $\text{FeRh} > \text{FeIr}$. Furthermore, the activation enthalpy was largest for **13a** despite the fact that it is generally easier to bridge two first row metals with CO.¹²⁻¹⁴ A similar trend was observed for $(\mu\text{-C}_7\text{H}_7)\text{M}'\text{M}(\text{CO})_4(\text{PPh}_3)$ ($\text{M}' = \text{Fe}, \text{Ru}$; $\text{M} = \text{Rh}, \text{Ir}$) compounds where the activation energy for intermetallic CO exchange followed $\text{FeIr} < \text{FeRh}$ and $\text{RuIr} < \text{RuRh}$.⁵⁴ The

authors noted that relatively few systematic studies of intermetallic exchange exist for dinuclear species and that often the relative ordering is dependent on the ancillary ligands.⁵³ In this regard, it is also curious that pair-wise exchange appears to be less facile in **13a-c** than **12b,c** as the former compounds incorporate Cp*, and electron releasing ligands are known to activate carbonyl migrations.^{44,55}

Table 5-11. Activation Parameters for Carbonyl Scrambling in **13a-c**.^{a,b}

	Pair-wise Exchange		Turnstile Exchange	
	ΔH^\ddagger (kJ·mol ⁻¹)	ΔS^\ddagger (J·mol ⁻¹ ·K ⁻¹)	ΔH^\ddagger (kJ·mol ⁻¹)	ΔS^\ddagger (J·mol ⁻¹ ·K ⁻¹)
13a	103 ^c	133 ^c	56 ± 3	-2 ± 10
13b	71 ± 9	61 ± 34	55 ± 5	14 ± 20
13c	51 ± 7	10 ± 29	58 ± 6	25 ± 23

^aA summary of the rate constants determined from spectral simulation at given temperatures is provided in Table 5-16. ^bErrors are the non-linear errors determined from non-linear least-squares analysis. ^cEstimated from two points.

In the present case, however, it must be remembered that the rate of intermetallic CO exchange is a property of the intermediate species **F/G** but the rate of broadening of the acyl resonance is a property of the dimetallacyclopentenones **13a-c**. Thus, the observed rate of exchange will be influenced by the rate of acyl ejection and accompanying Fe–C β bond rupture in **13a-c** to form **F**. In other words, if the rate of acyl ejection is the rate determining step, no conclusion can be drawn as to the *actual* rate of pair-wise CO exchange in **F/G**. Furthermore, it is interesting that while acyl ejection occurs at the Fe center, the activation energy is influenced profoundly by the nature of the ancillary group 9 metal. It has been argued that in mononuclear systems the rate of migratory insertion (and hence its microscopic reverse, acyl ejection) is affected by the level of back-donated electron density available to the carbonyl ligand.⁵⁶ Thus, carbonyls attached to electron poor metal centers are more electrophilic and consequently more susceptible to nucleophilic attack by the migrating alkyl ligand. Conversely, carbonyls attached to electron rich metal centers are

deactivated towards migratory insertion. Accordingly, one can infer that since **13c** is most activated towards acyl ejection, it is the system which favors the alkyne-bridged bimetallic **F/G** the most, and consequently is the system which imparts the greatest electron density to the Fe center. This agrees with the increased basicity of third row metals, and implies that Ir transfers proportionally more of its electron density to Fe than do either Rh or Co.

However, it should also be remembered that the product distribution is largely determined by the nature of the ligands on the ancillary metal, namely whether the substituents on the η^5 -cyclopentadienyl ligand are protons or methyl groups. In terms of electronic differences, the Cp ligand is less electron releasing than Cp* and would thus be expected to produce more electron poor group 9 metal centers. Consequently, electron poor iron centers would result because of electronic communication *via* the metal-metal bond. Thus, based on electronic arguments alone, we would expect the Cp systems to favor dimetallacyclopentenones, but the stable ground-state structure is that of a dimetallacyclobutene. Since electronic arguments do not explain the observed ground state structures, steric effects must therefore be considered. The presence of two symmetrically bridging CO ligands in **G** causes the Cp* ligand to reside directly under the somewhat bulky CF₃ group of the μ -HFB ligand in this structure. The resulting steric interference could be sufficient to assist migratory insertion, causing the CF₃ and Cp* groups to shift away from the metal-metal bond in opposite directions, thus relieving the steric interaction. However, the presence of both CO-inserted and alkyne-bridged isomers at ambient temperature in **13a-c** clearly demonstrates that the stereo-electronic boundary is easily crossed, and that minor changes at the group 9 metal center can be sufficient to dramatically alter the product distribution. Compounds **12b,c** and **13a-c** are thus much more structurally versatile than their Ru congeners which adopt the dimetallacyclobutene formulation without any evidence for rearrangements involving the alkyne ligand.^{1,2} In hindsight, the facility of migratory CO insertion at the Fe center is perhaps not surprisingly in light of the results presented in Chapter 3 and the fact that the vast majority of iron- and alkyne-containing bimetallic compounds have dimetallacyclopentenone structures.²⁶⁻³³

5.4. Low Temperature NMR Studies of the Reaction of **1a** with $\text{Cp}'\text{Rh}(\text{CO})_2$

5.4.1. Reaction of **1a** with $\text{CpRh}(\text{CO})_2$: Detection of an Intermediate Dimetallacyclopentenone in the Formation of a Dimetallacyclobutene

In order to gain some insight into the mode of formation of **12b,c**, the reaction between ^{13}C enriched **1a** and $\text{CpRh}(\text{CO})_2$ was monitored at low temperature by ^{13}C and ^{19}F NMR spectroscopy (Figures 5-7 and 5-8). Initially, only the resonances of the reactants were observed, but after the sample was warmed to -40°C , changes were detected in the ^{13}C NMR spectrum. The previously weak doublet at δ 191.76 ($^1J_{\text{RhC}} = 84$ Hz) for $\text{CpRh}(\text{CO})_2$ rapidly grew in intensity relative to the two multiplet resonances for **1a** (Figure 5-7(b)). The ^{19}F NMR spectrum remained unchanged with the only detectable signal being the singlet for the iron-alkyne species. Clearly, ^{13}C exchange was occurring in an intermolecular fashion between the reactants but without detectable product formation. Similar behavior was noted in the low temperature ^{13}C NMR monitoring of the reaction $\text{Os}(\text{CO})_4(\eta^2\text{-alkyne})$ with $\text{CpM}(\text{CO})_2$ species.⁸ After maintaining the temperature at -40°C for 45 minutes, the level of ^{13}C scrambling between the two reactants approached equilibrium and raising the temperature to -30°C did not produce any significant changes in the spectra.

Upon reaching -20°C , resonances due to bimetallic products were observed in both the ^{19}F and ^{13}C NMR spectra. Although free ^{13}C was detected at this stage, this cannot be taken as evidence of initial CO dissociation from **1a** as formation of **12b** occurs with liberation of carbon monoxide. Interestingly, although the characteristic resonances for **12b** were detected, a second species **14** was present in roughly 1.5 times greater concentration. The new compound was characterized by a pair of quartets in the ^{19}F NMR at δ -54.13 and -58.81 ($^5J_{\text{FF}} = 13.5$ Hz), indicating an unsymmetrical HFB moiety, with the lack of detectable coupling to Rh suggesting that the alkyne is not directly bonded to the rhodium center. In the carbonyl region of the ^{13}C NMR spectrum, **14** exhibited a 1:1:2:2 pattern of resonances (Figure 5-7(c)). The furthest downfield resonance, at δ 216.07, was a doublet ($^1J_{\text{RhC}} = 28$ Hz), as was the furthest upfield resonance at δ 202.22 ($^1J_{\text{RhC}} = 40$ Hz). The former had an integration of one and is comparable to the acyl resonance in $\text{Cp}_2\text{Rh}_2(\text{CO})_2(\mu\text{-$

$\eta^1:\eta^1\text{-C}_2(\text{CF}_3)_2\text{C}(\text{O})$) (δ 219.3, $^1J_{\text{RhC}} = 28$ Hz),²⁵ while the latter, of integration two, is characteristic of heterometallic compounds containing rhodium undergoing fast "merry-go-round" carbonyl migration.^{44,45} The remaining singlet resonances, in a 1:2 ratio, are consistent with a facial arrangement of terminal carbonyl ligands on the iron center. The most reasonable structure for **14** is thus $\text{CpRhFe}(\text{CO})_5(\mu\text{-}\eta^1:\eta^1\text{-C}(\text{O})\text{C}_2(\text{CF}_3)_2)$ (Scheme 5-4), a compound formed *without net ligand loss* from the reactants. It is also interesting that, in order to fit the NMR data, **14** must have the acyl group bonded to the Rh center while in **13a-c** the acyl moiety resides at the Fe center.

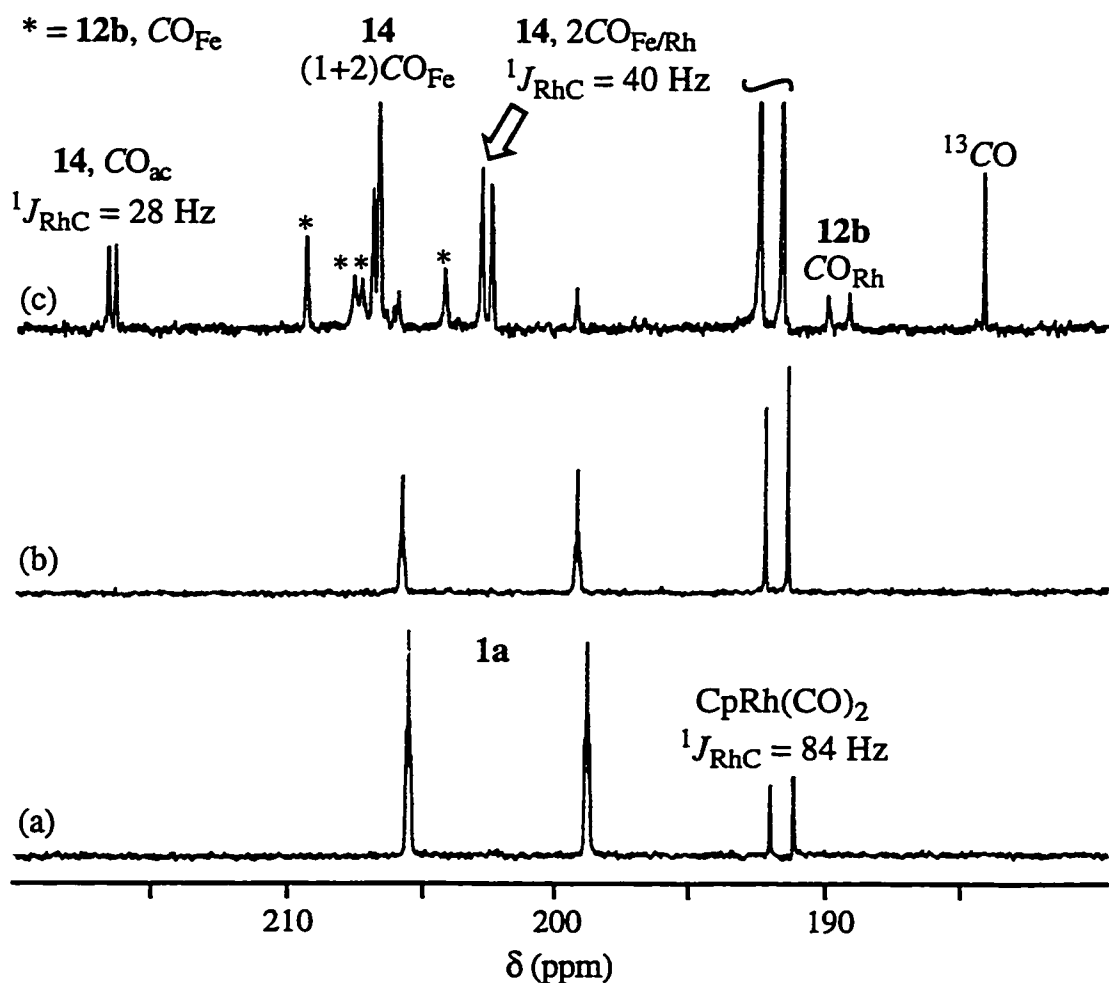


Figure 5-7. ^{13}C NMR Monitored Reaction of **1a** with $\text{CpRh}(\text{CO})_2$ in CD_2Cl_2 . (a) Initial, -80°C . (b) After Warming to -40°C . (c) at -80°C After Warming to 0°C .

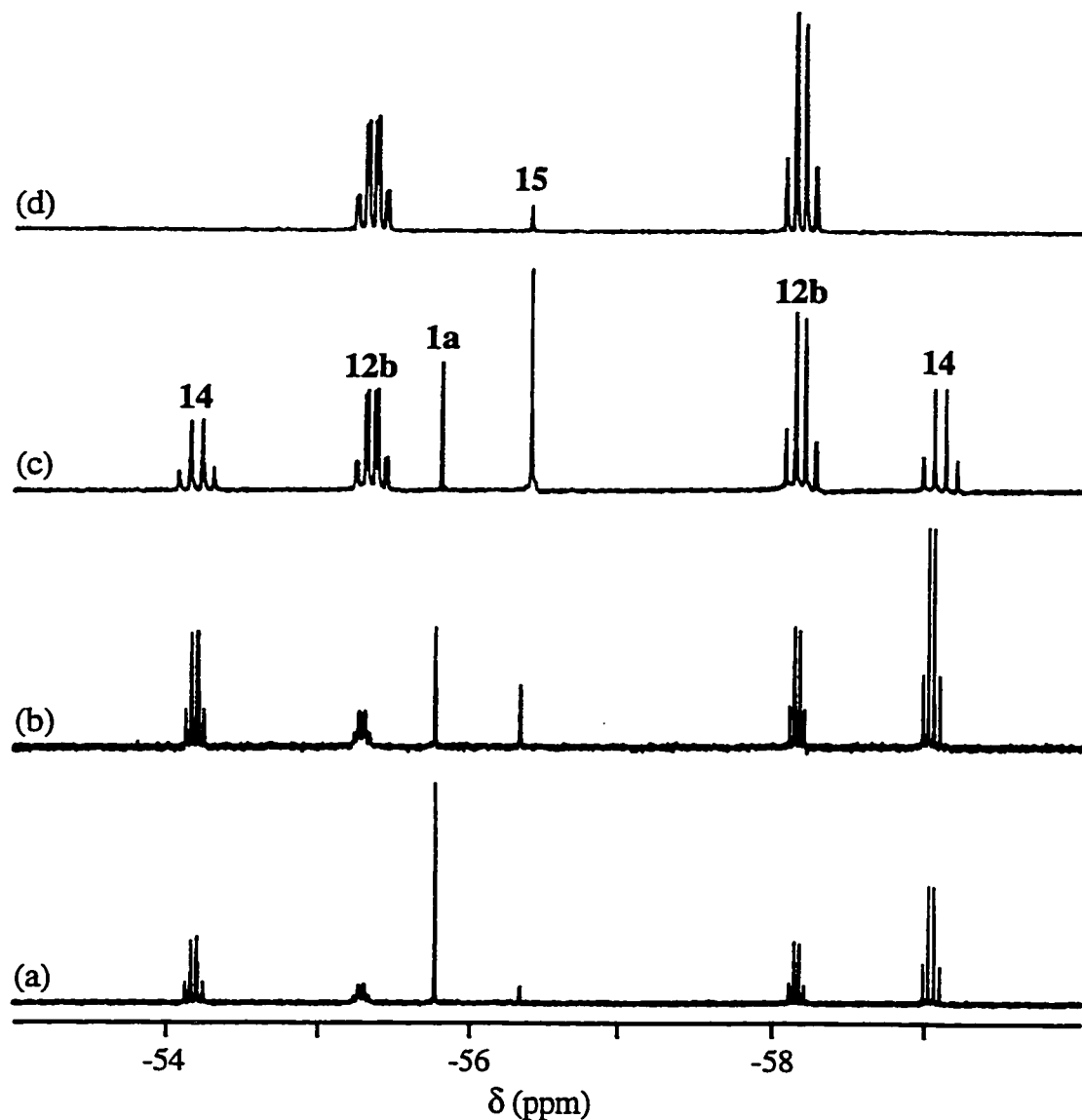


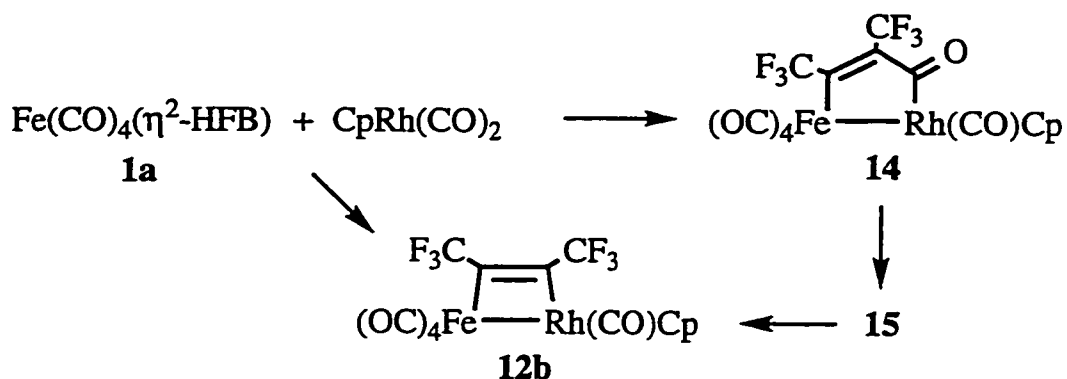
Figure 5-8. ^{19}F NMR Monitored Reaction of **1a** with $\text{CpRh}(\text{CO})_2$ in CD_2Cl_2 .

(a) at 0°C (376.5 MHz). (b) After 1.5 h at 0°C (376.5 MHz).

(c) at $+20^\circ\text{C}$ (188.3 MHz). (d) After 4 h at $+20^\circ\text{C}$ (188.3 MHz).

As the temperature was progressively raised to 0°C , a minor species (**15**) also grew in concentration, appearing in the ^{19}F NMR as a singlet at δ -56.07. As the sample was warmed to ambient temperature (Figure 5-8(c) and (d)), the remaining **1a** was consumed, and, more significantly, the amount of **14** dropped rapidly

while both **12b** and **15** increased in intensity. After four hours, **14** had been consumed entirely and **15** had also decreased in intensity.

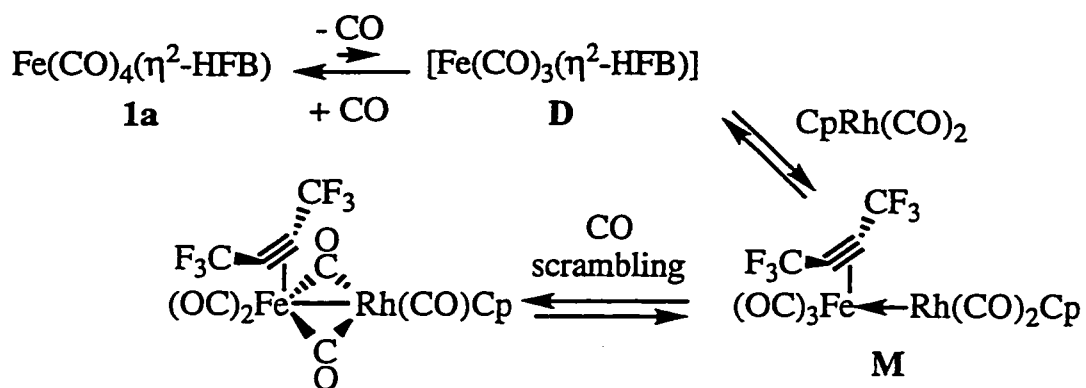


Scheme 5-4. Sequence of Appearance of Products in the Reaction of **1a** with CpRh(CO)_2 at Low Temperature in CD_2Cl_2 .

Compound **15** clearly contains a symmetrical HFB moiety as it displayed a singlet in the ^{19}F NMR. Although this intriguing intermediate was present in sufficiently high concentration to be detected in the ^{13}C NMR spectrum, apparent overlap of one of the signals with the remaining $\text{CpRh}(^{13}\text{CO})_2$ prevented complete identification of the signals. The solvent was stripped off the NMR sample at low temperature, and the excess $\text{CpRh}(^{13}\text{CO})_2$ was sublimed from the residue. Upon redissolution in cold CD_2Cl_2 , three signals were identified for **15**. A singlet of intensity two was detected at δ 205.61 for an Fe(CO)_2 group along with two doublets at δ 192.21 (d, $^1J_{\text{RhC}} = 21$ Hz), and 180.46 (d, $^1J_{\text{RhC}} = 82$ Hz) in a 2:1 ratio. The latter is clearly due to a terminal Rh-bonded carbonyl while the former has a $^1J_{\text{RhC}}$ coupling constant which is more typical of an acyl group. Unfortunately, a structure incorporating these features, a symmetrical HFB moiety, and two terminal Fe carbonyls was not obvious at this stage. A structure for **15** will be proposed in Section 6.4.1 where more supporting information will be presented.

From a mechanistic standpoint, several possible pathways can be suggested from the above data. The first result that requires justification is the ^{13}CO enrichment of CpRh(CO)_2 prior to product formation. Although free ^{13}CO

was not detected at this stage, the kinetic study conducted in Chapter 4 clearly established that CO dissociation occurs at measurable rates in the -30 to -40°C regime where exchange was observed (Figure 5-7(b)). The absence of detectable ^{13}C O may simply be the result of a smaller equilibrium constant between **1a** and the putative $[\text{Fe}(\text{CO})_3(\eta^2\text{-HFB})]$ (**D**) intermediate than in the Os chemistry mentioned previously. A probable mechanism for intermolecular carbonyl scrambling is given in Scheme 5-5.



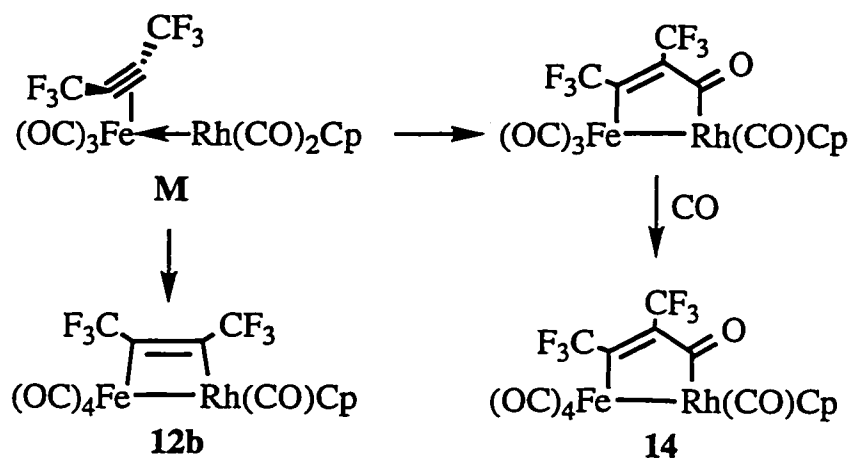
Scheme 5-5. Proposed Mechanism for Intermolecular Carbonyl Exchange Between **1a** and $\text{CpRh}(\text{CO})_2$.

Initial CO dissociation from the Fe center produces a 16-electron intermediate which can be stabilized by donation of an electron pair from $\text{CpRh}(\text{CO})_2$. Intermediate **M**, with a donor-acceptor metal-metal bond, allows intramolecular carbonyl scrambling and thereby exchange of ^{13}C O label from Fe to Rh. Subsequent dissociation of the dinuclear species reforms the reactants with differing ^{13}C O enrichment levels. Clearly, the concentration of intermediate **M** must be far less than what can be detected by ^{19}F NMR spectroscopy ($< \approx 1\%$).

A complex analogous to **M** has been reported between $\text{Cp}^*\text{Ir}(\text{CO})_2$ and the 16-electron $\text{W}(\text{CO})_5$ fragment.⁵⁷ The $\text{Ir} \rightarrow \text{W}$ dative bond was unsupported by bridging ligands in the solid state, but the carbonyls were fluxional in solution and a doubly-CO-bridged intermediate was proposed to account for the exchange behavior. Furthermore, when ^{13}C O enriched $\text{Cp}^*\text{Ir}(\text{CO})_2$ was reacted with natural-abundance $\text{W}(\text{CO})_5(\text{THF})$, the ^{13}C O label was incorporated

statistically in the bimetallic product as is observed for **12b**. Unlike **M**, $\text{Cp}^*(\text{OC})_2\text{IrW}(\text{CO})_5$ does not dissociate into its components in solution. As both species contain electron-precise $\text{Cp}'\text{M}(\text{CO})_2$ moieties, this difference likely reflects the formation of an unstable $\text{W}(\text{CO})_5$ fragment compared with stabilization of **D** by the four-electron donor alkyne.

The alkyne-bridged product **12b** can form by cleavage of one $\text{Fe}-\text{C}(\text{CF}_3)$ bond in intermediate **M** followed by formation of a $\text{Rh}-\text{C}(\text{CF}_3)$ bond. It is also conceivable that the alkyne could undergo migratory insertion to one of the carbonyls on the Rh center to form a dimetallacyclopentenone ring system.⁸ The resulting bimetallic compound would be electronically unsaturated and formation of **14** would be completed by scavenging of free CO from solution (Scheme 5-6).

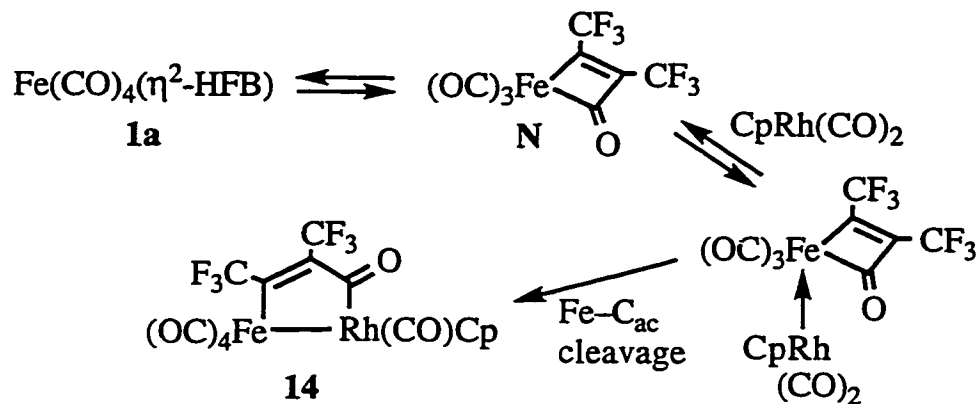


Scheme 5-6. Proposed Mechanism for Formation of **12c** and **14** from **M**.

However, it is unclear why CO would be scavenged so readily from solution to form **14** by this route, as this compound subsequently converts to **12c** at higher temperature with concomitant CO loss.

An alternate mechanism which can account for the formation of **14** directly from **1a** and $\text{CpRh}(\text{CO})_2$ without this requirement is presented in Scheme 5-7. In this case, the reaction is initiated by migratory insertion in **1a** to produce a tricarbonylferracyclobutenone which, as in Scheme 5-5, alleviates its unsaturation by accepting a dative bond from $\text{CpRh}(\text{CO})_2$. The iron-acyl bond then

undergoes cleavage accompanied by bridging and redistribution of a carbonyl ligand to the Fe center, thereby explaining why the acyl group is bonded to Rh in **14** while migratory insertion is preferred at the Fe center in **13a-c**.



Scheme 5-7. Proposed Mechanism for Formation of **14** from a Ferracyclobutenone Intermediate.

There is precedent for this type of rearrangement in the literature. In the reaction of $\text{Ru}_2(\text{CO})_5(\mu\text{-dmpm})_2$ with $\text{C}_2(\text{CO}_2\text{Me})_2$, Gladfelter observed an intermediate species $\text{Ru}_2(\text{CO})_5(\mu\text{-dmpm})_2(\text{C}_2(\text{CO}_2\text{Me})_2)$ whose spectroscopic properties were consistent with a metallacyclobutenone formulation at one ruthenium center; the intermediate later converted to the dimetallacyclopentenone $\text{Ru}_2(\text{CO})_4(\mu\text{-dmpm})_2(\mu\text{-}\eta^1:\eta^1\text{-C}_2(\text{CO}_2\text{Me})_2\text{C(O)})$ as proposed above.⁵⁸ Additionally, Mao has observed a species with a dative $\text{M} \rightarrow \text{M}'$ bond, analogous to intermediate **M**, in the reaction of $\text{Os}(\text{CO})_4(\eta^2\text{-C}_2\text{H}_2)$ with $\text{Ru}(\text{CO})_4(\eta^1\text{-dppm})$ (Scheme 1-7). Although this reaction was initiated by CO loss from the Os-alkyne species with coordination of the pendant phosphine, the $[\text{Ru}(\text{CO})_4(\mu\text{-dppm})\text{Os}(\text{CO})_2(\eta^1, \eta^1\text{-C}_2\text{H}_2\text{C(O)})]$ intermediate formed $\text{OsRu}(\text{CO})_6(\mu\text{-dppm})(\mu\text{-}\eta^1:\eta^1\text{-C}_2\text{H}_2\text{C(O)})$ on warming.⁵⁹ Importantly, it was the Os-acyl bond which cleaved to form the bridging organic group with the acyl carbonyl being relocated to the Ru center; a similar sequence of events is proposed in Scheme 5-7.

This mechanism has the additional advantage of explaining the formation of **14** without requiring ligand loss. Furthermore, the isolation of $\text{Fe}(\text{CO})_4(\eta^1, \eta^1\text{-C}_2(\text{CF}_3)_2\text{C}(\text{O}))$ (**5a**) from the reaction of **1a** with CO lends credence to the proposal. Admittedly, this reaction occurs slowly at room temperature, but this likely represents the poorer ability of CO to trap intermediate **N**. The tricarbonylferracyclobutenone is already quite electron poor and would be more likely to interact with a nucleophilic species such as $\text{CpRh}(\text{CO})_2$ than with a π -acid such as CO. Thus, in addition to being in equilibrium with a small amount of $[\text{Fe}(\text{CO})_3(\eta^2\text{-HFB})]$ (**D**) from CO dissociation, it appears that **1a** is also in equilibrium with a small quantity of $[\text{Fe}(\text{CO})_3(\eta^1, \eta^1\text{-C}_2(\text{CF}_3)_2\text{C}(\text{O}))]$ (**N**) which readily undergoes reaction with an added metal nucleophile such as $\text{CpRh}(\text{CO})_2$. As suggested in Scheme 5-4, the final step of the mechanism, conversion of **14** to **12b**, appears to proceed *via* intermediate **15** as this species clearly increased in concentration as **14** diminished, before being itself consumed. However, the fact that **14** and **12b** formed at the same constant ratio of *ca.* 1.5:1 at 0°C suggests that **12c** can form either from intermediate **M** (Scheme 5-6) or by CO dissociation from **14**.

In this context, it is interesting to note that **14** is the first $\mu\text{-}\eta^1:\eta^1$ -dimetallacyclopentenone species that has been detected as a kinetic product on the pathway to a dimetallacyclobutene generated from an $\text{M}(\text{CO})_4(\eta^2\text{-alkyne})$ species. Typically, the $\mu\text{-}\eta^1:\eta^1$ -dimetallacyclopentenones derived from $\text{Os}(\text{CO})_4(\eta^2\text{-C}_2\text{R}_2)$ ($\text{R} = \text{H}, \text{Me}$) and $\text{CpM}(\text{CO})_2$ ($\text{M} = \text{Co}, \text{Rh}, \text{Ir}$) are thermodynamically stable, and bimetallic complexes derived from π -acidic alkynes tend to be dimetallacyclobutenes.^{1,8,41} The more closely related $\text{Cp}_2\text{Rh}_2(\text{CO})_2(\mu\text{-}\eta^1:\eta^1\text{-C}_2(\text{CF}_3)_2\text{C}(\text{O}))$ is thermodynamically stable, and requires treatment with a decarbonylating agent such as Me_3NO to induce irreversible carbonyl deinsertion to alkyne-bridged products.²⁵

However, processes analogous to the **14** to **12b** conversion have been observed when pre-formed diruthenium complexes are reacted with alkynes. For instance, it is possible to convert $\text{Ru}_2(\text{CO})_4(\mu\text{-dmpm})_2(\mu\text{-}\eta^1:\eta^1\text{-C}_2(\text{CO}_2\text{Me})_2\text{C}(\text{O}))$ to $\text{Ru}_2(\text{CO})_4(\mu\text{-dmpm})_2(\mu\text{-}\eta^1:\eta^1\text{-C}_2(\text{CO}_2\text{Me})_2)$, but the former species must be heated to +90°C in toluene to initiate carbonyl

deinsertion.^{58,60} Additionally, $\text{Ru}_2(\text{CO})_4(\mu\text{-dppm})_2(\mu\text{-}\eta^1:\eta^1\text{-C}_2\text{H}_2)$ can be reversibly converted to $\text{Ru}_2(\text{CO})_4(\mu\text{-dppm})_2(\mu\text{-}\eta^1:\eta^1\text{-C}_2\text{H}_2\text{C}(\text{O}))$. In this system, however, the dimetallacyclopentenone species is the thermodynamically stable product as solutions of $\text{Ru}_2(\text{CO})_4(\mu\text{-dppm})_2(\mu\text{-}\eta^1:\eta^1\text{-C}_2\text{H}_2)$ slowly decompose to give $\text{Ru}_2(\text{CO})_4(\mu\text{-dppm})_2(\mu\text{-}\eta^1:\eta^1\text{-C}_2\text{H}_2\text{C}(\text{O}))$.⁶¹ In the present case, **12b** is thermodynamically stable, and no changes are observed when **12b** is stirred overnight under slight CO pressure at ambient temperature.

5.4.2. Reaction of **1a** with $\text{Cp}^*\text{Rh}(\text{CO})_2$

The detection of a dimetallacyclopentenone intermediate on the path to **12b** raises interesting questions as to how **13a-c** are formed, especially as there is evidence for these species existing in equilibrium with the dimetallacyclobutene isomer **G** at room temperature. Accordingly, the reaction between $\text{Fe}(\text{}^{13}\text{CO})_4(\eta^2\text{-HFB})$ and $\text{Cp}^*\text{Rh}(\text{CO})_2$ was monitored at low temperature by ^{19}F and ^{13}C NMR spectroscopy. At -60°C , only resonances for the two reactants were detected. As with the previous reaction, ^{13}CO enrichment of $\text{Cp}^*\text{Rh}(\text{CO})_2$ was observed on warming to -40°C . A small amount of free ^{13}CO was also detected, but after 15 minutes at this temperature, the ^{19}F NMR spectrum indicated that **13b** was present in 9% concentration; thus, the free ^{13}CO detected was liberated in the product-forming step and is not conclusive evidence for initial CO dissociation from **1a**.

The temperature was maintained at -40°C for 45 min, and the ^{13}CO enrichment level in $\text{Cp}^*\text{Rh}(\text{CO})_2$ approached the anticipated equilibrium level. Product formation also continued at a slow pace. Raising the temperature from -30°C through to 0°C resulted in greater quantities of **13b** along with two minor products in *ca.* 4% and 2% concentration, each of which contain unsymmetrical HFB ligands. At this point, the reaction appeared to be retarded by the presence of free CO. The solution was freeze-thaw degassed three times and warmed to room temperature to complete the reaction. Upon warming, one of the minor products disappeared, leaving a final product distribution of 98% **13b** with 2% of the second minor compound detected earlier in the reaction. Neither of the minor species could be characterized by ^{13}C NMR owing to their low concentrations.

However, the fact that one of the minor species appeared to convert to **13b** on warming suggests that it may be the $\eta^1:\eta^1$ -dimetallacyclopentenone species analogous to **14**.

In any case, the fact that the anticipated end product was the only significant species observed during the course of the reaction suggests that the pathway *via* initial carbonyl insertion at the Fe center (Scheme 5-7) is disfavored with a more strongly nucleophilic metal species. It would appear, rather, that the reaction occurs *via* the interaction of $\text{Cp}^*\text{Rh}(\text{CO})_2$ with **D** produced by CO dissociation from **1a** (Scheme 5-5). The intermediate analogous to **M** presumably converts initially to the dimetallacyclobutene **G** which undergoes migratory insertion to produce **13b**. Formation of a $\mu\text{-}\eta^1:\eta^1$ -dimetallacyclopentenone from the analog of **M** (Scheme 5-6) can be ruled out as migratory insertion would be less favored for $\text{Cp}^*\text{Rh}(\text{CO})_2$ than for its Cp analog; the greater electron density on the Rh center would make the attendant carbonyls less prone to nucleophilic attack than in the more electron poor $\text{CpRh}(\text{CO})_2$.

The absence of a significant route leading to a $\mu\text{-}\eta^1:\eta^1$ -dimetallacyclopentenone reflects the greater ease of formation of $[\text{Fe}(\text{CO})_3(\eta^2\text{-HFB})]$ (**D**) than $[\text{Fe}(\text{CO})_3(\eta^1,\eta^1\text{-C}_2(\text{CF}_3)_2\text{C}(\text{O}))]$ (**N**). Thus, $\text{Cp}^*\text{Rh}(\text{CO})_2$ apparently reacts with the small quantities of **D** produced at low temperature before **N** becomes accessible. Casey and co-workers have detected a similar compound to intermediate **M** proposed in Scheme 5-5. $\text{Cp}^*_2\text{Re}_2(\text{CO})_3(\mu\text{-CO})(\eta^2\text{-C}_2\text{Me}_2)$ was formed when $\text{Cp}^*(\text{OC})_2\text{Re}=\text{Re}(\text{CO})_2\text{Cp}^*$ was exposed to but-2-yne at -78°C . Upon warming to -40°C , the η^2 -alkyne compound formed $\text{Cp}^*_2\text{Re}_2(\text{CO})_3(\mu\text{-}\eta^1:\eta^3\text{-C}_2\text{Me}_2\text{C}(\text{O}))$ along with the fragmentation products $\text{Cp}^*\text{Re}(\text{CO})_3$ and $\text{Cp}^*\text{Re}(\text{CO})(\eta^2\text{-C}_2\text{Me}_2)$.⁶² The fluxional behavior of this $\mu\text{-}\eta^1:\eta^3$ -dimetallacyclopentenone was rationalized by invoking a dimetallacyclobutene intermediate as is proposed for **13b** presently.⁶³ Thus, although they are generated by different routes, **13a-c** behave in a similar fashion to $\text{Cp}^*_2\text{Re}_2(\text{CO})_3(\mu\text{-}\eta^1:\eta^3\text{-C}_2\text{Me}_2\text{C}(\text{O}))$.

5.5. Intermolecular CO Exchange Between **1a** and Os(CO)₅

An earlier experiment established that intermetallic ¹³CO exchange occurred between Ru(CO)₄(η²-HFB) and Os(CO)₅ prior to formation of RuOs(CO)₈(μ-η¹:η¹-HFB).² Although **1a** does not form a stable bimetallic product with M'(CO)₅, the fact that this same behavior was observed for **1a** and Cp'Rh(CO)₂ raises the question as to whether Os(CO)₅ would interact in the same fashion with **1a**. Thus, equimolar amounts of Fe(¹³CO)₄(η²-HFB) and Os(CO)₅ were introduced into an NMR tube in cold CD₂Cl₂. Initially, intense signals were observed for the equatorial and axial carbonyls of **1a** along with a weak singlet at δ 182.9 for Os(CO)₅ (Figure 5-9(a)). No change was observed on warming to -40 or -30°C, even though CO dissociation from **1a** is known to occur at measurable rates at these temperatures (Chapter 4), but upon reaching -20°C, the intensity of the δ 182.9 singlet began to grow in accord with intermolecular carbonyl scrambling (Figure 5-9(b)). After the tube had warmed and rested for one hour at 0°C, the ¹³CO label had been distributed statistically between the two discrete 18-electron metal fragments (Figure 5-9(c)). No other signals were observed.

Accordingly, a process similar to Scheme 5-5 is suggested, with the caveat that the intermediate analogous to **M** does not react to produce a stable bimetallic product. Pomeroy has reported that Os(CO)₅ can act as a donor ligand to the unsaturated Os(CO)₃(GeCl₃)(Cl) fragment,⁶⁴ and a related complex forms between Os(CO)₄(PR₃) and 16-electron M''(CO)₅ (M'' = Cr, Mo, W).^{65,66} In the present case, a clear influence of the heterobimetallic framework on the reaction is suggested, with Os(CO)₅ clearly being able to function as a donor to intermediate **D**, but failing to provide the correct conditions to afford an alkyne-bridged bimetallic product. The influence of the entering metal on the rate of reaction is also clear when it is recalled that CpRh(CO)₂ reacts more quickly with **1a** than CpCo(CO)₂ and CpIr(CO)₂. A similar sequence occurred for the Cp* analogs. It is not clear at this point what causes the 2nd row metal species to be the most reactive towards **1a** as the 3rd row congeners, Cp'Ir(CO)₂, would be expected to be the most nucleophilic of each series. A possible explanation is that the rate determining step is not formation of **M**, but rather is the subsequent step which

involves formation of the $M\text{-CCF}_3$ bond in **12b,c** or **F**. Although a dependence on the group 9 metal might be expected in this process, it is unclear why this step would be so much more rapid for the Rh species and faster for $\text{Cp}^*\text{M}(\text{CO})_2$ over $\text{CpM}(\text{CO})_2$.

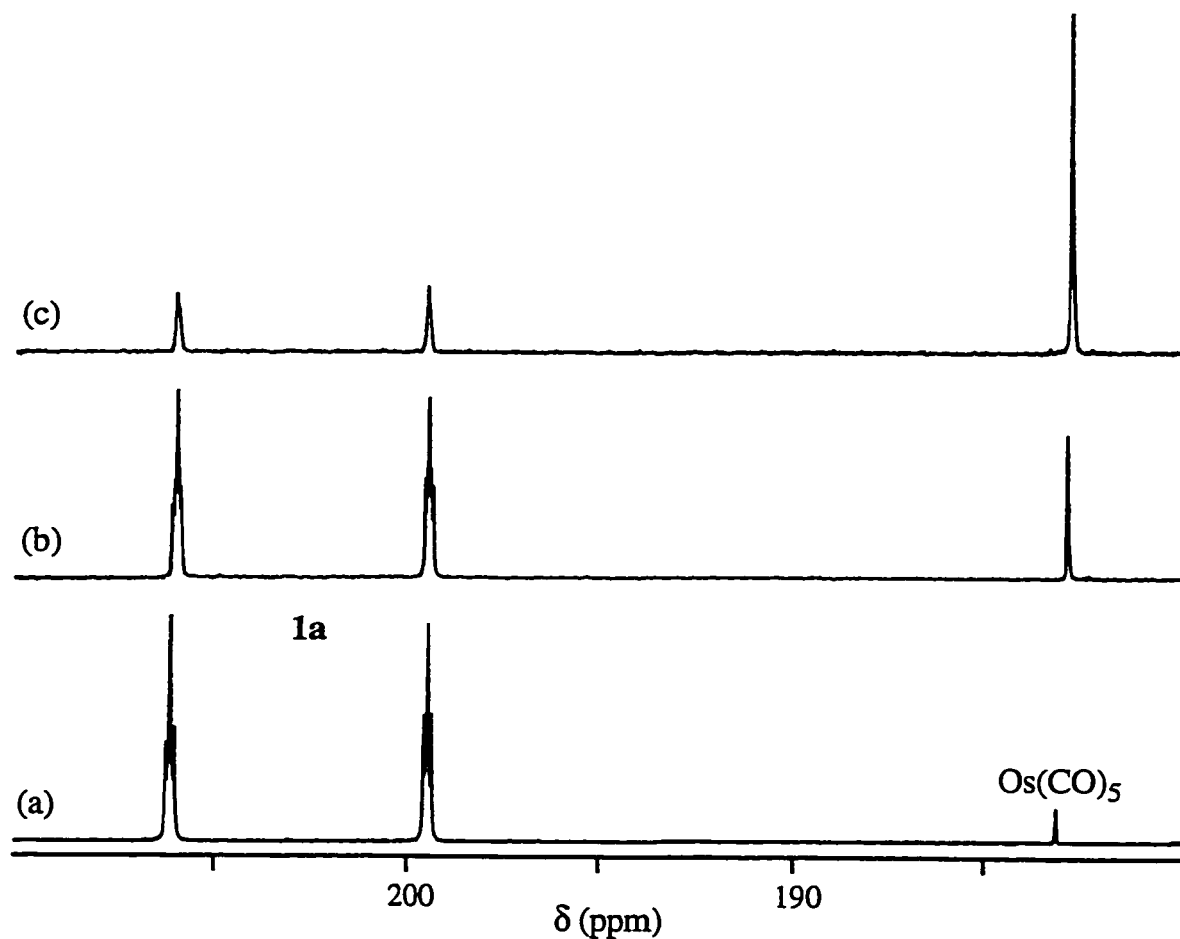


Figure 5-9. ^{13}C NMR Monitored Reaction of **1a** with $\text{Os}(\text{CO})_5$ in CD_2Cl_2 .
 (a) Initial, -60°C . (b) After Warming to -20°C . (c) After Warming to 0°C .

Nonetheless, the clear demonstration of metal-metal interaction without formation of a stable bimetallic species prompted an interesting suggestion - could a catalytic amount of **1a** be used to enrich $\text{Os}(\text{CO})_5$ with ^{13}C ? If so, this would provide a facile means of carrying out an otherwise difficult isotopic enrichment. Unfortunately, combining $\text{Os}(\text{CO})_5$ and 5 mol% **1a** under a ^{13}C atmosphere did

not introduce a noticeable amount of label into the osmium species even after several days stirring at room temperature. The reason for the lack of success appears to be that ^{13}CO competes effectively with $\text{Os}(\text{CO})_5$ for any intermediate **D** which may form, and thus the concentration of the weakly interacting dinuclear species analogous to **M** is negligibly small.

5.6. Conclusions

As with its Ru congener, $\text{Fe}(\text{CO})_4(\eta^2\text{-HFB})$ (**1a**) reacts with $\text{Cp}'\text{M}(\text{CO})_2$ ($\text{M} = \text{Co}, \text{Rh}, \text{Ir}; \text{Cp}' = \text{Cp}, \text{Cp}^*$) to produce bimetallic complexes. While the anticipated dimetallatetrahedrane (**11a**) and dimetallacyclobutene (**12a-c**) structures were formed from the Cp substituted compounds, the Cp^* variants (**13a-c**) had the $\mu\text{-}\eta^1\text{:}\eta^3$ -dimetallacyclopentenone form as ground state structures. However, the CO-inserted compounds entered into rapid equilibrium with alkyne-bridged species, demonstrating a relatively low energy barrier between the two isomers. The ease of rearrangement of dimetallacyclopentenone to dimetallacyclobutene can be rationalized by an electronic argument, but the steric influence of the ancillary cyclopentadienyl ring system on the group 9 metal appears to govern which ground state structure is preferred. A low temperature NMR study of the formation of the bimetallic compounds revealed facile intermolecular carbonyl scrambling prior to product formation, and detected a $\mu\text{-}\eta^1\text{:}\eta^1$ -dimetallacyclopentenone intermediate (**14**) in the reaction of **1a** with $\text{CpRh}(\text{CO})_2$, which readily lost CO on warming to form the dimetallacyclobutene **12b**. More interesting still was that intermetallic CO exchange was observed between **1a** and $\text{Os}(\text{CO})_5$ even though this combination of reagents did not yield a detectable bimetallic product. Thus, although some common features are shared with previously studied Ru and Os species, the heterobimetallic products derived from **1a** introduce a variety of new structural features to the class of $\text{Cp}'\text{MM}'(\text{CO})_5(\text{HFB})$ compounds.

5.7. Experimental Section

Unless otherwise noted, the general synthetic techniques and physical measurements employed are as described in Sections 2.6.1 and 2.6.2.

5.7.1. Reagents

Compound **1a** was prepared according to the procedures described in Chapter 2. $\text{CpM}(\text{CO})_2$ ($\text{M} = \text{Rh},^{67} \text{Ir}^{68}$) and $\text{Cp}^*\text{M}(\text{CO})_2$ ($\text{M} = \text{Co},^{69} \text{Rh},^{70} \text{Ir}^{71}$) were prepared according to published procedures. $\text{CpCo}(\text{CO})_2$ was purchased from Strem Chemical Co. and was used without further purification.

5.7.2. Synthetic Procedures

Preparation of $\text{Cp}'\text{CoFe}(\text{CO})_3(\mu\text{-CO})(\mu\text{-}\eta^2\text{:}\eta^2\text{-HFB})$ ($\text{Cp}' = \text{Cp}$, **11a; Cp^* , **11a***).** A pentane solution of $\text{CpCo}(\text{CO})_2$ (66 mg, 0.367 mmol) was added to **1a** (105 mg, 0.318 mmol) dissolved in 25 mL pentane at room temperature. The solution was stirred overnight. Removal of the solvent and excess $\text{CpCo}(\text{CO})_2$ *in vacuo* followed by recrystallization from pentane at -80°C afforded 119.6 mg of an analytically pure purple-black powder of $\text{CpCoFe}(\text{CO})_3(\mu\text{-CO})(\mu\text{-}\eta^2\text{:}\eta^2\text{-HFB})$ (**11a**) (0.263 mmol, 83 %). ^{13}C enriched material was prepared from $\text{Fe}(^{13}\text{CO})_4(\eta^2\text{-HFB})$. In an analogous fashion, **1a** (30 mg, 0.091 mmol) and $\text{Cp}^*\text{Co}(\text{CO})_2$ (26.3 mg, 0.105 mmol) formed 38.7 mg of a purple-black powder of $\text{Cp}^*\text{CoFe}(\text{CO})_3(\mu\text{-CO})(\mu\text{-}\eta^2\text{:}\eta^2\text{-HFB})$ (**11a***) (0.0738 mmol, 81 %) after stirring for three hours at ambient temperature *in vacuo* to remove traces of **13a**.

$\text{CpCoFe}(\text{CO})_3(\mu\text{-CO})(\mu\text{-}\eta^2\text{:}\eta^2\text{-HFB})$ (**11a**):

F.W. 454.0

Anal. Calcd for $\text{C}_{13}\text{H}_5\text{CoF}_6\text{FeO}_4$: C, 34.40; H, 1.11. Found: C, 34.29; H, 1.15.

IR (pentane) ν_{CO} 2079(vs), 2029(m), 2015(s), 1914(w).

^1H NMR (CD_2Cl_2 , 200.1 MHz) δ 5.32 (s, C_5H_5).

$^{13}\text{C}\{^1\text{H}\}$ NMR (CD_2Cl_2 , 100.6 MHz, ^{13}C enriched) (-100°C) δ 220.37 (s, $\mu\text{-CO}$), 206.11 (s, COFe), 202.84 (s, 2COFe). (-20°C) δ 221.27(s, $\mu\text{-CO}$), 204.52 (s, 3COFe(av)).

$^{13}\text{C}\{^{19}\text{F}\}$ NMR (CD_2Cl_2 , 100.6 MHz) δ 204.92 (s, CO_{av}), 128.50 (s, CF_3), 93.13 (s, C_5H_5), 73.54 (s, CCF_3).

^{19}F NMR (CD_2Cl_2 , 188.3 MHz) δ -50.38 (s).

EI-MS: M^+ (8.30% of base); $\text{M}^+ - n \text{CO}$ ($n = 1 - 4$); $\text{M}^+ - \text{Fe}(\text{CO})_4 - m \text{F}$ ($m = 0 - 2$); CpCo^+ (base peak).

$\text{Cp}^*\text{CoFe}(\text{CO})_3(\mu\text{-CO})(\mu\text{-}\eta^2\text{:}\eta^2\text{-HFB})$ (**11a***):

F.W. 524.1

Anal. Calcd for $\text{C}_{18}\text{H}_{15}\text{CoF}_6\text{FeO}_4$: C, 41.25; H, 2.88. Found: C, 41.16; H, 2.70.

IR (pentane) ν_{CO} 2071(vs), 2022(m), 2003(s), 1887(w).

^1H NMR (CD_2Cl_2 , 200.1 MHz) δ 1.74 (s, $\text{C}_5(\text{CH}_3)_5$).

$^{13}\text{C}\{^1\text{H}\}$ NMR (CD_2Cl_2 , 100.6 MHz, ^{13}CO enriched, -100°C) δ 228.17 (s, $\mu\text{-CO}$), 207.56 (s, COFe), 203.76 (s, 2COFe). (-40°C) δ 229.56(s, $\mu\text{-CO}$), 205.70 (s, 3COFe (av)).

$^{13}\text{C}\{^{19}\text{F}\}$ NMR (CD_2Cl_2 , 100.6 MHz) δ 206.28 (s, COFe), 128.82 (s, CF_3), 105.21 (s, C_5Me_5), 70.36 (s, CCF_3), 9.56 (q, $^1J_{\text{CH}} = 128$ Hz, CH_3).

^{19}F NMR (CD_2Cl_2 , 188.3 MHz) δ -48.85 (s).

EI-MS: M^+ (4.7% of base); $\text{M}^+ - n \text{CO}$ ($n = 1 - 4$); $\text{M}^+ - \text{Fe}(\text{CO})_4 - m \text{F}$ ($m = 0 - 2$) ($m = 2$; base peak).

Synthesis of 12b,c and 13a-c. The same simple procedure was followed, and thus only the quantities of starting materials, products and reaction times will be given.

$\text{CpRhFe}(\text{CO})_5(\mu\text{-}\eta^1\text{:}\eta^1\text{-HFB})$ (**12b**): $\text{CpRh}(\text{CO})_2$ (28 mg, 0.125 mmol) and **1a** (39 mg, 0.118 mmol) provided an analytically pure bright orange powder of **12b** (59.6 mg, 0.113 mmol, 96 %) after 1 h at room temperature.

F.W. 525.9

Anal. Calcd for $\text{C}_{14}\text{H}_5\text{F}_6\text{FeO}_5\text{Rh}$: C, 31.97; H, 0.96. Found: C, 32.00; H, 0.90.

IR (pentane) ν_{CO} 2093(s), 2043(vs), 2028(vs), 2019(m), 2012(m); $\nu_{\text{C-C}}$ 1635(vw).

(CH_2Cl_2) ν_{CO} 2092(s), 2038(s), 2027(vs), 2018(sh); $\nu_{\text{C-C}}$ 1630(vw).

^1H NMR (CD_2Cl_2 , 200.1 MHz) δ 5.64 (s, C_5H_5).

$^{13}\text{C}\{^1\text{H}\}$ NMR (CD_2Cl_2 , 100.6 MHz, ^{13}C enriched, -100°C) δ 208.72 (s, $\text{COFe}(\text{distinct})$), 207.05 (s, COFe), 206.64 (s, COFe), 203.67 (s, COFe), 189.19 (d, $^1J_{\text{RhC}} = 80$ Hz, CORh).

(toluene-*d*₈, 100.6 MHz, ^{13}C enriched) (-80°C) δ 208.99 (s, $\text{COFe}(\text{distinct})$), 207.94 (s, COFe), 207.19 (s, COFe), 204.49 (s, COFe), 190.05 (d, $^1J_{\text{RhC}} = 79$ Hz, CORh). (0°C) δ 209.60 (s, $\text{COFe}(\text{distinct})$), 205.84 (s, $2\text{COFe}(\text{av})$), 199 (br, $2\text{COFe/Rh}(\text{av})$). ($+80^\circ\text{C}$) δ 207.2 (br, $3\text{COFe}(\text{av})$), 198.8 (br, $2\text{COFe/Rh}(\text{av})$).
Slow decomposition occurred as the sample was warmed to $+100^\circ\text{C}$.

$^{13}\text{C}\{^{19}\text{F}\}$ NMR (CD_2Cl_2) (100.6 MHz, -20°C): δ 209.38 (s, COFe), 126.59 (d, $^2J_{\text{RhC}} = 10$ Hz, FeCCF_3), 122.19 (s, CF_3), 121.76 (d, $^1J_{\text{RhC}} = 28$ Hz, RhCCF_3), 120.43 (s, CF_3), 92.75 (d, $^1J_{\text{CH}} = 183$ Hz, C_5H_5). (125.7 MHz, ambient) δ 122.59 (s, CF_3), 122.18 (brd, $^1J_{\text{RhC}} = 26$ Hz, RhCCF_3), 120.86 (brs, CF_3), 93.06 (d, $^1J_{\text{CH}} = 183$ Hz, C_5H_5).

^{19}F NMR (CD_2Cl_2 , 188.3 MHz) δ -54.96 (qd, $^5J_{\text{FF}} = 11.7$ Hz, $^3J_{\text{RhF}} = 3.0$ Hz, RhCCF_3), -57.83 (q, $^5J_{\text{FF}} = 11.7$ Hz, FeCCF_3).

EI-MS: M^+ (0.1% of base); $\text{M}^+ - n \text{CO}$ ($n = 1 - 5$); $\text{M}^+ - \text{Fe}(\text{CO})_4 - 2\text{F}$; CpRh^+ (base peak).

$\text{CpIrFe}(\text{CO})_5(\mu\text{-}\eta^1\text{-}\eta^1\text{-HFB})$ (**12c**): $\text{CpIr}(\text{CO})_2$ (90 mg, 0.288 mmol) and **1a** (84 mg, 0.255 mmol) yielded yellow **12c** (113.6 mg, 0.185 mmol, 72 %) after 3 days stirring in pentane at ambient temperature.

F.W. 615.3

Anal. Calcd for $\text{C}_{14}\text{H}_5\text{F}_6\text{FeIrO}_5$: C, 27.33; H, 0.82. Found: C, 27.56; H, 0.73.

IR (pentane) ν_{CO} 2094(s), 2043(s), 2023(vs), 2015(s), 2004(m); ν_{CC} 1626 (w).

^1H NMR (CD_2Cl_2 , 200.1 MHz) δ 5.69 (s, C_5H_5).

$^{13}\text{C}\{^1\text{H}\}$ NMR (CD_2Cl_2 , 100.6 MHz, ^{13}C enriched, -100°C) δ 210.35 (s, $\text{COFe}(\text{distinct})$), 207.54 (s, 2COFe), 201.87 (s, COFe), 169.37 (s, COIr).

(toluene-*d*₈, 100.6 MHz, ^{13}C enriched) (-60°C) δ 211.20 (s, $\text{COFe}(\text{distinct})$), 208.41 (s, 2COFe), 202.83 (s, COFe), 169.03 (s, COIr). (-20°C) δ 211.40 (s, $\text{COFe}(\text{distinct})$), 208.5 (br), 202.7 (brs), 168.6 (br). ($+10^\circ\text{C}$) δ 211.2 (br, $\text{COFe}(\text{distinct})$), 205.5 (br, $2\text{COFe}(\text{av})$). ($+80^\circ\text{C}$) δ 207.1 (br, $3\text{COFe}(\text{av})$), 188 (vbr, $2\text{COFe/Ir}(\text{av})$).

$^{13}\text{C}\{^{19}\text{F}\}$ NMR (CD_2Cl_2 , 125.7 MHz) δ 129.7 (br, FeCCF_3), 125.04 (s, CF_3), 120.80 (s, CF_3), 105.21 (s, IrCCF_3), 88.92 (d, $^1J_{\text{CH}} = 184$ Hz, C_5H_5).

^{19}F NMR (CD_2Cl_2 , 376.5 MHz) δ -56.83 (q, $^5J_{\text{FF}} = 12.4$ Hz, IrCCF_3), -57.49 (q, $^5J_{\text{FF}} = 12.4$ Hz, FeCCF_3).

EI-MS: M^+ (0.3% of base); $\text{M}^+ - n \text{CO}$ ($n = 1 - 5$); $\text{M}^+ - \text{Fe}(\text{CO})_3 - 2\text{F}$; $\text{M}^+ - \text{Fe}(\text{CO})_4 - 2\text{F}$; (base peak).

$\text{Cp}^*\text{RhFe}(\text{CO})_4(\mu\text{-}\eta^1\text{:}\eta^3\text{-C}_2(\text{CF}_3)_2\text{C}(\text{O}))$ (**13b**): $\text{Cp}^*\text{Rh}(\text{CO})_2$ (19.8 mg, 0.067 mmol) and **1a** (20 mg, 0.061 mmol) reacted on warming from *ca.* -35°C to ambient temperature to afford a bright red powder of **13b** (34.1 mg, 0.057 mmol, 94 %).

F.W. 596.1

Anal. Calcd for $\text{C}_{19}\text{H}_{15}\text{F}_6\text{FeO}_5\text{Rh}$: C, 38.29; H, 2.54. Found: C, 38.26; H, 2.70.

IR (pentane) ν_{CO} 2082(m), 2063(vs), 2031(m), 2024(vs), 2012(m), 1996(w), 1957(m), 1790(w), 1761(w), 1753(sh); ν_{CC} 1625(vw).

(CH_2Cl_2) ν_{CO} 2078(mw), 2056(vs), 2021(s), 2000(m), 1961(mw,br), 1786(w), 1748(mw); ν_{CC} 1606(vw).

(KBr disk) ν_{CO} 2055(s), 2008(vs), 1957(m), 1788(w), 1749(mw).

^1H NMR (CD_2Cl_2 , 200.1 MHz) δ 1.87 (s, $\text{C}_5(\text{CH}_3)_5$).

$^{13}\text{C}\{^1\text{H}\}$ NMR (CD_2Cl_2 , 100.6 MHz, ^{13}CO enriched, -60°C) δ 216.62 (s, CO_{ac}), 212.81 (s, CO_{Fe}), 209.89 (s, CO_{Fe}), 204.09 (s, CO_{Fe}), 186.41 (d, $^1J_{\text{RhC}} = 81$ Hz, CORh).

(toluene-*dg*, 100.6 MHz, -60°C) δ 215.18 (s, CO_{ac}), 213.63 (s, CO_{Fe}), 210.09 (s, CO_{Fe}), 204.55 (s, CO_{Fe}), 187.26 (d, $^1J_{\text{RhC}} = 82$ Hz, CORh). ($+20^\circ\text{C}$) δ 209 (brs, $3\text{CO}_{\text{Fe}}(\text{av})$). ($+80^\circ\text{C}$, 50.3 MHz) δ 209.0 (s, $3\text{CO}_{\text{Fe}}(\text{av})$), 201 (brs, $2\text{CO}_{\text{Fe}}(\text{ac})\text{Rh}(\text{av})$). ($+110^\circ\text{C}$, 50.3 MHz) δ 208.5 (d, $^1J_{\text{RhC}} = 14$ Hz, global average) + decomposition products.

$^{13}\text{C}\{^{19}\text{F}\}$ NMR (CDCl_3 , 100.6 MHz, -50°C) δ 217.60 (s, CO_{ac}), 212.88 (s, CO_{Fe}), 209.34 (s, CO_{Fe}), 203.74 (s, CO_{Fe}), 186.38 (d, $^1J_{\text{RhC}} = 80$ Hz, CORh), 153.60 (d, $^1J_{\text{RhC}} = 38$ Hz, C_β), 126.75 (s, RhCCF_3), 121.58 (s, $\text{C}(\text{O})\text{CCF}_3$), 104.79 (s, C_5Me_5), 56.47 (s, C_α), 9.40 (q, $^1J_{\text{CH}} = 129$ Hz, CH_3).

^{19}F NMR (CD_2Cl_2 , 188.3 MHz) δ -53.74 (qd, $^5J_{\text{FF}} = 12.1$ Hz, $^3J_{\text{RhF}} = 3.4$ Hz, RhCCF_3), -58.69 (q, $^5J_{\text{FF}} = 12.1$ Hz, $\text{FeC}(\text{O})\text{CCF}_3$).

MS (+FAB): $M^+ - n \text{ CO}$ ($n = 1 - 4$); M^+ not obs.

$\text{Cp}^*\text{IrFe}(\text{CO})_4(\mu\text{-}\eta^1\text{:}\eta^3\text{-C}_2(\text{CF}_3)_2\text{C}(\text{O}))$ (**13c**): Reaction of **1a** (20 mg, 0.061 mmol) with $\text{Cp}^*\text{Ir}(\text{CO})_2$ (27.1 mg, 0.071 mmol) provided **13c** (37.4 mg, 0.0545 mmol, 90 %) after 4 h at ambient temperature.

F.W. 685.4

Anal. Calcd for $\text{C}_{19}\text{H}_{15}\text{F}_6\text{FeIrO}_5$: C, 33.30; H, 2.21. Found: C, 33.33; H, 1.97.

IR (pentane) ν_{CO} 2084(m), 2062(vs), 2032(m), 2016(vs), 2002(m), 1988(w), 1971(m), 1793(w), 1761(m); $\nu_{\text{C-C}}$ 1617(vw).

(CH_2Cl_2) ν_{CO} 2081(m), 2059(vs), 2009(vs), 1973(m), 1791(w), 1752(m); $\nu_{\text{C-C}}$ 1615 (vw).

(KBr disk) ν_{CO} 2048(s), 1999(s), 1980(s), 1974(s), 1792(m), 1757(s).

^1H NMR (CD_2Cl_2 , 200.1 MHz) δ 2.05 (s, $\text{C}_5(\text{CH}_3)_5$).

$^{13}\text{C}\{^1\text{H}\}$ NMR (CD_2Cl_2 , 100.6 MHz, ^{13}CO enriched, -70°C) δ 218.91 (s, CO_{ac}), 211.10 (s, CO_{Fe}), 210.70 (s, CO_{Fe}), 204.15 (s, CO_{Fe}), 165.73 (s, CO_{Ir}).

(toluene-*d*₈, 100.6 MHz) (-70°C) δ 217.69 (s, CO_{ac}), 212.47 (s, CO_{Fe}), 211.05 (s, CO_{Fe}), 204.69 (s, CO_{Fe}), 166.66 (s, CO_{Ir}). ($+20^\circ\text{C}$) δ 209.09 (s, $3\text{CO}_{\text{Fe}(\text{av})}$). ($+100^\circ\text{C}$) δ 208.95 (s, $3\text{CO}_{\text{Fe}(\text{av})}$), 191 (brs, $2\text{CO}_{\text{Fe}(\text{ac})/\text{Ir}(\text{av})}$).

$^{13}\text{C}\{^{19}\text{F}\}$ NMR (CDCl_3 , 100.6 MHz, -50°C) δ 219.94 (s, CO_{ac}), 211.56 (s, CO_{Fe}), 210.28 (s, CO_{Fe}), 203.89 (s, CO_{Fe}), 165.70 (s, CO_{Ir}), 130.53 s, C_β), 127.15 (s, CF_3), 124.47 (s, CF_3), 101.02 (s, C_5Me_5), 59.09 (s, C_α), 8.95 (q, $^1J_{\text{CH}} = 129$ Hz, CH_3).

^{19}F NMR (CD_2Cl_2 , 188.3 MHz) δ -55.51 (q, $^5J_{\text{FF}} = 12.5$ Hz, IrCCF_3), -57.69 (q, $^5J_{\text{FF}} = 12.5$ Hz, $\text{FeC}(\text{O})\text{CCF}_3$).

EI-MS: $M^+ - n \text{ CO}$ ($n = 1 - 5$), M^+ not obs.

Reaction of 11a,a* with CO. Compound **11a*** (25.3 mg, 0.0483 mmol) was dissolved in 10 mL pentane and the solution was freeze-thaw degassed three times. CO was admitted, and the dark purple solution was stirred overnight in a sealed flask. Crystallization at -80°C afforded a purple-black powder of $\text{Cp}^*\text{CoFe}(\text{CO})_4(\mu\text{-}\eta^1\text{:}\eta^3\text{-C}_2(\text{CF}_3)_2\text{C}(\text{O}))$ (**13a**) which was not isolated as a solid

owing to its instability in the absence of a CO atmosphere; NMR samples were prepared at low temperature to avoid conversion back to **11a***.

$\text{Cp}^*\text{CoFe}(\text{CO})_4(\mu\text{-}\eta^1\text{:}\eta^3\text{-C}_2(\text{CF}_3)_2\text{C}(\text{O}))$ (**13a**):

F.W. 552.1

IR (pentane) ν_{CO} 2064(s), 2019(s), 1972(m), 1790(w), 1762(w) 1754(sh).

(CH_2Cl_2) ν_{CO} 2060(s), 2014(s), 1970(m), 1786(w), 1755(sh) 1749(mw).

^1H NMR (CD_2Cl_2 , 200.1 MHz, -60°C) δ 1.65 (s, $\text{C}_5(\text{CH}_3)_5$).

$^{13}\text{C}\{^1\text{H}\}$ NMR (CD_2Cl_2 , 100.6 MHz, ^{13}CO enriched) (-60°C) δ 217.30 (s, CO_{ac}), 214.61 (s, CO_{Fe}), 208.42 (s, CO_{Fe}), 203.39 (s, CO_{Fe}), 198.88 (s, CO_{Co}). (+ 20°C) δ 216.88 (s, CO_{ac}), 209 (br s, $3\text{CO}_{\text{Fe}(\text{av})}$), 198.9 (br s, CO_{Co}) + signals from **11a***.

$^{13}\text{C}\{^{19}\text{F}\}$ NMR (CDCl_3 , 100.6 MHz, -50°C) δ 218.27 (s, CO_{ac}), 214.68 (s, CO_{Fe}), 207.83 (s, CO_{Fe}), 203.05 (s, CO_{Fe}), 198.88 (s, CO_{Co}), 155.92 (s, C_β), 126.67 (s, CF_3), 120.97 (s, CF_3), 99.60 (s, C_5Me_5), 57.90 (s, C_α), 9.25 (q, $^1J_{\text{CH}} = 129$ Hz, CH_3).

^{19}F NMR (CD_2Cl_2 , 188.3 MHz, -60°C) δ -51.51 (q, $^5J_{\text{FF}} = 11.5$ Hz, CoCCF_3), -58.74 (q, $^5J_{\text{FF}} = 11.5$ Hz, $\text{FeC}(\text{O})\text{CCF}_3$).

Similarly, reaction of **11a** with CO provided a mixture of three compounds (**12a:11a:?**) in roughly a 58:28:14% ratio by ^1H and ^{19}F NMR spectroscopy. When the mixture was dissolved in pentane, freeze-thaw degassed, and stirred *in vacuo* at room temperature for 2 hours, complete reversion to **11a** resulted.

IR (pentane, excluding peaks belonging to **11a**) ν_{CO} 2093(s), 2042(s), 2031(vs), 2024(vs), 2008(m), 1994(m), 1799(w); $\nu_{\text{C-C}}$ 1635(vw).

$\text{CpCoFe}(\text{CO})_5(\mu\text{-}\eta^1\text{:}\eta^1\text{-HFB})$ (**12a**):

F.W. 482.0

^1H NMR (CD_2Cl_2 , 400.1 MHz, -60°C) δ 5.08 (s, C_5H_5).

$^{13}\text{C}\{^1\text{H}\}$ NMR (CD_2Cl_2 , 100.6 MHz, ^{13}CO enriched, -60°C) δ 214.55 (s, CO_{Fe}), 212.02 (s, CO_{Fe}), 206.11 (s, CO_{Fe}), 202.36 (s, CO_{Fe}), 196.58 (s, CO_{Co}).

^{19}F NMR (CD_2Cl_2 , 376.5 MHz, -60°C) δ -52.66 (d, $^5J_{\text{FF}} = 10.9$ Hz, CoCCF_3),
-56.99 (q, $^5J_{\text{FF}} = 10.9$ Hz, FeCCF_3).

Unidentified minor product:

^1H NMR (CD_2Cl_2 , 400.1 MHz, -60°C) δ 5.27 (s, C_5H_5).

$^{13}\text{C}\{^1\text{H}\}$ NMR (CD_2Cl_2 , 100.6 MHz, ^{13}CO enriched, -60°C) δ 208.56 (s, CO),
206.11 (s, CO).

^{19}F NMR (CD_2Cl_2 , 376.5 MHz, -60°C) δ -55.06 (d, $^5J_{\text{FF}} = 11.4$ Hz, CF_3), -57.41
(q, $^5J_{\text{FF}} = 10.9$ Hz, CF_3).

5.7.3. X-ray Crystal Structure Determination of Compounds 12c and 13c

Yellow-orange single crystals of both compounds were grown by slow concentration of saturated pentane solutions at -20°C . The X-ray data collection and structure refinement were carried out by Dr. Bob McDonald at the Structure Determination Laboratory, Department of Chemistry, University of Alberta. A single crystal of 13c was mounted on a thin glass fibre and transferred to the goniometer of a Siemens P4/RA diffractometer⁷² where it was kept under a stream of cooled nitrogen gas. Reflection data for 12c was collected at room temperature as the crystals had a tendency to shatter when cooled in this fashion. The structures were solved using direct methods techniques (*SHELXS-86*⁷³) and refined by full-matrix least-squares on F^2 (*SHELXL-93*⁷⁴). All non-hydrogen atoms were located. The geometrically constrained hydrogen atoms were placed in appropriate calculated positions. A summary of data collection parameters is given in Tables 5-12 (12c) and 5-14 (13c). The final atomic coordinates and equivalent isotropic displacement parameters are given in Tables 5-13 (12c) and 5-15 (13c). Selected interatomic distances and angles are provided in Tables 5-5 through 5-8.

Table 5-12. Crystallographic Experimental Details for Compound 12c

Formula	C ₁₄ H ₅ F ₆ FeIrO ₅
Formula weight	615.23
Crystal dimensions (mm)	0.49 × 0.31 × 0.10
Crystal system	triclinic
Space group	$P\bar{1}$ (No. 2)
Unit cell parameters ^a	
<i>a</i> , Å	8.5452 (11)
<i>b</i> , Å	9.1953 (7)
<i>c</i> , Å	12.1348 (13)
α, deg	77.125 (7)
β, deg	82.357 (9)
γ, deg	64.274 (8)
<i>V</i> , Å ³	836.7 (2)
<i>Z</i>	2
ρ _{calc.} , g cm ⁻³	2.442
μ, mm ⁻¹	8.898
Radiation, λ (Å)	graphite-monochromated Mo Kα (0.71073)
Temperature, °C	22
Scan type	θ–2θ
Data collection 2θ limit, deg	50.0
Total data collected	5606 (–10 ≤ <i>h</i> ≤ 10, –14 ≤ <i>k</i> ≤ 10, –14 ≤ <i>l</i> ≤ –14)
Independent reflections	2803
Number of observations (<i>NO</i>)	2583 ($F_o^2 \geq 2\sigma(F_o^2)$)
Absorption correction method	semiempirical (ψ scans)
Range of transmission factors	0.6908–0.1728
Data/restraints/parameters	2803 [$F_o^2 \geq -3\sigma(F_o^2)$]/0/299
Extinction coefficient (<i>x</i>) ^b	0.0563 (25)
Goodness-of-fit (<i>S</i>) ^c	1.046 [$F_o^2 \geq -3\sigma(F_o^2)$]
Final <i>R</i> indices ^d	
$F_o^2 > 2\sigma(F_o^2)$	$R_1 = 0.0355$, $wR_2 = 0.0893$
all data	$R_1 = 0.0390$, $wR_2 = 0.0916$
Largest difference peak and hole	1.430 and –1.189 e Å ⁻³

^aObtained from least-squares refinement of 28 reflections with $26.9^\circ < 2\theta < 28.1^\circ$.

^b $F_c^* = kF_c[1 + x\{0.001F_c^2\lambda^3/\sin(2\theta)\}]^{-1/4}$ where *k* is the overall scale factor.

^c $S = [\sum w(F_o^2 - F_c^2)^2 / (n - p)]^{1/2}$ (*n* = number of data; *p* = number of parameters varied; $w = [\sigma^2(F_o^2) + (0.0696P)^2 + 0.1030P]^{-1}$ where $P = [\text{Max}(F_o^2, 0) + 2F_c^2]/3$).

^d $R_1 = \sum ||F_o| - |F_c|| / \sum |F_o|$; $wR_2 = [\sum w(F_o^2 - F_c^2)^2 / \sum w(F_o^4)]^{1/2}$.

Table 5-13. Atomic Coordinates and Equivalent Isotropic Displacement Parameters for Compound **12c**

Atom	<i>x</i>	<i>y</i>	<i>z</i>	<i>U</i> _{eq} , Å ²
Ir	-0.24179(3)	0.04643(3)	-0.19556(2)	0.0427(2)*
Fe	-0.33216(11)	-0.12658(12)	-0.30830(9)	0.0427(3)*
F1A ^b	0.1654(45)	-0.3249(49)	-0.0931(35)	0.176(21)*
F2A ^b	0.1615(26)	-0.0956(22)	-0.1554(25)	0.103(9)*
F3A ^b	0.2722(21)	-0.2846(42)	-0.2446(28)	0.143(13)*
F4A ^b	0.1729(38)	-0.4079(32)	-0.3814(31)	0.148(15)*
F5A ^b	-0.0321(27)	-0.4734(28)	-0.3662(31)	0.104(8)*
F6A ^b	0.1105(35)	-0.5330(19)	-0.2321(19)	0.103(6)*
F1B ^b	0.2169(32)	-0.3668(23)	-0.1231(33)	0.102(11)*
F2B ^b	0.1340(29)	-0.1422(27)	-0.0920(21)	0.110(8)*
F3B ^b	0.2500(37)	-0.1828(54)	-0.2520(21)	0.160(16)*
F4B ^b	0.1990(22)	-0.4469(41)	-0.3194(38)	0.162(20)*
F5B ^b	0.0073(29)	-0.3887(34)	-0.4322(19)	0.116(7)*
F6B ^b	-0.0024(62)	-0.5215(30)	-0.2767(52)	0.201(21)*
O1	-0.2873(11)	-0.1237(11)	0.0373(7)	0.097(2)*
O2	-0.3858(11)	-0.3230(11)	-0.0927(7)	0.095(2)*
O3	-0.4022(11)	-0.3292(10)	-0.4344(8)	0.085(2)*
O4	-0.1907(9)	0.0251(9)	-0.5116(6)	0.078(2)*
O5	-0.6856(7)	0.1398(8)	-0.3089(7)	0.074(2)*
C1	-0.2720(12)	-0.0618(12)	-0.0548(8)	0.062(2)*
C2	-0.3648(10)	-0.2449(11)	-0.1732(8)	0.059(2)*
C3	-0.3716(11)	-0.2533(11)	-0.3855(8)	0.058(2)*
C4	-0.2476(10)	-0.0281(10)	-0.4328(7)	0.051(2)*
C5	-0.5524(9)	0.0381(10)	-0.3079(7)	0.052(2)*
C6	0.1417(10)	-0.2164(11)	-0.1771(8)	0.059(2)*
C7	-0.0328(8)	-0.1660(8)	-0.2241(6)	0.043(2)*
C8	-0.0751(8)	-0.2497(9)	-0.2806(6)	0.0435(15)*
C9	0.0401(11)	-0.4086(12)	-0.3183(10)	0.070(3)*
C10	-0.1433(15)	0.2333(13)	-0.1998(13)	0.085(4)*
C11	-0.3040(16)	0.2840(11)	-0.1495(11)	0.083(3)*
C12	-0.4260(14)	0.3115(12)	-0.2212(13)	0.081(3)*
C13	-0.3430(21)	0.2822(13)	-0.3247(12)	0.098(4)*
C14	-0.1584(16)	0.2294(11)	-0.3102(11)	0.084(3)*

^aAnisotropically-refined atoms are marked with an asterisk (*). The form of the anisotropic displacement parameter is: $\exp[-2\pi^2(h^2a^*{}^2U_{11} + k^2b^*{}^2U_{22} + l^2c^*{}^2U_{33} + 2klb^*c^*U_{23} + 2hla^*c^*U_{13} + 2hka^*b^*U_{12})]$. ^bThe rotationally-disordered fluorine atoms were refined with an occupancy factor of 0.5.

Table 5-14. Crystallographic Experimental Details for Compound 13c

Formula	C ₁₉ H ₁₅ F ₆ FeIrO ₅
Formula weight	685.36
Crystal dimensions (mm)	0.21 × 0.20 × 0.08
Crystal system	monoclinic
Space group	<i>P</i> 2 ₁ / <i>n</i> (an alternate setting of <i>P</i> 2 ₁ / <i>c</i> [No. 14])
Unit cell parameters ^a	
<i>a</i> , Å	8.2816 (12)
<i>b</i> , Å	14.195 (2)
<i>c</i> , Å	18.514 (6)
β, deg	96.22 (2)
<i>V</i> , Å ³	2163.7 (9)
<i>Z</i>	4
ρ _{calc} , g cm ⁻³	2.104
μ, mm ⁻¹	6.894
Radiation, λ (Å)	graphite-monochromated Mo Kα (0.71073)
Temperature, °C	-60
Scan type	θ-2θ
Data collection 2θ limit, deg	50.0
Total data collected	3998 (0 ≤ <i>h</i> ≤ 9, 0 ≤ <i>k</i> ≤ 16, -22 ≤ <i>l</i> ≤ 21)
Independent reflections	3736
Number of observations (<i>NO</i>)	2793 (<i>F</i> _o ² ≥ 2σ(<i>F</i> _o ²))
Absorption correction method	semiempirical (ψ scans)
Range of transmission factors	0.8072-0.4305
Data/restraints/parameters	3735 [<i>F</i> _o ² ≥ -3σ(<i>F</i> _o ²)]/0/294
Goodness-of-fit (<i>S</i>) ^b	1.044 [<i>F</i> _o ² ≥ -3σ(<i>F</i> _o ²)]
Final <i>R</i> indices ^c	
<i>F</i> _o ² > 2σ(<i>F</i> _o ²)	<i>R</i> ₁ = 0.0451, <i>wR</i> ₂ = 0.0956
all data	<i>R</i> ₁ = 0.0714, <i>wR</i> ₂ = 0.1075
Largest difference peak and hole 1.737 and -1.404 e Å⁻³	

^aObtained from least-squares refinement of 26 reflections with 25.1° < 2θ < 25.9°.

^b*S* = [Σ*w*(*F*_o² - *F*_c²)²/(*n* - *p*)]^{1/2} (*n* = number of data; *p* = number of parameters varied; *w* = [σ²(*F*_o²) + (0.0576*P*)²]⁻¹ where *P* = [Max(*F*_o², 0) + 2*F*_c²]/3).

^c*R*₁ = Σ||*F*_o|| - ||*F*_c||/Σ||*F*_o||; *wR*₂ = [Σ*w*(*F*_o² - *F*_c²)²/Σ*w*(*F*_o⁴)]^{1/2}.

Table 5-15. Atomic Coordinates and Equivalent Isotropic Displacement Parameters for Compound 13c

Atom	x	y	z	$U_{eq}, \text{\AA}^2$
Ir	0.08687(5)	0.14507(3)	-0.13637(2)	0.02569(13)*
Fe	0.0195(2)	0.32506(10)	-0.10331(8)	0.0329(4)*
F1	0.3864(14)	0.4676(6)	-0.0952(6)	0.132(5)*
F2	0.5373(12)	0.3641(8)	-0.0621(11)	0.206(9)*
F3	0.3787(18)	0.4138(10)	0.0038(6)	0.188(8)*
F4	0.2484(11)	0.2741(6)	0.0613(3)	0.081(3)*
F5	0.2019(14)	0.1332(6)	0.0336(4)	0.119(4)*
F6	0.4288(11)	0.1922(7)	0.0194(4)	0.099(3)*
O1	-0.1509(11)	0.0791(6)	-0.0370(5)	0.067(3)*
O2	-0.2306(10)	0.2870(6)	-0.2236(4)	0.058(2)*
O3	-0.1511(12)	0.2940(7)	0.0287(5)	0.073(3)*
O4	-0.0358(13)	0.5276(6)	-0.1003(6)	0.094(4)*
O5	0.2191(10)	0.3761(5)	-0.2217(4)	0.055(2)*
C1	-0.0565(15)	0.1080(7)	-0.0736(6)	0.042(3)*
C2	-0.1374(14)	0.2963(8)	-0.1740(6)	0.045(3)*
C3	-0.0878(15)	0.3039(9)	-0.0218(7)	0.049(3)*
C4	-0.0110(14)	0.4492(8)	-0.1012(7)	0.053(3)*
C5	0.1847(13)	0.3442(6)	-0.1664(5)	0.034(2)*
C6	0.2734(12)	0.3176(7)	-0.0948(5)	0.033(2)*
C7	0.2122(11)	0.2359(7)	-0.0658(5)	0.030(2)*
C8	0.3936(15)	0.3876(9)	-0.0601(7)	0.049(3)*
C9	0.2686(15)	0.2085(8)	0.0115(6)	0.043(3)*
C10	0.2799(12)	0.1196(7)	-0.2120(6)	0.036(2)*
C11	0.1316(12)	0.1355(7)	-0.2576(5)	0.033(2)*
C12	0.0188(12)	0.0674(7)	-0.2414(5)	0.034(2)*
C13	0.0975(12)	0.0051(7)	-0.1868(5)	0.033(2)*
C14	0.2552(13)	0.0381(7)	-0.1672(6)	0.037(2)*
C15	0.4369(13)	0.1696(8)	-0.2156(7)	0.048(3)*
C16	0.1081(16)	0.2044(9)	-0.3188(5)	0.055(3)*
C17	-0.1498(14)	0.0547(9)	-0.2809(6)	0.057(3)*
C18	0.0193(15)	-0.0842(7)	-0.1597(6)	0.052(3)*
C19	0.3875(14)	-0.0118(8)	-0.1183(6)	0.054(3)*

^aAnisotropically-refined atoms are marked with an asterisk (*). The form of the anisotropic displacement parameter is: $\exp[-2\pi^2(h^2a^2U_{11} + k^2b^2U_{22} + l^2c^2U_{33} + 2klb^*c^*U_{23} + 2hla^*c^*U_{13} + 2hka^*b^*U_{12})]$.

5.7.4. Variable Temperature NMR Studies of Fluxional Processes

Temperature measurements were made with a Bruker B-VT1000 temperature control unit that had been previously calibrated with a Cu-Constantan thermocouple; the temperature at the NMR spectrometer probe is believed to be accurate to ± 2 K. Rate constants for the exchange processes were determined by comparison of computer-simulated and observed spectra. The best fit was determined by minimizing the variance of the calculated difference spectrum. The activation parameters for the dynamic processes studied were obtained by a non-linear least-squares fit to the exponential form of the Eyring equation. Computer simulation and calculation of activation parameters were carried out with local programs written by Professor R.E.D. McClung of this department.

Table 5-16. Summary of the Rate Constants^a for Pair-wise (k_1) and Turnstile(k_2) Carbonyl Scrambling in **12b,c** and **13a-c** as Determined by Spectral Simulation.

T (K) ^b	12b		12c		13a		13b		13c	
	k_1	k_2	k_1	k_2	k_1	k_2	k_1	k_2	k_1	k_2
203	25	—	—	—	—	—	—	—	—	—
213	74	—	—	—	—	—	—	—	—	3.0
223	200	—	—	—	—	—	—	2.8	—	15.5
233	470	—	37.5	—	—	1.2	—	15	—	88
243	1150	—	67	—	—	3.6	—	45	28	260
253	2250	2.0	300 ^c	7.0 ^c	—	13	18	205	110	675
263	4400	5.0	420	14	—	32	66 ^c	435 ^c	300	1500
273	8750	13.5	1000	50	—	97	285	1000	800	2500
283	2x10 ⁴	36	1800	110	5.0	230	750	2050	2000	5500
293	3.6x10 ⁴	77	3750	230	23	525	2000	4700	—	—
303	—	180	—	—	—	—	—	—	—	—
313	—	305	9000	650	—	—	—	—	—	—
323	—	475	—	—	—	—	—	—	—	—
333	—	850	2x10 ⁴	2000	—	—	—	—	—	—

^aThe estimated error in k_i is $\pm 10\%$ and is generally less accurate near the fast exchange limit. ^bThe estimated error in the temperature is ± 2 K (*vide supra*). ^cExcluded from the analysis of the data by least squares regression.

5.7.5. Variable Temperature NMR Reaction Monitoring

Typically, an 18.5 mg (0.056 mmol) sample of **1a** was dissolved in 0.5 mL cold CD₂Cl₂ before being transferred by cannula (pre-cooled with liquid nitrogen) into a serum-sealed NMR tube at -78°C containing a slight excess of the desired organometallic reagent dissolved in 0.2 mL CD₂Cl₂. The tube contents were carefully mixed by shaking while maintaining the NMR tube in the dry-ice acetone bath before being transferred to the NMR spectrometer which was pre-cooled to -80°C. The spectrometer probe was then warmed incrementally and spectra were recorded after each increase in temperature.

CpRhFe(CO)₅(μ-η¹:η¹-C(O)C₂(CF₃)₂) (**14**):

¹³C{¹H} NMR (CD₂Cl₂, 100.6 MHz, ¹³CO enriched, -80°C) δ 216.07 (d, ¹J_{RhC} = 28 Hz, CO_{ac}), 206.51 (s, CO_{Fe}), 206.28 (s, 2CO_{Fe}), 202.22 (d, ¹J_{RhC} = 40 Hz, CO_{Fe}/Rh(av)).

¹⁹F NMR (CD₂Cl₂, 400.1 MHz, -80°C) δ -54.13 (q, ⁵J_{FF} = 13.5 Hz), -58.81 (q, ⁵J_{FF} = 13.5 Hz).

15:

¹³C{¹H} NMR (CD₂Cl₂, 100.6 MHz, ¹³CO enriched, -80°C) δ 205.61 (s, 2CO_{Fe}), 192.21 (d, ¹J_{RhC} = 21 Hz, 2CO_{ac}), and 180.46 (d, ¹J_{RhC} = 82 Hz, CORh).

¹⁹F NMR (CD₂Cl₂, 400.1 MHz, -80°C) δ -56.07 (s).

5.8. References

1. Gagné, M. R.; Takats, J. *Organometallics* **1988**, *7*, 561.
2. Jacke, J.; Gagné, M.; Takats, J. unpublished results.
3. Cooke, J.; Takats, J. *J. Am. Chem. Soc.* **1997**, *119*, 11088.
4. Sweany, R. L. In *Comprehensive Organometallic Chemistry II*; E. W. Abel, F. G. A. Stone and G. Wilkinson, Eds.; Pergamon Press: Oxford, 1995; Vol. 8; pp 98-101.
5. Atwood, J. D. In *Comprehensive Organometallic Chemistry II*; E. W. Abel, F. G. A. Stone and G. Wilkinson, Eds.; Pergamon Press: Oxford, 1995; Vol. 8; pp 324-325.
6. Sharp, P. R. In *Comprehensive Organometallic Chemistry II*; E. W. Abel, F. G. A. Stone and G. Wilkinson, Eds.; Pergamon Press: Oxford, 1995; Vol. 8; pp 236-238.
7. Kruczynski, L.; Takats, J. *Inorg. Chem.* **1976**, *15*, 3140.
8. Washington, J. PhD Thesis, University of Alberta, 1994.
9. Silverstein, R. M.; Bassler, G. C.; Morrill, T. C. *Spectrometric Identification of Organic Compounds*; 5th ed.; Wiley: New York, 1991, pp 174, 239.
10. Corrigan, P. A.; Dickson, R. S. *Aust. J. Chem.* **1979**, *32*, 2147.
11. Guggolz, E.; Ziegler, M. L.; Kalcher, W.; Plank, J.; Riedel, D.; Herrmann, W. A. *Z. Naturforsch* **1981**, *36b*, 1053.
12. Cotton, F. A. *Prog. Inorg. Chem.* **1976**, *21*, 1.
13. Colton, R.; McCormick, M. J. *Coord. Chem. Rev.* **1980**, *31*, 1.
14. Band, E.; Muetterties, E. L. *Chem. Rev.* **1978**, *6*, 639.
15. Mann, B. E.; Taylor, B. F. *¹³C NMR Data for Organometallic Compounds*; Academic: New York, 1981, pp 2-5, 23 and 166-176.
16. Day, V.; Gagné, M.; Takats, J. unpublished results.
17. Jacke, J.; Santarsiero, B. D.; Takats, J. unpublished results.
18. Jenkins, J. A.; Cowie, M. *Organometallics* **1992**, *11*, 2774 and references therein.
19. Cooke, J.; McDonald, R.; Takats, J. unpublished results.
20. Crespi, A. M.; Sabat, M.; Shriver, D. F. *Inorg. Chem.* **1988**, *27*, 812.

21. Rausch, M. D.; Gastinger, R. G.; Gardner, S. A.; Brown, R. K.; Wood, J. S. *J. Am. Chem. Soc.* **1977**, *99*, 7870.
22. Krüger, C.; Barnett, B. L.; Brauer, D. In *The Organic Chemistry of Iron*; E. A. Koerner von Gustorf, F.-W. Grevels and I. Fischler, Eds.; Academic Press: New York, 1978; Vol. I; pp 4.
23. Bennett, M. J.; Graham, W. A. G.; Stewart, R. P.; Tuggle, R. M. *Inorg. Chem.* **1973**, *12*, 2944.
24. Marinelli, G.; Streib, W.; Huffman, J. C.; Caulton, K. G.; Gagné, M. R.; Takats, J.; Dartiguenave, M. *Polyhedron* **1990**, *9*, 1867.
25. Dickson, R. S.; Gatehouse, B. M.; Nesbit, M. C.; Pain, G. N. *J. Organomet. Chem.* **1981**, *215*, 97.
26. Dyke, A. F.; Knox, S. A. R.; Naish, P. J.; Taylor, G. E. *J. Chem. Soc., Chem. Commun.* **1980**, 409.
27. Dyke, A. F.; Knox, S. A. R.; Naish, P.; Taylor, G. E. *J. Chem. Soc., Dalton Trans.* **1982**, 1297.
28. Gracey, B. P.; Knox, S. A. R.; Macpherson, K. A.; Orpen, A. G.; Stobart, S. R. *J. Chem. Soc., Dalton Trans.* **1985**, 1935.
29. Otto, H.; Garcia Alonso, F. G.; Werner, H. *J. Organomet. Chem.* **1986**, *306*, C13.
30. Fontaine, X. L. R.; Jacobson, G. B.; Shaw, B. L.; Thornton-Pett, M. *J. Chem. Soc., Chem. Commun.* **1987**, 662.
31. Fontaine, X. L. R.; Jacobsen, G. B.; Shaw, B. L.; Thornton-Pett, M. *J. Chem. Soc., Dalton Trans.* **1988**, 741.
32. Hogarth, G.; Knox, S. A. R.; Lloyd, B. R.; Macpherson, K. A.; Morton, D. A. V.; Orpen, A. G. *J. Chem. Soc., Chem. Commun.* **1988**, 360.
33. Knox, S. A. R.; Lloyd, B. R.; Morton, D. A. V.; Orpen, A. G.; Turner, M. L.; Hogarth, G. *Polyhedron* **1995**, *14*, 2723.
34. Karel, K. J.; Tulip, T. H.; Ittel, S. D. *Organometallics* **1990**, *9*, 1276.
35. Hoffman, K.; Weiss, E. *J. Organomet. Chem.* **1977**, *128*, 399.
36. Aime, S.; Milone, L.; Sappa, E. *J. Chem. Soc. Dalton Trans.* **1979**, 1664.
37. Allen, F. H.; Kennard, O.; Watson, D. G.; Brammer, L.; Orpen, A. G.; Taylor, R. *J. Chem. Soc., Perkin Trans. II* **1987**, S1.

38. Crabtree, R. H. *The Organometallic Chemistry of the Transition Metals*; 2nd ed.; John Wiley & Sons: New York, 1994, pp 6.
39. Lawson, R. J.; Shapley, J. R. *Inorg. Chem.* **1978**, *17*, 2963.
40. Takats, J.; Washington, J.; Santarsiero, B. *Organometallics* **1994**, *13*, 1078.
41. Hoffman, K. MSc. Thesis, University of Alberta, 1994.
42. Adams, R. D.; Cotton, F. A. *J. Am. Chem. Soc.* **1973**, *95*, 6589.
43. Cotton, F. A.; Hunter, D. L. *Inorg. Chem. Acta* **1974**, *11*, L9.
44. Washington, J.; Takats, J. *Organometallics* **1990**, *9*, 925 and references therein.
45. Cooke, J.; Takats, J. *Organometallics* **1995**, *14*, 698.
46. Kruczynski, L.; LiShingMan, L. K. K.; Takats, J. *J. Am. Chem. Soc.* **1974**, *96*, 4006.
47. Wilson, S. T.; Coville, N. J.; Shapely, J. R.; Osborn, J. A. *J. Am. Chem. Soc.* **1974**, *96*, 4038.
48. Casey, C. P.; Cariño, R. S.; Hayashi, R. K.; Schladetzky, K. D. *J. Am. Chem. Soc.* **1996**, *118*, 1617.
49. Casey, C. P.; Boese, W. T.; Cariño, R. S.; Ford, P. C. *Organometallics* **1996**, *15*, 2189.
50. Sandström, J. *Dynamic NMR Spectroscopy*; Academic Press: London, 1982, Chp 7.
51. Riesen, A.; Einstein, F. W. B.; Ma, A. K.; Pomeroy, R. K.; Shipley, J. A. *Organometallics* **1991**, *10*, 3629.
52. Ball, R. G.; Edelmann, F.; Kiel, G.-Y.; Takats, J. *Organometallics* **1986**, *5*, 833.
53. Edelmann, F.; Takats, J. *J. Organomet. Chem.* **1988**, *344*, 351.
54. Astley, S. T.; Takats, J. *J. Organomet. Chem.* **1989**, *363*, 167.
55. Alex, R. F.; Pomeroy, R. K. *Organometallics* **1987**, *6*, 2437.
56. Collman, J. P.; Hegedus, L. S. *Principles and Applications of Organotransition Metal Chemistry*; University Science Books: Mill Valley, 1980, pp 286-288.
57. Einstein, F. W. B.; Pomeroy, R. K.; Rushman, P.; Willis, A. C. *Organometallics* **1985**, *4*, 250.

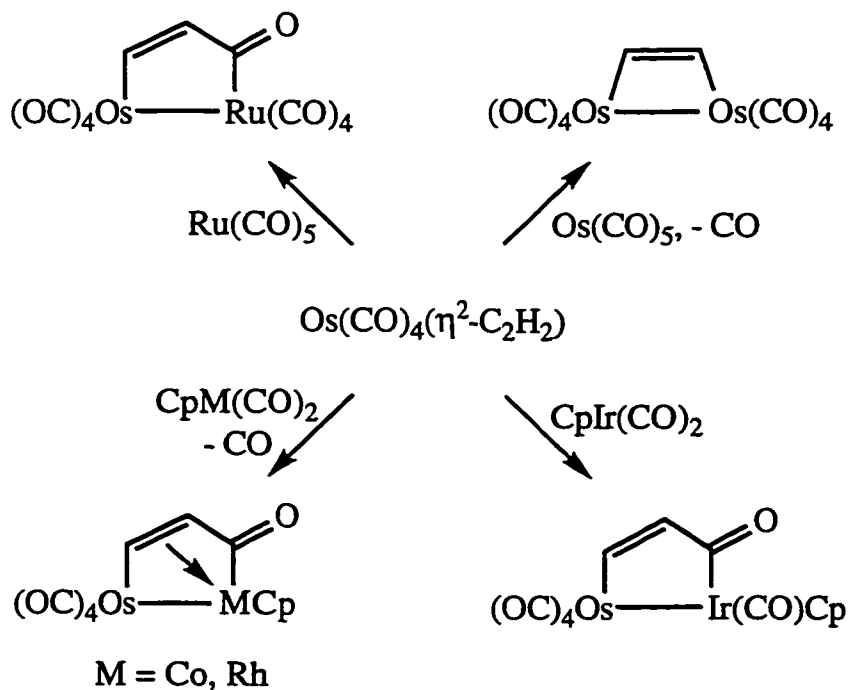
58. Johnson, K. A.; Gladfelter, W. L. *Organometallics* **1992**, *11*, 2534.
59. Mao, T. PhD Thesis, University of Alberta, 1996.
60. Johnson, K. A.; Gladfelter, W. L. *J. Am. Chem. Soc.* **1991**, *113*, 5097.
61. Mirza, H. A.; Vittal, J. J.; Puddephatt, R. J. *Organometallics* **1994**, *13*, 3063.
62. Casey, C. P.; Cariño, R. S.; Sakaba, H.; Hayashi, R. K. *Organometallics* **1996**, *15*, 2640.
63. Casey, C. P.; Cariño, R. S.; Sakaba, H. *Organometallics* **1997**, *16*, 419.
64. Einstein, F. W. B.; Pomeroy, R. K.; Rushman, P.; Willis, A. *J. Chem. Soc., Chem. Commun.* **1983**, 854.
65. Davis, H. B.; Einstein, F. W. B.; Glavina, P. G.; Jones, T.; Pomeroy, R. K.; Rushman, P. *Organometallics* **1989**, *8*, 1030.
66. Einstein, F. W. B.; Jones, T.; Pomeroy, R. K.; Rushman, P. *J. Am. Chem. Soc.* **1984**, *106*, 2707.
67. Dickson, R. S.; Tailby, G. R. *Aust. J. Chem.* **1970**, *23*, 1531.
68. Warner, S. A.; Andrews, P. S.; Rausch, M. D. *Inorg. Chem.* **1973**, *12*, 2396.
69. Frith, S. A.; Spencer, J. L. *Inorg. Synth.* **1985**, *23*, 15.
70. Werner, H.; Klingert, B. *J. Organomet. Chem.* **1981**, *218*, 395.
71. Ball, R. G.; Graham, W. A. G.; Heinekey, D. M.; Hoyano, J. K.; McMaster, A. D.; Mattson, B. M.; Michel, S. T. *Inorg. Chem.* **1990**, *29*, 2023.
72. Programs for diffractometer operation, data collection, data reduction, and absorption correction were those supplied by Siemens.
73. Sheldrick, G. M. *Acta Crystallogr.* **1990**, *A46*, 467.
74. Sheldrick, G.M. *SHELXL-93*. Program for crystal structure determination. University of Göttingen, Germany, 1993.

Chapter 6

**Reaction of $\text{Fe}(\text{CO})_4(\eta^2\text{-C}_2\text{H}_2)$ with $\text{Cp}'\text{M}(\text{CO})_2$ ($\text{M} = \text{Co}, \text{Rh}, \text{Ir}$;
 $\text{Cp}' = \text{Cp}, \text{Cp}^*$): Formation of Dimetallacyclopentenones**

6.1. Introduction

The previous chapter described the facile reaction of $\text{Fe}(\text{CO})_4(\eta^2\text{-HFB})$ (1a) with $\text{Cp}'\text{M}(\text{CO})_2$ ($\text{M} = \text{Co}, \text{Rh}, \text{Ir}$; $\text{Cp}' = \text{Cp}, \text{Cp}^*$) to produce heterobimetallic products. The compounds had surprisingly flexible structural characteristics which went beyond the simple dimetallacyclobutenes afforded by the heavier Ru and Os congeners.¹ The reactivity of $\text{M}(\text{CO})_4(\eta^2\text{-alkyne})$ compounds towards other late transition metal species is not limited to the thermally stable HFB derivatives, and although $\text{Ru}(\text{CO})_4(\eta^2\text{-C}_2\text{H}_2)$ is too thermally unstable to be used in such syntheses, its Os congener produces a variety of compounds, ranging from diosmacyclobutene to heterodimetallacyclopentenones, in reaction with $\text{M}'(\text{CO})_5$ ($\text{M}' = \text{Ru}, \text{Os}$) and $\text{CpM}(\text{CO})_2$ ($\text{M} = \text{Co}, \text{Rh}, \text{Ir}$) (Scheme 6-1).²



Scheme 6-1. Reaction of $\text{Os}(\text{CO})_4(\eta^2\text{-C}_2\text{H}_2)$ with Organometallic Reagents.

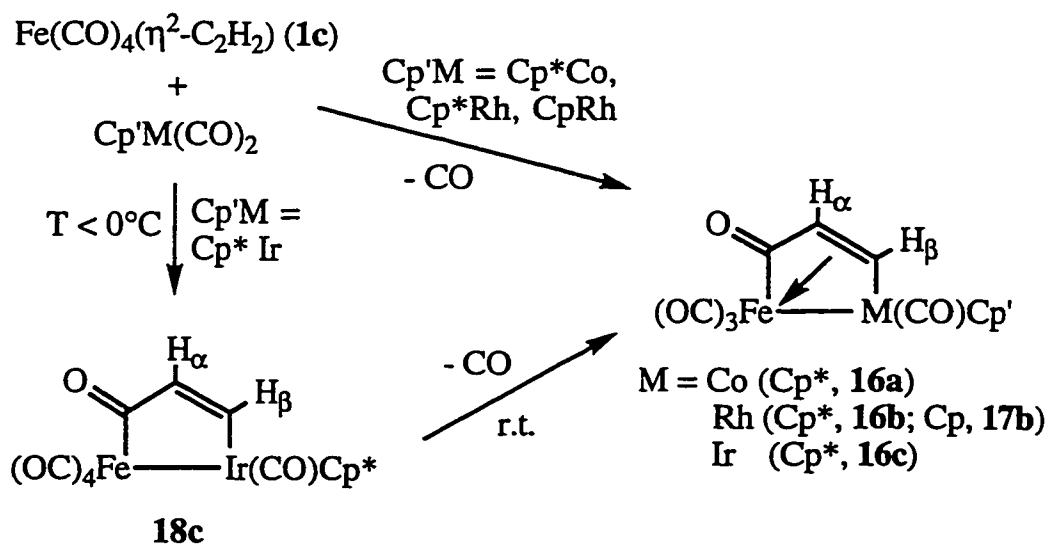
The most interesting compounds are the RuOs and OsIr μ - $\eta^1:\eta^1$ -dimetallacyclopentenones which are thermodynamically stable and form without net ligand loss from the reactants. In contrast, an analogous compound **14** forms initially in the reaction of **1a** with $\text{CpRh}(\text{CO})_2$ in CD_2Cl_2 , but subsequently converts to the stable alkyne-bridged compound **12b** (Chapter 5).

In light of the profound difference in reactivity of $\text{Os}(\text{CO})_4(\eta^2\text{-C}_2\text{H}_2)$ compared with its HFB analog (Eq. 5-1) and, given the interesting structural variety already afforded by the reaction of **1a** with $\text{Cp}'\text{M}(\text{CO})_2$, the bimetallic compounds available from $\text{Fe}(\text{CO})_4(\eta^2\text{-C}_2\text{H}_2)$ (**1c**) were investigated. A preliminary account of this study has been published.³

6.2. Reaction of **1c** with $\text{Cp}'\text{M}(\text{CO})_2$ ($\text{M} = \text{Co}, \text{Rh}, \text{Ir}$; $\text{Cp}' = \text{Cp}, \text{Cp}^*$)

6.2.1. Synthetic Aspects

As was the case for its HFB cousin, **1c** decomposed in the presence of $\text{M}'(\text{CO})_5$ ($\text{M}' = \text{Fe}, \text{Ru}, \text{Os}$) and did not produce tractable heterobimetallic products. However, facile reactions occurred at low temperature with the complete triad of $\text{Cp}^*\text{M}(\text{CO})_2$ ($\text{M} = \text{Co}, \text{Rh}, \text{Ir}$) reagents to produce thermally stable dimetallacyclopentenones, **16a-c** (Scheme 6-2).



Scheme 6-2. Reaction of $\text{Fe}(\text{CO})_4(\eta^2\text{-C}_2\text{H}_2)$ (**1c**) with $\text{Cp}'\text{M}(\text{CO})_2$.

Compounds **16a-c** had fairly low solubilities in hydrocarbon solvents and were easily separated from excess $\text{Cp}^*\text{M}(\text{CO})_2$ which remained in solution. In the case of $\text{Cp}^*\text{Ir}(\text{CO})_2$, a kinetic product **18c** could be isolated provided that the solution temperature was kept below *ca.* 0°C , as conversion to the thermodynamic product **16c** occurred above ice temperature.

As with **1a**, the $\text{CpM}(\text{CO})_2$ species were less reactive than their Cp^* congeners. When combined with the thermal instability of **1c** above 0°C , the result was that only the most reactive member, $\text{CpRh}(\text{CO})_2$, provided a heterobimetallic product, **17b**. In contrast, **1c** decomposed completely in the presence of $\text{CpCo}(\text{CO})_2$ and $\text{CpIr}(\text{CO})_2$, and the group 9 reagents were recovered quantitatively from the intractable decomposition products. This behavior roughly mirrors that of $\text{Os}(\text{CO})_4(\eta^2\text{-TFP})$, where $\text{Cp}^*\text{M}(\text{CO})_2$ ($\text{M} = \text{Co}, \text{Rh}, \text{Ir}$) gives stable products but only $\text{CpRh}(\text{CO})_2$ reacts from the $\text{CpM}(\text{CO})_2$ series.⁴ Conversely, $\text{Os}(\text{CO})_4(\eta^2\text{-C}_2\text{H}_2)$ reacts smoothly with $\text{CpM}(\text{CO})_2$ ($\text{M} = \text{Co}, \text{Rh}, \text{Ir}$)² but provides more complicated product distributions with the Cp^* reagents.⁵

Despite undergoing reactions which are superficially similar to those of $\text{Os}(\text{CO})_4(\eta^2\text{-C}_2\text{H}_2)$, several factors initially distinguish the reactivity of **1c** from its osmium counterpart. Firstly, $\text{Os}(\text{CO})_4(\eta^2\text{-C}_2\text{H}_2)$ reacts with $\text{CpM}(\text{CO})_2$ to produce CO insertion exclusively at the group 9 metal.² In contrast, **1c** produces the opposite sense of CO insertion with the acyl group bonded to the iron center, as is found in other reported heterobimetallic FeM ($\text{M} = \text{Ru},^6 \text{Rh},^7 \text{Pt}^{8,9}$) dimetallacyclopentenones. Secondly, while $\text{Os}(\text{CO})_4(\eta^2\text{-C}_2\text{H}_2)$ and $\text{CpIr}(\text{CO})_2$ form the stable $\text{Os}(\text{CO})_4\text{Ir}(\text{CO})\text{Cp}(\mu\text{-}\eta^1\text{:}\eta^1\text{-C}_2\text{H}_2\text{C}(\text{O}))$, **18c** readily loses a carbonyl to form **16c**.

6.2.2. Spectroscopic Characterization of **16a-c**

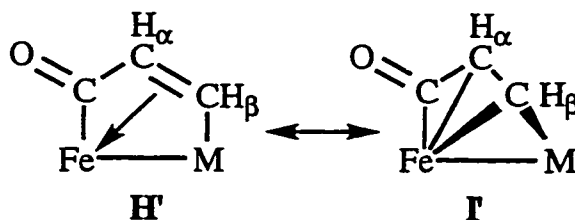
Elemental analysis and mass spectrometry provided molecular compositions $\text{Cp}^*\text{MFe}(\text{CO})_5(\text{C}_2\text{H}_2)$ for compounds **16a-c**. The ^1H and ^{13}C NMR spectra (Table 6-1) show two signals, widely separated in chemical shift, for the C_2H_2 moiety and thus confirm $\mu\text{-}\eta^1\text{:}\eta^3$ -dimetallacyclopentenone formulations analogous to **13a-c**.

Table 6-1. ^1H and $^{13}\text{C}\{^1\text{H}\}$ NMR Spectra of the C_2H_2 Moiety in **16a-c** and Representative $\text{MM}'\text{L}_n(\mu\text{-}\eta^1\text{:}\eta^3\text{-C}_2\text{H}_2\text{C(O)})$ Species.

$\text{MM}'\text{L}_n$	$\delta(\text{H}_\beta)$	$\delta(\text{H}_\alpha)$	$\delta(\text{C}_\beta)$	$\delta(\text{C}_\alpha)$
$\text{Cp}^*\text{CoFe}(\text{CO})_4$ (16a) ^a	9.56 ^b	3.42 ^b	176.00	40.77
$\text{Cp}^*\text{RhFe}(\text{CO})_4$ (16b) ^a	9.22 ^{b,c}	3.68 ^{b,d}	169.75 ^e	41.16
$\text{Cp}^*\text{IrFe}(\text{CO})_4$ (16c) ^a	8.73 ^b	4.65 ^b	139.21	41.35
$\text{Fe}_2(\text{CO})_5(\mu\text{-dppm})^{10}$	8.63	3.63	168.4	44.8
$(\text{Ph}_3\text{P})\text{PtFe}(\text{CO})_2(\mu\text{-dppm})^9$	8.28	3.98	—	—
$\text{Cp}_2\text{Fe}_2(\text{CO})(\mu\text{-CO})^{11}$	12.45	2.44	181.0	13.2

^aRecorded in CD_2Cl_2 ; ^1H at r.t.; $^{13}\text{C}\{^1\text{H}\}$ at -60°C . ^bdoublet, $^3J_{\text{HH}} = 6.5$ Hz. ^cadditional coupling $^2J_{\text{RhH}} = 3.5$ Hz. ^dadditional coupling $^3J_{\text{RhH}} = 4.5$ Hz. ^edoublet, $^1J_{\text{RhC}} = 34$ Hz.

In both the ^1H and ^{13}C NMR spectra, the upfield CH resonance is typical of a coordinated olefin and the downfield partner resembles a μ -alkylidene in resonance structure **I'** (Scheme 6-3).¹²



Scheme 6-3. Two Resonance Structures Describing the Bonding of the $\mu\text{-}\eta^1\text{:}\eta^3$ -Dimetallacyclopentenone Ring Systems in **16a-c**.

In accord with the proposed orientation of the bridging ring system, the C_α resonance is found at virtually the same position in **16a-c**, indicating that it has the same chemical environment regardless of the nature of M. On the other hand, the bridging carbon, C_β , shows a marked dependence on the group 9 metal center to which it is attached, and appears as a doublet in **16b**, $^1J_{\text{RhC}} = 34$ Hz. The trend for δC_β , $\text{Co} > \text{Rh} > \text{Ir}$, is as expected based on well preceded triad variation in ^{13}C chemical shift.¹³

Two trends are apparent in the ^1H NMR spectra. Both the H_α and H_β chemical shifts vary with M according to δH_α , $\text{Co} < \text{Rh} < \text{Ir}$ and δH_β , $\text{Co} > \text{Rh} > \text{Ir}$. Together, the trends suggest a dominant contribution from resonance form **I'** for the FeCo compound (**16a**) because δH_α will shift further upfield with stronger coordination of the olefin moiety and δH_β will shift further downfield as the alkylidene character increases in the bridging carbon. Conversely, the downfield shift of δH_α and upfield shift of δH_β in the FeIr species (**16c**) indicates a more significant contribution from **H'** in this compound. This feature is in line with the isolation of **18c** prior to **16c** as the olefin moiety is less strongly bonded to the Fe center in **16c** than in the FeCo and FeRh analogs. Additionally, it is interesting that $^3J_{\text{RhH}_\alpha} > ^2J_{\text{RhH}_\beta}$ in **16b**, as large $^2J_{\text{RhH}_\beta}$ values (19 Hz) were observed in $\text{CpRh}(\text{PR}_3)\text{Os}(\text{CO})_3(\mu\text{-}\eta^1\text{:}\eta^3\text{-C}_2\text{H}_2\text{C}(\text{O}))$ with smaller $^3J_{\text{RhH}_\alpha}$ (6 Hz).⁴ However, in $\text{Os}(\text{CO})_4\text{RhCp}(\mu\text{-}\eta^1\text{:}\eta^3\text{-C}_2\text{H}_2\text{C}(\text{O}))$, a compound where the orientation of the bridging moiety is opposite to that predicted currently, $^2J_{\text{RhH}_\beta}$ was not observed but $^2J_{\text{RhH}_\alpha}$ was 3.0 Hz.² It would thus appear that the variation of the rhodium-hydrogen coupling constant with structural changes is not reliable for the assignment of the orientation of the organic ring fragment with respect to the two metals.

To further corroborate the structural proposal, $^{13}\text{C}\{^1\text{H}\}$ NMR spectra of the carbonyl region were collected at the low temperature limit (Table 6-2).

Table 6-2. Limiting $^{13}\text{C}\{^1\text{H}\}$ NMR Spectra^a of **16a-c** in the Carbonyl Region.

	M	$\delta(\text{CO}_{\text{ac}})$	$\delta(\text{CO}_{\text{Fe}})$	$\delta(\text{CO}_{\text{M}})$
16a	Co	233.89	218.63, 213.81, 206.87	202.4 ^b
16b	Rh	234.06	216.65, 214.65, 207.13	189.86 ^c
16c	Ir	236.56	215.30, 214.38, 207.03	173.60

^aRecorded in CD_2Cl_2 at -60°C . ^bBroad. ^cdoublet, $^1J_{\text{RhC}} = 86$ Hz.

The orientation of the bridging moiety predicted in Scheme 6-2 is clearly established by the presence of a far downfield singlet for the acyl group attached to the Fe center.^{6,11} Also, a characteristic doublet resonance ($^1J_{\text{RhC}} = 86$ Hz) was observed for the terminal Rh-CO in **16b**. The chemical shift of the Ir-bonded

carbonyl is similarly diagnostic in **16c**, as is the broadened nature of the Co-bonded carbonyl due to quadrupolar interactions in **16a**.¹³

Bearing in mind the complexities of the IR spectra in **13a-c**, it was not surprising that the FT-IR spectra of **16a-c** showed more than the anticipated four terminal and single acyl carbonyl stretching bands (Table 6-3).

Table 6-3. FT-IR Spectra (CH₂Cl₂, cm⁻¹) of **16a-c**.

	νCO		νacyl
16a	2030(s), 1996(vs), 1963(m), 1940(sh)	1816(vw)	1744(m)
16b	2032(s), 2004(vs), 1961(s), 1936(m)	1812(w, br)	1742(m)
16c	2029(s), 1989(vs), 1963(s), 1941(sh)	1826(vw)	1750(m), 1728(w)

In fact, such features are quite common in $\mu\text{-}\eta^1\text{:}\eta^3$ -dimetallacyclopentenones derived from iron.^{6,10,11} Nonetheless, the infrared spectra of the three species are quite similar, suggesting that the nature of the heterobimetallic bond has little effect on the carbonyl stretching frequencies. The presence of additional weak bands in the bridging carbonyl region of the spectrum initially suggests that minor isomers analogous to Cp**M*Fe(CO)₃($\mu\text{-CO}$)₂($\mu\text{-}\eta^1\text{:}\eta^1$ -HFB) (**G**) might be present in solution. Further discussion of this possibility is deferred to Section 6.2.4.

6.2.3. Molecular Structure of Cp*RhFe(CO)₄($\mu\text{-}\eta^1\text{:}\eta^3$ -C₂H₂C(O)), **16b**

Although the spectroscopic data readily define the solution structures of **16a-c**, crystals of the FeRh compound were easily obtained and an X-ray diffraction study was performed. The molecular structure of **16b** is presented in Figure 6-1, and selected interatomic distances and angles are provided in Tables 6-4 and 6-5. The structure bears a close resemblance to **13c** which was discussed in detail in Chapter 5, with the exception that the Cp* ring is found on the same side of the molecule as the bridging carbon, C(7). Presumably, the lack of a substituent on C(7) in **16b** renders this the sterically favored orientation.

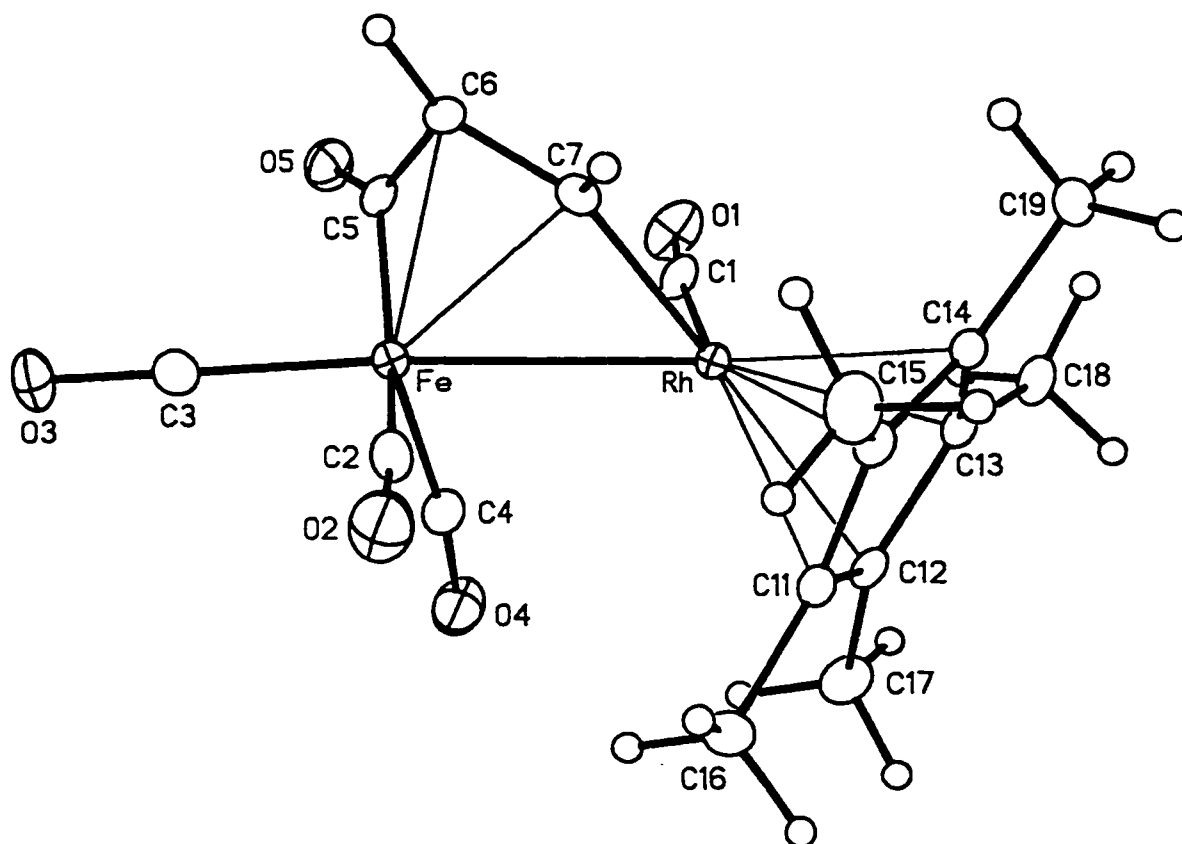


Figure 6-1. Molecular Structure of Compound **16b**.

Table 6-4. Selected Interatomic Distances (Å) in Compound **16b**.

Fe–Rh	2.6806(7)	Fe–C(7)	2.095(4)
Rh–C(1)	1.866(5)	C(1)–O(1)	1.137(5)
Rh–C(7)	2.011(4)	C(2)–O(2)	1.142(6)
Fe–C(2)	1.831(5)	C(3)–O(3)	1.152(6)
Fe–C(3)	1.769(5)	C(4)–O(4)	1.136(6)
Fe–C(4)	1.781(5)	C(5)–O(5)	1.199(5)
Fe–C(5)	1.936(4)	C(5)–C(6)	1.437(6)
Fe–C(6)	2.125(4)	C(6)–C(7)	1.393(6)

Table 6-5. Selected Interatomic Angles (deg.) in Compound **16b**.

Fe–Rh–C(1)	92.55(13)	C(2)–Fe–C(3)	92.9(2)
Fe–Rh–C(7)	50.62(11)	C(2)–Fe–C(4)	103.5(2)
Rh–Fe–C(2)	96.41(14)	C(2)–Fe–C(5)	155.5(2)
Rh–Fe–C(3)	167.4(2)	C(2)–Fe–C(6)	116.4(2)
Rh–Fe–C(4)	70.75(15)	C(2)–Fe–C(7)	92.8(2)
Rh–Fe–C(5)	88.23(12)	C(3)–Fe–C(4)	98.9(2)
Rh–Fe–C(6)	77.92(11)	C(3)–Fe–C(5)	86.8(2)
Rh–Fe–C(7)	47.90(11)	C(3)–Fe–C(6)	105.4(2)
Rh–C(7)–C(6)	126.5(3)	C(3)–Fe–C(7)	140.1(2)
Rh–C(1)–O(1)	173.6(4)	C(4)–Fe–C(5)	100.7(2)
Fe–C(2)–O(2)	175.7(4)	C(4)–Fe–C(6)	131.3(2)
Fe–C(3)–O(3)	178.1(5)	C(4)–Fe–C(7)	117.9(2)
Fe–C(4)–O(4)	172.7(4)	C(5)–Fe–C(6)	41.1(2)
Fe–C(5)–O(5)	144.1(3)	C(5)–Fe–C(7)	72.6(2)
Fe–C(5)–C(6)	76.5(3)	C(6)–Fe–C(7)	38.5(2)
Fe–C(6)–C(7)	69.6(2)	C(1)–Rh–C(7)	93.5(2)
Fe–C(7)–C(6)	71.9(2)	C(5)–C(6)–C(7)	115.2(3)
Fe–C(7)–Rh	81.49(14)	O(5)–C(5)–C(6)	138.3(4)

The Fe–Rh bond length, 2.6806(7) Å, is 0.02 Å shorter than in CpRh(P^{*i*}Pr)₃Fe(CO)₃(μ-η¹:η³-CHCPhC(O)) (2.698(1) Å),⁷ but longer than in CpRh(P^{*i*}Pr)₃Fe(CO)₃(μ-CO)(μ-C=CH₂) (2.604(1) Å).¹⁴ The metal-metal separation is significantly shorter than is found in the family of μ-C_nH_n (n = 7, 8) iron/rhodium compounds which range from 2.7638(7) Å in (μ-C₇H₇)FeRh(CO)₄¹⁵ to 2.907(1) Å in [(μ-C₈H₈)FeRh(CO)₃(C₇H₈)]BF₄,¹⁶ although the bonding requirements of the bridging C_nH_n ligand are believed to play a significant role in determining the metal-metal separation in these complexes.¹⁷ The Rh–C(7) bond distance, 2.011(4) Å, is slightly longer than that in CpRh(PMe₂Ph)Os(CO)₃(μ-η¹:η³-C₂H₂C(O)) (1.98(1) Å),⁴ but identical to the distances between the Rh center and the bridging alkylidene carbons in

$\text{CpRh}(\text{P}^i\text{Pr}_3)\text{Fe}(\text{CO})_3(\mu\text{-}\eta^1\text{:}\eta^3\text{-CHCPhC(O)})$ (2.016(6) Å)⁷ and $\text{CpRh}(\text{P}^i\text{Pr}_3)\text{Fe}(\text{CO})_3(\mu\text{-CO})(\mu\text{-C=CH}_2)$ (2.011(3) Å).¹⁴

As in **13c**, the unsaturated organic fragment has short Fe–C(6) and Fe–C(7) contacts which comparable well with those in other iron-containing $\mu\text{-}\eta^1\text{:}\eta^3$ -dimetallacyclopentenones (Table 6-6).

Table 6-6. Comparison of Metrical Parameters in $\text{MM}'\text{L}_n(\mu\text{-}\eta^1\text{:}\eta^3\text{-C}_2\text{R}_2\text{C(O)})$.

	Fe–C(5)	Fe–C(6)	Fe–C(7)	C(5)–C(6)	C(6)–C(7)	O(5)–C(5)–C(6)
16b	1.936(4)	2.125(4)	2.095(4)	1.437(6)	1.393(6)	138.3(4)
Fe_2^{a}	1.928(3)	2.111(3)	2.084(3)	1.447(5)	1.396(5)	138.3(3)
PtFe^{b}	1.913(9)	2.095(9)	2.114(9)	1.451(12)	1.408(12)	135.3(7)
RhFe^{c}	1.957(7)	2.124(5)	2.063(6)	1.469(8)	1.393(9)	138.6(6)
13c	1.913(11)	2.094(10)	2.096(9)	1.493(13)	1.396(13)	136.5(10)

^a $\text{Fe}_2(\text{CO})_5(\mu\text{-dppm})(\mu\text{-}\eta^1\text{:}\eta^3\text{-C}_2\text{H}_2\text{C(O)})$, Ref. 10. ^b $(\text{Ph}_3\text{P})\text{PtFe}(\text{CO})_2(\mu\text{-dppm})(\mu\text{-}\eta^1\text{:}\eta^3\text{-C}_2\text{H}_2\text{C(O)})$, Ref. 9. ^c $\text{CpRh}(\text{P}^i\text{Pr}_3)\text{Fe}(\text{CO})_3(\mu\text{-}\eta^1\text{:}\eta^3\text{-CHCPhC(O)})$, Ref. 7.

Indeed, there are no significant differences in the metrical parameters among the three examples in which a $(\mu\text{-}\eta^1\text{:}\eta^3\text{-C}_2\text{H}_2\text{C(O)})$ ring system is bonded to an Fe center. Compared with the more π -acidic bridging moieties in $\text{CpRh}(\text{P}^i\text{Pr}_3)\text{Fe}(\text{CO})_3(\mu\text{-}\eta^1\text{:}\eta^3\text{-CHCPhC(O)})$ and **13c**, the most significant differences lie in the C(5)–C(6) bond length which is some 0.03 - 0.055 Å shorter in **16b**, perhaps suggesting more ketene character (resonance structure **J** in Scheme 5-3). Interestingly, the C(6)–C(7) distances are identical despite the significant difference in substituents.

The general similarity of the bonding of the bridging moiety in **16b** and **13c** is further reflected in the similar geometries of the two Fe centers which show only minor differences in internuclear angles and interatomic distances. However, one source of differentiation between the two structures is in the parameters which involve the group 9 metal. The M–C(7)–C(6) and M–Fe–C(5) angles differ, being some 9° more acute in **13c**. This initially suggests a slight difference in the orientation of the bridging organic moiety with respect to the metal-metal bond, which is also reflected in the M–Fe–C(6)–C(5) torsion angles, 90.5(5) and

101.4(2)° in **13c** and **16b**, respectively. Thus, the C(6)–C(5) bond lies perpendicular to the metal-metal bond in **13c**, but is skewed roughly 10° from perpendicularity in **16b**. This subtle change in the orientation of the bridging moiety may be brought about by steric interaction of the trifluoromethyl group on C(7) with the methyl groups of the Cp* ring in **13c**, which causes the bridging moiety to realign itself above the iron center to compensate.

The general coordination geometry about Fe is also similar to that in CpRh(P^{*i*}Pr₃)Fe(CO)₃(μ-η¹:η³-CHCPhC(O)) with the important exception that the carbonyl corresponding to C(4)O(4) was characterized as semibridging in this compound, with an Rh–C(O) distance of 2.569(7) Å and a non-linear Fe–C–O angle of 166.5(6)°. ⁷ However, the Fe–C(4)–O(4) angle in **16b**, 172.7(4)°, is not overly skewed from linearity and compares with the Rh–C(1)–O(1) angle, 173.6(4)°. Also, the Rh–C(4) separation, 2.685(5) Å, is 0.12 Å longer in **16b**. The lack of a significant interaction is also reflected in the ¹³C NMR spectrum where there was no evidence of coupling between any of the Fe-bonded carbonyls and rhodium. The fact that the analogous carbonyl in CpRh(P^{*i*}Pr₃)Fe(CO)₃(μ-η¹:η³-CHCPhC(O)) appears to have slight semibridging character can be traced to the greater electron density at Rh in this species, afforded by the presence of a strongly donating phosphine ligand. However, Rh coupling was also not detected in the ¹³C NMR spectrum of this compound, but this may be due to the fact that the spectrum was collected at ambient temperature where the iron carbonyls were rapidly exchanging. ⁷

6.2.4. Characterization of **17b**: Detection of an Isomeric Pair Related by the Orientation of Ligands on the Ancillary Metal Center

The product from the reaction of **1c** and CpRh(CO)₂ (**17b**) had the molecular composition CpRhFe(CO)₅(C₂H₂), and the FT-IR spectrum showed some of the same complications as its Cp* congener. Five terminal carbonyl stretches were observed along with two weaker bands of approximately the same intensity in the bridging/acyl region of the spectrum. Surprisingly, two sets of resonances were observed in the ¹H NMR spectrum in a *ca.* 2:1 ratio. Each set consisted of a downfield doublet of doublets, a Cp singlet, and an upfield doublet

of doublets, indicating that two isomeric dimetallacyclopentenones were present (Table 6-7). The isomers appeared in a 2:1 ratio in CD_2Cl_2 , but had roughly equal concentrations in toluene-*d*₈.

Table 6-7. Selected ^1H and $^{13}\text{C}\{^1\text{H}\}$ NMR Data for **17b/b'** and **16b**.^a

	$\delta(\text{H}_\beta)$	$\delta(\text{H}_\alpha)$	$\delta(\text{C}_\beta)$	$\delta(\text{C}_\alpha)$	$\delta(\text{CO}_{\text{ac}})$	$\delta(\text{CO}_{\text{Rh}})$
17b	10.17 ^{b,c}	3.79 ^d	165.09 ^e	41.17	233.46	187.88 ^f
17b'	9.42 ^{b,g}	3.79 ^d	158.23 ^e	45.29	230.34	187.46 ^f
16b	9.22 ^{b,c}	3.68 ^{c,h}	169.75 ^e	41.16	234.06	189.86 ^f

^aIn CD_2Cl_2 . ^bdoublet, $^3J_{\text{HH}} = 6.5$ Hz. ^cdoublet, $^2J_{\text{RhH}} = 3.5$ Hz. ^dmultiplet. ^edoublet, $^1J_{\text{RhC}} = 34$ Hz. ^fdoublet, $^1J_{\text{RhC}} = 86$ Hz. ^gdoublet, $^2J_{\text{RhH}} \approx 1$ Hz. ^hdoublet, $^3J_{\text{RhH}} = 4.5$ Hz.

$^{13}\text{C}\{^1\text{H}\}$ NMR spectroscopy confirmed that both isomers have an acyl carbonyl bonded to iron, an $\text{Fe}(\text{CO})_3$ group, and a terminal Rh carbonyl. Furthermore, the carbons of the acetylene moiety are similar to **16b**, demonstrating that **17b** consists of two $\text{CpRhFe}(\text{CO})_4(\mu\text{-}\eta^1\text{:}\eta^3\text{-C}_2\text{H}_2\text{C}(\text{O}))$ isomers. An analysis of the molecular geometry reveals that the only possible source of the isomerization is the disposition of the Cp ligand with respect to the bridging moiety (Figure 6-2).

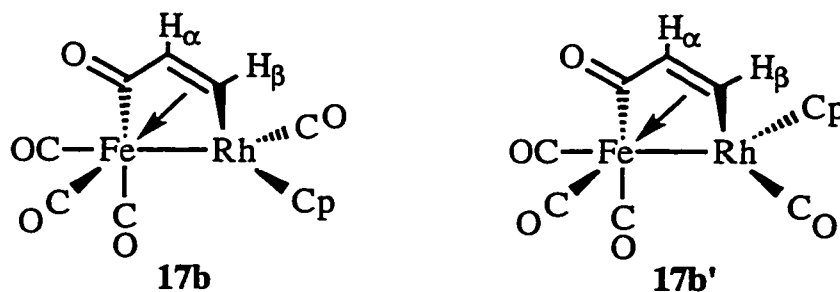


Figure 6-2. Isomeric Forms of $\text{CpRhFe}(\text{CO})_4(\mu\text{-}\eta^1\text{:}\eta^3\text{-C}_2\text{H}_2\text{C}(\text{O}))$ (**17b/b'**).

The major isomer, **17b**, is presumed to have the same orientation of ligands as **16b** while the minor isomer, **17b'**, has the Cp ligand on the opposite side of the molecule.

Thus, the additional features in the FT-IR spectra of **17b** are not due to the presence of a dimetallacyclobutene isomer. In particular, the two bands at 1813 and 1753 cm^{-1} belong to the acyl groups of the distinct dimetallacyclopentenone isomers, Figure 6-2. The change in intensity in moving from pentane to CH_2Cl_2 solvent, mirrors the isomer distributions from ^1H NMR in CD_2Cl_2 or toluene- d_8 . Accordingly, it is also possible that the minor bands observed at *ca.* 1810 - 1825 cm^{-1} in **16a-c** are due to an isomer in which the Cp^* ligand is found on the opposite side of the molecule. Indeed, when the NMR spectra of **16b,c** were collected with good signal to noise ratios, the minor isomers **16b',c'** could be detected in *ca.* 8% and 5% abundance, respectively. It also proved possible to detect **16b',c'** in the $^{13}\text{C}\{^1\text{H}\}$ NMR of ^{13}CO enriched samples (Figure 6-3).

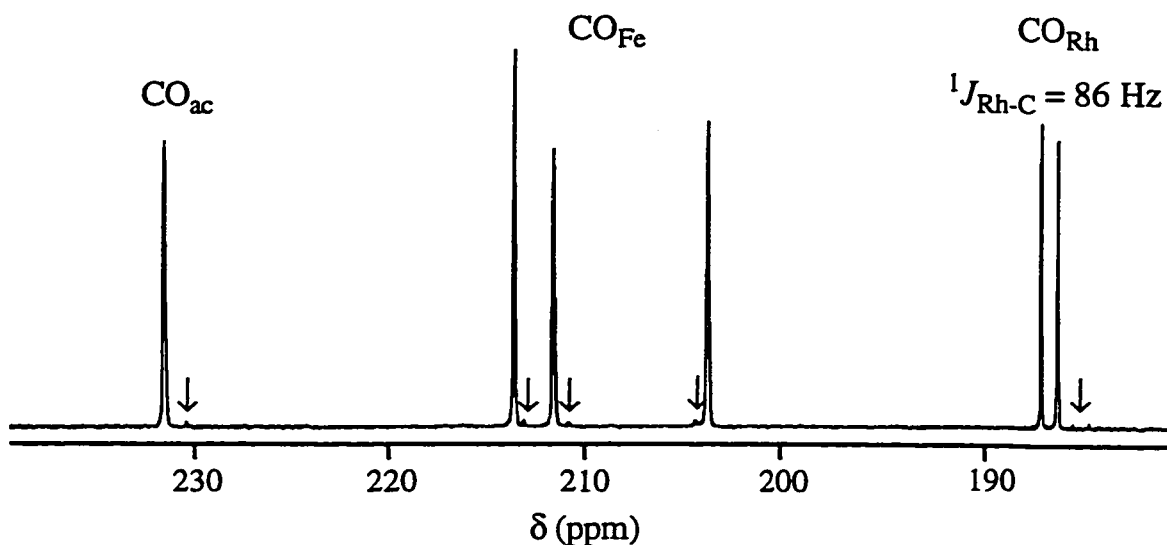


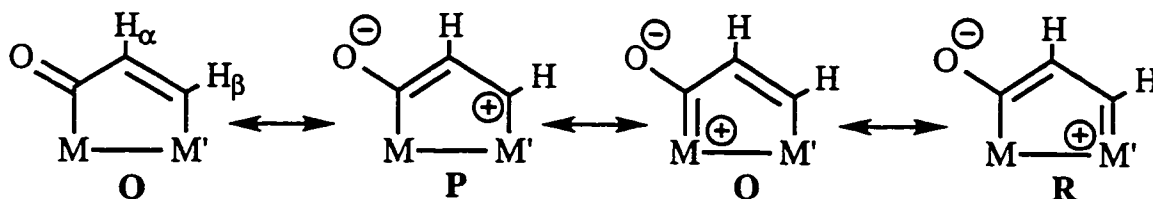
Figure 6-3. $^{13}\text{C}\{^1\text{H}\}$ NMR of **16b** in the Carbonyl Region at -80°C ($\downarrow = \mathbf{16b'}$).

As with **17b'**, the spectral pattern was identical to the major isomer, confirming that the ligand connectivity was retained but that the arrangement in space was different. Furthermore, the fact that **16b'** is found in far lower concentration than **17b'** supports the contention that the isomers are related by the disposition of Cp' with respect to the bridging ligand. The bulkier Cp^* ring is less likely to occupy the sterically hindered site on the same side of the molecule as the acyl group, and consequently **16b'** is less favored than **17b'**, the latter of which contains the

smaller Cp ligand. Indeed, when a crystal from the crop used in the X-ray crystallography study of compound **16b** was dissolved in CD_2Cl_2 at -78°C , the signals for **16b'** were absent in the ^1H NMR spectrum, confirming that the major isomer in solution is identical to that in the solid state. Although the minor isomer of **16c** was detected by ^1H and ^{13}C NMR spectroscopy, the IR spectrum contained a third weak band in the acyl region that remains unexplained (1728 cm^{-1} in Table 6-3).

6.2.5. Initial Characterization of **18c**

The kinetic product from the reaction of **1c** with $\text{Cp}^*\text{Ir}(\text{CO})_2$ (**18c**) has the molecular composition $\text{Cp}^*\text{IrFe}(\text{CO})_6(\text{C}_2\text{H}_2)$ judging from its mass spectrum and elemental analysis, although the weak molecular ion in the mass spectrum and less than 0.3% difference in carbon analysis do not conclusively differentiate from a $\text{Cp}^*\text{IrFe}(\text{CO})_5(\text{C}_2\text{H}_2)$ formulation. In the IR spectrum, the four carbonyl stretches are all typical of terminal carbonyl bands and the low frequency position of the acyl stretching band, 1613 cm^{-1} , suggests an α,β -unsaturated organic fragment as a result of resonance delocalization of electron density to the acyl group (Scheme 6-4).¹⁸



Scheme 6-4. Resonance Structures Describing the Bonding of the Unsaturated Organic Fragment in a $\mu\text{-}\eta^1\text{:}\eta^1$ -Dimetallacyclopentenone.

The ^1H and ^{13}C NMR characteristics of the C_2H_2 moiety confirm that it belongs to a $\mu\text{-}\eta^1\text{:}\eta^1\text{-C}_2\text{H}_2\text{C}(\text{O})$ group on the basis of the similarity of the chemical shifts of H_α , H_β and C_α , C_β , and their similarity to those in previously reported analogs (Table 6-8). Furthermore, the observation that H_α , C_α are generally upfield of H_β , C_β in these compounds is consistent with resonance structure **P** in which C_β bears a partial positive charge.

Table 6-8. ^1H and $^{13}\text{C}\{^1\text{H}\}$ NMR Data for $\text{MM}'\text{L}_n(\mu\text{-}\eta^1\text{:}\eta^1\text{-C}_2\text{H}_2\text{C}(\text{O}))$.

$\text{MM}'\text{L}_n$	$\delta(\text{H}_\beta)$	$\delta(\text{H}_\alpha)$	$\delta(\text{C}_\beta)$	$\delta(\text{C}_\alpha)$
$\text{Cp}^*\text{IrFe}(\text{CO})_5$ (18c)	7.95	6.35	152.78	148.40
$\text{Os}(\text{CO})_4\text{Ir}(\text{CO})\text{Cp}^2$	7.98	7.51	166.9	132.1
$\text{OsRu}(\text{CO})_8^2$	8.17	7.46	166.5	131.4
$\text{OsFe}(\text{CO})_6(\mu\text{-dppm})^{19}$	8.47	7.4	139.6	161.3
$\text{Ru}_2(\text{CO})_4(\mu\text{-dppm})_2^{20}$	8.0	7.4	176.8	170.8
$\text{OsCo}(\text{CO})_4(\text{PMe}_3)\text{Cp}^4$	7.84	5.98	154.0	144.3
$\text{OsCo}(\text{CO})_4(\text{PMe}_2\text{Ph})\text{Cp}^4$	7.72	6.02	154.6	145.3
$\text{OsRh}(\text{CO})_4(\text{PMe}_3)(\eta^5\text{-C}_9\text{H}_7)^4$	7.81	6.53	153.6	152.2
2-cyclopenten-1-one ¹⁸	7.71	6.10	165.1	133.8

Four carbonyl resonances were also detected in a 1:2:1:2 ratio in the $^{13}\text{C}\{^1\text{H}\}$ NMR spectrum at -60°C , the furthest downfield of which, δ 248.94, is assigned to the acyl group. The assignment was confirmed *via* a proton-coupled ^{13}C NMR spectrum because the downfield resonance appeared as a doublet ($^3J_{\text{CH}} = 20$ Hz). The ^1H NMR spectrum of ^{13}CO enriched material also showed this coupling at the δ 7.95 signal. The magnitude of the $^3J_{\text{CH}}$ coupling constant (20 Hz) between H_β and the acyl carbon is somewhat larger than that reported for $^3J_{\text{CH}}$ in similar *trans* configurations in olefins bearing a carbonyl substituent (14 - 16 Hz),²¹ but the absence of observable $^2J_{\text{CH}}$ coupling between H_α and the acyl carbon is consistent with the typically small value of the geminal coupling constant. This bears direct comparison with the more familiar large *trans* $^3J_{\text{HH}}$ and smaller *gem* $^2J_{\text{HH}}$ coupling patterns commonly observed in substituted olefins.²¹

The CH groups expectedly appeared as doublets in the proton-coupled spectrum with $^1J_{\text{CH}} = 153$ and 156 Hz, respectively. The magnitude of $^1J_{\text{CH}}$ compares identically with that in ethylene ($^1J_{\text{CH}} = 156$ Hz),¹⁸ and thus supports the formulation of a carbon-carbon double bond. The $^{13}\text{C}\{^1\text{H}\}$ NMR spectrum of a sample with *ca.* 50% ^{13}CO enrichment identified the δ 148.40 signal as being due to the carbon bonded to the acyl group *via* the appearance of ^{13}C satellites,

$^1J_{CC} = 40$ Hz. The magnitude of the coupling constant is comparable to that seen in $\text{Os}(\text{CO})_4\text{M}(\text{CO})\text{Cp}(\mu\text{-}\eta^1\text{:}\eta^1\text{-CMeCHC(O)})$ ($\text{M} = \text{Co}$, 42 Hz; $\text{M} = \text{Rh}$, 49 Hz; $\text{M} = \text{Ir}$, 51 Hz).⁴

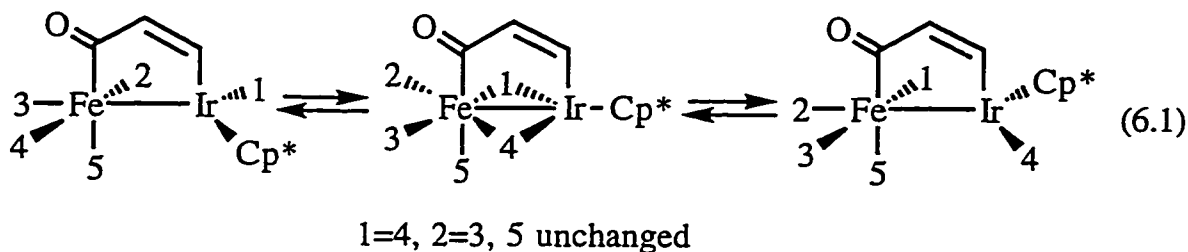
The fact that the Fe and Ir centers in **18c** are NMR silent renders an accurate determination of the metal connectivity of the $\mu\text{-}\eta^1\text{:}\eta^1\text{-C}_2\text{H}_2\text{C(O)}$ ring somewhat ambiguous, but the bonding of the acyl group to iron is suggested by its chemical shift, δ 248.94.¹³ An increased contribution from resonance structure **Q** (Scheme 6-4) could account for the far downfield shift of the acyl carbon in **18c** as it introduces metal-carbene character. Additionally, the downfield shift of the acyl carbon in **18c** compared to **16c**, δ 236.56, has precedence. In $\text{OsRu}(\text{CO})_6(\mu\text{-dppm})(\mu\text{-}\eta^1\text{:}\eta^1\text{-C}_2\text{H}_2\text{C(O)})$ and $\text{OsRu}(\text{CO})_5(\mu\text{-dppm})(\mu\text{-}\eta^1\text{:}\eta^3\text{-C}_2\text{H}_2\text{C(O)})$, the only other known pair of $\mu\text{-}\eta^1\text{:}\eta^1\text{-}$ and $\mu\text{-}\eta^1\text{:}\eta^3\text{-}$ dimetallacyclopentenones related by CO loss, the acyl resonances were found at δ 250.7 and 233.2 respectively.¹⁹

The 2:1:2 pattern of the remaining carbonyls in the natural abundance $^{13}\text{C}\{^1\text{H}\}$ NMR spectrum is curious given that the solution IR spectrum clearly indicates the presence of terminal carbonyls only as all bands were between 2065 and 1964 cm^{-1} . Interestingly, a ^{13}C NMR spectrum recorded on a ^{13}CO enriched sample at -100°C displayed four singlet resonances at δ 209.68, 204.39, 203.06, and 202.97 in a 2:1:0.8:0.8 ratio, relative to the acyl integration of one. The chemical shifts are all typical of Fe-bonded carbonyls, and are roughly 30 ppm downfield of the normal range for terminal Ir carbonyls.¹³ It was also intriguing that the upfield signals integrated roughly to 80% of the downfield signals. Relaxation effects were eliminated as a source of this discrepancy by including a long relaxation delay between pulses. The remaining possibility is that ^{13}CO enrichment did not occur in a statistical fashion, contrary to **16a-c** where complete scrambling of the ^{13}C label was observed. Should this be the reason, it suggests that these resonances should be associated with Ir, as $\text{Cp}^*\text{Ir}(\text{CO})_2$ contained only natural abundance CO ligands at the outset of the reaction, and that the acyl group is derived from **1c**, as it integrates normally to 1.0 CO.

The possibility of fluxionality was also investigated, but no lineshape changes were observed between -100°C and 0°C , above which the complex

readily lost CO to form **16c**. The only changes observed were due to temperature dependent chemical shifts. The acyl carbonyl signal shifted progressively upfield from δ 250.12 at -100°C to δ 246.20 at 0°C , and the resonance at δ 204.04 (-100°C) shifted downfield slightly to δ 205.35 at 0°C . The singlet of intensity two did not change position with temperature, while the remaining two singlets of integration 0.8 merged into a single band by -60°C .

The variable temperature ^{13}C NMR series does not rule out the possibility of fluxionality, but it indicates that if the molecule is fluxional, the process has an extremely low activation energy. In this scenario, the -100°C spectrum would still be considered as the fast exchange limit. $\text{Os}(\text{CO})_4\text{Ir}(\text{CO})\text{Cp}(\mu\text{-}\eta^1\text{:}\eta^1\text{-C}_2\text{H}_2\text{C}(\text{O}))$ undergoes fluxional carbonyl exchange by the truncated merry-go-round mechanism, but the low temperature limiting spectrum was achieved at -30°C .⁴ The possibility of a more rapid fluxional process in **18c** has precedence as the first row metals generally tend to form bridging carbonyls.^{22,23} Applied to **18c**, merry-go-round exchange would involve migration of specific terminal carbonyls on Fe and Ir through bridging intermediates (Eq. 6.1).



Thus, one would expect the time-averaged spectrum to be a 2:2:1 signal pattern which is inconsistent with the -100°C spectrum on ^{13}CO enriched **18c**. Furthermore, even if such a process was occurring, the averaging of carbonyls *1* and *4* at *ca.* δ 202 ppm would require the resonance for carbonyl *4* to be found at roughly δ 230 ppm given that Ir-bonded CO ligands resonate at *ca.* δ 170 ppm.¹³ This is 15 - 20 ppm further downfield than has been observed for the Fe carbonyls in **12**, **13** and **16**. In light of the clear structural ambiguities with respect to the arrangement of the carbonyl ligands about the dimetallacyclopentenone core, the molecular structure of **18c** was determined by X-ray crystallography.

6.2.6. Molecular Structure of 18c

The molecular structure of **18c** is presented in Figure 6-4, and selected interatomic distances and angles are provided in Tables 6-9 and 6-10. The structure reveals several features that were anticipated from the spectroscopic data, namely the presence and orientation of the $\mu\text{-}\eta^1\text{:}\eta^1\text{-C}_2\text{H}_2\text{C(O)}$ moiety. However, the remaining carbonyl ligands take on a surprising orientation around the bimetallic framework. The Fe center supports three terminal carbonyls and one which spans the two metals in a semi-bridging fashion. In addition to interacting weakly with the semi-bridging carbonyl that is bonded primarily to Fe, the Ir center also supports a terminal carbonyl ligand. At first glance, the solid state structure appears to be at odds with the solution spectroscopic data, namely the ^{13}C NMR spectra which did not detect a terminal Ir carbonyl. We shall return to this point following a discussion of the salient metrical parameters of **18c**.

The Fe-Ir separation of 2.7457(10) Å is slightly longer, by 0.04 Å, than that reported in **12c** and **13c**. Despite the slight expansion, a metal-metal single bond is still suggested as the Fe-Ir distance is some 0.2 Å shorter than in $(\mu\text{-PPh}_2)\text{FeIr(CO)}_5(\text{PPh}_3)_2$ where a dative Fe→Ir bond is present.²⁴ The iron center is roughly octahedral, but the main distortions are the Ir-Fe-C(2) angle, which is compressed to 58.2(2)°, while the Ir-Fe-C(3) angle is expanded to 110.8(2)°. The C(4)-Fe-C(6) angle is essentially linear at 177.9(3)°, and the angles between the four carbonyl ligands are slightly greater than 90°, ranging between 94.0(3) and 96.5(3)°. While this is in part due to the distortion of the structure caused by the semi-bridging CO ligand (*vide infra*), the C(2)-Fe-C(6) and C(3)-Fe-C(6) angles are slightly acute and show a similar distortion discussed for the structure of **12c** (Chapter 5).

The five-membered ring is essentially flat, with an Fe-C(6)-C(7)-C(8) torsion angle of 2.4(9)° and a C(6)-C(7)-C(8)-Ir torsion angle of 7.1(10)°. The dimetallacyclopentenone ring in $\text{Ru}_2(\text{CO})_4(\mu\text{-dppm})_2(\mu\text{-}\eta^1\text{:}\eta^1\text{-C}_2\text{H}_2\text{C(O)})$ is also reported to be planar.²⁰ The C(6)-C(7) bond distance is 1.464(10) Å, which is identical to that expected for the $\text{C}(sp^2)\text{-C}(sp^2)$ single bond length in an α , β -unsaturated ketone.²⁵ Similarly, the C(7)-C(8) distance of 1.329(9) Å is identical, within error, to that found in organic analogs (1.340(13) Å), as is the C(6)-O(6)

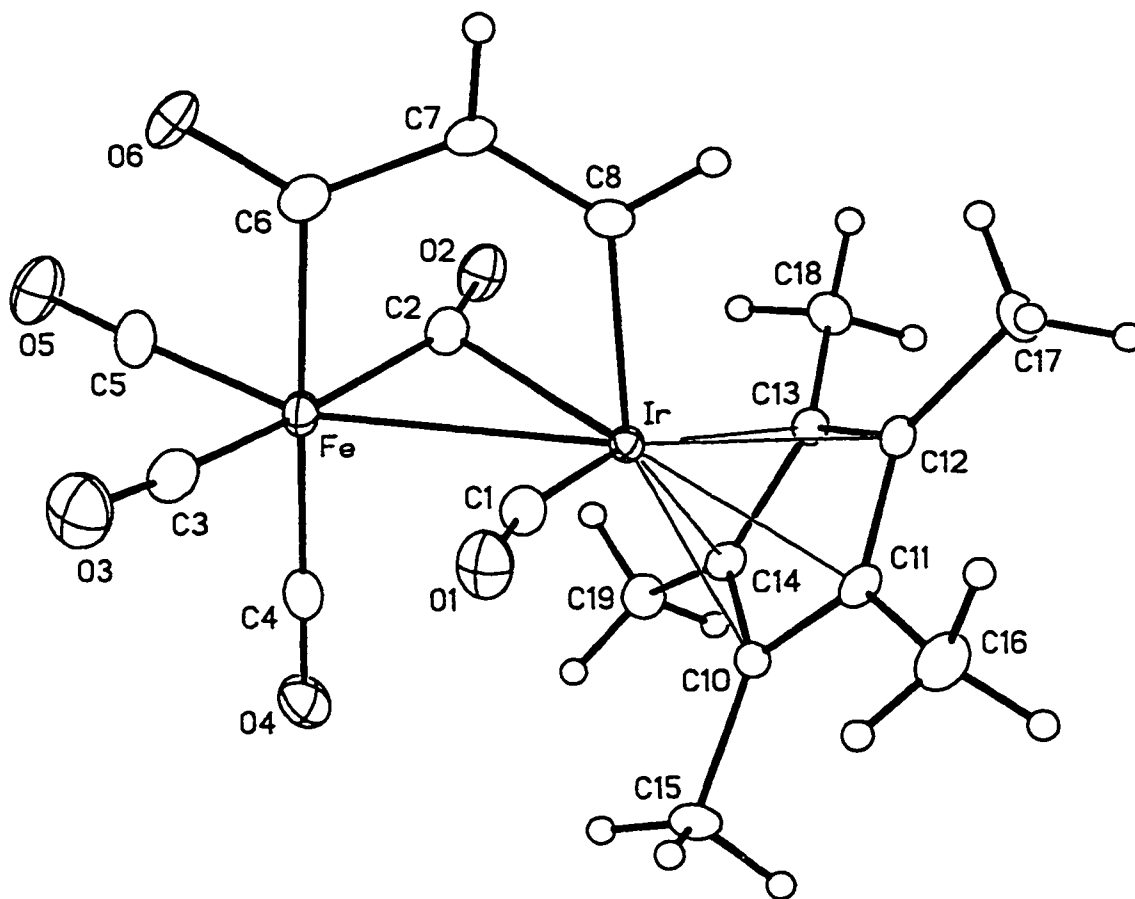


Figure 6-4. Molecular Structure of Compound 18c.

Table 6-9. Selected Interatomic Distances (Å) in Compound 18c.

Fe–Ir	2.7457(10)	C(1)–O(1)	1.135(8)
Ir–C(1)	1.868(7)	C(2)–O(2)	1.145(9)
Ir–C(2)	2.367(7)	C(3)–O(3)	1.134(9)
Ir–C(8)	2.034(6)	C(4)–O(4)	1.144(8)
Fe–C(2)	1.849(7)	C(5)–O(5)	1.142(9)
Fe–C(3)	1.818(8)	C(6)–O(6)	1.211(8)
Fe–C(4)	1.822(8)	C(6)–C(7)	1.464(10)
Fe–C(5)	1.777(7)	C(7)–C(8)	1.329(9)
Fe–C(6)	2.057(7)		

Table 6-10. Selected Interatomic Angles (deg.) in Compound **18c**.

Fe–Ir–C(1)	70.2(2)	C(3)–Fe–C(4)	96.5(3)
Fe–Ir–C(2)	41.6(2)	C(3)–Fe–C(5)	95.7(3)
Fe–Ir–C(8)	82.9(2)	C(3)–Fe–C(6)	82.8(3)
Ir–Fe–C(1)	39.76(14)	C(4)–Fe–C(5)	96.4(3)
Ir–Fe–C(2)	58.2(2)	C(4)–Fe–C(6)	177.9(3)
Ir–Fe–C(3)	110.8(2)	C(5)–Fe–C(6)	85.7(3)
Ir–Fe–C(4)	89.5(2)	Ir–C(1)–O(1)	167.0(6)
Ir–Fe–C(5)	152.0(2)	Ir–C(2)–O(2)	124.9(5)
Ir–Fe–C(6)	88.8(2)	Fe–C(2)–O(2)	154.8(6)
C(1)–Ir–C(2)	110.7(3)	Fe–C(3)–O(3)	175.8(7)
C(1)–Ir–C(8)	86.4(3)	Fe–C(4)–O(4)	178.7(7)
C(2)–Ir–C(8)	76.6(2)	Fe–C(5)–O(5)	178.3(8)
C(1)–Fe–C(2)	97.1(3)	Fe–C(6)–O(6)	122.8(6)
C(2)–Fe–C(3)	163.8(3)	Fe–C(6)–C(7)	116.5(4)
C(2)–Fe–C(4)	95.2(3)	Ir–C(8)–C(7)	127.0(5)
C(2)–Fe–C(5)	94.0(3)	O(6)–C(6)–C(7)	120.7(6)
C(2)–Fe–C(6)	85.1(3)	C(6)–C(7)–C(8)	123.8(6)

separation, 1.211(8) Å, compared with 1.222(10) Å.²⁵ Finally, the Fe–C(6) and Ir–C(8) distances of 2.057(7) Å and 2.034(6) Å indicate metal-carbon single bonds. The former is within the range of Fe–C(*sp*²) bond lengths,²⁶ but longer than in Fe(CO)₄{η¹,η¹-(O)CCHCHC(O)}, 2.016(3) Å, where partial Fe–C(O) double bonding was suggested.²⁷ The latter compares with the Ir–C(*sp*²) bond lengths in **12c** and **13c**. Combined with the similarity to α, β-unsaturated ketones, these features suggest contributions from resonance structures **O** and **P** in Scheme 6-4.

Within the ring, the Ir–C(8)–C(7) and C(8)–C(7)–C(6) bond angles are slightly greater than would be expected for ideal *sp*² hybridization while the Fe–C(6)–C(7) angle is slightly compressed. By comparison, the O(6)–C(6)–C(7) angle is 120.7(6)°. The Ir–Fe–C(6) angle is 88.8(2)° in good agreement with the octahedral geometry at the Fe center, while the Fe–Ir–C(8) angle is more

compressed at 82.9(2)°. The metrical parameters of the dimetallacyclopentenone ring compare well with those reported previously (Table 6-11).

Table 6-11. Comparison of Metrical Parameters in $MM'L_n(\mu-\eta^1:\eta^1-C_2H_2C(O))$.

$MM'L_n$	C(6)–C(7)	C(7)–C(8)	C(6)–O(6)	C(6)–C(7)–C(8)	O(6)–C(6)–C(7)
18c	1.464(10)	1.329(9)	1.211(8)	123.8(6)	120.7(6)
OsIr ^a	1.45(4)	1.31(4)	1.24(3)	122(3)	122(2)
OsRh ^b	1.51(1)	1.32(1)	1.19(1)	122.9(9)	120.7(9)
RuRu ^c	1.49(2)	1.33(2)	1.21(2)	126(1)	114(1)

^aOs(CO)₄Ir(CO)Cp(μ-η¹:η¹-C₂H₂C(O)); ^bOs(CO)₂(PMe₃)(μ-CO)₂Rh(η⁵-C₉H₇)(μ-η¹:η¹-C₂H₂C(O)), Ref. 4. ^cRu₂(CO)₄(μ-dppm)₂(μ-η¹:η¹-C₂H₂C(O)), Ref. 20.

The C(6)–C(7)–C(8) angle is fairly constant across all examples, indicating that the central angle of the bridge does not change significantly despite differences in the metal-metal bond lengths. The differences in bond angles involving the acyl carbonyl in Ru₂(CO)₄(μ-dppm)₂(μ-η¹:η¹-C₂H₂C(O)) are most likely the result of increased steric restrictions in this system. The slightly longer C(6)–C(7) and shorter C(6)–O(6) bond distances in Os(CO)₂(PMe₃)(μ-CO)₂Rh(η⁵-C₉H₇)(μ-η¹:η¹-C₂H₂C(O)) suggest a greater contribution from resonance structure **O** than is found in **18c**.

One of the more interesting features of the structure is the presence of the semi-bridging CO ligand, C(2)O(2), which is absent in Os(CO)₄Ir(CO)Cp(μ-η¹:η¹-C₂H₂C(O)).⁴ This carbonyl is best characterized as semi-bridging as the Fe–C(2) bond length, 1.849(7) Å, is over 0.5 Å shorter than the Ir–C(2) separation, 2.367(7) Å. Furthermore, the C(2)–O(2) vector is not perpendicular to the metal-metal bond and intersects with the Fe–Ir vector at an angle of 113.2°. Additionally, the Fe–C(2)–O(2) bond angle is 154.8(6)° and the Ir–Fe–C(2) angle is 58.2(2)°, both of which are characteristic of a semi-bridging interaction.^{28,29} It is also noteworthy that the Fe–C(2) bond length is the longest of the Fe-bonded carbonyls. The presence of a semi-bridging CO ligand in **18c** compared with all-terminal COs in Os(CO)₄Ir(CO)Cp(μ-η¹:η¹-C₂H₂C(O)) can be justified in two ways. Firstly, the Ir center in the latter bears an electronegative acyl carbonyl

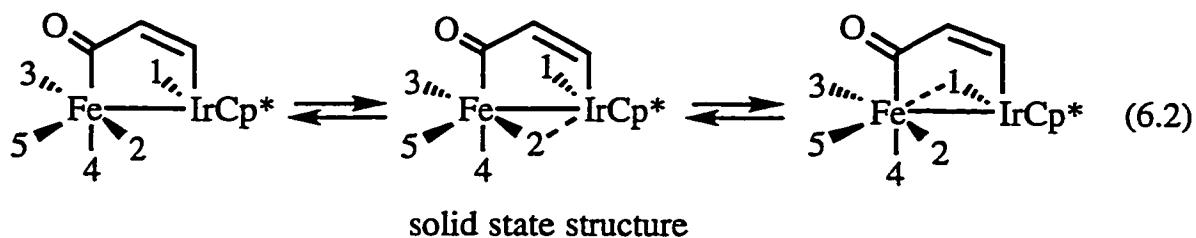
while the former is bonded to a CH group, rendering the Ir center more electron rich in **18c** and more receptive to interaction with a π -acidic carbonyl from the Fe center. Secondly, the Fe–Ir bond is slightly shorter than the Os–Ir bond, 2.785(2) Å,⁴ which also more readily supports a bridging interaction. Although the Ir-bonded carbonyl in **18c** also shows a departure from linearity (Ir–C(1)–O(1) = 167.0(6)°), the Fe–C(1) separation, 2.748(7) Å, is some 0.4 Å longer than Ir–C(2) and thus does not indicate a significant interaction. A compensating pair of semi-bridging carbonyls were reported to exist in Fe₃(CO)₈(C₄H₈S)₂,³⁰ and, although the Fe–C–O angles were identical to Ir–C(1)–O(1), the Fe–C(O) separation (2.55 Å) was 0.2 Å shorter than is found for Fe–C(1) in **18c**.

The metrical parameters describing the semi-bridging C(2)O(2) ligand are very similar to those observed in CpFe(CO)(μ -CO)(μ -CF₂)Ir(CO)(Cl)(PMe₂Ph)₂,³¹ which is interesting as the ancillary ligands are quite different. The separation corresponding to Fe–C(2) is slightly shorter in this compound (1.807(6) Å), and the Ir–C(2) separation is slightly longer (2.392(5) Å) but the Fe–C(2)–O(2) angle is identical at 154.2(5)°. These values are quite different than those observed for the bridging carbonyls in Cp*Ir(μ -CO)₂Fe₂(CO)₇, where one carbonyl bridges the metals symmetrically (Fe–C–O = 131(3)°; Fe–C = 1.89(5) Å; Ir–C = 1.91(5) Å) and the other bridges in a more unsymmetrical fashion (Fe–C–O = 142(4)°; Fe–C = 2.13(4) Å; Ir–C = 1.89(5) Å).³²

6.2.7. Further Spectroscopic Characterization of **18c**

A KBr disk IR spectrum of **18c** revealed a band at 1815 cm⁻¹ due to the semi-bridging C(2)O(2) ligand in Figure 6-4, a feature that was not detected in solution. This band is some 150 cm⁻¹ lower than the lowest frequency CO stretching band in CH₂Cl₂ and is also 80 cm⁻¹ lower in frequency than the μ -CO band in CpFe(CO)(μ -CO)(μ -CF₂)Ir(CO)(Cl)(PMe₂Ph)₂ (1897 cm⁻¹).³¹ Thus, it is clear that the molecule possesses different solution and solid-state structures. Returning to the problem of reconciling the ¹³C NMR data, one potential rationalization relies on a slight modification of Eq. 6.1. In the modified proposal, Eq. 6.2, the carbonyls oscillate rapidly between an isomer in which all carbonyls

are terminal and isomers in which C(2)O(2) and C(1)O(1) take on semi-bridging character.



In this case, none of the carbonyls are rendered formally equivalent, but it is presumed that COs 3 and 5 give rise to coincidentally superimposed ^{13}C resonances due to the similarity of their chemical environments. Since CO 1 fluctuates between semi-bridging and terminal modes, we can begin to rationalize the *ca.* 30 - 35 ppm downfield displacement from its anticipated δ 170 ppm position in the ^{13}C NMR spectrum, as a bridging carbonyl would be expected to resonate to lower field, *cf.* δ 216 ppm in $\text{CpFe}(\text{CO})(\mu\text{-CO})(\mu\text{-CF}_2)\text{Ir}(\text{CO})(\text{Cl})(\text{PMe}_2\text{Ph})_2$.³¹ A downfield shift of *ca.* 10-15 ppm was also observed when terminal Ir carbonyls were aimed between the two metals in a series of heterodinuclear RhIr compounds. A weak bridging interaction was suggested to account for the downfield shift.³³ Carbonyl 2 similarly migrates between a semi-bridging position and a terminal position on Fe, and would be expected to resonate downfield of the terminal Fe-CO resonances (δ 209.68 and 204.39 ppm). Thus, both arguments suggest that there should be a significant difference in chemical shift between CO 1 and 2, whereas the two resonate at almost identical positions in the ^{13}C NMR spectrum of **18c**. Accordingly, the behavior of **18c** in solution is not easily reconciled with the solid state structure in Figure 6-4.

6.3. Variable Temperature NMR Studies of Molecular Rearrangements

6.3.1. Fluxional Turnstile Exchange in 16a-c and 17b,b'

Compounds **16a-c** and **17b/b'** are fluxional in solution and their ^{13}C NMR spectra reflect the familiar turnstile, or trigonal twist, exchange mechanism which

was observed in **12b,c** and **13a-c** and is common to *fac*-M(CO)₃ groups in bimetallic and cluster compounds.³⁴ The fluxional process was characterized by the broadening of the three distinct iron carbonyl resonances observed in the low-temperature limiting spectra (Table 6-2) followed by coalescence to a single broad resonance at room temperature. The acyl and M–CO signals remained sharp over the temperature range studied and are thus not involved in the fluxional process. The Co-carbonyl resonance in **16a** broadened from a linewidth of 6 Hz at 213 K to 30 Hz at 293 K as a result of the influence of the ⁵⁹Co quadrupole,¹³ but the change in linewidth was independent of the turnstile exchange. Lineshape simulation was employed to determine activation parameters (Table 6-12).

Table 6-12. Activation Parameters for Turnstile Exchange in **16a-c** and **17b/b'**.^{a,b}

	ΔH^\ddagger (kJ·mol ⁻¹)	ΔS^\ddagger (J·mol ⁻¹ ·K ⁻¹)
16a	57 ± 6	22 ± 24
16b	54 ± 1	5 ± 4
16c	53 ± 6	-5 ± 23
17b	62 ± 4	32 ± 16
17b'	39 ± 5	-22 ± 21

^aA summary of the rate constants determined from spectral simulation is provided in Table 6-17. ^bErrors are non-linear errors from non-linear least-squares analysis.

Expectedly, the ΔH^\ddagger and ΔS^\ddagger parameters are quite similar for the three heterobimetallic complexes **16a-c**, again demonstrating that the nature of the ancillary metal has very little influence on the energy barrier for turnstile rotation of carbonyls on the Fe center.

The isomers **17b** and **17b'**, however, showed different behavior in the ¹³C NMR (Figure 6-5) and thus have distinctly different activation parameters. The minor isomer, **17b'**, displays a decrease in ΔH^\ddagger by some 23 kJ·mol⁻¹ (Table 6-12) compared to **17b** and undergoes turnstile migration at much lower temperature. Referring to the proposed structures in Figure 6-2, it may be that this is because

the Cp ring lies adjacent to the $\text{Fe}(\text{CO})_3$ group in **17b** and thus sterically impedes the rotation.

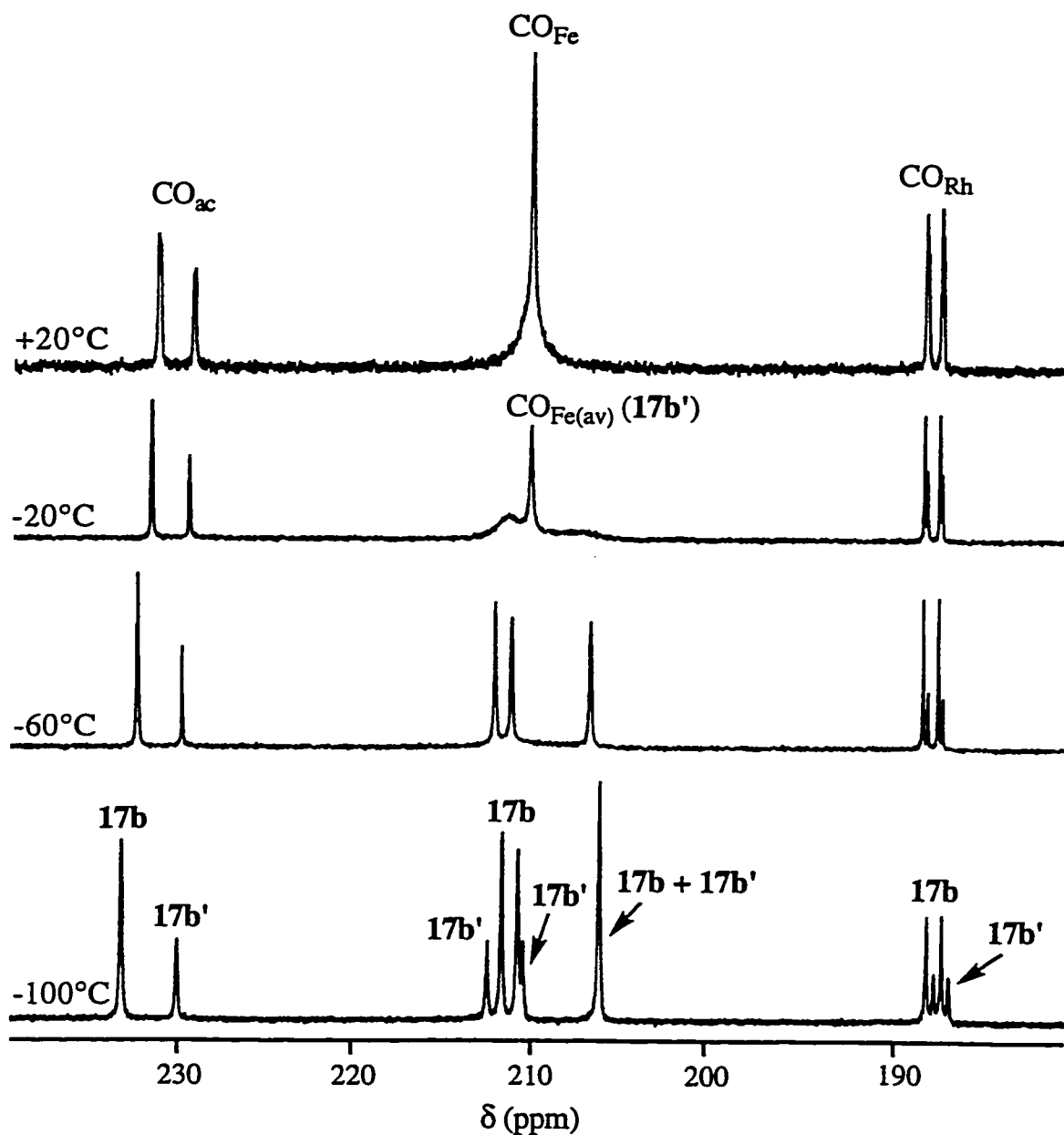


Figure 6-5. Variable Temperature ^{13}C NMR of **17b/b'** in the Carbonyl Region.

In **17b'**, the Cp ring is on the opposite side of the molecule and the facial arrangement of carbonyls on the Fe center is more free to rotate. The minor isomers **16b',c'** show similar behavior in their ^{13}C NMR spectra and enter into

turnstile exchange at lower temperature than the major isomers. However, steric arguments would predict a larger ΔH^\ddagger for **16b** than **17b**, contrary to observation, and suggests that the increase in electron density in the bimetallic framework afforded by the Cp* ligand in the latter may counteract the increase in ΔH^\ddagger from increased steric interference.

6.3.2. Isomerization of **17b,b'**

Although the isomers **17b/b'** were distinct below *ca.* 0°C, at room temperature the resonances in the ^1H NMR spectra began to broaden. At higher temperatures, the intense singlets for the Cp ligands coalesced and sharpened to a single resonance, indicating that isomer interconversion was occurring (Figure 6-6). Concomitant with the change in the Cp resonances, the upfield resonances for the H_α protons also broadened, coalesced and sharpened to a doublet of doublets signal pattern centered at δ 3.15. The downfield resonances for the H_β protons similarly coalesced, forming a broadened singlet by +80°C, the larger difference in frequency between the two H_β signals than the H_α and Cp resonances requiring a higher temperature to achieve coalescence. Thus, the exchange process serves to interconvert $\text{H}_\alpha(\mathbf{17b})$ with $\text{H}_\alpha(\mathbf{17b}')$ and $\text{H}_\beta(\mathbf{17b})$ with $\text{H}_\beta(\mathbf{17b}')$ but does not cause exchange *between* the H_α and H_β protons. Lineshape simulation of the coalescence of the Cp resonances gave activation parameters $\Delta H^\ddagger = 73 \pm 4 \text{ kJ}\cdot\text{mol}^{-1}$ and $\Delta S^\ddagger = 21 \pm 13 \text{ J}\cdot\text{mol}^{-1}\cdot\text{K}^{-1}$ for the isomerization process.

In the toluene-*d*₈ ^{13}C NMR spectra, two sharp singlets were observed for the acyl and Rh–CO signals at ambient temperature. The $\text{Fe}(\text{CO})_3$ groups appeared as a single overlapped resonance as a result of the fast turnstile exchange discussed above. Upon warming to +60°C, the acyl singlets and Rh–CO doublets collapsed to broad resonances concurrent with broadening of the averaged $\text{Fe}(\text{CO})_3$ resonance at δ 210.9 (Figure 6-7). A carbon-carbon bond cleavage mechanism similar to that in **13a-c** can account for these observations (Eq. 6.3). While intervening pair-wise carbonyl exchange is not required to bring about exchange between the two isomers, the broadening of the Rh–CO

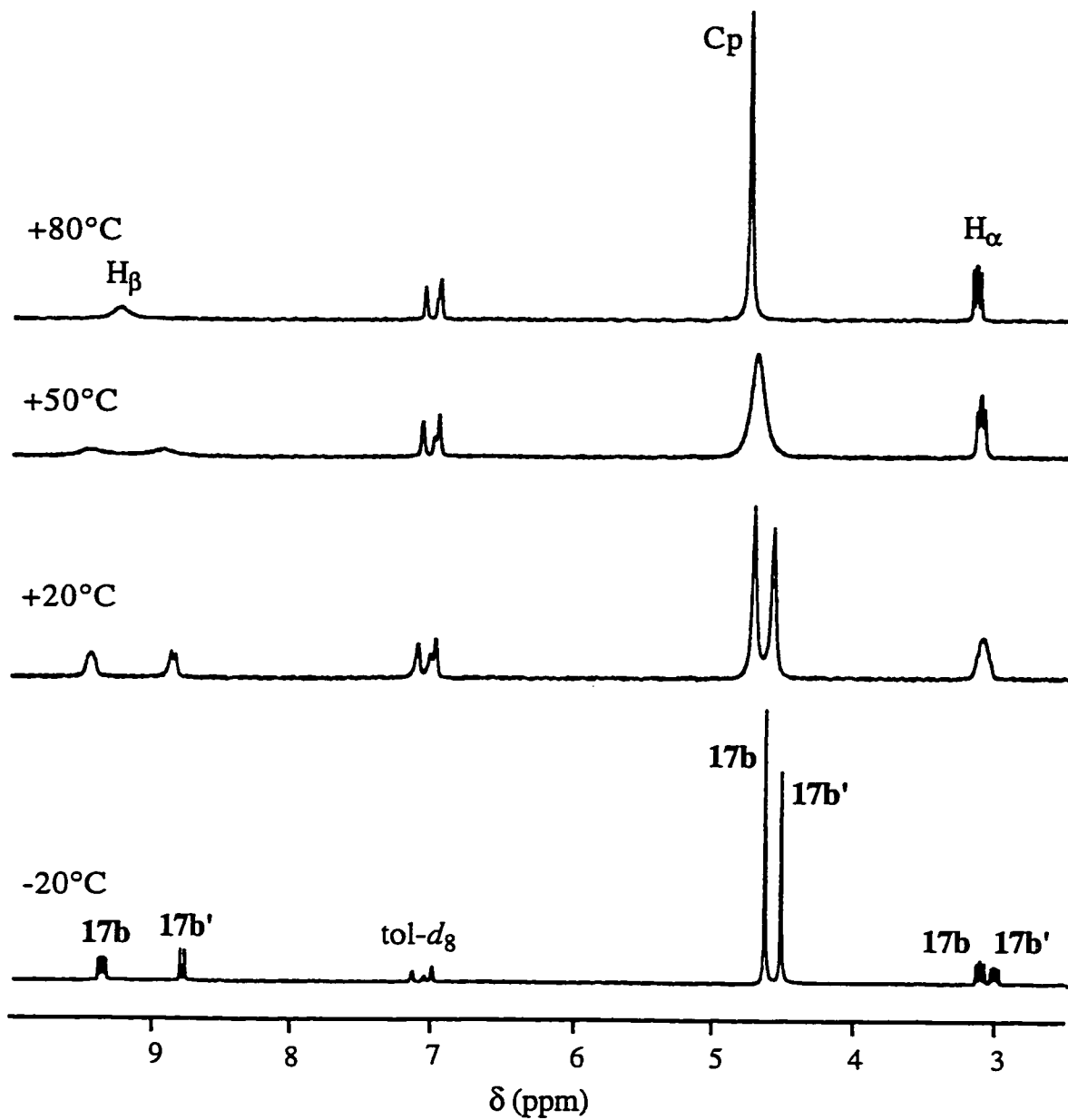
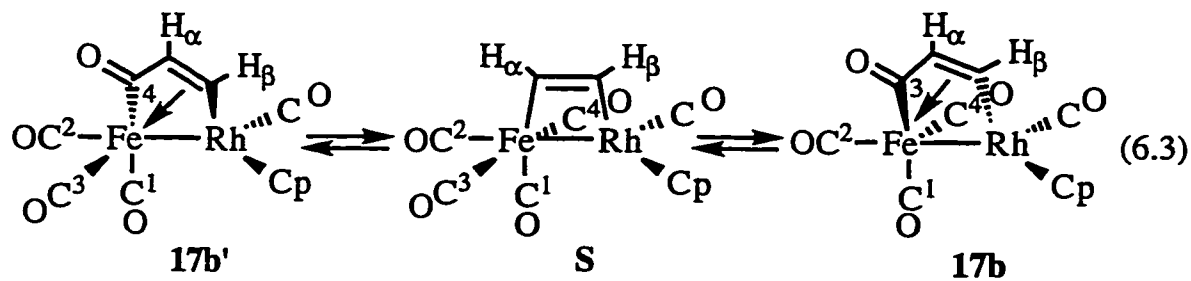


Figure 6-6. Variable Temperature ^1H NMR of 17b/b' (tol- d_8 , 200.1 MHz).



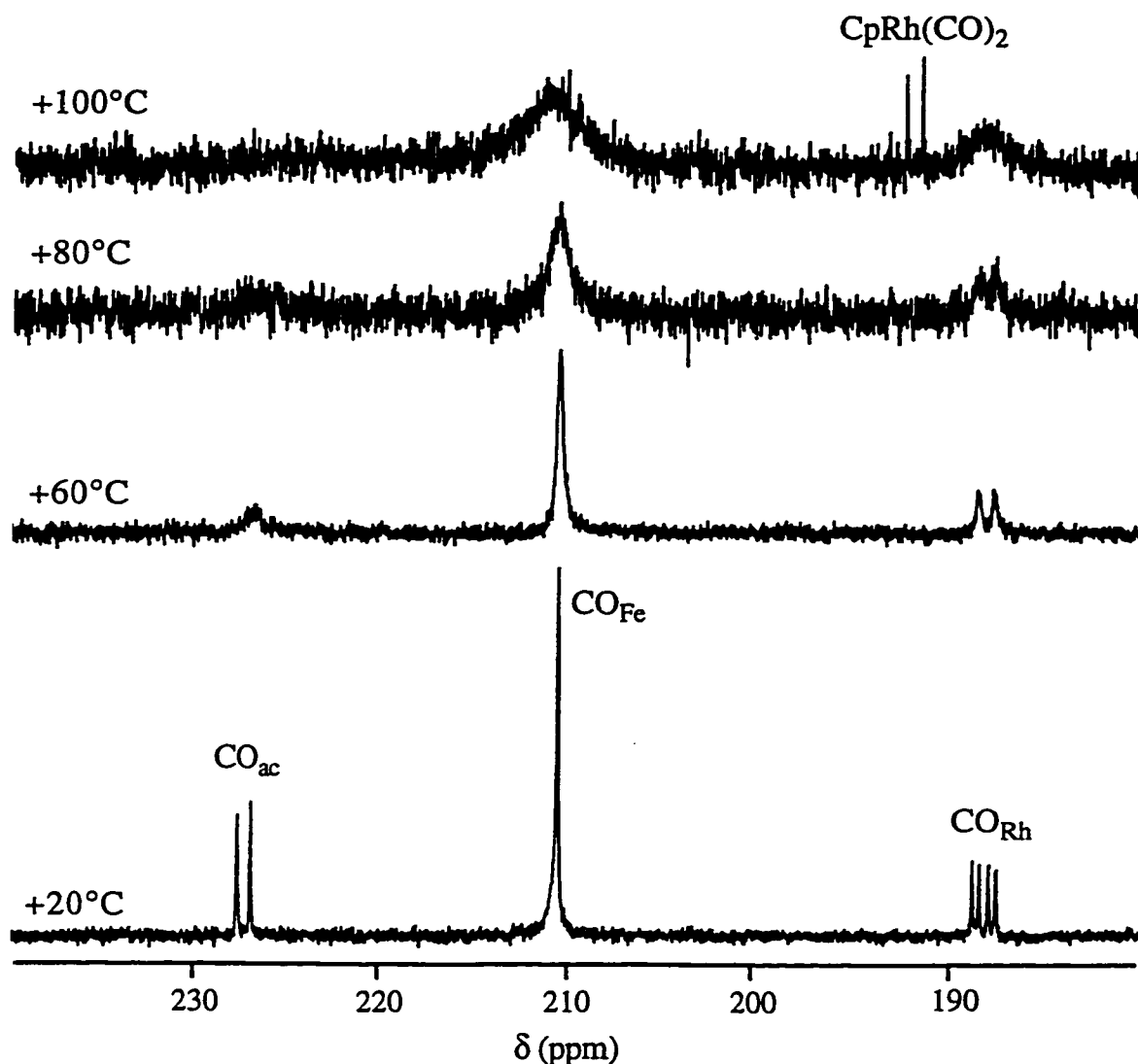
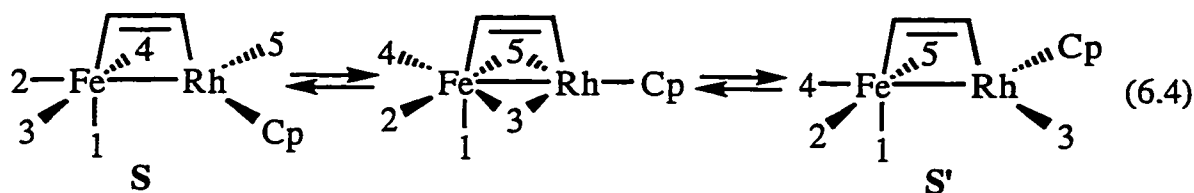


Figure 6-7. High Temperature ^{13}C NMR Spectra of **17b/b'** (tol-*d*₈, 100.6 MHz).

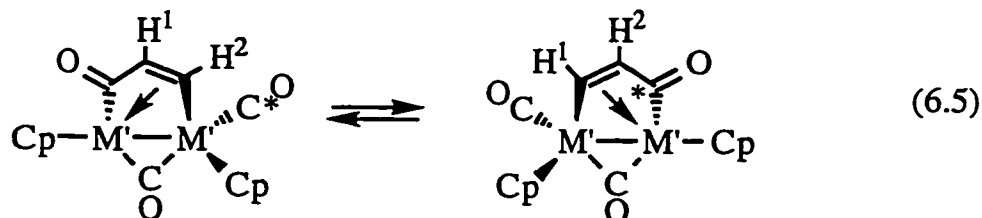
resonances indicates that a truncated merry-go-round mechanism brings the Rh-CO into exchange with the remaining carbonyls (Eq. 6.4). As with **13a-c**, however, it is not possible to delineate the actual rate of pair-wise exchange of the carbonyls as the competing isomer exchange process is rate limiting. It is likely that a process analogous to Eq. 6.3 forms the minor isomers **16b'** and **16c'** in the Cp* analogs, but that the rate of interconversion is slower than would produce line broadening in the ^1H or ^{13}C NMR.

Upon raising the temperature through +80°C to +100°C, all signals broadened into the baseline, but the fast exchange limit was not achieved. The

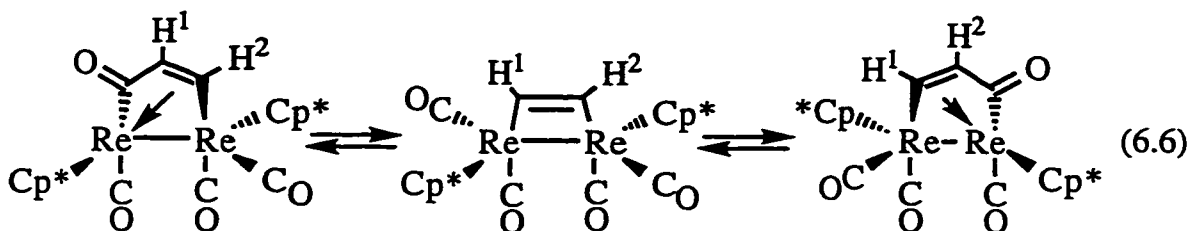
appearance of the characteristic doublet for $\text{CpRh}(\text{CO})_2$ at δ 192 ($^1J_{\text{RhC}} = 82$ Hz) also suggested that some decomposition was occurring at high temperature. In order to confirm that the acyl and Rh–CO resonances were also exchanging near ambient temperature, a Spin Saturation Transfer (SST) experiment was conducted. Irradiation of any of the four signals at $+20^\circ\text{C}$ in Figure 6-5 caused a decrease in intensity in the remaining signals, confirming that global carbonyl exchange was occurring.



The behaviour of **17b/b'** contrasts markedly with that routinely observed for homonuclear dimetallacyclopentenones such as $\text{Cp}_2\text{M}'_2(\text{CO})(\mu\text{-CO})(\mu\text{-}\eta^1\text{:}\eta^3\text{-C}_2\text{H}_2\text{C}(\text{O}))$ ($\text{M}' = \text{Fe}, \text{Ru}$),^{11,12} $\text{Fe}_2(\text{CO})_5(\mu\text{-dppm})(\mu\text{-}\eta^1\text{:}\eta^3\text{-C}_2\text{H}_2\text{C}(\text{O}))$,¹⁰ and $\text{Cp}^*\text{Re}_2(\text{CO})_3(\mu\text{-}\eta^1\text{:}\eta^3\text{-C}_2\text{H}_2\text{C}(\text{O}))$ ³⁵ where exchange between the α and β protons was observed at high temperature. Knox has described this exchange in terms of ejection of CO from the metallacycle with synchronous migratory insertion of CO into the formerly bridging carbon-metal bond to regenerate the dimetallacyclopentenone (Eq. 6.5)¹¹ and has referred to the molecular structures of the enantiomeric pair of $\text{Fe}_2(\text{CO})_5(\mu\text{-dppm})(\mu\text{-}\eta^1\text{:}\eta^3\text{-C}_2\text{H}_2\text{C}(\text{O}))$ to demonstrate how little motion need occur to accomplish this transformation.¹⁰



Casey preferred to view the process in terms of a stepwise mechanism that involved the formation of an intermediate dimetallacyclobutene (Eq. 6.6).^{35,36}



The above is similar to the process occurring in **17b/b'** with the exception that migratory CO insertion occurs exclusively at the Fe center. The reported activation free energies for $\text{Cp}_2\text{M}'_2(\text{CO})(\mu\text{-CO})(\mu\text{-}\eta^1\text{:}\eta^3\text{-C}_2\text{H}_2\text{C}(\text{O}))$ ($\text{M}' = \text{Fe}$, $\Delta G^\ddagger_{399} = 84.8 \text{ kJ}\cdot\text{mol}^{-1}$; Ru , $\Delta G^\ddagger_{371} = 79.4 \text{ kJ}\cdot\text{mol}^{-1}$)^{11,12} and $\text{Cp}^*_2\text{Re}_2(\text{CO})_3(\mu\text{-}\eta^1\text{:}\eta^3\text{-C}_2\text{H}_2\text{C}(\text{O}))$ ($\Delta G^\ddagger_{343} = 69.9 \text{ kJ}\cdot\text{mol}^{-1}$)³⁵ are somewhat higher than that which governs the behavior of **17b/b'**, $\Delta G^\ddagger_{343-399} = 65 - 66 \text{ kJ}\cdot\text{mol}^{-1}$ from $\Delta H^\ddagger = 73 \pm 4 \text{ kJ}\cdot\text{mol}^{-1}$ and $\Delta S^\ddagger = 21 \pm 13 \text{ J}\cdot\text{mol}^{-1}\cdot\text{K}^{-1}$.

6.4. Low Temperature NMR Reaction Monitoring

6.4.1. Reaction of **1c** with $\text{Cp}^*\text{Rh}(\text{CO})_2$

The reaction between **1c** and $\text{Cp}^*\text{Rh}(\text{CO})_2$ was quite rapid at low temperature, and the first ^1H NMR spectrum recorded after mixing the two reagents at -78°C showed evidence of initial product formation (Figure 6-8). After approximately one hour at -60°C , **1c** had been consumed and two products (**18b**:**19b**) were present in a 37:63% ratio. The minor species, **18b**, displayed two doublets of doublets at δ 7.83 and 5.63 ppm which shared a common $^3J_{\text{HH}}$ coupling constant of 6.5 Hz, but had slightly dissimilar J_{RhH} values of 3.0 and 2.5 Hz, respectively. The major species, **19b**, gave rise to two equal intensity doublets at δ 7.90 and 5.93, $^3J_{\text{HH}} = 8.0 \text{ Hz}$. The similarity of the chemical shifts of the CH protons in **18b** and **19b** are characteristic of a $\mu\text{-}\eta^1\text{:}\eta^1\text{-C}_2\text{H}_2\text{C}(\text{O})$ bridged bimetallic species (*vide supra*) and the coupling to rhodium in **18b** indicates that the CH terminus is bonded to Rh, while the lack of Rh-H coupling in **19b** suggests the alternate scenario. In order to confirm the assignments, a $^{13}\text{C}\{^1\text{H}\}$ NMR spectrum was collected at this juncture.

Both species displayed a doublet of intensity two (δ 234.90, $^1J_{\text{RhC}} = 43 \text{ Hz}$, **18b**; δ 229.36, $^1J_{\text{RhC}} = 48 \text{ Hz}$, **19b**) in addition to two singlets in a 2:1 ratio to

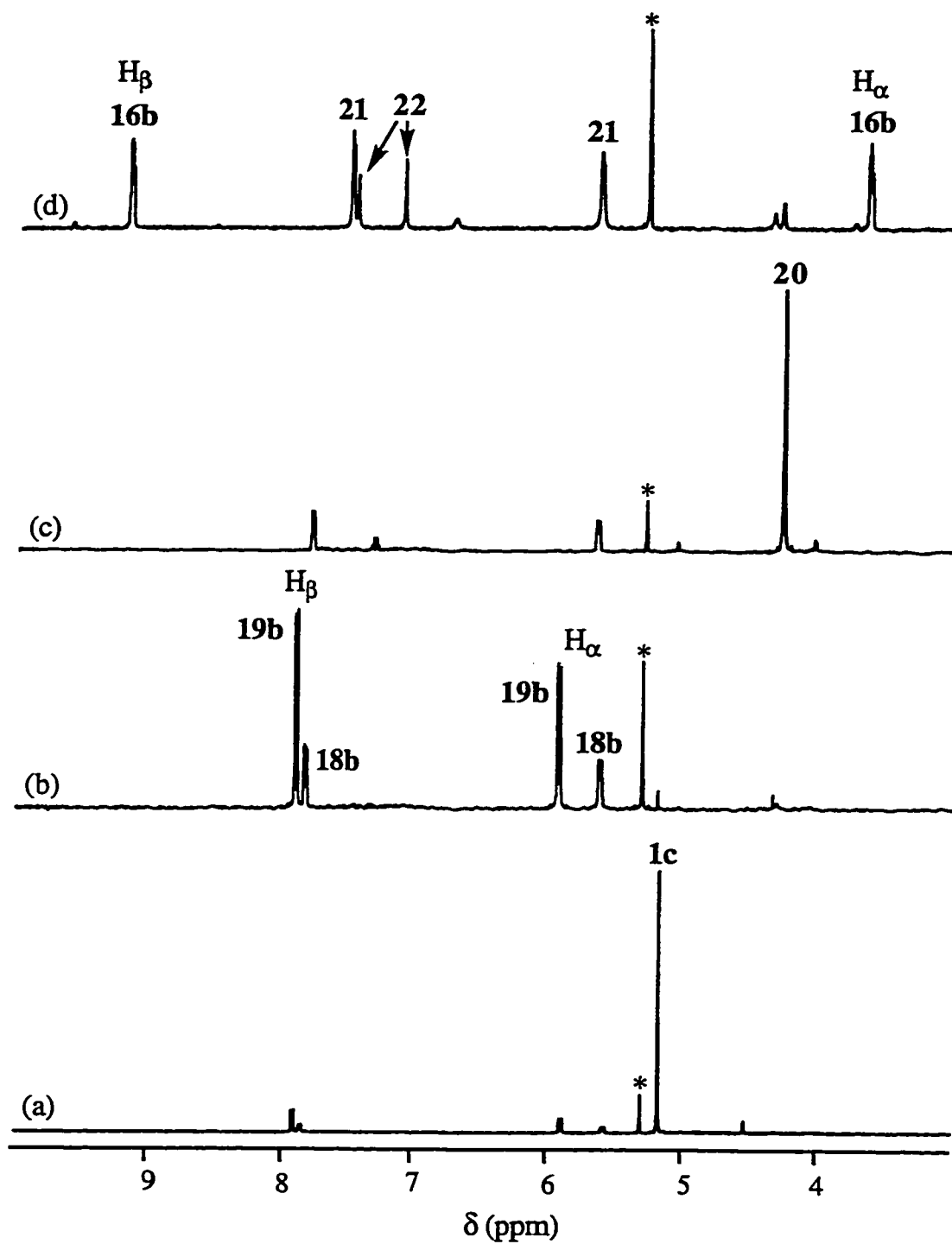
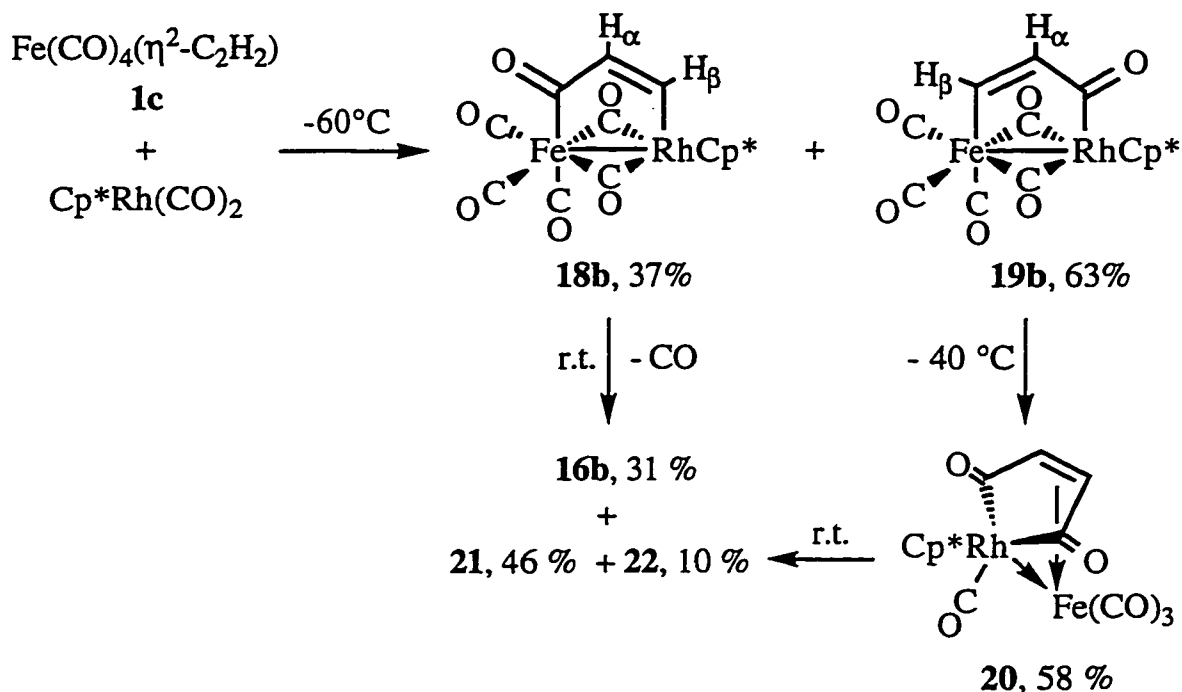


Figure 6-8. ^1H NMR Monitored Reaction of **1c** with $\text{Cp}^*\text{Rh}(\text{CO})_2$ in CD_2Cl_2 (*). (a) Initial, -80°C . (b) After 1 h at -60°C . (c) At -30°C . (d) At -60°C , after 1 day at r.t.

higher field (δ 208.42, 198.81, **18b**; δ 209.18, 201.98, **19b**). The low field doublet indicates a pair of CO ligands symmetrically bridging the Fe and Rh centers while the latter pattern is typical of an $\text{Fe}(\text{CO})_3$ group with C_s symmetry. The key difference between the two compounds lies in the remaining CO resonance which was found as a singlet at δ 248.73 in **18b** and as a doublet ($^1J_{\text{RhC}} = 26$ Hz) at δ 229.36 in **19b**. Both are characteristic of acyl groups in dimetallacyclopentenones, with the former bonded to Fe and the latter to Rh.^{4,37} Compound **18b** is therefore analogous to **18c**, with the exception that the carbonyl ligands symmetrically bridge the two metals as would be expected as one ascends a triad.^{22,23,28} Compound **19b** has the reverse sense of coordination of the bridging organic group (Scheme 6-5).



Scheme 6-5. Low Temperature Reaction of **1a** with $\text{Cp}^*\text{Rh}(\text{CO})_2$ in CD_2Cl_2 .
 Product yields are given as a percentage of all species in solution.

The assignment is supported by the fact that the CH carbons in **19b** gave singlets at δ 176.26 and 146.91. The former resonance was a further 24 ppm downfield than the corresponding CH_β resonance in **18c**, agreeing with expectations as one

moves from a third row to first row metal of attachment.¹³ In **18b**, the analogous resonances were found at δ 180.70 and 141.52. Importantly, the downfield signal, C_{β} , was split into a doublet ($^1J_{RhC} = 31$ Hz) due to coupling to the Rh center.

No further spectral changes were observed at -60°C , but upon warming to -40°C , **19b** underwent a relatively clean conversion to a new species **20** within 1.5 h. In addition to a singlet for the Cp^* group, compound **20** is characterized by a sharp singlet at δ 4.32 ppm in the ^1H NMR spectrum, indicating a highly symmetrical structure. In the ^{13}C NMR spectrum, a pair of singlets were observed at δ 210.15 and 208.19 in a 2:1 ratio for an $\text{Fe}(\text{CO})_3$ group of C_s symmetry. Additionally, a pair of doublets were observed at δ 202.71 and 186.32, also in a 2:1 ratio. The doublet of intensity one had a large $^1J_{RhC}$ coupling constant of 83 Hz, distinctive of a terminal rhodium-bonded carbonyl, while the doublet of intensity two had a smaller coupling constant of 20 Hz which is more typical of an acyl group bonded to Rh.^{4,37}

The CH carbon initially escaped detection, but a more detailed examination of the spectrum revealed that it was hidden at δ 54.25 beneath the intense quintet for the CD_2Cl_2 resonance. In order to confirm the location of the signal, an APT spectrum was collected and the CH resonance appeared in the opposite phase to the solvent quintet. The far upfield chemical shift indicates significant rehybridization of the carbon atom from sp^2 towards sp^3 and compares well to the CH carbon of the coordinated olefinic moiety in **6c** (Chapter 3). A structure compatible with the spectroscopic data is presented in Scheme 6-5, the most interesting feature being that a second migratory CO insertion has occurred at the Rh center. A dative $\text{Rh}\rightarrow\text{Fe}$ bond is implied by electron counting as the Rh-bonded carbonyl is clearly terminally-bonded from its chemical shift and the magnitude of the $^1J_{RhC}$ coupling constant. A structure similar to that of **20** is thus proposed for intermediate **15** seen in the NMR monitored reaction of **1a** with $\text{CpRh}(\text{CO})_2$ in Chapter 5, with the assumption that the signal due to one iron carbonyl moiety went undetected due to the low concentration of this species.

Few changes were apparent upon warming the sample to 0°C , but significant developments occurred upon standing at ambient temperature.

Within 1.5 h, compound **18b** converted completely to **16b**. Species **20** also began to diminish with concomitant formation of new products **21** and **22**. After 8 h at ambient temperature, the disappearance of **20** was 50% complete. At this point, the solution was freeze-thaw degassed three times and allowed to sit overnight at ambient temperature. The final product distribution was determined to be **16b**, 31%:**20**, 5%:**21**, 46%:**22**, 10%: Σ (minor products), 8%. Based on this distribution of products in comparison to the initial 37:63% ratio of **18b** and **19b**, it appears that all of the anticipated product **16b** was derived from **18b** while **19b** produced both **21** and **22**. The minor products appear to be derived in part from each of the two initial intermediates, but their low concentration made proper characterization impossible.

Compounds **21** and **22** have proven to be difficult to characterize owing to the complexity of the final spectra. In particular, carbonyl resonances due to **22** were difficult to detect in the $^{13}\text{C}\{^1\text{H}\}$ spectrum owing to the low concentration of this species. Even for compound **21**, only the following signals could be detected. A pair of doublets were found in the ^1H NMR spectrum at δ 7.52 and 5.64 with a common J_{HH} coupling constant of 4.5 Hz. In the $^{13}\text{C}\{^1\text{H}\}$ NMR, the carbonyls appeared as a doublet at δ 158.20 ($^1J_{\text{RhC}} = 37$ Hz) and equal intensity singlets at δ 210.66 and 173.62. Two singlets were also observed at δ 171.24 and 104.29 ppm, and were assigned to CH groups as they were inverted in the corresponding APT spectrum. Unfortunately, no firm structural assignment could be obtained from this data.

6.4.2. Proposed Mechanisms in the Reaction of **1c** with $\text{Cp}^*\text{Rh}(\text{CO})_2$

In order to obtain further mechanistic information, a second reaction monitoring was undertaken with ^{13}CO enriched **1c** (Figure 6-9). In the first ^{13}C NMR spectrum recorded, **1c** appeared as a broad singlet at δ 210.9 and a sharp doublet was displayed at δ 194.68 ($^1J_{\text{RhC}} = 83$ Hz) for $\text{Cp}^*\text{Rh}(\text{CO})_2$. The integration ratio of the two resonances was 7.2:1, suggesting that some of the ^{13}CO label had already been incorporated into $\text{Cp}^*\text{Rh}(\text{CO})_2$ *via* intermolecular exchange. As with the reaction between **1a** and $\text{CpRh}(\text{CO})_2$ (Chapter 5), there was no evidence of free ^{13}CO in solution at this stage, but it is possible that the

scrambling of the isotopic label could have occurred *via* a process analogous to that in Scheme 5-5. Upon warming the sample to -60°C , the intensities of **1c** and $\text{Cp}^*\text{Rh}(\text{CO})_2$ had become roughly equal in integration and the signals for the products had increased dramatically in intensity. The ^1H NMR spectrum indicated a product distribution of **18b** and **19b** identical to that in the previous reaction, and ^{13}C satellites ($^3J_{\text{CH}} \approx 18$ Hz) were detected for the δ 7.83 and 7.90 resonances, respectively, in support of their dimetallacyclopentenone formulations. Additionally, the assignment of the structures were further supported by the fact that the C_α carbons (δ 141.05, **18b**; 146.48, **19b**) in each were flanked by ^{13}C satellites ($^1J_{\text{CC}} = 39$ Hz, **18b**; 45 Hz, **19b**), confirming their attachment to the acyl group. However, the remaining carbonyl resonances did not correlate with the previous assignments in terms of integrated intensity.

Two contrasting features were noted. In **18b**, the doublet for the symmetrically bridging CO ligands integrated at a value of 0.8 relative to the other signals, implying that the μ -COs contained only 40% of the ^{13}C label that was incorporated into the other signals. This compares quite well in a qualitative sense with the ^{13}C incorporation pattern in **18c**, wherein the resonances attributed to the semi-bridging CO ligands were found to contain only 80% of the ^{13}C label found in the remaining sites. Conversely, in **19b**, the acyl resonance contained 30% greater ^{13}C content than the remaining carbonyl ligands, which integrated in the anticipated 2:2:1 pattern. The mechanistic implications of both results, coupled with the fact that **18b** and **19b** form without net ligand loss, are summarized in Scheme 6-6. It is proposed that migratory CO insertion initiates the reaction in an analogous fashion to that presented in Scheme 5-7. This is not without foundation as **1c** reacts readily with excess acetylene at the remarkably low temperature of -60°C to form $\text{Fe}(\text{CO})_3\{\eta^4\text{-C}_6\text{H}_6\text{C}(\text{O})\}$ (**3**) in which acetylene and CO are linked (Chapter 3).

Following the initial migratory CO insertion step, the reaction can follow two pathways. Nucleophilic attack by $\text{Cp}^*\text{Rh}(\text{CO})_2$ at the electron-deficient β -position of the metallacyclobutenone ring produces **18b** after proceeding through an intermediate in which the two carbonyls originating from the Rh reagent form the bridging carbonyls of the resulting bimetallic. This explains the low

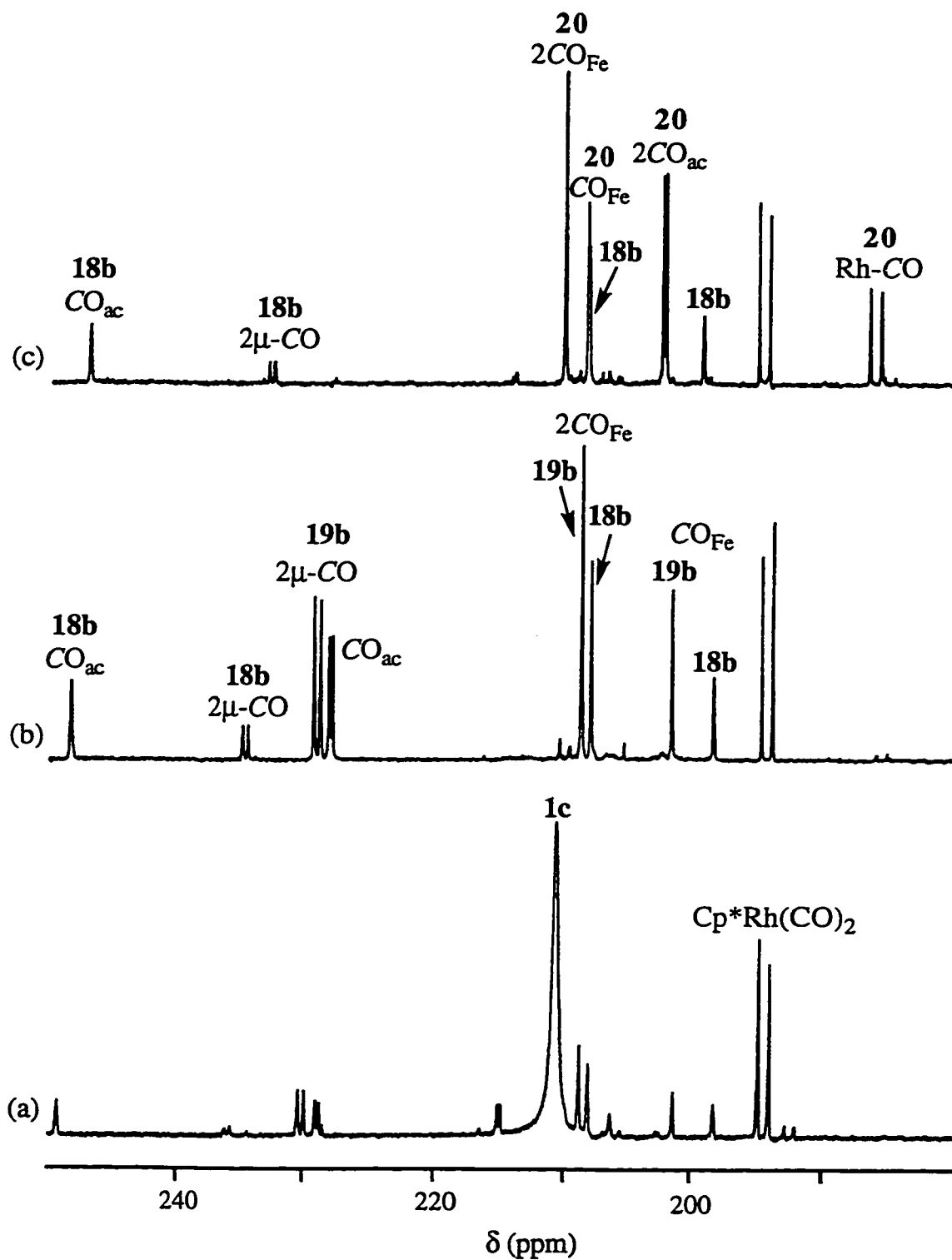
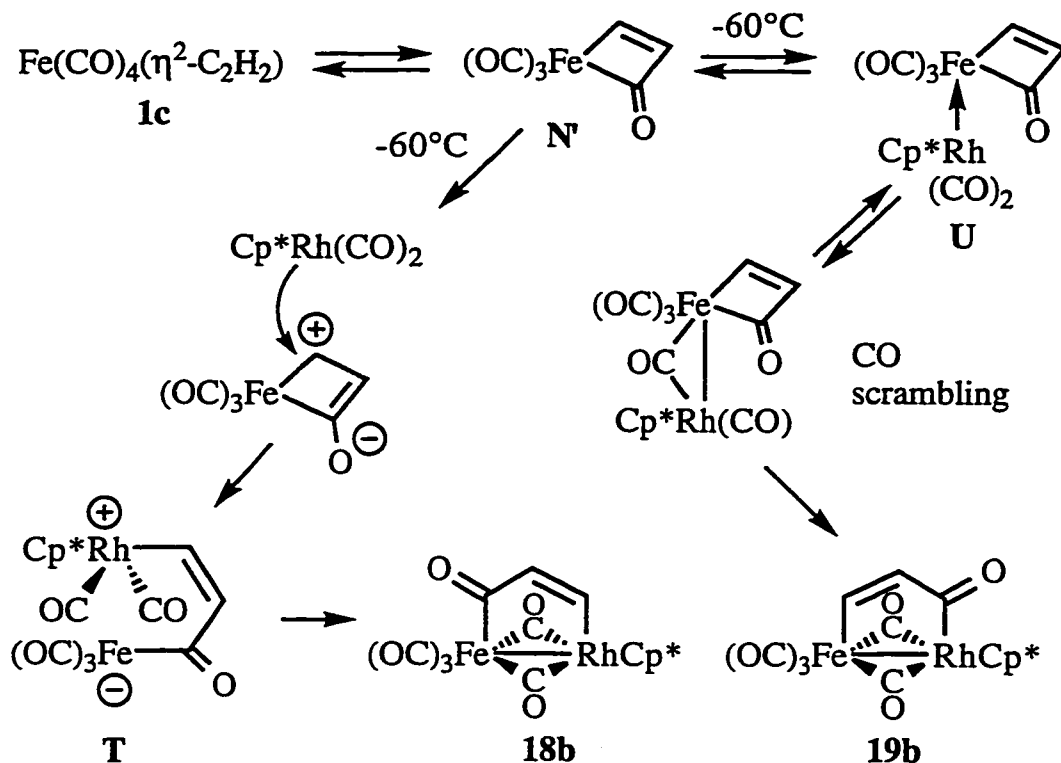


Figure 6-9. ^{13}C NMR Monitored Reaction of **1c** with $\text{Cp}^*\text{Rh}(\text{CO})_2$ in CD_2Cl_2 .
 (a) Initial, -80°C . (b) After 1 h at -60°C . (c) At -20°C .



Scheme 6-6. Proposed Mechanism of Formation for **18b** and **19b**.

integration of the pair of μ -CO ligands as they are originating from a species which originally contained ^{12}CO ligands; the partial ^{13}CO enrichment of the μ -COs is accounted for by the initial ^{13}CO enrichment of $\text{Cp}^*\text{Rh}(\text{CO})_2$ by the reversible dissociative pathway analogous to Scheme 5-5.

The second route involves attack by $\text{Cp}^*\text{Rh}(\text{CO})_2$ at the iron center in order to alleviate coordinative unsaturation. In a manner similar to that in Scheme 5-5, intermediate U can rapidly exchange its carbonyls with the three terminal COs on the iron center. However, the acyl carbonyl does not enter into exchange and thus carries a higher abundance of ^{13}CO than the remaining sites. In a similar manner to that in Scheme 5-7, cleavage of the $\text{Fe}-\text{C}_{\text{acyl}}$ bond results in formation of the $\mu\text{-}\eta^1:\eta^1\text{-C(O)C}_2\text{H}_2$ bridge, with accompanying formation of a metal-metal bond supported by a pair of symmetrically bridging CO ligands.

The key feature in formation of **19b** is that the initial CO insertion serves to "lock in" the ^{13}CO enrichment level of the acyl group while the remaining sites are free to exchange with the ^{12}CO label from $\text{Cp}^*\text{Rh}(\text{CO})_2$. The initial

equilibrium in the pathway leading to **U** can also explain the initial ^{13}C O enrichment of $\text{Cp}^*\text{Rh}(\text{CO})_2$ providing that formation of **19b** is slower than intermetallic ^{13}C O scrambling. The absence of detectable free ^{13}C O in solution certainly favors this proposal, but does not entirely discount the possibility of the CO-dissociation route mentioned earlier as the magnitude of the equilibrium constant between **1c** and $[\text{Fe}(\text{CO})_3(\eta^2\text{-C}_2\text{H}_2)]$ (**D'**) is not known. If CO scrambling between metal centers was rapid, even a small concentration of **D'** could account for the initial ^{13}C O enrichment of $\text{Cp}^*\text{Rh}(\text{CO})_2$.

The two pathways are similar in the sense that tricarbonylferracyclobutenone **N'** acts as an electrophile towards $\text{Cp}^*\text{Rh}(\text{CO})_2$, but they differ in the location where the entering nucleophile attacks. The formation of **18b** is rationalized by the electrophilic center residing on the β -carbon of the organic ring system while production of **19b** is more readily explained by the iron center acting as the site of attack. Thus, intermediate **N'** is best thought of as ambident electrophile which presents two clear reactive sites to an entering metal nucleophile.

It is important to note that although **1c** displays remarkable CO lability, it is not easy to rationalize formation of **18b** and **19b** by initial CO dissociation from the iron-acetylene species. Indeed, if this were the case, a CO-dissociated bimetallic intermediate would be unlikely to re-coordinate CO to form **18b** or **19b** after migratory insertion to form the $\text{C}_2\text{H}_2\text{C}(\text{O})$ moiety, but would be expected, rather, to collapse immediately to **16b** or its $\text{Cp}^*\text{RhFe}(\text{CO})_4(\mu\text{-}\eta^3\text{:}\eta^1\text{-C}(\text{O})\text{C}_2\text{H}_2)$ isomer. However, a reversible dissociative pathway can explain the initial ^{13}C O enrichment of $\text{Cp}^*\text{Rh}(\text{CO})_2$, but the dissociative route does not appear to be important in the formation of bimetallic products. In this sense, the behavior of **1c** towards $\text{Cp}^*\text{Rh}(\text{CO})_2$ can be likened to that of **1a** towards $\text{Os}(\text{CO})_5$ (Section 5.5). An additional experiment showed that ^{13}C O enriched **1c** exchanged its ^{13}C O label with $\text{Os}(\text{CO})_5$ upon warming to -30°C , but the iron-alkyne compound underwent significant decomposition in CD_2Cl_2 during the course of the exchange. Thus, although CO dissociation from the iron-alkyne species can promote a facile interaction with a saturated transition metal species, the resulting interaction need not form a bimetallic product. This behavior differs markedly

from the corresponding Os chemistry where carbonyl dissociation is proposed to account for all reactivity with both transition metal and phosphine nucleophiles.^{4,19}

As in the previous reaction, warming the sample to -30°C converted **19b** to **20** while leaving **18b** unchanged. The acyl resonance in **20** integrated 10% greater than expected indicating that the $\text{CO}_{\text{ac}}-\text{CH}_{\alpha}$ bond in **19b** is retained upon conversion to **20**, which most likely occurs by migration of CH_{β} to a bridging carbonyl with concomitant formation of a terminal Rh–CO bond from the other μ -CO ligand. Upon warming to room temperature, **20** slowly decayed with formation of **21** and **22** along with minor products as before and **18b** converted to **16b**. The ^{13}C O label was statistically distributed in **16b**, presumably by intramolecular carbonyl migration. Unfortunately, the ^{13}C O enriched sample did not shed further light on the structures of **20** and **21**.

6.4.3. Solvent Dependence of the Reaction of **1c** with $\text{Cp}^*\text{Rh}(\text{CO})_2$

It is clear that the change in solvent from pentane, used in the benchtop preparation of **16b**, to CD_2Cl_2 has a marked influence on the outcome of the reaction. Thus, the benchtop reaction of **1c** with $\text{Cp}^*\text{Rh}(\text{CO})_2$ was carried out in CH_2Cl_2 for comparison. As with the NMR-monitored reaction, the benchtop conditions did not lead cleanly to **16b**, but produced species **21** and a mixture of several other products which could not be separated or identified. Washington also noted a difference in product distribution when $\text{Os}(\text{CO})_4(\eta^2\text{-C}_2\text{H}_2)$ was reacted with $\text{CpRh}(\text{CO})_2$ in CD_2Cl_2 or pentane. In this case, the reaction proceeded cleanly but yielded two different products, $\text{CpRhOs}(\text{CO})_5(\mu\text{-}\eta^1\text{:}\eta^1\text{-C}(\text{O})\text{C}_2\text{H}_2)$ and $\text{CpRhOs}(\text{CO})_4(\mu\text{-}\eta^3\text{:}\eta^1\text{-C}(\text{O})\text{C}_2\text{H}_2)$, respectively, and demonstrated an interesting lack of conversion between related dimetallacyclopentenones.⁴ Presently, it is difficult to rationalize the formation of **19b** only in CD_2Cl_2 , especially as the zwitterionic route leading to **18b** and thus **16b** would be expected to be favored in a polar medium. It is also possible that differences in concentration play a role, as NMR requires much greater reagent concentrations than were used in the benchtop preparation of **16b**.

6.4.4. Reaction of **1c** with $\text{Cp}^*\text{Ir}(\text{CO})_2$

Given the clear differences encountered between the NMR monitored reaction in CD_2Cl_2 and the preparative route to **16b** in pentane, the reaction of **1c** with $\text{Cp}^*\text{Ir}(\text{CO})_2$ was also monitored by low temperature NMR spectroscopy in CD_2Cl_2 . As with the previous case, the initial spectrum recorded at -80°C following mixing showed evidence of product formation, and **1c** was consumed after roughly one hour at -60°C . However, the only resonances detected in the ^1H and ^{13}C NMR spectra corresponded to those for **18c**. The only difference observed was that the reaction employing $\text{Fe}(^{13}\text{CO})_4(\eta^2\text{-C}_2\text{H}_2)$ proceeded to give even less ^{13}CO enrichment in the bridging carbonyls, 30% relative to the 1:2:1 pattern of the carbonyls attached solely to the Fe center. This value did not change, even after keeping the sample at -20°C for 1.5 h and at -10°C for 6 h. As with the reaction with $\text{Cp}^*\text{Rh}(\text{CO})_2$, ^{13}CO incorporation into the excess $\text{Cp}^*\text{Ir}(\text{CO})_2$ was observed, suggesting a similar mechanism for the production of **18b,c**. Warming the sample to room temperature produced **18c** in 91% yield, with two minor products in 6 and 3% yield. Curiously, then, it appears that $\text{Cp}^*\text{Ir}(\text{CO})_2$ exclusively attacks the CH_β position in **N'** in both pentane and CD_2Cl_2 in contrast to $\text{Cp}^*\text{Rh}(\text{CO})_2$ which also coordinates to the electron deficient Fe center. The preference for ligand attack by $\text{Cp}^*\text{Ir}(\text{CO})_2$ falls in line with the expectation that the third row metal would be more nucleophilic than its second row congener, but it remains unexplained why $\text{Cp}^*\text{Rh}(\text{CO})_2$ reacts by different routes in CD_2Cl_2 and pentane.

One unexplained difference between runs employing $\text{Fe}(\text{CO})_4(\eta^2\text{-C}_2\text{H}_2)$ and $\text{Fe}(^{13}\text{CO})_4(\eta^2\text{-C}_2\text{H}_2)$ was that, in the latter case, one of the minor products was characterized by a singlet in the ^1H NMR at δ 6.69, and was present in 15% concentration after warming to room temperature. Although it is not clear why this product, **23**, formed in greater quantities in the ^{13}CO enriched sample, it was present at sufficient concentration to allow for characterization by ^{13}C NMR spectroscopy. Interestingly, a 2:2:2:1 pattern of carbonyl resonances was present at δ 217.69, 210.61, 208.98, and 169.72. Further, in the ^1H -coupled ^{13}C NMR spectrum, the furthest downfield resonance appeared as a doublet ($^3J_{\text{CH}} = 19$ Hz), suggesting that it belonged to a pair of equivalent acyl groups. The chemical

shift is too far upfield to be due to Fe-bonded acyl groups, thus suggesting attachment to the Ir center. The furthest upfield signal, at δ 169.72, is due to a terminal Ir-CO, which leaves the remaining pair of resonances, each of intensity two, as belonging to an $\text{Fe}(\text{CO})_4$ group. Additionally, a single CH resonance was detected at δ 162.08 in agreement with the singlet in the ^1H NMR. The chemical shift agrees with the CH group in an $\text{M}\{\eta^1, \eta^1\text{-(O)CCHCHC(O)}\}$ ring system (Table 3-1).²⁷ A structure that reconciles all of the above data is presented in Figure 6-10, and is closely related to **20**.

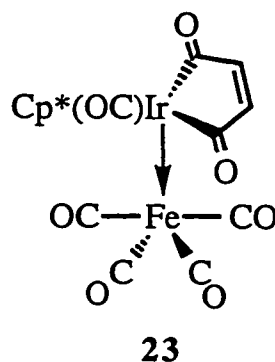


Figure 6-10. Plausible Structure for Compound **23**.

Presumably, the $\text{Fe}(\text{CO})_4$ group rotates rapidly so as to render the inequivalent axial carbonyls time-averaged to give a 1:1 pattern. As in **20**, it is interesting that a dative $\text{Ir} \rightarrow \text{Fe}$ bond is apparently preferred over a covalent metal-metal bond in which case the terminal Ir-CO would bridge the two centers. The fact that **23** contains 7 carbonyl ligands suggests that it may have been formed from further reaction of **18c** with CO since **16c** does not reversibly react with carbon monoxide. However, warming a CH_2Cl_2 solution of **18c** from -20°C under a CO atmosphere induced no reaction, and prolonged stirring at ambient temperature only served to retard the rate of formation of **16c**. The mechanism of formation of **23** is thus unclear.

6.4.5. Conversion of $\mu\text{-}\eta^1\text{:}\eta^1\text{-}$ and $\mu\text{-}\eta^1\text{:}\eta^3\text{-}$ Dimetallacyclopentenones

Despite the added complication in the FeRh chemistry, the conversion of **18b,c** to **16b,c** is interesting because the transformation of a $\mu\text{-}\eta^1\text{:}\eta^1\text{-}$ to an $\mu\text{-}$

$\eta^1:\eta^3$ -dimetallacyclopentenone is rarely observed despite its apparent simplicity. For instance, the $\mu\text{-}\eta^1:\eta^1$ -dimetallacyclopentenones generated from the reaction of $\text{Os}(\text{CO})_4(\eta^2\text{-C}_2\text{R}_2)$ ($\text{R} = \text{H}, \text{Me}$) and $\text{CpM}(\text{CO})_2$ ($\text{M} = \text{Co}, \text{Rh}, \text{Ir}$) are all thermodynamically stable and resistant to CO loss. Even $\text{CpRhOs}(\text{CO})_5(\mu\text{-}\eta^1:\eta^1\text{-C}(\text{O})\text{C}_2\text{H}_2)$, which is generated only when $\text{Os}(\text{CO})_4(\eta^2\text{-C}_2\text{H}_2)$ and $\text{CpRh}(\text{CO})_2$ are combined as concentrated solutions in CD_2Cl_2 , stubbornly refuses to dissociate a carbonyl to form $\text{CpRhOs}(\text{CO})_4(\mu\text{-}\eta^3:\eta^1\text{-C}(\text{O})\text{C}_2\text{H}_2)$, the only product when the reaction is carried out in pentane.⁴ Apart from **18b,c**, the only other known example of this behavior is $\text{OsRu}(\text{CO})_6(\mu\text{-dppm})(\mu\text{-}\eta^1:\eta^1\text{-C}_2\text{H}_2\text{C}(\text{O}))$ which converts to $\text{OsRu}(\text{CO})_5(\mu\text{-dppm})(\mu\text{-}\eta^1:\eta^1\text{-C}_2\text{H}_2\text{C}(\text{O}))$.¹⁹ Interestingly, the latter process is reversible, with the $\mu\text{-}\eta^1:\eta^3$ -dimetallacyclopentenone also being the thermodynamically stable product.

In contrast to the OsRu system and **18b,c**, $\text{OsFe}(\text{CO})_6(\mu\text{-dppm})(\mu\text{-}\eta^1:\eta^1\text{-C}_2\text{H}_2\text{C}(\text{O}))$ is stable towards CO loss.¹⁹ A possible explanation of this result is that the bonding of the terminal iron carbonyls in this compound would be expected to be enhanced by the presence of a donating phosphine ligand. Conversely, the presence of only π -acidic carbonyl ligands in addition to the acyl moiety in **18b,c** would be expected to weaken the Fe–CO bonding sufficiently to promote carbonyl dissociation and allow for the coordination of the more electron-rich olefinic moiety from the cyclopentenone ring. Steric effects should be unimportant in hindering the formation of " $\text{OsFe}(\text{CO})_5(\mu\text{-dppm})(\mu\text{-}\eta^1:\eta^3\text{-C}_2\text{H}_2\text{C}(\text{O}))$ " as the OsRu analog is thermodynamically stable. Although the Fe center would be smaller than Ru, there is no evidence for any steric interaction between the phenyl groups of the dppm ligand and the η^3 -organic moiety in the X-ray crystal structure of $\text{OsRu}(\text{CO})_5(\mu\text{-dppm})(\mu\text{-}\eta^1:\eta^3\text{-C}_2\text{H}_2\text{C}(\text{O}))$.¹⁹

6.5. Conclusions

$\text{Fe}(\text{CO})_4(\eta^2\text{-C}_2\text{H}_2)$ (**1c**) reacts with $\text{Cp}^*\text{M}(\text{CO})_2$ ($\text{M} = \text{Co}, \text{Rh}, \text{Ir}$) and $\text{CpRh}(\text{CO})_2$ to produce dimetallacyclopentenone products (**16a-c**, **17b**, **18c**). At a cursory glance, this is superficially similar to the reactivity of $\text{Os}(\text{CO})_4(\eta^2\text{-C}_2\text{H}_2)$, but the iron systems are distinguished by the fact that the opposite sense of CO insertion occurs so that the acyl group is bonded to iron in almost all cases. The

dimetallacyclopentenones showed a variety of fluxional and structural characteristics, the most interesting of which was the formation of isomers which differed in the orientation of the cyclopentadienyl ring on the ancillary metal center. The reaction of **1c** with $\text{Cp}^*\text{M}(\text{CO})_2$ ($\text{M} = \text{Rh}, \text{Ir}$) was studied by low temperature multinuclear NMR spectroscopy. With $\text{Cp}^*\text{Rh}(\text{CO})_2$, a $\mu\text{-}\eta^1\text{:}\eta^1$ -dimetallacyclopentenone intermediate (**18b**) was detected on the pathway to the stable CO-dissociated product. More interestingly, an isomer with a Rh-bonded acyl group (**19b**) was found to be favored in CD_2Cl_2 . This species did not form a $\mu\text{-}\eta^1\text{:}\eta^3$ -dimetallacyclopentenone on warming, but rather underwent a second migratory insertion at the Rh center to produce compound **20**. The reactions were initiated by migratory CO insertion in **1c**, and non-statistical incorporation of ^{13}CO into the carbonyl sites in the isomeric products enabled the elucidation of competing pathways which differed in the site of attack by the entering metal nucleophile, $\text{Cp}^*\text{Rh}(\text{CO})_2$, on the tricarbonylferracyclobutenone intermediate. In contrast, $\text{Cp}^*\text{Ir}(\text{CO})_2$ appeared to follow only one reaction path in both pentane and CD_2Cl_2 , demonstrating an intriguing metal and solvent dependence of the reaction.

6.6. Experimental Section

Unless otherwise noted, the general synthetic techniques and physical measurements employed are as described in Sections 2.6.1 and 2.6.2.

6.6.1. Reagents

Compound **1c** was prepared according to the procedures described in Chapter 2. $\text{CpRh}(\text{CO})_2$ ³⁸ and $\text{Cp}^*\text{M}(\text{CO})_2$ ($\text{M} = \text{Co}$,³⁹ Rh ,⁴⁰ Ir ⁴¹) were prepared according to published procedures.

6.6.2. Synthetic Procedures

Synthesis of $\text{Cp}'\text{MFe}(\text{CO})_4(\mu\text{-}\eta^1\text{:}\eta^3\text{-C}_2\text{H}_2\text{C}(\text{O}))$ ($\text{Cp}' = \text{Cp}^*$; $\text{M} = \text{Co}$, **16a; Rh , **16b**. $\text{Cp}' = \text{Cp}$; $\text{M} = \text{Rh}$, **17b**).** The same general procedure was followed in each case. Compound **1c** and a slight excess of $\text{Cp}'\text{M}(\text{CO})_2$ were combined in pentane at -78°C and allowed to warm slowly. Analytically pure **16a,b** were obtained by recrystallizing from CH_2Cl_2 /pentane. ^{13}C O enriched material was prepared from $\text{Fe}(^{13}\text{CO})_4(\eta^2\text{-C}_2\text{H}_2)$.

$\text{Cp}^*\text{CoFe}(\text{CO})_4(\mu\text{-}\eta^1\text{:}\eta^3\text{-C}_2\text{H}_2\text{C}(\text{O}))$ (**16a**): Compound **1c** (59 mg, 0.304 mmol) and $\text{Cp}^*\text{Co}(\text{CO})_2$ (82.9 mg, 0.351 mmol) gave dark purple microcrystals of **16a** (86.3 mg, 0.207 mmol, 68 %). The solid was somewhat air sensitive in solution.

F.W. 416.1

Anal. Calcd for $\text{C}_{17}\text{H}_{17}\text{FeCoO}_5$: C, 49.07; H, 4.12. Found: C, 48.80; H, 3.98.

IR (CH_2Cl_2) ν_{CO} 2030(s), 1996(vs), 1963(m), 1940(sh); ν_{acyl} 1816(vw), 1744(m).

^1H NMR (CD_2Cl_2 , 400.1 MHz) δ 9.56 (d, $^3J_{\text{HH}} = 6.5$ Hz, H_β), 3.42 (dd, $^3J_{\text{HH}} = 6.5$ Hz, H_α), 1.88 (s, C_5Me_5).

$^{13}\text{C}\{^1\text{H}\}$ NMR (CD_2Cl_2 , 100.6 MHz, -60°C) δ 233.89 (s, CO_{ac}), 218.63 (s, CO_{Fe}), 213.81 (s, CO_{Fe}), 206.87 (s, CO_{Fe}), 202.4 (br s, CO_{Co}), 176.00 (s, CH_β), 98.37 (s, C_5Me_5), 40.77 (s, CH_α), 9.20 (s, Me).

$^{13}\text{C}\{^1\text{H}\}$ NMR (CD_2Cl_2 , 100.6 MHz, ^{13}C O enriched) (-60°C) δ 233.94 (s, CO_{ac}), 218.63 (s, CO_{Fe}), 213.81 (s, CO_{Fe}), 206.86 (s, CO_{Fe}), 202.42 (s, CO_{Co}). ($+20^\circ\text{C}$) δ 232.86 (s, CO_{ac}), 213.6 (brs, $3\text{CO}_{\text{Fe}(\text{av})}$), 203.2 (br s, CO_{Co}).

EI-MS: M^+ not obs; $M^+ - n \text{ CO} - m\text{H}$ ($m = 0$; $n = 2, 3$; $m = 2$; $n = 1 - 5$); $M^+ - \text{C}_2\text{H}_2 - 5\text{CO}$; $\text{Cp}^*\text{Co}^+/\text{Fe}(\text{CO})_4(\text{C}_2\text{H}_2)^+$ (base peak).

$\text{Cp}^*\text{RhFe}(\text{CO})_4(\mu\text{-}\eta^1\text{-}\eta^3\text{-C}_2\text{H}_2\text{C}(\text{O}))$ (**16b**): $\text{Cp}^*\text{Rh}(\text{CO})_2$ (95.8 mg, 0.326 mmol) and compound **1c** (59 mg, 0.304 mmol) afforded a brick red powder of **16b** (112.6 mg, 0.245 mmol, 81 %). The reaction mixture changed color from orange to deep red at *ca.* -35°C and began to deposit red precipitate soon after.

F.W. 460.1

Anal. Calcd for $\text{C}_{17}\text{H}_{17}\text{FeRhO}_5$: C, 44.38; H, 3.72. Found: C, 44.30; H, 3.45.

IR (CH_2Cl_2) ν_{CO} 2032(s), 2004(vs), 1961(s), 1936(m); ν_{acyl} 1812(w, br), 1742(m).

^1H NMR (CD_2Cl_2 , 400.1 MHz) **16b**: δ 9.22 (dd, $^3J_{\text{HH}} = 6.5$ Hz, $^2J_{\text{RhH}} = 3.5$ Hz, H_β), 3.68 (dd, $^3J_{\text{HH}} = 7$ Hz, $^3J_{\text{RhH}} = 4.5$ Hz, H_α), 2.02 (s, C_5Me_5). **16b'**: δ 9.61 (br, H_β), 3.81 (br, H_α), 1.86 (s, C_5Me_5). **16b**:**16b'** = 12:1.

$^{13}\text{C}\{^1\text{H}\}$ NMR (CD_2Cl_2 , 100.6 MHz, -60°C) δ 234.06 (s, CO_{ac}), 216.65 (s, CO_{Fe}), 214.65 (s, CO_{Fe}), 207.13 (s, CO_{Fe}), 189.86 (d, $^1J_{\text{RhC}} = 86$ Hz, CORh), 169.75 (d, $^1J_{\text{RhC}} = 34$ Hz, CH_β), 103.42 (d, $^1J_{\text{RhC}} = 4$ Hz, C_5Me_5), 41.16 (s, CH_α), 9.29 (s, Me). Signals for **16b'** were not observed.

$^{13}\text{C}\{^1\text{H}\}$ NMR (CD_2Cl_2 , 100.6 MHz, ^{13}CO enriched) **16b**: (-80°C) δ 234.31 (s, CO_{ac}), 216.56 (s, CO_{Fe}), 214.59 (s, CO_{Fe}), 206.92 (s, CO_{Fe}), 189.62 (d, $^1J_{\text{RhC}} = 84$ Hz, CORh). ($+20^\circ\text{C}$) δ 233.09 (s, CO_{ac}), 213.5 (brs, $3\text{CO}_{\text{Fe}(\text{av})}$), 190.49 (d, $^1J_{\text{RhC}} = 85$ Hz, CORh). **16b'**: (-80°C) δ 233.21 (s, CO_{ac}), 216.09 (s, CO_{Fe}), 213.82 (s, CO_{Fe}), 207.56 (s, CO_{Fe}), 188.00 (d, $^1J_{\text{RhC}} = 83$ Hz, CORh). ($+20^\circ\text{C}$) δ 232.13 (s, CO_{ac}), 212.8 (s, $3\text{CO}_{\text{Fe}(\text{av})}$), 189.01 (d, $^1J_{\text{RhC}} = 83$ Hz, CORh).

EI-MS: M^+ (2.2% of base); $M^+ - n \text{ CO}$ ($n = 1 - 5$); ($n = 5$; base peak).

$\text{CpRhFe}(\text{CO})_4(\mu\text{-}\eta^1\text{-}\eta^3\text{-C}_2\text{H}_2\text{C}(\text{O}))$ (**17b**): Compound **1c** (21 mg, 0.108 mmol) and $\text{CpRh}(\text{CO})_2$ (27.5 mg, 0.122 mmol) produced an analytically pure bright orange-red powder of **17b** (35.1 mg, 0.0900 mmol, 83 %).

F.W. 389.9

Anal. Calcd for $C_{12}H_7FeRhO_5$: C, 36.96; H, 1.81. Found: C, 36.96; H, 1.96.

IR (pentane) ν_{CO} 2055(vs), 2023(s), 2013(vs) 1989(m), 1979 (s); ν_{acyl} 1815(w), 1762(w).

IR (CH_2Cl_2) ν_{CO} 2049(s), 2015(vs), 1979(s, br); ν_{acyl} 1813(w), 1753(m).

1H NMR (CD_2Cl_2 , 400.1 MHz, $-40^\circ C$) δ 10.17 (dd, $^3J_{HH} = 6.5$ Hz, $^2J_{RhH} = 3.5$ Hz, H_β , **17b**), 9.42 (dd, $^3J_{HH} = 6.5$ Hz, $^2J_{RhH} \approx 1$ Hz, H_β , **17b'**), 5.67 (s, 5H, Cp, **17b**), 5.26 (s, 5H, Cp, **17b'**), 3.79 (m, H_α , **17b + 17b'**); **17b:17b'** = 2.3:1.

(toluene-*dg*, 200.1 MHz, $-20^\circ C$) δ 9.34 (dd, $^3J_{HH} = 6.5$ Hz, $^2J_{RhH} = 3.5$ Hz, H_β , **17b**), 8.77 (d, $^3J_{HH} = 6.5$ Hz, H_β , **17b'**), 4.64 (s, 5H, Cp, **17b**), 4.53 (s, 5H, Cp, **17b'**), 3.14 (dd, $^3J_{HH} = 6.5$ Hz, $^3J_{RhH} = 5.0$ Hz, H_α , **17b**), 3.04 (dd, $^3J_{HH} = 6.5$ Hz, $^3J_{RhH} = 4.0$ Hz, H_α , **17b'**); **17b:17b'** = 1.3:1. ($+80^\circ C$) δ 9.22 (brs, $H_\beta(av)$), 4.78 (s, 5H, Cp_{av}), 3.21 (dd, $^3J_{HH} = 6.5$ Hz, $^3J_{RhH} = 4.5$ Hz, $H_\alpha(av)$).

$^{13}C\{^1H\}$ NMR (CD_2Cl_2 , 75.5 MHz) δ 210.9 (s, $CO_{Fe(av)}$), 165.09 (d, $^1J_{RhC} = 34$ Hz, CH_β , **17b**), 158.23 (d, $^1J_{RhC} = 34$ Hz, CH_β , **17b'**), 92.25 (brs, C_5H_5 , **17b'**), 92.15 (brs, C_5H_5 , **17b**), 45.29 (s, CH_α , **17b'**), 41.17 (s, CH_α , **17b**).

$^{13}C\{^1H\}$ NMR (CD_2Cl_2 , 100.6 MHz, ^{13}CO enriched, $-100^\circ C$) δ 233.46 (s, CO_{ac} , **17b**), 230.34 (s, CO_{ac} , **17b'**), 212.92 (s, CO_{Fe} , **17b'**), 212.11 (s, CO_{Fe} , **17b**), 211.24 (s, CO_{Fe} , **17b**), 210.94 (s, CO_{Fe} , **17b'**), 206.64 (s, CO_{Fe} , **17b + 17b'**), 187.88 (d, $^1J_{RhC} = 86$ Hz, CO_{Rh} , **17b**), 187.46 (d, $^1J_{RhC} = 84$ Hz, CO_{Rh} , **17b'**); **17b:17b'** = 2.4:1. ($+20^\circ C$) δ 231.54 (s, CO_{ac} , **17b**), 229.66 (s, CO_{ac} , **17b'**), 210.9 (s, $CO_{Fe(av)}$), 188.31 (d, $^1J_{RhC} = 86$ Hz, CO_{Rh} , **17b + 17b'**); **17b:17b'** = 1.6:1.

(toluene-*dg*, 100.6 MHz) ($+20^\circ C$) δ 227.82 (s, CO_{ac} , **17b**), 227.05 (s, CO_{ac} , **17b'**), 210.9 (s, $CO_{Fe(av)}$), 188.50 (d, $^1J_{RhC} = 84$ Hz, CO_{Rh} , **17b'**), 188.12 (d, $^1J_{RhC} = 86$ Hz, CO_{Rh} , **17b**); **17b:17b'** = 1:1. ($+60^\circ C$) δ 227.0 (v br, CO_{ac}), 210.9 (br s, $CO_{Fe(av)}$), 188.3 (br d, $^1J_{RhC} = 81$ Hz, CO_{Rh}). ($+100^\circ C$) δ 211.5 (v br), 188.3 (br) + decomposition products.

EI-MS: M^+ (4.9% of base); $M^+ - n CO$ ($n = 1 - 5$); ($n = 5$; base peak), $M^+ - C_2H_2 - 5CO$, $CpRh^+$.

Synthesis of $Cp^*IrFe(CO)_5(\mu-\eta^1-\eta^1-C_2H_2C(O))$ (18c**).** Under similar conditions, compound **1c** (47 mg, 0.242 mmol) and $Cp^*Ir(CO)_2$ (100.9 mg, 0.263

mmol) afforded a bright yellow powder of **18c** (109.6 mg, 0.190 mmol, 79 %). The initial yellow color began to darken at *ca.* -20°C and warming the solution above *ca.* 0°C began conversion to **16c**.

F.W. 577.4

IR (CH₂Cl₂) ν_{CO} 2065(s), 2007(s), 1994(s), 1964(sh); ν_{acyl} 1613(w, br).

(KBr disk) ν_{CO} 2055(s), 1993(sh), 1985(s), 1951(sh), 1815(w); ν_{acyl} 1604(m).

¹H NMR (CD₂Cl₂, 400.1 MHz, -60°C) δ 7.95 (d, ³J_{HH} = 6.5 Hz, H_β), 6.35 (d, ³J_{HH} = 6.5 Hz, H_α), 1.96 (s, C₅Me₅). (¹³CO enriched) δ 7.95 (d, with ¹³C satellites, ³J_{CH} = 19 Hz, ³J_{HH} = 6.5 Hz, H_β), 6.35 (d, ³J_{HH} = 6.5 Hz, H_α), 1.96 (s, C₅Me₅).

¹³C NMR (CD₂Cl₂, 100.6 MHz, -60°C) δ 248.94 (d, ³J_{CH} = 20 Hz, CO_{ac}), 210.24 (s, 2CO), 205.17 (s, CO), 203.28 (s, 2CO), 152.78 (d, ¹J_{CH} = 153 Hz, CH_β), 148.40 (d, ¹J_{CH} = 156 Hz, CH_α), 101.77 (s, C₅Me₅), 9.17 (q, ¹J_{CH} = 118 Hz, Me).

¹³C{¹H} NMR (CD₂Cl₂, 100.6 MHz, ¹³CO enriched, -100°C) δ 249.10 (s, CO_{ac}), 209.68 (s, 2CO), 204.39 (s, CO), 203.06 (s, CO), 202.97 (s, CO), 152.44 (s, CH_β), 148.40 (s with ¹³C satellites, ¹J_{CC} = 40 Hz, CH_α), 101.10 (s, C₅Me₅), 8.14 (s, Me).

EI-MS: M⁺ (0.5% of base); M⁺ - n CO (n = 1 - 6); M⁺ - C₂H₂ - m CO (m = 5, 6); M⁺ - 6CO - 2H (base peak).

Synthesis of Cp*IrFe(CO)₄(μ-η¹:η³-C₂H₂C(O)) 16c. Compound **18c** was formed *in situ* from **1c** (59 mg, 0.304 mmol) and Cp*Ir(CO)₂ (128.1 mg, 0.334 mmol). After completing crystallization at -80°C, the yellow powder was dissolved in 20 mL CH₂Cl₂ and stirred overnight at ambient temperature. Concentration of the solution, addition of pentane and crystallization at -80°C gave **16c** (131.1 mg, 0.239 mmol, 79 %) as an orange powder. Compound **16c** *did not* revert to **18c** upon stirring under CO.

F.W. 549.4

Anal. Calcd for C₁₇H₁₇FeIrO₅: C, 37.17; H, 3.12. Found: C, 37.15; H, 2.90.

IR (CH₂Cl₂) ν_{CO} 2029(s), 1989(vs), 1963(s), 1941(sh); ν_{acyl} 1826(vw), 1750(m), 1728(w).

¹H NMR (CD₂Cl₂, 400.1 MHz) **16c**: δ 8.73 (d, ³J_{HH} = 6.5 Hz, H_β), 4.65 (d, ³J_{HH} = 6.5 Hz, H_α), 2.20 (s, C₅Me₅). **16c'**: δ 9.35 (brd, ³J_{HH} = 6.5 Hz, H_β), 4.67 (d, ³J_{HH} = 6.5 Hz, H_α), 2.01 (s, C₅Me₅). **16c**:**16c'** = 21:1.

¹³C NMR (CD₂Cl₂, 100.6 MHz, -60°C) δ 236.56 (d, ²J_{CH} = 16 Hz, CO_{ac}), 215.30 (s, CO_{Fe}), 214.38 (s, CO_{Fe}), 207.03 (s, CO_{Fe}), 173.60 (s, CO_{Ir}), 139.21 (d, ¹J_{CH} = 152 Hz, CH_β), 99.77 (s, C₅Me₅), 41.35 (d, ¹J_{CH} = 166 Hz, CH_α), 8.90 (q, ¹J_{CH} = 128 Hz, Me). Signals for **16c'** were not observed.

¹³C{¹H} NMR (CD₂Cl₂, 100.6 MHz, ¹³CO enriched) **16c**: (-60°C) δ 236.57 (s, CO_{ac}), 215.30 (s, CO_{Fe}), 214.38 (s, CO_{Fe}), 207.03 (s, CO_{Fe}), 173.60 (s, CO_{Ir}). (+20°C) δ 235.60 (s, CO_{ac}), 214.0 (brs, 3CO_{Fe(av)}), 173.98 (s, CO_{Ir}). **16c'**: (+20°C) δ 235.92 (s, CO_{ac}), 212.67 (s, 3CO_{Fe(av)}), 178.51 (s, CO_{Ir}).

EI-MS: M⁺ (1.1% of base); M⁺ - n CO (n = 1 - 5); M⁺ - C₂H₂ - 5CO; Cp*Ir(CO)⁺ - 2H (base peak).

6.6.3. X-ray Crystal Structure Determination of Compounds **16b** and **18c**

Deep red single crystals of compound **16b** were grown from a CH₂Cl₂/pentane solution at -80°C. Yellow-orange single crystals of **18c** were grown by slow evaporation of a CH₂Cl₂/pentane solution at -35°C under a CO atmosphere. The X-ray data collection and structure refinement were carried out by Dr. Bob McDonald at the Structure Determination Laboratory, Department of Chemistry, University of Alberta. The crystals were mounted on a thin glass fibre and transferred to the goniometer of a Siemens P4/RA diffractometer⁴² where they were kept under a stream of cooled nitrogen gas. The structures were solved using direct methods techniques (*SHELXS-86*⁴³) and refined by full-matrix least-squares on *F*² (*SHELXL-93*⁴⁴). All non-hydrogen atoms were located. The geometrically constrained hydrogen atoms were placed in appropriate calculated positions. A summary of data collection parameters is given in Tables 6-13 (**16b**) and 6-15 (**18c**). The final atomic coordinates and equivalent isotropic displacement parameters are given in Tables 6-14 (**16b**) and 6-16 (**18c**). Selected interatomic distances and angles are provided in Tables 6-4, 6-5, 6-9, and 6-10.

Table 6-13. Crystallographic Experimental Details for Compound 16b

Formula	C ₁₇ H ₁₇ FeO ₅ Rh
Formula weight	460.07
Crystal dimensions (mm)	0.40 × 0.14 × 0.10
Crystal system	triclinic
Space group	<i>P</i> $\bar{1}$ (No. 2)
Unit cell parameters ^a	
<i>a</i> , Å	8.2524 (2)
<i>b</i> , Å	8.7016 (2)
<i>c</i> , Å	12.9448 (3)
α , deg	93.363 (2)
β , deg	94.316 (2)
γ , deg	108.284 (2)
<i>V</i> , Å ³	876.79(4)
<i>Z</i>	2
ρ_{calc} , g cm ⁻³	1.743
μ , mm ⁻¹	14.453
Radiation, λ (Å)	graphite-monochromated Cu K α (1.54178)
Temperature, °C	-60
Scan type	θ -2 θ
Data collection 2 θ limit, deg	113.5
Total data collected	4656 (-8 ≤ <i>h</i> ≤ 8, -9 ≤ <i>k</i> ≤ 9, -14 ≤ <i>l</i> ≤ 14)
Independent reflections	2329
Number of observations (<i>NO</i>)	2241 ($F_o^2 \geq 2\sigma(F_o^2)$)
Absorption correction method	empirical (face-indexed)
Range of transmission factors	0.3718–0.1466
Data/restraints/parameters	2329 [$F_o^2 \geq -3\sigma(F_o^2)$]/0/218
Extinction coefficient (<i>x</i>) ^b	0.0033 (3)
Goodness-of-fit (<i>S</i>) ^c	1.104 [$F_o^2 \geq -3\sigma(F_o^2)$]
Final <i>R</i> indices ^d	
$F_o^2 > 2\sigma(F_o^2)$	<i>R</i>₁ = 0.0280, <i>wR</i>₂ = 0.0736
all data	<i>R</i>₁ = 0.0290, <i>wR</i>₂ = 0.0742
Largest difference peak and hole	0.658 and -0.807 e Å ⁻³

^aObtained from least-squares refinement of 44 reflections with 57.5° < 2 θ < 59.1°.

^b $F_c^* = kF_c[1 + x\{0.001F_c^2\lambda^3/\sin(2\theta)\}]^{-1/4}$ where *k* is the overall scale factor.

^c $S = [\sum w(F_o^2 - F_c^2)^2 / (n - p)]^{1/2}$ (*n* = number of data; *p* = number of parameters varied; $w = [\sigma^2(F_o^2) + (0.0327P)^2 + 1.1861P]^{-1}$ where $P = [\text{Max}(F_o^2, 0) + 2F_c^2] / 3$).

^d $R_1 = \sum ||F_o| - |F_c|| / \sum |F_o|$; $wR_2 = [\sum w(F_o^2 - F_c^2)^2 / \sum w(F_o^4)]^{1/2}$.

Table 6-14. Atomic Coordinates and Equivalent Isotropic Displacement Parameters for Compound 16b

Atom	<i>x</i>	<i>y</i>	<i>z</i>	<i>U</i> _{eq} , Å ²
Rh	0.24908(3)	0.15474(3)	-0.30580(2)	0.0232(2)*
Fe	0.16313(8)	-0.02569(8)	-0.14539(5)	0.0287(2)*
O1	0.1062(5)	-0.1244(4)	-0.4693(3)	0.0574(10)*
O2	0.3036(5)	0.2378(5)	0.0250(3)	0.0630(10)*
O3	0.0955(5)	-0.2759(5)	0.0011(3)	0.0613(10)*
O4	0.4690(5)	-0.0822(5)	-0.2144(4)	0.0707(12)*
O5	-0.0644(4)	-0.3190(4)	-0.2770(3)	0.0490(8)*
C1	0.1579(5)	-0.0248(5)	-0.4031(4)	0.0351(10)*
C2	0.2493(6)	0.1410(6)	-0.0430(4)	0.0421(11)*
C3	0.1227(6)	-0.1752(6)	-0.0553(4)	0.0410(11)*
C4	0.3501(6)	-0.0537(6)	-0.1926(4)	0.0442(12)*
C5	-0.0145(5)	-0.1813(5)	-0.2391(3)	0.0333(10)*
C6	-0.0806(5)	-0.0483(5)	-0.2229(3)	0.0320(10)*
C7	0.0352(5)	0.1051(5)	-0.2319(3)	0.0307(9)*
C10	0.3547(5)	0.4211(5)	-0.2550(3)	0.0326(9)*
C11	0.4968(5)	0.3561(5)	-0.2453(4)	0.0362(10)*
C12	0.5155(5)	0.2917(5)	-0.3442(4)	0.0338(10)*
C13	0.3877(5)	0.3143(5)	-0.4182(3)	0.0301(9)*
C14	0.2907(5)	0.3982(5)	-0.3619(3)	0.0295(9)*
C15	0.2967(7)	0.5091(6)	-0.1710(4)	0.0519(13)*
C16	0.6145(6)	0.3705(6)	-0.1487(4)	0.0549(14)*
C17	0.6547(6)	0.2215(7)	-0.3692(5)	0.0580(15)*
C18	0.3700(6)	0.2753(6)	-0.5318(4)	0.0444(11)*
C19	0.1607(6)	0.4667(6)	-0.4095(4)	0.0432(11)*

^aAnisotropically-refined atoms are marked with an asterisk (*). The form of the anisotropic displacement parameter is: $\exp[-2\pi^2(h^2a^{*2}U_{11} + k^2b^{*2}U_{22} + l^2c^{*2}U_{33} + 2klb^{*c^*}U_{23} + 2hla^{*c^*}U_{13} + 2hka^{*b^*}U_{12})]$.

Table 6-15. Crystallographic Experimental Details for Compound **18c**

Formula	C ₁₈ H ₁₇ FeIrO ₆
Formula weight	577.37
Crystal dimensions (mm)	0.32 × 0.21 × 0.10
Crystal system	triclinic
Space group	<i>P</i> $\bar{1}$ (No. 2)
Unit cell parameters ^a	
<i>a</i> , Å	8.2247 (10)
<i>b</i> , Å	9.0985 (14)
<i>c</i> , Å	14.163 (2)
α , deg	92.820 (12)
β , deg	104.416 (10)
γ , deg	114.051 (10)
<i>V</i> , Å ³	923.6 (2)
<i>Z</i>	2
ρ_{calc} , g cm ⁻³	2.076
μ , mm ⁻¹	8.012
Radiation, λ (Å)	graphite-monochromated Mo K α (0.71073)
Temperature, °C	-60
Scan type	θ - 2θ
Data collection 2θ limit, deg	50.0
Total data collected	3501 ($0 \leq h \leq 9, -10 \leq k \leq 9, -16 \leq l \leq 16$)
Independent reflections	3251
Number of observations (<i>NO</i>)	3050 ($F_o^2 \geq 2\sigma(F_o^2)$)
Absorption correction method	Gaussian integration (face-indexed)
Range of transmission factors	0.4836–0.2814
Data/restraints/parameters	3251 [$F_o^2 \geq -3\sigma(F_o^2)$]/0/240
Goodness-of-fit (<i>S</i>) ^b	1.111 [$F_o^2 \geq -3\sigma(F_o^2)$]
Final <i>R</i> indices ^c	
$F_o^2 > 2\sigma(F_o^2)$	$R_1 = 0.0303, wR_2 = 0.0770$
all data	$R_1 = 0.0331, wR_2 = 0.0786$
Largest difference peak and hole	2.194 and -1.948 e Å ⁻³

^aObtained from least-squares refinement of 28 reflections with $27.1^\circ < 2\theta < 28.0^\circ$.

^b $S = [\sum w(F_o^2 - F_c^2)^2 / (n - p)]^{1/2}$ (*n* = number of data; *p* = number of parameters varied; $w = [\sigma^2(F_o^2) + (0.0562P)^2 + 0.1647P]^{-1}$ where $P = [\text{Max}(F_o^2, 0) + 2F_c^2] / 3$).

^c $R_1 = \sum |F_o| - |F_c| / \sum |F_o|$; $wR_2 = [\sum w(F_o^2 - F_c^2)^2 / \sum w(F_o^4)]^{1/2}$.

Table 6-16. Atomic Coordinates and Equivalent Isotropic Displacement Parameters for Compound **18c**

Atom	x	y	z	$U_{eq}, \text{\AA}^2$
Ir	0.21400(3)	0.40438(2)	0.290030(14)	0.02327(10)*
Fe	0.43534(13)	0.62653(11)	0.19801(7)	0.0340(2)*
O1	0.6036(7)	0.4794(7)	0.4056(4)	0.0503(13)*
O2	0.0476(7)	0.5773(6)	0.1305(4)	0.0501(13)*
O3	0.8354(8)	0.7347(8)	0.2978(5)	0.071(2)*
O4	0.3816(8)	0.3541(7)	0.0514(4)	0.0590(15)*
O5	0.4971(8)	0.8728(7)	0.0695(4)	0.065(2)*
O6	0.5787(8)	0.9520(6)	0.3089(5)	0.0593(15)*
C1	0.4647(9)	0.4649(8)	0.3557(5)	0.0375(15)*
C2	0.1842(10)	0.5728(8)	0.1710(5)	0.040(2)*
C3	0.6805(11)	0.6874(9)	0.2602(5)	0.045(2)*
C4	0.4039(10)	0.4589(9)	0.1087(5)	0.041(2)*
C5	0.4734(9)	0.7750(9)	0.1188(5)	0.044(2)*
C6	0.4715(10)	0.8106(8)	0.3030(5)	0.0388(15)*
C7	0.3603(9)	0.7627(7)	0.3719(5)	0.0348(14)*
C8	0.2453(9)	0.6094(7)	0.3719(4)	0.0333(14)*
C10	0.1046(8)	0.1321(7)	0.2374(4)	0.0261(12)*
C11	0.1037(8)	0.1622(7)	0.3368(4)	0.0276(12)*
C12	-0.0215(8)	0.2349(7)	0.3380(4)	0.0275(12)*
C13	-0.0957(8)	0.2525(7)	0.2378(4)	0.0269(12)*
C14	-0.0175(8)	0.1859(7)	0.1760(4)	0.0269(12)*
C15	0.2032(10)	0.0425(8)	0.2035(5)	0.0388(15)*
C16	0.2026(10)	0.1121(9)	0.4260(5)	0.043(2)*
C17	-0.0776(9)	0.2770(8)	0.4253(5)	0.039(2)*
C18	-0.2491(9)	0.3027(9)	0.2031(5)	0.040(2)*
C19	-0.0710(9)	0.1645(8)	0.0650(4)	0.0360(14)*

^aAnisotropically-refined atoms are marked with an asterisk (*). The form of the anisotropic displacement parameter is: $\exp[-2\pi^2(h^2a^{*2}U_{11} + k^2b^{*2}U_{22} + l^2c^{*2}U_{33} + 2klb^{*c^{*}}U_{23} + 2hla^{*c^{*}}U_{13} + 2hka^{*b^{*}}U_{12})]$.

6.6.4. Variable Temperature NMR Studies of Fluxional Processes

The general procedures were the same as in Section 5.7.4. The rate constants determined from lineshape simulation of the turnstile processes are summarized in Table 6-17. The rate data for the 17b/17b' isomerization are k (T): 6.0 s⁻¹ (293 K), 19 s⁻¹ (303 K), 50 s⁻¹ (313 K), 115 s⁻¹ (323 K), 260 s⁻¹ (333 K), 600 s⁻¹ (343 K), 1700 s⁻¹ (353 K).

Table 6-17. Summary of the Rate Constants Determined by Spectral Simulation for Turnstile Carbonyl Scrambling in 16a-c and 17b,b'.

T (K) ^a	k (s ⁻¹) ^b				
	16a	16b	16c	17b	17b'
193	–	–	–	–	12.5
203	–	–	–	–	32.5
213	–	–	–	–	105
223	–	–	–	–	275
233	12.5	7.5	4.5	–	575
243	41	24	9.0	13	1700
253	165	78	32	48	4500
263	380	200	80	150	11000
273	1000	530	225	400	–
283	2300	1250	525	1200	–
293	8600	2800	1200	–	–

^aThe estimated error in the temperature is ± 2 K. ^bThe estimated error in k_i is $\pm 10\%$ and generally less accurate near the fast exchange limit.

6.6.5. Variable Temperature NMR Reaction Monitoring

The general technique was the same as in Section 5.7.5, and typically a 14 mg (0.072 mmol) sample of 1c was combined with a slight excess of Cp*M(CO)₂ in cold CD₂Cl₂. ¹H NMR spectra were recorded at 400.1 MHz and ¹³C NMR spectra were recorded at 100.6 MHz.

Cp*RhFe(CO)₃(μ-CO)₂(μ-η¹:η¹-C₂H₂C(O)) (18b):

¹H NMR (-60°C) δ 7.83 (dd, ³J_{HH} = 6.5 Hz, ²J_{RhH} = 3.0 Hz, H_β), 5.63 (dd, ³J_{HH} = 6.5 Hz, ³J_{RhH} = 2.5 Hz, H_α), 1.80 (s, C₅Me₅). (¹³CO enriched) δ 7.83 (dd

with ^{13}C satellites, $^3J_{\text{CH}} = 19$ Hz, $^3J_{\text{HH}} = 6.5$ Hz, $^2J_{\text{RhH}} = 3.0$ Hz, $\text{H}\beta$), 5.63 (dd, $^3J_{\text{HH}} = 6.5$ Hz, $^3J_{\text{RhH}} = 2.5$ Hz, $\text{H}\alpha$), 1.80 (s, C_5Me_5).

$^{13}\text{C}\{^1\text{H}\}$ NMR (-60°C) δ 248.73 (s, CO_{ac}), 234.90 (d, $^1J_{\text{RhC}} = 43$ Hz, $2\mu\text{-CO}$), 208.42 (s, 2CO_{Fe}), 198.81 (s, CO_{Fe}), 180.70 (d, $^1J_{\text{RhC}} = 31$ Hz, $\text{CH}\beta$), 141.52 (s, $\text{CH}\alpha$), 105.78 (d, $^1J_{\text{RhC}} = 4$ Hz, C_5Me_5), 8.17 (s, Me).

$^{13}\text{C}\{^1\text{H}\}$ NMR (^{13}C enriched, -80°C) δ 249.24 (s, CO_{ac}), 235.79 (d, $^1J_{\text{RhC}} = 43$ Hz, $2\mu\text{-CO}$), 208.29 (s, 2CO_{Fe}), 198.50 (s, CO_{Fe}), 181.09 (m, $\text{CH}\beta$), 141.05 (s with ^{13}C satellites, $^1J_{\text{CC}} = 39$ Hz, $\text{CH}\alpha$), 105.81 (s, C_5Me_5), 8.08 (s, Me). The integration of the ^{13}C resonances was 1:0.8:2:1.

$\text{Cp}^*\text{RhFe}(\text{CO})_3(\mu\text{-CO})_2(\mu\text{-}\eta^1\text{:}\eta^1\text{-}(\text{O})\text{CC}_2\text{H}_2)$ (**19b**):

^1H NMR (-60°C) δ 7.90 (d, $^3J_{\text{HH}} = 8.0$ Hz, $\text{H}\beta$), 5.93 (d, $^3J_{\text{HH}} = 8.0$ Hz, $\text{H}\alpha$), 1.75 (s, C_5Me_5). (^{13}C enriched) δ 7.90 (d, with ^{13}C satellites, $^3J_{\text{CH}} = 20$ Hz, $^3J_{\text{HH}} = 8.0$ Hz, $\text{H}\beta$), 5.93 (d, $^3J_{\text{HH}} = 8.0$ Hz, $\text{H}\alpha$), 1.75 (s, C_5Me_5).

$^{13}\text{C}\{^1\text{H}\}$ NMR (-60°C) δ 229.36 (d, $^1J_{\text{RhC}} = 48$ Hz, $2\mu\text{-CO}$), 228.37 (d, $^1J_{\text{RhC}} = 26$ Hz, CO_{ac}), 209.18 (s, 2CO_{Fe}), 201.98 (s, CO_{Fe}), 176.26 (s, $\text{CH}\beta$), 146.91 (s, $\text{CH}\alpha$), 107.31 (d, $^1J_{\text{RhC}} = 4$ Hz, C_5Me_5), 7.96 (s, Me).

$^{13}\text{C}\{^1\text{H}\}$ NMR (^{13}C enriched, -80°C) δ 230.09 (d, $^1J_{\text{RhC}} = 48$ Hz, $2\mu\text{-CO}$), 228.84 (d, $^1J_{\text{RhC}} = 26$ Hz, CO_{ac}), 209.01 (s, 2CO_{Fe}), 201.60 (s, CO_{Fe}), 176.39 (s, $\text{CH}\beta$), 146.48 (s with ^{13}C satellites, $^1J_{\text{CC}} = 45$ Hz, $\text{CH}\alpha$), 107.15 (s, C_5Me_5), 7.86 (s, Me). The integration of the ^{13}C resonances was 2:1.3:2:1.

$\text{Cp}^*\text{Rh}(\text{CO})(\sigma\text{-}\eta^1\text{:}\eta^1\text{:}\mu\text{-}\eta^2\text{-}(\text{O})\text{CCHCHC}(\text{O}))\text{Fe}(\text{CO})_3$ (**20**):

^1H NMR (-60°C) δ 4.32 (s, CH), 1.86 (s, C_5Me_5). (^{13}C enriched) δ 4.32 (s, with ^{13}C satellites, $^3J_{\text{CH}} = 11$ Hz, CH), 1.86 (s, C_5Me_5).

$^{13}\text{C}\{^1\text{H}\}$ NMR (-60°C) δ 210.15 (s, 2CO_{Fe}), 208.19 (s, CO_{Fe}), 202.71 (d, $^1J_{\text{RhC}} = 20$ Hz, 2CO_{ac}), 186.32 (d, $^1J_{\text{RhC}} = 83$ Hz, CORh), 106.91 (d, $^1J_{\text{RhC}} = 2$ Hz, C_5Me_5), 54.25 (s, CH), 9.35 (s, Me).

$^{13}\text{C}\{^1\text{H}\}$ NMR (^{13}C enriched, -30°C) δ 210.43 (s, 2CO_{Fe}), 208.51 (s, CO_{Fe}), 202.68 (d, $^1J_{\text{RhC}} = 20$ Hz, 2CO_{ac}), 186.73 (d, $^1J_{\text{RhC}} = 85$ Hz, CORh), 107.23 (s, C_5Me_5), 9.35 (s, Me). The integration of the ^{13}C resonances was 2:1:2.2:1 and the CH resonance was not detected.

21:

^1H NMR (-60°C) δ 7.52 (d, $J_{\text{HH}} = 4.5$ Hz), 5.64 (d, $J_{\text{HH}} = 4.5$ Hz), 1.90 (s, C_5Me_5).

$^{13}\text{C}\{^1\text{H}\}$ NMR (-60°C) δ 210.66 (s, CO), 173.62 (s, CO), 171.24 (s, CH), 158.20 (d, $^1J_{\text{RhC}} = 37$ Hz, CO), 104.29 (s, CH).

22:

^1H NMR (-60°C) δ 7.47 (s), 7.11 (s), 1.75 (s, C_5Me_5).

$\text{Cp}^*\text{Ir}(\text{CO})(\eta^1:\eta^1\text{-}(\text{O})\text{CCHCHC}(\text{O}))\text{Fe}(\text{CO})_4$ (**23**):

^1H NMR (-60°C) δ 6.69 (brs), 2.03 (s, C_5Me_5).

$^{13}\text{C}\{^1\text{H}\}$ NMR (^{13}CO enriched, -60°C) δ 217.69 (s, 2CO_{ac}), 210.61 (s, 2CO), 208.98 (s, 2CO), 169.72 (s, CO_{Ir}), 162.08 (s, CH), 100.38 (s, C_5Me_5), 8.57 (s, Me).

^{13}C NMR (^{13}CO enriched, -60°C) δ 217.72 (d, $^3J_{\text{CH}} = 19$ Hz, 2CO_{ac}), 210.61 (s, 2CO), 209.01 (s, 2CO), 169.72 (s, CO_{Ir}), 100.38 (s, C_5Me_5).

6.7. References

1. Gagné, M. R.; Takats, J. *Organometallics* **1988**, *7*, 561.
2. Burn, M. J.; Kiel, G.-Y.; Seils, F.; Takats, J.; Washington, J. *J. Am. Chem. Soc.* **1989**, *111*, 6850.
3. Cooke, J.; Takats, J. *J. Am. Chem. Soc.* **1997**, *119*, 11088.
4. Washington, J. PhD Thesis, University of Alberta, 1994.
5. Washington, J. unpublished results.
6. Gracey, B. P.; Knox, S. A. R.; Macpherson, K. A.; Orpen, A. G.; Stobart, S. R. *J. Chem. Soc., Dalton Trans.* **1985**, 1935.
7. Otto, H.; Garcia Alonso, F. G.; Werner, H. *J. Organomet. Chem.* **1986**, *306*, C13.
8. Fontaine, X. L. R.; Jacobson, G. B.; Shaw, B. L.; Thornton-Pett, M. *J. Chem. Soc., Chem. Commun.* **1987**, 662.
9. Fontaine, X. L. R.; Jacobsen, G. B.; Shaw, B. L.; Thornton-Pett, M. *J. Chem. Soc., Dalton Trans.* **1988**, 741.
10. Knox, S. A. R.; Lloyd, B. R.; Morton, D. A. V.; Orpen, A. G.; Turner, M. L.; Hogarth, G. *Polyhedron* **1995**, *14*, 2723.
11. Dyke, A. F.; Knox, S. A. R.; Naish, P.; Taylor, G. E. *J. Chem. Soc., Dalton Trans.* **1982**, 1297.
12. Dyke, A. F.; Knox, S. A. R.; Naish, P. J.; Taylor, G. E. *J. Chem. Soc., Chem. Commun.* **1980**, 409.
13. Mann, B. E.; Taylor, B. F. *¹³C NMR Data for Organometallic Compounds*; Academic: New York, 1981, pp 2-5, 166-176, 180.
14. Werner, H.; Garcia Alonso, F. J.; Otto, H.; Peters, K.; von Schnering, H. G. *Chem. Ber.* **1988**, *121*, 1565.
15. Bennett, M. J.; Pratt, J. L.; Simpson, K. A.; LiShingMan, K. K.; Takats, J. *J. Am. Chem. Soc.* **1976**, *98*, 4810.
16. Bieri, J. H.; Egolf, T.; von Philipsborn, W.; Piantini, U.; Prewo, R.; Ruppli, U.; Salzer, A. *Organometallics* **1986**, *5*, 2413.
17. Ball, R. G.; Edelmann, F.; Kiel, G.-Y.; Takats, J. *Organometallics* **1986**, *5*, 833.

18. Silverstein, R. M.; Bassler, G. C.; Morrill, T. C. *Spectrometric Identification of Organic Compounds*; 5th ed.; Wiley: New York, 1991, pp 113-116, 239, 247.
19. Mao, T. PhD Thesis, University of Alberta, 1996.
20. Mirza, H. A.; Vittal, J. J.; Puddephatt, R. J. *Organometallics* **1994**, *13*, 3063.
21. Breitmaier, E.; Voelter, W. *Carbon-13 NMR Spectroscopy*; VCH: Weinheim, 1987, pp 133-155.
22. Colton, R.; McCormick, M. J. *Coord. Chem. Rev.* **1980**, *31*, 1.
23. Band, E.; Muetterties, E. L. *Chem. Rev.* **1978**, *6*, 639.
24. Roberts, D. A.; Steinmetz, G. R.; Breen, M. J.; Shulman, P. M.; Morrision, E. D.; Duttera, M. R.; DeBrosse, C. W.; Whittle, R. R.; Geoffrey, G. L. *Organometallics* **1983**, *2*, 846.
25. Allen, F. H.; Kennard, O.; Watson, D. G.; Brammer, L.; Orpen, A. G.; Taylor, R. *J. Chem. Soc., Perkin Trans. II* **1987**, S1.
26. Krüger, C.; Barnett, B. L.; Brauer, D. In *The Organic Chemistry of Iron*; E. A. Koerner von Gustorf, F.-W. Grevels and I. Fischler, Eds.; Academic Press: New York, 1978; Vol. I; pp 4.
27. Hoffman, K.; Weiss, E. *J. Organomet. Chem.* **1977**, *128*, 399.
28. Cotton, F. A. *Prog. Inorg. Chem.* **1976**, *21*, 1.
29. Crabtree, R. H.; Lavin, M. *Inorg. Chem.* **1986**, *25*, 805.
30. Cotton, F. A.; Troup, J. M. *J. Am. Chem. Soc.* **1974**, *96*, 5070.
31. Crespi, A. M.; Sabat, M.; Shriver, D. F. *Inorg. Chem.* **1988**, *27*, 812.
32. Guggolz, E.; Ziegler, M. L.; Kalcher, W.; Plank, J.; Riedel, D.; Herrmann, W. A. *Z. Naturforsch* **1981**, *36b*, 1053.
33. George, D. S. A.; McDonald, R.; Cowie, M. *Organometallics* **1998**, *17*, 2553.
34. Deeming, A. J. *Adv. Organomet. Chem.* **1986**, *26*, 1.
35. Casey, C. P.; Cariño, R. S.; Sakaba, H.; Hayashi, R. K. *Organometallics* **1996**, *15*, 2640.
36. Casey, C. P.; Cariño, R. S.; Sakaba, H. *Organometallics* **1997**, *16*, 419.
37. Dickson, R. S.; Gatehouse, B. M.; Nesbit, M. C.; Pain, G. N. *J. Organomet. Chem.* **1981**, *215*, 97.
38. Dickson, R. S.; Tailby, G. R. *Aust. J. Chem.* **1970**, *23*, 1531.

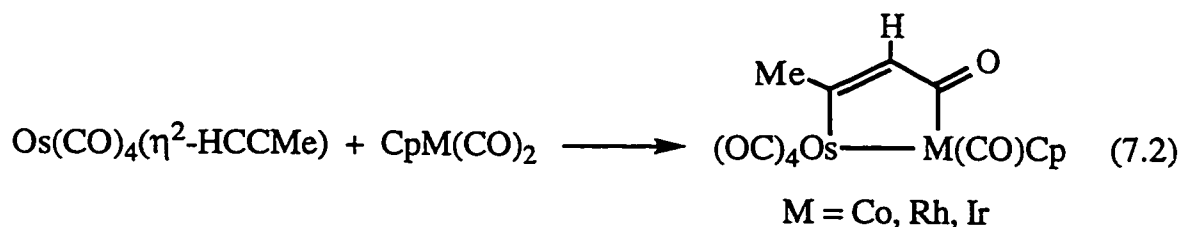
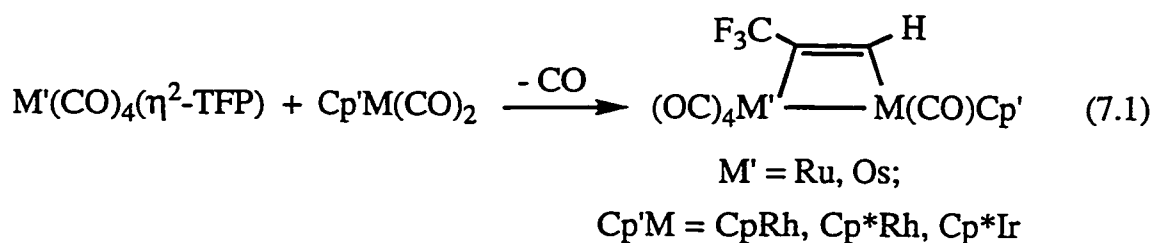
39. Frith, S. A.; Spencer, J. L. *Inorg. Synth.* **1985**, *23*, 15.
40. Werner, H.; Klingert, B. *J. Organomet. Chem.* **1981**, *218*, 395.
41. Ball, R. G.; Graham, W. A. G.; Heinekey, D. M.; Hoyano, J. K.; McMaster, A. D.; Mattson, B. M.; Michel, S. T. *Inorg. Chem.* **1990**, *29*, 2023.
42. Programs for diffractometer operation, data collection, data reduction, and absorption correction were those supplied by Siemens.
43. Sheldrick, G. M. *Acta Crystallogr.* **1990**, *A46*, 467.
44. Sheldrick, G.M. *SHELXL-93*. Program for crystal structure determination. University of Göttingen, Germany, 1993.

Chapter 7

**Heterobimetallic Compounds Derived from
Fe(CO)₄(η²-RCCR') (R = H, R' = CF₃, Me; R, R' = Me)**

7.1. Introduction

Previous chapters have established that Fe(CO)₄(η²-C₂R₂) (R = CF₃, **1a**; H, **1c**) produce a diverse array of heterobimetallic compounds when reacted with Cp'M(CO)₂ (M = Co, Rh, Ir; Cp' = Cp, Cp*). Dimetallacyclopentenones predominated when Cp' = Cp*, and a high degree of regioselectivity was observed, with migratory CO insertion occurring at the Fe center in the majority of cases. However, the coordinated alkynes were symmetrical in **1a,c**, and it was of interest to discover whether the unsymmetrical alkynes in **1b,d** might also introduce substituent control to the regiochemistry of the heterobimetallic products, as was the case when M'(CO)₄(η²-TFP) (M' = Ru,¹ Os²) and Os(CO)₄(η²-HCCMe)² were reacted with Cp'M(CO)₂ (Eqs. 7.1 and 7.2).



In order to complete the study of the bimetallic products available from Fe(CO)₄(η²-alkyne) compounds, the but-2-yne complex **1e** was also reacted with Cp'M(CO)₂.

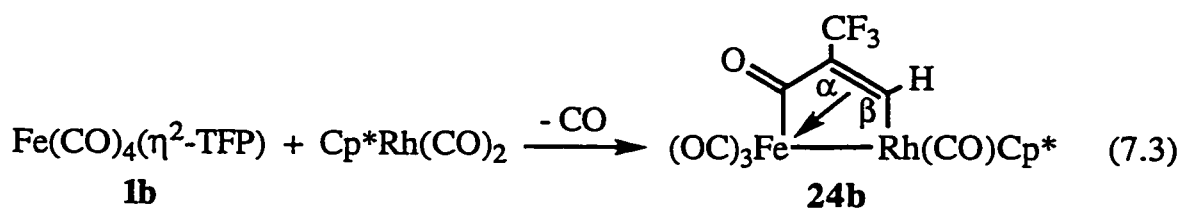
7.2. Reaction of $\text{Fe}(\text{CO})_4(\eta^2\text{-TFP})$ (**1b**) with $\text{Cp}'\text{M}(\text{CO})_2$ ($\text{M} = \text{Co}, \text{Rh}, \text{Ir}$; $\text{Cp}' = \text{Cp}, \text{Cp}^*$): Competing Formation of Dimetallacyclopentenones

7.2.1. Initial Observations

$\text{Fe}(\text{CO})_4(\eta^2\text{-TFP})$ (**1b**) reacted cleanly with the three $\text{Cp}^*\text{M}(\text{CO})_2$ ($\text{M} = \text{Co}, \text{Rh}, \text{Ir}$) reagents and $\text{CpRh}(\text{CO})_2$, but decomposed in the presence of $\text{CpCo}(\text{CO})_2$ and $\text{CpIr}(\text{CO})_2$, thus showing similar reactivity to the acetylene complex **1c** rather than the HFB complex **1a**, the latter of which reacted cleanly with all six $\text{Cp}'\text{M}(\text{CO})_2$ species. $\text{Cp}^*\text{Co}(\text{CO})_2$ and $\text{CpRh}(\text{CO})_2$ gave a mixture of two different bimetallic species, and the reaction with $\text{Cp}^*\text{Ir}(\text{CO})_2$ was even more complicated, generating a thermally unstable mixture of one major product, one minor product, and a number of trace species. The compound derived from $\text{Cp}^*\text{Rh}(\text{CO})_2$ shall be discussed first as it was the only reaction which afforded a single product.

7.2.2. Reaction of $\text{Fe}(\text{CO})_4(\eta^2\text{-TFP})$ (**1b**) with $\text{Cp}^*\text{Rh}(\text{CO})_2$

Elemental analysis and mass spectrometry suggested that the product (**24b**) obtained from the reaction of **1b** and $\text{Cp}^*\text{Rh}(\text{CO})_2$ had the molecular formulation $\text{Cp}^*\text{RhFe}(\text{CO})_5(\text{TFP})$. The CH proton appeared as a doublet ($^2J_{\text{RhH}} = 3 \text{ Hz}$) at $\delta 9.23$, outside the range ($\delta 8.1 - 6.8$) observed in the TFP-bridged complexes from Eq. 7.1.^{1,2} Additionally, $^4J_{\text{HF}}$ was typically on the order of 2 Hz in these compounds and no such coupling was detected in **24b**. On the other hand, the chemical shift of the CH proton is almost identical to that in **16b** ($\delta 9.22$), suggesting a dimetallacyclopentenone structure (Eq. 7.3).



The ^{13}C NMR spectrum proved invaluable in confirming the structure, the most telling features being the characteristic doublet resonance for a terminal Rh carbonyl at $\delta 188.42$ ($^1J_{\text{RhC}} = 84 \text{ Hz}$) and the widely separated resonances for

the TFP carbons. The δ 164.60 signal (C_β) was a doublet, $^1J_{RhC} = 35$ Hz, and the δ 49.57 signal (C_α) was a quartet, $^2J_{CF} = 35$ Hz. When a $^{13}C\{^{19}F\}$ NMR spectrum was collected, the downfield signal was not observed in the baseline noise, and the δ 49.57 resonance collapsed to a singlet. Thus, C_β bears a proton and C_α is substituted by CF_3 . As expected, three resonances were observed in the Fe–CO region (δ 214.95, 211.72, 204.98), and the acyl signal was some 11 ppm further downfield, δ 226.12.

The FT-IR spectrum of **24b** in pentane resembled that of **13b**, showing five terminal CO bands and two lower frequency bands due to acyl or bridging carbonyls, implying that **24b** exists in dynamic equilibrium with a CO-bridged dimetallacyclobutene (Eq. 5.3). The variable temperature ^{13}C NMR spectra also possessed all the hallmarks of a similar mechanism for CO exchange as the one exhibited by **13b**. The three Fe–CO resonances broadened above $-20^\circ C$, agreeing with the anticipated turnstile exchange mechanism, and the acyl and Rh–CO signals also broadened noticeably by $0^\circ C$, suggesting an acyl ejection route followed by merry-go-round carbonyl exchange in the resulting dimetallacyclobutene. However, the instability of **24b** above $0^\circ C$ prevented reaching the fast-exchange limit.

7.2.3. Molecular Structure of $Cp^*RhFe(CO)_4(\mu-\eta^1:\eta^3-CHC(CF_3)C(O))$, **24b**

Although the spectroscopic data readily defined the solution structure of **24b**, crystals were easily obtained and an X-ray diffraction study was performed. The molecular structure of **24b** is presented in Figure 7-1, and selected interatomic distances and angles are provided in Tables 7-1 and 7-2. The structure is analogous to **16b** and the substitution pattern is as predicted from the spectroscopic data. The two compounds have identical orientations of ligands, the only difference being the replacement of a proton by a CF_3 group on C(6). A comparison of important metrical parameters between the two species reveals but a few significant differences within the dimetallacyclopentenone ring.

The FeRh bond length in **24b** is slightly longer than in **16b**, but by only 0.013 Å. Interestingly, there are only subtle differences in the metrical parameters in the two bridging organic moieties, despite the fact that different alkynes are

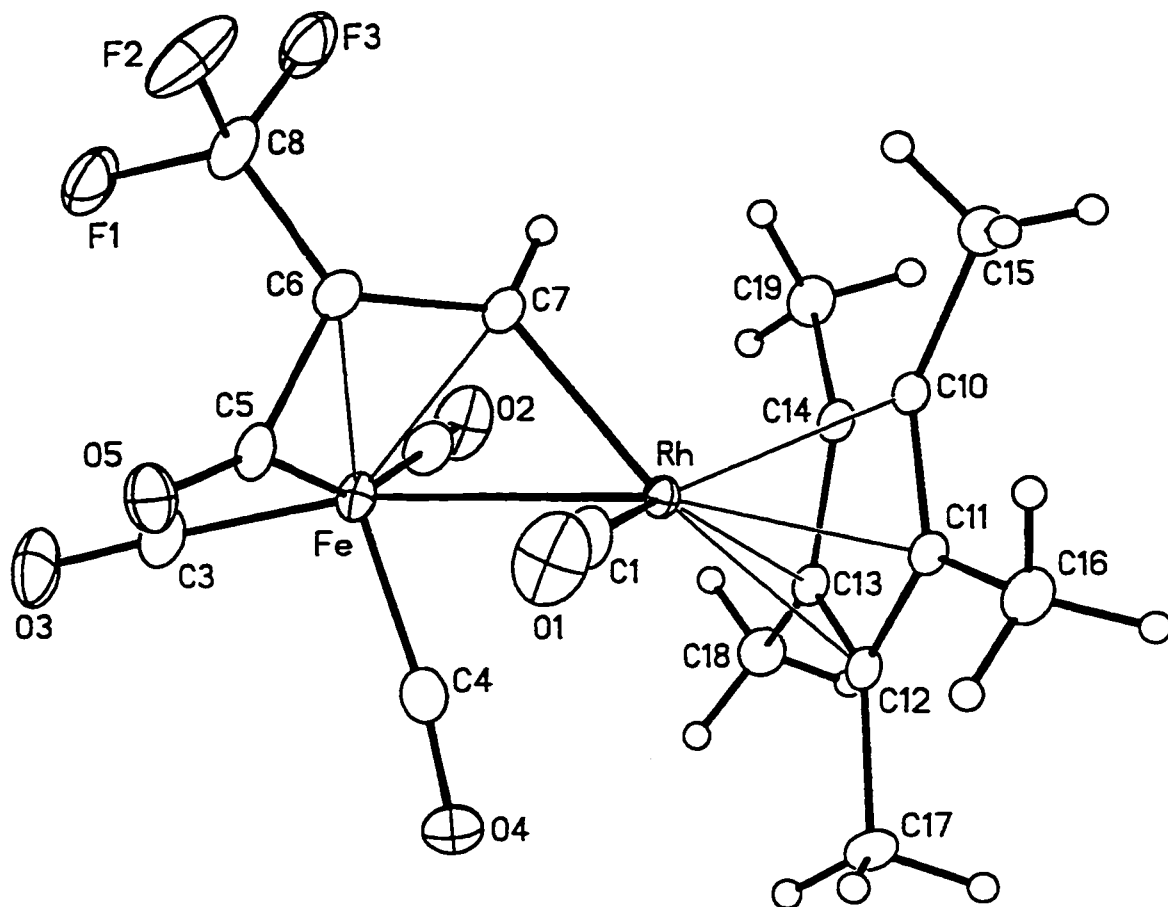


Figure 7-1. Molecular Structure of Compound **24b**.

The numbering scheme up to C(7) is identical to that of **16b** (Figure 6-1).

Table 7-1. Selected Interatomic Distances (Å) in Compound **24b**.^a

Fe–Rh	2.6940(10)	[2.6806(7)]	Fe–C(7)	2.116(6)	[2.095(4)]
Rh–C(1)	1.874(6)	[1.866(5)]	C(1)–O(1)	1.137(7)	[1.137(5)]
Rh–C(7)	2.011(6)	[2.011(4)]	C(2)–O(2)	1.143(8)	[1.142(6)]
Fe–C(2)	1.836(8)	[1.831(5)]	C(3)–O(3)	1.143(8)	[1.152(6)]
Fe–C(3)	1.768(7)	[1.769(5)]	C(4)–O(4)	1.153(7)	[1.136(6)]
Fe–C(4)	1.781(8)	[1.781(5)]	C(5)–O(5)	1.206(7)	[1.199(5)]
Fe–C(5)	1.916(6)	[1.936(4)]	C(5)–C(6)	1.477(9)	[1.437(6)]
Fe–C(6)	2.103(6)	[2.125(4)]	C(6)–C(7)	1.378(8)	[1.393(6)]

^aValues in brackets are for **16b**. Statistically significant differences are in *italics*.

Table 7-2. Selected Interatomic Angles (deg.) in Compound **24b**.

Fe–Rh–C(1)	94.9(2)	[92.55(13)]	C(2)–Fe–C(4)	102.2(3)	[103.5(2)]
Fe–Rh–C(7)	51.0(2)	[50.62(11)]	C(2)–Fe–C(5)	155.0(3)	[155.5(2)]
Fe–C(7)–Rh	81.5(2)	[81.49(14)]	C(2)–Fe–C(6)	114.1(3)	[116.4(2)]
Rh–Fe–C(2)	96.7(2)	[96.41(14)]	C(2)–Fe–C(7)	92.0(3)	[92.8(2)]
Rh–Fe–C(3)	166.4(2)	[167.4(2)]	C(3)–Fe–C(4)	97.8(3)	[98.9(2)]
Rh–Fe–C(4)	70.9(2)	[70.75(15)]	C(3)–Fe–C(5)	87.3(3)	[86.8(2)]
Rh–Fe–C(5)	87.7(2)	[88.23(12)]	C(3)–Fe–C(6)	106.6(3)	[105.4(2)]
Rh–Fe–C(6)	77.9(2)	[77.92(11)]	C(3)–Fe–C(7)	141.6(3)	[140.1(2)]
Rh–Fe–C(7)	47.6(2)	[47.90(11)]	C(4)–Fe–C(5)	102.5(3)	[100.7(2)]
Rh–C(7)–C(6)	127.2(5)	[126.5(3)]	C(4)–Fe–C(6)	134.3(3)	[131.3(2)]
Rh–C(1)–O(1)	174.5(6)	[173.6(4)]	C(4)–Fe–C(7)	118.1(3)	[117.9(2)]
Fe–C(2)–O(2)	176.6(7)	[175.7(4)]	C(5)–Fe–C(6)	42.8(3)	[41.1(2)]
Fe–C(3)–O(3)	177.0(7)	[178.1(5)]	C(5)–Fe–C(7)	72.9(3)	[72.6(2)]
Fe–C(4)–O(4)	172.1(6)	[172.7(4)]	C(6)–Fe–C(7)	38.1(2)	[38.5(2)]
Fe–C(5)–O(5)	147.2(6)	[144.1(3)]	C(1)–Rh–C(7)	92.3(3)	[93.5(2)]
Fe–C(5)–C(6)	75.4(4)	[76.5(3)]	C(5)–C(6)–C(7)	114.4(5)	[115.2(3)]
Fe–C(6)–C(7)	71.5(4)	[69.6(2)]	O(5)–C(5)–C(6)	136.2(6)	[138.3(4)]
Fe–C(7)–C(6)	70.4(4)	[71.9(2)]	C(5)–C(6)–C(8)	120.3(6)	–
C(2)–Fe–C(3)	93.2(3)	[92.9(2)]	C(7)–C(6)–C(8)	124.3(6)	–

^aValues in brackets are for **16b**. Statistically significant differences are in *italics*.

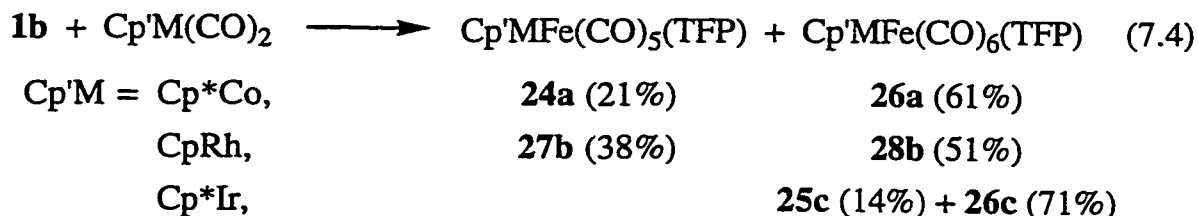
employed. The C(6)–C(7) distances are 1.378(8) (**24b**) and 1.393(6) Å (**16b**), but the difference is of borderline statistical significance. The Fe–C(7) distance in **24b** is slightly longer than the Fe–C(6) separation, which reverses the situation found in **16b**. In the present case, this indicates stronger bonding to C(6) which bears an electron withdrawing CF₃ group, polarizing the alkene double bond toward C(6) at the expense of marginally weaker bonding with C(7). However, the average of the Fe–C(6) and Fe–C(7) distances in both compounds is identical at 2.110 Å, implying that the electronic differences largely balance one another. A more significant difference is found in the C(5)–C(6) separation which is some

0.04 Å longer in **24b**. This feature resembles **13c**, which contains a dimetallacyclopentenone derived from the π -acidic HFB ligand. Thus, the TFP moiety in **24b** confers properties in between HFB and acetylene.

Although structurally characterized dimetallacyclopentenones derived from TFP are unknown, a comparable compound, $\text{CpRh}(\text{P}^i\text{Pr}_3)\text{Fe}(\text{CO})_3(\mu\text{-}\eta^1\text{:}\eta^3\text{-CHCPhC(O)})$, has been prepared by Werner and co-workers.³ As has been noted in Chapter 6, the metrical parameters of this complex are comparable with **16b**, and thus, by extension, to **24b**. The Fe–Rh bond length in Werner's compound, 2.698(1) Å, is virtually identical to that in **24b** (2.694(1) Å), as is the Rh–C(7) distance of 2.016(6) Å compared to 2.011(6) Å.³ However, differences do exist in the manner in which the bridging organic moiety is bonded to the iron center. Namely, while the Fe–C(6) bond is slightly shorter than the Fe–C(7) bond in **24b**, the situation is quite different in Werner's compound, where the corresponding bond lengths are 2.124(5) Å and 2.063(6) Å.³ The olefinic carbon-carbon bond length, 1.393(9) Å, is also somewhat longer than in **24b**.³ In these respects, Werner's compound more closely resembles **16b** than **24b**, suggesting that phenyl group perturbs the basic dimetallacyclopentenone structure to a lesser extent than does the more electronegative trifluoromethyl substituent.

7.2.4. Reaction of **1b** with $\text{Cp}'\text{M}(\text{CO})_2$ ($\text{Cp}'\text{M} = \text{Cp}^*\text{Co}, \text{CpRh}, \text{Cp}^*\text{Ir}$)

Although reaction of **1b** with $\text{Cp}^*\text{Rh}(\text{CO})_2$ afforded a single product, subsequent reactions carried out with the remaining reactive group 9 reagents produced mixtures (Eq. 7.4).



Unfortunately, the mixtures could not be separated because the heterobimetallic products had similar solubility properties, decomposed on silica gel and alumina, and were all somewhat thermally unstable. Consequently, isolation and characterization of the mixtures were conducted at low temperature.

Based on the corresponding reaction of **1c** (Chapter 6), a pair of $\text{CpRhFe(CO)}_4(\mu\text{-}\eta^1\text{:}\eta^3\text{-CHC(CF}_3\text{)C(O)})$ isomers were anticipated from the reaction of **1b** with CpRh(CO)_2 . Although initial characterization suggested that at least two species were present, they had markedly different spectroscopic properties and did not appear to be isomers. Elemental and mass spectral analysis confirmed that the species were bimetallic, but could not differentiate between $\text{CpRhFe(CO)}_5(\text{TFP})$ and $\text{CpRhFe(CO)}_6(\text{TFP})$ formulations. The FT-IR spectrum was expectedly complex, showing 10 CO stretching bands in pentane. Of these, the stretches at highest and lowest frequencies, 2089 and 1667 cm^{-1} , are distinctive of a CpRhFe(CO)_5 framework (eg. **12b**) and a $\mu\text{-}\eta^1\text{:}\eta^1\text{-CRCR'C(O)}$ ring system (eg. **18c**), respectively. The band at 1794 cm^{-1} may be due to the acyl group of a $\mu\text{-}\eta^1\text{:}\eta^3\text{-CRCR'C(O)}$ dimetallacyclopentenone, while a weaker band at 1749 cm^{-1} suggests that a second dimetallacyclopentenone species may be present in minor concentration.

The ^{19}F NMR spectrum revealed three species in roughly a 53:38:9 % ratio, but the chemical shifts were too similar to provide any structural differentiation. In the ^1H NMR spectrum, the major species (**28b**) displayed a quartet at δ 6.58 ($^4J_{\text{HF}} = 2.5$ Hz) for the *CH* proton, which is quite comparable to that of the α -proton in **18c**, δ 6.35. The *CH* protons in the remaining two species, **27b** and **27b'**, were found downfield at δ 10.39 (d, $^2J_{\text{RhH}} = 3.5$ Hz) and 9.66 (s), respectively, and are similar to the β -proton resonances in **17b/b'**. Thus, **27b/b'** are a pair of $\text{CpRhFe(CO)}_4(\mu\text{-}\eta^1\text{:}\eta^3\text{-CHC(CF}_3\text{)C(O)})$ isomers, and the source of the isomerization is presumably analogous to that found in **17b/b'**.

The ^{13}C NMR spectra provided confirmatory spectroscopic proof for the structure of **28b**. At -60°C , carbonyl resonances were found at δ 218.25 (d, $^1J_{\text{RhC}} = 26$ Hz), 207.31, 206.98, and 203.95 (d, $^1J_{\text{RhC}} = 39$ Hz) in a 1:2:1:2 ratio. The farthest downfield resonance is typical of an acyl group bonded to rhodium,⁴ and the remaining resonances are characteristic of a CpRhFe(CO)_5 bimetallic framework undergoing fast, time-averaged, pair-wise merry-go-round carbonyl exchange.² Resonances were also found at δ 163.87 (q, $^2J_{\text{CF}} = 31$ Hz), 157.70 (q, $^3J_{\text{CF}} = 7$ Hz), and 127.00 (q, $^1J_{\text{CF}} = 272$ Hz). The latter is due to the CF_3 group, and the former two resonances are assigned to the CCF_3 and *CH* carbons

respectively on the basis of the decreasing magnitude of J_{CF} over two and three bonds as in **1b**. The assignment was confirmed by a $^{13}\text{C}\{^{19}\text{F}\}$ NMR experiment wherein the quartets at δ 163.8 and 127.0 were reduced to singlets while the quartet at δ 157.7 became a 158 Hz doublet due to coupling to an attached proton. Furthermore, the lack of Rh coupling in the olefinic carbons confirms that neither is bonded to the rhodium center. Finally, when the $^{13}\text{C}\{^1\text{H}\}$ NMR spectrum was recorded on ^{13}CO enriched **28b**, the signal at δ 157.70 showed clear ^{13}C satellites ($^1J_{C\alpha C\beta} = 36$ Hz), confirming its connectivity to the acyl carbonyl and completing the spectroscopic proof of **28b** as $\text{CpRhFe}(\text{CO})_5(\mu\text{-}\eta^1\text{:}\eta^1\text{-C}(\text{O})\text{CHC}(\text{CF}_3))$ (Figure 7-2).

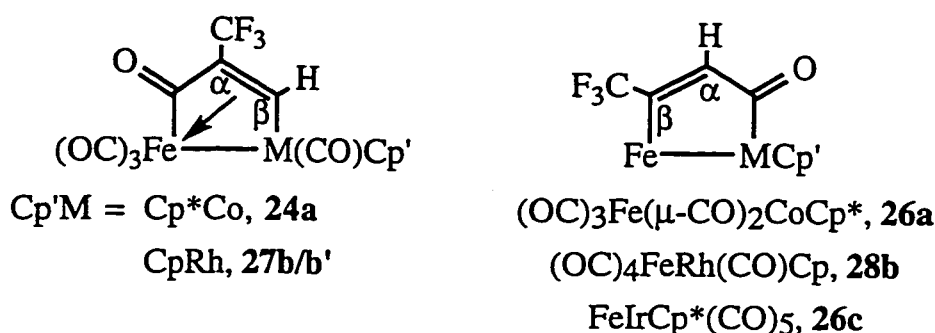


Figure 7-2. Proposed Structures for **24a**, **26a,c**, **27b**, and **28b**.

^{13}C NMR was also instrumental in characterizing **27b**, which displayed resonances analogous to **24b** (Table 7-3) and thus has a corresponding structure. Although the minor isomer was not detected in the natural abundance ^{13}C NMR spectrum, the anticipated pattern of five equal intensity carbonyl resonances was observed in the ^{13}CO enriched sample. As with **17b'**, the signals for the three terminal carbonyls on the Fe center were not detected until the sample was cooled to -80°C because fast turnstile exchange occurred at higher temperature, rendering the three singlets broad at -60°C and undetectable at -40°C .

$\text{Cp}^*\text{Co}(\text{CO})_2$ produced a mixture of dimetallacyclopentenones, **24a** and **26a**, in reaction with **1b** (Eq. 7.4 and Figure 7-2). The important spectroscopic characteristics of the compounds are summarized in Tables 7-3 and 7-4. The $\mu\text{-}\eta^1\text{:}\eta^1\text{-}$ dimetallacyclopentenone **26a** is analogous to **28b**, with the exception that

the prominent band at 1828 cm^{-1} in the FT-IR spectrum indicates the presence of bridging carbonyls. This was confirmed by ^{13}C NMR spectroscopy, wherein a far-downfield singlet of intensity two was detected at δ 241.10 for the symmetrically bridging CO ligands. The chemical shift of the acyl group, δ 239.50, agrees with the proposed structure in Figure 7-2 and compares to the δ 235.2 value in $\text{CpCoOs}(\text{CO})_5(\mu\text{-}\eta^1\text{:}\eta^1\text{-C}(\text{O})\text{CHCMe})$.² The δ 241.10 and 239.50 signals broadened upon warming, without change in the linewidth of the upfield CO resonances on the Fe center. As has been noted before, this broadening is due to interaction with the ^{59}Co quadrupole⁹ and confirms that the acyl group is bonded to the Co center, rather than the Fe center which would also give a downfield resonance, *eg.* δ 248.94 in 18c.

Table 7-3. Selected NMR Data for $\text{MM}'\text{L}_n(\mu\text{-}\eta^1\text{:}\eta^3\text{-CH}_\beta\text{CRC}(\text{O}))$ Species.

$\text{MM}'\text{L}_n$	R	δ (H_β)	δ (C_{ac})	δ (C_β)	δ (C_α)
$\text{Cp}^*\text{CoFe}(\text{CO})_4$ (24a) ^a	CF_3	9.60	225.25	171.28	–
$\text{Cp}^*\text{CoFe}(\text{CO})_4$ (16a)	H	9.56	233.94	176.00	40.77
$\text{Cp}^*\text{RhFe}(\text{CO})_4$ (24b) ^a	CF_3	9.23 ^b	226.12	164.60 ^c	49.57 ^d
$\text{Cp}^*\text{RhFe}(\text{CO})_4$ (16b)	H	9.22 ^b	234.06	169.75 ^c	41.16
$\text{CpRhFe}(\text{CO})_4$ (27b) ^a	CF_3	10.39 ^b	225.00	162.08 ^c	50.66 ^d
$\text{CpRhFe}(\text{CO})_4$ (17b)	H	10.17 ^b	233.46	165.09 ^c	41.17
$\text{CpRhFe}(\text{CO})_4$ (27b') ^a	CF_3	9.66	222.93	–	–
$\text{CpRhFe}(\text{CO})_4$ (17b')	H	9.42	230.34	158.23 ^c	45.29
$\text{Cp}^*\text{IrFe}(\text{CO})_4$ (24c) ^a	CF_3	8.95	228.27	136.28	–
$\text{Cp}^*\text{IrFe}(\text{CO})_4$ (16c)	H	8.73	236.56	139.21	41.35
$\text{CpRh}(\text{P}^i\text{Pr}_3)\text{Fe}(\text{CO})_3$ ³	Ph	9.62	228.26	156.33 ^c	63.10
$\text{Fe}_2(\text{CO})_5(\mu\text{-dppm})$ ⁵	Ph	9.11	211.3	161.4	40.9
$(\text{Ph}_3\text{P})\text{PtFe}(\text{CO})_2(\mu\text{-dppm})$ ⁶	Ph	8.42	–	–	–
$\text{Cp}_2\text{Fe}_2(\text{CO})(\mu\text{-CO})$ ⁷	Ph	12.83	–	–	–
$\text{CpRu}(\text{CO})(\mu\text{-CO})\text{FeCp}$ ⁸	Ph	12.14	235.1	185.7	31.5
$\text{Cp}_2\text{Ru}_2(\text{CO})(\mu\text{-CO})$ ⁷	Ph	11.33	221.2	152.1	43.7

^a CD_2Cl_2 , -60°C . ^bdoublet, $^2J_{\text{RhH}} = 3$ Hz. ^cdoublet, $^1J_{\text{RhC}} = 34\text{-}35$ Hz. ^dquartet, $^2J_{\text{CF}} = 35\text{-}36$ Hz.

Table 7-4. Selected NMR Data for $MM'L_n(\mu-\eta^1:\eta^1-C(O)CH_\alpha CR)$ Species.

$MM'L_n$	R	$\delta(C_{ac})$	$\delta(C_\beta)$	$\delta(C_\alpha)$	$\delta(H_\alpha)$
$Cp^*Co(\mu-CO)_2Fe(CO)_3$ (26a) ^a	CF ₃	239.50	169.62 ^b	144.57	5.81
$CpCoOs(CO)_5$ ²	Me	235.2	157.5	155.8	6.74
$CpRhFe(CO)_5$ (28b) ^a	CF ₃	218.25 ^c	163.87 ^b	157.70 ^d	6.58 ^e
$CpRhOs(CO)_5$ ²	Me	215.3 ^f	156.7	158.9	6.95
$Cp^*RhFe(CO)_5$ (19b)	H	228.37 ^c	176.26	146.91	7.90
$Cp^*IrFe(CO)_5$ (26c) ^a	CF ₃	206.53	170.07 ^b	153.48 ^d	6.40 ^g
$CpIrOs(CO)_5$ ²	Me	199.4	151.4	162.7	7.21
$Ru_2(CO)_7(PMe_3)^1$	CF ₃	247.15	148.64	163.40	6.83 ^h
$RuOs(CO)_7(PMe_3)^1$	CF ₃	247.44	131.27	164.63	7.29 ^h

^aCD₂Cl₂, -60°C. ^bquartet, ²J_{CF} = 30-32 Hz. ^cdoublet, ¹J_{RhC} = 26 Hz. ^dquartet, ³J_{CF} = 7 Hz. ^equartet, ⁴J_{HF} = 2.5 Hz. ^fdoublet, ¹J_{RhC} = 24 Hz. ^gquartet, ⁴J_{HF} = 1.0 Hz. ^hquartet, ⁴J_{HF} = 1.6 Hz.

Interestingly, both species from the reaction of **1b** with Cp*Ir(CO)₂ had a Cp*IrFe(CO)₆(TFP) formulation and gave rise to two singlets of intensity one and two singlets of intensity two in the carbonyl region of the natural abundance ¹³C{¹H} NMR spectrum. The major species, **26c**, displayed spectroscopic characteristics similar to those of **26a** and **28b**, and is proposed to have an analogous dimetallacyclopentenone core. The arrangement of the carbonyl ligands, though, appears to resemble **18c** (Chapter 6). The 2:1:2 array of singlets in the natural abundance spectrum of **26c** resolved to a 2:1:1:1 pattern in the ¹³CO enriched material, and all signals were too far downfield to be due to a terminal Ir carbonyl. Also, although the overall ¹³CO enrichment pattern resembled that of **18b**, namely as the acyl group contained a 50% excess of ¹³C label (*vide infra*), compound **26c** does not have a pair of symmetrically bridging CO ligands because five distinct terminal CO stretching bands were observed in the FT-IR spectrum between 2076 and 2003 cm⁻¹.

The minor component, **25c**, was present in too low a concentration to allow for identification of the resonances arising from the TFP ligand in the ¹³C NMR spectrum, but is proposed to be Cp*IrFe(CO)₅(μ-η¹:η¹-CHC(CF₃)C(O))

(Figure 7-3) on the basis of the downfield shifts of the acyl carbonyl, δ 242.23, and CH proton δ 8.88, which compare to δ 248.94 and δ 7.95, respectively, in **18c**.

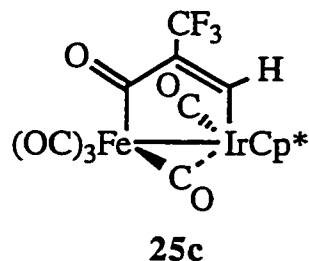


Figure 7-3. Proposed Structure for **25c**.

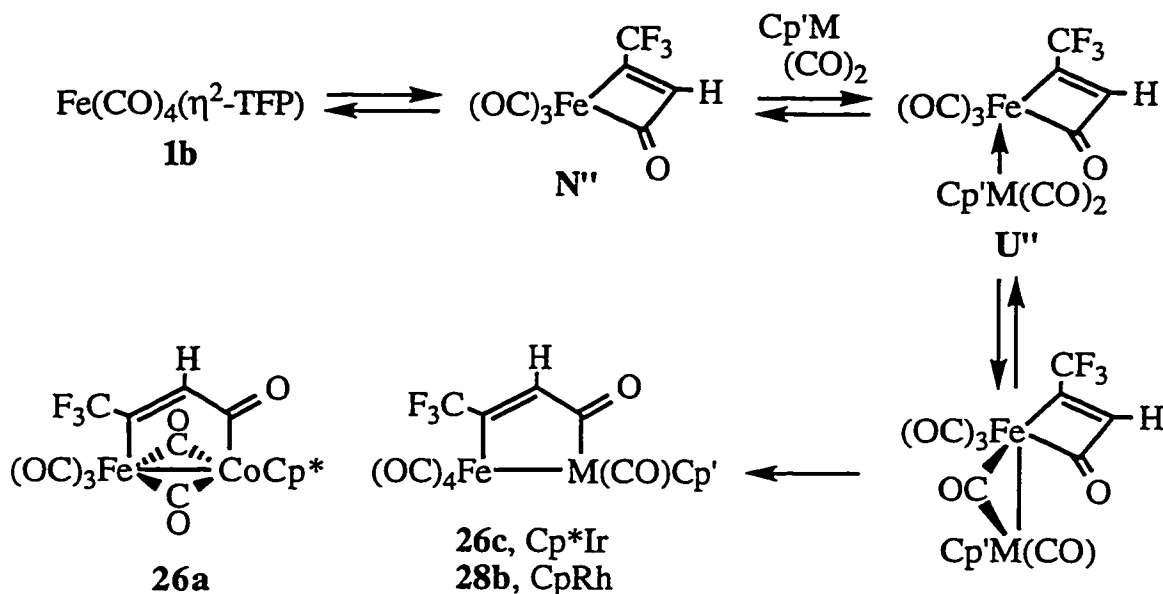
Also, compound **25c** showed anomalous carbonyl integrations in the ^{13}C O enriched material, *i.e.* 1:2:1: \approx 1 compared with 1:2:1:2 from the natural abundance spectrum, agreeing with the ^{13}C NMR features of **18c** which also had non-statistical incorporation of ^{13}C O. Furthermore, the lack of a terminal Ir carbonyl resonance and downfield shift of the resonances of intensity two suggest similar bridging interactions as were proposed for **18c**.

A comparison of the data in Table 7-4 introduces an interesting contradiction. Although compounds **26a,c** and **28b** have acyl carbonyl chemical shifts which are similar to those of their $\text{CpMOs}(\text{CO})_5(\mu\text{-}\eta^1\text{:}\eta^1\text{-C}(\text{O})\text{CHCMe})$ analogs, C_β is generally *upfield* of C_α in these compounds and in $\text{RuM}'(\text{CO})_7(\text{PMe}_3)(\mu\text{-}\eta^1\text{:}\eta^1\text{-C}(\text{O})\text{CHC}(\text{CF}_3))$ ($\text{M}' = \text{Ru}, \text{Os}$). It was noted that this result is not explained by resonance arguments such as Scheme 6-4.^{1,2} Thus, a comparison of the chemical shifts of the olefinic carbons in a $\mu\text{-}\eta^1\text{:}\eta^1$ -dimetallacyclopentenone ring does not provide an accurate determination of the substitution pattern. Accordingly, the orientation of the substituents in **26a,c** was confirmed by preparing ^{13}C O enriched material and noting the presence of ^{13}C satellites ($^1J_{\text{C}\alpha\text{C}\beta} = 39 \text{ Hz}$) at the CH resonance.

7.2.5. Mechanistic Implications of the Product Distributions

The formation of a mixture of $\mu\text{-}\eta^1\text{:}\eta^1$ - and $\mu\text{-}\eta^1\text{:}\eta^3$ -dimetallacyclopentenones, which differ in both the regiochemistry of substituents and

orientation of the bridging moiety with respect to the bimetallic framework, suggests competing reaction pathways. An interesting observation was that ^{13}CO enriched **26a,c** and **28b** displayed atypically high integrations (1.33 - 1.5) for the acyl resonances. Relaxation differences were excluded as the source of the phenomenon, implying that the acyl groups contained 33 - 50% greater ^{13}C label than the remaining carbonyl ligands. The same scenario was encountered for compound **18b** (Chapter 6), a species that also has the acyl group of the dimetallacyclopentenone ring coordinated to the group 9 metal center. That is, the products are formed by a similar mechanism *via* a tricarbonylferracyclobutenone intermediate (N'') (Scheme 7-1).



Scheme 7-1. Proposed Reaction Sequence for Formation of **26a,c** and **28b**.

As with **18b**, the initial migratory insertion forming N'' locks in the ^{13}CO label in the acyl group while the terminal carbonyls exchange with the ^{12}CO ligands in $\text{Cp}'\text{M}(\text{CO})_2$, leading to a lower overall level of ^{13}CO in the $\text{Cp}'\text{MFe}(\text{CO})_5$ bimetallic framework. Gratifyingly, the regiochemistry of the intermediate ferracyclobutenone N'' agrees with that of compound **5b** which formed from **1b** under a CO atmosphere (Chapter 3). As was proposed for the formation of **5b**, the substituent pattern can be rationalized by migratory insertion into the CH

terminus of the alkyne with retention of the stronger Fe–C(CF₃) bond. However, in contrast to **18b**, which was observed only in CD₂Cl₂, **26a,c** and **28b** formed in pentane and carrying out the reaction in CH₂Cl₂ did not significantly alter the product distributions.

Interestingly, upon warming the ¹³CO enriched sample of **28b** to ambient temperature, the downfield doublet for the acyl group broadened noticeably and slowly *decreased in integration* relative to the upfield signals until the statistically expected 1:2:1:2 ratio was achieved. The linewidths of the remaining signals did increase subtly, but not to as great a degree as was observed for that of the acyl group, suggesting that a very slow dynamic process was redistributing the ¹³CO label. As there are no immediately obvious molecular rearrangements that could accommodate the exchange without violating the 18-electron rule, a reasonable explanation would be full reversibility of the equilibria in Scheme 7-1. The conversion of OsRu(CO)₈(μ-η¹:η¹-C(Me)CHC(O)) to its OsRu(CO)₈(μ-η¹:η¹-CHC(Me)C(O)) isomer is equally difficult to rationalize.¹⁰

The formation of **24a,b** and **27b** can be justified by a competing pathway initiated by CO dissociation from **1b**. In an analogous manner to **13a-c** (Chapter 5), the initial product of the reaction is a dimetallacyclobutene **F''** which undergoes migratory insertion to produce the observed dimetallacyclopentenone product (Scheme 7-2). The regioselectivity of the reaction is rationalized by the retention of the stronger Fe–C(CF₃) bond in **M''** while the weaker Fe–CH bond is cleaved and migrates to the group 9 metal center. In the case of **24b**, the above route also agrees with the observation of additional IR bands attributed to a dimetallacyclobutene isomer.

Thus, as with its HFB analog, compound **1b** reacts along competing pathways initiated either by CO dissociation to form **D''** (Scheme 7-2) or migratory insertion to form **N''** (Scheme 7-1), with regiochemistry defined by retention of the stronger Fe–C(CF₃) bond in each case. The reactivity of the Cp'Rh(CO)₂ species is comparable to that of **1a**, as the Cp* compound exclusively affords a μ-η¹:η³-dimetallacyclopentenone product, **24b**, while CpRh(CO)₂ also provides a μ-η¹:η¹-dimetallacyclopentenone in which the acyl carbonyl is bonded to Rh, **28b**. An interesting contrast, though, is that while **28b**

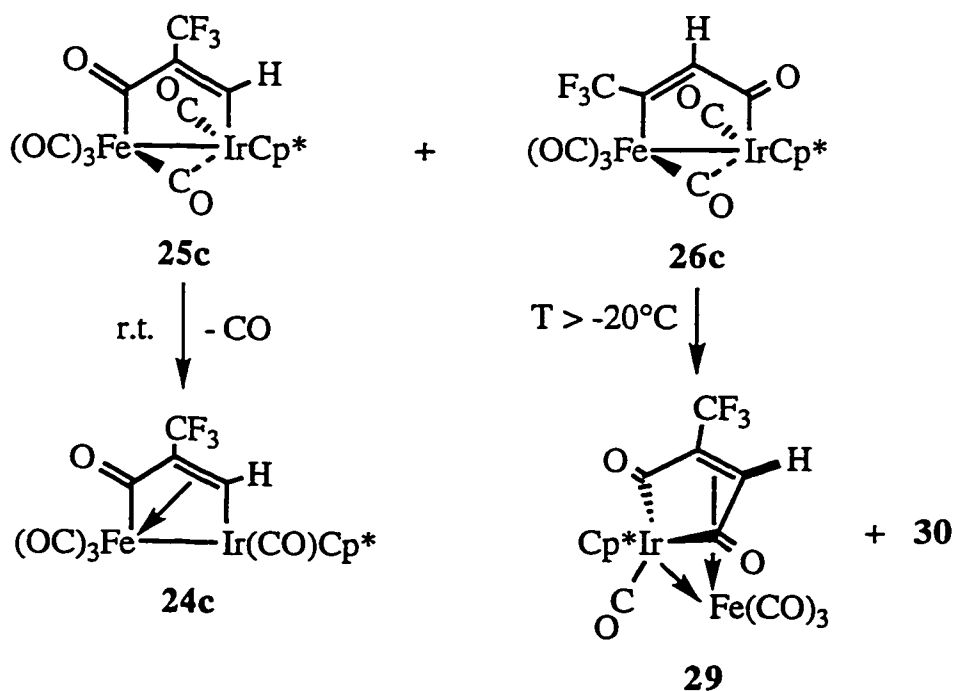
The proposed regiochemistry of the ring is inconsistent with **25c** forming from attack at the C β position in N'' (Scheme 7-1), and can only be rationalized if the ferracyclobutenone (N''*) has the opposite orientation of substituents. The lack of a product derived in a similar fashion from N'' is possibly due to steric hindrance by the bulky CF₃ group in the opposite substituent orientation, which would effectively prevent attack by the entering metal nucleophile. Also, the electron withdrawing CF₃ substituent would tend to destabilize a charge-separated resonance structure in N''. Although similar products were not detected in the other reactions involving Cp'M(CO)₂ (Cp'M = Cp*Co, Cp*Rh, CpRh), the minor nature of this pathway with Cp*Ir(CO)₂ still supports the notion that migratory CO insertion into the Fe–CH bond is preferable to the Fe–C(CF₃) bond in **1b**. Finally, while it is possible that compounds **24a** and **27b** form *via* undetectable intermediates analogous to **25c**, it is extremely unlikely that compound **24b** does as this would require that Cp*Rh(CO)₂ react entirely with N''* while remaining unreactive towards D'' and N'' which are the major accessible intermediates from **1b**.

Thus, Fe(CO)₄(η^2 -TFP) (**1b**) exhibits reactivity intermediate between its HFB and acetylene analogs, which is not entirely unexpected given the mixture of electronic and steric properties imparted by the presence of a single CF₃ substituent on the coordinated alkyne. Unlike **1a**, however, none of the products adopt stable dimetallacyclobutene configurations, but rather exist as the isomeric μ - η^1 : η^3 -dimetallacyclopentenones. Although M'(CO)₄(η^2 -TFP) (M' = Ru, Os) primarily form alkyne-bridged compounds (Eq. 7.1), a connection exists to the corresponding iron chemistry as almost all of the reactions proceed with regioselective retention of the stronger M'–C(CF₃) bond. One of the defining differences appears to be that μ - η^1 : η^3 -dimetallacyclopentenones are favored over dimetallacyclobutenes as one ascends the triad. Accordingly, it is possible to justify why the reaction of Os(CO)₄(η^2 -TFP) with Cp*Co(CO)₂ leads to Os(CO)₄Cp*Co(μ - η^1 : η^3 -C(CF₃)CHC(O)), a dimetallacyclopentenone with the opposite sense of CO insertion and substituent orientation to **24a-c**. In this case, migratory insertion at the first row metal is preferred over the alkyne-bridged configuration of Eq. 7.1. Thus, all combinations of 2nd and 3rd row metals

provide dimetallacyclobutenes, but combinations involving a first row metal appear to favor dimetallacyclopentenones. Finally, the lack of compounds analogous to **26a,c** and **28b** in the Ru and Os chemistry can be traced to the inability of $M'(CO)_4(\eta^2\text{-TFP})$ ($M' = \text{Ru}, \text{Os}$) to undergo initial migratory CO insertion to produce intermediates analogous to N'' .

7.2.6. Identification of the Thermodynamic Products from **25c** and **26c**

Compounds **26a** and **28b** were relatively stable upon warming to ambient temperature, and appeared to decompose more slowly than **24a** and **27b**, respectively. However, **26c** underwent a dramatic change upon warming above -20°C , and converted to two new species, **29** and **30**. Compound **25c**, also in the mixture, was initially unfettered by the increase in temperature. Compound **30** persisted upon warming to ambient temperature, but **29** decomposed and **25c** converted to the anticipated $\mu\text{-}\eta^1\text{:}\eta^3\text{-dimetallacyclopentenone}$ **24c** (Table 7-3), mirroring the conversion of **18c** to **16c** (Scheme 7-4).



Scheme 7-4. Further Reaction of the Mixture of **25c** and **26c**.

Although the minor component, **30**, could not be conclusively identified, compound **29** was characterized by a singlet at δ 5.00 ppm in the ^1H NMR spectrum and six carbonyl singlets (δ 209.74, 209.16, 207.65, 178.12, 177.87, 163.49) in the ^{13}C NMR spectrum. In the ^{13}CO enriched species, one of these, δ 178.12, had an integration 50% higher than the others, clearly indicating its origin as the acyl group in **26c**. Given the presence of a second acyl carbonyl of similar chemical shift (δ 177.87), a terminal Ir-CO (δ 163.49) and three terminal Fe carbonyls to lower field, the most consistent formulation is a structure analogous to **20** (Chapter 6); the latter was derived from **18b**, an FeRh dimetallacyclopentenone analogous to **26c**. The assignment was confirmed by the observation of $^3J_{\text{CH}}$ coupling of 10 Hz to the δ 177.9 acyl carbonyl in the ^1H coupled ^{13}C NMR spectrum. The δ 178.2 signal remained a singlet in accord with it remaining attached to the CH carbon since $^2J_{\text{CH}}$ is negligibly small.¹¹ Although the CH and C(CF₃) resonances were not detected, the upfield shift of the acyl carbonyls and the CH proton relative to compound **23** (Chapter 6) clearly indicate that the olefinic portion of the five membered metallacycle is coordinated to the Fe center.

7.3. Reaction of $\text{Fe}(\text{CO})_4(\eta^2\text{-RCCMe})$ (R = H, **1d**; Me, **1e**) with $\text{Cp}'\text{M}(\text{CO})_2$

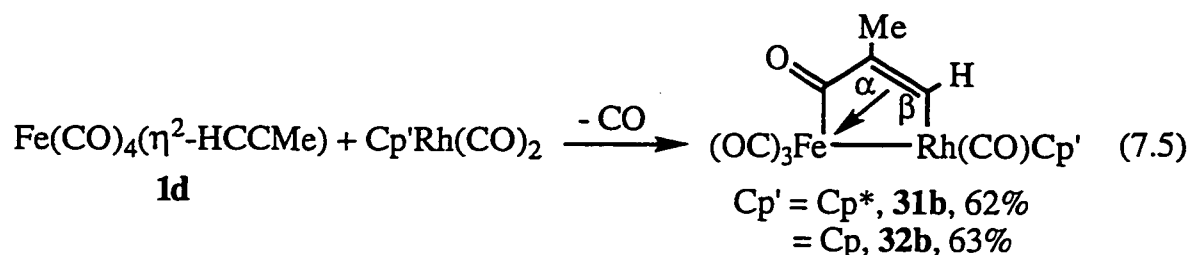
7.3.1. Initial Observations

The $\text{Fe}(\text{CO})_4(\eta^2\text{-RCCMe})$ (R = H, **1d**; Me, **1e**) complexes were less reactive towards $\text{Cp}'\text{M}(\text{CO})_2$ than their HFB, TFP and acetylene cousins. Of the six possible reactants, only $\text{Cp}^*\text{Co}(\text{CO})_2$, $\text{Cp}'\text{Rh}(\text{CO})_2$ (Cp' = Cp, Cp*) and $\text{Cp}^*\text{Ir}(\text{CO})_2$ underwent a reaction with **1d**, and only the Cp*-substituted reagents reacted with **1e**. Additionally, the thermal instability of **1d,e** meant that all of the reactions were complicated by competing decomposition of the iron-alkyne compounds, and intractable, often pyrophoric, brown/black residues formed in the reaction flasks. As a result, any bimetallic complexes which formed were isolated in lower yields than with **1a-c**, especially in the case of the compounds derived from $\text{Cp}^*\text{Ir}(\text{CO})_2$, where the reaction was quite sluggish and decomposition predominated. The reactions between **1d** and $\text{Cp}'\text{Rh}(\text{CO})_2$ proceeded to give one product which could be separated from the intractable

material which formed also, but **1e** was unreactive towards $\text{CpRh}(\text{CO})_2$ and produced a complicated mixture of species with $\text{Cp}^*\text{Rh}(\text{CO})_2$ which proved impossible to properly characterize; $\text{Cp}^*\text{Ir}(\text{CO})_2$ and **1d,e** similarly gave complicated mixtures which were not studied further. $\text{Cp}^*\text{Co}(\text{CO})_2$ was the only reagent to afford one product in reaction with the thermally unstable **1e**.

7.3.2. Characterization of the Products from the Reaction of **1d** with $\text{Cp}'\text{Rh}(\text{CO})_2$ ($\text{Cp}' = \text{Cp}, \text{Cp}^*$)

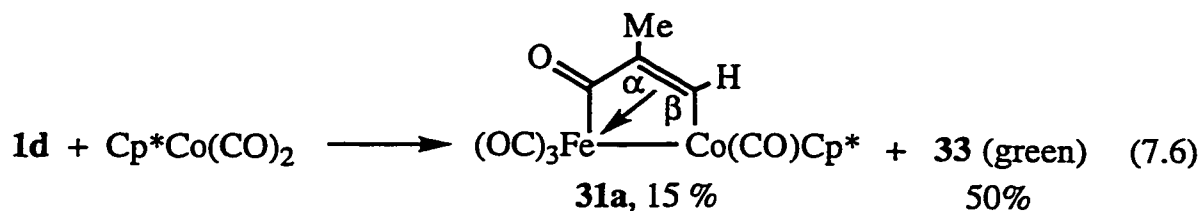
Compound **1d** reacted with $\text{Cp}'\text{Rh}(\text{CO})_2$ to produce reddish-brown dimetallacyclopentenones **31b** ($\text{Cp}' = \text{Cp}^*$) and **32b** ($\text{Cp}' = \text{Cp}$), which were separated from intractable brown/black residues by extraction with CH_2Cl_2 and pentane, respectively (Eq. 7.5).



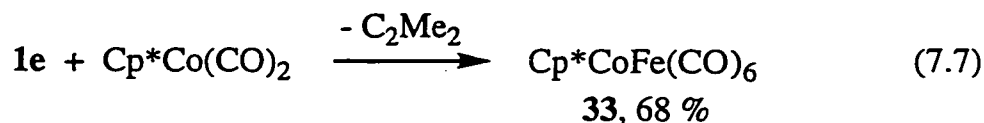
The IR, ^1H and ^{13}C NMR spectra of the compounds agree with the proposed structures, and the regiochemistry of the ring was confirmed by APT experiments which clearly demonstrated that the bridging carbons had attached protons. As with its TFP and acetylene analogs, the compound derived from $\text{CpRh}(\text{CO})_2$ existed as a pair of isomers, **32b/b'**. However, unlike the corresponding reaction of **1b** with $\text{CpRh}(\text{CO})_2$, no evidence was found for a dimetallacyclopentenone in which the acyl group was bonded to Rh. Interestingly, the regiochemistry of the ring was identical to that in the TFP analogs, despite the different electronic characteristics of the substituents.

7.3.3. Unexpected Formation of $\text{Cp}^*\text{CoFe}(\mu\text{-CO})_2(\text{CO})_4$, **33**, *via* Alkyne Loss

The reaction of **1d** with $\text{Cp}^*\text{Co}(\text{CO})_2$ gave two inseparable products which were isolated by pentane extraction at 0°C (Eq. 7.6).



The minor component had similar spectral characteristics to **31b** and is assigned a corresponding dimetallacyclopentenone structure, but the major component, **33**, differed significantly from expectations in that it was a dark green color and *did not contain any ^1H or ^{13}C NMR resonances for the propyne moiety*. Intriguingly, the dark green compound formed exclusively in the reaction of the butyne analog, **1e**, with $\text{Cp}^*\text{Co}(\text{CO})_2$, and elemental analysis provided the molecular formulation $\text{Cp}^*\text{CoFe}(\text{CO})_6$ (Eq. 7.7).



The product was thermally unstable and slowly decomposed above *ca.* 0°C in solution, but formed dark green needles from pentane at -80°C and could be handled as a solid in air at ambient temperature for short periods.

It is quite interesting that **33** formed as the net result of alkyne loss from **1d,e** as the alkyne ligand is retained in all other reactions of $\text{Fe}(\text{CO})_4(\eta^2\text{-alkyne})$ species discussed thus far. Indeed, **1d,e** react with CO at low temperature to produce the dimeric compounds **6d,e** rather than dissociating the alkyne and coordinating CO to form $\text{Fe}(\text{CO})_5$. A reaction initiated by CO loss from **1d,e** would require subsequent alkyne loss and CO scavenging to form **33**, which also seems unlikely. Based on the reactivity of **1b,c**, it is possible that **33** forms by decomposition of a $\mu\text{-}\eta^1\text{:}\eta^1$ -dimetallacyclopentenone analogous to **18b** or **26a**, perhaps *via* FeCo analogs of compounds such as **20** or **29**, both of which are thermally unstable and decompose on warming to unknown products.

The pentane IR spectrum of **33** displayed four terminal CO stretches at 2050, 2018, 1977 and 1974 cm^{-1} , and a pair of bands were observed in the bridging region at 1831 and 1815 cm^{-1} . However, electron counting suggests

that only a single bridging CO is necessary to support a covalent metal-metal bond (structure V in Figure 7-4).

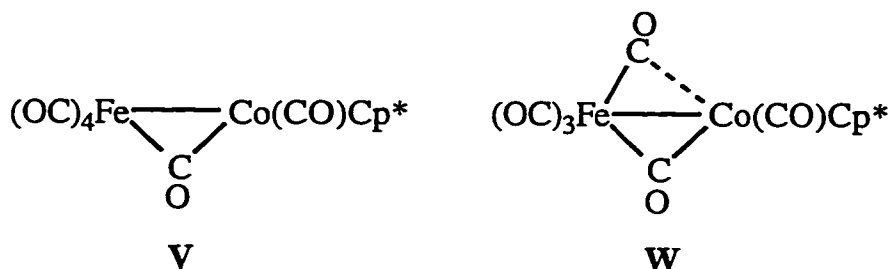


Figure 7-4. Possible Structures for Compound 33.

The second μ -CO band could be accounted by the semi-bridging interaction of a terminal Fe carbonyl with the electron rich Co center, structure W. However, the μ -CO bands occur at quite similar frequencies, implying that both COs should have similar bridging character.

The ^{13}C NMR spectrum of **33** was largely uninformative, as a single resonance was observed at δ 224.02 ppm for the carbonyl ligands at -20°C , suggesting a highly fluxional structure. In accord with this suggestion, cooling the sample to -100°C caused the singlet to broaden and become asymmetric. Thus, the -20°C spectrum is the fast exchange limit for global carbonyl exchange while the broad asymmetric resonance at -100°C represents decoalescence or an intermediate rate of exchange. Unfortunately, the low temperature limiting spectrum was not accessible. The averaged chemical shift of δ 224 ppm agrees with some of the carbonyl ligands adopting bridging positions in the ground state, thereby accounting for the downfield shift. In order to further probe the structure of this interesting bimetallic compound, single crystals were grown from a pentane solution of **33** at -35°C .

7.3.4. Molecular Structure of $\text{Cp}^*\text{CoFe}(\mu\text{-CO})_2(\text{CO})_4$, **33**

The molecular structure of compound **33** is presented in Figure 7-5, and selected interatomic distances and angles are provided in Tables 7-5 and 7-6. Interestingly, and contrary to simple electron counting arguments but in accord

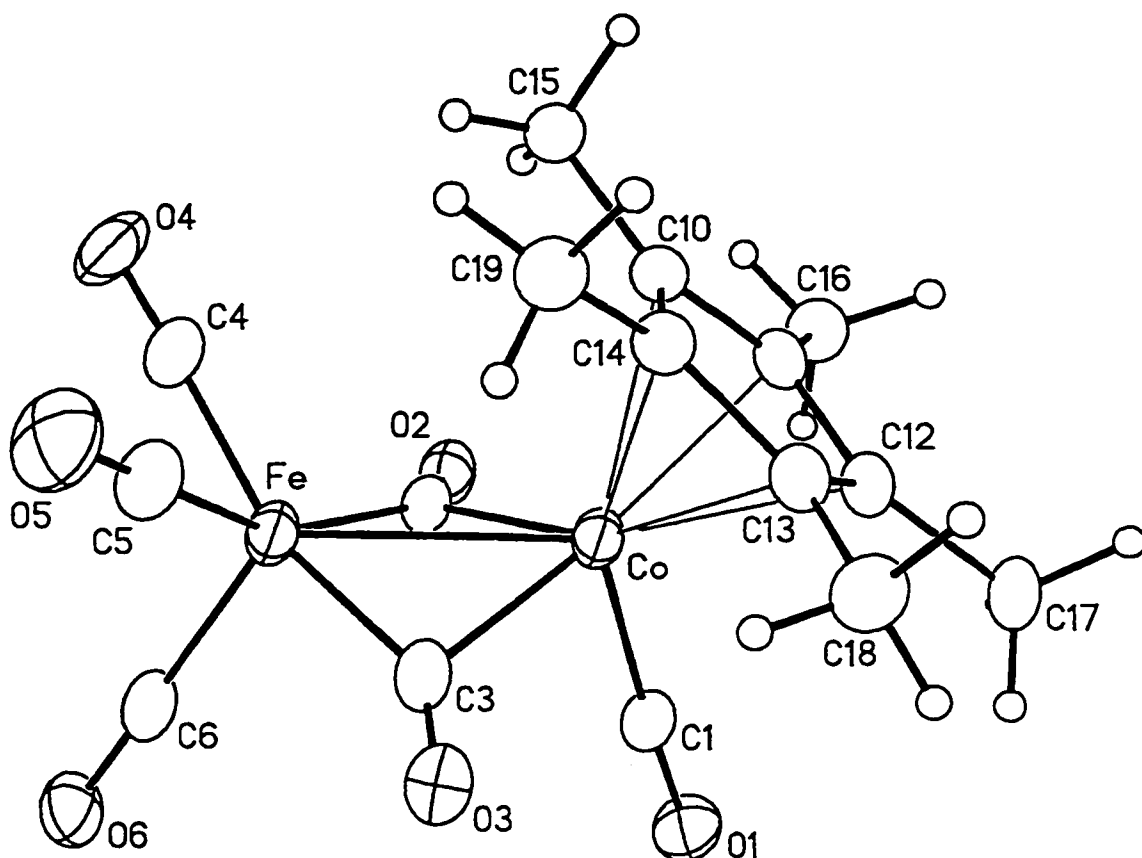


Figure 7-5. Molecular Structure of Compound 33.

Table 7-5. Selected Interatomic Distances (Å) in Compound 33.^a

Fe–Co	2.5459(9)	[2.591(1)]	Fe–C(6)	1.798(5)	[1.801(3)] ^d
Co–C(1)	1.768(5)	[1.762(3)]	C(1)–O(1)	1.132(5)	
Co–C(2)	2.017(5)	[1.941(3)]	C(2)–O(2)	1.171(5)	
Co–C(3)	2.006(5)	[1.834(3)]	C(3)–O(3)	1.161(6)	
Fe–C(2)	1.883(5)	[1.943(3)]	C(4)–O(4)	1.131(6)	
Fe–C(3)	1.910(5)	[2.225(3)]	C(5)–O(5)	1.136(6)	
Fe–C(4)	1.802(6)	[1.771(4)] ^b	C(6)–O(6)	1.136(6)	
Fe–C(5)	1.808(6)	[1.802(4)] ^c			

^aValues in brackets are for Cp*FeCo(μ -CO)₂(CO)₄ (Figure 7-7, Ref. 14) with the metal labels reversed. ^bC(5), ^cC(6), ^dC(4) in Figure 7-7.

Table 7-6. Selected Interatomic Angles (deg.) in Compound **33**.^a

Fe–Co–C(1)	105.43(14)		Fe–C(5)–O(5)	177.3(5)	
Fe–Co–C(2)	47.00(13)	[48.21(9)]	Fe–C(6)–O(6)	178.5(4)	
Fe–Co–C(3)	47.81(14)	[57.4(1)]	C(1)–Co–C(2)	87.0(2)	
Co–Fe–C(2)	51.57(13)	[48.14(8)]	C(1)–Co–C(3)	89.1(2)	
Co–Fe–C(3)	51.12(14)	[43.95(8)]	C(2)–Co–C(3)	89.2(2)	[101.0(1)]
Co–Fe–C(4)	117.7(2)		C(2)–Fe–C(3)	96.3(2)	[88.4(1)]
Co–Fe–C(5)	116.2(2)		C(2)–Fe–C(4)	83.5(2)	
Co–Fe–C(6)	121.64(14)		C(2)–Fe–C(5)	156.7(2)	
Co–C(2)–Fe	81.4(2)	[83.7(1)]	C(2)–Fe–C(6)	99.6(2)	
Co–C(3)–Fe	81.1(2)	[78.7(1)]	C(3)–Fe–C(4)	160.3(2)	
Co–C(1)–O(1)	176.9(4)		C(3)–Fe–C(5)	85.1(2)	
Co–C(2)–O(2)	128.5(3)	[137.5(2)]	C(3)–Fe–C(6)	95.1(2)	
Co–C(3)–O(3)	130.7(4)	[153.3(3)]	C(4)–Fe–C(5)	87.5(2)	
Fe–C(2)–O(2)	149.8(4)	[138.9(2)]	C(4)–Fe–C(6)	104.4(2)	
Fe–C(3)–O(3)	147.9(4)	[128.0(2)]	C(5)–Fe–C(6)	103.4(2)	
Fe–C(4)–O(4)	177.7(5)				

^aValues in brackets are for Cp*FeCo(μ -CO)₂(CO)₄ with the metal labels reversed.

with the IR spectrum, the heterobimetallic contains two bridging and four terminal carbonyl ligands. Three of the terminal COs are on the Fe center while the fourth resides on Co. Interestingly, the bridging carbonyls are quite symmetrical with respect to the pseudo-mirror plane through C(6), Fe, Co, and C(1) (torsion angle = 5.5(2)°). The coordination geometry of the Fe center is difficult to describe, but can be thought of as a square-based pyramid, with C(6) as the apex, if the metal-metal bond is neglected.¹² The coordination geometry also resembles the Co centers in Co₂(CO)₈.¹³ Indeed, the C(4)–Fe–C(5) angle of 87.5(2)° and C(4)–Fe–C(6) and C(5)–Fe–C(6) angles of 104.4(2) and 103.4(2)°, respectively, in **33** compare to the corresponding angles between terminal carbonyls in Co₂(CO)₈ (93.3, 101.6, and 108.3°; the indicated values are the average from the two independent molecules in the crystal of the dicobalt

compound).¹³ The apical carbonyl in **33**, C(6)O(6), is related to the bridging carbonyls, C(2)O(2) and C(3)O(3), by angles of 99.6(2) and 95.1(2)°, respectively, which compare with 96.9 and 93.2° in Co₂(CO)₈.¹³

The bridging carbonyls, C(2)O(2) and C(3)O(3), adopt an interesting configuration. Both have shorter Fe–C(O) bonds than Co–C(O) bonds by *ca.* 0.12 Å, and the Fe–C–O angles (*ca.* 149°) are larger than the Co–C–O angles (*ca.* 130°) by approximately 19°. As a result, the bridging C–O vectors are not perpendicular to the Fe–Co bond and intersect at angles of 98.2(2) and 96.8(2)° respectively. As such, the μ -COs in **33** appear to be semi-bridging as asymmetrically bridging carbonyls are typically normal with respect to the metal-metal bond.¹⁵ Yet, asymmetrically bridging carbonyls tend to have more similar M–C(O) distances than semi-bridging carbonyls, and a deviation of *ca.* 0.25 Å has been suggested as a practical borderline between the two possibilities.¹⁶ The difference of *ca.* 0.12 Å between the Fe– and Co–C(O) bond distances in **33** appears to be at odds with the latter criterion, but the 0.25 Å value was suggested from a study of polynuclear iron compounds and is not easily applied to heterobimetallics. Namely, differences in metal covalent radii will affect the observed bond lengths. Based on the well recognized decrease in metallic radii as one proceeds across a row of the periodic table, it is reasonable to suggest that an Fe(0) center will have a larger covalent radius than a Co(0) center, which will in turn be larger than the oxidized Co(I) center in **33**.¹⁷ Accordingly, a correction for the difference in metal radii would show more disparate M–C(O) bond lengths. The structure of **33** can thus be described as a highly distorted Fe(CO)₅ moiety coordinated to an unsaturated Cp*Co(CO) fragment through an Fe→Co dative bond which is stabilized by a pair of similar, strongly semi-bridging carbonyls originating from the Fe center (Figure 7-6).

Stone and co-workers have structurally characterized an isoelectronic compound, Cp(OC)Mn(μ -CO)₂Rh(CO)Cp*, which also possesses a pair of similar semi-bridging carbonyl ligands.¹⁸ The Mn–C(O) and Rh–C(O) distances were 1.866(7) and 2.172(7) Å, and the Mn–C–O and Rh–C–O angles were 153.0(6) and 123.3(5)°, respectively. The larger difference in the M–C–O angles and the fact that the bridging C–O vectors intersect the Mn–Rh bond at an angle of

100.0(6)° suggest a slightly weaker interaction with the Rh center than is found for the Co center in **33**. The increased length of the Rh–C(O) bond is mostly due to the increase of *ca.* 0.16 Å in the Mn–Rh bond length compared with the Fe–Co bond length in **33**. Also, the reaction of Cp*Rh(CO)₂ with Fe₂(CO)₉ provided the FeRh analog of **33** in 29% yield relative to the major product, Fe₂Rh(CO)₇(μ-CO)₂Cp*.¹⁸ Although definitive data, such as ¹³C NMR, was not presented, a structure analogous to that in Figure 7-6 was proposed for Cp*RhFe(μ-CO)₂(CO)₄ on the basis of similar characteristics in its IR spectrum to the isoelectronic Cp*Rh(CO)(μ-CO)₂Mn(CO)Cp*.¹⁸ Indeed, the IR spectrum, 2053(vs), 2017(vs), 1979(s), 1961(sh), 1835(sh), 1825(s) cm⁻¹ in hexane, is virtually identical to **33**.

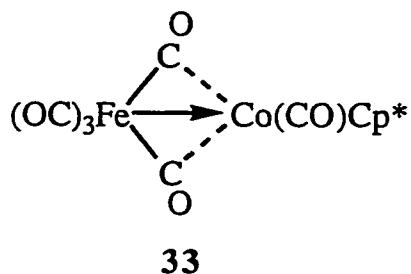


Figure 7-6. Bonding Description of Compound **33**.

An intriguing comparison can also be drawn with an isomeric compound to **33** in which the Cp* ring is found on the Fe center (Figure 7-7).¹⁴ The formation of Cp*FeCo(μ-CO)₂(CO)₄ was also serendipitous, being isolated as one of two low yield products from the thermolysis of (μ-η²:η²-Cp*Fe(CO)₂-C≡CH)Co₂(CO)₆ at +70°C.¹⁴ Interestingly, the thermal stability of Cp*FeCo(μ-CO)₂(CO)₄ is contrary to **33** which decomposes above 0°C in solution. The structure is similar to that of **33** in a number of respects, and a comparison of pertinent metrical parameters is provided in Tables 7-5 and 7-6; for ease of comparison with the corresponding values in **33**, the Co and Fe labels have been transposed in the Tables. For example, the "Co–C(1)" bond in Table 7-5 refers to the Fe–C(1) bond from Figure 7-7.

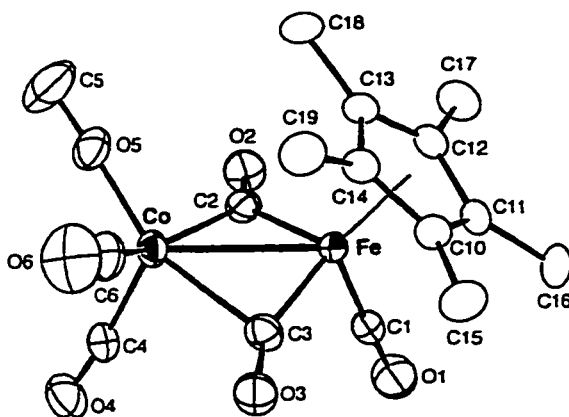


Figure 7-7. Molecular Structure of $\text{Cp}^*\text{FeCo}(\mu\text{-CO})_2(\text{CO})_4$ (Fig. 5 in Ref. 14).

Although the coordination geometries about the Fe and Co centers in $\text{Cp}^*\text{FeCo}(\mu\text{-CO})_2(\text{CO})_4$ resemble the Co and Fe centers, respectively, in **33**, the bridging CO ligands are quite different. $\text{C}(2)\text{O}(2)$ bridges the metal-metal bond in an essentially symmetrical manner as its vector intersects the metal-metal bond at a near-right angle, $90.8(1)^\circ$. Conversely, the $\text{C}(3)\text{O}(3)$ ligand is bonded strongly to the Fe center and has a weaker semi-bridging interaction to Co. The $\text{Fe}-\text{C}(3)$ and $\text{Co}-\text{C}(3)$ separations differ by 0.39 \AA , and $\text{C}(3)\text{O}(3)$ is tilted towards the Co center so that its vector intersects the metal-metal bond at an angle of $95.9(1)^\circ$. The presence of the symmetrically bridging $\text{C}(2)\text{O}(2)$ ligand also requires an $\text{Fe} \rightarrow \text{Co}$ dative bond under the 18 electron rule (Figure 7-8). This feature persists in solution as the $\mu\text{-CO}$ stretching bands ($1858, 1776 \text{ cm}^{-1}$) are separated by greater than 80 cm^{-1} .¹⁴

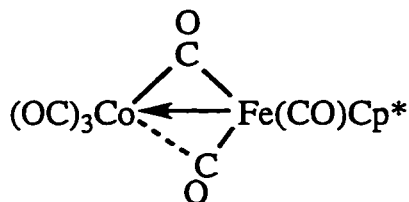


Figure 7-8. Bonding Model for $\text{Cp}^*\text{FeCo}(\mu\text{-CO})_2(\text{CO})_4$.

Thus, the electronic characteristics of the two isomers are quite different, as might be expected by transposing the group eight and group nine metals. The alignment of the semi-bridging CO ligands in both compounds can be rationalized by considering the direction of electron transfer implied from the orientation of the dative bonds. The semi-bridging carbonyls serve to take up the additional electron density conferred to the Co center in each case. Interestingly, the Fe–Co bond is 0.045 Å shorter in **33** than in Cp*FeCo(μ -CO)₂(CO)₄. The metal-metal separation is similar to that in CpFeCo(μ -CO)₂(CO)₃L (L = CO, 2.545(1);¹² PMePh₂, 2.540(4) Å¹⁹). The former compound (L = CO) was described as having a pair of asymmetrically bridging carbonyls, implying a covalent metal-metal bond, while the latter has symmetrically and semi-bridging carbonyls analogous to those in Figure 7-7.¹⁵ Compound **33** and Cp'FeCo(μ -CO)₂(CO)₃L compounds thus demonstrate an interesting continuum of structural types, and the flexibility of bridging carbonyls on the bimetallic framework serve as a reminder of the formality of bonding descriptions such as those in Figures 7-6 and 7-8.

7.4. Conclusions

The trifluoropropyne complex **1b** produced two types of bimetallic compounds in reaction with Cp'M(CO)₂. The first were μ - η^1 : η^3 -dimetallacyclopentenones which had similar traits to the dinuclear compounds derived from the symmetrical HFB and acetylene complexes **1a,c**. The CF₃ substituent was located adjacent to the acyl group, and the regiochemistry was rationalized by retention of the stronger Fe–C(CF₃) bond in forming an intermediate dimetallacyclobutene. However, the major products in most reactions were μ - η^1 : η^1 -dimetallacyclopentenones in which the acyl group was bonded to the group 9 metal center and the substituent orientation was reversed, a result rationalized by initial migratory CO insertion into the Fe–CH bond of **1b**. The propyne and but-2-yne compounds, **1d,e**, proved to be less reactive towards Cp'M(CO)₂ and decomposition products predominated in many of the reactions. Nonetheless, μ - η^1 : η^3 -dimetallacyclopentenones were isolated from **1d** when M = Rh, and the reactions were regioselective, with the methyl substituent adjacent to the acyl group on the Fe center. More interesting was the reaction of **1e** with

$\text{Cp}^*\text{Co}(\text{CO})_2$, which produced the bimetallic complex $\text{Cp}^*\text{CoFe}(\mu\text{-CO})_2(\text{CO})_4$ (33) *via* net alkyne loss. Although novel from the viewpoint that all other reactions of $\text{Fe}(\text{CO})_4(\eta^2\text{-alkyne})$ thus far have proceeded with retention of the alkyne ligand, the latter compound is also interesting in that it contains an $\text{Fe}\rightarrow\text{Co}$ dative bond supported by a pair of similar semi-bridging carbonyl ligands.

7.5. Experimental Section

Unless otherwise noted, the general synthetic techniques and physical measurements employed are as described in Sections 2.6.1 and 2.6.2.

7.5.1. Reagents

Compounds **1b,d,e** were prepared according to the procedures described in Chapter 2. $\text{CpRh}(\text{CO})_2^{20}$ and $\text{Cp}^*\text{M}(\text{CO})_2$ ($\text{M} = \text{Co},^{21} \text{Rh},^{22} \text{Ir}^{23}$) were prepared according to published procedures.

7.5.2. Synthetic Procedures

Reaction of $\text{Fe}(\text{CO})_4(\eta^2\text{-TFP})$ (1b**) with $\text{Cp}^*\text{Co}(\text{CO})_2$.** Compound **1b** (46 mg, 0.176 mmol), dissolved in 20 mL pentane, was added to $\text{Cp}^*\text{Co}(\text{CO})_2$ (49.3 mg, 0.197 mmol) at -78°C and allowed to warm slowly to room temperature. The solvent was removed *in vacuo* and the residue was extracted exhaustively with pentane. The combined extracts were concentrated to 10 mL, and crystallization at -80°C afforded a dark purple powder of a *ca.* 75:25% mixture of $\text{Cp}^*\text{CoFe}(\text{CO})_3(\mu\text{-CO})_2(\mu\text{-}\eta^1\text{:}\eta^1\text{-C}(\text{O})\text{CHC}(\text{CF}_3))$ (**26a**) and $\text{Cp}^*\text{CoFe}(\text{CO})_4(\mu\text{-}\eta^1\text{:}\eta^3\text{-CHC}(\text{CF}_3)\text{C}(\text{O}))$ (**24a**) (72.9 mg, 0.144 mmol, 82 %), which was isolated by inverse filtration at -78°C . ^{13}C O enriched material was prepared from $\text{Fe}(^{13}\text{CO})_4(\eta^2\text{-TFP})$. Attempts to separate the species by fractional crystallization and chromatography failed, respectively, due to their similar solubilities and low stability on silica gel and alumina. Exhaustive washing with pentane afforded a clean IR spectrum of **24a**, but insufficient material was recovered for characterization by NMR. The material was thus characterized as a mixture.

Anal. Calcd for $\text{C}_{19}\text{H}_{16}\text{F}_3\text{CoFeO}_6$: C, 44.56; H, 3.15.

Anal. Calcd for $\text{C}_{19}\text{H}_{16}\text{F}_3\text{CoFeO}_5$: C, 44.66; H, 3.33.

Found: C, 44.41; H, 2.83.

EI-MS: $\text{Cp}^*\text{CoFe}(\text{CO})_6(\text{HCC}(\text{CF}_3))^+ - n \text{CO}$ ($n = 1 - 6$), $n = 1$ is 1.1% of base peak intensity; $\text{Cp}^*\text{Co}(\text{CO})_2^+$ (base peak).

$\text{Cp}^*\text{CoFe}(\text{CO})_4(\mu\text{-}\eta^1\text{:}\eta^3\text{-CHC}(\text{CF}_3)\text{C}(\text{O}))$ (**24a**):

F.W. 484.1

IR (CH₂Cl₂) ν_{CO} 2043(s), 2010(vs), 1984(m), 1952(w); ν_{acyl} 1776(w), 1747(w).
¹H NMR (CD₂Cl₂, 400.1 MHz, -60°C) δ 9.60 (s, H β) 1.86 (s, C₅Me₅).
¹³C{¹H} NMR (CD₂Cl₂, 100.6 MHz, -60°C) δ 225.25 (s, CO_{ac}), 216.96 (s, COFe),
 210.75 (s, COFe), 204.70 (s, COFe), 201.23 (s, COCo), 171.28 (s, CH β), 99.31 (s,
 C₅Me₅), 9.27 (s, Me). Neither the CF₃ nor C(CF₃) resonances were observed.
¹³C{¹H} NMR (CD₂Cl₂, 100.6 MHz, ¹³CO enriched) (-60°C) δ 225.93 (s, CO_{ac}),
 216.96 (s, COFe), 210.75 (s, COFe), 204.70 (s, COFe), 201.22 (s, COCo). (0°C)
 δ 224.26 (s, CO_{ac}), 216.5 (br, COFe), 210.0 (br, COFe), 204.4 (br, COFe), 201.0
 (br, COCo).
¹⁹F NMR (CD₂Cl₂, 188.3 MHz, -60°C) δ -63.34 (s, CF₃).

Cp*CoFe(CO)₃(μ -CO)₂(μ - η^1 : η^1 -C(O)CHC(CF₃)) (**26a**):

F.W. 512.1

IR (CH₂Cl₂) ν_{CO} 2083(s), 2036(m), 2012(m), 1828(m); ν_{acyl} 1645(w); the band
 positions were extrapolated by subtracting those of **24a**.

¹H NMR (CD₂Cl₂, 400.1 MHz, -60°C) δ 5.81 (s, H α) 1.60 (s, C₅Me₅).

¹³C{¹H} NMR (CD₂Cl₂, 100.6 MHz, -60°C) δ 241.10 (s, 2 μ -CO), 239.50 (s,
 CO_{ac}), 206.98 (s, 2COFe), 201.57 (s, COFe), 169.62 (q, ²J_{CF} = 32 Hz,
 C β (CF₃)), 144.57 (s, C α H), 128.07 (q, ¹J_{CF} = 274 Hz, CF₃) 105.26 (s, C₅Me₅),
 7.83 (s, Me).

¹³C{¹H} NMR (CD₂Cl₂, 100.6 MHz, ¹³CO enriched, -60°C) δ 241.08 (s, 2 μ -CO),
 239.49 (s, CO_{ac}, integration 1.33), 206.97 (s, 2COFe), 201.57 (s, COFe), 169.62
 (q, ²J_{CF} = 32 Hz, C β (CF₃)), 144.57 (s, with ¹³C satellites, ¹J_{C α C_{ac}} = 39 Hz,
 C α H), 128.07 (q, ¹J_{CF} = 274 Hz, CF₃) 105.26 (s, C₅Me₅), 7.83 (s, Me).

¹⁹F NMR (CD₂Cl₂, 188.3 MHz, -60°C) δ -59.04 (s, CF₃).

Synthesis of Cp*RhFe(CO)₄(μ - η^1 : η^3 -CHC(CF₃)C(O)) (24b**).**

Compound **1b** (46 mg, 0.176 mmol) and Cp*Rh(CO)₂ (60.6 mg, 0.206 mmol)
 afforded a brick red powder of **24b** (78.9 mg, 0.149 mmol, 85 %), which was
 unstable in solution at room temperature, but was obtained analytically pure by
 recrystallizing from CH₂Cl₂/pentane.

F.W. 528.1

Anal. Calcd for $C_{18}H_{16}F_3FeRhO_5$: C, 40.94; H, 3.05. Found: C, 40.74; H, 2.74.
 IR (CH_2Cl_2) ν_{CO} 2044(s), 2018(vs), 1982(s), 1947(br); ν_{acyl} 1773(m), 1743(m).
 IR (pentane) ν_{CO} 2054(s), 2024(vs), 2013(s), 1986(s), 1957(br); ν_{acyl} 1791(w),
 1778(vw).

1H NMR (CD_2Cl_2 , 200.1 MHz) δ 9.23 (d, $^2J_{RhH} = 3$ Hz, H_β) 1.98 (s, C_5Me_5).
 $^{13}C\{^1H\}$ NMR (CD_2Cl_2 , 100.6 MHz, $-60^\circ C$) δ 226.12 (br s, CO_{ac}), 214.95 (s, CO_{Fe}), 211.72 (s, CO_{Fe}), 204.98 (s, CO_{Fe}), 188.42 (d, $^1J_{RhC} = 84$ Hz, CO_{Rh}),
 164.60 (d, $^1J_{RhC} = 35$ Hz, CH_β), 122.66 (q, $^1J_{CF} = 278$ Hz, CF_3), 104.30 (d, $^1J_{RhC} = 4.5$ Hz, C_5Me_5), 49.57 (q, $^2J_{CF} = 35$ Hz, $C_\alpha(CF_3)$), 9.45 (s, Me).

$^{13}C\{^{19}F\}$ NMR (CD_2Cl_2 , 100.6 MHz, $-60^\circ C$) δ 226.12 (br s, CO_{ac}), 214.95 (s, CO_{Fe}), 211.72 (s, CO_{Fe}), 204.98 (s, CO_{Fe}), 188.42 (d, $^1J_{RhC} = 84$ Hz, CO_{Rh}),
 122.65 (s, CF_3) 104.31 (br s, C_5Me_5), 49.57 (s, $C_\alpha(CF_3)$), 9.45 (q, $^1J_{CH} = 128$
 Hz, Me).

$^{13}C\{^1H\}$ NMR (CD_2Cl_2 , 100.6 MHz, ^{13}CO enriched) ($-60^\circ C$) δ 226.12 (s, CO_{ac}),
 214.93 (s, CO_{Fe}), 211.69 (s, CO_{Fe}), 204.95 (s, CO_{Fe}), 188.71 (d, $^1J_{RhC} = 84$
 Hz, CO_{Rh}). ($0^\circ C$) δ 225.26 (s, CO_{ac}), 215.3 (br, CO_{Fe}), 211.9 (br, CO_{Fe}), 205.4
 (br, CO_{Fe}), 189.19 (d, $^1J_{RhC} = 84$ Hz, CO_{Rh}).

^{19}F NMR (CD_2Cl_2 , 188.3 MHz $-60^\circ C$) δ -63.47 (s, CF_3).

EI-MS: M^+ (0.5% of base); $M^+ - n CO$ ($n = 1 - 5$); $Cp^*Rh(CO)_2^+$ (base peak).

Reaction of $Fe(CO)_4(\eta^2-TFP)$ (1b) with $CpRh(CO)_2$. Under similar conditions, compound **1b** (48 mg, 0.183 mmol) and $CpRh(CO)_2$ (49 mg, 0.220 mmol) afforded an analytically pure reddish orange powder of an inseparable mixture (*ca.* 43:57%) of **27b** and **28b** (76.6 mg, 0.162 mmol, 89 %).

Anal. Calcd for $C_{14}H_6F_3FeO_6Rh$: C, 34.60; H, 1.24.

Anal. Calcd for $C_{13}H_6F_3FeO_5Rh$: C, 34.10; H, 1.32.

Found: C, 34.18; H, 1.16.

IR (pentane) ν_{CO} 2089(s), 2066(m), 2041(vs), 2025(m), 2019(m), 2015(m),
 2007(m), 1988(w); ν_{acyl} 1794(w, br), 1667(m).

IR (CH_2Cl_2) ν_{CO} 2088(s), 2063(ms), 2033(vs), 2021(vs), 2001(sh), 1979(sh);
 ν_{acyl} 1780(mw), 1749(w), 1648(m).

EL-MS: $\text{CpRhFe(CO)}_6(\text{HCCCF}_3)^+ - n \text{ CO}$ ($n = 1 - 5$), $n = 1$ is 22.0% of base peak intensity; CpRh(CO)_2^+ (base peak); CpRh^+ (69.1% of base).

$\text{CpRhFe(CO)}_4(\mu\text{-}\eta^1\text{:}\eta^3\text{-CHC(CF}_3\text{)C(O)})$ (**27b**, major isomer; **27b'**, minor isomer):

F.W. 457.9

$^1\text{H NMR}$ (CD_2Cl_2 , 400.1 MHz, -60°C) δ 10.39 (d, $^2J_{\text{RhH}} = 3.5$ Hz, H_β , **27b**), 9.66 (s, H_β , **27b'**), 5.80 (s, C_5H_5 , **27b**), 5.32 (s, C_5H_5 , **27b'**). **27b:27b'** = 4:1.

$^{13}\text{C}\{^1\text{H}\}$ NMR (CD_2Cl_2 , 100.6 MHz, -60°C) δ 225.00 (s, CO_{ac}), 210.88 (s, CO_{Fe}), 209.10 (s, CO_{Fe}), 204.82 (s, CO_{Fe}), 186.72 (d, $^1J_{\text{RhC}} = 85$ Hz, CO_{Rh}), 162.08 (d, $^1J_{\text{RhC}} = 34$ Hz, CH_β), 92.14 (s, C_5H_5), 50.66 (q, $^2J_{\text{CF}} = 36$ Hz, $\text{C}_\alpha(\text{CF}_3)$).

None of the resonances for **27b'** were observed.

$^{13}\text{C}\{^{19}\text{F}\}$ NMR (CD_2Cl_2 , 100.6 MHz, -60°C) δ 225.06 (d, $^3J_{\text{CH}} = 12$ Hz, CO_{ac}), 210.83 (s, CO_{Fe}), 209.06 (s, CO_{Fe}), 204.76 (s, CO_{Fe}), 186.69 (d, $^1J_{\text{RhC}} = 85$ Hz, CO_{Rh}), 162.04 (dd, $^1J_{\text{CH}} = 160$ Hz, $^1J_{\text{RhC}} = 34$ Hz, CH_β), 92.08 (d, $^1J_{\text{CH}} = 182$ Hz, C_5H_5), 122.20 (s, CF_3), 50.60 (s, $\text{C}_\alpha(\text{CF}_3)$).

$^{13}\text{C}\{^1\text{H}\}$ NMR (CD_2Cl_2 , 100.6 MHz, ^{13}CO enriched) (-80°C) **27b**: δ 225.35 (s, CO_{ac}), 211.43 (s, CO_{Fe}), 209.00 (s, CO_{Fe}), 204.66 (s, CO_{Fe}), 186.66 (d, $^1J_{\text{RhC}} = 84$ Hz, CO_{Rh}). **27b'**: δ 222.93 (s, CO_{ac}), 211.43 (s, CO_{Fe}), 208.80 (s, CO_{Fe}), 204.60 (s, CO_{Fe}), 186.32 (d, $^1J_{\text{RhC}} = 82$ Hz, CO_{Rh}). (0°C) **27b**: δ 225 (vbr, CO_{ac}), 211 (br s, CO_{Fe}), 186.8 (br d, $^1J_{\text{RhC}} = 80$ Hz, CO_{Rh}). **27b'**: δ 222.5 (br s, CO_{ac}), 186.8 (br d, $^1J_{\text{RhC}} = 80$ Hz, CO_{Rh}) + decomposition products.

$^{19}\text{F NMR}$ (CD_2Cl_2 , 188.3 MHz, -60°C) δ -63.70 (s, **27b**), -64.10 (s, **27b'**).

$\text{CpRhFe(CO)}_5(\mu\text{-}\eta^1\text{:}\eta^1\text{-C(O)CHC(CF}_3\text{)})$ (**28b**):

F.W. 486.0

$^1\text{H NMR}$ (CD_2Cl_2 , 400.1 MHz, -60°C) δ 6.58 (q, $^4J_{\text{HF}} = 2.5$ Hz, H_α), 5.66 (s, C_5H_5).

$^{13}\text{C}\{^1\text{H}\}$ NMR (CD_2Cl_2 , 100.6 MHz, -60°C) δ 218.25 (d, $^1J_{\text{RhC}} = 26$ Hz, CO_{ac}), 207.31 (s, 2CO_{Fe}), 206.98 (s, CO_{Fe}), 203.95 (d, $^1J_{\text{RhC}} = 39$ Hz, $2\text{CO}_{\text{Fe/Rh(av)}}$), 163.87 (q, $^2J_{\text{CF}} = 31$ Hz, $\text{C}_\beta(\text{CF}_3)$), 157.70 (q, $^3J_{\text{CF}} = 7$ Hz, C_αH), 127.00 (q, $^1J_{\text{CF}} = 272$ Hz, CF_3), 96.14 (s, C_5H_5).

$^{13}\text{C}\{^{19}\text{F}\}$ NMR (CD_2Cl_2 , 100.6 MHz, -60°C) δ 218.36 (d, $^1J_{\text{RhC}} = 25$ Hz, CO_{ac}), 207.28 (s, 2CO_{Fe}), 206.91 (s, CO_{Fe}), 203.90 (d, $^1J_{\text{RhC}} = 39$ Hz,

$2\text{CO}_{\text{Fe/Rh(av)}}$, 163.79 (s, $\text{C}_{\beta}(\text{CF}_3)$), 157.70 (d, $^1J_{\text{CH}} = 158$ Hz, $\text{C}_{\alpha}\text{H}$), 126.95 (s, CF_3), 96.14 (d, $^1J_{\text{CH}} = 178$ Hz, C_5H_5).
 $^{13}\text{C}\{^1\text{H}\}$ NMR (CD_2Cl_2 , 100.6 MHz, ^{13}C enriched) (-60°C) δ 218.31 (d, $^1J_{\text{RhC}} = 25$ Hz, CO_{ac}), 207.32 (s, 2CO_{Fe}), 207.00 (s, CO_{Fe}), 203.97 (d, $^1J_{\text{RhC}} = 39$ Hz, $2\text{CO}_{\text{Fe/Rh(av)}}$), 157.61 (s, with ^{13}C satellites, $^1J_{\text{CC}} = 36$ Hz, $\text{C}_{\alpha}\text{H}$), 96.16 (s, C_5H_5). ($+20^\circ\text{C}$) δ 216.48 (brd, $^1J_{\text{RhC}} = 25$ Hz, CO_{ac}), 207.76 (s, 3CO_{Fe}), 204.66 (d, $^1J_{\text{RhC}} = 39$ Hz, $2\text{CO}_{\text{Fe/Rh(av)}}$) 96.73 (s, C_5H_5). The CCF_3 and CF_3 resonances were not observed. The integration of the acyl peak was 1.50 relative to the 2:1:2 ratio of the other resonances in the initial spectrum at -60°C , but this ratio slowly changed to 1:2:1:2 after the sample was warmed to room temperature.

^{19}F NMR (CD_2Cl_2 , 188.3 MHz, -60°C) δ -62.90 (d, $^4J_{\text{HF}} = 2.5$ Hz, CF_3).

Reaction of $\text{Fe}(\text{CO})_4(\eta^2\text{-TFP})$ (1b) with $\text{Cp}^*\text{Ir}(\text{CO})_2$. Compound **1b** (46 mg, 0.176 mmol) and $\text{Cp}^*\text{Ir}(\text{CO})_2$ (72.3 mg, 0.189 mmol) afforded a deep yellow powder of a *ca.* 17:83% mixture of **25c** and **26c** (96.3 mg, 0.149 mmol, 85 %) when warmed to -20°C .

F.W. 645.4

Anal. Calcd for $\text{C}_{19}\text{H}_{16}\text{F}_3\text{FeIrO}_6$: C, 35.36; H, 2.50. Found: C, 35.10; H, 2.24.

IR (CH_2Cl_2) ν_{CO} 2076(s), 2052(m), 2042(m), 2022(s), 2003(s), 1826(w,br); ν_{acyl} 1752(vw), 1617(m).

EI-MS: $\text{M}^+ - n\text{CO}$ ($n = 1 - 5$); $\text{Cp}^*\text{Ir}(\text{CO})_2^+$ (base peak); $\text{Cp}^*\text{Ir}(\text{CO})^+$, Cp^*Ir^+ .

$\text{Cp}^*\text{IrFe}(\text{CO})_5(\mu\text{-}\eta^1\text{-}\eta^1\text{-CHC}(\text{CF}_3)\text{C}(\text{O}))$ (**25c**):

^1H NMR (CD_2Cl_2 , 400.1 MHz, -60°C) δ 8.88 (s, H_{β}), 2.01 (s, C_5Me_5).

$^{13}\text{C}\{^1\text{H}\}$ NMR (CD_2Cl_2 , 100.6 MHz, -60°C) δ 242.23 (s, CO_{ac}), 208.27 (s, 2CO), 204.95 (s, CO), 199.53 (s, 2CO), 104.63 (s, C_5Me_5), 8.16 (s, Me). Neither the CH, CF_3 , nor CCF_3 resonances were identified.

$^{13}\text{C}\{^1\text{H}\}$ NMR (CD_2Cl_2 , 100.6 MHz, ^{13}C enriched, -60°C) δ 242.14 (s, CO_{ac}), 208.25 (s, 2CO), 204.96 (s, CO), 199.57 (s, 2CO , integrated 0.5 per CO).

^{19}F NMR (CD_2Cl_2 , 188.3 MHz, -60°C) δ -64.91 (s, CF_3).

$\text{Cp}^*\text{IrFe}(\text{CO})_5(\mu\text{-}\eta^1\text{:}\eta^1\text{-C(O)CHC(CF}_3\text{)})$ (**26c**):

^1H NMR (CD_2Cl_2 , 400.1 MHz, -60°C) δ 6.40 (q, $^4J_{\text{HF}} = 1.0$ Hz, H_α), 1.92 (s, C_5Me_5).

$^{13}\text{C}\{^1\text{H}\}$ NMR (CD_2Cl_2 , 100.6 MHz, -60°C) δ 208.58 (s, 2CO), 206.53 (s, CO_{ac}), 206.28 (s, CO), 202.82 (s, 2CO), 170.07 (q, $^2J_{\text{CF}} = 30$ Hz, $\text{C}_\beta(\text{CF}_3)$), 153.48 (q, $^3J_{\text{CF}} = 7$ Hz, C_αH), 128.01 (q, $^1J_{\text{CF}} = 273$ Hz, CF_3) 104.23 (s, C_5Me_5), 7.72 (s, Me).

$^{13}\text{C}\{^1\text{H}\}$ NMR (CD_2Cl_2 , 100.6 MHz, ^{13}C enriched, -60°C) δ 208.56 (s, 2CO), 206.49 (s, CO_{ac} , integration 1.5), 206.29 (s, CO), 202.92 (s, CO), 202.81 (s, CO), 170.0 (q, $^2J_{\text{CF}} = 30$ Hz, $\text{C}_\beta(\text{CF}_3)$), 153.5 (q, with ^{13}C satellites, $^1J_{\text{CC}} = 39$ Hz, $^3J_{\text{CF}} = 7$ Hz, C_αH), 104.19 (s, C_5Me_5), 7.73 (s, Me).

^{19}F NMR (CD_2Cl_2 , 188.3 MHz, -60°C) δ -60.15 (d, $^4J_{\text{HF}} = 1.0$ Hz, CF_3).

When a CD_2Cl_2 NMR sample of the initial mixture of **25c** and **26c** was warmed above -20°C to room temperature, **25c** persisted in solution at the same concentration, while **26c** decreased with concomitant formation of **29** and a minor species **30**, the final ratio being 52:16:16:16 % for **29:25c:26c:30**.

$\text{Cp}^*\text{Ir}(\text{CO})\{\sigma\text{-}\eta^1\text{:}\eta^1\text{:}\mu\text{-}\eta^2\text{-C(O)CHC(CF}_3\text{)C(O)}\}\text{Fe}(\text{CO})_3$ (**29**):

F.W. 645.4

^1H NMR (CD_2Cl_2 , 200.1 MHz) δ 5.00 (s, CH) 2.08 (s, C_5Me_5).

$^{13}\text{C}\{^1\text{H}\}$ NMR (CD_2Cl_2 , 100.6 MHz, ^{13}C enriched, -20°C): δ 209.74 (s, CO_{Fe}), 209.16 (s, CO_{Fe}), 207.65 (s, CO_{Fe}), 178.12 (s, CO_{ac} , integration *ca.* 1.5), 177.87 (s, CO_{ac}), 163.49 (s, CO_{Ir}).

^{13}C NMR (CD_2Cl_2 , 50.2 MHz, ^{13}C enriched, -20°C): δ 209.67 (s, CO_{Fe}), 209.13 (s, CO_{Fe}), 207.62 (s, CO_{Fe}), 178.23 (s, CHCO_{ac} , integration *ca.* 1.5), 177.92 (d, $^3J_{\text{CH}} = 10$ Hz, $(\text{F}_3\text{C})\text{CCO}_{\text{ac}}$), 163.46 (s, CO_{Ir}).

^{19}F NMR (CD_2Cl_2 , 188.3 MHz) δ -60.48 (s, CF_3).

When the NMR sample was isolated and stirred overnight in 10 mL CH_2Cl_2 at ambient temperature, an intractable brown solid formed. The CH_2Cl_2 extract contained **24c** and **30** in roughly a 30:70% ratio.

Anal. Calcd for $C_{18}H_{16}F_3FeIrO_5$: C, 35.02; H, 2.61. Found: C, 34.84; H, 1.86.

IR (CH_2Cl_2) ν_{CO} 2041(s), 2000(m), 1977(m); ν_{acyl} 1751(w), 1659(vw), 1642(vw).

EI-MS: M^+ ; $M^+ - n CO$ ($n = 1 - 5$); $Cp^*Ir(CO)_2^+$ (base peak); $Cp^*Ir(CO)^+$, Cp^*Ir^+ .

$Cp^*IrFe(CO)_4(\mu-\eta^1:\eta^3-CHC(CF_3)C(O))$ (**24c**):

1H NMR (CD_2Cl_2 , 400.1 MHz, $-60^\circ C$) δ 8.95 (br s, H_β) 2.01 (s, C_5Me_5).

$^{13}C\{^1H\}$ NMR (CD_2Cl_2 , 100.6 MHz, ^{13}CO enriched, $-60^\circ C$) δ 228.27 (s, CO_{ac}), 212.41 (s, CO_{Fe}), 209.60 (s, CO_{Fe}), 204.72 (s, CO_{Fe}), 172.37 (s, CO_{Ir}), 136.28 (s, CH_β), 100.60 (s, C_5Me_5), 8.71 (s, Me). The CCF_3 signal was not observed.

^{19}F NMR (CD_2Cl_2 , 188.3 MHz, $-60^\circ C$) δ -62.96 (br s, CF_3).

30: 1H NMR (CD_2Cl_2 , 400.1 MHz, $-60^\circ C$) δ 6.95 (br s) 1.88 (s, C_5Me_5).

$^{13}C\{^1H\}$ NMR (CD_2Cl_2 , 100.6 MHz, ^{13}CO enriched, $-60^\circ C$) δ 214.96 (s), 212.45 (s), 210.66 (s), 168.80 (s, CO_{Ir}).

^{19}F NMR (CD_2Cl_2 , 188.3 MHz, $-60^\circ C$) δ -64.19 (br s, CF_3).

Synthesis of $Cp^*RhFe(CO)_4(\mu-\eta^1:\eta^3-CHCMeC(O))$ ($Cp' = Cp^*$, **31b; Cp , **32b**).** Compound **1d** (64 mg, 0.308 mmol) and $Cp^*Rh(CO)_2$ (110 mg, 0.374 mmol) afforded **31b** as a red-brown powder (89.9 mg, 0.190 mmol, 62 %) after CH_2Cl_2 extraction from an intractable black powder. Compound **32b** was isolated in 63% yield using pentane for the extraction.

$Cp^*RhFe(CO)_4(\mu-\eta^1:\eta^3-CHCMeC(O))$ (**31b**):

F.W. 474.1

Anal. Calcd for $C_{18}H_{19}FeRhO_5$: C, 45.60; H, 4.04. Found: C, 45.61; H, 4.07.

IR (CH_2Cl_2) ν_{CO} 2029(s), 2000(vs), 1957(s), 1933(sh); ν_{acyl} 1763(sh), 1734(m).

1H NMR (CD_2Cl_2 , 400.1 MHz, $-60^\circ C$) δ 8.87 (d, $^2J_{RhH} = 3.5$ Hz, H_β), 1.96 (s, C_5Me_5), 1.60 (s, 3H, CH_3).

$^{13}C\{^1H\}$ NMR (CD_2Cl_2 , 100.6 MHz, $-60^\circ C$) δ 234.59 (s, CO_{ac}), 216.76 (s, CO_{Fe}), 213.88 (s, CO_{Fe}), 207.70 (s, CO_{Fe}), 189.91 (d, $^1J_{RhC} = 86$ Hz, CO_{Rh}), 166.82 (d, $^1J_{RhC} = 34$ Hz, CH_β), 103.10 (d, $^1J_{RhC} = 4$ Hz, C_5Me_5), 54.79 (s, C_α), 20.86 (s, $C(O)CMe$), 9.37 (s, C_5Me_5).

EI-MS: M^+ (1.3% of base); $M^+ - n CO$ ($n = 1 - 5$) ($n = 5$, base peak).

CpRhFe(CO)₄(μ-η¹:η³-CHCMeC(O)) (32b):

F.W. 403.9

Anal. Calcd for C₁₃H₉FeRhO₅: C, 38.65; H, 2.25. Found: C, 38.60; H, 1.99.

IR (CH₂Cl₂) ν_{CO} 2048(s), 2011(vs), 1974(s); ν_{acyl} 1762(m), 1743(m).

¹H NMR (CD₂Cl₂, 400.1 MHz, -60°C) **32b**: δ 9.71 (d, ²J_{RhH} = 3.5 Hz, H_β), 5.63 (s, 5H, C₅H₅), 1.62 (s, 3H, CH₃). **32b'**: δ 8.91 (s, H_β), 5.22 (s, 5H, C₅H₅), 1.60 (s, 3H, CH₃). **32b**:**32b'** = 1.6:1.

¹³C{¹H} NMR (CD₂Cl₂, 100.6 MHz, -60°C) δ 233.74 (s, CO_{ac}, **32b**), 230.67 (s, CO_{ac}, **32b'**), 212.54 (s, CO_{Fe}, **32b/b'**), 210.78 (s, CO_{Fe}, **32b/b'**), 207.58 (s, CO_{Fe}, **32b/b'**), 188.24 (d, ¹J_{RhC} = 86 Hz, CO_{Rh}, **32b**), 188.11 (d, ¹J_{RhC} = 85 Hz, CO_{Rh}, **32b'**), 160.51 (d, ¹J_{RhC} = 34 Hz, CH_β, **32b**), 153.40 (d, ¹J_{RhC} = 33 Hz, CH_β, **32b'**), 91.48 (s, C₅H₅, **32b**), 91.46 (s, C₅H₅, **32b'**), 59.88 (s, C_α, **32b'**), 55.32 (s, C_α, **32b**), 20.52 (s, CH₃, **32b**), 20.39 (s, CH₃, **32b'**).

EI-MS: M⁺ (0.5% of base); M⁺ - n CO (n = 1 - 5) (n = 5, base peak), CpRh(CO)₂⁺, CpRh⁺.

Synthesis of Cp*CoFe(μ-CO)₂(CO)₄ (33) from Fe(CO)₄(η²-RCCMe).

Method A. Fe(CO)₄(η²-C₂Me₂) (**1e**) (66 mg, 0.297 mmol) dissolved in 20 mL pentane was added to a pentane solution of Cp*Co(CO)₂ (78.3 mg, 0.313 mmol) at -78°C. After stirring at -5°C for 1 h, the solution was filtered and stored at -80°C. The resulting dark green needles were isolated by inverse filtration and recrystallized from a minimum of cold pentane at -80°C to afford analytically pure Cp*CoFe(μ-CO)₂(CO)₄ (**33**) (84.3 mg, 0.202 mmol, 68 %). The compound was somewhat thermally unstable and decomposed above *ca.* 0°C in solution, but could be handled briefly in air as a solid at ambient temperature.

Method B. In a similar manner, Fe(CO)₄(η²-MeCCH) (**1d**) (39 mg, 0.188 mmol) and Cp*Co(CO)₂ (53.7 mg, 0.215 mmol) afforded **33** (51.1 mg, 0.122 mmol, 65 %) as a mixture containing *ca.* 15% Cp*CoFe(CO)₄(μ-η¹:η³-CHCMeC(O)) (**31a**).

Cp*CoFe(CO)₄(μ-η¹:η³-CHCMeC(O)) (31a):

¹H NMR (CD₂Cl₂, 400.1 MHz) δ 9.04 (s, H_β), 1.82 (s, C₅Me₅), 1.63 (s, Me).

$^{13}\text{C}\{^1\text{H}\}$ NMR (CD_2Cl_2 , 100.6 MHz, -100°C) δ 235.15 (s, CO_{ac}), 218.62 (s, CO_{Fe}), 213.01 (s, CO_{Fe}), 207.14 (s, CO_{Fe}), 202.02 (s, CO_{Co}), 172.48 (s, $\text{CH}\beta$), 97.77 (s, C_5Me_5), 20.47 (s, $\text{C}(\text{O})\text{CMe}$), 9.13 (s, C_5Me_5). C_α was not observed.

$\text{Cp}^*\text{CoFe}(\mu\text{-CO})_2(\text{CO})_4$ (**33**):

F.W. 418.1

Anal. Calcd for $\text{C}_{16}\text{H}_{15}\text{CoFeO}_6$: C, 45.97; H, 3.62. Found: C, 45.98; H, 3.51.

IR (pentane) ν_{CO} 2050(s), 2018(s), 1977(m), 1974(sh), 1831(w), 1815(m).

(CH_2Cl_2) ν_{CO} 2046(s), 2016(s), 1962(m), 1816(sh), 1799(m).

^1H NMR (CD_2Cl_2 , 400.1 MHz, -60°C) δ 1.74 (s, Cp^*).

$^{13}\text{C}\{^1\text{H}\}$ NMR (CD_2Cl_2 , 100.6 MHz, -20°C) δ 224.02 (s, CO_{av}), 102.48 (s, C_5Me_5), 9.50 (s, C_5Me_5).

EI-MS: M^+ (7.8% of base); $\text{M}^+ - n \text{CO}$ ($n = 1 - 6$); $\text{Cp}^*\text{Co}(\text{CO})_m^+$ ($m = 0 - 2$, $m = 0$, base peak).

7.5.3. X-ray Crystal Structure Determination of Compounds **24b** and **33**.

Deep red single crystals of compound **24b** and dark green single crystals of compound **33** were grown from CH_2Cl_2 /pentane and saturated pentane solutions, respectively, at -35°C . The X-ray data collection and structure refinement were carried out by Dr. Bob McDonald at the Structure Determination Laboratory, Department of Chemistry, University of Alberta. The crystals were mounted on a thin glass fibre and transferred to the goniometer of a Siemens P4/RA diffractometer²⁴ where they were kept under a stream of cold nitrogen gas. The structures were solved using direct methods techniques (**24b**, *SHELXS-86*²⁵; **33**, *DIRDIF-96*²⁶) and refined by full-matrix least-squares on F^2 (*SHELXL-93*²⁷). All non-hydrogen atoms were located. The geometrically constrained hydrogen atoms were placed in appropriate calculated positions. A summary of data collection parameters is given in Tables 7-7 (**24b**) and 7-9 (**33**). The final atomic coordinates and equivalent isotropic displacement parameters are given in Tables 7-8 (**24b**) and 7-10 (**33**). Selected interatomic distances and angles are provided in Tables 7-1 and 7-2 (**24b**) and 7-5 and 7-6 (**33**).

Table 7-7. Crystallographic Experimental Details for Compound 24b

Formula	C ₁₈ H ₁₆ F ₃ FeO ₅ Rh
Formula weight	528.07
Crystal dimensions (mm)	0.16 × 0.15 × 0.14
Crystal system	monoclinic
Space group	<i>P</i> 2 ₁ / <i>c</i> (No. 14)
Unit cell parameters ^a	
<i>a</i> , Å	9.7038 (9)
<i>b</i> , Å	12.6526 (15)
<i>c</i> , Å	15.957 (2)
β, deg	91.929 (11)
<i>V</i> , Å ³	1958.1 (4)
<i>Z</i>	4
ρ _{calc} , g cm ⁻³	1.791
μ, mm ⁻¹	1.637
Radiation, λ (Å)	graphite-monochromated Mo Kα (0.71073)
Temperature, °C	-60
Scan type	θ-2θ
Data collection 2θ limit, deg	50.0
Total data collected	3660 (0 ≤ <i>h</i> ≤ 11, 0 ≤ <i>k</i> ≤ 15, -18 ≤ <i>l</i> ≤ 18)
Independent reflections	3445
Number of observations (<i>NO</i>)	2477 (<i>F</i> _o ² ≥ 2σ(<i>F</i> _o ²))
Absorption correction method	Gaussian integration (face-indexed)
Range of transmission factors	0.8348-0.7841
Data/restraints/parameters	3444 [<i>F</i> _o ² ≥ -3σ(<i>F</i> _o ²)]/0/258
Goodness-of-fit (<i>S</i>) ^b	1.053 [<i>F</i> _o ² ≥ -3σ(<i>F</i> _o ²)]
Final <i>R</i> indices ^c	
<i>F</i> _o ² > 2σ(<i>F</i> _o ²)	<i>R</i> ₁ = 0.0490, <i>wR</i> ₂ = 0.0846
all data	<i>R</i> ₁ = 0.0814, <i>wR</i> ₂ = 0.0961
Largest difference peak and hole	0.592 and -0.431 e Å ⁻³

^aObtained from least-squares refinement of 28 reflections with 20.5° < 2θ < 25.9°.

^b*S* = [Σ*w*(*F*_o² - *F*_c²)²/(*n* - *p*)]^{1/2} (*n* = number of data; *p* = number of parameters varied; *w* = [σ²(*F*_o²) + (0.0295*P*)² + 0.9723*P*]⁻¹ where *P* = [Max(*F*_o², 0) + 2*F*_c²]/3).

^c*R*₁ = Σ||*F*_o - *F*_c||/Σ|*F*_o|; *wR*₂ = [Σ*w*(*F*_o² - *F*_c²)²/Σ*w*(*F*_o⁴)]^{1/2}.

Table 7-8. Atomic Coordinates and Equivalent Isotropic Displacement Parameters for Compound 24b

Atom	x	y	z	$U_{eq}, \text{\AA}^2$
Rh	-0.13260(5)	0.17561(4)	-0.14271(3)	0.02427(14)*
Fe	0.09628(9)	0.28743(7)	-0.10210(6)	0.0321(2)*
F1	0.3838(4)	0.2594(4)	-0.2222(3)	0.0709(14)*
F2	0.3304(5)	0.1175(4)	-0.2851(3)	0.090(2)*
F3	0.2378(4)	0.2626(4)	-0.3226(3)	0.076(2)*
O1	-0.0181(6)	-0.0381(4)	-0.0961(4)	0.074(2)*
O2	-0.0030(6)	0.4980(4)	-0.1616(4)	0.073(2)*
O3	-0.0521(5)	0.2635(4)	0.0535(3)	0.0497(13)*
O4	0.3409(5)	0.3766(5)	-0.0187(4)	0.077(2)*
O5	0.2711(5)	0.0943(4)	-0.0731(3)	0.0508(13)*
C1	-0.0566(7)	0.0449(5)	-0.1110(4)	0.037(2)*
C2	0.0320(7)	0.4157(6)	-0.1402(5)	0.046(2)*
C3	-0.0004(7)	0.2682(5)	-0.0104(5)	0.039(2)*
C4	0.2452(7)	0.3435(5)	-0.0531(5)	0.046(2)*
C5	0.1980(6)	0.1581(5)	-0.1090(4)	0.035(2)*
C6	0.1652(6)	0.1871(5)	-0.1970(4)	0.0323(15)*
C7	0.0284(6)	0.2106(5)	-0.2138(4)	0.0286(14)*
C8	0.2776(7)	0.2075(6)	-0.2558(5)	0.045(2)*
C10	-0.3125(5)	0.1648(5)	-0.2289(3)	0.0259(14)*
C11	-0.3439(6)	0.1141(5)	-0.1510(4)	0.0274(14)*
C12	-0.3429(6)	0.1917(5)	-0.0865(4)	0.0267(14)*
C13	-0.3089(6)	0.2904(5)	-0.1230(4)	0.0287(15)*
C14	-0.2896(6)	0.2738(5)	-0.2110(4)	0.0262(14)*
C15	-0.3181(6)	0.1145(5)	-0.3142(4)	0.039(2)*
C16	-0.3891(7)	0.0018(5)	-0.1406(4)	0.043(2)*
C17	-0.3816(7)	0.1731(5)	0.0022(4)	0.040(2)*
C18	-0.3103(7)	0.3962(5)	-0.0801(4)	0.040(2)*
C19	-0.2625(7)	0.3577(5)	-0.2758(4)	0.040(2)*

^aAnisotropically-refined atoms are marked with an asterisk (*). The form of the anisotropic displacement parameter is: $\exp[-2\pi^2(h^2a^2U_{11} + k^2b^2U_{22} + l^2c^2U_{33} + 2klb^*c^*U_{23} + 2hla^*c^*U_{13} + 2hka^*b^*U_{12})]$.

Table 7-9. Crystallographic Experimental Details for Compound 33

Formula	C ₁₆ H ₁₅ CoFeO ₆
Formula weight	418.06
Crystal dimensions (mm)	0.37 × 0.24 × 0.18
Crystal system	triclinic
Space group	<i>P</i> $\bar{1}$ (No. 2)
Unit cell parameters ^a	
<i>a</i> , Å	8.2363 (5)
<i>b</i> , Å	9.0399 (9)
<i>c</i> , Å	12.0416 (11)
α , deg	91.362 (6)
β , deg	90.316 (6)
γ , deg	109.519 (9)
<i>V</i> , Å ³	844.71 (13)
<i>Z</i>	2
ρ_{calc} , g cm ⁻³	1.644
μ , mm ⁻¹	14.83
Radiation, λ (Å)	graphite-monochromated Cu K α (1.54178)
Temperature, °C	-60
Scan type	θ -2 θ
Data collection 2 θ limit, deg	115.0
Total data collected	4470 ($-9 \leq h \leq 9$, $-9 \leq k \leq 9$, $-12 \leq l \leq 13$)
Independent reflections	2282
Number of observations (<i>NO</i>)	2049 ($F_o^2 \geq 2\sigma(F_o^2)$)
Absorption correction method	semiempirical (ψ scans)
Range of transmission factors	0.3447–0.0078
Data/restraints/parameters	2282 [$F_o^2 \geq -3\sigma(F_o^2)$]/0/223
Extinction coefficient (<i>x</i>) ^b	0.0033 (3)
Goodness-of-fit (<i>S</i>) ^c	1.121 [$F_o^2 \geq -3\sigma(F_o^2)$]
Final <i>R</i> indices ^d	
$F_o^2 > 2\sigma(F_o^2)$	$R_1 = 0.0563$, $wR_2 = 0.1393$
all data	$R_1 = 0.0601$, $wR_2 = 0.1440$
Largest difference peak and hole	0.666 and -0.478 e Å ⁻³

^aObtained from least-squares refinement of 30 reflections with $56.7^\circ < 2\theta < 58.0^\circ$.

^b $F_c^* = kF_c[1 + x\{0.001F_c^2\lambda^3/\sin(2\theta)\}]^{-1/4}$ where *k* is the overall scale factor.

^c $S = [\sum w(F_o^2 - F_c^2)^2 / (n - p)]^{1/2}$ (*n* = number of data; *p* = number of parameters varied; $w = [\sigma^2(F_o^2) + (0.1068P)^2]^{-1}$ where $P = [\text{Max}(F_o^2, 0) + 2F_c^2] / 3$).

^d $R_1 = \sum \|F_o\| - |F_c| / \sum |F_o|$; $wR_2 = [\sum w(F_o^2 - F_c^2)^2 / \sum w(F_o^4)]^{1/2}$.

Table 7-10. Atomic Coordinates and Equivalent Isotropic Displacement Parameters for Compound 33

Atom	x	y	z	$U_{eq}, \text{\AA}^2$
Co	0.22015(8)	0.41431(7)	0.22397(5)	0.0563(3)*
Fe	-0.02796(8)	0.15447(7)	0.21978(5)	0.0604(3)*
O1	0.1311(5)	0.6133(4)	0.0662(3)	0.0823(9)*
O2	-0.0924(4)	0.4272(4)	0.3259(3)	0.0711(8)*
O3	0.2141(5)	0.2119(4)	0.0324(3)	0.0802(9)*
O4	-0.1995(6)	0.0390(5)	0.4288(3)	0.1004(12)*
O5	0.0613(7)	-0.1347(5)	0.2078(4)	0.1131(14)*
O6	-0.3155(5)	0.0859(4)	0.0600(3)	0.0871(10)*
C1	0.1628(6)	0.5321(5)	0.1263(4)	0.0642(10)*
C2	-0.0250(6)	0.3512(5)	0.2767(4)	0.0617(10)*
C3	0.1483(6)	0.2344(5)	0.1130(4)	0.0666(11)*
C4	-0.1302(7)	0.0848(6)	0.3493(5)	0.0762(13)*
C5	0.0306(7)	-0.0212(6)	0.2113(5)	0.0808(13)*
C6	-0.2034(6)	0.1144(5)	0.1215(4)	0.0701(12)*
C10	0.3245(5)	0.4141(5)	0.3860(4)	0.0636(10)*
C11	0.3481(5)	0.5689(5)	0.3559(4)	0.0623(10)*
C12	0.4485(5)	0.5981(5)	0.2562(4)	0.0649(11)*
C13	0.4896(5)	0.4608(5)	0.2265(4)	0.0655(11)*
C14	0.4116(5)	0.3464(5)	0.3053(4)	0.0643(11)*
C15	0.2372(6)	0.3375(6)	0.4872(4)	0.0724(12)*
C16	0.2861(7)	0.6851(6)	0.4153(4)	0.0784(13)*
C17	0.5153(7)	0.7522(6)	0.2003(5)	0.0782(13)*
C18	0.6012(6)	0.4433(7)	0.1331(4)	0.0780(13)*
C19	0.4306(7)	0.1872(6)	0.3095(4)	0.0771(13)*

^aAnisotropically-refined atoms are marked with an asterisk (*). The form of the anisotropic displacement parameter is: $\exp[-2\pi^2(h^2a^{*2}U_{11} + k^2b^{*2}U_{22} + l^2c^{*2}U_{33} + 2klb^{*c^*}U_{23} + 2hla^{*c^*}U_{13} + 2hka^{*b^*}U_{12})]$.

7.6. References

1. Hoffman, K. MSc. Thesis, University of Alberta, 1994.
2. Washington, J. PhD Thesis, University of Alberta, 1994.
3. Otto, H.; Garcia Alonso, F. G.; Werner, H. *J. Organomet. Chem.* **1986**, *306*, C13.
4. Dickson, R. S.; Gatehouse, B. M.; Nesbit, M. C.; Pain, G. N. *J. Organomet. Chem.* **1981**, *215*, 97.
5. Knox, S. A. R.; Lloyd, B. R.; Morton, D. A. V.; Orpen, A. G.; Turner, M. L.; Hogarth, G. *Polyhedron* **1995**, *14*, 2723.
6. Fontaine, X. L. R.; Jacobsen, G. B.; Shaw, B. L.; Thornton-Pett, M. *J. Chem. Soc., Dalton Trans.* **1988**, 741.
7. Dyke, A. F.; Knox, S. A. R.; Naish, P.; Taylor, G. E. *J. Chem. Soc., Dalton Trans.* **1982**, 1297.
8. Gracey, B. P.; Knox, S. A. R.; Macpherson, K. A.; Orpen, A. G.; Stobart, S. R. *J. Chem. Soc., Dalton Trans.* **1985**, 1935.
9. Mann, B. E.; Taylor, B. F. *¹³C NMR Data for Organometallic Compounds*; Academic: New York, 1981, pp 2-5.
10. Takats, J. *J. Cluster Science* **1992**, *3*, 479.
11. Breitmaier, E.; Voelter, W. *Carbon-13 NMR Spectroscopy*; VCH: Weinheim, 1987, pp 133-155.
12. Campbell, I. L. C.; Stephens, F. S. *J. Chem. Soc., Dalton Trans.* **1975**, 22.
13. Leung, P. C.; Coppens, P. *Acta Cryst.* **1983**, *B39*, 535.
14. Akita, M.; Terada, M.; Ishii, N.; Hirakawa, H.; Moro-oka, Y. *J. Organomet. Chem.* **1994**, *473*, 175.
15. Colton, R.; McCormick, M. J. *Coord. Chem. Rev.* **1980**, *31*, 1.
16. Cotton, F. A. *Prog. Inorg. Chem.* **1976**, *21*, 1.
17. Huheey, J. E.; Keiter, E. A.; Keiter, R. L. *Inorganic Chemistry: Principles of Structure and Reactivity*; 4th ed.; HarperCollins: New York, 1993, pp 112-113 and 578.
18. Aldridge, M. L.; Green, M.; Howard, J. A. K.; Pain, G. N.; Porter, S. J.; Stone, F. G. A. *J. Chem. Soc., Dalton Trans.* **1982**, 1333.

19. Davey, G.; Stephens, F. S. *J. Chem. Soc., Dalton Trans.* **1974**, 698.
20. Dickson, R. S.; Tailby, G. R. *Aust. J. Chem.* **1970**, *23*, 1531.
21. Frith, S. A.; Spencer, J. L. *Inorg. Synth.* **1985**, *23*, 15.
22. Werner, H.; Klingert, B. *J. Organomet. Chem.* **1981**, *218*, 395.
23. Ball, R. G.; Graham, W. A. G.; Heinekey, D. M.; Hoyano, J. K.; McMaster, A. D.; Mattson, B. M.; Michel, S. T. *Inorg. Chem.* **1990**, *29*, 2023.
24. Programs for diffractometer operation, data collection, data reduction, and absorption correction were those supplied by Siemens.
25. Sheldrick, G. M. *Acta Crystallogr.* **1990**, *A46*, 467.
26. Beurskens, P. T.; Beurskens, G.; Bosman, W.P.; de Gelder, R.; Garcia Granda, S.; Gould, R. O.; Israel, R; Smits, J.M.M. (1996). The *DIRDIF-96* program system. Crystallography Laboratory, University of Nijmegen, The Netherlands.
27. Sheldrick, G.M. *SHELXL-93*. Program for crystal structure determination. University of Göttingen, Germany, 1993.

Chapter 8

Conclusions

The aim of this Thesis was to investigate the low temperature photochemistry of $\text{Fe}(\text{CO})_5$ with the goal of providing a general synthesis of $\text{Fe}(\text{CO})_4(\eta^2\text{-alkyne})$ compounds and to survey the chemistry of these hitherto elusive species.¹⁻⁴ The objective seemed reasonable as it had been suggested that the paucity of such compounds in the literature was not necessarily due to the thermodynamic instability of the Fe-alkyne bond, but was rather a reflection of the "hyper-reactivity" of these compounds with alkynes.³ Gratifyingly, the proposal proved to be correct, and slight but important modifications of the methodology applied to the low temperature photochemical synthesis of Ru and Os($\text{CO})_4(\eta^2\text{-alkyne})$ compounds⁴⁻⁷ generated a range of $\text{Fe}(\text{CO})_4(\eta^2\text{-RCCR'})$ (R = R' = CF_3 , **1a**; H, **1c**; Me, **1e**; R = H, R' = CF_3 , **1b**; R = H, R' = Me, **1d**) complexes (Chapter 2). The isolation of the compounds was limited to gaseous or liquid alkynes with low boiling points,⁸ but compounds containing higher boiling alkynes such as C_2Et_2 could be generated *in situ* with the limitation that any further reactions would have to take place in the presence of excess alkyne. Nonetheless, the alkynes incorporated in **1a-e** possessed a range of electronic and steric traits and provided a suitable starting point for a survey of the reactivity of $\text{Fe}(\text{CO})_4(\eta^2\text{-alkyne})$ species towards alkynes, CO, phosphines, and electronically saturated group 8/9 transition metal complexes.

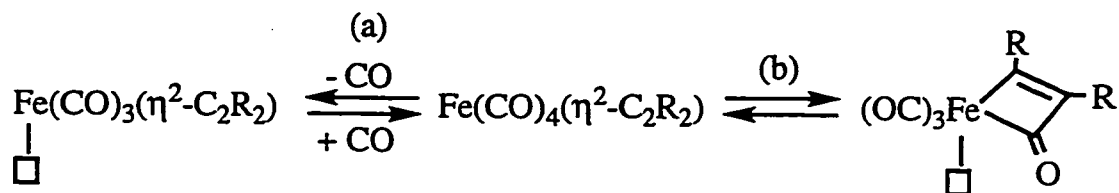
The reactivity of the isolated compounds **1** towards alkynes vindicated early proposals that $\text{Fe}(\text{CO})_4(\eta^2\text{-alkyne})$ species were intermediates in the iron carbonyl mediated coupling of alkynes with carbon monoxide to produce unsaturated cyclic organic molecules (Chapter 3).^{1,9} The exceptionally low temperatures at which the reactions occurred readily justified why compounds **1** were not detected in earlier studies. Interestingly, the type of cyclic organic ligands formed was strongly dependent on the nature of the alkyne substituent, and a diverse array of products, ranging from the cyclopentadienone complex **2**

to the tropone complex **3** and the *p*-quinone compounds **4**, demonstrated a remarkable range of possible transformations.

The discovery that **1a-e** were also independently reactive towards carbon monoxide, in the absence of added alkyne, provided initial clues as to the pathways by which compounds **2-4** formed. More importantly, it was found that $\text{Fe}(\text{CO})_4(\eta^2\text{-RCCMe})$ ($\text{R} = \text{H}$, **1d**; Me , **1e**) underwent spontaneous migratory carbonyl insertions to produce tricarbonyl-3,4-dimethylferracyclopenta-3-en-2,5-dione dimers (**6d,e**). The isolated dimers then reacted further with alkynes to provide a general synthesis of a modest range of substituted tricarbonyl(*p*-quinone)iron complexes (**4c-h**). Thus, the identity of a second heretofore unknown and unproven intermediate was detected in the elegantly simple synthesis of $\text{Fe}(\text{CO})_3\{\eta^4\text{-(O)CC}_4\text{Me}_4\text{C(O)}\}$ from $\text{Fe}(\text{CO})_5$ and C_2Me_2 under gentle sunlight irradiation (Eq. 1.2), a reaction that was first discovered at the dawn of modern organometallic chemistry¹⁰ and one whose mechanism has been a source of speculation and debate.^{1,9,11}

Apart from the ability of the $\text{Fe}(\text{CO})_4(\eta^2\text{-alkyne})$ complexes to undergo facile migratory CO insertions, the carbonyl ligands were also found to be very labile and would readily exchange with ^{13}CO in solution (Scheme 8-1). The exchange reactions became synthetically useful at the remarkably low temperature of -40°C and ^{13}CO incorporation was even observed at temperatures as low as -78°C over longer time periods. Interestingly, migratory CO insertion was found to compete with ^{13}CO exchange for the more electron rich alkyne in compound **1e**, resulting in low yields of $\text{Fe}(^{13}\text{CO})_4(\eta^2\text{-C}_2\text{Me}_2)$ and preferential formation of the isotopically enriched dimer **6e**. This feature may explain the fact that **1e** produced the *p*-quinone compound **4a** while $\text{Fe}(\text{CO})_4(\eta^2\text{-HFB})$ (**1a**) afforded the cyclopentadienone complex **2**. Thus, migratory CO insertion becomes less facile as the coordinated alkyne becomes more π -acidic, resulting in the production of cyclic organic ligands containing only one ketone function. This notion is reinforced by the observation that **1e** did not produce tropone or cyclopentadienone complexes in the absence of added CO, but rather underwent two sequential migratory insertions to produce compound **4a** along with

decomposition products resulting from the necessary scavenging of an extra mole of CO to produce the *p*-quinone ring.



Scheme 8-1. Modes of Reaction Initiation in $\text{Fe}(\text{CO})_4(\eta^2\text{-alkyne})$ Chemistry.
(a) Carbonyl Dissociation. (b) Migratory CO Insertion.

However, the lability of the carbonyl ligands was found to dominate the chemistry of the π -acidic HFB complex **1a** in reaction with phosphines (Chapter 4). Carbonyl substitution was observed exclusively with PR_3 ($\text{R} = \text{Me}, \text{Ph}, \text{Cy}$), and no products resulting from migratory CO insertion were observed. A kinetic study¹² quantified the rate of CO loss from **1a**, and revealed an astounding 3×10^{13} fold increase in reactivity relative to the parent $\text{Fe}(\text{CO})_5$. More interesting still was the fact that $\text{Fe}(\text{CO})_4(\eta^2\text{-HFB})$ was found to be much more reactive than its Ru and Os counterparts, providing an interesting exception to the usual triad trend for CO substitution in transition metal carbonyl compounds, (1st row) < (2nd row) > (3rd row).¹³ The phenomenal acceleration of the rate of CO dissociation has been rationalized by stabilization of the $[\text{Fe}(\text{CO})_3(\eta^2\text{-HFB})]$ intermediate by interaction of the second π set of the alkyne with the vacated metal orbital. The source of the metal dependence of carbonyl lability is believed to reside in better stabilization of the $[\text{Fe}(\text{CO})_3(\eta^2\text{-HFB})]$ intermediate due to stronger interactions between the empty $3d$ and filled π_{\perp} orbital on the alkyne than is possible for the Os and Ru analogs.

Similar to the 2nd and 3rd row metals, though, the rate of carbonyl substitution was found to be even further accelerated for the initial monophosphine substituted complexes **8**, resulting in the eventual production of *trans*-diaxially substituted products **9**. However, unlike the heavier members of the triad, the $\text{Fe}(\text{CO})_2(\text{PR}_3)_2(\eta^2\text{-HFB})$ ($\text{R} = \text{Ph}$, **9b**; Cy , **9c**) compounds were affected

by the steric bulk of the phosphine ligand, resulting in reversible dissociation of PR_3 in solution. In the case of the tricyclohexylphosphine ligand, a felicitous combination of steric and electronic characteristics allowed the isolation of $\text{Fe}(\text{CO})_2(\text{PCy}_3)(\eta^2\text{-HFB})$ (**10**), a compound containing a four electron-donor alkyne which provided a model for the putative $[\text{Fe}(\text{CO})_3(\eta^2\text{-HFB})]$ intermediate following CO dissociation from **1a**.

The $\text{Fe}(\text{CO})_4(\eta^2\text{-alkyne})$ species were also found to be useful precursors in the synthesis of alkyne-bridged heterobimetallic compounds, adding the missing members to a series of group 8/group 9 complexes already thoroughly investigated for Ru and Os with Co, Rh, and Ir (Chapters 5-7).^{5,6,8,14} A variety of structural types, including dimetallatetrahedranes, dimetallacyclobutenes, $\mu\text{-}\eta^1\text{:}\eta^3\text{-dimetallacyclopentenones}$, and $\mu\text{-}\eta^1\text{:}\eta^1\text{-dimetallacyclopentenones}$, were accessible when compounds **1** were combined with $\text{Cp}'\text{M}(\text{CO})_2$ ($\text{Cp}' = \text{Cp}, \text{Cp}^*$; $\text{M} = \text{Co}, \text{Rh}, \text{Ir}$) reagents. However, unlike the Ru and Os species, low temperature multinuclear NMR studies revealed that the reactions were not all initiated by facile CO loss from the iron-alkyne complex. Although carbonyl dissociation did rationalize some of the reactions of the π -acidic HFB and TFP species, in the majority of cases it was found that an alternate pathway, initiated by migratory CO insertion, better explained the product distributions. The isotope enrichment pattern of the dinuclear species resulting from $\text{Fe}(\text{}^{13}\text{CO})_4(\eta^2\text{-HCCR})$ ($\text{R} = \text{CF}_3$, **1b**; H, **1c**) provided strong support for the migratory insertion route. The reaction of **1c** and $\text{Cp}^*\text{Rh}(\text{CO})_2$ was particularly interesting as it followed different pathways in pentane and CD_2Cl_2 . Although the product distributions implied that the intermediate tricarbonylferracyclobutenone provided two different electrophilic sites to the entering metal nucleophile, further work is warranted to gain a better understanding of the solvent dependence of this system. Another feature of the reactions that deserves further study is the dependence of the reactions on the nature of the entering metal species. In all cases, a clear trend was established for the reactivity of the $\text{Cp}'\text{M}(\text{CO})_2$ reagents, $\text{Co} < \text{Rh} > \text{Ir}$ and $\text{Cp}^* > \text{Cp}$.

In most cases, the reactions occurred in a regioselective fashion. Indeed, with the exception of the reaction of **1c** and $\text{Cp}^*\text{Rh}(\text{CO})_2$ in CD_2Cl_2 , the $\mu\text{-}$

$\eta^1:\eta^3$ -dimetallacyclopentenones (**13**, **16**) resulting from the reaction of **1a** and **1c** with $\text{Cp}^*\text{M}(\text{CO})_2$ ($\text{M} = \text{Co}, \text{Rh}, \text{Ir}$) produced migratory CO insertion exclusively at the Fe center. The reaction of **1a** also showed an interesting dependence on the nature of the ancillary metal ligands, for $\text{CpM}(\text{CO})_2$ afforded the dimetallacyclobutenes **12** rather than $\mu\text{-}\eta^1:\eta^3$ -dimetallacyclopentenones. A study of the fluxional behavior of **12** and **13** revealed similar features connecting the two intimately related structural types.

The reactions of the unsymmetrical $\text{Fe}(\text{CO})_4(\eta^2\text{-HCCCF}_3)$ (**1b**) were more complicated, but, despite the fact that the major products often had the acyl group bonded to the ancillary metal center, a common theme was that the reaction occurred by migratory CO insertion at the iron center in **1b**. Furthermore, although the reactions of **1b** followed two different pathways, the regiochemistry of the products was rationalized by the retention of the stronger $\text{Fe-C}(\text{CF}_3)$ bond in each mechanism. The propyne analog, **1d**, gave only one type of $\mu\text{-}\eta^1:\eta^3$ -dimetallacyclopentenone product, but was much less reactive than **1a-c**. The but-2-yne complex, **1e**, was the least reactive member of the series towards $\text{Cp}^*\text{M}(\text{CO})_2$ reagents. Only $\text{Cp}^*\text{Co}(\text{CO})_2$ afforded a single product with **1e**, and it was most intriguing that the resulting bimetallic compound, $\text{Cp}^*\text{CoFe}(\mu\text{-CO})_2(\text{CO})_4$ (**33**), did not incorporate the alkyne ligand. Rather, an $\text{Fe}\rightarrow\text{Co}$ dative bond was supported by a pair of similar semi-bridging carbonyl ligands. Although the reaction pathway was not elucidated, this example was unique as all other reactions investigated thus far proceeded with retention and modification of the alkyne ligand.

An interesting contrast was also apparent in the reactivity of the $\text{Fe}(\text{CO})_4(\eta^2\text{-alkyne})$ compounds. As the coordinated alkyne became more electron rich (**1e**) the species became less reactive towards entering metal nucleophiles but more reactive towards CO. Conversely, as the alkyne became more electron poor (**1a**), a greater range of compounds was available from $\text{Cp}^*\text{M}(\text{CO})_2$ reagents but the reactions with CO proceeded sluggishly. Intermediate reactivity was observed for the acetylene compound **1c**. The decreasing ease of formation of bimetallic compounds as the alkyne donor strength increased likely reflects the decreasing thermal stability of compounds **1**

and increasing competitiveness of CO, relative to the incoming ML_n species, for the putative $[Fe(CO)_3(\eta^2\text{-alkyne})]$ intermediate. Conversely, the increasing ability to undergo migratory insertion reactions is best rationalized by the increased four-electron destabilization which is absent in the resulting metallacycloketones.

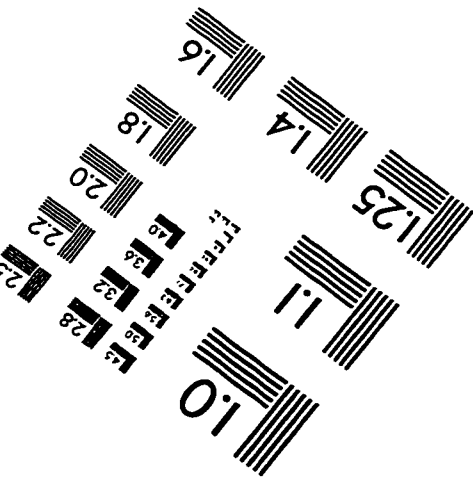
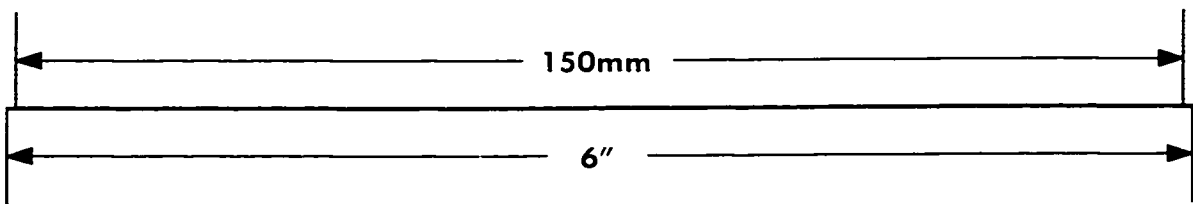
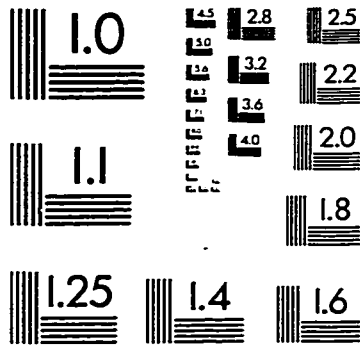
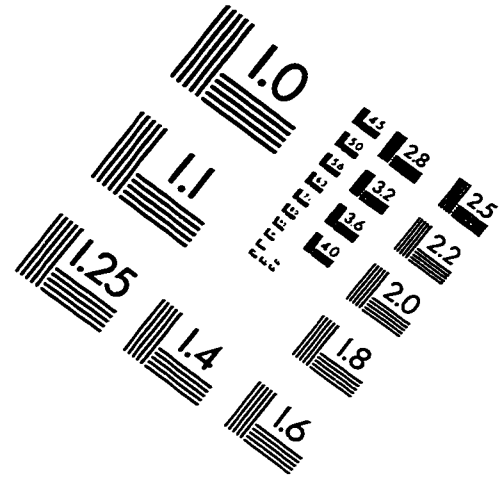
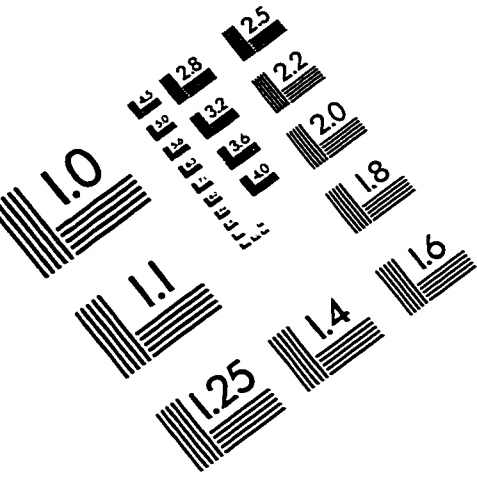
In conclusion, we have demonstrated that the long elusive $Fe(CO)_4(\eta^2\text{-alkyne})$ complexes can be successfully synthesized under suitable conditions. The ready reaction of the compounds with excess alkyne vindicates early proposals that they are intermediates in the iron carbonyl mediated coupling of alkynes with carbon monoxide. However, the remarkable acceleration toward CO substitution and the ability to form dimetallacyclic complexes clearly take the compounds beyond the realm of chemistry anticipated by Hübel and his school, justifying the somewhat playful claim of this Thesis representing an "organometallic renaissance". Furthermore, the clear structural differences seen in the products obtained by using the iron- or osmium-alkyne complexes as starting materials has enabled an initial evaluation of the factors which control the differing chemistry within the triad.

The primary difference appears to be that the $Fe(CO)_4(\eta^2\text{-alkyne})$ complexes can initiate reactions through facile migratory insertion while the Os analogs display chemistry governed entirely by a carbonyl dissociation pathway.⁸ This distinction is blurred somewhat by the realization that the carbonyl ligands in the $Fe(CO)_4(\eta^2\text{-alkyne})$ compounds are even more labile than in the Os species, a result that has been rationalized by better $4e^-$ stabilization of the $[Fe(CO)_3(\eta^2\text{-alkyne})]$ intermediate than is possible for the 3rd row transition metal. An interesting contrast is that the effects of four electron destabilization appear to cause the competing migratory insertion route, becoming especially clear for $Fe(CO)_4(\eta^2\text{-C}_2\text{Me}_2)$ (**1e**) which more readily undergoes migratory insertion than CO dissociation. Accordingly, the chemistry of the $Fe(CO)_4(\eta^2\text{-alkyne})$ complexes is governed by the competing influences of stabilizing and destabilizing four-electron interactions, a feature that is becoming more widely recognized in organometallic chemistry as a whole.¹⁵

8.1. References

1. Hübel, W. In *Organic Synthesis via Metal Carbonyls*; I. Wender and P. Pino, Eds.; Wiley-Interscience: New York, 1968; Vol. 1; pp 273 and references therein.
2. Pannell, K. H.; Crawford, G. M. *J. Coord. Chem.* **1973**, *2*, 251.
3. Carty, A. J.; Smith, W. F.; Taylor, N. J. *J. Organomet. Chem.* **1978**, *146*, C1.
4. Ball, R. G.; Burke, M. R.; Takats, J. *Organometallics* **1987**, *6*, 1918.
5. Gagné, M. R.; Takats, J. *Organometallics* **1988**, *7*, 561.
6. Burn, M. J.; Kiel, G.-Y.; Seils, F.; Takats, J.; Washington, J. *J. Am. Chem. Soc.* **1989**, *111*, 6850.
7. Washington, J.; McDonald, R.; Takats, J.; Menashe, N.; Reshef, D.; Shvo, Y. *Organometallics* **1995**, *14*, 3996.
8. Washington, J. PhD Thesis, University of Alberta, 1994.
9. Orgel, L. E. In *International Conference on Co-ordination Chemistry*; Spec. Publ. No. 13, The Chemical Society: London, 1959; pp 93.
10. Sternberg, H. W.; Markby, R.; Wender, I. *J. Am. Chem. Soc.* **1958**, *80*, 1009.
11. Parshall, W.; Ittel, S. D. *Homogeneous Catalysis*; Wiley-Interscience: New York, 1992; Vol. 2, pp 205-207.
12. Pearson, J.; Cooke, J.; Takats, J.; Jordan, R. B. *J. Am. Chem. Soc.* **1998**, *120*, 1434.
13. Basolo, F. *Polyhedron* **1990**, *9*, 1503.
14. Hoffman, K. MSc. Thesis, University of Alberta, 1994.
15. Caulton, K. G. *New. J. Chem.* **1994**, *18*, 25.

IMAGE EVALUATION TEST TARGET (QA-3)



APPLIED IMAGE, Inc.
1653 East Main Street
Rochester, NY 14609 USA
Phone: 716/482-0300
Fax: 716/288-5989

© 1993, Applied Image, Inc., All Rights Reserved

